Mechanical Engineering Series

Dietmar Gross
Thomas Seelig

Fracture Mechanics

With an Introduction to Micromechanics

Second Edition

Springer

Mechanical Engineering Series

Frederick F. Ling
Editor-in-Chief

For further volumes:
http://www.springer.com/series/1161

Dietmar Gross • Thomas Seelig

Fracture Mechanics

With an Introduction to Micromechanics

Second Edition

Springer

Prof. Dr.-Ing. Dietmar Gross
Division of Solid Mechanics
TU Darmstadt
Hochschulstrasse 1
D-64289 Darmstadt
Germany
gross@mechanik.tu-darmstadt.de

Prof. Dr.-Ing. Thomas Seelig
Institute of Mechanics
Karlsruhe University (KIT)
Kaiserstrasse 12
D-76131 Karlsruhe
Germany
thomas.seelig@kit.edu

ISSN 0941-5122 e-ISSN 2192-063X
ISBN 978-3-642-19239-5 e-ISBN 978-3-642-19240-1
DOI 10.1007/978-3-642-19240-1
Springer Heidelberg Dordrecht London New York

Library of Congress Control Number: 2011932493

Cover design: SPi Publisher Services

Printed on acid-free paper

Springer is part of Springer Science+Business Media (www.springer.com)

Preface

This book has evolved from lectures on fracture mechanics and micromechanics which we held for students of engineering and natural sciences over the years. It is primarily meant as an aid for students learning the foundations of these subjects. At the same time this book may also serve as an introduction into these fields for researchers and practitioners in industry and to provide the theoretical background for solving respective problems.

The book covers the most important areas of fracture mechanics and gives an introduction into micromechanics. Our major concern was the presentation of principal concepts and methods in a clear and sound manner as a basis for a deeper entry into the matter. The presentation mainly focuses on the mechanical description of fracture processes; yet, material specific aspects are also discussed. To keep the text self-contained, continuum mechanical and phenomenological foundations are recapitulated first. They are followed by a brief survey of classical fracture and failure hypotheses. A major part of the book is devoted to linear fracture mechanics and elastic-plastic fracture mechanics. Further chapters deal with creep fracture and dynamic fracture mechanics. An extensive chapter treats foundations of micromechanics and homogenization. Finally, elements of damage mechanics and probabilistic fracture mechanics are presented. Suggestions for further reading are listed at the end of each chapter.

The first edition was well accepted by the readers making a new edition necessary. We have used this chance to incorporate a number of extensions which partly are influenced by new developments in the field of fracture mechanics. Discussed are, among others, the crack initiation at notches, cohesive zone models, the peel test, fragmentation, and strain localization due to damage and material softening. Furthermore, following suggestions from many students, supplementary examples have been added as problems at the end of some chapters.

The authors are indebted to all who have contributed to this book. This particularly includes those from whom we have learned or, as Roda Roda has put it ironically: “Copying from four books yields a fifth profound book”. Special thanks go to Mrs. Dipl.-Ing. H. Herbst who has prepared most of the figures. Finally, the pleasant cooperation with the publisher is gratefully acknowledged.

Darmstadt and Karlsruhe in June 2011,

Dietmar Gross
Thomas Seelig

Contents

Introduction 1

1 Elements of solid mechanics 5
1.1 Stress 5
1.1.1 Stress vector 5
1.1.2 Stress tensor 7
1.1.3 Equilibrium conditions 10
1.2 Deformation and strain 11
1.2.1 Strain tensor 11
1.2.2 Strain rate 13
1.3 Constitutive laws 14
1.3.1 Elasticity 15
1.3.2 Viscoelasticity 19
1.3.3 Plasticity 22
1.4 Energy principles 27
1.4.1 Energy balance 27
1.4.2 Principle of virtual work 28
1.4.3 Theorems of Clapeyron and Betti 30
1.5 Plane problems 31
1.5.1 Plane stress, plane strain, longitudinal shear 31
1.5.2 Linear elasticity, complex method 33
1.5.3 Perfectly plastic material, slip-line fields 35
1.6 Further reading 38

2 Classical fracture and failure hypotheses 39
2.1 Basic concepts 39
2.2 Failure hypotheses 41
2.2.1 Principal stress hypothesis 41
2.2.2 Principal strain hypothesis 42
2.2.3 Strain energy hypothesis 42
2.2.4 Coulomb-Mohr hypothesis 43

2.2.5 Drucker-Prager hypothesis 46
2.2.6 Johnson-Cook criterion 47
2.3 Deformation behavior during failure 48
2.4 Problems 49
2.5 Further reading 49

3 Micro and macro phenomena of fracture 51
3.1 Microscopic aspects 51
3.1.1 Surface energy, theoretical strength 51
3.1.2 Microstructure and defects 53
3.1.3 Crack formation 56
3.1.4 Percolation 57
3.2 Macroscopic aspects 59
3.2.1 Crack growth 59
3.2.2 Types of fracture 60
3.3 Further reading 61

4 Linear fracture mechanics 63
4.1 General remarks 63
4.2 Crack-tip field 64
4.2.1 Two-dimensional crack-tip fields 64
4.2.2 Mode-I crack-tip field 70
4.2.3 Three-dimensional crack-tip field 71
4.3 K-concept 72
4.4 K-factors 73
4.4.1 Examples 74
4.4.2 Integral equation formulation 80
4.4.3 Method of weight functions 82
4.4.4 Crack interaction 85
4.4.5 Stress intensity factors and stress concentration factors 90
4.5 Fracture toughness K_{Ic} 92
4.6 Energy balance 94
4.6.1 Energy release during crack propagation 94
4.6.2 Energy release rate 96
4.6.3 Compliance, energy release rate, and K-factors 99
4.6.4 Energy balance, Griffith's fracture criterion 100
4.6.5 $J-$integral 106
4.7 Small-scale yielding 113
4.7.1 Plastic zone size, Irwin's crack length correction 113
4.7.2 Qualitative remarks on the plastic zone 115
4.8 Stable crack growth 116
4.9 Mixed-mode loading 119
4.10 Crack initiation at cavities and notches 124
4.11 Fatigue crack growth 126
4.12 Interface cracks 128

4.13 Piezoelectric materials . . . 136
4.13.1 Basic principles . . . 136
4.13.2 The crack in a ferroelectric material . . . 138
4.14 Problems . . . 140
4.15 Further reading . . . 143

5 Elastic-plastic fracture mechanics . . . 145
5.1 Introduction . . . 145
5.2 Dugdale model . . . 146
5.3 Cohesive zone models . . . 150
5.4 Crack-tip field . . . 153
5.4.1 Perfectly plastic material . . . 153
5.4.2 Total strain theory, HRR−field . . . 159
5.5 Fracture criterion . . . 164
5.6 Determination of J . . . 166
5.7 Determination of J_c . . . 167
5.8 Crack propagation . . . 171
5.8.1 J–controlled crack growth . . . 171
5.8.2 Stable crack growth . . . 173
5.8.3 Steady-state crack growth . . . 175
5.9 Essential work of fracture . . . 181
5.10 Problems . . . 183
5.11 Further reading . . . 184

6 Creep fracture . . . 185
6.1 Introduction . . . 185
6.2 Fracture of linear viscoelastic materials . . . 186
6.2.1 Crack-tip field, elastic-viscoelastic analogy . . . 186
6.2.2 Fracture concept . . . 188
6.2.3 Crack propagation . . . 190
6.3 Creep fracture of nonlinear materials . . . 194
6.3.1 Secondary creep, constitutive law . . . 194
6.3.2 Stationary crack, crack-tip field, loading parameters . . . 195
6.3.3 Creep crack growth . . . 199
6.4 Further reading . . . 204

7 Dynamic fracture mechanics . . . 207
7.1 Introduction . . . 207
7.2 Some foundations of elastodynamics . . . 208
7.3 Dynamic loading of a stationary crack . . . 209
7.3.1 Crack-tip field, *K*-concept . . . 209
7.3.2 Energy release rate, energetic fracture criterion . . . 210
7.3.3 Examples . . . 211
7.4 Crack propagation . . . 214
7.4.1 Crack-tip field . . . 214

7.4.2 Energy release rate . . . 217
7.4.3 Fracture concept, crack-tip speed, crack branching, crack arrest . . . 220
7.4.4 Examples . . . 223
7.5 Fragmentation . . . 227
7.6 Further reading . . . 228

8 Micromechanics and homogenization . . . 229
8.1 Introduction . . . 229
8.2 Selected defects and fundamental solutions . . . 231
8.2.1 Eigenstrain . . . 231
8.2.2 Inhomogeneities . . . 240
8.3 Effective elastic properties . . . 245
8.3.1 Foundations . . . 245
8.3.2 Analytical approximations . . . 254
8.3.3 Energy methods and bounds . . . 273
8.4 Homogenization of elastic-plastic materials . . . 280
8.4.1 Foundations . . . 280
8.4.2 Approximations . . . 289
8.5 Thermoelastic material . . . 294
8.6 Problems . . . 296
8.7 Further reading . . . 298

9 Damage mechanics . . . 301
9.1 Introduction . . . 301
9.2 Foundations . . . 302
9.3 Brittle damage . . . 304
9.4 Ductile damage . . . 307
9.4.1 Void growth . . . 307
9.4.2 Damage models . . . 310
9.4.3 Fracture concept . . . 312
9.5 Material softening and strain localization . . . 312
9.6 Further reading . . . 316

10 Probabilistic fracture mechanics . . . 317
10.1 Introduction . . . 317
10.2 Foundations . . . 318
10.3 Statistical fracture concept of Weibull . . . 320
10.3.1 Fracture probability . . . 320
10.3.2 Fracture stress . . . 323
10.3.3 Generalizations . . . 324
10.4 Probabilistic fracture mechanical analysis . . . 325
10.5 Further reading . . . 326

Index . . . 329

Introduction

Fracture in science and technology is understood as the total or partial separation of an originally intact body or structure. The characterization of corresponding mechanical phenomena is the subject of fracture mechanics. From an engineering point of view, in many cases a macroscopic approach is sufficient. But also microscopic aspects became of increasing interest during the past years. For both, the macroscopic and microscopic approach, continuum mechanics has proven to be an effective tool. Using this well-developed instrument, fracture criteria and concepts may be established, which allow a prediction of the fracture behavior.

In general, separation of a body occurs by propagation of one or several cracks through the material. Therefore, fracture mechanics deals to a large extent with the behavior of cracks. In a real structure or material, cracks or other defects of different size which possibly evolve to cracks, are virtually always present. One of the main questions which fracture mechanics shall answer is as follows: under what circumstances does a crack in a body start to propagate and subsequently lead to fracture? Other topics are the conditions for crack nucleation, crack path prediction, or the velocity of a propagating crack.

In continuum mechanics, usually stresses and strains are used to describe the mechanical behavior of a solid. These quantities, likewise very important in fracture mechanics, can not always be directly applied for the characterization of fracture processes. One reason for this is that stresses or strains might become infinitely large at a crack tip. Another one follows from the simple fact that two cracks of different lengths behave differently when loaded by the same external stress. Under increasing load the longer crack will start to propagate at a lower stress than the shorter one. For these reasons additional quantities like *stress intensity factors* or the *energy release rate* have been introduced in fracture mechanics. They are able to characterize the local state at a crack tip and the global behavior of the crack during propagation, respectively.

For the understanding of fracture processes, at least a partial insight into the underlying micromechanisms is useful. For example, from observing the changes in the microstructure it becomes understandable how a material defect may increase until it can be regarded as a microscopic or a macroscopic crack. The relevance of

micromechanisms also explains the important role that material science has played in the past and still plays in the evolution of fracture mechanics. Increasingly, microscopic processes are mechanically modeled nowadays and incorporated into continuum theories. Special fields like damage mechanics or micromechanics have been developed from these efforts and have become important tools in fracture mechanics. In particular, micromechanics offers a theoretical framework for a systematic treatment of defects and their influence on different length scales.

Fracture mechanics may be classified from different points of view. Usually it is divided into *linear elastic fracture mechanics* and *nonlinear fracture mechanics.* The first describes fracture processes by using linear elasticity. Since this is appropriate particularly for brittle fracture, linear fracture mechanics also is understood as *brittle fracture mechanics*. In contrast, nonlinear fracture mechanics characterizes fracture processes which are dominated by inelastic material behavior. Depending on whether the material is elastic-plastic or considerable viscous effects are present, a further partition into *elastic-plastic fracture mechanics* and *creep fracture mechanics* is common practice. Another classification is rather material oriented. Accordingly, fracture mechanics sometimes is divided into fracture mechanics of metals, of polymers, or of composites. If, in contrast to a deterministic approach, probabilistic methods are used to characterize fracture processes, we call this *probabilistic fracture mechanics.*

The roots of fracture mechanics reach back to the beginnings of modern mechanics. Already GALILEO GALILEI (1564-1642) in 1638 reflected about the fracture of beams, which led him to the conclusion that the bending moment is the crucial loading measure. In parallel with the evolution of continuum mechanics in the 19th century, a number of different strength hypotheses had been proposed which partly are still in use as fracture or failure criteria. They directly employ stresses or strains to characterize the loading of the material. Corresponding efforts took place at the beginning of the last century in conjunction with the development of plasticity theory. But only in 1920 the first cornerstone of a fracture theory of cracks was set through A.A. GRIFFITH (1893–1963) by introducing the necessary energy for crack growth in the energy balance and by formulating an energetic fracture concept. A further milestone was the statistical theory of fracture formulated in 1939 by W. WEIBULL (1887-1979). But the actual breakthrough was achieved in 1951 by G.R. IRWIN (1907-1998) who was the first to characterize the state at a crack tip by stress intensity factors. The so-called K–concept of linear fracture mechanics rapidly found entrance into practical applications and is meanwhile firmly established. In the early 60s the first concepts for an elastic-plastic fracture mechanics were proposed and a rapid development set in. First steps towards an integration of damage mechanics and micromechanics into fracture mechanics have been attempted in the 80s. Despite substantial progress, fracture mechanics is by no means an already completed field but still a subject of intensive research.

The development of fracture mechanics is driven to a large extent by the ambition to prevent failure of technical constructions and components. Therefore, fracture mechanics is used as a design tool in all fields where fracture and an accompanying failure of a component with serious, or in the worst case, catastrophic consequences

must be prevented. Typical fields of application can be found in aerospace engineering, microsystems technology, nuclear power techniques, pressure vessel construction, automotive engineering, or in steel and solid construction. Moreover, fracture mechanics is used in many other fields for the solution of problems where separation processes play a dominant role. Some examples are comminution technology, earthquake research, and materials science.

Chapter 1
Elements of solid mechanics

This chapter summarizes basic concepts and equations of solid mechanics. It is self-evident that this outline cannot be complete but is limited to a necessary minimum. For more detailed descriptions the reader is referred to the literature, and selected textbooks are listed at the end of the chapter (Section 1.6). The reader with some knowledge of elasticity and plasticity may skip this part and jump directly to the next chapter.

As the term already suggests, it is the aim of solid mechanics to make the behavior of solids accessible to a mechanical analysis. Solid mechanics is based on the idealization of the real discontinuous material by a continuum. Doing so, the material properties and the appearing mechanical quantities in general may be represented by continuous functions. It is understood that a theory on this basis has its limits when the real material's discontinuous character plays an important role. Concepts like macroscopic stresses or strains are physically meaningful only when applied to sufficiently large regions compared with existing inhomogeneities. For example, in case of structural components made of polycrystalline materials, the region under consideration has to be large compared with the grain size. This always should be considered when applying conventional continuum mechanics to microscopic domains.

The representation in this chapter primarily uses cartesian coordinates and the index notation. In parallel also the symbolic notation is applied which often makes the interrelation of quantities easier to read and to understand. Accordingly, vectors and tensors are represented either through their components or by their symbols. Finally, this outline is restricted mostly to isotropic materials and small (infinitesimal) deformations.

1.1 Stress

1.1.1 Stress vector

If a body is loaded by external forces (volume forces $\boldsymbol{f}$, surface forces $\boldsymbol{t}$), distributed internal forces - the *stresses* - will be caused. For their definition we intersect the body in its actual deformed state by a fictitious cut (Fig. 1.1a). Both parts then interact through area forces of equal magnitude and opposite direction. Let $\Delta \boldsymbol{F}$ be

D. Gross and T. Seelig, *Fracture Mechanics: With an Introduction to Micromechanics*, Mechanical Engineering Series, DOI 10.1007/978-3-642-19240-1_1,

the total force acting on an area element ΔA of the cross section, then $\Delta \boldsymbol{F}/\Delta A$ is the average surface traction on this element. The limit

$$\boldsymbol{t} = \lim_{\Delta A \to 0} \frac{\Delta \boldsymbol{F}}{\Delta A} = \frac{\mathrm{d}\boldsymbol{F}}{\mathrm{d}A} \tag{1.1}$$

is called the *stress vector* in a point of the cross section. Its component $\sigma = \boldsymbol{t} \cdot \boldsymbol{n}$ in the direction of the *unit normal vector* $\boldsymbol{n}$, i.e., perpendicular to the area element $\mathrm{d}A$, is the *normal stress*; the component $\tau = \sqrt{t^2 - \sigma^2}$ acting perpendicular to $\boldsymbol{n}$ and tangential to the element $\mathrm{d}A$ is called *shear stress* (Fig. 1.1b).

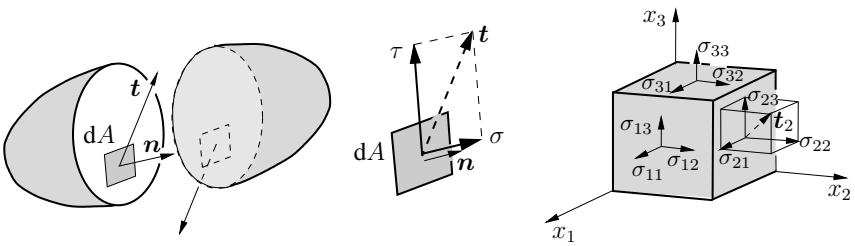

a) b) c)

Fig. 1.1 Stress vector

The stress vector $\boldsymbol{t}$ at a point depends on the orientation of the cross section, i.e., on the unit normal vector: $\boldsymbol{t} = \boldsymbol{t}(\boldsymbol{n})$. We now consider the three stress vectors $\boldsymbol{t}_1$, $\boldsymbol{t}_2$, $\boldsymbol{t}_3$, which are assigned to the three specific sections perpendicular to the coordinate axes x_1, x_2, x_3 (Fig. 1.1c). Their cartesian components are denoted by σ_{ij} where the indices i, j attain the values $1, 2, 3$. The first subscript indicates the orientation of the section, i.e., the direction of its normal $\boldsymbol{n}$, while the second subscript expresses the direction of the stress component itself. Accordingly, σ_{11}, σ_{22}, σ_{33} are normal stresses and σ_{12}, σ_{23} etc. are shear stresses. It should be mentioned that sometimes another notation will be preferred. With reference to the coordinates x,y,z the normal stresses often are denoted by σ_x, σ_y, σ_z, while the shear stresses are designated by τ_{xy}, τ_{yz} etc.

The sign of the stresses is given by the following sign convention: components at an area element whose normal vector points into the positive (negative) coordinate direction are defined as positive if they act in the positive (negative) direction.

For example, the stress vector $\boldsymbol{t}_2$ may be expressed by the components as $\boldsymbol{t}_2 = \sigma_{21}\boldsymbol{e}_1 + \sigma_{22}\boldsymbol{e}_2 + \sigma_{23}\boldsymbol{e}_3 = \sigma_{2i}\boldsymbol{e}_i$. Analogous, $\boldsymbol{t}_1 = \sigma_{1i}\boldsymbol{e}_i$ holds and consequently in general

$$\boldsymbol{t}_j = \sigma_{ji}\, \boldsymbol{e}_i \ . \tag{1.2}$$

Here $\boldsymbol{e}_1, \boldsymbol{e}_2, \boldsymbol{e}_3$ are the unit vectors in coordinate directions x_1, x_2, x_3. In addition, the *summation convention* has been adopted. According to this rule a repeated subscript indicates a summation where this subscript in turn attains the values $1, 2, 3$.

1.1.2 Stress tensor

The nine scalar quantities σ_{ij} form the cartesian components of Cauchy's *stress tensor* $\boldsymbol{\sigma}$ (A.L. CAUCHY, 1789-1857). It can be represented by the matrix

$$\boldsymbol{\sigma} = \begin{pmatrix} \sigma_{11} & \sigma_{12} & \sigma_{13} \\ \sigma_{21} & \sigma_{22} & \sigma_{23} \\ \sigma_{31} & \sigma_{32} & \sigma_{33} \end{pmatrix} . \tag{1.3}$$

The stress tensor characterizes the *stress state* at a point of the body, i.e., it uniquely determines the stress vector for an arbitrary section through the material. This can be shown by considering the infinitesimal tetrahedron in Fig. 1.2a. The orientation of the area $\mathrm{d}A$ is given by its normal $\boldsymbol{n}$ or by its components n_i, respectively. Taking into account that possible body forces are of higher order small, equilibrium requires $\boldsymbol{t}\,\mathrm{d}A = \boldsymbol{t}_1 \mathrm{d}A_1 + \boldsymbol{t}_2 \mathrm{d}A_2 + \boldsymbol{t}_3 \mathrm{d}A_3$. Introducing $\boldsymbol{t} = t_i\,\boldsymbol{e}_i$, $\mathrm{d}A_j = \mathrm{d}A\,n_j$ and (1.2) yields in index notation and in symbolic notation, respectively

$$t_i = \sigma_{ij} n_j \qquad \text{or} \qquad \boldsymbol{t} = \boldsymbol{\sigma} \cdot \boldsymbol{n} \tag{1.4}$$

where the dot in the symbolic notation indicates a summation over one subscript (in this case the subscript j). Thus, the stress tensor $\boldsymbol{\sigma}$ determines the stress vector $\boldsymbol{t}$ for each direction $\boldsymbol{n}$. It should be mentioned that (1.4) represents a linear mapping of two vectors by which $\boldsymbol{\sigma}$ is characterized as a second rank tensor.

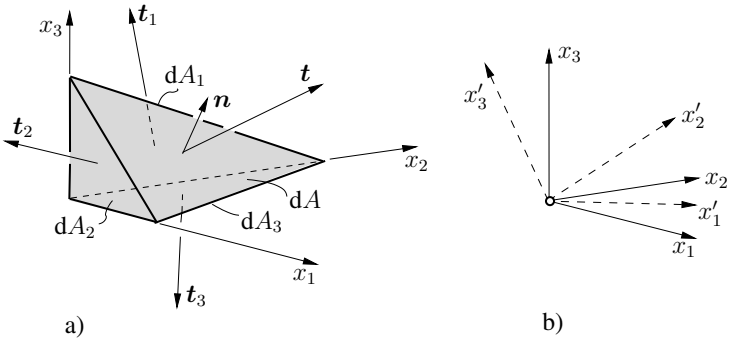

Fig. 1.2 Stress state

On account of the equilibrium condition of moments (which we will not discuss here), the stress tensor is symmetric:

$$\sigma_{ij} = \sigma_{ji} \, . \tag{1.5}$$

As a consequence, the shear stresses in two perpendicular cuts are pairwise equal to each other.

Sometimes it is necessary or useful to represent the components of the stress tensor in a coordinate system x_1', x_2', x_3' which is rotated with respect to the original system x_1, x_2, x_3 (Fig. 1.2b). The relationship between the components with respect to the first and the second system is given by the *transformation relation*

$$\sigma'_{kl} = a_{ki} a_{lj}\, \sigma_{ij} \ . \tag{1.6}$$

Herein a_{ki} denotes the cosine of the angle between the x'_k- and the x_i-axis: $a_{ki} = \cos(x'_k, x_i) = \boldsymbol{e}'_k \cdot \boldsymbol{e}_i$.

A particular coordinate system is given by the *principal axes*. They are characterized by the special feature that solely normal stresses and no shear stresses appear in sections perpendicular to these axes. In this case, the stress vector t_i and the accompanying normal vector n_i have the same direction: $t_i = \sigma n_i = \sigma \delta_{ij} n_j$. Here σ is the normal stress in the section and δ_{ij} the so-called *Kronecker-symbol* which is defined as $\delta_{ij} = 1$ for $i = j$ and $\delta_{ij} = 0$ for $i \neq j$. Introducing this into (1.4) we get the homogeneous linear system of equations

$$(\sigma_{ij} - \sigma\, \delta_{ij}) n_j = 0 \qquad \text{or} \qquad (\boldsymbol{\sigma} - \sigma\, \boldsymbol{I}) \cdot \boldsymbol{n} = \boldsymbol{0} \tag{1.7}$$

where $\boldsymbol{I}$ is the unit tensor with the components δ_{ij}. The system of equations (1.7) has a nontrivial solution for the unknown n_j only if its determinant vanishes: $\det(\sigma_{ij} - \sigma\, \delta_{ij}) = 0$. This leads to the cubic equation

$$\sigma^3 - I_\sigma\, \sigma^2 - II_\sigma\, \sigma - III_\sigma = 0 \tag{1.8}$$

where the quantities I_σ, II_σ, III_σ are independent of the chosen coordinate system. They are the *invariants* of the stress tensor and given by

$$\begin{aligned} I_\sigma &= \sigma_{ii} = \sigma_{11} + \sigma_{22} + \sigma_{33} \ , \\ II_\sigma &= (\sigma_{ij}\sigma_{ij} - \sigma_{ii}\sigma_{jj})/2 \\ &= -(\sigma_{11}\sigma_{22} + \sigma_{22}\sigma_{33} + \sigma_{33}\sigma_{11}) + \sigma_{12}^2 + \sigma_{23}^2 + \sigma_{31}^2 \ , \\ III_\sigma &= \det(\sigma_{ij}) = \begin{vmatrix} \sigma_{11} & \sigma_{12} & \sigma_{13} \\ \sigma_{21} & \sigma_{22} & \sigma_{23} \\ \sigma_{31} & \sigma_{32} & \sigma_{33} \end{vmatrix} \ . \end{aligned} \tag{1.9}$$

The three solutions σ_1, σ_2, σ_3 of (1.8) are all real and called the *principal stresses*. Each principal stress corresponds to a *principal direction* (normal vector n_j directed along the principal axis) which may be determined from (1.7). It can be shown that the principal directions are perpendicular to each other and that the principal stresses are stationary (extreme) values of normal stresses at a point of the body. With respect to the principal axes the stress tensor can be represented by

$$\boldsymbol{\sigma} = \begin{pmatrix} \sigma_1 & 0 & 0 \\ 0 & \sigma_2 & 0 \\ 0 & 0 & \sigma_3 \end{pmatrix} \ . \tag{1.10}$$

In sections whose normal is perpendicular to one principal axis and forms angles of 45° with the remaining two axes, extreme shear stresses appear. For example, in such a section with the normal perpendicular to the σ_3-direction a shear stress $\tau_3 = \pm(\sigma_1 - \sigma_2)/2$ acts. In general, the three extreme shear stresses are given by

$$\tau_1 = \pm\frac{\sigma_2 - \sigma_3}{2}\,, \quad \tau_2 = \pm\frac{\sigma_3 - \sigma_1}{2}\,, \quad \tau_3 = \pm\frac{\sigma_1 - \sigma_2}{2}\,. \tag{1.11}$$

Thus, if σ_1 is the maximum and σ_3 the minimum principal stress, the maximum shear stress results as

$$\tau_{\max} = \frac{\sigma_1 - \sigma_3}{2}\,. \tag{1.12}$$

Of practical relevance are also the *octahedral stresses*. They are defined as normal and shear stress in cross sections whose normal forms the same angle with all three principal axes:

$$\begin{aligned} \sigma_{\rm oct} &= \frac{\sigma_1 + \sigma_2 + \sigma_3}{3} = \frac{\sigma_{ii}}{3} = \frac{I_\sigma}{3}\,, \\ \tau_{\rm oct} &= \frac{1}{3}\sqrt{(\sigma_1 - \sigma_2)^2 + (\sigma_2 - \sigma_3)^2 + (\sigma_3 - \sigma_1)^2}\,. \end{aligned} \tag{1.13}$$

The stress component $\sigma_{\rm oct}$ can be interpreted as the average normal stress: $\sigma_m = \sigma_{kk}/3 = \sigma_{\rm oct}$.

In many cases it is useful to decompose the stress tensor additively:

$$\sigma_{ij} = \frac{\sigma_{kk}}{3}\,\delta_{ij} + s_{ij} \qquad \text{or} \qquad \boldsymbol{\sigma} = \sigma_m\,\boldsymbol{I} + \boldsymbol{s}\,. \tag{1.14}$$

Therein $\frac{1}{3}\sigma_{kk}\delta_{ij}$ characterizes a loading by an all-side equal stress σ_m. Because of the analogy with a static stress state in a fluid, this part is referred to as a *hydrostatic stress state*. The tensor $\boldsymbol{s}$ is called *deviatoric stress state*. By this part and its invariants

$$\begin{aligned} I_s &= 0\,, \\ II_s &= \frac{1}{2}\,s_{ij}s_{ij} = \frac{1}{6}\left[(\sigma_1 - \sigma_2)^2 + (\sigma_2 - \sigma_3)^2 + (\sigma_3 - \sigma_1)^2\right] \\ &= \frac{1}{6}[(\sigma_{11} - \sigma_{22})^2 + (\sigma_{22} - \sigma_{33})^2 + (\sigma_{33} - \sigma_{11})^2] + \sigma_{12}^2 + \sigma_{23}^2 + \sigma_{31}^2\,, \\ III_s &= \frac{1}{3}\,s_{ij}s_{jk}s_{ki} \end{aligned} \tag{1.15}$$

the deviation of the stress state from a hydrostatic state is characterized. Comparison with (1.13) yields: $II_s = \frac{3}{2}\tau_{\rm oct}^2$.

A graphical visualization of the stress state is possible by the so-called *Mohr's circles* (O. MOHR, 1835-1918). This is a representation of normal stresses σ and corresponding shear stresses τ as points in a σ-τ-diagram for all possible cross sections and directions, respectively. With respect to principal axes, we get from

equation (1.4)

$$\sigma^2 + \tau^2 = t_i t_i = \sigma_1^2 n_1^2 + \sigma_2^2 n_2^2 + \sigma_3^2 n_3^2 \,,$$
$$\sigma = t_i n_i = \sigma_1 n_1^2 + \sigma_2 n_2^2 + \sigma_3 n_3^2 \,.$$

Inserting this into the identity

$$(\sigma - \frac{\sigma_2 + \sigma_3}{2})^2 + \tau^2 = -\sigma(\sigma_2 + \sigma_3) + (\frac{\sigma_2 + \sigma_3}{2})^2 + (\sigma^2 + \tau^2)$$

and taking into account $n_i n_i = 1$, it may be written as

$$(\sigma - \frac{\sigma_2 + \sigma_3}{2})^2 + \tau^2 = n_1^2(\sigma_1 - \sigma_2)(\sigma_1 - \sigma_3) + (\frac{\sigma_2 - \sigma_3}{2})^2 \,. \tag{1.16}$$

This equation formally may be interpreted as the equation of a "circle" with its center at $\sigma = (\sigma_2 + \sigma_3)/2$, $\tau = 0$ and a radius depending on n_1. Because of $0 \le n_1^2 \le 1$ the minimum stress distance from the center is $(\sigma_2 - \sigma_3)/2 = \tau_1$ (for $n_1 = 0$), while the maximum distance is $\sigma_1 + (\sigma_2 - \sigma_3)/2$ (for $n_1 = \pm 1$). Analogous considerations can be performed for two further equations which follow from (1.16) by a cyclic permutation of subscripts. Arranging the principal stresses according to their magnitude ($\sigma_1 \ge \sigma_2 \ge \sigma_3$), we finally get the condensed representation of Fig. 1.3. Accordingly, stress points (σ, τ) are possible only in the shaded region and on the circles of radii τ_i. The circles themselves correspond to cross sections with a normal perpendicular to one of the three principal axes.

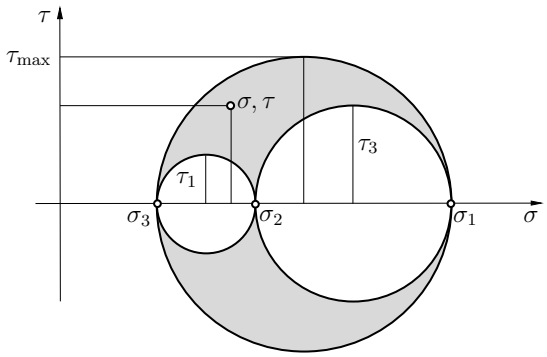

Fig. 1.3 Mohr's circles

1.1.3 Equilibrium conditions

An arbitrary material region is in general loaded by body forces f_i which are distributed over the volume V and surface forces (stress vector) t_i acting along the

surface ∂V. Force equilibrium is ensured if the resultant of these forces vanishes:

$$\int_{\partial V} t_i \, \mathrm{d}A + \int_V f_i \, \mathrm{d}V = 0 \; . \tag{1.17}$$

Using $t_i = \sigma_{ij} n_j$, see (1.7), and applying the divergence theorem $\int_{\partial V} \sigma_{ij} n_j \, \mathrm{d}A = \int_V \sigma_{ij,j} \, \mathrm{d}V$ this equation can be rewritten as

$$\int_V (\sigma_{ij,j} + f_i) \, \mathrm{d}V = 0 \; . \tag{1.18}$$

Here we have assumed that the stresses and their derivatives are continuous. The latter are indicated by a subscript after a comma: $\sigma_{ij,j} = \partial \sigma_{ij} / \partial x_j$. Since the volume V is arbitrary, it follows from (1.18) that for each point of the body the local *equilibrium conditions*

$$\sigma_{ij,j} + f_i = 0 \qquad \text{or} \qquad \nabla \cdot \boldsymbol{\sigma} + \boldsymbol{f} = \boldsymbol{0} \tag{1.19}$$

must be fulfilled. Within the symbolic notation, we have used the vector operator $\nabla = (\partial / \partial x_j) \, \boldsymbol{e}_j$.

From (1.19) the *equations of motion* directly can be derived if the motion-induced *inertia forces* $-\rho \ddot{u}_i$ are considered as additional volume forces:

$$\sigma_{ij,j} + f_i = \rho \, \ddot{u}_i \; . \tag{1.20}$$

Here ρ is the mass density and dots above a quantity denote derivatives with respect to time.

We will not discuss the equilibrium of moments. It only should be noted that this condition leads to the already mentioned symmetry of the stress tensor (1.5).

1.2 Deformation and strain

1.2.1 Strain tensor

The kinematics of a deformable body usually is described in terms of the displacement vector and a strain tensor. These quantities can be introduced by considering an arbitrary material point P whose position in the undeformed state (e.g., at time $t = 0$) is given by the coordinates (position vector) X_i, see Fig. 1.4. A point Q at a distance $\mathrm{d}S$ adjacent to P has the coordinates $X_i + \mathrm{d}X_i$. On account of a load-induced deformation, P is displaced to P' and Q to Q', respectively. Their current position (at time t) is given by the space coordinates x_i and $x_i + \mathrm{d}x_i$, respectively. The displacement from P to P' is expressed by the *displacement vector*

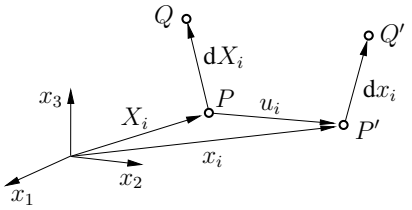

Fig. 1.4 Deformation

$$u_i = x_i - X_i \ . \tag{1.21}$$

Assuming a uniquely invertible mapping between x_i and X_i, the displacement vector u_i and the position vector x_i can be regarded as functions of the *material coordinates* X_i:

$$u_i = u_i(X_j, t) \ , \qquad x_i = x_i(X_j, t) \ . \tag{1.22}$$

In order to derive a suitable deformation measure we compare the distances of adjacent points in the deformed and undeformed state. It is convenient to consider for this purpose the squared distances

$$\mathrm{d}s^2 = \mathrm{d}x_k \mathrm{d}x_k = \frac{\partial x_k}{\partial X_i} \frac{\partial x_k}{\partial X_j} \, \mathrm{d}X_i \mathrm{d}X_j \ ,$$
$$\mathrm{d}S^2 = \mathrm{d}X_k \mathrm{d}X_k = \mathrm{d}X_i \mathrm{d}X_j \, \delta_{ij} \ .$$

Using (1.21) and (1.22) one obtains

$$\mathrm{d}s^2 - \mathrm{d}S^2 = 2 \, E_{ij} \, \mathrm{d}X_i \mathrm{d}X_j \tag{1.23}$$

where

$$E_{ij} = \frac{1}{2} \left(\frac{\partial u_i}{\partial X_j} + \frac{\partial u_j}{\partial X_i} + \frac{\partial u_k}{\partial X_i} \frac{\partial u_k}{\partial X_j} \right) \tag{1.24}$$

is a symmetric second rank tensor which is called *Green's strain tensor* (G. GREEN, 1793-1841).

It can be shown that for sufficiently small (infinitesimal) displacement gradients ($\partial u_i / \partial X_j \ll 1$) the derivatives with respect to material coordinates X_j can be replaced by derivatives with respect to space coordinates x_j, i.e., $\partial u_i / \partial X_j \to \partial u_i / \partial x_j = u_{i,j}$. Taking into account that in this case the product of the displacement gradients in E_{ij} vanishes (being small of higher order), we get from (1.24) the *infinitesimal strain tensor*

$$\varepsilon_{ij} = \frac{1}{2} (u_{i,j} + u_{j,i}) \ . \tag{1.25}$$

It may be represented as the matrix

$$\boldsymbol{\varepsilon} = \begin{pmatrix} \varepsilon_{11} & \varepsilon_{12} & \varepsilon_{13} \\ \varepsilon_{21} & \varepsilon_{22} & \varepsilon_{23} \\ \varepsilon_{31} & \varepsilon_{32} & \varepsilon_{33} \end{pmatrix} \tag{1.26}$$

which is symmetric because of $\varepsilon_{ij} = \varepsilon_{ji}$, see (1.25).

Geometrically, the *normal strains* ε_{11}, ε_{22}, ε_{33} can be interpreted as relative length changes and the *shear strains* ε_{12}, ε_{23}, ε_{31} as angle changes. In this context also the engineering notation should be mentioned. With reference to x, y, z-coordinates often the notation ε_x, ε_y, ε_z for normal strains and $\gamma_{xy}/2$, $\gamma_{yz}/2$, $\gamma_{zx}/2$ for shear strains is used.

The properties of the strain tensor can be transferred from the stress tensor. There exists a system of principal axes where shear strains vanish and solely *principal strains* ε_1, ε_2, ε_3 appear. Furthermore, the strain tensor has the three invariants I_ε, II_ε, III_ε. The first invariant characterizes the *volumetric strain*, i.e., the relative volume change:

$$I_\varepsilon = \varepsilon_V = \varepsilon_{kk} = \varepsilon_1 + \varepsilon_2 + \varepsilon_3 \; . \tag{1.27}$$

If the strain tensor is decomposed according to

$$\varepsilon_{ij} = \frac{\varepsilon_{kk}}{3}\,\delta_{ij} + e_{ij} \qquad \text{or} \qquad \boldsymbol{\varepsilon} = \frac{\varepsilon_V}{3}\,\boldsymbol{I} + \boldsymbol{e} \tag{1.28}$$

then the first part describes the volume change while the second part, the strain deviator $\boldsymbol{e}$, expresses a *distorsion*, i.e., a deformation at constant volume. Of particular importance is the second invariant of the deviator which in analogy to (1.15) reads

$$II_e = \frac{1}{2}\,e_{ij}e_{ij} = \frac{1}{6}\left[(\varepsilon_1 - \varepsilon_2)^2 + (\varepsilon_2 - \varepsilon_3)^2 + (\varepsilon_3 - \varepsilon_1)^2\right] . \tag{1.29}$$

For given strain components (1.25) forms a system of six equations for the three displacement components. Thus, the strain components cannot be independent of each other if the displacement field in a simply connected domain shall be unique (apart from a rigid body motion). They have to satisfy the *compatibility conditions* which can be derived from (1.25) by eliminating the displacements:

$$\varepsilon_{ij,kl} + \varepsilon_{kl,ij} - \varepsilon_{ik,jl} - \varepsilon_{jl,ik} = 0 \; . \tag{1.30}$$

1.2.2 Strain rate

The strain tensor is not always suitable to describe the deformation and motion of a deformable body. In some cases, as for example in plasticity, it is more appropriate to use strain changes and strain rates, respectively. To introduce these quantities we start from the velocity field $v_i(x_j, t)$ (Fig. 1.5). The relative velocity of two particles, located at time t at adjacent points P' und Q' in space is expressed by

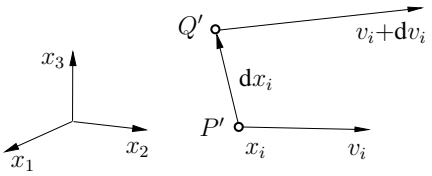

Fig. 1.5 Strain rate

$$\mathrm{d}v_i = \frac{\partial v_i}{\partial x_j}\,\mathrm{d}x_j = v_{i,j}\,\mathrm{d}x_j \ . \tag{1.31}$$

Through this equation, the velocity gradient $v_{i,j}$ is defined as a second rank tensor which can be decomposed as follows:

$$v_{i,j} = \frac{1}{2}(v_{i,j} + v_{j,i}) + \frac{1}{2}(v_{i,j} - v_{j,i}) = D_{ij} + W_{ij} \ . \tag{1.32}$$

The symmetric part

$$D_{ij} = \frac{1}{2}(v_{i,j} + v_{j,i}) \tag{1.33}$$

is known as the *strain rate tensor*. It characterizes the temporal strain change of the current configuration. Multiplying it with the time increment yields the so-called *natural strain increment*:

$$\mathrm{d}\epsilon_{ij} = D_{ij}\,\mathrm{d}t \ . \tag{1.34}$$

If the strains remain small during the whole deformation history, then D_{ij} and $\mathrm{d}\epsilon_{ij}$ can be replaced by the time derivative of the strain tensor $\dot{\varepsilon}_{ij}$ and by the strain increment $\mathrm{d}\varepsilon_{ij}$, respectively. In the following, we will mostly employ this assumption. It also should be mentioned that all properties of the stress tensor analogously can be transferred to D_{ij} and $\mathrm{d}\epsilon_{ij}$. In addition, the compatibility conditions (1.30) can be applied by replacing ε_{ij} by D_{ij} and $\mathrm{d}\epsilon_{ij}$, respectively.

The skew-symmetric part W_{ij} in (1.32) characterizes the current rotation (spin) which will not be further discussed here.

1.3 Constitutive laws

In the following we will assume small (infinitesimal) strains which is appropriate for a wide range of problems. This assumption also considerably simplifies the formulation of constitutive laws by which the deformation behavior of the material is characterized.

1.3.1 Elasticity

1.3.1.1 Linear elastic behavior

Generalizing the uniaxial Hooke's law $\sigma = E\,\varepsilon$ (R. HOOKE, 1635-1703) for a linear elastic material, stresses and strains in the three-dimensional case are related as

$$\boldsymbol{\sigma} = \boldsymbol{C} : \boldsymbol{\varepsilon} \qquad \text{or} \qquad \sigma_{ij} = C_{ijkl}\,\varepsilon_{kl}\ . \tag{1.35a}$$

Here the two dots in the symbolic notation indicate a summation over two index pairs (in this case k, l). The *elasticity tensor* $\boldsymbol{C}$ is a fourth rank tensor which characterizes through its components C_{ijkl}, i.e., through the elasticity constants, the elastic properties of the material. It can be shown that $\boldsymbol{C}$ in the most general anisotropic case consists of 21 independent constants and that the symmetries $C_{ijkl} = C_{jikl} = C_{ijlk} = C_{klij}$ hold. Inverting (1.35a), the elasticity law alternatively can be written as

$$\boldsymbol{\varepsilon} = \boldsymbol{M} : \boldsymbol{\sigma} \qquad \text{or} \qquad \varepsilon_{ij} = M_{ijkl}\,\sigma_{kl} \tag{1.35b}$$

where $\boldsymbol{M} = \boldsymbol{C}^{-1}$ is the *compliance tensor*. Its components M_{ijkl} have identical symmetry properties as C_{ijkl}.

An isotropic material shows the same behavior in all directions. In this case, $\boldsymbol{C}$ is an isotropic tensor which is determined by solely two independent constants:

$$C_{ijkl} = \lambda\,\delta_{ij}\delta_{kl} + \mu\,(\delta_{ik}\delta_{jl} + \delta_{il}\delta_{jk})\ . \tag{1.36}$$

Inserting this representation into (1.35a) the elasticity law reads

$$\sigma_{ij} = \lambda\,\varepsilon_{kk}\,\delta_{ij} + 2\,\mu\,\varepsilon_{ij} \tag{1.37}$$

where λ and μ are the so-called Lamé constants (G. LAMÉ, 1795-1870). Their relation with Young's modulus E (T. YOUNG, 1773-1829), shear modulus G, Poisson's ratio ν (S.D. POISSON, 1781-1840) and the bulk modulus K is given in Table 1.1.

Inverting (1.37) according to (1.35b) and using the relations in Table 1.2, the elasticity law can be rewritten as

$$\varepsilon_{ij} = -\frac{\nu}{E}\,\sigma_{kk}\,\delta_{ij} + \frac{1+\nu}{E}\,\sigma_{ij}\ . \tag{1.38}$$

Another possibility of representation is the decomposition of the isotropic elasticity law into its hydrostatic (volumetric) and deviatoric part. Using (1.14), (1.28) and the relations of Table 1.1 yields

$$\sigma_{kk} = 3\,K\,\varepsilon_{kk}\ , \qquad s_{ij} = 2\,\mu\,e_{ij}\ . \tag{1.39}$$

An anisotropic material is characterized by its different behavior in different directions. In the following we restrict our attention to two specific cases. An *or-*

	basic pair			
	$\lambda,\ \mu$	$\mu,\ K$	$E,\ G$	$E,\ \nu$
λ	λ	$K-\frac{2}{3}\,\mu$	$\frac{G(E-2G)}{3G-E}$	$\frac{E\nu}{(1+\nu)(1-2\nu)}$
μ	μ	μ	G	$\frac{E}{2(1+\nu)}$
K	$\lambda+\frac{2}{3}\,G$	K	$\frac{G\,E}{3(3G-E)}$	$\frac{E}{3(1-2\nu)}$
E	$\frac{\mu(3\lambda+2\mu)}{\lambda+\mu}$	$\frac{9K\,\mu}{3K+\mu}$	E	E
ν	$\frac{\lambda}{2(\lambda+\mu)}$	$\frac{3K-2\mu}{2(3K+\mu)}$	$\frac{E}{2G}-1$	ν

Table 1.1 Relations between elastic constants

thotropic material has three principal material directions which are perpendicular to each other. If they coincide with the chosen coordinate axes, the elasticity law can be expressed in matrix notation as

$$\begin{bmatrix} \varepsilon_{11} \\ \varepsilon_{22} \\ \varepsilon_{33} \\ 2\,\varepsilon_{23} \\ 2\,\varepsilon_{31} \\ 2\,\varepsilon_{12} \end{bmatrix} = \begin{bmatrix} h_{11} & h_{12} & h_{13} & 0 & 0 & 0 \\ h_{12} & h_{22} & h_{23} & 0 & 0 & 0 \\ h_{13} & h_{23} & h_{33} & 0 & 0 & 0 \\ 0 & 0 & 0 & h_{44} & 0 & 0 \\ 0 & 0 & 0 & 0 & h_{55} & 0 \\ 0 & 0 & 0 & 0 & 0 & h_{66} \end{bmatrix} \begin{bmatrix} \sigma_{11} \\ \sigma_{22} \\ \sigma_{33} \\ \sigma_{23} \\ \sigma_{31} \\ \sigma_{12} \end{bmatrix} . \tag{1.40}$$

The nine independent compliances h_{ij} are related to the tensor components M_{ijkl} and the engineering elasticity constants E_i (Young's moduli), ν_{ij} (Poisson's ratios), μ_{ij} (shear moduli) as follows:

$$\begin{aligned} h_{11} &= M_{1111} = \frac{1}{E_1}\,, \quad h_{12} = M_{1122} = -\frac{\nu_{12}}{E_1} = -\frac{\nu_{21}}{E_2}\,, \quad h_{44} = M_{2323} = \frac{1}{\mu_{23}}\,, \\ h_{22} &= M_{2222} = \frac{1}{E_2}\,, \quad h_{23} = M_{2233} = -\frac{\nu_{23}}{E_2} = -\frac{\nu_{32}}{E_3}\,, \quad h_{55} = M_{3131} = \frac{1}{\mu_{31}}\,, \\ h_{33} &= M_{3333} = \frac{1}{E_3}\,, \quad h_{13} = M_{1133} = -\frac{\nu_{13}}{E_1} = -\frac{\nu_{31}}{E_3}\,, \quad h_{66} = M_{1212} = \frac{1}{\mu_{12}}\,. \end{aligned} \tag{1.41}$$

If the material constants of an orthotropic material are not changed when the material is rotated with respect to one of its principal directions (e.g., the x_3-axis), it is called *transversely isotropic*. Since the compliances in this case are interrelated by

$$h_{11} = h_{22}\,, \quad h_{13} = h_{23}\,, \quad h_{44} = h_{55}\,, \quad h_{66} = 2(h_{11} - h_{12})\,, \tag{1.42}$$

such a material is characterized by only five independent elasticity constants.

When a stress-free material is heated, thermal strains $\boldsymbol{\varepsilon}^{th}$ appear. They are, at a good approximation, proportional to the temperature change ΔT:

$$\boldsymbol{\varepsilon}^{th} = \boldsymbol{k}\,\Delta T \qquad \text{or} \qquad \varepsilon_{ij}^{th} = k_{ij}\,\Delta T\ . \tag{1.43}$$

Here $\boldsymbol{k}$ denotes a tensor given by thermal expansion coefficients. For a thermally isotropic material it is determined by only a single parameter: $k_{ij} = k\,\delta_{ij}$. Defining total strains $\boldsymbol{\varepsilon}$ as the sum of elastic and thermal strains, the elasticity law attains the form of the so-called Duhamel-Neumann law (J.M. DUHAMEL, 1797-1872, F. NEUMANN, 1798-1895)

$$\boldsymbol{\sigma} = \boldsymbol{C} : (\boldsymbol{\varepsilon} - \boldsymbol{\varepsilon}^{th})\ . \tag{1.44}$$

1.3.1.2 Strain energy density

The work per unit volume, done during deformation of an elastic material

$$U = \int_0^{\varepsilon_{kl}} \sigma_{ij}\,\mathrm{d}\varepsilon_{ij} \tag{1.45}$$

is independent of the deformation path. In this case the integrand $\mathrm{d}U = \sigma_{ij}\mathrm{d}\varepsilon_{ij}$ is a total differential, i.e., $\mathrm{d}U = \frac{\partial U}{\partial \varepsilon_{ij}}\mathrm{d}\varepsilon_{ij}$, and

$$\sigma_{ij} = \frac{\partial U}{\partial \varepsilon_{ij}} \tag{1.46}$$

holds. The function $U = U(\varepsilon_{ij})$ is called *strain energy density*.

In addition to $U(\varepsilon_{ij})$, the *complementary energy density* $\widetilde{U}(\sigma_{ij})$ may be introduced. It is defined as

$$\widetilde{U} = \sigma_{ij}\varepsilon_{ij} - U = \int_0^{\sigma_{kl}} \varepsilon_{ij}\,\mathrm{d}\sigma_{ij}\ . \tag{1.47}$$

Analogous to (1.46), the relation

$$\varepsilon_{ij} = \frac{\partial \widetilde{U}}{\partial \sigma_{ij}} \tag{1.48}$$

is valid.

Specifically for a linear elastic material, by introducing (1.35a) and (1.35b) into (1.45) and (1.47), the strain energy density and complementary energy density can be determined as

$$U = \widetilde{U} = \frac{1}{2}\,\sigma_{ij}\varepsilon_{ij} = \frac{1}{2}\,\boldsymbol{\varepsilon} : \boldsymbol{C} : \boldsymbol{\varepsilon} = \frac{1}{2}\,\boldsymbol{\sigma} : \boldsymbol{M} : \boldsymbol{\sigma}\ . \tag{1.49}$$

Using (1.14), (1.28), and (1.39) the strain energy density can be decomposed into two parts:

$$U = \frac{1}{2}\, K\, \varepsilon_{kk}^2 + \mu\, e_{ij} e_{ij} = U_V + U_D \ . \tag{1.50}$$

Here $U_V = \frac{1}{2} K \varepsilon_{kk}^2 = \frac{1}{2} K I_\varepsilon^2$ is the pure *volumetric strain energy density* (= portion of energy on account of a volumetric strain) while $U_D = \mu\, e_{ij} e_{ij} = 2\,\mu\, II_e$ is the *distortional energy density* (= portion of energy on account of purely deviatoric strains).

1.3.1.3 Nonlinear elastic material behavior

The strain energy density U of an isotropic material depends solely on the invariants I_ε, II_ε, III_ε of the strain tensor. Since II_ε and III_ε can be expressed by the invariants II_e, III_e of the deviator and by I_ε, the functional dependence can be written as $U = U(I_\varepsilon, II_e, III_e)$. Consequently, using (1.46) and $I_\varepsilon = \varepsilon_{ij}\, \delta_{ij}$, $II_e = \frac{1}{2} e_{ij} e_{ij}$, $III_e = \frac{1}{3} e_{ij} e_{jk} e_{ki}$, a general nonlinear elasticity law may be represented as

$$\sigma_{ij} = \frac{\partial U}{\partial I_\varepsilon}\, \delta_{ij} + \frac{\partial U}{\partial II_e}\, e_{ij} + \frac{\partial U}{\partial III_e}\, e_{ik} e_{kj} \ . \tag{1.51}$$

For many materials it may be assumed that the strain energy density, analogous to the linear elastic case, is additively composed of a volumetric part and a distortional part: $U = U_1(I_\varepsilon) + U_2(II_e)$. In this case (1.51) reduces to

$$\sigma_{ij} = \frac{\mathrm{d}U_1}{\mathrm{d}I_\varepsilon}\, \delta_{ij} + \frac{\mathrm{d}U_2}{\mathrm{d}II_e}\, e_{ij} \ . \tag{1.52}$$

Splitting the stresses into the hydrostatic and deviatoric parts we obtain the relations

$$\sigma_{kk} = 3\, \frac{\mathrm{d}U_1}{\mathrm{d}I_\varepsilon} = f(\varepsilon_{kk}) \ , \qquad s_{ij} = \frac{\mathrm{d}U_2}{\mathrm{d}II_e}\, e_{ij} = g(II_e)\, e_{ij} \ . \tag{1.53}$$

If the material additionally can be regarded as incompressible, i.e., $\varepsilon_{kk} = 0$, the first equation in (1.53) can be omitted. In this case the function $g(II_e)$ can be simply expressed by the material's uniaxial stress-strain curve $\sigma(\varepsilon)$. For this purpose we first define a uniaxial *equivalent stress* or *effective stress* σ_e as follows: with respect to the material response, a three-dimensional stress state $\boldsymbol{\sigma}$ (respectively $\boldsymbol{s}$) is equivalent to a uniaxial stress state σ_e, if the second invariants II_s of the deviator are equal in both stress states. This leads with (1.15) and $\sigma_1 = \sigma_\mathrm{e}$, $\sigma_2 = \sigma_3 = 0$ to

$$\sigma_\mathrm{e}^2 = \frac{3}{2}\, s_{ij} s_{ij} = \frac{3}{2}\, \boldsymbol{s} : \boldsymbol{s} \ . \tag{1.54a}$$

In case of an incompressible material, analogously, a three-dimensional strain state $\boldsymbol{\varepsilon}$ (respectively $\boldsymbol{e}$) is considered equivalent to a uniaxial strain state ε_e if the second invariants II_e are equal in both strain states. Inserting this in conjunction with $\varepsilon_1 = \varepsilon_\mathrm{e}$, $\varepsilon_2 = \varepsilon_3 = -\varepsilon_1/2$ into (1.29) results in the following definition of a uniaxial *equivalent strain* or *effective strain*

$$\varepsilon_{\mathrm{e}}^2 = \frac{2}{3}\, e_{ij} e_{ij} = \frac{2}{3}\, \boldsymbol{e} : \boldsymbol{e} \ . \tag{1.54b}$$

If we now consider the product $s_{ij} s_{ij}$ and introduce (1.53), (1.54a), (1.54b) we obtain $g = \frac{2}{3}\sigma_{\mathrm{e}}/\varepsilon_{\mathrm{e}}$ and the material law reads

$$s_{ij} = \frac{2}{3}\, \frac{\sigma_{\mathrm{e}}}{\varepsilon_{\mathrm{e}}}\, e_{ij} \ . \tag{1.55}$$

As an example we consider a uniaxial stress-strain curve, represented by the power law

$$\varepsilon = B\, \sigma^n \qquad \text{or} \qquad \sigma = b\, \varepsilon^N \tag{1.56}$$

where $n = 1/N$ and $B = 1/b^n$ are material constants. Assuming incompressibility, its three-dimensional generalization is given by

$$e_{ij} = \frac{3}{2}\, B\, \sigma_{\mathrm{e}}^{n-1} s_{ij} \qquad \text{or} \qquad s_{ij} = \frac{2}{3}\, b\, \varepsilon_{\mathrm{e}}^{N-1} e_{ij} \ . \tag{1.57}$$

The strain energy density and complementary energy density in this case are

$$U = \frac{n}{n+1}\, s_{ij} e_{ij} \ , \qquad \widetilde{U} = \frac{1}{n+1}\, s_{ij} e_{ij} \ . \tag{1.58}$$

1.3.2 Viscoelasticity

Viscoelastic materials combine elastic and viscous behavior. They are characterized by a time-dependent response and by a dependence of stresses and strains on the load or deformation history, respectively. Typical viscoelastic effects are creep and relaxation phenomena as they appear for example in polymers. But creep effects are also relevant in metals such as steel in the high temperature regime.

1.3.2.1 Linear viscoelastic material behavior

The uniaxial linear viscoelastic material behavior can be described by the constitutive law

$$\varepsilon(t) = \int_{-\infty}^{t} J(t-\tau)\, \frac{\mathrm{d}\sigma}{\mathrm{d}\tau}\, \mathrm{d}\tau \qquad \text{or} \qquad \sigma(t) = \int_{-\infty}^{t} E(t-\tau)\, \frac{\mathrm{d}\varepsilon}{\mathrm{d}\tau}\, \mathrm{d}\tau \ . \tag{1.59}$$

Here $J(t)$ and $E(t)$ are material functions, representing the response to an instantaneously applied constant stress σ_0 or constant strain ε_0, respectively. The function $J(t) = \varepsilon(t)/\sigma_0$ is called *creep function* or *creep compliance* while $E(t) = \sigma(t)/\varepsilon_0$ is referred to as *relaxation function* (Fig. 1.6). They are interrelated through

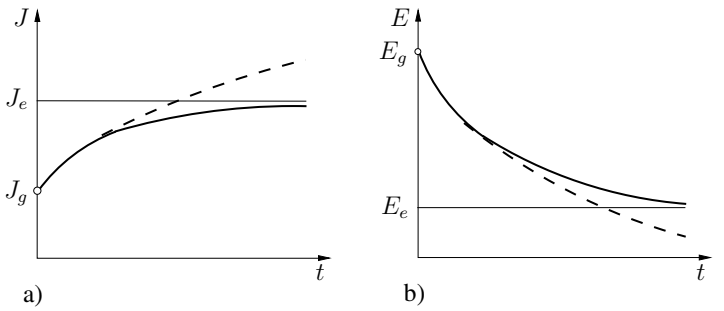

Fig. 1.6 a) Creep function, b) relaxation function

$$\frac{\mathrm{d}}{\mathrm{d}t}\int_0^t J(t-\tau)\,E(\tau)\,\mathrm{d}\tau = 1\ . \tag{1.60}$$

The lower limit of the integrals in (1.59) indicates that the material behavior at time t depends on the entire preceding stress and strain history, respectively.

In case of an isotropic material, a three-dimensional generalization of (1.59) can be obtained by separating the hydrostatic (volumetric) and deviatoric (distortional) parts. In addition, for many viscoelastic materials it may be assumed that the response to volumetric strains is purely elastic: $\sigma_{kk} = 3K\varepsilon_{kk}$. In this case, the constitutive law for the remaining deviatoric part is given by

$$e'_{ij} = \frac{1}{2}\int_{-\infty}^t J_d(t-\tau)\,\frac{\mathrm{d}s_{ij}}{\mathrm{d}\tau}\,\mathrm{d}\tau\ , \qquad s_{ij} = 2\int_{-\infty}^t G(t-\tau)\,\frac{\mathrm{d}e_{ij}}{\mathrm{d}\tau}\,\mathrm{d}\tau\ . \tag{1.61}$$

The creep function $J_d(t)$ and relaxation function $G(t)$ again are related as in the uniaxial case, see (1.60).

Integrals of the type (1.59), (1.61) are known as *convolution integrals*. They are treated conveniently by *Laplace transform*. The Laplace transformed function $\bar{f}(p)$ of a function $f(t)$ is defined as

$$\bar{f}(p) = \int_0^\infty f(t)\,\mathrm{e}^{-pt}\,\mathrm{d}t\ . \tag{1.62}$$

For instance, applying this transformation to the second equation of (1.61) and assuming that the strain history starts at time $\tau = 0$ we obtain

$$\bar{s}_{ij} = 2\,p\,\bar{G}(p)\,\bar{e}_{ij}\ . \tag{1.63}$$

Comparing this result with (1.39) we observe that, apart from the material constant, the transformed viscoelastic law and the elastic law are of the same form. This is valid also for all further relevant equations such as equilibrium conditions and

kinematic relations. This property is known as *elastic–viscoelastic analogy* which is the basis of the so-called *correspondence principle*. According to this principle the Laplace-transformed solution of a viscoelastic problem can be obtained from the corresponding elastic solution by replacing the elastic constants appropriately by the Laplace-transformed creep and relaxation functions, respectively (e.g., $G \rightarrow p\,\bar{G}(p)$). The final solution of the viscoelastic problem then follows by the inverse transformation.

1.3.2.2 Nonlinear viscoelastic material response, creep

Nonlinear viscoelastic behavior is often described by pragmatic approaches which are applicable only to specific materials or in a restricted loading regime. One of these is Leaderman's approach for polymers (H. LEADERMAN, 1943)

$$\varepsilon(t) = \int_{-\infty}^{t} J(t-\tau)\,\frac{\mathrm{d}(\sigma f)}{\mathrm{d}\tau}\,\mathrm{d}\tau \tag{1.64}$$

where $f(\sigma)$ is an additional material function. It characterizes the dependence of creep strains on an applied constant stress σ_0 in the form $\varepsilon(t) = \sigma_0 f(\sigma_0) J(t)$. A generalization of (1.64) to the three-dimensional case may be accomplished analogously to the linear case.

Because of its practical relevance, creep of metallic materials under constant stress shall briefly be discussed. Usually the three stages of primary, secondary, and tertiary creep are distinguished, where secondary creep often is the dominant stage. This stage is characterized by an approximately constant strain rate (creep rate) $\dot{\varepsilon}$ under a fixed uniaxial stress σ. The strain rate only depends on the stress level: $\dot{\varepsilon} = \dot{\varepsilon}(\sigma)$. For the characterization of such a stationary creep deformation different approaches are in use such as, for example, Norton-Bailey's creep law (F.H. NORTON, R.W. BAILEY, 1929)

$$\dot{\varepsilon} = B\,\sigma^n\ , \tag{1.65}$$

Prandtl's approach (L. PRANDTL, 1875-1953)

$$\frac{\dot{\varepsilon}}{\dot{\varepsilon}_\star} = [\sinh(\frac{\sigma}{\sigma_\star})]^n \tag{1.66}$$

or modified approaches of the type

$$\frac{\dot{\varepsilon}}{\dot{\varepsilon}_\star} = C\,\frac{\mathrm{d}}{\mathrm{d}t}(\frac{\sigma}{\sigma_\star})^m + (\frac{\sigma}{\sigma_\star})^n \tag{1.67}$$

where B, C, n, m, $\sigma_\star$, and $\dot{\varepsilon}_\star$ are material parameters.

The constitutive laws for viscous flow and elastic response often have a similar structure. For instance, (1.65) can formally be obtained from (1.56) by simply

replacing strains by strain rates. If one assumes that the quantities (work rates)

$$\widetilde{D} = \int_0^{\sigma_{kl}} \dot{\varepsilon}_{ij}\,\mathrm{d}\sigma_{ij}\ , \qquad D = \int_0^{\dot{\varepsilon}_{kl}} \sigma_{ij}\,\mathrm{d}\dot{\varepsilon}_{ij} = \sigma_{ij}\dot{\varepsilon}_{ij} - \widetilde{D} \tag{1.68}$$

are independent of the integration path, then the relations

$$\dot{\varepsilon}_{ij} = \frac{\partial \widetilde{D}}{\partial \sigma_{ij}}\ , \qquad \sigma_{ij} = \frac{\partial D}{\partial \dot{\varepsilon}_{ij}} \tag{1.69}$$

hold which are analogous to (1.48) and (1.46). The function $\widetilde{D}(\sigma_{ij})$ is known as *flow potential*, $D(\dot{\varepsilon}_{ij})$ is the *strain energy rate density* and $\sigma_{ij}\dot{\varepsilon}_{ij}$ is called *dissipation rate*.

Assuming an incompressible material ($\dot{\varepsilon}_{kk} = 0$) and a dependence of the flow potential solely on $I\!I_s$, equation (1.69) yields

$$\dot{e}_{ij} = \frac{\mathrm{d}\widetilde{D}}{\mathrm{d}I\!I_s}\, s_{ij} = \frac{3}{2}\,\frac{\dot{\varepsilon}_\mathrm{e}}{\sigma_\mathrm{e}}\, s_{ij} \tag{1.70}$$

where $\sigma_\mathrm{e} = (\frac{3}{2}\, s_{ij}s_{ij})^{1/2}$ and $\dot{\varepsilon}_\mathrm{e} = (\frac{2}{3}\,\dot{e}_{ij}\dot{e}_{ij})^{1/2}$. For example, Norton's creep law for the three-dimensional case then attains the form

$$\dot{e}_{ij} = \frac{3}{2}\, B\, \sigma_\mathrm{e}^{n-1}\, s_{ij}\ . \tag{1.71}$$

The corresponding strain energy rate density and the flow potential read

$$D = \frac{n}{n+1}\, s_{ij}\dot{e}_{ij}\ , \qquad \widetilde{D} = \frac{1}{n+1}\, s_{ij}\dot{e}_{ij}\ . \tag{1.72}$$

These equations are fully analogous to equations (1.57), (1.58) for a nonlinear elastic power law. Both sets of equations can be transformed into each other by replacing strains by strain rates and vice versa. Consequently, also the solutions of corresponding boundary value problems are analogous. According to this analogy, the solution of a nonlinear elastic problem can be transferred to the corresponding creep problem by replacing strains by strain rates.

1.3.3 Plasticity

If stresses or strains exceed a certain limit, plastic yielding may be observed especially in metallic materials. In this case, in contrast to viscoelasticity, a load change mostly leads to an immediate (time independent) deformation change. One effect of plastic yielding are remaining plastic deformations after unloading.

For the characterization of an elastic-plastic material in conventional plasticity theory one usually assumes that the strains and strain increments are additively composed of an elastic and a plastic part:

$$\boldsymbol{\varepsilon} = \boldsymbol{\varepsilon}^e + \boldsymbol{\varepsilon}^p \,, \qquad \mathrm{d}\boldsymbol{\varepsilon} = \mathrm{d}\boldsymbol{\varepsilon}^e + \mathrm{d}\boldsymbol{\varepsilon}^p \,. \tag{1.73a}$$

By relating the strain increments to a corresponding time increment $\mathrm{d}t$ the additive split also can be expressed as

$$\dot{\boldsymbol{\varepsilon}} = \dot{\boldsymbol{\varepsilon}}^e + \dot{\boldsymbol{\varepsilon}}^p \,. \tag{1.73b}$$

For the elastic part a linear stress-strain relationship, as given e.g. by (1.35a), may be assumed. In conjunction with (1.73a) the elasticity law then attains the form

$$\boldsymbol{\sigma} = \boldsymbol{C} : \boldsymbol{\varepsilon}^e = \boldsymbol{C} : (\boldsymbol{\varepsilon} - \boldsymbol{\varepsilon}^p) \,. \tag{1.74}$$

As a constitutive law for the plastic part, formulations in terms of plastic strain increments as well as in terms of total plastic strains are in use. The corresponding representations are known as *incremental plasticity* and *deformation plasticity* (*total strain theory*), respectively. Both approaches usually assume plastic incompressibility, i.e., vanishing plastic volumetric strains: $\varepsilon^p_{kk} = 0$. As a consequence $\boldsymbol{\varepsilon}^p = \boldsymbol{e}^p$ holds.

1.3.3.1 Yield criterion

It is feasible to assume that yielding occurs only if a certain state prevails which is determined by the stresses σ_{ij}. Such a *yield criterion* can be expressed by

$$F(\boldsymbol{\sigma}) = 0 \tag{1.75a}$$

which may be interpreted as a surface (= *yield surface*) in the nine-dimensional space of stresses σ_{ij}. A stress state on the yield surface ($F = 0$) then characterizes yielding while stress states within the yield surface ($F < 0$) correspond to an elastic response. Accordingly, the extended yield criterion

$$F(\boldsymbol{\sigma}) \leq 0 \tag{1.75b}$$

defines the set of all possible (admissible) stress states.

The yield surface may change its location and its shape during plastic deformation. Special cases are the self similar growth of the yield surface, known as *isotropic hardening*, and a pure translation, known as *kinematic hardening*. If the yield surface remains unchanged, the material response is called *perfectly plastic*. As we will discuss later in conjunction with the principle of maximum plastic work, the yield surface is convex.

For an isotropic material, the yield criterion can only depend on the invariants I_σ, II_σ, III_σ which is equivalent to a dependence only on I_σ, II_s, III_s. When loaded by a hydrostatic stress state many materials, especially metals, show a purely elastic

response by volumetric strains, i.e., I_σ does not influence yielding. Thus, the yield criterion (1.75a) reduces to

$$F(II_s, III_s) = 0 \; . \tag{1.76}$$

Equation (1.76) offers a multitude of possible criteria from which only two well-established and widely-used yield criteria shall be mentioned here. The VON MISES yield criterion (R. VON MISES, 1883–1953) is given by

$$F = II_s - k^2 = 0 \qquad \text{or} \qquad F = \frac{1}{2}\, s_{ij} s_{ij} - k^2 = 0 \; . \tag{1.77a}$$

In conjunction with (1.15) it can also be written as

$$F = \frac{1}{6}\left[(\sigma_1 - \sigma_2)^2 + (\sigma_2 - \sigma_3)^2 + (\sigma_3 - \sigma_1)^2\right] - k^2 = 0 \; . \tag{1.77b}$$

Accordingly, the material yields if II_s attains the critical value k^2. Equivalent are the statements that yielding requires a certain octahedral shear stress τ_{oct} or that the linear elastic response is limited by a critical distortional strain energy density U_G. Equation (1.77b) defines a cylindrical surface of radius $\sqrt{2}k$ around the *"hydrostatic" axis* $\sigma_1 = \sigma_2 = \sigma_3$ in the three-dimensional space of principal stresses (Fig. 1.7a). For a perfectly plastic material k is constant. Introducing the yield stress σ_Y for uniaxial tension ($\sigma_1 = \sigma_Y$, $\sigma_2 = \sigma_3 = 0$) and τ_Y for pure shear ($\sigma_1 = -\sigma_3 = \tau_Y$, $\sigma_2 = 0$), the relation $k = \sigma_Y/\sqrt{3} = \tau_Y$ holds. In case of isotropic hardening, k depends on the plastic deformation. The constant σ_Y then has to be replaced by the actual yield stress: $k = \sigma/\sqrt{3}$. By comparison with (1.77a) we obtain the already known uniaxial equivalent stress $\sigma_{\mathrm{e}} = (\frac{3}{2}\, s_{ij} s_{ij})^{1/2}$, see (1.54a), which is also known as the *von Mises stress*.

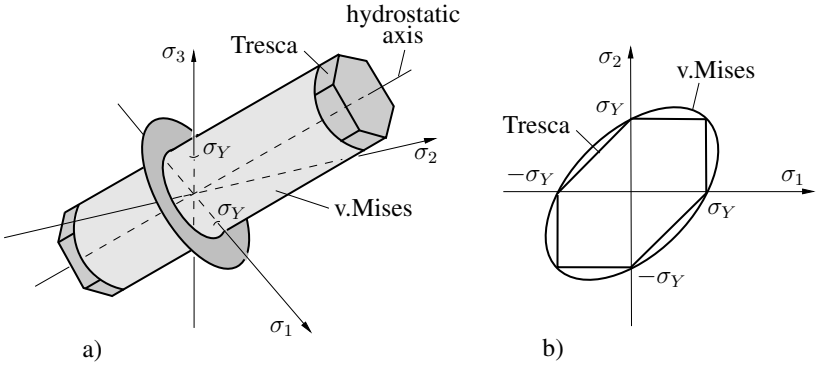

Fig. 1.7 Yield criteria according to von Mises and Tresca

For the special case of plane stress ($\sigma_3 = 0$) we obtain from (1.77b) the yield condition

$$\sigma_1^2 + \sigma_2^2 - \sigma_1 \sigma_2 = \sigma_Y^2 \; . \tag{1.78}$$

The associated yield curve is an ellipse, see Fig. 1.7b.

The yield condition according to H.E. TRESCA (1868) is based on the assumption that plastic flow occurs if the maximum shear stress reaches a certain critical value: $F = \tau_{\max} - k = 0$. Introducing the extreme shear stresses according to (1.11), one of the conditions

$$\sigma_1 - \sigma_3 \pm 2k = 0 \quad , \qquad \sigma_2 - \sigma_1 \pm 2k = 0 \quad , \qquad \sigma_3 - \sigma_2 \pm 2k = 0 \tag{1.79}$$

must be fulfilled. The associated yield surface in principal stress space is a hexagonal prism whose middle axis coincides with the hydrostatic axis (Fig. 1.7). For a perfectly plastic material, the relation between k and the flow stresses σ_Y (uniaxial tension) and τ_Y (pure shear) is given by $k = \sigma_Y/2 = \tau_Y$.

1.3.3.2 Incremental theory

In the following we assume that the material satisfies the *principle of maximum plastic work:*

$$(\sigma_{ij} - \sigma_{ij}^0)\, \mathrm{d}\varepsilon_{ij}^p \geq 0 \,. \tag{1.80}$$

Here, σ_{ij} is the actual stress state on the yield surface, while σ_{ij}^0 represents an initial state within or on the yield surface. This principle can be interpreted such that among all stress states $\tilde{\sigma}_{ij}$ which fulfill the yield condition, the actual stresses σ_{ij} render the plastic work $\tilde{\sigma}_{ij}\mathrm{d}\varepsilon_{ij}^p$ an extremum. This extremum statement can be formulated as

$$\frac{\partial}{\partial \tilde{\sigma}_{ij}} [\tilde{\sigma}_{ij}\mathrm{d}\varepsilon_{ij}^p - \mathrm{d}\lambda\, F(\tilde{\sigma}_{ij})] = 0 \qquad \text{for} \qquad \tilde{\sigma}_{ij} = \sigma_{ij} \tag{1.81}$$

where $\mathrm{d}\lambda \geq 0$ is a free Lagrange multiplier. From this follows the *flow rule*

$$\mathrm{d}\varepsilon_{ij}^p = \mathrm{d}\lambda \frac{\partial F}{\partial \sigma_{ij}} \tag{1.82a}$$

which alternatively can be written as

$$\dot{\varepsilon}_{ij}^p = \dot{\lambda} \frac{\partial F}{\partial \sigma_{ij}} \qquad \text{or} \qquad \dot{\boldsymbol{\varepsilon}}^p = \dot{\lambda} \frac{\partial F}{\partial \boldsymbol{\sigma}} \,. \tag{1.82b}$$

Without going into details it should be mentioned that from the principle of maximum plastic work some consequences arise. One of them is the already mentioned convexity of the yield surface. Another consequence is the *normality rule* which states that the plastic strain increment points outward of the yield surface in normal direction, cf. (1.82a,b).

If we take von Mises yield condition (1.77a,b) as the basis, then (1.82a,b) yields $\mathrm{d}\boldsymbol{\varepsilon}^p = \mathrm{d}\lambda\, \boldsymbol{s}$. In this case, the principal axes of $\mathrm{d}\boldsymbol{\varepsilon}^p$ coincide with those of the stress deviator $\boldsymbol{s}$ and consequently also with those of $\boldsymbol{\sigma}$. The multiplier $\mathrm{d}\lambda$ can be determined by introducing the equivalent stress $\sigma_{\mathrm{e}} = (\frac{3}{2} s_{ij} s_{ij})^{1/2}$ and

– taking into account plastic incompressibility – the equivalent strain increment $\mathrm{d}\varepsilon_{\mathrm{e}}^p = (\frac{2}{3}\mathrm{d}\varepsilon_{ij}^p \mathrm{d}\varepsilon_{ij}^p)^{1/2}$. From $\mathrm{d}\varepsilon_{ij}^p \mathrm{d}\varepsilon_{ij}^p = (\mathrm{d}\lambda)^2 s_{ij} s_{ij}$ we then get $\mathrm{d}\lambda = \frac{3}{2}\mathrm{d}\varepsilon_{\mathrm{e}}^p/\sigma_{\mathrm{e}}$ and finally

$$\mathrm{d}\varepsilon_{ij}^p = \frac{3}{2}\frac{\mathrm{d}\varepsilon_{\mathrm{e}}^p}{\sigma_{\mathrm{e}}} s_{ij} \qquad \text{or} \qquad \dot{\boldsymbol{\varepsilon}}^p = \frac{3}{2}\frac{\dot{\varepsilon}_{\mathrm{e}}^p}{\sigma_{\mathrm{e}}} \boldsymbol{s} \; . \tag{1.83a}$$

For a perfectly plastic material, the equivalent stress is constant: $\sigma_{\mathrm{e}} = \sigma_Y$. This is not the case for strain hardening materials and it is then appropriate to introduce into (1.83a) the *plastic tangent modulus* $g = \mathrm{d}\sigma_{\mathrm{e}}/\mathrm{d}\varepsilon_{\mathrm{e}}^p = \dot{\sigma}_{\mathrm{e}}/\dot{\varepsilon}_{\mathrm{e}}^p$ and to write the flow rule as follows

$$\mathrm{d}\varepsilon_{ij}^p = \frac{3}{2}\frac{s_{ij}}{g\,\sigma_{\mathrm{e}}}\mathrm{d}\sigma_{\mathrm{e}} \qquad \text{or} \qquad \dot{\boldsymbol{\varepsilon}}^p = \frac{3}{2}\frac{\dot{\sigma}_{\mathrm{e}}}{g\,\sigma_{\mathrm{e}}} \boldsymbol{s} \; . \tag{1.83b}$$

Combining the elastic and plastic strain increments according to (1.73a,b) we obtain as the constitutive law during yielding ($F = 0$, $\mathrm{d}\sigma_{\mathrm{e}} > 0$) the so-called *Prandtl-Reuss law*

$$\dot{\varepsilon}_{kk} = \frac{1}{3K}\dot{\sigma}_{kk} \; , \qquad \dot{\boldsymbol{e}} = \frac{1}{2\,\mu}\dot{\boldsymbol{s}} + \frac{3}{2}\frac{\dot{\sigma}_{\mathrm{e}}}{g\,\sigma_{\mathrm{e}}} \boldsymbol{s} \; . \tag{1.83c}$$

In contrast, if Tresca's yield condition in the form $F = \sigma_1 - \sigma_3 - k = 0$ with $\sigma_1 \geq \sigma_2 \geq \sigma_3$ is employed the plastic increments in principal directions follow from flow rule (1.82a) as

$$\mathrm{d}\varepsilon_1^p = \mathrm{d}\lambda \; , \qquad \mathrm{d}\varepsilon_2^p = 0 \; , \qquad \mathrm{d}\varepsilon_3^p = -\mathrm{d}\lambda \; . \tag{1.84}$$

As before, they satisfy the condition of plastic incompressibility.

1.3.3.3 Deformation theory

In deformation theory (also referred to as total strain theory) it is assumed that between plastic strains and deviatoric stresses the relation

$$\boldsymbol{\varepsilon}^p = \lambda\, \boldsymbol{s} \tag{1.85}$$

holds where the multiplier λ depends on the stress state and plastic deformation. On the basis of von Mises' yield condition in conjunction with the equivalent stress $\sigma_{\mathrm{e}} = (\frac{3}{2}s_{ij}s_{ij})^{1/2}$ and the equivalent plastic strain $\varepsilon_{\mathrm{e}}^p = (\frac{2}{3}\varepsilon_{ij}^p \varepsilon_{ij}^p)^{1/2}$ it is determined as $\lambda = 3\varepsilon_{\mathrm{e}}^p/2\sigma_{\mathrm{e}}$. Combining elastic and plastic strains according to (1.73a) we obtain the finite *Hencky-Ilyushin law*

$$\varepsilon_{kk} = \frac{1}{3K}\sigma_{kk} \; , \qquad \boldsymbol{e} = \left[\frac{1}{2\,\mu} + \frac{3}{2}\frac{\varepsilon_{\mathrm{e}}^p}{\sigma_{\mathrm{e}}}\right] \boldsymbol{s} \; . \tag{1.86}$$

Comparing (1.86) with (1.55) it can be recognized that deformation theory describes the plastic material behavior like a nonlinear elastic behavior. Consequently, deformation theory is not able to adequately model unloading processes. Therefore,

to be physically meaningful, it is only applicable in a monotonic loading regime. Under such circumstances this theory is especially appropriate if *proportional loading* is present, i.e., if the condition

$$\boldsymbol{s} = P\,\boldsymbol{s}^0 \tag{1.87}$$

is fulfilled. Here, $\boldsymbol{s}^0$ is a reference stress state (e.g., for the final load) and P is a scalar load parameter. It can be shown that in this case deformation theory and incremental theory are equivalent.

As a sufficiently good approximation of the real material behavior, the general relation (1.85) often is specified by the power laws (1.56) and (1.57), respectively. This leads always to proportional loading according to (1.87) as long as the external load of the body or a sub-body is prescribed by solely one load parameter P (e.g., by a single force). In this case, the strains and displacements are given by

$$\boldsymbol{\varepsilon}^p = P^n\,\boldsymbol{\varepsilon}^{p\,0}\,, \qquad \boldsymbol{u} = P^n\,\boldsymbol{u}^0\,. \tag{1.88}$$

Here $\boldsymbol{\varepsilon}^{p\,0}$ and $\boldsymbol{u}^0$ are the plastic strains and displacements associated with the reference stress state $\boldsymbol{s}^0$. As a consequence, if the stresses and strains are known for a certain load, they are known for all other loading stages.

It should be mentioned that these properties arising from the power law can analogously be transferred from deformation theory of plasticity to creep processes. Due to the analogy of constitutive laws for nonlinear elastic behavior and for creep (see Sect. 1.3.2.2), only strains must be replaced by strain rates and displacements by velocities. Then the following relations apply:

$$\boldsymbol{s} = P\,\boldsymbol{s}^0\,, \qquad \dot{\boldsymbol{\varepsilon}}^p = P^n\,\dot{\boldsymbol{\varepsilon}}^{p\,0}\,, \qquad \dot{\boldsymbol{u}} = P^n\,\dot{\boldsymbol{u}}^0\,. \tag{1.89}$$

1.4 Energy principles

In the following some classical energy principles for deformable bodies are shortly discussed. Here we assume that during state changes the material surface of a body remains unchanged. This means that any crack growth is precluded. For brevity we further assume that the body is externally loaded solely by surface tractions and no volume forces are present. The latter can easily be taken into account if necessary.

1.4.1 Energy balance

The energy balance or first law of thermodynamics, applied to continuum mechanics, states that the change of total energy (internal energy + kinetic energy) of a body is equal to the energy flux into the body. This can be expressed through the equations

$$\dot{E} + \dot{K} = P + Q \quad , \qquad (E+K)_2 - (E+K)_1 = \int_{t_1}^{t_2} (P+Q)\,\mathrm{d}t \; . \tag{1.90}$$

Here E, K, and P are the internal energy, the kinetic energy, and the power of external forces, respectively. They are given by

$$E = \int_V \rho\, e \,\mathrm{d}V \; , \qquad K = \frac{1}{2} \int_V \rho\, \dot{\boldsymbol{u}} \cdot \dot{\boldsymbol{u}} \,\mathrm{d}V \; , \qquad P = \int_{\partial V} \boldsymbol{t} \cdot \dot{\boldsymbol{u}} \,\mathrm{d}A \tag{1.91}$$

where e is the specific internal energy. The quantity Q describes an energy transport into the body which is not covered by P, as e.g., heat flux. We will not further specify this term.

For an elastic material $\rho\, e$ can be identified as the strain energy density U. In the special case of quasi-static loading ($K = 0$) and for $Q = 0$ the energy balance reads

$$\mathit{\Pi}_2^{int} - \mathit{\Pi}_1^{int} = W_{12}^{ext} \; . \tag{1.92}$$

Here the terms

$$\mathit{\Pi}^{int} = \int_V U \,\mathrm{d}V \; , \qquad W_{12}^{ext} = \int_{\partial V} [\int_{\boldsymbol{u}_1}^{\boldsymbol{u}_2} \boldsymbol{t} \cdot \mathrm{d}\boldsymbol{u}] \,\mathrm{d}A \tag{1.93}$$

for the body's strain energy and for the work done by external forces between the states 1 and 2 have been introduced. The term $\mathit{\Pi}^{int}$ is also called *elastic potential*.

1.4.2 Principle of virtual work

We consider a body in equilibrium with prescribed tractions $\hat{\boldsymbol{t}}$ and displacements $\hat{\boldsymbol{u}}$ on the partial surfaces ∂V_t and ∂V_u. The static and kinematic basic equations for this case read

$$\begin{aligned} &\sigma_{ij,j} = 0 && \text{in } V, \quad && \sigma_{ij} n_j = \hat{t}_i && \text{on } \partial V_t \; , \\ &\varepsilon_{ij} = \tfrac{1}{2}(u_{i,j} + u_{j,i}) && \text{in } V, \quad && u_i = \hat{u}_i && \text{on } \partial V_u \; . \end{aligned} \tag{1.94}$$

A statically admissible stress field $\boldsymbol{\sigma}^{(1)}$ satisfies the equilibrium conditions and boundary conditions on ∂V_t. Analogously, a kinematically admissible displacement field $\boldsymbol{u}^{(2)}$ and strain field $\boldsymbol{\varepsilon}^{(2)}$ satisfy the kinematic relations and boundary conditions on ∂V_u. By multiplying the equilibrium conditions for $\boldsymbol{\sigma}^{(1)}$ by the displacements $\boldsymbol{u}^{(2)}$ and subsequent integration over the volume V in conjunction with the divergence theorem, from (1.94) the *general work theorem*

$$\int_V \boldsymbol{\sigma}^{(1)} : \boldsymbol{\varepsilon}^{(2)} \, \mathrm{d}V = \int_{\partial V_t} \hat{\boldsymbol{t}}^{(1)} \cdot \boldsymbol{u}^{(2)} \, \mathrm{d}A + \int_{\partial V_u} \boldsymbol{t}^{(1)} \cdot \hat{\boldsymbol{u}}^{(2)} \, \mathrm{d}A \tag{1.95}$$

is obtained.

From (1.95) various specific theorems can be derived. If we use as force quantities (e.g., stresses) the actual quantities associated with an equilibrium state and as kinematic quantities the so-called virtual displacements $\delta \boldsymbol{u}$ and virtual strains $\delta \boldsymbol{\varepsilon}$ relative to the equilibrium configuration, we obtain the *principle of virtual work* (*principle of virtual displacements*)

$$\delta W^{int} = \delta W^{ext} \tag{1.96}$$

where

$$\delta W^{int} = \int_V \boldsymbol{\sigma} : \delta \boldsymbol{\varepsilon} \, \mathrm{d}V \, , \qquad \delta W^{ext} = \int_{\partial V_t} \hat{\boldsymbol{t}} \cdot \delta \boldsymbol{u} \, \mathrm{d}A \, . \tag{1.97}$$

Here, the virtual displacements are understood as infinitesimal and kinematically admissible. According to this principle the work δW^{int} done by internal forces and δW^{ext} done by external forces during a virtual displacement must be equal for a body in equilibrium.

For an elastic material the work of internal forces is equivalent to the change of the elastic potential. This is valid since according to (1.45) $\boldsymbol{\sigma} : \delta \boldsymbol{\varepsilon} = \delta U$ from which in conjunction with (1.97) and (1.93) the relation $\delta W^{int} = \delta \Pi^{int}$ follows. If additionally the external forces can be derived from a potential, the relation $\delta W^{ext} = -\delta \Pi^{ext}$ holds and we obtain from (1.96)

$$\delta \Pi = \delta (\Pi^{int} + \Pi^{ext}) = 0 \, . \tag{1.98}$$

Thus, in an equilibrium state the total potential Π is stationary. It can be shown that the corresponding value is a minimum if the potential is convex:

$$\Pi = \Pi^{int} + \Pi^{ext} = \text{minimum} \, . \tag{1.99}$$

This is the *principle of minimum potential energy*. It can be phrased as follows: among all admissible deformations (compatible with kinematic boundary conditions) the actual deformations render the total potential Π stationary (minimum). It should be mentioned that the potential for a linear elastic material and fixed traction or displacement boundary conditions is in fact convex, i.e., it attains an absolute minimum in an equilibrium state.

From (1.95) also the *principle of virtual complementary work* (*principle of virtual forces*) can be obtained. In this case, the kinematic quantities are chosen to be the actual displacements and strains while virtual changes from the equilibrium state are taken as statically admissible force quantities. This yields

$$\delta \widetilde{W}^{int} = \delta \widetilde{W}^{ext} \tag{1.100}$$

where

$$\delta\widetilde{W}^{int} = \int_V \boldsymbol{\varepsilon} : \delta\boldsymbol{\sigma}\,\mathrm{d}V\ , \qquad \delta\widetilde{W}^{ext} = \int_{\partial V_u} \hat{\boldsymbol{u}} \cdot \delta\boldsymbol{t}\,\mathrm{d}A \tag{1.101}$$

are the *complementary work* of internal and external forces, respectively. Analogous to the previous principle the *internal complementary potential*

$$\widetilde{\Pi}^{int} = \int_V \widetilde{U}\,\mathrm{d}V \tag{1.102}$$

can be introduced for elastic materials. In addition, if an external complementary potential exists where $\widetilde{\Pi}^{ext} = -\widetilde{W}^{ext}$ we obtain from (1.100)

$$\delta\widetilde{\Pi} = \delta(\widetilde{\Pi}^{int} + \widetilde{\Pi}^{ext}) = 0\ . \tag{1.103}$$

Hence, in an equilibrium state also the complementary potential attains a stationary value. It is a minimum if $\widetilde{\Pi}$ is convex, which in fact holds for linear elastic systems:

$$\widetilde{\Pi} = \widetilde{\Pi}^{int} + \widetilde{\Pi}^{ext} = \text{minimum}\ . \tag{1.104}$$

This is the *principle of stationary (minimum) complementary potential*. Accordingly, among all admissible stress fields (compatible with the static boundary conditions) the actual stresses render the complementary potential $\widetilde{\Pi}$ stationary (minimum).

1.4.3 Theorems of Clapeyron and Betti

As the static and kinematic quantities in (1.95) we now introduce the actual (true) quantities. Provided that the external forces are dead loads ($\boldsymbol{t} = \boldsymbol{t}(\boldsymbol{x})$), the right-hand side of (1.95) represents the work W^{ext} of those forces done from the undeformed to the current deformed state. Since dead loads have a potential, $W^{ext} = -\Pi^{ext}$ holds. Furthermore, for a linear elastic material, the left-hand side of (1.95) in conjunction with $\boldsymbol{\sigma} : \boldsymbol{\varepsilon} = 2\,U$ and (1.93) becomes $2\,\Pi^{int}$. As a consequence we obtain *Clapeyron's theorem* (B.P.E. CLAPEYRON, 1799-1864)

$$2\,\Pi^{int} + \Pi^{ext} = 0\ . \tag{1.105}$$

In contrast, for the special case of an incompressible nonlinear elastic material which is described by the power law (1.56), (1.57) we first obtain for the left-hand side of (1.95) $\frac{n+1}{n}\Pi^{int}$ and finally

$$\frac{n+1}{n}\,\Pi^{int} + \Pi^{ext} = 0\ . \tag{1.106}$$

We now consider again the case of a linear elastic material which is described by the elasticity law $\sigma_{ij} = C_{ijkl}\varepsilon_{kl}$, see (1.35a). On account of the symmetry of the elasticity tensor ($C_{ijkl} = C_{jikl} = C_{ijlk} = C_{klij}$) the general relation $\sigma_{ij}^{(1)}\varepsilon_{ij}^{(2)} = \sigma_{ij}^{(2)}\varepsilon_{ij}^{(1)}$ holds. Integration over the volume in conjunction with the general work theorem (1.95) yields *Betti's theorem* (E. BETTI, 1823-1892)

$$\int_{\partial V} \boldsymbol{t}^{(1)} \cdot \boldsymbol{u}^{(2)} \, \mathrm{d}A = \int_{\partial V} \boldsymbol{t}^{(2)} \cdot \boldsymbol{u}^{(1)} \, \mathrm{d}A \tag{1.107}$$

which is also called *reciprocity relation*. Accordingly, for two different load configurations (1), (2) of the same body, the work done by the first force system on the displacements of the second system is equal to the work done by the second force system on the displacements of the first system.

1.5 Plane problems

1.5.1 Plane stress, plane strain, longitudinal shear

Problems of solid mechanics may often be approximated as plane (two-dimensional) problems. Particularly important for applications are the *plane strain* and the *plane stress* state. Besides, the *longitudinal* (*anti-plane*) stress state has a somewhat minor importance. For their representation we use in the following the engineering notation with coordinates x, y, z, displacements u, v, w, strains $\varepsilon_x, \gamma_{xy}, \ldots$ and stresses $\sigma_x, \tau_{xy}, \ldots$.

A *plane strain* state is characterized by constrained strains and displacements in one direction (e.g., in z-direction). In this case w, ε_z, γ_{xz}, γ_{yz}, τ_{xz}, τ_{yz} are zero and all other quantities depend solely on x and y. The equilibrium conditions (without volume forces), kinematic relations and compatibility conditions then reduce to

$$\frac{\partial \sigma_x}{\partial x} + \frac{\partial \tau_{xy}}{\partial y} = 0 \,, \qquad \frac{\partial \tau_{xy}}{\partial x} + \frac{\partial \sigma_y}{\partial y} = 0 \,, \tag{1.108}$$

$$\varepsilon_x = \frac{\partial u}{\partial x} \,, \qquad \varepsilon_y = \frac{\partial v}{\partial y} \,, \qquad \gamma_{xy} = \frac{\partial u}{\partial y} + \frac{\partial v}{\partial x} \,, \tag{1.109}$$

$$\frac{\partial^2 \varepsilon_x}{\partial y^2} + \frac{\partial^2 \varepsilon_y}{\partial x^2} = \frac{\partial^2 \gamma_{xy}}{\partial x \partial y} \,. \tag{1.110}$$

Also the constitutive law becomes more simple. For example, from (1.38) we obtain for an isotropic linear elastic material

$$\varepsilon_x = \frac{1-\nu^2}{E}(\sigma_x - \frac{\nu}{1-\nu}\sigma_y) \,, \quad \varepsilon_y = \frac{1-\nu^2}{E}(\sigma_y - \frac{\nu}{1-\nu}\sigma_x) \,, \quad \gamma_{xy} = \frac{\tau_{xy}}{G} \tag{1.111}$$

and $\sigma_z = \nu(\sigma_x + \sigma_y)$.

In a *plane stress* situation it is assumed that σ_z, τ_{xz}, τ_{yz}, γ_{xz}, γ_{yz} vanish and that the remaining stresses and strains are independent of z. A corresponding state appears approximately (not exact) in plates whose thickness is small compared with their in-plane dimensions and which are loaded solely by forces parallel to the plate. The equilibrium conditions, kinematic relations, and compatibility conditions are identical with equations (1.108 – 1.110) for plane strain. In contrast to the latter state, the displacements u, v, w now may be dependent on z in general. The constitutive law for a linear elastic isotropic material reduce to

$$\varepsilon_x = \frac{1}{E}\left(\sigma_x - \nu\sigma_y\right), \qquad \varepsilon_y = \frac{1}{E}\left(\sigma_y - \nu\sigma_x\right), \qquad \gamma_{xy} = \frac{\tau_{xy}}{G} \tag{1.112}$$

and $E\varepsilon_z = -\nu(\sigma_x + \sigma_y)$. Equations (1.112) differ from (1.111) only through somewhat different elastic constants. Therefore, solutions of plane strain boundary value problems can simply be transferred to plane stress by changing the elastic constants, and vice versa.

Often it is necessary to describe the stresses in a coordinate system ξ, η which is rotated with respect to the x, y-system by an angle φ, see Fig. 1.8. The respective transformation relations can be obtained from (1.6) as

$$\begin{aligned}
\sigma_\xi &= \frac{1}{2}(\sigma_x + \sigma_y) + \frac{1}{2}(\sigma_x - \sigma_y)\cos 2\varphi + \tau_{xy}\sin 2\varphi\,, \\
\sigma_\eta &= \frac{1}{2}(\sigma_x + \sigma_y) - \frac{1}{2}(\sigma_x - \sigma_y)\cos 2\varphi - \tau_{xy}\sin 2\varphi\,, \\
\tau_{\xi\eta} &= -\frac{1}{2}(\sigma_x - \sigma_y)\sin 2\varphi + \tau_{xy}\cos 2\varphi\,.
\end{aligned} \tag{1.113}$$

They can be visualized by Mohr's circle in Fig. 1.8.

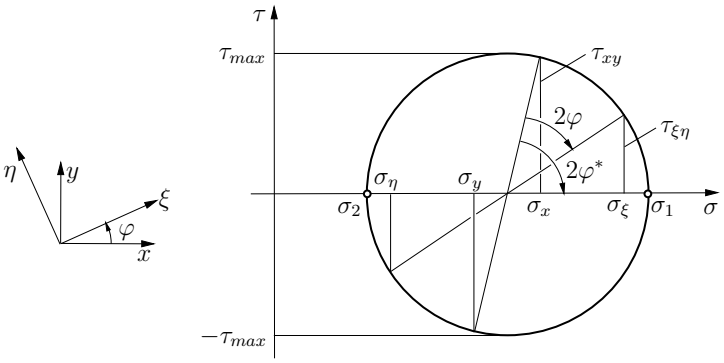

Fig. 1.8 Mohr's circle

One principal direction in plane strain as well as in plane stress is given by the z-direction. The other two are in the x, y-plane. The associated principal stresses

and principal directions are given by

$$\sigma_{1,2} = \frac{\sigma_x + \sigma_y}{2} \pm \sqrt{(\frac{\sigma_x - \sigma_y}{2})^2 + \tau_{xy}^2}\,, \qquad \tan 2\varphi^* = \frac{2\tau_{xy}}{\sigma_x - \sigma_y}\,. \tag{1.114}$$

In sections under $\varphi^{**} = \varphi^* \pm \pi/4$ the principal shear stress

$$\tau_3 = \frac{\sigma_1 - \sigma_2}{2} = \sqrt{(\frac{\sigma_x - \sigma_y}{2})^2 + \tau_{xy}^2} \tag{1.115}$$

appears. For $\sigma_1 \geq \sigma_z \geq \sigma_2$ it is the maximum shear stress $\tau_{\max}$.

The here specified formulas for the stresses can analogously be transferred to the strains, the strain increments, and the strain rates.

In *anti-plane strain* or *longitudinal shear*, the only non-vanishing field quantities are w, γ_{xz}, γ_{yz}, τ_{xz}, τ_{yz}, which are again independent of z. In this case, the equilibrium condition, kinematic relations, and compatibility condition reduce to

$$\frac{\partial \tau_{xz}}{\partial x} + \frac{\partial \tau_{yz}}{\partial y} = 0\,, \qquad \gamma_{xz} = \frac{\partial w}{\partial x}\,, \qquad \gamma_{yz} = \frac{\partial w}{\partial y}\,, \qquad \frac{\partial \gamma_{xz}}{\partial y} = \frac{\partial \gamma_{yz}}{\partial x}\,. \tag{1.116}$$

For a linear elastic behavior, the constitutive law is given by

$$\gamma_{xz} = \tau_{xz}/G\,, \qquad \gamma_{yz} = \tau_{yz}/G\,. \tag{1.117}$$

Because of its simplicity, longitudinal shear is often used as a model case.

In plasticity and viscoelasticity, deformations usually are not directly described through total displacements and strains but through their increments and velocities, respectively. In this case the kinematic quantities in the forgoing equations must be replaced adequately.

1.5.2 Linear elasticity, complex method

For the analytical solution of plane problems of linear elasticity a number of methods are available. The probably most powerful and elegant tool is the *complex variable method* which shortly shall be introduced.

In this method, the stresses and displacements are considered as functions of the complex variable $z = x + \mathrm{i}y = re^{\mathrm{i}\varphi}$ and the conjugate complex variable $\overline{z} = x - \mathrm{i}y = re^{-\mathrm{i}\varphi}$, respectively. It can then be shown that solutions of the basic equations of plane strain and plane stress can be constructed from solely two complex functions $\Phi(z)$ and $\Psi(z)$. Their relation with the cartesian components of stresses and displacements is given by *Kolosov's formulas* (J.V. KOLOSOV, 1867-1936)

$$\begin{aligned} \sigma_x + \sigma_y &= 2[\Phi'(z) + \overline{\Phi'(z)}] \,, \\ \sigma_y - \sigma_x + 2\mathrm{i}\tau_{xy} &= 2[\overline{z}\Phi''(z) + \Psi'(z)] \,, \\ 2\,\mu\,(u + \mathrm{i}v) &= \kappa\Phi(z) - z\overline{\Phi'(z)} - \overline{\Psi(z)} \,, \end{aligned} \tag{1.118a}$$

where

$$\kappa = \begin{cases} 3 - 4\nu & \text{plane strain} \,, \\ (3-\nu)/(1+\nu) & \text{plane stress} \,. \end{cases} \tag{1.118b}$$

Frequently it is appropriate to use polar coordinates r, φ instead of cartesian coordinates (Fig. 1.9). Then Kolosov's formulas attain the form

$$\begin{aligned} \sigma_r + \sigma_\varphi &= 2[\Phi'(z) + \overline{\Phi'(z)}] \,, \\ \sigma_\varphi - \sigma_r + 2\mathrm{i}\tau_{r\varphi} &= 2[z\Phi''(z) + \Psi'(z)z/\overline{z}] \,, \\ 2\,\mu\,(u_r + \mathrm{i}u_\varphi) &= [\kappa\Phi(z) - z\overline{\Phi'(z)} - \overline{\Psi(z)}]e^{-\mathrm{i}\varphi} \,. \end{aligned} \tag{1.119}$$

In order to formulate the boundary conditions, often the relations between Φ, Ψ and the resultant force components X, Y along the curve $\overline{AB}$ and their moment M with respect to the origin are needed (Fig. 1.9):

$$\begin{aligned} X + \mathrm{i}Y &= \int_A^B (t_x + \mathrm{i}t_y)\mathrm{d}s = -\mathrm{i}\left[\Phi(z) + \overline{\Psi(z)} + z\overline{\Phi'(z)}\right]_A^B \,, \\ M &= \int_A^B (x\,t_y - y\,t_x)\mathrm{d}s = -\mathrm{Re}\,[z\overline{z}\Phi'(z) + z\Psi(z) - \int \Psi(z)\mathrm{d}z]_A^B \,. \end{aligned} \tag{1.120}$$

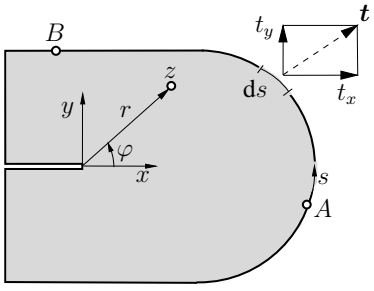

Fig. 1.9 Body in complex plane

In particular, solutions for longitudinal shear (anti-plane shear) can easily be represented. The stresses and the displacement in this case can be derived from solely one complex function $\Omega(z)$:

$$\begin{aligned} \tau_{xz} - \mathrm{i}\tau_{yz} &= (\tau_{rz} - \mathrm{i}\tau_{\varphi z})e^{-\mathrm{i}\varphi} = \Omega'(z) \,, \\ \mu\, w &= \mathrm{Re}\ \Omega(z) \,. \end{aligned} \tag{1.121}$$

A certain class of plane problems, including straight cracks located on the x-axis, can be treated more simple by using *Westergaard's* single stress function $Z(z)$ (H.M. WESTERGAARD, 1939). If the displacement field is symmetric with respect to the x-axis, i.e. $u(x,-y) = u(x,y)$, $v(x,-y) = -v(x,y)$, and $\tau_{xy} = 0$ along $y = 0$, the stresses and displacements are given by

$$\begin{aligned} &\sigma_x = \mathrm{Re}Z - y\,\mathrm{Im}Z', \quad \sigma_y = \mathrm{Re}Z + y\,\mathrm{Im}Z', \quad \tau_{xy} = -y\,\mathrm{Re}Z', \\ &4\mu\, u = (\kappa-1)\mathrm{Re}\bar{Z} - 2y\,\mathrm{Im}Z \,, \quad 4\mu\, v = (\kappa+1)\mathrm{Im}\bar{Z} - 2y\,\mathrm{Re}Z \end{aligned} \tag{1.122}$$

where $\bar{Z} = \int Z\mathrm{d}z$. Such fields appear e.g. at mode I cracks, see Sections 4.1 and 4.2. Similarly, if the displacement field is antisymmetric with respect to the x-axis, i.e. $u(x,-y) = -u(x,y)$, $v(x,-y) = v(x,y)$, and $\sigma_y = 0$ along $y = 0$, the stresses and displacements are given by

$$\begin{aligned} &\sigma_x = 2\,\mathrm{Im}Z + y\,\mathrm{Re}Z', \quad \sigma_y = -y\,\mathrm{Re}Z', \quad \tau_{xy} = \mathrm{Re}Z - y\,\mathrm{Im}Z', \\ &4\mu\, u = (\kappa+1)\mathrm{Im}\bar{Z} + 2y\,\mathrm{Re}Z \,, \quad 4\mu\, v = -(\kappa-1)\mathrm{Re}\bar{Z} - 2y\,\mathrm{Im}Z \end{aligned} \tag{1.123}$$

where again $\bar{Z} = \int Z\mathrm{d}z$. Such fields characterize, among others, mode-II cracks.

1.5.3 Perfectly plastic material, slip-line fields

In plasticity the solution of boundary value problems is in most cases only possible by using numerical methods such as the finite element method. One of the few methods allowing for an analytical treatment of such problems is the *slip line theory*. It enables the investigation of stresses and deformations in case of plane strain, presuming a rigid perfectly plastic material for which we will employ the von Mises yield condition.

From the condition $\mathrm{d}\varepsilon_z^p = 0$ in conjunction with $\mathrm{d}\varepsilon_{ij}^p = \mathrm{d}\varepsilon_{ij}$ and (1.83a) we first obtain for the stress $s_z = 0$ and $\sigma_z = \sigma_3 = (\sigma_x + \sigma_y)/2 = \sigma_m$, respectively. The yield condition (1.77b) then reduces to

$$(\sigma_x - \sigma_y)^2 + 4\tau_{xy}^2 = 4k^2 \,. \tag{1.124}$$

From this we obtain for the principal stresses $\sigma_1 = \sigma_m + k$, $\sigma_2 = \sigma_m - k$ and for the maximum shear stress $\tau_{\max} = k$. The yield condition in combination with the equilibrium conditions (1.108) form a hyperbolic system of three equations for the three unknowns σ_x, σ_y, and τ_{xy}.

It is now appropriate to introduce an orthogonal mesh of α- and β-lines, whose directions in each point coincide with the direction of maximum shear stress

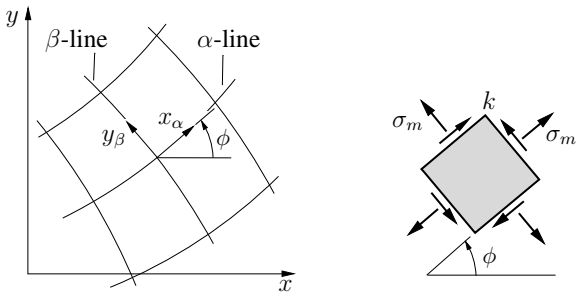

Fig. 1.10 Slip lines

(Fig. 1.10). Since the latter coincides with the direction of maximum shear strain increment or rate, i.e., maximum slip (see e.g., (1.83a)) they are called *slip lines*. It should be mentioned that these lines are the *characteristics* of the hyperbolic system of equations. Denoting the angle between the x-axis and the tangent of the α-line (= direction of maximum shear stress) as ϕ, from (1.114) the relations

$$\sigma_x = \sigma_m - k \sin 2\phi \,, \qquad \sigma_y = \sigma_m + k \sin 2\phi \,, \qquad \tau_{xy} = k \cos 2\phi \tag{1.125}$$

are obtained. They identically fulfill the yield condition. Inserting them into the equilibrium conditions (1.108) yields

$$\begin{aligned} \frac{\partial \sigma_m}{\partial x} - 2\,k \cos 2\phi \, \frac{\partial \phi}{\partial x} - 2\,k \sin 2\phi \, \frac{\partial \phi}{\partial y} = 0 \,, \\ \frac{\partial \sigma_m}{\partial y} - 2\,k \sin 2\phi \, \frac{\partial \phi}{\partial x} + 2\,k \cos 2\phi \, \frac{\partial \phi}{\partial y} = 0 \,. \end{aligned}$$

Since the choice of the coordinate system x, y is arbitrary, we can also use the local system x_α, y_β whose axes coincide with the tangents of the α- and β-line (Fig. 1.10). Setting $\phi = 0$ in the equations above reduces them to ordinary differential equations along the slip lines:

$$\frac{\mathrm{d}}{\mathrm{d}x_\alpha} (\sigma_m - 2\,k\,\phi) = 0 \,, \qquad \frac{\mathrm{d}}{\mathrm{d}y_\beta} (\sigma_m + 2\,k\,\phi) = 0 \,.$$

Integration yields *Hencky's equations* (H. HENCKY, 1885-1952)

$$\begin{aligned} \sigma_m - 2\,k\,\phi &= C_\alpha = \text{const} \quad \text{along } \alpha\text{-lines} \,, \\ \sigma_m + 2\,k\,\phi &= C_\beta = \text{const} \quad \text{elong } \beta\text{-lines} \,. \end{aligned} \tag{1.126}$$

They allow to determine C_α, C_β for prescribed traction boundary conditions and subsequently the entire slip line field and stress field. For kinematic boundary conditions, equations (1.126) are not sufficient. In this case the kinematic relations have to be taken into account which is not further discussed here.

Without derivation two geometric properties of the slip line field shall be mentioned. According to Hencky's *first theorem* the angle between two slip lines of one family (e.g. α-lines) is constant in the region of intersection with slip lines of the other family (β). That means that if one family contains a straight line then the whole family consists of straight lines (e.g., parallel lines, fan). Hencky's second theorem states the following: if one moves along a slip line of one family the curvature radius of the other family changes proportional to the covered arc length. It also should be mentioned that a slip line can be a discontinuity line for the normal stress component in tangential direction and for the tangential velocity.

The anti-plane shear stress state can be treated analogous to plane strain. In this case the yield criterion and the equilibrium condition are given by

$$\tau_{xz}^2 + \tau_{yz}^2 = k^2 = \tau_Y^2 \ , \qquad \frac{\partial \tau_{xz}}{\partial x} + \frac{\partial \tau_{yz}}{\partial y} = 0 \ . \tag{1.127}$$

Again we introduce α-lines whose direction ϕ is given by the direction in which the yield stress τ_Y occurs. β-lines are not needed in this case. The equilibrium condition in conjunction with

$$\tau_{xz} = -\tau_Y \sin\phi \ , \qquad \tau_{yz} = \tau_Y \cos\phi \tag{1.128}$$

attains the form

$$\frac{\mathrm{d}\phi}{\mathrm{d}x_\alpha} = 0 \quad . \tag{1.129}$$

Thus, the α-lines are straight.

The flow rule $\mathrm{d}\varepsilon_{ij} = \mathrm{d}\varepsilon_{ij}^p = \mathrm{d}\lambda\, s_{ij}$ (see Section 1.3.3.2), taking into account

$$2\,\varepsilon_{13} = \gamma_{xz} = \frac{\partial w}{\partial x} \ , \qquad 2\,\varepsilon_{23} = \gamma_{yz} = \frac{\partial w}{\partial y} \ , \tag{1.130}$$

in this case can be written as

$$\mathrm{d}\left(\frac{\partial w}{\partial x}\right) = \frac{\partial(\mathrm{d}w)}{\partial x} = 2\,\mathrm{d}\lambda\ \tau_{xz} \ , \qquad \mathrm{d}\left(\frac{\partial w}{\partial y}\right) = \frac{\partial(\mathrm{d}w)}{\partial y} = 2\,\mathrm{d}\lambda\ \tau_{yz} \ . \tag{1.131}$$

Replacing the x, y-coordinates by the more appropriate x_α, y_β-system, and subsequently introducing (1.128) and $\phi = 0$, it attains the form

$$\frac{\partial(\mathrm{d}w)}{\partial x_\alpha} = 0 \ , \qquad \frac{\partial(\mathrm{d}w)}{\partial y_\beta} = 2\,\mathrm{d}\lambda\ \tau_Y \ . \tag{1.132}$$

Accordingly, along the α-line the displacement increments $\mathrm{d}w$ are constant. As a consequence, if the initial state is undeformed, all material points along an α-line experience the same displacement w.

1.6 Further reading

Betten, J. *Creep Mechanics*. Springer, Berlin (2008)

Chakrabarty, J. *Theory of Plasticity*. Butterworth-Heinemann, New York (2006)

Christensen, R.M. *Theory of Viscoelasticity*. Academic Press, New York (1982)

Doghri, I. *Mechanics of Deformable Solids*. Springer, Berlin (2000)

Fung, Y.C. *Foundations of Solid Mechanics*. Prentice-Hall, Englewood Cliffs (1965)

Gould, P.L. *Introduction to Linear Elasticity*. Springer, New York (1993)

Hill, R. *The Mathematical Theory of Plasticity*. Oxford University Press, Oxford (1998)

Kachanov, L.M. *Fundamentals of Theory of Plasticity*. North-Holland, 1971

Khan, A.S. and Huang, S. *Continuum Theory of Plasticity*. John Wiley & Sons, New York (1995)

Lemaitre, J. and Chaboche, J.-L. *Mechanics of Solid Materials*. Cambridge University Press, Cambridge (2000)

Lubliner, J. *Plasticity Theory*. Macmillan Publ. Comp., New York (1998)

Maugin, G.A. *The Thermomechanics of Plasticity and Fracture*. Cambridge University Press, Cambridge (1992)

Muskhelisvili, N.I. *Some Basic Problems of the Mathematical Theory of Elasticity*. Noordhoff, Leyden (2010)

Nadai, A. *Theory of Flow and Fracture of Solids*, Vol. 1 & 2. McGraw-Hill, New York (1963)

Rabotnov, Y.N. *Creep Problems in Structural Members*. North Holland, Amsterdam (1969)

Sokolnikoff, I.S. *The Mathematical Theory of Elasticity*. McGraw-Hill, New York (1956)

Chapter 2
Classical fracture and failure hypotheses

In this chapter, a brief outline on classical fracture and failure hypotheses for materials under static loading will be given. The word *classical* this context means in that most of these so-called *strength hypotheses* are already quite old. Partially they date back to considerations made at the end of the 19th or the beginning of the 20th century and they are inseparably associated with the development of solid mechanics at that time. Through modern fracture mechanics they have been pushed into the background, as far as research is regarded. However, because of their wide spreading which, last but not least, is due to their simplicity, they are still of remarkable importance.

2.1 Basic concepts

Strength hypotheses are intended to make a statement about the circumstances under which a material fails. Their basis are experiments conducted under specific, mostly simple, loading conditions. As an example, two typical stress-strain curves for materials under uniaxial tension are schematically shown in Fig. 2.1. Up to a

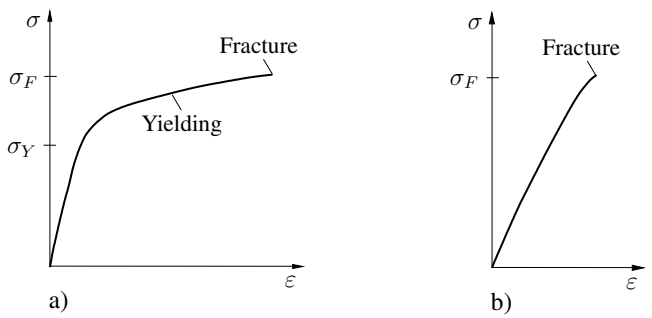

Fig. 2.1 Material behavior: a) ductile, b) brittle

D. Gross and T. Seelig, *Fracture Mechanics: With an Introduction to Micromechanics*, Mechanical Engineering Series, DOI 10.1007/978-3-642-19240-1_2,

certain limit the response of many materials is essentially elastic. *Ductile* behavior is characterized through plastic deformations which occur when the stress exceeds the *yield strength* σ_Y. In this case, the *ultimate stress* at fracture will be attained only after sufficiently large inelastic deformations. In contrast, *brittle* material behavior is characterized by the fact that no significant inelastic deformations occur prior to fracture.

Depending on the problem at hand, the *strength* of a material is often characterized by either the yield stress or the ultimate stress at fracture. The associated material parameters are the yield strength and the ultimate tensile strength. A common feature of both is that the material behavior changes drastically at these limits. In this context it should be emphasized that ductile or brittle behavior is not a pure material property. The stress state also has an essential influence onto the material behavior. To illustrate this fact it should be mentioned that in general, a hydrostatic stress state does not lead to inelastic deformations of most materials which usually are considered as plastically deformable. Thus, under certain loading conditions, such a material can behave as absolutely brittle.

We now assume that for uniaxial loading as well as for any complex loading the actual state of the material which determines its behavior inclusive its failure limit can be characterized simply by the current stress or strain state. Then the failure condition can be expressed as

$$F(\sigma_{ij}) = 0 \qquad \text{or} \qquad G(\varepsilon_{ij}) = 0 \; . \tag{2.1}$$

Just like the yield condition which is described by an analogous equation, the failure condition $F(\sigma_{ij}) = 0$ can be interpreted as a *failure surface* in the six-dimensional stress space or alternatively in the three-dimensional space of principal stresses. Accordingly, a stress state σ_{ij} on the surface $F = 0$ characterizes failure as a result of yielding or fracture.

A failure condition of the type (2.1) implies that the material state at failure is independent of the deformation history. With sufficient accuracy this applies to the onset of plastic yielding in ductile materials or to the fracture of brittle materials. Furthermore, such a failure condition is acceptable only if until failure the material can be considered as a continuum without macroscopic defects. This means in particular that macroscopic cracks must not appear and influence the behavior of the material through their presence.

The deformation process of plastically deformable materials such as metals (also concrete or geological materials often are considered as plastically deformable) after reaching the yield strength can be described by a flow rule. Such a flow rule however, by no means characterizes the kinematics of brittle fracture. In general, simple kinematic statements for fracture processes are possible only for specific stress states.

2.2 Failure hypotheses

Formally it is possible to establish infinitely many failure hypotheses of the type (2.1). In what follows, some common hypotheses are presented, part of which can be applied with sufficient accuracy (from an engineer's point of view) to certain classes of materials. Some of them, however, are only of historical relevance. In this context we will not again discuss the VON MISES and TRESCA yield condition since this has already been done in Section 1.3.3.1.

2.2.1 Principal stress hypothesis

This hypothesis dates back to W.J.M. RANKINE (1820–1872), G. LAMÉ (1795–1870), and C.L. NAVIER (1785–1836). According to this hypothesis, the material behavior is characterized by two characteristic values, the tensile strength σ_t and the compressive strength σ_p. Failure is expected to take place when the maximum principal stress reaches σ_t or when the minimum principal stress reaches $-\sigma_p$, i.e., when one of the following conditions is fulfilled:

$$\sigma_1 = \begin{cases} \sigma_t \\ -\sigma_p \end{cases} \qquad \sigma_2 = \begin{cases} \sigma_t \\ -\sigma_p \end{cases} \qquad \sigma_3 = \begin{cases} \sigma_t \\ -\sigma_p \end{cases} \quad . \tag{2.2}$$

The associated failure surface in principal stress space is represented by a cube (Fig. 2.2a). The corresponding failure curve for a plane stress state ($\sigma_3 = 0$) is a square (Fig. 2.2b).

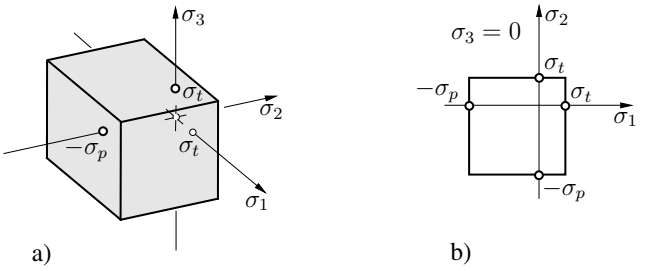

Fig. 2.2 Principal stress hypothesis

The principal stress hypothesis predominantly serves to describe brittle failure of materials. For tensile loading we generally associate with it the process of decohesion along cross sections perpendicular to the largest principal stress. The hypothesis neglects the influence of the two other principal stresses onto failure, its applicability hence is quite limited.

2.2.2 Principal strain hypothesis

According to the hypothesis suggested by DE SAINT-VENANT (1797–1886) and C. BACH (1889), failure occurs when the maximum principle strain reaches the critical value ε_t. If we assume linear elastic behavior until failure and introduce the critical tensile stress $\sigma_t = E\varepsilon_t$, we get the following failure conditions:

$$\sigma_1 - \nu(\sigma_2 + \sigma_3) = \sigma_t \ , \quad \sigma_2 - \nu(\sigma_3 + \sigma_1) = \sigma_t \ , \quad \sigma_3 - \nu(\sigma_1 + \sigma_2) = \sigma_t \ . \tag{2.3}$$

In this case, the failure surface is represented by a pyramid with three planes centered around the hydrostatic axis with its apex at $\sigma_1 = \sigma_2 = \sigma_3 = \sigma_t/(1-2\nu)$ (Fig. 2.3a). The failure curve for plane stress is shown in Fig. 2.3b.

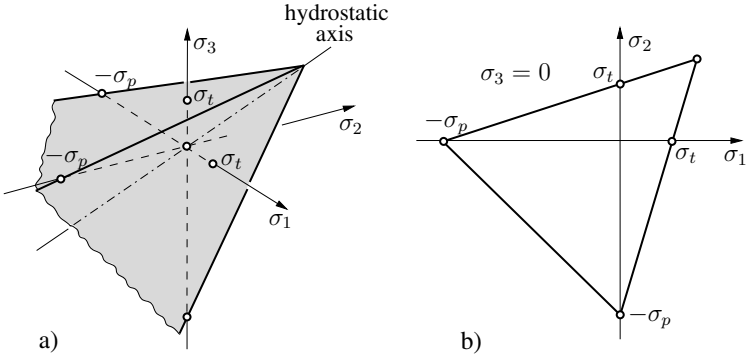

Fig. 2.3 Principal strain hypothesis

According to this hypothesis, failure under uniaxial compression should occur at $\sigma_p = \sigma_t/\nu$. This contradicts experimental experiences for most materials.

2.2.3 Strain energy hypothesis

The hypothesis by E. BELTRAMI (1835-1900) postulates failure when the strain energy density U reaches a material-specific critical value U_c, i.e., at $U = U_c$. Usually this assumption implies that the material behaves linearly elastic until failure. If we introduce with $U_c = \sigma_c^2/2E$ a uniaxial failure stress σ_c and express $U = U_V + U_G$ through the principal stresses by using (1.50), we obtain the following representation of the hypothesis:

$$(1+\nu)[(\sigma_1-\sigma_2)^2+(\sigma_2-\sigma_3)^2+(\sigma_3-\sigma_1)^2]+(1-2\nu)(\sigma_1+\sigma_2+\sigma_3)^2 = 3\sigma_c^2 \ . \tag{2.4}$$

The corresponding failure surface is an ellipsoid around the hydrostatic axis with the apex at $\sigma_1 = \sigma_2 = \sigma_3 = \pm\sigma_c/\sqrt{3(1-2\nu)}$.

According to this hypothesis, a sufficiently high hydrostatic pressure always leads to failure; this is in contradiction with experimental results. If the volumetric part U_V of the strain energy density U is omitted, Beltrami's hypothesis reduces to the von Mises yield condition.

In conjunction with modern fracture mechanics, the strain energy hypothesis in a somewhat modified form has been suggested for application as a crack initiation and propagation criterion, see S-criterion in Sect. 4.9.

2.2.4 Coulomb-Mohr hypothesis

This hypothesis predominantly serves to describe failure due to slip of geological and granular materials, such as sand, rock, or soils. These materials can carry only relatively small or, in the limit, no tensile stresses.

For a physical explanation we consider an arbitrary cross section which is loaded by the normal stress $-\sigma$ (pressure) and the shear stress τ. *Coulomb's friction law*, applied to the stresses, postulates sliding when τ attains a critical value proportional to the pressure $-\sigma$: $\mid \tau \mid = -\sigma \tan \rho$. Here ρ is the material-dependent *friction angle*. For $-\sigma \to 0$ it follows that $\mid \tau \mid \to 0$; tensile stresses are not possible in this case. In many cases however, even for $\sigma = 0$, onset of sliding requires a nonzero, finite shear stress. In addition, materials frequently are able to carry tensile stresses to a certain extent. Therefore it is reasonable to modify the sliding condition as follows:

$$\mid \tau \mid = -\sigma \tan \rho + c \,. \tag{2.5}$$

This relation is known as the *Coulomb-Mohr hypothesis* (C.A. COULOMB (1736–1806); O. MOHR (1835–1918)). The parameter c is called *cohesion*.

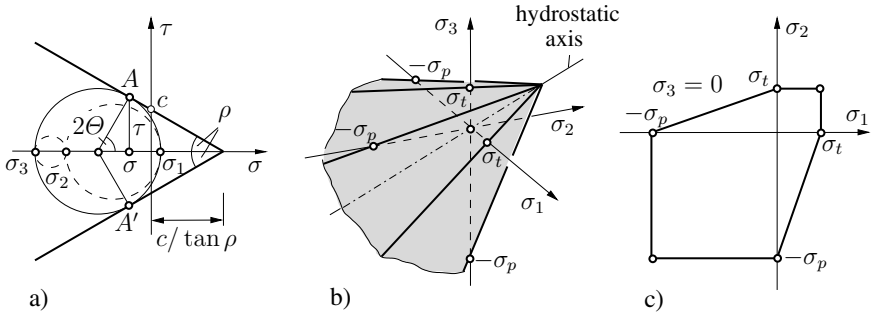

Fig. 2.4 Coulomb-Mohr hypothesis

In the σ-τ diagram, equation (2.5) is represented by two straight lines which form the envelop of admissible Mohr's circles (Fig. 2.4a). Sliding occurs for those stress states for which the largest of the three Mohr's circles just touches the envelope. In

terms of principal stresses this leads to the condition

$$\frac{|\,\sigma_1 - \sigma_3\,|}{2} = \left[\frac{c}{\tan\rho} - \frac{\sigma_1 + \sigma_3}{2}\right]\sin\rho\;. \tag{2.6}$$

If we introduce into this equation for instance $\sigma_1 = \sigma_t$ and $\sigma_3 = 0$, we obtain for the uniaxial tensile strength $\sigma_t = 2c\cos\rho/(1+\sin\rho)$. Analogously, with $\sigma_1 = 0$ and $\sigma_3 = -\sigma_p$ the compressive strength follows to $\sigma_p = 2c\cos\rho/(1-\sin\rho)$. It should also be mentioned that (2.6) includes as a special case for $\rho \to 0$ Tresca's yield condition (cf. Sect. 1.3.3.1).

Sometimes it is appropriate to use the characteristic material parameters σ_p and $\kappa = \sigma_p/\sigma_t$ instead of the parameters ρ and c. In this case it follows from (2.6) that for the onset of sliding, one of the following conditions must be fulfilled:

$$\left.\begin{matrix}\kappa\sigma_1 - \sigma_3\\ -\sigma_1 + \kappa\sigma_3\end{matrix}\right\} = \sigma_p\;,\quad \left.\begin{matrix}\kappa\sigma_2 - \sigma_1\\ -\sigma_2 + \kappa\sigma_1\end{matrix}\right\} = \sigma_p\;,\quad \left.\begin{matrix}\kappa\sigma_3 - \sigma_2\\ -\sigma_3 + \kappa\sigma_1\end{matrix}\right\} = \sigma_p\;. \tag{2.7}$$

Here, the principal stresses are *not* a priori ordered according to their magnitude. The associated failure surface is a pyramid formed by six planes around the hydrostatic axis (Fig. 2.4b). Its apex is located at $\sigma_1 = \sigma_2 = \sigma_3 = \sigma_p/(\kappa - 1)$. The failure curve for a plane stress state is shown as the hexagon in Fig. 2.4c.

As already mentioned, sliding is supposed to take place in cross sections where relation (2.5) is fulfilled. They are characterized by the corresponding points A and A' in Fig. 2.4a. Accordingly, the normal of the slip plane lies in the plane given by the maximum principal stress σ_1 and the minimum principal stress σ_3. The unit normal vector and the direction of σ_1 form an angle of

$$\Theta_{1,2} = \pm(45^\circ - \rho/2)\;. \tag{2.8}$$

According to this hypothesis, the intermediate principle stress σ_2 has no effect on the onset of failure and the failure angle. It finally should be noted that failure along the cross section determined by relation (2.8) occurs only when it is kinematically possible.

The result (2.8) for the orientation of the failure cross section is used among others in geology to explain different types of faults of the earth's crust. Here it is

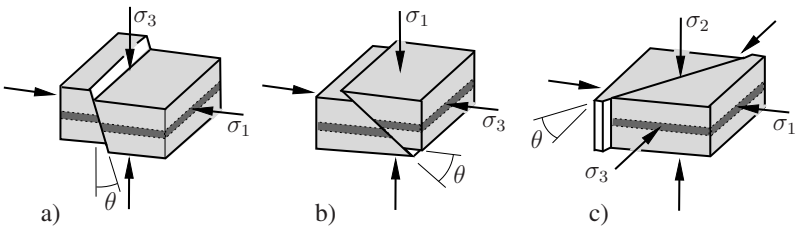

Fig. 2.5 Faults

assumed that all principal stresses are compressive stresses ($|\sigma_3| \geq |\sigma_2| \geq |\sigma_1|$) and act in vertical (perpendicular to the earth' surface) and in horizontal direction, respectively. A *normal fault* then is explained with a situation where the vertical principal stress if larger than the principal stresses acting in horizontal direction (Fig. 2.5a). In contrast, for a *reverse fault* it is supposed that the value of the vertical pressure is the smallest one (Fig. 2.5b). Finally, a *strike-slip fault* is associated with a vertical pressure σ_2 whose magnitude lies between the maximum and the minimum values of the principal stresses (Fig. 2.5c).

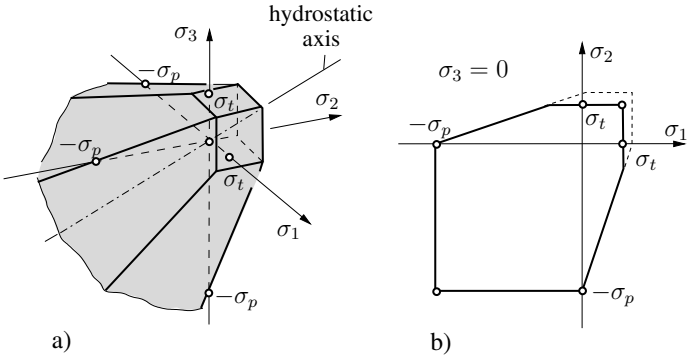

Fig. 2.6 Tension cut-off

Experiments show that the Coulomb-Mohr hypothesis describes the behavior of different materials sufficiently well in the compression regime but worse in the tension regime. Responsible for this is in most cases a change of the failure mechanism. This holds particularly when failure in the tension regime occurs not due to the sliding but is rather associated with a decohesion of the cross sections perpendicular to the maximum principal stress. A possibility to improve the failure condition consists, for instance, in a modification of the failure surface through so-called *tension cut-offs* (Fig. 2.6).

The hypothesis (2.5) assumes a linear relation between τ and σ. A generalization of the form

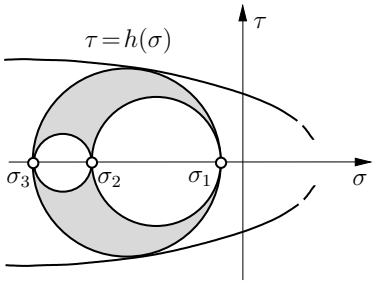

Fig. 2.7 Mohr's failure hypothesis

$$| \tau | = h(\sigma) \tag{2.9}$$

where the function $h(\sigma)$ must be determined experimentally was proposed by O. MOHR (1900). In the σ-τ diagram it represents the envelope of admissible Mohr's circles (Fig. 2.7). As in hypothesis (2.5), the intermediate principal stress σ_2 has no effect on failure. In this respect, both hypotheses may be considered as special (not general) cases of a failure condition $F(\sigma_1, \sigma_3) = 0$.

2.2.5 Drucker-Prager hypothesis

According to the hypothesis by D.C. DRUCKER (1918-2001) and W. PRAGER (1903-1980), a material fails when the condition

$$F(I_\sigma, II_s) = \alpha\, I_\sigma + \sqrt{II_s} - k = 0 \tag{2.10a}$$

is fulfilled. Here, I_σ, II_s are the invariants of the stress tensor and of its deviator, respectively, and α and k are material parameters. If we introduce $\sigma_m = \sigma_{\rm oct} = I_\sigma/3$ and $\tau_{\rm oct} = \sqrt{2\, II_s/3}$ the condition (2.10a) can be interpreted similar to the Mohr-Coulomb hypothesis. Accordingly, failure occurs when the octahedral shear stress $\tau_{\rm oct}$ reaches a value which is linearly dependent on the normal stress σ_m (cf. (2.5)):

$$\tau_{\rm oct} = -\sqrt{6}\, \alpha\, \sigma_m + \sqrt{2/3}\, k\ . \tag{2.10b}$$

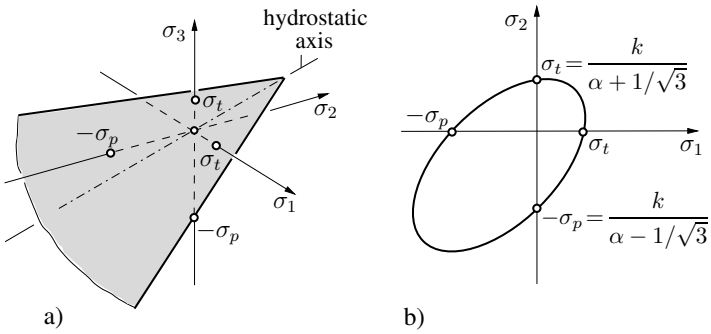

Fig. 2.8 Drucker-Prager hypothesis

The failure surface defined by (2.10a,b) in principal stress space forms a cone around the hydrostatic axis with the apex at $\sigma_1 = \sigma_2 = \sigma_3 = k/3\alpha$ (Fig. 2.8a). The associated failure curve for plane stress ($\sigma_3 = 0$) is an ellipse (Fig. 2.8b). As the Coulomb-Mohr hypothesis, the Drucker-Prager criterion is used as a yield or as a fracture condition, predominantly for granular and geological materials. For $\alpha = 0$ it reduces to the von Mises yield condition.

Experiments show that in some cases a description of the failure condition by means of only two material parameters is not sufficient. It then must be suitably modified. A frequently used extension of the Drucker-Prager hypothesis is given by

$$F(I_\sigma, II_s) = \alpha\, I_\sigma + \sqrt{II_s + \beta\, I_\sigma^2} - k = 0\ . \tag{2.11}$$

Here, β is an additional material parameter.

2.2.6 Johnson-Cook criterion

While the failure hypotheses discussed so far are primarily intented to describe brittle failure or the onset of plastic flow, the criterion by JOHNSON and COOK (1985) addresses ductile failure after pronounced plastic deformation. Ultimate failure in many ductile materials proceeds by the formation and coalescence of microscopic voids (as discussed in more detail in Sections 3.1.3 and 9.4) which is essentially driven by hydrostatic stress. Correspondingly, the plastic strain at failure in these materials is assumed to be a decreasing function of the ratio of hydrostatic to deviatoric stress as sketched in Fig. 2.9 and approximated by the relation:

$$\varepsilon_{fail} = D_1 + D_2 \exp\left(D_3\, \frac{\sigma_m}{\sigma_\mathrm{e}}\right) \quad . \tag{2.12}$$

Here, ε_{fail} is the value of the equivalent plastic strain $\varepsilon_\mathrm{e}^p = \sqrt{\frac{2}{3}\,\varepsilon_{ij}^p \varepsilon_{ij}^p}$ at failure, $\sigma_m = \frac{1}{3}\,\sigma_{kk}$ is the hydrostatic stress, $\sigma_\mathrm{e} = \sqrt{\frac{3}{2}\,s_{ij}s_{ij}}$ the equivalent (von Mises) stress, and D_1, D_2, D_3 are material constants.

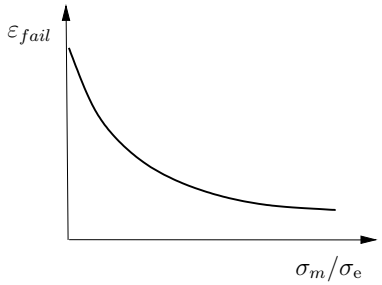

Fig. 2.9 Johnson-Cook criterion

It should be mentioned that the direct relation between the accumulated plastic strain at failure and the stress state in the failure criterion (2.12) is meaningful only if proportional loading prevails throughout the entire deformation history, i.e. when the ratio $\sigma_m/\sigma_\mathrm{e}$ is constant (see also Section 1.3.3.3). The model can be extended to

account for non-proportional loading by supplementing it with a damage evolution law. More elaborate models for ductile failure, however, are discussed in Sect. 9.4.

2.3 Deformation behavior during failure

On the basis of the failure criterion alone no direct conclusion can be drawn for the deformation behavior or the kinematics during failure. Respective statements are only possible when a specified kinematic idea is a priori associated with the failure hypothesis or when a physically meaningful assumption is introduced.

During failure due to fracture, a body is separated into two or more parts. This process is accompanied with the creation of new surfaces, i.e., with the formation of *fracture surfaces*. The associated kinematics can not be described in a simple manner. Only for sufficiently uniform stress states statements are possible which are guided by experimental results. They show two basic patterns for the formation of fracture surfaces. For a *normal stress dominated fracture*, the fracture plane coincides with the cross section normal to the maximum principal stress which necessarily must be tension (Fig. 2.10a). If the fracture surface is formed by cross sections in which a certain shear stress (e.g., $\tau_{\max}$, τ_{oct}, etc.) reaches a critical value, this is called *shear dominated fracture* (Fig. 2.10b). Dependent on the stress state and the material behavior, both types occur also in various mixed forms.

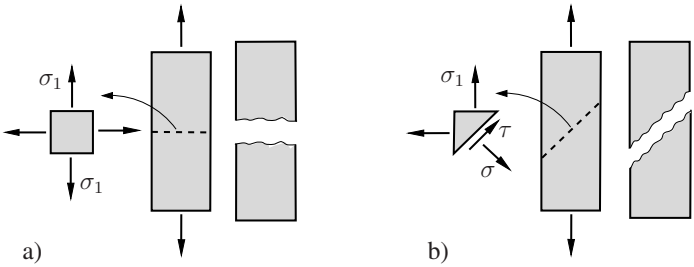

Fig. 2.10 Fracture surfaces

If "failure" denotes the onset of yielding, the failure criterion is equivalent to a yield criterion. Within the framework of incremental plasticity, deformations appearing during yielding can be described by means of the flow rule $\mathrm{d}\varepsilon_{ij}^{p} = \mathrm{d}\lambda\, \partial F/\partial\sigma_{ij}$ (cf. Sect. 1.3.3.2). The respective equations for the von Mises and Tresca yield conditions are assembled in (1.83a) and (1.84). As a further example, the incremental stress-strain relations for the Drucker-Prager model shall be specified here. We assume that the yield surface is independent of the deformation history (perfectly plastic material). In this case, the flow rule in conjunction with (2.10a,b) and $I_\sigma = \sigma_{kk} = \sigma_{ij}\delta_{ij}$ and $II_s = \frac{1}{2}s_{ij}s_{ij}$ yields

$$\mathrm{d}\varepsilon_{ij}^{p} = \mathrm{d}\lambda \left(\alpha\, \delta_{ij} + \frac{s_{ij}}{2\sqrt{II_s}} \right) . \tag{2.13}$$

The determination of $\mathrm{d}\lambda$ is not further discussed here. It should be noted that according to (2.12) volume changes generally occur; the corresponding increment is given by $\mathrm{d}\varepsilon_{kk}^{p} = 3\alpha\, \mathrm{d}\lambda$. However, experiments suggest that the associated flow rule is not valid for granular materials. Thus, yielding then takes place not perpendicular to the yield surface. Therefore, equation (2.13) should not be used for such materials.

2.4 Problems

Problem 2.1 a) Determine the stress distribution in a linear elastic thick-walled cylinder (radii a and b) subjected to an internal pressure p by using the complex potentials

$$\Phi(z) = A\, z\,, \qquad \Psi(z) = \frac{B}{z}\,.$$

b) Find the potential failure loci according to the maximum principal stress criterion and the maximum shear stress criterion.

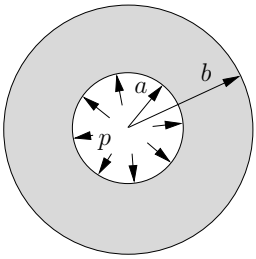

Fig. 2.11

Solution

a)

$$\sigma_\varphi = p\,\frac{(b/r)^2+1}{(b/a)^2-1} = \sigma_1 > 0\,, \quad \sigma_r = p\,\frac{(b/r)^2-1}{(b/a)^2-1} = \sigma_2 < 0\,, \quad \tau_{r\varphi} = 0\,.$$

b) Maximum principal stress criterion: Since $\sigma_\varphi = \sigma_1$ is the maximum principal stress, failure should occur perpendicular to the hoop stress, i.e. in radial sections.

Maximum shear stress criterion: On account of $\tau_{r\varphi} = 0$, the maximum shear direction is everywhere inclined by 45° with respect to the radial direction. This can be expressed by the differential relation $\mathrm{d}r = r\,\mathrm{d}\varphi$ which has the solution $\varphi(r) = \varphi_0 + \ln(r/a)$; i.e. failure takes place along logarithmic spirals.

2.5 Further reading

Gould, P.L. *Introduction to Linear Elasticity*. Springer, New York, 1993

Paul, B. *Macroscopic Criteria for Plastic Flow and Brittle Fracture*. In *Fracture – A Treatise*, Vol. 2, ed. H. Liebowitz, pp. 315-496, Academic Press, London, 1968

Nadai, A. *Theory of Flow and Fracture of Solids*, Vol. 1. McGraw-Hill, New York, 1963

Chapter 3
Micro and macro phenomena of fracture

Origins and phenomena of fracture are manifold. The reason for this can be found in the fact that the phenomena are predominantly determined by the microscopic properties of a material which in turn vary extensively from material to material. In this book, emphasis is placed on a continuum-mechanical description of macroscopic fracture behavior. Nevertheless, it is beneficial to have a certain understanding of microscopic events. Therefore, both microscopic and macroscopic aspects are briefly discussed in this chapter. The former have only exemplary character and focus on phenomena in crystalline or polycrystalline materials which includes the large class of metals.

3.1 Microscopic aspects

3.1.1 Surface energy, theoretical strength

Fracture is the separation of a body into two or more parts. During this process the bonds between the components of the material are broken. At the microscopic level, these are for instance bonds between atoms, ions, molecules, etc. The bonding force between two of those elements can be expressed by means of the relation

$$F = -\frac{a}{r^m} + \frac{b}{r^n} \tag{3.1}$$

(Fig. 3.1a). Here, the first term represents attractive forces, while the second term describes repulsive ones. The parameters a, b, m, and n ($m < n$) are constants which depend on the bond type. For small displacements from the equilibrium configuration d_0, the bonding force $F(r)$ can be approximated by a linear function. This is equivalent to a material behavior which macroscopically is described by Hooke's law.

D. Gross and T. Seelig, *Fracture Mechanics: With an Introduction to Micromechanics*, Mechanical Engineering Series, DOI 10.1007/978-3-642-19240-1_3,

During the release of bonds, i.e., the separation of elements, a negative material-specific work W^B is done by the bonding force. As a consequence of separation, for instance in a perfect crystal, the lattice geometry changes in the immediate neighborhood of the newly created surface. This change is confined to a few lattice spacings into the bulk. If dissipative processes are neglected and the material is, from the macroscopic point of view, considered as a continuum, the work of bonding forces is transferred into *surface energy* of the body (i.e., the energy stored at the body's surface). It is defined as

$$\Gamma^0 = \gamma^0 A \tag{3.2}$$

where A is the newly created surface and γ^0 is the *surface energy density*.

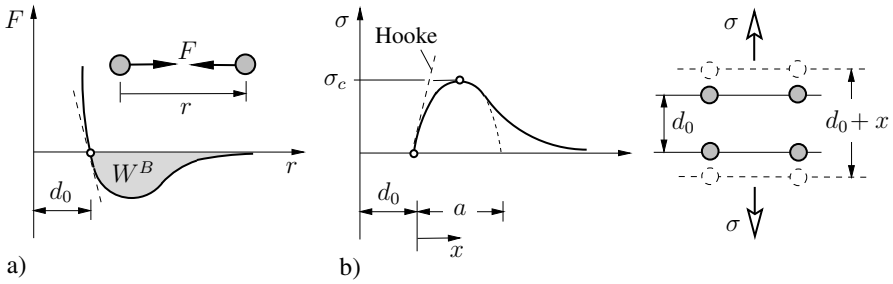

Fig. 3.1 Theoretical strength

In what follows, we consider in a somewhat simplified manner the separation process of two atomic lattice planes of a crystal. For the separation stress $\sigma(x)$ we assume a dependence on the separation displacement x similar to the bonding force (Fig. 3.1b). In the tensile regime it can be approximated by the relation $\sigma_c \sin(\pi x/a)$. For small displacements x this leads to $\sigma \approx \sigma_c \pi x/a$. Equating the latter with Hooke's law $\sigma = E\varepsilon = Ex/d_0$ yields for the so-called *theoretical strength*, i.e., the *cohesive stress* that has to be overcome during separation

$$\sigma_c \approx E\frac{a}{\pi d_0} \,. \tag{3.3}$$

If we further assume that the bonds are completely broken for $a \approx d_0$ we obtain the rough estimate

$$\sigma_c \approx \frac{E}{\pi} \,. \tag{3.4}$$

From the work of stresses in conjunction with the foregoing assumptions the surface energy γ^0 can be determined. Taking into account that *two* new surfaces are created during separation we get

$$2\gamma^0 = \int_0^\infty \sigma(x)\mathrm{d}x \approx \int_0^a \sigma_c \sin\frac{\pi x}{a}\mathrm{d}x = \sigma_c \frac{2a}{\pi} \,. \tag{3.5}$$

With $a \approx d_0$ and (3.4) it follows herefrom that

$$\gamma^0 \approx \frac{E d_0}{\pi^2} \,. \tag{3.6}$$

If the relations (3.4) and (3.6) are applied to iron or steel, using the data $E = 2.1 \cdot 10^5\,\mathrm{MPa}$ and $d_0 = 2.5 \cdot 10^{-10}\,\mathrm{m}$, we obtain $\sigma_c \approx 0.7 \cdot 10^5\,\mathrm{MPa}$ and $\gamma^0 \approx 5\,\mathrm{J/m^2}$. However, corresponding values can only be reached for defect-free single crystals (whiskers). For real polycrystalline materials, the fracture strength is 2-3 orders of magnitude less. In parallel, the energy necessary for the creation of new fracture surfaces exceeds the value in (3.6) by several orders of magnitude. The reasons for this can be found in the inhomogeneous structure of the material and, first of all, in its defect structure.

As a side note it should be mentioned that the bonding force (3.1) can be derived from an interaction potential $\Phi(r)$ as $F = -\partial\Phi/\partial r$. A typical standard potential for interatomic interaction is the *Lennard-Jones potential* (J. LENNARD-JONES, 1894-1954)

$$\Phi_{LJ}(r) = -\frac{A}{r^6} + \frac{B}{r^{12}} \,. \tag{3.7}$$

Its first term describes the attractive *van der Waals* forces while the second term is responsible for the short-range repulsive forces. This potential is widely used for fundamental investigations and molecular dynamic simulations including separation processes on the microscale.

3.1.2 Microstructure and defects

A polycrystalline material consists of crystals (grains) which are joined with one another along grain boundaries. The individual grains have anisotropic properties and the orientation of their crystallographic planes and axes differ from grain to grain. Furthermore, e.g., due to segregation, the properties of grain boundaries differ substantially from those of the grains.

In addition to these irregularities of the material's structure, a real material contains from the beginning on a number of defects of different size. Defects with the characteristic length of one or several grains, e.g., induced by the manufacturing process, are for instance inclusions with strongly different material properties, cavities, or microcracks. From the physical point of view, they are mostly viewed as defects on the *mesoscale*. In addition, there are faults on the *microscale* which are understood as defects in the crystal lattice. Usually they are classified according to their dimension as point imperfections (e.g., vacancies, interstitials, impurity atoms), line imperfections (dislocations), and area imperfections (e.g., stacking faults, phase boundaries, twin boundaries).

A particular role regarding the mechanical behavior is played by *dislocations*. The geometry of these lattice imperfections is shown in Fig. 3.2a for an *edge dislocation* and in Fig. 3.2b for a *screw dislocation*. A dislocation can be characterized by

the *Burgers vector* $\boldsymbol{b}$ (J.M. BURGERS, 1895-1981) as follows: $\boldsymbol{b}$ is perpendicular to the *dislocation line* for an edge dislocation while $\boldsymbol{b}$ is parallel to the dislocation line for the screw dislocation (Fig. 3.2a, b). It should be noted that a dislocation induces an eigenstress field which is accompanied by an elastic energy (cf. Section 8.2.1).

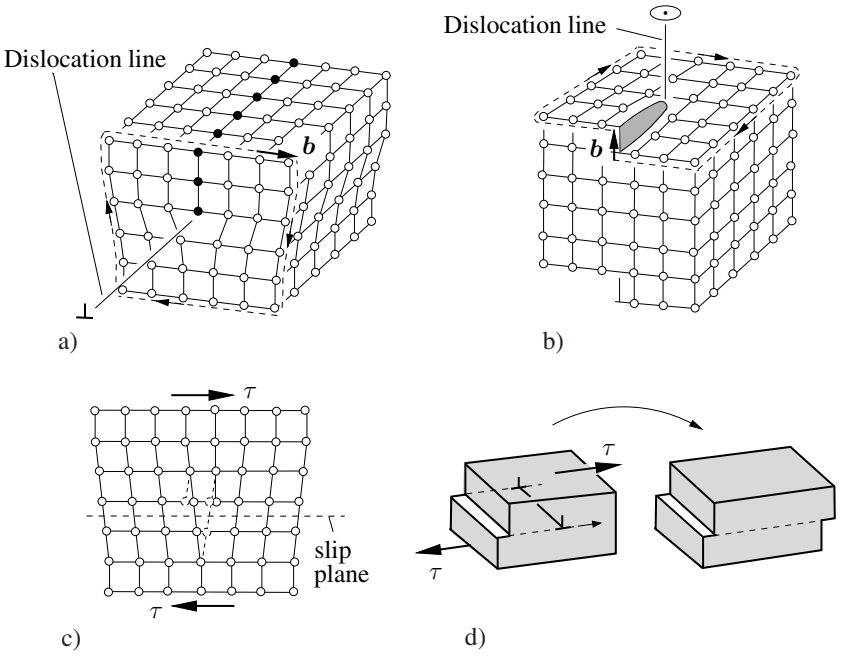

Fig. 3.2 Dislocations

Under the action of sufficiently high shear stresses the atoms in the vicinity of the dislocation line rearrange their bonds which leads to a displacement of the dislocation (Fig. 3.2c). The work done during this process is mainly dissipated as heat (= lattice vibration). The dislocation movement results in a relative "slip" of the lattice planes and may lead to the formation of a new surface (Fig. 3.2d). This microscopic mechanism is the origin of macroscopic plastic material behavior. The dislocation movement within a crystal is often not uniformly distributed but rather localized in *slip bands*. In general, dislocations can not move unlimited. At obstacles such as grain boundaries or inclusions they may stop and accumulate. Macroscopically such a dislocation pile-up is observed as strain hardening.

In contrast to crystalline materials, the molecules and atoms are completely disordered in amorphous solids such as glasses or many polymers. While in these materials no disturbances of a regular lattice, e.g. by dislocations or grain boundaries can be identified, the defects are essentially given by foreign particles and microvoids. The characteristic feature of polymeric materials (plastics) is their composition of long molecular chains which, in case of an amorphous microstructure, are randomly

entangled. Two kinds of forces and bonds, respectively, can be distinguished in such a material: a) the intramolecular forces between neighboring atoms within a polymer chain due to covalent chemical bonds and b) the considerably weaker intermolecular van der Waals forces between atoms of different chains. On account of local entanglements and/or chemical bonds, the molecular chains form a complex three-dimensional network. Under external tensile loading, the microscopic deformations initially comprise rotations and stretching of single chain segments. Subsequently, debonding of intermolecular cross-links and straining as well as rupture of chains may occur. This microscopic damage mechanism preferably takes place at heterogeneities of the molecular network and at foreign particles (e.g. dust particles). Similar to the situation in crystalline materials, this process is accompanied by the formation of microvoids. With increasing deformation, void formation localizes in thin zones perpendicular to the macroscopic loading direction. In these zones, the polymer material between the voids is stretched into fibrils, i.e. oriented bundles of molecular chains (Fig. 3.3). This damage mechanism on the mesoscale is called *crazing*. It is in most cases the precursor of microcracks in polymeric materials where the cracks develop from crazes due to rupture of the fibrils.

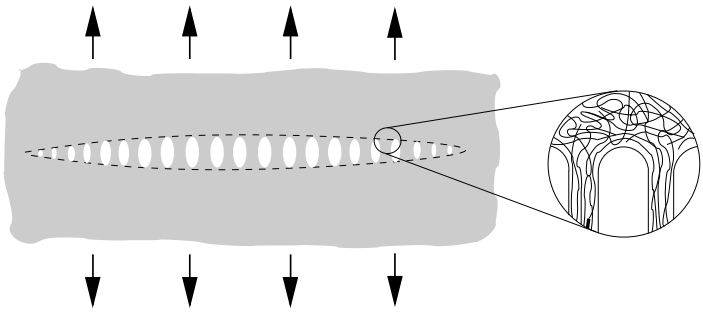

Fig. 3.3 Craze zone in a thermoplastic polymer

In two-phase or multi-phase materials like fiber or particle-reinforced composites but also concrete and asphalt, the fracture mechanical relevant microstructure is characterized by the specific heterogeneous composition. The dominant microscopic damage mechanisms that may lead to crack formation are local fracture of the usually brittle reinforcement particles, fiber pull-out and breakage, and failure of the interface to the surrounding matrix. The coalescence of these microscopic defects to a macroscopic crack generally takes place in a significantly larger region than in unreinforced plastics or in polycrystalline materials.

3.1.3 Crack formation

In initially crack-free polycrystalline materials there are different mechanisms of microcrack formation. A separation of atomic planes without any accompanying dislocation movement hardly occurs. The formation of microcracks and their subsequent propagation practically always is combined with more or less pronounced microplastic processes.

A rather important mechanism of microcrack formation is the dislocation pile-up at obstacles. It causes high stress concentrations which can lead to bond breaking along preferred lattice planes and as a consequence to *cleavage*. If such a crack runs through several grains, the orientation of the separation surface changes according to the local lattice planes and axes (Fig. 3.4a). Such a type of fracture is called *transcrystalline cleavage*.

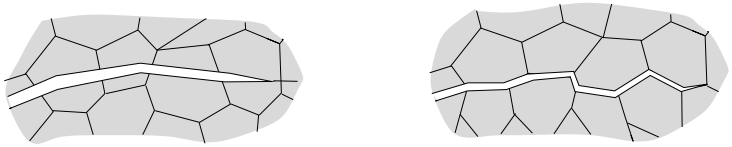

Fig. 3.4 a) Transcrystalline crack, b) intercrystalline crack

If the grain boundaries are sufficiently weak, the separation on account of dislocation pile-up and (or) grain boundary sliding will take place along these boundaries. This is called *intercrystalline fracture* (Fig. 3.4b). Both fracture processes are macroscopically *brittle*. They are accompanied by none or very small macroscopically inelastic deformations and they need very low energy.

A dislocation pile-up causes not only stress concentrations. It also can be the responsible source for the formation of microscopic voids and cavities. This mechanism is schematically shown in Fig. 3.5: the coalescence (concentration) of dislocations leads to the formation and growth of microcavities.

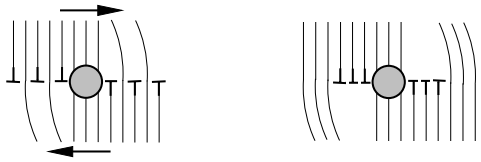

Fig. 3.5 Formation and growth of voids

Crystalline materials often contain a large number of second phase particles embedded at the grain boundaries or in the crystals. In their vicinity, presuming a sufficiently high mobility of dislocations, micro-plastic deformations occur prior to

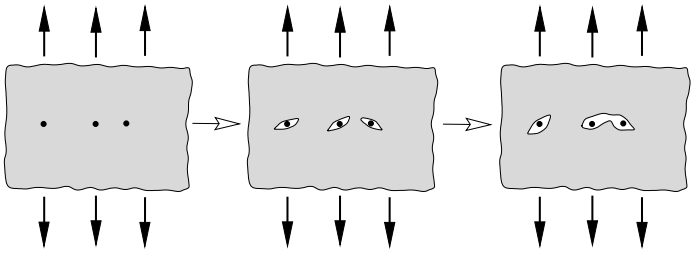

Fig. 3.6 Fracture due to formation and coalescence of voids

the formation of microcracks. The accompanying dislocation pile-up subsequently leads to the formation and growth of cavities around the particles and as a consequence to a loss of their bonds with the matrix. With increasing macroscopic deformation the voids grow due to micro-plastic yielding, they coalesce, and finally lead to separation (Fig. 3.6). Corresponding fracture surfaces show a typical structure of *honeycombs* or *dimples* which are separated by micro-plastically highly deformed zones. The energy needed for such a type of fracture is a multiple higher than that for cleavage.

Localization of slip processes in slip bands can also be the origin of crack formation. For instance, a sufficiently high cyclic load can lead to *extrusions* and *intrusions* at the body's free surface or at inhomogeneities (Fig. 3.7). A result of the increasing "surface roughness" is the formation of a *fatigue crack*.

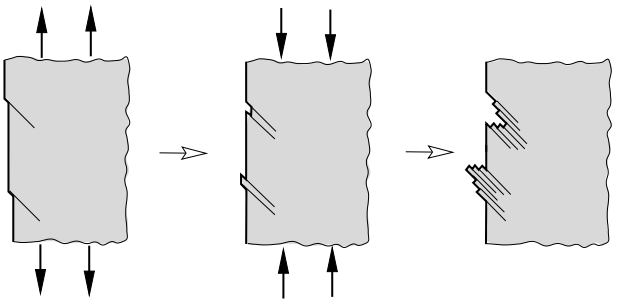

Fig. 3.7 Formation of a fatigue crack

3.1.4 Percolation

Defects in most real materials are distributed in an irregular spatial pattern (Fig. 3.8a). As a consequence, with increasing fraction f of defects (e.g. void volume fraction or microcrack density) local defect agglomerations, so-called *clusters*, will inevitably

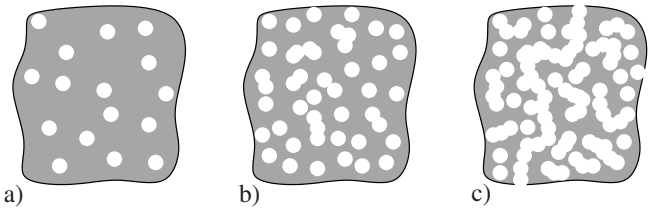

Fig. 3.8 Increasing defect fraction f in an irregular microstructure: a) isolated defects: $f_1 \ll f_c$, b) isolated clusters: $f_2 < f_c$, c) percolation threshold $f = f_c$

be formed (Fig. 3.8b, see also Fig. 3.6). In such a cluster, several defects are physically interconnected (e.g. nearly or already coalesced microcracks or voids) so that they act as a single larger defect. As long as clusters are still isolated in the surrounding matrix, their influence on the macroscopic behavior of the heterogeneous material is limited. However, at a critical defect fraction f_c, the so-called *percolation threshold* or *percolation limit*, the situation occurs that a single cluster extends throughout the entire microstructure (Fig. 3.8c). Depending on the defect type, this is accompanied by a drastic change of the macroscopic physical properties of a material. For example, in case of microvoids or microcracks, the macroscopic permeability of a solid to fluid flow may jump from zero to a finite value at the percolation threshold $f = f_c$ and further increase for $f > f_c$. Analogously, the macroscopic elastic stiffness continuously decreases with increasing f as long as $f < f_c$ but vanishes for $f > f_c$.

Dimension	Defect type	f_c
3D	Spheres	0.289
	Cubes, parallel faces	0.277
	Cubes, random orientation	0.217
	Ellipsoids of revolution, aspect ratio 5	0.163
	Ellipsoids of revolution, aspect ratio 1/5	0.176
2D	Discs	0.676
	Squares, parallel edges	0.667
	Squares, random orientation	0.625
	Ellipses, aspect ratio 5	0.455
	Ellipses, aspect ratio 20	0.178

Table 3.1 Percolation threshold

The percolation threshold strongly depends on the defect geometry but also on the spatial dimension, i.e. whether the defect distribution is considered as plane (two-dimensional) or spatial (three-dimensional). Because of its manifold physical importance, the percolation phenomenon is studied in many investigations experimentally as well as theoretically by means of statistical methods, and also numerically with massive computer simulations. Table 3.1 shows a collection of percolation threshold values that have been found by these methods. Aspects of the percolation

limit in conjunction with analytical micromechanical models will also be discussed in Section 8.3.

3.2 Macroscopic aspects

3.2.1 Crack growth

In what follows the material is macroscopically considered as a continuum which a priori contains cracks. This can be either an actually existing macroscopic crack of a given geometric configuration or a supposed, hypothetical crack of eventually very small size. The latter serves as a model for macroscopically invisible but always existing defects and microcracks in a real material. The question of crack formation in an initially undamaged material is not considered in this approach. It cannot be answered in the framework of classical continuum mechanics. A description of crack formation is possible only by means of continuum damage mechanics which takes into account the microscopic defect structure and its evolution (cf. Chapter 9).

A fracture process is always connected with crack growth. Both, fracture and crack growth, can be classified from different phenomenological viewpoints. The typical stages in the behavior of a loaded crack are characterized as follows. As long as the crack does not change its length, the crack is called *stationary*. At a specific critical load or deformation, respectively, *crack initiation* takes place, i.e., the crack starts to propagate and becomes non-stationary.

One can distinguish different types of *crack propagation*. Crack growth is called *stable* if an increase of crack length requires an increase of external load. In contrast, crack growth is *unstable* if the crack, starting from a specific configuration, advances spontaneously without any increase of the external load. It should be noted here that stable or unstable crack growth is governed not solely by material properties. In fact, the geometry and the type of loading have a significant influence on the crack behavior.

Very slow crack propagation under constant loading in a creeping manner (e.g., at a velocity of 1 mm/s or less) is called *subcritical*. Under cyclic loading the crack can propagate in small "steps" (e.g., of about 10^{-6} mm per cycle). This type of crack propagation is called *fatigue crack growth*. If the crack propagates with a velocity which approaches the order of the speed of sound in the solid material (e.g., 600 m/s or more), the crack is called *fast*. If such a fast crack comes to rest, we call this *crack arrest*. As a further classification, we distinguish between *quasistatic* and *dynamic* crack propagation. While inertia forces play no role in the former they cannot be neglected in the latter.

3.2.2 Types of fracture

The fracture process is finished when crack growth comes to an end or, what occurs more often, a complete break-through of the body into two or more parts has taken place. According to typical phenomena, the entire event of *fracture* is classified by different types. *Ductile fracture* is characterized by large plastic deformations which occur before and (or) during the fracture process. Here, the inelastic deformations of uncracked metal specimen under uniaxial tension may reach more than 10%. In cracked bodies, these strains often are not only concentrated in the immediate vicinity of the crack tip or the fracture surface. The related microscopic failure mechanism in metals is plastic flow accompanied by void nucleation and coalescence.

A fracture event is called *brittle* if macroscopically only a small amount of inelastic deformations occur or if they vanish at all. In this case, plastic strains in uncracked specimen under tension immediately prior to fracture are less than 2...10%. Inelastic strains in cracked components are confined to the immediate vicinity of the crack tip or the fracture surface. Here, the microscopic failure mechanism in metals is either confined plastic flow combined with void growth or cleavage.

Fracture resulting from crack growth due to cyclic loading is called *fatigue fracture*. Fracture due to creep crack growth is known as *creep fracture*.

An additional distinguishing feature is the orientation of the fracture surface (cf. Section 2.3). Fracture is called *normal stress dominated* if the fracture surface is oriented perpendicular to the largest principal stress (tension). In contrast, fracture is *shear dominated* if the fracture surface coincides with a cross section of high shear stress. Both types can also occur in a mixed form. A typical example is the normal stress dominated fracture with *shear lips* at the specimen edges (Fig. 3.9).

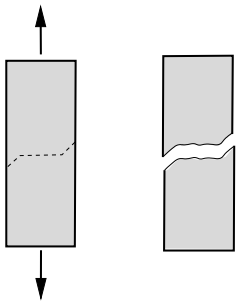

Fig. 3.9 Fracture with shear lips

The actual fracture behavior is highly dependent on various factors such as temperature, stress state, or loading rate. For instance, the behavior of many materials is brittle at sufficiently low temperatures and ductile above a *transition temperature*. Furthermore, depending on the stress state, plastic flow can be more or less constrained. Accordingly, fracture will tend more to a brittle or more to a ductile behavior. This also affects the orientation of the fracture surface. For instance, the

occurrence of the above-mentioned shear lips is a result of the stress state in the boundary area (close to plane stress) where plastic flow is less constrained.

A characteristic fracture quantity is the work done by the bonding forces during creation of a fracture surface. This applies especially when all processes of bond release related to fracture (e.g., void nucleation and growth with large micro-plastic deformations) are confined to the immediate vicinity of the macroscopic fracture surface. Due to microscopic irregularities, this macroscopic surface is smaller than the true fracture surface. Analogous to the surface energy, it is then reasonable to introduce an *effective fracture surface energy* Γ:

$$\Gamma = \gamma A \, . \tag{3.8}$$

Here, γ is the *fracture surface energy density* and A is the macroscopic fracture surface.

3.3 Further reading

Anderson, T.L., *Fracture Mechanics; Fundamentals and Application*. CRC Press, Boca Raton, 2004

Broberg, K.B., *Cracks and Fracture*. Academic Press, London, 1999

Cotterell, B. and Mai, Y.-W. *Fracture Mechanics of Cementitious Materials*. Blackie Academic & Professional, 1996

Gittus, J., *Creep, Viscoelasticity and Creep Fracture in Solids*. Applied Science Publishers, London, 1975

Hellan, K., *Introduction to Fracture Mechanics*. McGraw-Hill, New York, 1985

Herzberg, R.W., *Deformation and Fracture Mechanics of Engineering Materials*. John Wiley & Sons, New York, 1996

Janssen, M., Zuidema, J. and Wanhill, R.J.H., Fracture Mechanics. DUP Blue Print, Delft 2002

Knott, J.F., *Fundamentals of Fracture Mechanics*. Butterworth, London, 1973

Lawn, B., *Fracture of Brittle Solids*. Cambridge University Press, Cambridge, 1993

Liebowitz, H. (ed.), *Fracture – A Treatise*, Vol. 1. Academic Press, London, 1968

Riedel, H., *Fracture at High Temperature*. Springer, Berlin, 1987

Suresh, S., *Fatigue of Materials*. Cambridge University Press, Cambridge, 1998

Yang, W. and Lee, W.B., *Mesoplasticity and its Applications*. Springer, Berlin, 1993

Chapter 4
Linear fracture mechanics

4.1 General remarks

We now turn to the description of the crack behavior. From a macroscopic, continuum mechanical viewpoint, we consider a crack as a cut in a body. Its opposite boundaries are the *crack surfaces* which are also called *crack faces* or *crack flanks* (Fig. 4.1). In general they are traction-free. The crack ends at the *crack front* or *crack tip*.

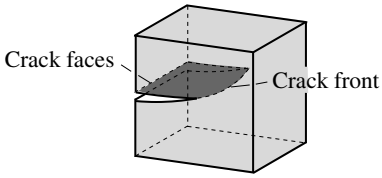

Fig. 4.1 Cracked body

Concerning the deformation of a crack, there exist three types of *crack opening* which are shown in Fig. 4.2. *Mode I* denotes a symmetric crack opening with respect to the x, z-plane. *Mode II* is characterized by an antisymmetric separation of the crack surfaces due to relative displacements in x-direction (normal to the crack front). Finally, *mode III* describes a separation due to relative displacements in z-direction (tangential to the crack front). The symmetries associated with the

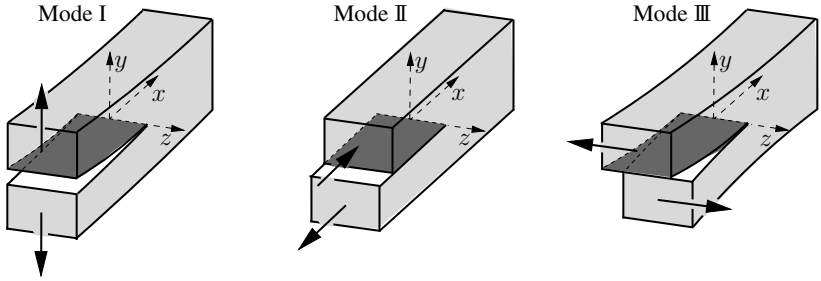

Fig. 4.2 Crack opening modes

D. Gross and T. Seelig, *Fracture Mechanics: With an Introduction to Micromechanics*, Mechanical Engineering Series, DOI 10.1007/978-3-642-19240-1_4,

different types of crack opening are only locally defined, i.e., for the region close to the crack tip. In special cases, however, they may hold for the entire body.

An important role for the continuum mechanical description is played by the size of the *process zone*. The latter denotes the region close to a crack front (crack tip) in which microscopically quite complex processes of bond breaking occur that generally cannot be described in terms of classical continuum mechanics. If continuum mechanics shall be applicable to the whole cracked body, it must be assumed that the extension of the process zone is negligibly small compared to all characteristic macroscopic dimensions of the body. Such a localization of the fracture process exists in many cases. For instance, this feature is typical for metals and for the majority of brittle materials. However, the process zone in concrete or in granular materials may have a considerable size and under some circumstances include the entire body.

In *linear fracture mechanics*, a cracked body is regarded as linear elastic in the whole region. Possible inelastic processes within or outside the process zone around the crack tip must be restricted to a small region which can be neglected from a macroscopic point of view. Accordingly, linear fracture mechanics is predominantly applicable for the description of brittle fracture (cf. Section 3.2.2).

Of fundamental importance is the *crack-tip field*, i.e., the stresses and strains close to a crack tip. Although this field, as already mentioned, does not directly describe the state within the process zone, it indirectly controls the processes taking place there. In what follows, the crack-tip field for the case of an isotropic, linearly elastic material under static loading will be investigated.

4.2 Crack-tip field

4.2.1 Two-dimensional crack-tip fields

We consider the two-dimensional problem of a body which contains a straight crack. Here, we focus only on the field within a small region of radius R around one of the crack tips (Fig. 4.3). For this purpose it is appropriate to introduce the depicted coordinate system with its origin at the crack tip.

Longitudinal shear, mode III

The simplest two-dimensional problem is the longitudinal shear stress state (anti-plane shear). In this case, the only non-vanishing displacement component w is perpendicular to the x, y-plane which leads to a mode-III crack opening. The corresponding crack-tip field can be determined using a complex function $\Omega(z)$ (cf. Section 1.5.2). As an appropriate function for the solution we choose

$$\Omega(z) = Az^{\lambda} \tag{4.1}$$

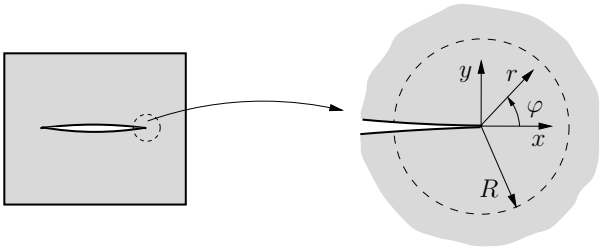

Fig. 4.3 Vicinity of the crack tip

where A is a free, in general complex constant. The likewise unknown exponent λ is assumed to be real. In order to render the displacements at the crack tip nonsingular, $\lambda > 0$ is assumed. As a consequence, the strain energy will also be finite. The special case $\lambda = 0$ will be excluded at this stage. According to (1.121), it corresponds to a stress-free rigid body displacement.

From (4.1), using (1.121) and $z = re^{\mathrm{i}\varphi}$, we get

$$2\mathrm{i}\tau_{yz} = \overline{\Omega'(z)} - \Omega'(z) = \overline{A}\lambda r^{\lambda-1} e^{-\mathrm{i}(\lambda-1)\varphi} - A\lambda r^{\lambda-1} e^{\mathrm{i}(\lambda-1)\varphi} \, .$$

The boundary conditions require that the crack faces ($\varphi = \pm\pi$) are traction-free, i.e., $\tau_{yz}(\pm\pi) = 0$. This leads to the homogeneous system of equations

$$\begin{aligned} \overline{A}e^{-\mathrm{i}\lambda\pi} - Ae^{\mathrm{i}\lambda\pi} &= 0 \, , \\ \overline{A}e^{\mathrm{i}\lambda\pi} - Ae^{-\mathrm{i}\lambda\pi} &= 0 \, . \end{aligned} \tag{4.2}$$

A non-trivial solution exists if the determinant of the system vanishes. Hence, the "eigenvalues" λ are determined as follows:

$$\sin 2\lambda\pi = 0 \quad \rightarrow \quad \lambda = n/2 \qquad n = 1, 2, 3, \ldots \, . \tag{4.3}$$

Substitution of this result into one of the equations (4.2) finally yields: $\overline{A} = (-1)^n A$.

To each λ of the infinite set of eigenvalues corresponds an eigenfunction of the type (4.1) which fulfills the boundary conditions. The eigenfunctions can be arbitrarily superimposed:

$$\Omega = A_1 z^{1/2} + A_2 z + A_3 z^{3/2} + \ldots \, . \tag{4.4}$$

Accordingly, the stresses $\tau_{\alpha z}$, $\alpha = x, y$ and the displacement w can be represented in the following form:

$$\begin{aligned} \tau_{\alpha z} &= r^{-1/2}\hat{\tau}_{\alpha z}^{(1)}(\varphi) + \hat{\tau}_{\alpha z}^{(2)}(\varphi) + r^{1/2}\hat{\tau}_{\alpha z}^{(3)}(\varphi) + \ldots \, , \\ w - w_0 &= r^{1/2}\hat{w}^{(1)}(\varphi) + r\hat{w}^{(2)}(\varphi) + r^{3/2}\hat{w}^{(3)}(\varphi) + \ldots \, . \end{aligned} \tag{4.5}$$

Here, $\hat{\tau}_{\alpha z}^{(1)}(\varphi)$, $\hat{w}^{(1)}(\varphi)$, ... are functions of the angle φ which are each determined up to a factor. A possible rigid body displacement is described by w_0.

If the crack tip is approached (i.e., $r \to 0$), the field can solely be described by the dominant first term in (4.4) or (4.5), respectively. It corresponds to the smallest eigenvalue $\lambda = 1/2$. The associated stresses and displacements are given by the expressions

$$\left\{ \begin{array}{c} \tau_{xz} \\ \tau_{yz} \end{array} \right\} = \frac{K_{III}}{\sqrt{2\pi r}} \left\{ \begin{array}{c} -\sin(\varphi/2) \\ \cos(\varphi/2) \end{array} \right\} , \qquad w = \frac{2K_{III}}{G} \sqrt{\frac{r}{2\pi}} \sin(\varphi/2) . \tag{4.6}$$

Thus, the stresses at the crack tip have a singularity of the type $r^{-1/2}$.

The singular crack-tip field is determined by means of (4.6) up to a factor K_{III}. This factor is called *stress intensity factor* or, shorter, *K-factor* where the subscript indicates the mode III crack opening. The stress intensity factor K_{III} can be regarded as a measure for the "strength" of the crack-tip field. The latter is fully characterized once the stress intensity factor is known. Vice versa, K_{III} can be determined from (4.6) if the stresses or displacements close to the crack tip are known. For example, it follows from (4.6) that

$$K_{III} = \lim_{r \to 0} \sqrt{2\pi r}\, \tau_{yz}(\varphi = 0) . \tag{4.7}$$

Like the stresses and displacements, the magnitude of the K-factor depends on the geometry of the body and its loading.

The second term in (4.5) corresponds to the eigenvalue $\lambda = 1$. It leads to the nonsingular stresses and displacements

$$\left\{ \begin{array}{c} \tau_{xz} \\ \tau_{yz} \end{array} \right\}^{(2)} = \left\{ \begin{array}{c} \tau_{\mathrm{T}} \\ 0 \end{array} \right\} , \qquad w^{(2)} = \frac{\tau_{\mathrm{T}}}{G}\, r \cos\varphi = \frac{\tau_{\mathrm{T}}}{G}\, x \tag{4.8}$$

where τ_{T} is a yet undetermined constant shear stress. This contribution to the complete field is of minor importance immediately at the crack tip but it becomes relevant at some distance from the tip.

Plane strain and plane stress, mode I and mode II

For plane strain and plane stress, the crack-tip field can be determined by using two complex functions $\Phi(z)$ and $\Psi(z)$ (cf. Section 1.5.2). The approach is analogous to that in the foregoing section for longitudinal shear. For the solution we use the functions

$$\Phi(z) = Az^{\lambda} , \qquad \Psi(z) = Bz^{\lambda} \tag{4.9}$$

where the exponent λ again is assumed to be real and positive. From (4.9) and according to (1.119) we obtain in a first step

$$\begin{aligned}\sigma_\varphi + \mathrm{i}\tau_{r\varphi} &= \Phi'(z) + \overline{\Phi'(z)} + z\Phi''(z) + \Psi'(z)z/\overline{z} \\ &= A\lambda r^{\lambda-1}e^{\mathrm{i}(\lambda-1)\varphi} + \overline{A}\lambda r^{\lambda-1}e^{-\mathrm{i}(\lambda-1)\varphi} \\ &\quad + A\lambda(\lambda-1)r^{\lambda-1}e^{\mathrm{i}(\lambda-1)\varphi} + B\lambda r^{\lambda-1}e^{\mathrm{i}(\lambda+1)\varphi}\,.\end{aligned} \tag{4.10}$$

Along the crack faces $\varphi = \pm\pi$, the boundary conditions $\sigma_\varphi + \mathrm{i}\tau_{r\varphi} = 0$ must be fulfilled. From them, taking into account $e^{-\mathrm{i}\pi} = e^{\mathrm{i}\pi} = -1$, the following homogeneous system of equations is obtained:

$$\begin{aligned} A\lambda e^{-\mathrm{i}\lambda\pi} &+\overline{A}e^{\mathrm{i}\lambda\pi} &+Be^{-\mathrm{i}\lambda\pi} & &= 0\,,\\ A\lambda e^{\mathrm{i}\lambda\pi} &+\overline{A}e^{-\mathrm{i}\lambda\pi} &+Be^{\mathrm{i}\lambda\pi} & &= 0\,,\\ Ae^{-\mathrm{i}\lambda\pi} &+\overline{A}\lambda e^{\mathrm{i}\lambda\pi} & &+\overline{B}e^{\mathrm{i}\lambda\pi} &= 0\,,\\ Ae^{\mathrm{i}\lambda\pi} &+\overline{A}\lambda e^{-\mathrm{i}\lambda\pi} & &+\overline{B}e^{-\mathrm{i}\lambda\pi} &= 0\,. \end{aligned} \tag{4.11}$$

Here, the last two equations are the complex conjugate of the first two equations. The condition that the system's determinant must be zero, leads to the same eigenvalues as for longitudinal shear:

$$\cos 4\lambda\pi = 1 \quad\rightarrow\quad \lambda = n/2 \qquad n = 1, 2, 3, \ldots\,. \tag{4.12}$$

Substitution into one of the equations (4.11) yields $B = -nA/2 - (-1)^n\overline{A}$.

The stresses σ_{ij} and displacements u_i, where $i, j = x, y$, can be represented as the sum of the eigenfunctions which correspond to the above eigenvalues:

$$\begin{aligned}\sigma_{ij} &= r^{-1/2}\hat{\sigma}_{ij}^{(1)}(\varphi) + \;\hat{\sigma}_{ij}^{(2)}(\varphi) + r^{1/2}\hat{\sigma}_{ij}^{(3)}(\varphi) + \ldots\,,\\ u_i - u_{i0} &= r^{1/2}\hat{u}_i^{(1)}(\varphi) \;\; + r\hat{u}_i^{(2)}(\varphi) + r^{3/2}\hat{u}_i^{(3)}(\varphi) + \ldots\,.\end{aligned} \tag{4.13}$$

Here, u_{i0} describes a possible rigid body displacement. For $r \to 0$, the first term dominates which is singular in the stresses. It is appropriate to split the associated field into a symmetric and an antisymmetric part with respect to the x-axis. The symmetric singular field corresponds to a mode-I crack opening while the antisymmetric field leads to a mode-II crack opening. Accordingly, the *crack-tip field* (near field) can be written as follows:

Mode I:

$$\begin{aligned}\begin{Bmatrix}\sigma_x\\ \sigma_y\\ \tau_{xy}\end{Bmatrix} &= \frac{K_I}{\sqrt{2\pi r}}\cos(\varphi/2)\begin{Bmatrix}1 - \sin(\varphi/2)\sin(3\varphi/2)\\ 1 + \sin(\varphi/2)\sin(3\varphi/2)\\ \sin(\varphi/2)\cos(3\varphi/2)\end{Bmatrix}\,,\\ \begin{Bmatrix}u\\ v\end{Bmatrix} &= \frac{K_I}{2G}\sqrt{\frac{r}{2\pi}}\,(\kappa - \cos\varphi)\begin{Bmatrix}\cos(\varphi/2)\\ \sin(\varphi/2)\end{Bmatrix}\,,\end{aligned} \tag{4.14}$$

Mode II:

$$\begin{Bmatrix}\sigma_x\\ \sigma_y\\ \tau_{xy}\end{Bmatrix}=\frac{K_{II}}{\sqrt{2\pi r}}\begin{Bmatrix}-\sin(\varphi/2)[2+\cos(\varphi/2)\cos(3\varphi/2)]\\ \sin(\varphi/2)\cos(\varphi/2)\cos(3\varphi/2)\\ \cos(\varphi/2)[1-\sin(\varphi/2)\sin(3\varphi/2)]\end{Bmatrix},$$
$$\begin{Bmatrix}u\\ v\end{Bmatrix}=\frac{K_{II}}{2G}\sqrt{\frac{r}{2\pi}}\begin{Bmatrix}\sin(\varphi/2)[\kappa+2+\cos\varphi]\\ \cos(\varphi/2)[\kappa-2+\cos\varphi]\end{Bmatrix}, \tag{4.15}$$

where

$$\begin{array}{lll}\text{plane strain:} & \kappa=3-4\nu\,, & \sigma_z=\nu(\sigma_x+\sigma_y)\,,\\ \text{plane stress:} & \kappa=(3-\nu)/(1+\nu)\,, & \sigma_z=0\,.\end{array} \tag{4.16}$$

According to these representations, the distribution of stresses and deformations close to the crack tip is uniquely determined. It will be exemplarily discussed in Section 4.2.2 for mode I. The "strength" (amplitude) of the crack-tip field is characterized by the *stress-intensity factors* K_I and K_{II}. They depend on the geometry of the body (including the crack) and its loading. The K-factors can be determined from the stresses and deformations provided these are known. For example, the following relations result from (4.14) and (4.15):

$$K_I=\lim_{r\to 0}\sqrt{2\pi r}\;\sigma_y(\varphi=0)\,,\qquad K_{II}=\lim_{r\to 0}\sqrt{2\pi r}\;\tau_{xy}(\varphi=0)\,. \tag{4.17}$$

For larger distances r from the crack tip the second term in (4.13) has to be taken into account which belongs to the eigenvalue $\lambda=1$. The corresponding nonsingular stresses and displacements are given by

$$\begin{Bmatrix}\sigma_x\\ \sigma_y\\ \tau_{xy}\end{Bmatrix}^{(2)}=\begin{Bmatrix}\sigma_{\mathrm{T}}\\ 0\\ 0\end{Bmatrix},\qquad \begin{Bmatrix}u\\ v\end{Bmatrix}^{(2)}=\frac{\sigma_{\mathrm{T}}}{8G}\begin{Bmatrix}(\kappa+1)\,x\\ (\kappa-3)\,y\end{Bmatrix}, \tag{4.18}$$

where σ_{T} is a constant stress which commonly is called T-stress (transversal stress). It can be seen that this part of the field is symmetric with respect to the x-axis and contributes solely to the mode-I crack opening. The T-stress becomes important especially when K_I is zero or sufficiently small. It then represents the dominant part of the mode-I field.

The field in the vicinity of the tip of a *straight* crack with *traction-free* crack faces is, according to (4.5) and (4.13), composed as a sum of the eigenfunctions. Among them, the first term (i.e., the crack-tip field) dominates if the crack tip is approached ($r\to 0$). But it should be emphasized that for larger distances r, the higher-order terms can not be neglected. Furthermore, it can be shown that the crack-tip field has exactly the same form as (4.6) or (4.14) and (4.15), respectively, if the crack faces

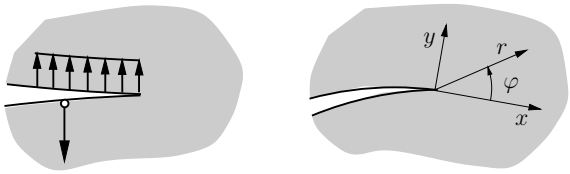

a) b)

Fig. 4.4 a) Loaded crack faces, b) curved crack

are loaded (Fig. 4.4a) or if volume forces are present. This also applies to a crack which is curved in the region close to the crack tip (Fig. 4.4b).

The singularity of the order $r^{-1/2}$ is typical for a crack tip. Singular stresses of eventually a different type of singularity can also appear in many other problems of linear elasticity. As an example, a "crack-similar" V-notch is considered whose edges form an angle 2α (Fig. 4.5a). The functions (4.9) in conjunction with (4.10) and the boundary conditions $(\sigma_\varphi + \mathrm{i}\tau_{r\varphi})_{\varphi=\pm\alpha} = 0$ again lead to a homogeneous system of equations. It differs from (4.11) only in that now the angle α appears instead of π. Setting the determinant of the system to zero, we obtain the equation for the eigenvalues

$$\sin 2\lambda\alpha = \pm\lambda \sin 2\alpha \; . \tag{4.19}$$

The smallest eigenvalue λ_0 resulting from (4.19) is shown in Fig. 4.5b (higher eigenvalues and eigenfunctions shall not be considered). For $2\alpha \le \pi$ we get $\lambda_0 = 1$. In this case no stress singularity follows from (4.9). For notch angles $\pi < 2\alpha < 2\pi$, the eigenvalue λ_0 lies in the range $1/2 < \lambda < 1$ and the already known result $\lambda_0 = 1/2$ is obtained in the limit case $2\alpha = 2\pi$, i.e., for a crack. The corresponding stress singularities are of the type $\sigma_{ij} \sim r^{\lambda-1}$ which can be seen, e.g., from (4.9). For instance, in case of a mode-I loading the stress σ_y ahead of the notch tip can be represented as

$$\sigma_y = \frac{K_I^*}{\sqrt{2\pi}}\, x^{\lambda-1} \qquad (y = 0,\ x > 0) \tag{4.20}$$

where K_I^* is a generalized mode I stress intensity factor.

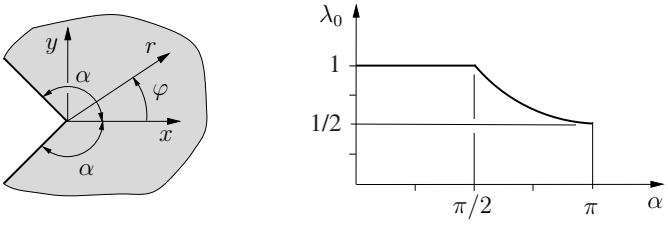

a) b)

Fig. 4.5 a) V-notch, b) smallest eigenvalue

At blunt notches with a finite notch radius, also very high stresses can occur. However, in contrast to a crack or a sharp V-notch, the stresses at the notch root then remain finite and do not tend to infinity (see Section 4.4.5).

4.2.2 Mode-I crack-tip field

The mode-I crack-tip field can be described by the relations (4.14). Thus, the stresses σ_{ij} and, according to Hooke's law, the strains ε_{ij} have singularities of the type $r^{-1/2}$, i.e., they increase infinitely as $r \to 0$. As an example, the distribution of σ_y ahead of the crack tip ($\varphi = 0$) is schematically depicted in Fig. 4.6a. In contrast, the displacements show a behavior of the type $r^{1/2}$. For a positive K_I this leads to a parabola-shaped crack opening along the crack faces $\varphi = \pm\pi$ (Fig. 4.6a):

$$v^{\pm} = v(\pm\pi) = \pm\frac{K_I}{2G}\sqrt{\frac{r}{2\pi}}\,(\kappa+1)\,. \tag{4.21}$$

If K_I is negative, the crack faces formally "overlap" or penetrate each other, respectively, which is physically impossible. Actually, the crack faces are in contact during *crack closure* and contact forces act along the contact zone.

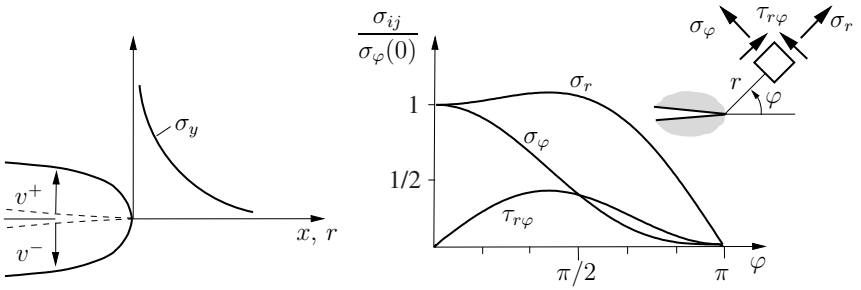

Fig. 4.6 Mode-I crack-tip field

It is sometimes appropriate to describe the crack-tip field not by its cartesian components (4.14) but by equivalent quantities. For example, the stress components in polar coordinates can be found by applying the transformation (1.113):

$$\begin{Bmatrix}\sigma_r\\ \sigma_\varphi\\ \tau_{r\varphi}\end{Bmatrix} = \frac{K_I}{4\sqrt{2\pi r}}\begin{Bmatrix}5\cos(\varphi/2)-\cos(3\varphi/2)\\ 3\cos(\varphi/2)+\cos(3\varphi/2)\\ \sin(\varphi/2)+\sin(3\varphi/2)\end{Bmatrix}\,. \tag{4.22}$$

Their dependence on the angle φ is shown in Fig. 4.6b.

The principal stresses in the x, y-plane and the principal directions, here characterized by the angle α, can be determined from (1.114) as follows

$$\begin{Bmatrix}\sigma_1\\ \sigma_2\end{Bmatrix} = \frac{K_I}{\sqrt{2\pi r}}\cos(\varphi/2)\begin{Bmatrix}1+\sin(\varphi/2)\\ 1-\sin(\varphi/2)\end{Bmatrix}, \qquad \alpha = \pm\frac{\pi}{4}+\frac{3}{4}\varphi\,. \tag{4.23}$$

The third principal stress is given by σ_z. According to (4.16), it is different for plane strain and plane stress:

$$\sigma_3 = 2\nu\frac{K_I}{\sqrt{2\pi r}}\cos(\varphi/2) \quad \text{(plane strain)}\,, \qquad \sigma_3 = 0 \quad \text{(plane stress)}\,. \tag{4.24}$$

Thus, σ_1 is the largest principal stress, the smallest one can be σ_3 or σ_2, depending on the stress state and the angle φ.

From the principal stresses the maximum shear stress can directly be determined. Using $\tau_{\max} = (\sigma_{\max} - \sigma_{\min})/2$ we obtain

$$\begin{aligned}&\text{plane stress: } \tau_{\max} = \sigma_1/2\\ &\text{plane strain: } \tau_{\max} = \begin{cases}(\sigma_1-\sigma_2)/2 & \text{for} \quad \sin(\varphi/2) \geq 1-2\nu\,,\\ (\sigma_1-\sigma_3)/2 & \text{for} \quad \sin(\varphi/2) \leq 1-2\nu\,.\end{cases}\end{aligned} \tag{4.25}$$

4.2.3 Three-dimensional crack-tip field

In various cases the three-dimensional character of a crack problem must be taken into account. This is generally the case if the crack front is curved. Examples of such problems are the penny-shaped internal crack or a half-elliptical surface crack (Fig. 4.7a). But also the problem of a crack with the straight crack front in a flat plate of finite thickness is, strictly speaking, a three-dimensional problem. Here, the stress state varies near the crack front along the thickness of the plate.

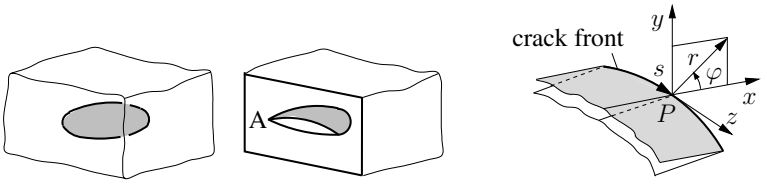

Fig. 4.7 Three-dimensional crack field

It can be shown that the crack-tip field in a three-dimensional case *locally* is of the same type as in a two-dimensional problem. In general, it is composed of the

fields corresponding to the three crack opening modes. Regarding the mode-I and mode-II deformations, the plane strain case has to be considered. If an arbitrary point P on the crack front is chosen as origin of a local coordinate system (Fig. 4.7b), the stresses for $r \to 0$ are given by

$$\sigma_{ij} = \frac{1}{\sqrt{2\pi r}}[K_I \tilde{\sigma}_{ij}^{I}(\varphi) + K_{II} \tilde{\sigma}_{ij}^{II}(\varphi) + K_{III} \tilde{\sigma}_{ij}^{III}(\varphi)] \tag{4.26}$$

where $\tilde{\sigma}_{ij}^{I}(\varphi), \ldots$ are known functions of the angle φ which are determined by (4.14), (4.15), and (4.6). Thus, the field close to the crack front is fully characterized by the stress-intensity factors K_I, K_{II}, and K_{III}. The latter can vary with the arc length s along the crack front, i.e., $K_I = K_I(s), \ldots$.

The representation (4.26) is valid along the crack front except some special (singular) points. Such a singular point is, for example, a kink of the crack front or a point where the crack front intersects a free surface (point A in Fig. 4.7a). In these points stress singularities occur which are *not* of the type $r^{-1/2}$.

4.3 K-concept

In the following we restrict our attention to the case of a pure mode-I crack opening which is the most important case for practical applications. As already mentioned, the corresponding crack-tip field is fully characterized by the stress intensity factor K_I. This K_I-determined field dominates in an outwards limited region around the crack tip. It is schematically characterized in Fig. 4.8 by a circle of radius R. Outside R the higher-order terms can not be neglected.

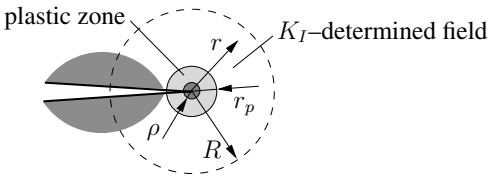

Fig. 4.8 K-concept

The validity of the K_I-determined field is limited also inwards because linear elasticity does not provide a realistic description of the actual stress and deformation state below a certain limit of r. One reason for this is that no real material can sustain infinite stresses. In addition, the infinitely high strains appearing there contradict the assumptions of linear elasticity (small deformations). For most real materials, plastic flow or, more generally, inelastic deformations appear at the crack tip on account of the strongly increasing stresses. In addition, there is always a small but

finite process zone at the crack tip where debonding takes place. Its characteristic dimension is denoted by ρ in Fig. 4.8, that of the *plastic zone* is described by r_p.

We now suppose that the K_I-dominated region is large compared to the enclosed domain which is not described by the crack-tip field ($\rho,\ r_p \ll R$) and thus may be regarded as a 'black box'. Under these circumstances it can be assumed that the processes in this 'black box' are controlled by the surrounding K_I-determined field. This hypothesis is the basis of the *K-concept*: the state within the process zone or at the crack tip, respectively, can indirectly be characterized by K_I. The stress-intensity factor, similar to the stresses themselves, is considered as a state variable or a 'loading parameter' of the region close to the crack tip.

By introducing the stress intensity factor we now are able to formulate a fracture criterion. Accordingly, crack propagation (fracture) starts when the stress intensity factor K_I reaches a material-specific critical value K_{Ic}:

$$\boxed{K_I = K_{Ic}}\ . \tag{4.27}$$

Under these circumstances, a critical state exists in the process zone which leads to material separation. We have tacitly assumed here that the state in the process zone is determined by the actual value of K_I and does not depend on the loading history of the crack tip.

The quantity K_{Ic} on the right-hand side of (4.27) is called *fracture toughness*. It is a material parameter which is determined by appropriate experiments (cf. Section 4.5). From (4.22) it can be seen that the K-factor has the dimension [stress]·[length]$^{1/2}$. It is specified as a multiple of the unit Nmm$^{-3/2}$ or MPa mm$^{1/2}$, respectively. The use of stress-intensity factors in a fracture criterion dates back to G.R. IRWIN (1951).

In the fracture criterion (4.27) for pure mode I, the crack-tip loading is characterized by the single parameter K_I. Corresponding one-parameter fracture criteria can also be formulated for pure mode II or pure mode III, respectively:

$$K_{II} = K_{IIc} \quad (\text{mode II})\ , \qquad K_{III} = K_{IIIc} \quad (\text{mode III})\ . \tag{4.28}$$

The case of a mixed crack-tip loading by K_I, K_{II}, and K_{III} is more involved. Then a generalized fracture criterion

$$f(K_I, K_{II}, K_{III}) = 0 \tag{4.29}$$

must be formulated (see Section 4.9).

4.4 K-factors

There exist many methods to determine K-factors. Since these are directly tied to the field quantities, generally all techniques of linear elasticity applicable for the determination of stresses and deformations can be utilized. But sometimes it is neces-

sary to tailor them according to the specific characteristics of crack problems (stress singularities).

Analytical methods are mainly used when closed form solutions are of interest or needed. They can be obtained only for relatively simple boundary value problems. The analysis of more complex problems usually relies on *numerical methods*. Here, in most cases the finite element method or the boundary element method are applied, but also finite difference method or other schemes are in use. Moreover, also *experimental methods* such as strain measurements in the crack-tip region or photoelasticity can be applied.

A discussion of all methods would go beyond the scope of this book. In this respect, the reader is referred to the special literature. In what follows, only a few analytical solutions for selected crack configurations and loadings are discussed. Subsequently, we will shortly introduce an integral equation formulation of crack problems, the method of weight functions, and finally a procedure for the investigation of interacting cracks.

4.4.1 Examples

As the simplest example, we first consider a straight crack Γ of length $2a$ in an infinite plate under uniaxial remote stress σ (Fig. 4.9a). It is convenient for this and many other problems to represent the solution as a superposition of two partial solutions. Partial problem (1) considers the elastic plate *without* a crack under the prescribed load σ. Here, along the line Γ the stress $\sigma_y^{(1)}|_\Gamma = \sigma$ appears. Partial problem

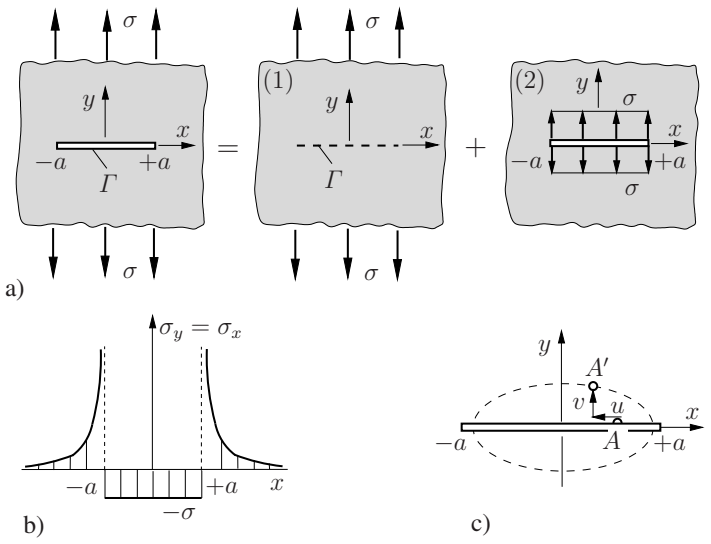

Fig. 4.9 Single crack under remote stress σ

(2) is concerned with the elastic plate, now containing a crack which is loaded along the crack faces by exactly the same stress but with the opposite sign: $\sigma_y^{(2)}|_\Gamma = -\sigma$. The boundary condition of the original problem (i.e., traction-free crack faces) is fulfilled by superposition of the two partial solutions: $\sigma_y|_\Gamma = \sigma_y^{(1)}|_\Gamma + \sigma_y^{(2)}|_\Gamma = 0$. In partial problem (1) there is no crack and since no stress singularity appears, no stress intensity factor is present. As a consequence, the K-factor of the original problem is given by that of the partial problem (2).

Using the complex method, the solutions of the partial problems and the original problem can be represented as follows:

$$\begin{aligned} &\Phi = \Phi^{(1)} + \Phi^{(2)} \ , \ \Phi^{(1)}(z) = \tfrac{1}{4}\sigma z \ , \ \Phi^{(2)}(z) = \tfrac{1}{2}\sigma[\sqrt{z^2-a^2} - z] \ , \\ &\Psi = \Psi^{(1)} + \Psi^{(2)} \ , \ \Psi^{(1)}(z) = \tfrac{1}{2}\sigma z \ , \ \Psi^{(2)}(z) = -\tfrac{1}{2}\sigma a^2/\sqrt{z^2-a^2} \ . \end{aligned} \tag{4.30}$$

For the partial problem (2) we get for the stresses along the x-axis (Fig. 4.9b)

$$\tau_{xy}^{(2)} = 0 \ , \qquad \sigma_y^{(2)} = \sigma_x^{(2)} = \sigma \begin{cases} -1 & |x| < a \\ \dfrac{x}{\sqrt{x^2-a^2}} - 1 & |x| > a \ . \end{cases} \tag{4.31}$$

The displacements of the upper $(+)$ and the lower $(-)$ crack surfaces ($|x| \le a$) are given by (Fig. 4.9c)

$$4Gu^{\pm} = -(1+\kappa)\sigma x \ , \qquad 4Gv^{\pm} = \pm(1+\kappa)\sigma\sqrt{a^2-x^2} \ . \tag{4.32}$$

The stress-intensity factor may be determined directly from the complex potential Φ. To show this we consider a crack tip which is located at an arbitrary point z_0. From Kolosov's formulas in conjunction with (4.14), (4.15) we get for $r \to 0$ or $z \to z_0$, respectively,

$$\begin{aligned} 2\Phi'(z) + 2\overline{\Phi'(z)} &= \sigma_x + \sigma_y \\ &= 2(2\pi r)^{-1/2}[K_I \cos(\varphi/2) - K_{II} \sin(\varphi/2)] \\ &= (2\pi r)^{-1/2}[(K_I - \mathrm{i}K_{II})e^{-\mathrm{i}\varphi/2} + \overline{(K_I - \mathrm{i}K_{II})e^{-\mathrm{i}\varphi/2}}] \ . \end{aligned}$$

This leads with $re^{\mathrm{i}\varphi} = z - z_0$ to the representation

$$2\Phi'(z) = (K_I - \mathrm{i}K_{II})[2\pi(z-z_0)]^{-1/2} \qquad (z \to z_0)$$

and finally to

$$K_I - \mathrm{i}K_{II} = 2\sqrt{2\pi} \lim_{z \to z_0} \sqrt{z - z_0}\, \Phi'(z) \ . \tag{4.33}$$

For our specific example, due to the symmetry, only a mode-I loading appears ($K_{II} = 0$) which is equal at both crack tips. Inserting (4.30) into (4.33) we get the stress intensity factor

$$K_I = \sigma\sqrt{\pi a} \ . \tag{4.34}$$

In the next example, the same crack now will be loaded by a pair of opposite single forces at the crack faces as shown in Fig. 4.10a. If only P ($Q = 0$) acts, the complex potentials are

$$\Phi'(z) = \frac{P}{2\pi(z-b)}\sqrt{\frac{a^2-b^2}{z^2-a^2}}\,, \qquad \Psi'(z) = -z\Phi''(z)\,. \tag{4.35}$$

They fulfill all boundary conditions. The corresponding K_I-factors (K_{II} is zero on account of the symmetry) at the right ($+$) and the left ($-$) crack tip are obtained from (4.33) as

$$K_I^{\pm} = \frac{P}{\sqrt{\pi a}}\sqrt{\frac{a \pm b}{a \mp b}}\,. \tag{4.36}$$

Analogous, for a crack face loading solely by Q (pure mode II), we obtain

$$K_I^{\pm} = 0\,, \qquad K_{II}^{\pm} = \frac{Q}{\sqrt{\pi a}}\sqrt{\frac{a \pm b}{a \mp b}}\,. \tag{4.37}$$

The solutions (4.36) and (4.37) can be used as *fundamental solutions* from which further solutions can be constructed. For instance, for a crack loading as depicted in Fig. 4.10b it follows by superposition

$$K_I = \frac{P}{\sqrt{\pi a}}\left[\sqrt{\frac{a+b}{a-b}} + \sqrt{\frac{a-b}{a+b}}\right] = \frac{P}{\sqrt{\pi a}}\frac{2a}{\sqrt{a^2-b^2}}\,. \tag{4.38}$$

Using this result, we get for the loading according to Fig. 4.10c

$$K_I = 2\sigma\sqrt{\frac{a}{\pi}}\int_c^a \frac{\mathrm{d}x}{\sqrt{a^2-x^2}} = 2\sigma\sqrt{\frac{a}{\pi}}\left[\frac{\pi}{2} - \arcsin\frac{c}{a}\right]\,. \tag{4.39}$$

For the special case $c = 0$ this leads to the already known result (4.34). In a similar way, using (4.36), the solution for a crack under an arbitrary load $p(x)$, see Fig. 4.10d, is obtained:

$$K_I^{\pm} = \frac{1}{\sqrt{\pi a}}\int_{-a}^{+a} p(x)\sqrt{\frac{a \pm x}{a \mp x}}\,\mathrm{d}x\,. \tag{4.40}$$

In the same manner, shear loaded cracks can be treated. For example, using (4.37) we obtain for a crack under a pure shear load (mode II) as depicted in Fig. 4.10e

$$K_{II} = \tau\sqrt{\pi a}\,. \tag{4.41}$$

The K_{II}-factors here and for the case in Fig. 4.10f are the same.

Figure 4.11a shows a periodic configuration of collinear cracks of equal length $2a$ in an infinite domain under remote tension σ. The solution for this case in terms

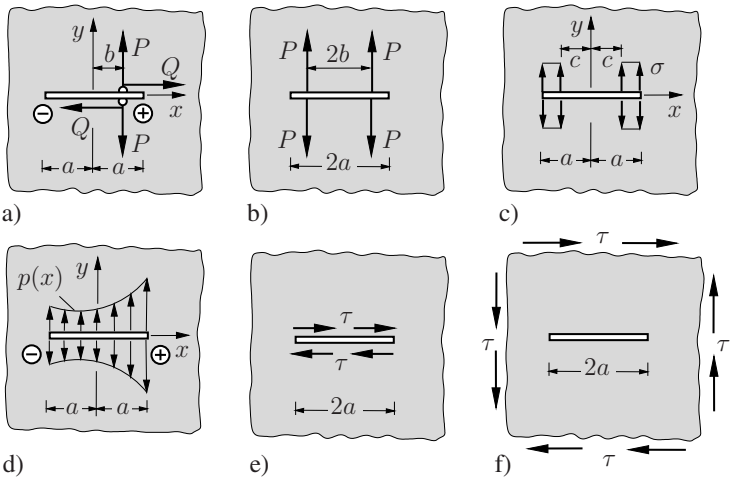

Fig. 4.10 Crack under different types of loading

of complex potential is given by

$$\Phi'(z) = \frac{\sigma}{2} \frac{1}{\sqrt{1 - \left[\dfrac{\sin(\pi a/2b)}{\sin(\pi z/2b)}\right]^2}} , \qquad \Psi'(z) = -z\Phi''(z) . \tag{4.42}$$

From Φ' in conjunction with (4.33) the stress intensity factor K_I is determined as

$$K_I = \sigma\sqrt{\pi a}\,\sqrt{\frac{2b}{\pi a}\tan\frac{\pi a}{2b}} . \tag{4.43}$$

Accordingly, K_I strongly increases if the crack tips approach each other. The reason for this behavior is the interaction of the cracks (cf. Section 4.4.4). If the distance between the crack tips gets very small ($a \to b$), equation (4.43) with the notation

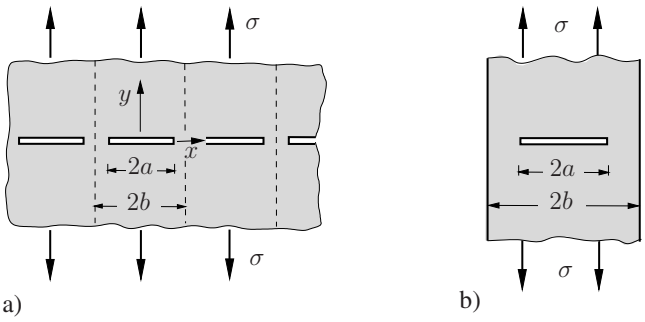

Fig. 4.11 a) Collinear cracks, b) center crack in a strip

Table 4.1 K-factors

1	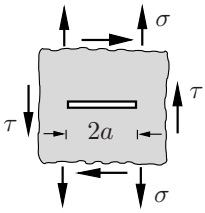	$\left\{ \begin{matrix} K_I \\ K_{II} \end{matrix} \right\} = \left\{ \begin{matrix} \sigma \\ \tau \end{matrix} \right\} \sqrt{\pi a}$
2	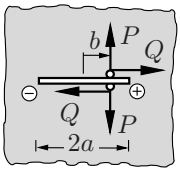	$\left\{ \begin{matrix} K_I^{\pm} \\ K_{II}^{\pm} \end{matrix} \right\} = \left\{ \begin{matrix} P \\ Q \end{matrix} \right\} \frac{1}{\sqrt{\pi a}} \sqrt{\frac{a \pm b}{a \mp b}}$
3	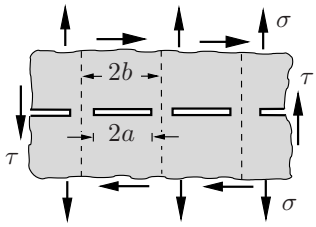	$\left\{ \begin{matrix} K_I \\ K_{II} \end{matrix} \right\} = \left\{ \begin{matrix} \sigma \\ \tau \end{matrix} \right\} \sqrt{2b \tan \frac{\pi a}{2b}}$
4	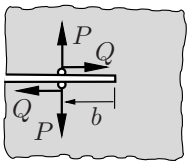	$\left\{ \begin{matrix} K_I \\ K_{II} \end{matrix} \right\} = \left\{ \begin{matrix} P \\ Q \end{matrix} \right\} \frac{2}{\sqrt{2\pi b}}$
5	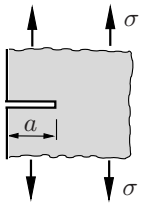	$K_I = 1.1215\, \sigma \sqrt{\pi a}$
6	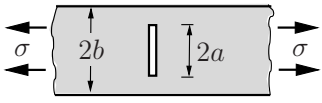	$K_I = \sigma \sqrt{\pi a}\, F_I(a/b)$ $F_I = \dfrac{1 - 0.025(a/b)^2 + 0.06(a/b)^4}{\sqrt{\cos\left(\pi a/2b\right)}}$

Table 4.1 K-factors (continued)

7	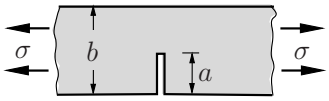	$K_I = \sigma\sqrt{\pi a}\,\sqrt{\frac{2b}{\pi a}\tan\frac{\pi a}{2b}}\,G_I(a/b)$ $G_I = \frac{0.752+2.02\frac{a}{b}+0.37(1-\sin\frac{\pi a}{2b})^3}{\cos\frac{\pi a}{2b}}$
8	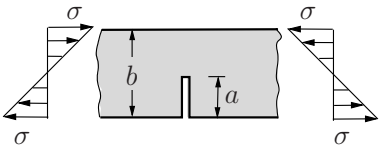	$K_I = \sigma\sqrt{\pi a}\,\sqrt{\frac{2b}{\pi a}\tan\frac{\pi a}{2b}}\,G_I(a/b)$ $G_I = \frac{0.923+0.199(1-\sin\frac{\pi a}{2b})^4}{\cos\frac{\pi a}{2b}}$
9	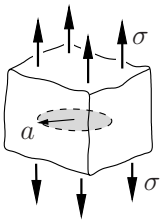	$K_I = \frac{2}{\pi}\sigma\sqrt{\pi a}$
10	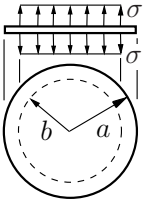	$K_I = \frac{2}{\pi}\sigma\sqrt{\pi a}\,\left[1-\sqrt{1-(b/a)^2}\,\right]$
11	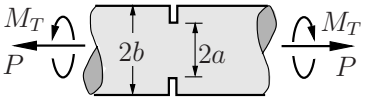	$K_I = \frac{P}{\pi a^2}\sqrt{\pi a}\sqrt{1-a/b}\,G_I(a/b)$ $K_{III} = \frac{2M_T}{\pi a^3}\sqrt{\pi a}\sqrt{1-a/b}\,G_{III}(a/b)$ $G_I = \frac{1}{2}(1+\frac{\varepsilon}{2}+\frac{3}{8}\varepsilon^2-0.363\varepsilon^3+0.731\varepsilon^4)$ $G_{III} = \frac{3}{8}(1+\frac{\varepsilon}{2}+\frac{3}{8}\varepsilon^2+\frac{5}{16}\varepsilon^3+\frac{35}{128}\varepsilon^4$ $+0.208\varepsilon^5)\,, \quad \varepsilon = a/b$
12	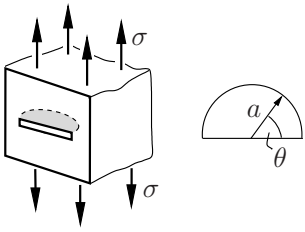	$K_I(\theta) = \sigma\sqrt{\pi a}\,F_I(\theta)$ $F_I = \frac{2}{\pi}(1.211-0.186\sqrt{\sin\theta}\,)$ $10^\circ < \theta < 170^\circ$

$c = b - a$ leads to

$$K_I = \sigma\sqrt{\frac{4b}{\pi}}\sqrt{\frac{b}{c}} \qquad \text{for} \qquad c \ll b\,. \tag{4.44}$$

The result (4.43) can also be used as an approximation for the configuration in Fig. 4.11b as long as the boundaries are sufficiently far away from the crack tips.

In Table 4.1, the stress intensity factors for various configurations are shown. Solutions for many other cases can be found in the relevant handbooks of stress-intensity factors listed at the end of this chapter.

4.4.2 Integral equation formulation

A possible starting point for the solution of crack problems is their formulation through integral equations. Of the various existing and different formulations only one shall be discussed here. Its basic idea is the representation of a crack by a continuous distribution of dislocations.

As a preparation of the formulation, we first consider the displacements and stresses obtained from the complex potentials

$$\Phi(z) = A \ln z\,, \qquad \Psi(z) = \overline{A} \ln z \tag{4.45}$$

where A here is specifically replaced by the real parameter $A = -Gb_y/\pi(\kappa+1)$:

$$\begin{Bmatrix} u \\ v \end{Bmatrix} = \frac{-b_y}{2\pi(\kappa+1)} \begin{Bmatrix} (\kappa-1)\ln r - \cos 2\varphi \\ (\kappa+1)\,\varphi - \sin 2\varphi \end{Bmatrix}\,,$$

$$\begin{Bmatrix} \sigma_x \\ \sigma_y \\ \tau_{xy} \end{Bmatrix} = \frac{-b_y G}{\pi(\kappa+1)\,r} \begin{Bmatrix} \cos\varphi + \cos 3\varphi \\ 3\cos\varphi - \cos 3\varphi \\ -\sin\varphi + \sin 3\varphi \end{Bmatrix}\,. \tag{4.46}$$

While the displacement u does not experience any change along a full circle enclosing the origin from $\varphi = 0$ to $\varphi = 2\pi$, the displacement v exhibits a *displace-*

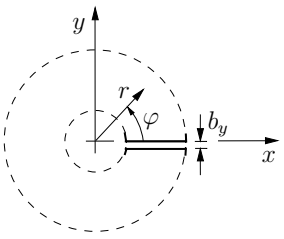

Fig. 4.12 Displacement jump due to an edge dislocation

ment jump (discontinuity) of the magnitude $v(0) - v(2\pi) = v^+ - v^- = b_y$. Thus, the potentials (4.45) describe an *edge dislocation* with a displacement jump in y-direction (Fig. 4.12, cf. Section 3.1.2). This dislocation is accompanied with stresses $\sigma_y = \sigma_x = -2Gb_y/\pi(\kappa+1)x$ and $\tau_{xy} = 0$ acting along the x-axis. If a general displacement jump b_y in y-direction and b_x in x-direction shall be described, the constant A in (4.45) must be replaced by $A = G(b_y - ib_x)/\pi(\kappa+1)$.

As a specific problem, we again consider in the following the already investigated crack under constant crack-face loading σ (pressure) (Fig. 4.13a). The crack now is represented as a continuous distribution of dislocations which are located in the interval $-a \le t \le +a$ on the x-axis (Fig. 4.13b). After renaming $b_y \to \mathrm{d}b_y = \mu \mathrm{d}t$, $x \to x - t$, $z \to z - t$, we obtain from (4.45) and (4.46) for the stress σ_y along the x-axis and for the potential Φ' the representations

$$\sigma_y(x,0) = -\frac{2G}{\pi(\kappa+1)} \int_{-a}^{+a} \frac{\mu(t)\mathrm{d}t}{x-t} \,, \tag{4.47}$$

$$\Phi'(z) = -\frac{G}{\pi(\kappa+1)} \int_{-a}^{+a} \frac{\mu(t)\mathrm{d}t}{z-t} \,. \tag{4.48}$$

In our case, the left-hand side of (4.47), i.e., the stress σ_y along the crack, is known: $\sigma_y = -\sigma$. Accordingly, (4.47) is a singular integral equation for the unknown distribution μ. Its solution is given by

$$\mu(x) = \frac{\sigma(\kappa+1)}{2G} \frac{x}{\sqrt{a^2 - x^2}} \,. \tag{4.49}$$

Knowing $\mu(x)$ the problem is practically solved because the potentials Φ and Ψ can be found from $\mu(x)$ by integration. For example, from (4.48) we obtain

$$\Phi'(z) = -\frac{\sigma}{2\pi} \int_{-a}^{+a} \frac{x\mathrm{d}x}{(z-x)\sqrt{a^2-x^2}} = \frac{\sigma}{2} \left[\frac{z}{\sqrt{z^2-a^2}} - 1 \right] \,, \tag{4.50}$$

from which the stress intensity factor can be determined.

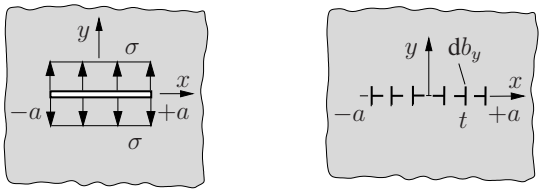

a) b)

Fig. 4.13 Crack represented as distribution of dislocations

If only the stress intensity factor is of interest, this quantity can directly be determined from μ. Along the crack, $\mu = \mathrm{d}b_y/\mathrm{d}x = \mathrm{d}(v^+ - v^-)/\mathrm{d}x$ is valid. Combining this with the crack-tip field formulas (4.14), the following relation for the right crack tip yields:

$$K_I = \lim_{x \to a} \frac{2G}{\kappa + 1} \sqrt{2\pi} \sqrt{a - x}\, \mu(x) \; . \tag{4.51}$$

When introducing the distribution (4.49), we get the already known result $K_I = \sigma\sqrt{\pi a}$.

The integral equation formulation is applicable not only for straight cracks. It can easily be extended to curved cracks, bounded domains, and arbitrary loadings. In addition, it can be used as a starting point for numerical methods, tailored specifically for the solution of crack problems.

4.4.3 Method of weight functions

For many geometrical configurations, the K-factors are known for particular loadings, for example, from handbooks. How they can be used to obtain K-factors for the same geometry but for other loadings will be shown in the following. For simplicity we restrict the discussion to plane mode-I problems.

Starting point is Betti's theorem (cf. Section 1.4.3)

$$\int_A t_i^{(1)} u_i^{(2)} \mathrm{d}A = \int_A t_i^{(2)} u_i^{(1)} \mathrm{d}A \tag{4.52}$$

with $t_i = \sigma_{ij} n_j$ which we apply to the two configurations in Fig. 4.14. Except for the loading, they differ from each other only by slightly different crack lengths: the crack in configuration (2) is by a *small* amount ε longer than that in configuration (1). Since relation (4.52) can be applied only to configurations with identical geometry, we assume that in configuration (1) a cut of the length ε is made in front of the crack along the x-axis. The stresses acting there are given by the crack-tip field formulas (4.14): $\sigma_y^{(1)}(\xi) = K_I^{(1)}(a)/\sqrt{2\pi\xi}$. Analogous, the crack face displacement v in the traction-free region $0 \le \xi \le \varepsilon$ of configuration (2) is

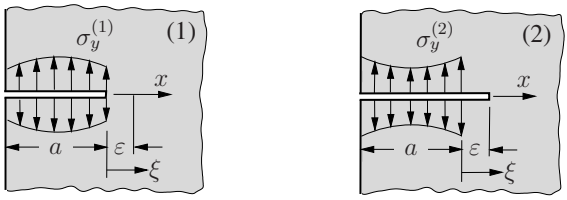

Fig. 4.14 Application of Betti's theorem

$v^{(2)}(\xi) = \frac{\kappa+1}{2G} K_I^{(2)}(a+\varepsilon)\sqrt{(\varepsilon-\xi)/2\pi}$. Adopting the notation from Fig. 4.14 and taking into account the symmetry, it follows from (4.52) that

$$\int_0^a \sigma_y^{(1)}(x)\, v^{(2)}(x,a+\varepsilon)\mathrm{d}x + \int_0^\varepsilon \frac{K_I^{(1)}(a)}{\sqrt{2\pi\xi}}\, \frac{\kappa+1}{2G} K_I^{(2)}(a+\varepsilon)\sqrt{\frac{\varepsilon-\xi}{2\pi}}\,\mathrm{d}\xi = \int_0^a \sigma_y^{(2)}(x)\, v^{(1)}(x)\,\mathrm{d}x\ .$$

With the expansions

$$v^{(2)}(x,a+\varepsilon) = v^{(2)}(x,a) + \frac{\partial v^{(2)}}{\partial a}\,\varepsilon + \dots\ , \qquad K_I^{(2)}(a+\varepsilon) = K_I^{(2)}(a) + \frac{\mathrm{d}K_I^{(2)}}{\mathrm{d}a}\,\varepsilon + \dots$$

and under consideration of

$$\int_0^a \sigma_y^{(1)}\, v^{(2)}(x,a)\,\mathrm{d}x = \int_0^a \sigma_y^{(2)}\, v^{(1)}(x,a)\,\mathrm{d}x \quad , \qquad \int_0^\varepsilon \sqrt{\frac{\varepsilon-\xi}{\xi}}\,\mathrm{d}\xi = \frac{\pi\varepsilon}{2}$$

we get, after taking the limit $\varepsilon \to 0$, the result

$$\int_0^a \sigma_y^{(1)} \frac{\partial v^{(2)}}{\partial a}\,\mathrm{d}x + \frac{\kappa+1}{8G} K_I^{(1)}(a)\, K_I^{(2)}(a) = 0\ . \tag{4.53}$$

We now consider configuration (2) as the known reference configuration while the stress intensity factor for configuration (1) is unknown. Renaming the known and unknown quantities as

$$K_I^{(2)}\ ,\ v^{(2)}\ \to\ K_I^r\ ,\ v^r\ , \qquad K_I^{(1)}\ ,\ \sigma_y^{(1)}\ \to\ K_I\ ,\ \sigma_y$$

equation (4.53) yields

$$K_I = -\frac{8G}{\kappa+1}\,\frac{1}{K_I^r}\int_0^a \sigma_y\,\frac{\partial v^r}{\partial a}\,\mathrm{d}x\ . \tag{4.54}$$

Here, the term $[8G/(\kappa+1)K_I^r]\partial v^r/\partial a$ is called *weight function*. It "weights" the prescribed crack load σ_y during integration to determine the related stress intensity factor. Formula (4.54) here is valid for a crack with *one* crack tip. When applied to a crack with two crack tips the integration has to be performed along the whole crack length and the derivative $\partial v^r/\partial a$ has to be taken with respect to the crack tip where the stress intensity factor shall be determined (i.e., the other crack tip then has to be held fixed). For a symmetrically loaded crack with $K_I^+ = K_I^-$, formula (4.54) reduces to an integration along the half-length of the crack.

As an example, we will determine K_I for the crack in Fig. 4.15a with a crack-face loading $\sigma_y = -\sigma_0\sqrt{1 - x^2/a^2}$. As the reference case, we use the crack with a constant traction $\sigma_y^r = -\sigma$ (cf. Section 4.4.1). For the latter the expressions $K_I^r = \sigma\sqrt{\pi a}$ and $4Gv^r = (1+\kappa)\sigma\sqrt{a^2 - x^2}$ apply. Substitution into (4.54), with the symmetry taken into account, leads to

$$K_I = \frac{8G}{\kappa+1}\frac{1}{\sigma\sqrt{\pi a}}\int_0^a \sigma_0\sqrt{1-\frac{x^2}{a^2}}\,\frac{1+\kappa}{4G}\,\frac{\sigma a}{\sqrt{a^2-x^2}}\,\mathrm{d}x = \frac{2}{\pi}\sigma_0\sqrt{\pi a}\,. \tag{4.55}$$

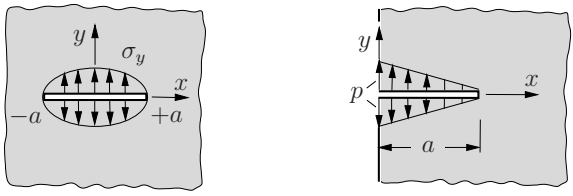

a) b)

Fig. 4.15 Weight function method: examples

Often the situation is met that the stress intensity factor K_I^r for a reference load σ_y^r is known but the reference displacement v^r is unknown. In such cases it is possible to obtain an approximate solution for K_I by using a displacement approach. In order to show this we assume for simplicity that the reference load is constant along the crack: $\sigma_y^r = -\sigma = \text{const}$. For the reference displacement we employ the two-terms approach (Petroski & Achenbach, 1995)

$$v^r = \frac{1+\kappa}{8\sqrt{2}}\frac{\sigma}{G}\left[4f(a)\sqrt{a}\,(a-x)^{1/2} + h(a)\frac{(a-x)^{3/2}}{\sqrt{a}}\right] \tag{4.56}$$

with

$$K_I^r = \sigma\sqrt{\pi a}\; f(a) \tag{4.57}$$

which is motivated by the crack-tip field solution. The function $h(a)$ is determined from the condition of *self-consistency* which requires $K_I = K_I^r$ for $\sigma_y = \sigma_y^r$. Thus, from (4.54) it follows that

$$(K_I^r)^2 = \frac{8G}{1+\kappa}\,\sigma\int_0^a \frac{\partial v^r}{\partial a}\,\mathrm{d}x \qquad \text{or} \qquad \int_0^a (K_I^r)^2\,\mathrm{d}a = \frac{8G}{1+\kappa}\,\sigma\int_0^a v^r\,\mathrm{d}x$$

and finally

$$h(a) = \frac{5\sqrt{2}\pi}{2a^2}\int_0^a a f^2(a)\,\mathrm{d}a - \frac{20}{3}f(a)\,. \tag{4.58}$$

As an example, we consider an edge crack with a linear crack face loading (see Fig. 4.15b). For the reference case under constant load distribution, the stress intensity factor is $K_I^r = 1.1215\ \sigma\sqrt{\pi a}$, i.e., $f = 1.1215 = \text{const}$ (cf. Table 4.1, No. 5). Introducing (4.56) and the crack loading $\sigma_y = -p(1 - x/a)$ into (4.54) finally gives as an approximation for the K-factor

$$K_I \simeq 0.435\ p\sqrt{\pi a}\ . \tag{4.59}$$

The exact value is $K_I^{ex} = 0.439\ p\sqrt{\pi a}$. If only the first term of (4.56) is taken into account ($h = 0$), the coarser approximation $K_I \simeq 0.480\ p\sqrt{\pi a}$ is obtained.

4.4.4 Crack interaction

Often one has to deal not only with a single crack but with a certain number of cracks, e.g., two or three, or even with a system consisting of many cracks. If the distances between the cracks are large compared to their length, they affect each other only a little. In a first approximation each crack then can be treated as if the others were absent. But if the cracks are close the interaction between them can lead, depending on the geometrical configuration, to an increase or to a reduction of the crack-tip loading, i.e., of the K-factors. This is known as an amplification or shielding effect. Exact solutions for such problems are possible only in specific cases. But also numerical methods are in some sort limited. Generally, they are practicable only if the number of the cracks is sufficiently small. One example, for which an exact solution exists, is the row of collinear cracks in Fig. 4.11a or in Table 4.1, No 3, respectively. If the adjacent crack tips in this case approach each other ($a \to b$), the K-factors grow infinitely (amplification).

In what follows, we will discuss the principle of a method which goes back to M. KACHANOV (1983) and which allows the construction of rather good approximate solutions for complex crack systems. As a preparation, we consider a crack 1 (see Fig. 4.16) the crack faces of which are loaded by a constant unit traction. The solution of this problem is known (cf. Section 4.4.1) and we can determine the stresses in each point or along an arbitrary line. For example, according to (4.31), along the line 2 (x-axis) the normal stress is given by (the shear stress is zero)

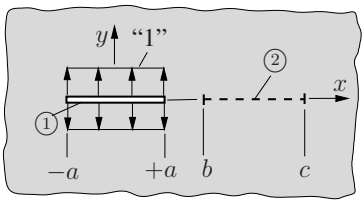

Fig. 4.16 Definition of the transmission factor

$$\sigma_y(x) = f_{12}(x) = \frac{x}{\sqrt{x^2 - a^2}} - 1 \,. \tag{4.60}$$

We denote its mean value in the interval (b, c) as the *transmission factor:*

$$\Lambda_{12} = \langle f_{12} \rangle = \frac{1}{c-b} \int_b^c f_{12}(x) \mathrm{d}x = \frac{\sqrt{c^2 - a^2} - \sqrt{b^2 - a^2}}{c-b} - 1 \,. \tag{4.61}$$

It describes the average loading of line 2 due to a unit load of crack 1 and it is determined solely by the geometrical configuration.

The explanation of Kachanov's method is restricted here, for simplicity, to two collinear cracks under a pure mode-I loading due to the remote tension σ_0 (Fig. 4.17). Because we are interested only in the stress intensity factors, it is sufficient to investigate the system with the crack face loadings $p_1^\infty = p_2^\infty = \sigma_0$. The solution of this problem can formally be obtained from the superposition of two partial problems. The first one refers to a situation where only crack 1 is loaded by an unknown crack face traction $p_1(x) = p_1^\infty + \widetilde{p}_1(x)$. Here, $\widetilde{p}_1(x)$ describes the deviation of the crack 1 loading due to existence of crack 2. Along its line, the stress $\sigma_2(x)$ appears on account of the loading $p_1(x)$. We now replace σ_2 approximately by the stress $\langle p_1 \rangle f_{12}(x)$ which appears as a result of a constant crack loading by the mean value $\langle p_1 \rangle$. Thus, regarding the effect onto crack 2, we take into account only the mean (average) loading of crack 1. The second partial problem is treated in the

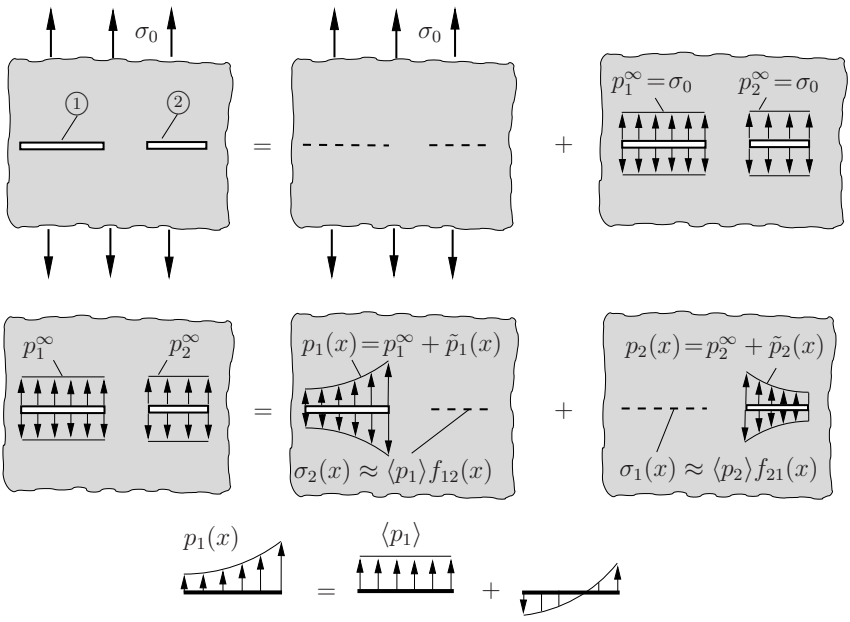

Fig. 4.17 Kachanov's method

same manner. After superposition, the boundary conditions for both cracks

$$p_1(x) - \langle p_2 \rangle f_{21}(x) = p_1^\infty \ , \qquad p_2(x) - \langle p_1 \rangle f_{12}(x) = p_2^\infty$$

lead to the representations

$$p_1(x) = p_1^\infty + \langle p_2 \rangle f_{21}(x) \ , \qquad p_2(x) = p_2^\infty + \langle p_1 \rangle f_{12}(x) \ . \tag{4.62}$$

The unknown mean values $\langle p_1 \rangle$ and $\langle p_2 \rangle$ are determined from the condition that equations (4.62) must be *self-consistent*, i.e., they must be applicable also for the determination of the mean values:

$$\langle p_1 \rangle = p_1^\infty + \langle p_2 \rangle \langle f_{21} \rangle \ , \qquad \langle p_2 \rangle = p_2^\infty + \langle p_1 \rangle \langle f_{12} \rangle \ .$$

These *self-consistency equations* represent a linear system of equations for $\langle p_1 \rangle$, $\langle p_2 \rangle$ which, using the transmission factors according to (4.61), can be written as

$$\begin{aligned} \langle p_1 \rangle - \Lambda_{21} \langle p_2 \rangle &= p_1^\infty \ , \\ -\Lambda_{12} \langle p_1 \rangle + \langle p_2 \rangle &= p_2^\infty \ . \end{aligned} \tag{4.63}$$

After its solution, the crack loadings $p_1(x)$ and $p_2(x)$ according to (4.62) are known and the stress intensity factors $K_I^\pm$ for each crack can be determined by means of (4.40).

If the system consists not only of two but of n cracks under a mode-I loading, generalizing equations (4.63), the following system of equations is obtained

$$(\delta_{ji} - \Lambda_{ji}) \langle p_j \rangle = p_i^\infty \ , \qquad i = 1, \ldots, n \tag{4.64}$$

where $\Lambda_{ij} = 0$ for $i = j$. If the cracks experience also a mode-II loading, this must be taken into account for the transmission factors and boundary conditions. In this case, a configuration of n cracks leads to a system of $2n$ equations for n mean values of the normal tractions and n mean values for the shear tractions, respectively.

As an example, we consider two collinear cracks of the same length as shown in Fig. 4.18a. For this case, taking into account that $\Lambda_{12} = \Lambda_{21} = \Lambda$, $\langle p_1 \rangle = \langle p_2 \rangle = \langle p \rangle$ (symmetry!), we obtain from (4.63)

$$\langle p \rangle - \Lambda \langle p \rangle = p^\infty \qquad \text{or} \qquad \langle p \rangle = \frac{p^\infty}{1 - \Lambda}$$

where

$$\Lambda = \frac{\sqrt{2(1+\kappa)}}{1+\sqrt{\kappa}} - 1 \ .$$

According to (4.62) and (4.60), the crack loading, e.g. of the right crack, is determined as

$$p(x) = p^\infty + \langle p \rangle \left[\frac{2x + 1 + \kappa}{2\sqrt{(x+\kappa)(x+1)}} - 1 \right] \ .$$

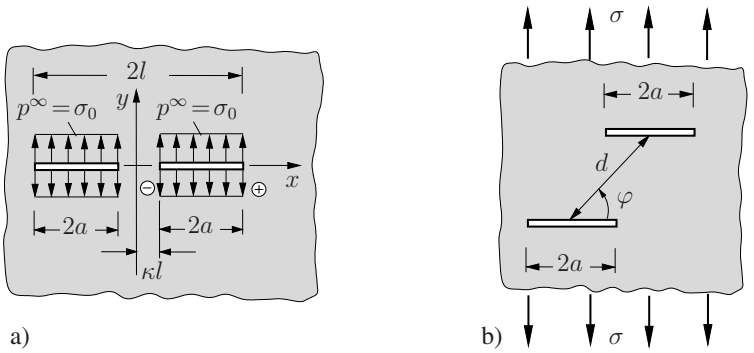

Fig. 4.18 Two interacting cracks of equal length

Substitution into (4.40) finally yields the approximate solution for the K-factors

$$K_I^{\pm} = K_I^0 \left\{ 1 + \frac{1}{1-\Lambda} \frac{1}{2\pi(1-\kappa)} \left[\pm 4\mathcal{E}(\alpha) \mp 2\kappa(\kappa+1)\mathcal{K}(\alpha) - \pi(1-\kappa) \right] \right\}. \quad (4.65)$$

Here, $K_I^0 = \sigma_0\sqrt{\pi a}$ is the K-factor for a single (undisturbed) crack and $\mathcal{K}(\alpha)$ and $\mathcal{E}(\alpha)$ are the complete elliptic integrals of the first and the second kind, respectively, with the argument $\alpha = \sqrt{1-\kappa^2}$. Table 4.2 shows a comparison of some results of the approximate solution with the exact values. As can be seen, the error is very small even for the case when the distances between the cracks are quite small.

κ	K_I^+/K_I^0 (approx.)	K_I^+/K_I^0 (exact)	K_I^-/K_I^0 (approx.)	K_I^-/K_I^0 (exact)
0.2	1.052	1.052	1.112	1.112
0.05	1.118	1.120	1.452	1.473
0.01	1.175	1.184	2.134	2.372

Table 4.2 Comparison of approximate solutions with exact values

For this specific example, we now will consider the case when the distance $d = 2(\kappa l + a)$ between the midpoints of the cracks is large compared to the crack lengths: $d \gg a$. Then, from (4.60) by series expansion for $x \gg a$ we obtain along the x-axis the stress $f_{12} = \sigma_y \approx \frac{1}{2}(a/x)^2$. With $x \approx d$, this stress can be considered as constant in the region of the crack line 2: $f_{12} = \Lambda_{12} = \sigma_y \approx \frac{1}{2}(a/d)^2$. Herewith, it follows $p \approx p^\infty[1 + \frac{1}{2}(a/d)^2]$, and we obtain for the K-factors

$$K_I \approx K_I^0 \left[1 + \frac{1}{2} \left(\frac{a}{d} \right)^2 \right] . \quad (4.66)$$

In this first approximation, they are equal at the left and at the right crack tip.

In the same manner we can determine the K-factors for the generalized crack configuration depicted in Fig. 4.18b:

$$K_I \approx K_I^0 \left[1 + \frac{a^2}{2d^2}(2\cos 2\varphi - \cos 4\varphi)\right] ,$$
$$K_{II} \approx K_I^0 \frac{a^2}{2d^2}(-\sin 2\varphi + \sin 4\varphi) . \tag{4.67}$$

It can be recognized that the interaction of the cracks decreases rapidly with increasing distance d. For collinear cracks ($\varphi = 0$) with a distance $d = 10a$ only a small increase of K_I of $1/200$ can be observed. For stacked cracks ($\varphi = \pi/2$), a small K_I-decrease of $3/200$ occurs. The reason for this phenomenon lies in the decay behavior of the stresses around a crack which is loaded according to Fig. 4.16. For $r \gg a$, this decay is in the plane (2D) case of the type $(a/r)^2$. In contrast, in the equivalent three-dimensional case of a circular crack, the stress decay for larger distances ($r \gg a$) is of the type $(a/r)^3$, i.e., disturbances decay faster than in the 2D case. Accordingly, for the same distances between the cracks, the interaction in the three-dimensional case is weaker than in the plane problem.

When interacting cracks propagate, interesting and partly unexpected phenomena may occur. One of them shall briefly be discussed. For this purpose we consider a plate under uniaxial tension containing two nearly collinear straight cracks (Fig. 4.19). Experiments show that these cracks, when propagating, in a first phase approach each other, as expected. But as the distance becomes shorter, the crack tips in a second phase deviate slightly and do not coalesce along the shortest path. Due to their interaction, both crack tips run around each other in a certain distance until, at some later instant, each of them merges with the other crack. Figure 4.19 shows the results of a numerical simulation which provides a realistic impression of this process.

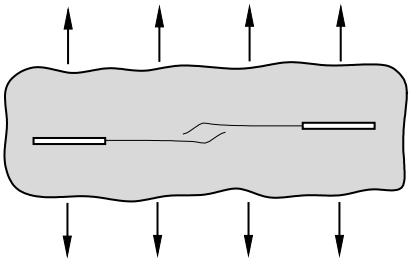

Fig. 4.19 Interaction between two cracks propagating towards each other

Even though such curved crack paths can be determined only numerically, the observed phenomenon can qualitatively be explained from the results (4.67) for the crack configuration in Fig. 4.18b. As will be discussed in Section 4.9, the angle at which a propagating crack is deviated from a straight path, is mainly controlled by the K_{II}-factor. The latter changes, according to (4.67), with the angle φ, i.e.,

with the relative position of the crack tips and experiences a sign change. For small angles φ, the K_{II}-factor is positive which causes initially a downward deviation of the left crack in Fig. 4.19 and an upward deviation of the right crack, i.e., the crack tips repel each other. For larger angles φ, the K_{II}-factor becomes negative and both cracks are directed towards each other.

4.4.5 Stress intensity factors and stress concentration factors

Similar as in the vicinity of crack tips, very high stresses prevail at notches with a sufficiently small notch radius. However, in contrast to the crack tip, the stresses at the root of a blunt notch are always finite, or in other words, they are non-singular. The increase of stresses at notches commonly is called *stress concentration* and the stress amplification due to the notch in relation to the nominal stress is described by a so-called *stress concentration factor*. A more detailed analysis shows that there are close relationships between the stress fields near a crack tip and near a notch root which in the following shall be briefly discussed.

As a typical example we first consider an elliptical cavity with semiaxes a and b in an infinite domain under uniaxial tension σ perpendicular to the semimajor axis a (Fig. 4.20a). Without going into the derivation, it can be shown that the maximum boundary stress occurs at the apexes $x = \pm a$ of the ellipse and is given by

$$\sigma_{\max} = \sigma \left(1 + 2\frac{a}{b}\right) = \sigma \left(1 + 2\sqrt{\frac{a}{\rho}}\right) . \tag{4.68}$$

Here, $\rho = b^2/a$ is the radius of curvature at the apex, see Fig. 4.20b. It can be seen that the stress amplification increases with decreasing ratio b/a of the semiaxes or ρ/a, respectively. For very narrow ellipses, i.e. $b \ll a$ or $\rho \ll a$, (4.68) reduces to

$$\sigma_{\max} = 2\sigma\sqrt{\frac{a}{\rho}} . \tag{4.69}$$

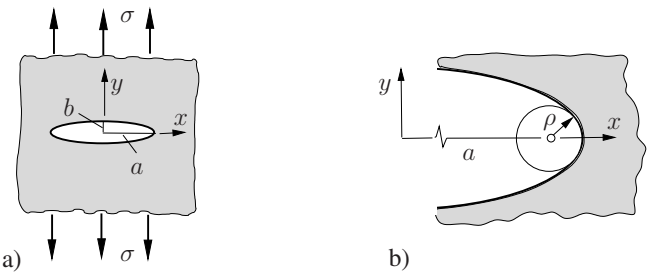

Fig. 4.20 Elliptic cavity under uniaxial tension

In the limit case $b \to 0$ or $\rho \to 0$, the elliptic cavity degenerates to a crack of length $2a$ and the maximum stress tends to infinity.

In order to show the relationship between the crack tip field and the stress field at a blunt notch, we now take a closer look at the direct surrounding of the apex, see Fig. 4.21a. Here, the boundary of the ellipse coincides with that of a deep notch of parabolic shape. If the origin of coordinates is put into the focal point of the parabola, it can alternatively be described by

$$x = \frac{\rho}{2} + \frac{y^2}{2\rho} \quad \text{or} \quad z = \frac{\rho}{2}(1 - i\,\eta)^2, \quad -\infty < \eta < \infty \tag{4.70}$$

where $z = x + iy = r\,\mathrm{e}^{i\varphi}$. The corresponding mode I notch stress-field is obtained by the superposition of two fields. The first one is the crack tip field of a crack tip at the origin which is given by (4.15). This field generates boundary tractions along the contour of the parabola which are compensated to zero by a second field with the complex potentials

$$\Phi'(z) = 0\,, \qquad \Psi'(z) = \frac{\rho K_I}{2z\sqrt{2\pi z}}\,, \tag{4.71}$$

i.e. the boundary of the parabolic notch then is traction-free. Hence, the stress field near the notch root is given by the sum of (4.15) and the stresses from (4.71):

$$\begin{Bmatrix} \sigma_x \\ \sigma_y \\ \tau_{xy} \end{Bmatrix} = \frac{K_I}{\sqrt{2\pi r}} \left[\cos\frac{\varphi}{2} \begin{Bmatrix} 1 - \sin\frac{\varphi}{2}\sin\frac{3\varphi}{2} \\ 1 + \sin\frac{\varphi}{2}\sin\frac{3\varphi}{2} \\ \sin\frac{\varphi}{2}\cos\frac{3\varphi}{2} \end{Bmatrix} - \frac{\rho}{2r} \begin{Bmatrix} \cos\frac{3\varphi}{2} \\ -\cos\frac{3\varphi}{2} \\ \sin\frac{3\varphi}{2} \end{Bmatrix} \right]. \tag{4.72}$$

Consequently, the intensity of the stress field near the notch root is uniquely given by the stress intensity factor K_I of a corresponding crack. In particular, the maximum boundary stress $\sigma_{\max} = \sigma_y$ at the notch root ($r = \rho/2$, $\varphi = 0$) can be written as

$$\sigma_{\max} = \frac{2K_I}{\sqrt{\pi\rho}}\,. \tag{4.73}$$

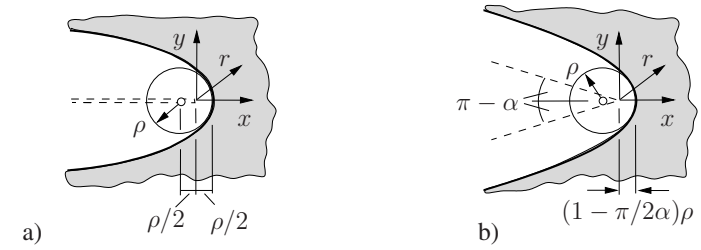

Fig. 4.21 a) Parabolic notch, b) V-notch

From this generally valid relationship, the maximum stress at a deep notch of prescribed notch radius can be determined for a given load from the mode I stress intensity factor. In reverse, from

$$K_I = \lim_{\rho \to 0} \frac{1}{2} \sqrt{\pi \rho}\, \sigma_{\max} \tag{4.74}$$

the stress intensity factor can be obtained if $\sigma_{\max}(\rho)$ is known. Analogous relationships are valid in pure mode II and mode III, respectively:

$$K_{II} = \lim_{\rho \to 0} \frac{1}{2} \sqrt{\pi \rho}\, \sigma_{\max}\,, \qquad K_{III} = \lim_{\rho \to 0} \frac{1}{2} \sqrt{\pi \rho}\, \tau_{\max}\,. \tag{4.75}$$

A similar relationship exists between the generalized stress intensity factor K^* for a sharp V-notch as shown in Fig. 4.5 (see also (4.20)) and the maximum boundary stress $\sigma_{\max}$ at the root of a blunt V-shaped notch with a notch radius ρ according to Fig. 4.21b:

$$\sigma_{\max} = \frac{K_I^*}{\sqrt{2\pi}}\, f(\alpha)\, \rho^{\lambda - 1}\,. \tag{4.76}$$

Here, $f(\alpha)$ and λ depend on the notch opening angle. For $\alpha = \pi$ (crack), $f = 2\sqrt{2}$ and $\lambda = 1/2$ hold.

4.5 Fracture toughness K_{Ic}

The determination of the fracture toughness K_{Ic} of a material usually is performed in standardized tests (e.g., ASTM–Standard E399-90) the details of which will not be discussed here. In such tests different specimen types are in use. Two of them are shown in Fig. 4.22. The test specimen must have a starter crack which is produced in metals by loading the initially notched specimen by a suitable oscillating load. From the measured loading at which the crack starts to propagate, the fracture toughness can be determined by means of the relation between the stress intensity factor, the loading and the crack length.

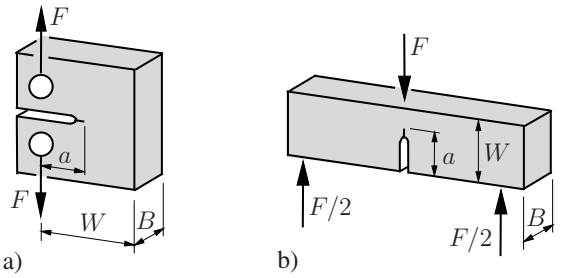

Fig. 4.22 Test specimens: a) compact tension (CT), b) 3-point bending (3PB)

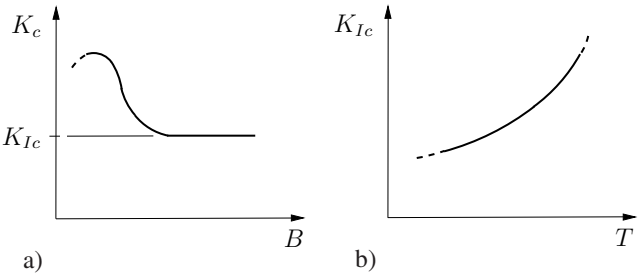

Fig. 4.23 a) Influence of sample thickness, b) influence of temperature

In order to extract from measurements fracture toughness values that can in fact be regarded as geometry-independent material parameters, the samples must satisfy the requirements of linear fracture mechanics. Accordingly, the plastic zone must be small compared to all relevant length parameters including the size of the K_I-determined region (cf. Sections 4.3 and 4.7). This is provided by the *size condition*

$$a,\ W-a,\ B \geq 2.5\left(\frac{K_{Ic}}{\sigma_Y}\right)^2 \tag{4.77}$$

where σ_Y is the yield strength. Under these circumstances, it is ensured that predominantly a plane strain state prevails in the region close to the crack front. How a decrease of the sample thickness affects the critical stress intensity factor is shown in Fig. 4.23a. The essential reason for the increase of K_c is the decrease of yield constraint which is associated with the change of the stress state (cf. Section 4.7.2).

material	K_{Ic} [MPa$\sqrt{\text{m}}$]	$R_{p0,2}$ [MPa]
high-strength steel	25...95	1600...2000
30CrNiMo8 (20^o)	115	1100
30CrNiMo8 (-20^o)	65	
construction steel	30...125	<500
Ti alloys	40...95	800...1200
Ti6Al4V	90	900
Al alloys	20...65	200...600
AlCuMg	30	450
AlZnMgCu1,5	30	500
Al_2O_3 ceramics	3...9	
marble	1.2...2	
glass	0.6...1.3	
concrete	0.15...1.4	
PMMA	0.7...1.6	
Douglas fir (TL, RL)	0.32, 0.36	

Table 4.3 Fracture toughness of some materials

The fracture toughness of a material strongly depends on a number of influence parameters. Among them are the characteristics of the microstructure (e.g., the grain size), the loading history, the heat treatment, or the environment (e.g., air or water). Figure 4.23b schematically shows the significant influence of the temperature observed for many materials. In Table 4.3 reference data for the fracture toughness of some materials are given. However, reliable data for structural applications in any case have to be measured directly at the particular material that is used.

4.6 Energy balance

4.6.1 Energy release during crack propagation

We consider an elastic body containing a crack with the boundary ∂V_t subjected to external tractions and where along the boundary ∂V_u displacements are prescribed (Fig. 4.24). The external tractions are assumed to have a potential Π^{ext} which applies, for example, to dead loading or spring forces.

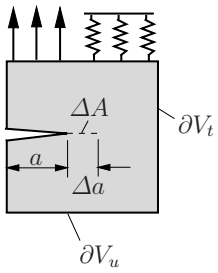

Fig. 4.24 Crack growth and energy release

Let us suppose that due to crack advance by an area ΔA (or the length Δa in the two-dimensional case, respectively), the system passes from the initial equilibrium state 1 in a new equilibrium state 2. This transition is imagined to be realized as follows: we assume that the body in state 1 is cut along ΔA and the stresses acting there are understood as external forces. They subsequently are released quasi-statically to zero such that state 2 is reached at the end. The work ΔW_σ done by these forces during this process is negative (or utmost zero) since forces and displacements are opposite directed. Simultaneously, the external forces along ∂V_t accomplish the work W_{12}^{ext} during the transition from state 1 to state 2. It can be expressed by the difference of the potential: $W_{12}^{ext} = -\Delta\Pi^{ext} = -(\Pi_2^{ext} - \Pi_1^{ext})$. Thus, the energy balance (cf. Section 1.4.1) yields

$$\Delta\Pi^{int} = \Pi_2^{int} - \Pi_1^{int} = W_{12}^{ext} + \Delta W_\sigma = -\Pi_2^{ext} + \Pi_1^{ext} + \Delta W_\sigma \ ,$$

and with $\Pi = \Pi^{int} + \Pi^{ext}$ we get

$$\Delta\Pi = \Delta W_\sigma \leq 0 \,. \tag{4.78}$$

Therefore, the mechanical energy Π of the system decreases during crack advance. The released energy is available for the fracture process. It should be emphasized that ΔW_σ must *not* be confused with the work ΔW^B of the bonding forces during crack propagation. The latter is done during the separation process between the components (atoms, molecules, etc.) of the material, i.e., ΔW^B is a material-specific quantity (cf. Sections 3.1.1 and 3.2.2).

We will briefly consider two special cases. If the displacements along the whole boundary ∂V are kept constant, then $\Delta\Pi^{ext} = 0$ and $\Delta\Pi^{int} = \Delta W_\sigma$. In contrast, if the external load is a dead loading and the material is linear elastic, from Clapeyron's theorem ($2\Pi^{int} + \Pi^{ext} = 0$) the result $-\Delta\Pi^i = \Delta\Pi^a/2 = \Delta W_\sigma$ follows.

As an example, we will determine the energy change of the system when a crack of the length $2a$ is created in an initially crack-free infinite plate under remote tension σ (Fig. 4.25). Using the displacement $v = (1+\kappa)\sigma\sqrt{a^2 - x^2}/4G$ of the upper crack face, first the work ΔW_σ during crack formation is calculated as (the same work is done at the upper and lower crack faces):

$$\Delta W_\sigma = -2\int_{-a}^{a} \frac{1}{2}\sigma v \mathrm{d}x = -\sigma^2 a^2 \pi \frac{1+\kappa}{8G} \,. \tag{4.79}$$

From this, in case of constant loading at infinity (dead loading), we obtain

$$\Delta\Pi = -\Delta\Pi^{int} = \Delta\Pi^{ext}/2 = -\sigma^2 a^2 \pi (1+\kappa)/8G \,. \tag{4.80}$$

If, in contrast, the displacements at infinity are kept constant, we get

$$\Delta\Pi = \Delta\Pi^{int} = -\sigma^2 a^2 \pi (1+\kappa)/8G \,. \tag{4.81}$$

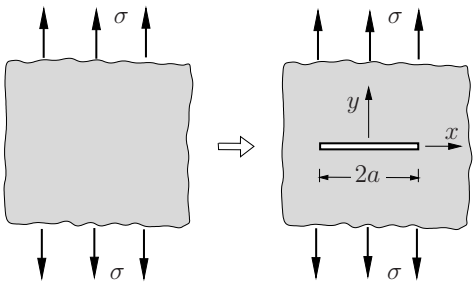

Fig. 4.25 Energy release during crack formation

Indeed, $\Delta\Pi$ in both cases is the same. However, $\Delta\Pi^{int}$ differs by the sign. It should be noted here that without any restriction, the system's potential for the initial state (plate without a crack) can be chosen to be zero. Then, (4.80) or (4.81), respectively, describes the potential Π of the plate with a crack. It also should be mentioned that (4.79)–(4.81) describe the work and energy changes per unit thickness (plane problem).

4.6.2 Energy release rate

The released energy $-\mathrm{d}\Pi$ during an infinitesimally small crack advance $\mathrm{d}A$, related to $\mathrm{d}A$, is called *energy release rate*:

$$\mathcal{G} = -\frac{\mathrm{d}\Pi}{\mathrm{d}A} \,. \tag{4.82a}$$

For a plane problem, $\mathrm{d}\Pi$ is related to the unit thickness and thus we define

$$\mathcal{G} = -\frac{\mathrm{d}\Pi}{\mathrm{d}a} \,, \tag{4.82b}$$

where $\mathrm{d}a$ is an infinitesimally small crack extension. The energy release rate has the dimension of a force (per unit thickness). Therefore it is also denoted as the *crack extension force*.

In the linear elastic case, the energy release rate can be expressed in terms of stress intensity factors. We show this for the situation of pure mode I. Again, a crack extension of the *small* length Δa is thought to be generated by the quasi-static reduction of stresses acting along the cut Δa (Fig. 4.26). *Before* crack extension, there acts, according to (4.14), the normal stress $\sigma_y(x) = K_I(a)/\sqrt{2\pi x}$ (higher order terms can be omitted because subsequently we will let $\Delta a \to 0$). According to (4.21), the displacement of the upper and lower crack face along Δa *after* crack extension is $v^{\pm}(x) = \pm\frac{\kappa+1}{2G}K_I(a+\Delta a)\sqrt{(\Delta a - x)/2\pi}$. Thus, the energy release results as

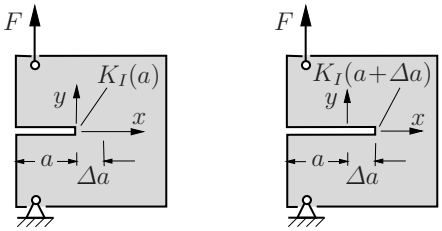

Fig. 4.26 Energy release rate for mode I

$$\begin{aligned} \Delta W_\sigma = \Delta \Pi &= -\frac{1}{2}\int_0^{\Delta a} \sigma_y \,(v^+ - v^-)\,\mathrm{d}x \\ &= -\int_0^{\Delta a} \frac{K_I(a)}{\sqrt{2\pi x}}\,\frac{\kappa+1}{2G}\,K_I(a+\Delta a)\sqrt{\frac{\Delta a - x}{2\pi}}\,\mathrm{d}x \\ &= -\frac{\kappa+1}{8G}\,K_I(a)\,K_I(a+\Delta a)\,\Delta a\,. \end{aligned} \tag{4.83}$$

Taking the limit $\Delta a \to 0$, we obtain

$$\mathcal{G} = -\frac{\mathrm{d}\Pi}{\mathrm{d}a} = \frac{\kappa+1}{8G}\,K_I^2 = \begin{cases} K_I^2/E & \text{for plane stress,} \\ (1-\nu^2)K_I^2/E & \text{for plane strain.} \end{cases} \tag{4.84}$$

In the same manner, the energy release rates for pure mode-II and pure mode-III loading can be determined:

$$\mathcal{G} = \frac{\kappa+1}{8G}K_{II}^2 \quad (\text{mode II})\,, \qquad \mathcal{G} = \frac{1}{2G}K_{III}^2 \quad (\text{mode III})\,. \tag{4.85}$$

In case of a general crack loading, when all three modes are present, we obtain for the energy release rate per unit length of the crack front

$$\mathcal{G} = \frac{1}{E'}(K_I^2 + K_{II}^2) + \frac{1}{2G}K_{III}^2\,. \tag{4.86}$$

Here, $E' = E/(1-\nu^2)$ for plane strain and for the three-dimensional case while $E' = E$ for plane stress.

In the pure mode-I case, according to (4.74), there is a unique relation between K_I and $\mathcal{G}$. This applies also for the pure mode-II and the pure mode-III case. Thus, within the framework of linear fracture mechanics, the K-concept and the criterion

$$\boxed{\mathcal{G} = \mathcal{G}_c} \tag{4.87}$$

are equivalent for pure modes. Here, $\mathcal{G}_c$ is a material parameter which is called *crack resistance* or *crack resistance force*. Because of the direct relation $\mathcal{G}_c = K_{Ic}^2/E'$ it is, like K_{Ic}, frequently also called *fracture toughness*. The condition (4.87) can be interpreted as follows: fracture is initiated if the energy release during crack growth is equal to the required energy. This *energy criterion* was proposed by A.A. GRIFFITH (1921) in a slightly different form. We will come back to it again in Section 4.6.4. In another perspective of (4.87) the interpretation of $\mathcal{G}$ as a (generalized) force is emphasized. Accordingly, at crack initiation the crack extension force must be equal to the crack resistance force.

As examples we will determine the energy release rates for two crack configurations which are of relevance for different applications. The configuration shown in Fig. 4.27a can be regarded as a model of two adhesively bonded or welded thin

layers (strips) under tension F. At sufficiently large distances from the crack tips, for $h \ll 2b$, the stress states outside and within the bonded region do not vary with x. A crack advance $\mathrm{d}a$ of the left or the right crack tip leads to a length decrease of the bonded region of exactly the same amount as the length increase of the outside region. Presuming the load F as a dead load and applying the relations of beam theory (which are exact in this case), with the bending moment $M = Fh/2$ and the moment of inertia $I = Bh^3/12$, we obtain in a first step

$$\mathrm{d}\Pi^{int} = \left[\left(\frac{F^2}{2\,E'(B\,h)} + \frac{M^2}{2\,E'I}\right) - \frac{F^2}{2\,E'(2\,B\,h)}\right]\,\mathrm{d}a = \frac{7\,F^2}{4\,E'\,B\,h}\,\mathrm{d}a\;.$$

Here, B is the width of the layer in the third direction. Because of $\mathrm{d}\Pi = -\mathrm{d}\Pi^i = \mathrm{d}\Pi^a/2$ and $\mathrm{d}A = B\,\mathrm{d}a$, equation (4.82a) yields for plane strain

$$\mathcal{G} = \frac{7\,(1-\nu^2)\,F^2}{4\,E\,B^2\,h} \qquad \text{or} \qquad \mathcal{G} = \frac{7\,(1-\nu^2)\,\sigma^2\,h}{4\,E} \tag{4.88}$$

where $\sigma = F/Bh$ is the mean stress in a layer. It should be mentioned that in this case, contrary to a first impression, no pure mode-II loading occurs. Thus, the stress intensity factors cannot be determined from $\mathcal{G}$. Without going into the details of the calculation, the K-factors are $K_I \approx -K_{II} \approx \sqrt{7/9}\,\sigma\sqrt{h}$.

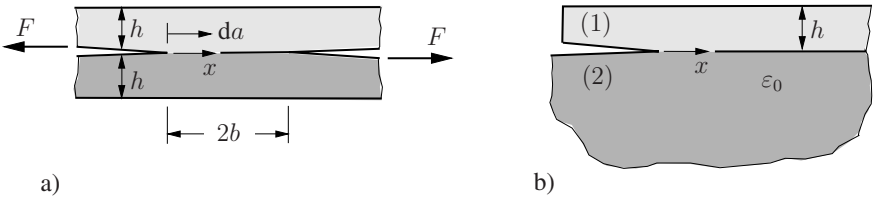

Fig. 4.27 Energy release rate: two examples

Figure 4.27b shows a crack in the interface (bonding plane) between a thin layer (1) and a base material or substrate (2). We suppose that the substrate (2) experiences a constant strain $\varepsilon_x = \varepsilon_0$ which is imposed to the layer (1). This leads for $|x| \gg h$, plane strain presumed, far ahead of the crack tip to the constant stress $\sigma = E\varepsilon_0/(1-\nu^2)$ while the left-hand side of the layer is stress-free. If the crack advances by $\mathrm{d}a$, the layer region with the constant stress decreases by the same amount and the state in the substrate remains unchanged. As a consequence,

$$\mathrm{d}\Pi^{int} = -\frac{1}{2}\,\sigma\,\varepsilon_0\,B\,h\,\mathrm{d}a = -\frac{\sigma^2(1-\nu^2)\,B\,h}{2\,E}\,\mathrm{d}a\;.$$

Since no external forces are present, $\mathrm{d}\Pi = \mathrm{d}\Pi^{int}$ holds and (4.82a) in conjunction with $\mathrm{d}A = B\mathrm{d}a$ yields

$$\mathcal{G} = \frac{(1-\nu^2)\,\sigma^2\,h}{2\,E}\;. \tag{4.89}$$

As in the forgoing example, no pure mode-II is present. Thus, the stress intensity factors cannot be determined from $\mathcal{G}$. It also should be noted that this configuration frequently is used to model the *delamination* of a thin layer (film) from a substrate. Cracks in the interface between two different materials will more thoroughly be considered in Section 4.11.

4.6.3 Compliance, energy release rate, and K-factors

In the linear elastic case, the energy release rate is related to the compliance of a body or its overall stiffness, respectively. We will show this for the example of a plane mode-I problem of a body which is loaded by a prescribed force F (dead load) (Fig. 4.28a). With $\Pi^{ext} = -F u_F$ and $\Pi^{int} = F u_F/2$, the total potential in this case is

$$\Pi = \Pi^{int} + \Pi^{ext} = -\frac{1}{2} F\, u_F \ .$$

Between the displacement u_F and the load F, the linear relationship

$$u_F = C\, F$$

holds where C is the *compliance* (i.e., the inverse stiffness) of the body. If the crack advances, C and u_F change (Fig. 4.28b): $C = C(a)$, $u_F = u_F(a)$. Therefore, the potential can be written as $\Pi = -F^2 C(a)/2$ and the energy release rate takes the form

$$\mathcal{G} = -\frac{\mathrm{d}\Pi}{B\,\mathrm{d}a} = \frac{F^2}{2B}\,\frac{\mathrm{d}C}{\mathrm{d}a} \tag{4.90}$$

where B is the thickness of the body. It can be shown that this result is independent of the loading type. For instance, it applies also if the force acts to the body via a spring or if instead of the force the displacement u_F is held constant.

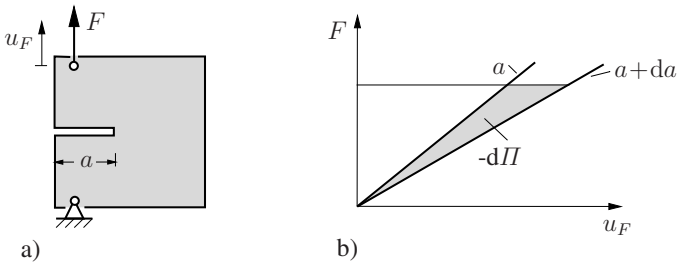

Fig. 4.28 Change of compliance on account of crack advance

In pure mode-I, from (4.90) in conjunction with (4.84) we obtain for the stress intensity factor

$$K_I^2 = \frac{F^2 E'}{2B} \frac{\mathrm{d}C}{\mathrm{d}a} \tag{4.91}$$

where $E' = E$ in plane stress and $E' = E/(1-\nu^2)$ in plane strain. This relation, for example, can be used to determine stress intensity factors experimentally. For this purpose, the compliances of a body are determined for crack lengths which differ by a small amount Δa.

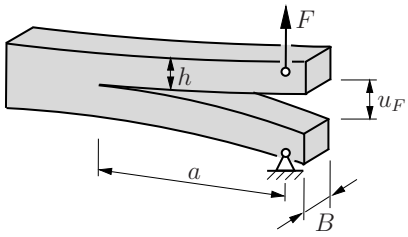

Fig. 4.29 DCB specimen

The relation (4.90) can also be used for the derivation of approximate analytical solutions for K-factors in certain cases. As an example of such a formula we consider a DCB specimen (double cantilever beam specimen) which is used in fracture experiments (Fig. 4.29). If both arms are considered as cantilever beams of length a, from beam theory (without taking shear into account) we get $u_F = 2Fa^3/3EI$. With $I = Bh^3/12$ this leads to the compliance $C = u_F/F = 8a^3/EBh^3$. Inserting this into (4.91) and assuming plane stress yields

$$K_I = 2\sqrt{3}\, \frac{F\, a}{B\, h^{3/2}} \ . \tag{4.92}$$

4.6.4 Energy balance, Griffith's fracture criterion

A fracture event in a body is accompanied by irreversible processes of bond-breaking. It is appropriate to represent all energies which are exclusively associated with the fracture process by a separate term in the energy balance (1.90). Among these are the surface energy, the energy needed for the large microplastic deformations in the process zone, and possible chemical and electromagnetic energies (cf. Chapter 3). Without specifying them in detail, they are summarized as the fracture energy Γ. The energy balance then can be written in the general form

$$\dot{E} + \dot{K} + \dot{\Gamma} = P + Q \ . \tag{4.93}$$

It must be satisfied at initiation and during the fracture process. Due to the irreversibility of the process, $\dot{\Gamma} \geq 0$ holds.

The fracture process takes place in the process zone whose volume in many cases can be considered as negligibly small compared to the volume of the body (Fig. 4.30). It is then obvious to split the energy balance (4.93) into one part for the process zone and another part for the rest of the body:

$$\begin{aligned} &\text{process zone:} && \dot{\Gamma} = -P^* \,, \\ &\text{body:} && \dot{E} + \dot{K} = P + Q + P^* \,. \end{aligned} \tag{4.94}$$

Here, $-P^*$ describes the energy transport into the process zone. If we restrict ourselves to solely mechanical energy terms, it is given by

$$P^* = \int\limits_{A_P} t_i \, \dot{u}_i \, \mathrm{d}A \,. \tag{4.95}$$

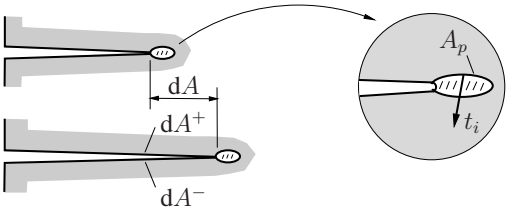

Fig. 4.30 Fracture process and energy balance

A fracture process is associated with the creation of a new surface. Between two adjacent states 1 and 2 at times t and $t + \mathrm{d}t$, the material is separated along the fracture surface $\mathrm{d}A$. During this time, the process zone moves and all material points of $\mathrm{d}A$ pass through an "unloading history" from state 1 to the state 2 where the bonding forces are fully released ($t_i = 0$). The work done by the bonding forces (i.e., the energy flow into the process zone) can be expressed by

$$\mathrm{d}W_\sigma = P^* \mathrm{d}t = \int\limits_{\mathrm{d}A^\pm} [\int\limits_{(1)}^{(2)} t_i \, \mathrm{d}u_i] \, \mathrm{d}\overline{A} \,. \tag{4.96}$$

Here, $\mathrm{d}A^\pm$ indicates that the work of the bonding forces on both opposite surfaces has to be taken into account. Simultaneously, during creation of $\mathrm{d}A$, the fracture energy is changed by an amount $\mathrm{d}\Gamma$ which is proportional to $\mathrm{d}A$: $\mathrm{d}\Gamma \propto \mathrm{d}A$. If $\mathrm{d}\Gamma$ is thought to be distributed in state 2 (after full separation) as *fracture surface energy* along the surface $\mathrm{d}A^\pm$, it can be written as (cf. Section 3.2.2)

$$\mathrm{d}\Gamma = \dot{\Gamma} \, \mathrm{d}t = 2 \, \gamma \, \mathrm{d}A \,. \tag{4.97}$$

The specific fracture surface energy γ is often considered to be constant. But in general, it can also be a function of the fracture history, i.e., for example, a function of the crack extension Δa: $\gamma = \gamma(\Delta a)$.

Again, the different physical meaning of $\dot{\Gamma}$ and P^* shall be emphasized. During the motion of the process zone by $\mathrm{d}A$ (i.e., crack extension), the energy $\mathrm{d}\Gamma$ on account of the creation of new fracture surfaces is transformed into energy terms like heat and surface energy. This takes place within the process zone. In contrast, P^* describes the energy flux into the process zone or, in other words, the effect of the surrounding continuum onto the process zone.

We now come back to the special case of an elastic body where a "slow", quasi-static fracture process is taking place. Here, we identify the process zone with the plastic zone, i.e., with the entire *small* area around the crack tip where inelastic processes occur. Accordingly, Γ now contains the energy needed both for the separation process and for the inelastic deformation process in the plastic zone. The kinetic energy K and the non-mechanical energy transport Q do not play a role. The internal energy E can be replaced by the strain energy Π^{int}. Additionally, it is presumed that the external forces have a potential Π^{ext}. With $\dot{\Pi}^{int}\mathrm{d}t = \mathrm{d}\Pi^{int}$, $\dot{\Gamma}\mathrm{d}t = \mathrm{d}\Gamma$ and $P\mathrm{d}t = -\mathrm{d}\Pi^{ext}$, the energy balance (4.93) reads

$$\boxed{\mathrm{d}\Pi^{int} + \mathrm{d}\Pi^{ext} + \mathrm{d}\Gamma = 0} \qquad \text{or} \qquad \boxed{\frac{\mathrm{d}\Pi}{\mathrm{d}A} + \frac{\mathrm{d}\Gamma}{\mathrm{d}A} = 0}\,. \tag{4.98}$$

Thus, during the fracture process, the change of the sum of the potential Π of external and internal forces and of the fracture energy Γ is zero. If, according to (4.82a), the energy release rate is introduced, equation (4.98) with (4.97) and the notation $\mathcal{G}_c = 2\gamma$ attains the form of (4.87), i.e.

$$\boxed{\mathcal{G} = \mathcal{G}_c}\,. \tag{4.99}$$

In other words, at initiation and during the subsequent progression of quasi-static crack advance, the released energy must be equal to the energy needed for the fracture process. The energy relation (4.98) was first applied as a fracture condition by A.A. GRIFFITH, why it is called *Griffith's fracture criterion*. However, Griffith regarded Γ not as the fracture surface energy (incorporating all inelastic terms associated with fracture) but as the pure surface energy. Formally, he treated the fracture process as *reversible*. Furthermore, he applied the energy balance (4.98) only to initiation of crack growth and not to its subsequent evolution.

In Section 4.6.2 it has been already mentioned that the K-concept and the energy criterion are fully equivalent in linear fracture mechanics. However, in most applications, the K-concept is preferred. An essential reason for that is its simpler applicability. For instance, K-factors are available in handbooks for many geometrical configurations and loading cases. Another reason is the transferability of the fundamental idea of dominant, singular crack-tip fields to nonlinear fracture mechanics, i.e., to inelastic, nonlinear material behavior. Nevertheless, there are a number of cases in linear fracture mechanics in which the energy criterion is preferred. One

example are interface cracks as they appear frequently in composite materials or laminates (cf. Section 4.12).

For an illustration of Griffith's fracture criterion (4.98), again a straight crack in an infinite plate under remote uniaxial tension σ is considered, see Fig. 4.31a. According to (4.80) and (4.97) the energy terms per unit thickness are

$$\Pi = -\sigma^2 a^2 \pi \, \frac{1+\kappa}{8G} \,, \qquad \Gamma = 4a\gamma$$

where γ is assumed to be constant (Fig. 4.31b). Introducing them into (4.98) yields the fracture condition

$$\frac{\mathrm{d}(\Pi + \Gamma)}{\mathrm{d}a} = 0 \qquad \rightsquigarrow \qquad 4\gamma = 2\sigma^2 \pi a \, \frac{1+\kappa}{8G} \quad . \tag{4.100}$$

If the actual crack length is prescribed, it determines the critical stress needed for the fracture process:

$$\sigma_c = \sqrt{\frac{16G\gamma}{\pi(1+\kappa)a}} \quad . \tag{4.101a}$$

Contrary, if the stress σ is given, from (4.100) the critical crack length a_c at which the crack starts to grow can be obtained (Fig. 4.31b):

$$a_c = \frac{16G\gamma}{\pi(1+\kappa)\sigma^2} \,. \tag{4.101b}$$

It is self-evident that identical results are obtained by using the K-concept.

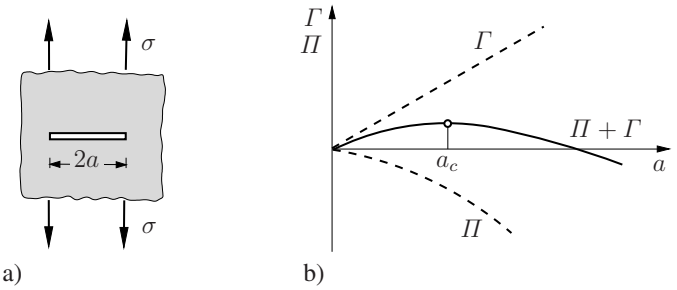

Fig. 4.31 Griffith's fracture criterion

In another example, we will address the question under which circumstances a so-called *channel crack* is formed in a thin layer (film) (1) of thickness h which is bonded on a substrate (2), see Fig. 4.32. We suppose that before failure, the uncracked layer is loaded by a constant tension σ and that the bond between layer and substrate remains intact during crack formation. In a good approximation, the layer then can be treated as a shear-compliant beam in plane strain whose axis remains straight. Without going into details of the derivation, the change of strain energy or

total potential, respectively, as well as the fracture energy during complete formation of the channel crack are determined as

$$\Pi \approx \frac{\sqrt{2}}{16}\,\frac{\sigma^2\,h^2\,(1-\nu^2)}{E}\,, \qquad \Gamma = 2\,\gamma\,h = \mathcal{G}_c\,h\,. \tag{4.102}$$

Then, if stress and fracture toughness are known, Griffith's energy criterion (4.98) leads to the critical layer thickness

$$h_c \approx 4\sqrt{2}\,\frac{\mathcal{G}_c E}{\sigma^2(1-\nu^2)}\,. \tag{4.103}$$

Thus, if channeling of a thin layer under tension shall be prevented (i.e., $\mathrm{d}\Pi + \mathrm{d}\Gamma < 0$), its thickness h must be below the critical value h_c: $h < h_c$. In this context it should be noted that tensile stresses due to the fabrication process or as a result of thermal effects in many cases cannot be avoided.

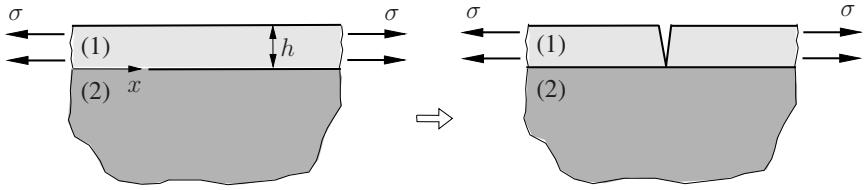

Fig. 4.32 Channeling in a thin layer

As a final example of an application of the energy criterion, the so-called *Peel-Test* is investigated. This test is frequently used to experimentally evaluate adhesive bonds or to determine the specific fracture surface energy of a thin film (layer) on a substrate. For this purpose, an elastic film of thickness h and width B (cross section $A = Bh$) is considered which is peeled-off from a rigid substrate, see Fig. 4.33a. We assume that the separation process takes place under steady state conditions, i.e. the force F (dead load) and the peel angle φ are constant.

When the film is peeled-off by a distance Δa, the point of application of F is displaced in the direction of the force by $\Delta u = \Delta a(1-\cos\varphi+\varepsilon)$. Here, $\varepsilon = F/EA$ is the constant strain in the already debonded part of the film. Hence, the work done by F, i.e. the change of the external potential, is given by $\Delta W = -\Delta\Pi^a = F\Delta u$, while the change of stored elastic energy (internal potential) is $\Delta U = \Delta\Pi^i = F^2/(2EA)\Delta a$. With the fracture surface energy $\Delta\Gamma = \gamma B\Delta a$, the energy balance (cf. (4.98))

$$\Delta U - \Delta W + \Delta\Gamma = 0$$

yields

$$\frac{F^2}{2EA} - F(1-\cos\varphi + \frac{F}{EA}) + \gamma B = 0\,. \tag{4.104}$$

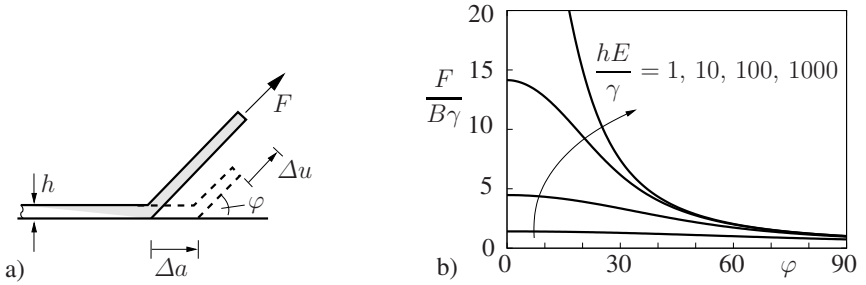

Fig. 4.33 Peel Test

This equation can be resolved for γ to determine the fracture surface energy. Vice versa, F is obtained as

$$F = EA\left(\sqrt{\frac{2\gamma}{Eh} + (1-\cos\varphi)^2} - (1-\cos\varphi)\right) . \tag{4.105}$$

In the special case of an infinitely stiff film ($E \to \infty$), (4.104) leads to $F = \gamma B/(1-\cos\varphi)$. Fig. 4.33b shows in dimensionless form the peel force $F/B\gamma$ as a function of the peel angle φ for different values of dimensionless parameter hE/γ. Accordingly, the necessary force increases with the film stiffness EA and decreases with angle φ.

It should be mentioned that there exists a different interpretation of the energy criterion which is based upon the generalized force concept. Here, $\mathcal{G}$ is understood as a force which acts to drive the crack (= crack extension force). Crack propagation is counteracted by the material resistance $\mathcal{G}_c$ (= crack resistance force). A quasi-static crack growth can only take place if the "equilibrium condition" (4.99) is fulfilled. The latter can also be reformulated in terms of the (generalized) principle of virtual displacements. For this purpose, a virtual (i.e., only thought and infinitesimal) crack advance δA is considered. Then the crack extension force does the virtual work $\mathcal{G}\,\delta A = -\delta \Pi$ and the crack resistance force the work $\mathcal{G}_c \delta A = 2\gamma \delta A = \delta \Gamma$, respectively. Thus equation (4.99) leads to

$$\delta(\Pi + \Gamma) = 0 . \tag{4.106}$$

Finally, a simple model (analogy) of crack propagation shall be discussed. It consists of Coulomb's dry friction of a body on a rough support (Fig. 4.34) where movement of the body is identified with crack propagation. The body remains at rest as long as the acting driving force is less than the limiting adhesive force ($\widehat{=}$ no

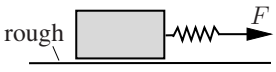

Fig. 4.34 Coulomb's friction as a model of crack propagation

crack propagation for $\mathcal{G} < \mathcal{G}_c$). If the driving force is equal to the limiting adhesive or frictional force, respectively, movement is initiated and further movement under equilibrium conditions takes place ($\widehat{=}$ crack initiation and propagation for $\mathcal{G} = \mathcal{G}_c$).

The energy balance (4.93) is also valid when large inelastic regions are present. In this case, however, the entire plastic region cannot be regarded as the process zone. It is then necessary to separate clearly the energy needed for the fracture process ($\dot{\Gamma}$) and that consumed by inelastic deformations outside the process zone. This can be done, for example, within the framework of a *cohesive zone model* (see Section 5.3). In such a model, the volume of the process zone is neglected and the latter is regarded as a 'process surface' A_P. Outside of the process zone A_P, the material behaves inelastic (e.g., elastic-plastic). The fracture process (separation) takes place along the surface A_P where a material-specific separation law governs the cohesive stresses. According to this separation law, the cohesive stresses accomplish a certain fracture work.

4.6.5 J−integral

With the K-factors and the energy release rate $\mathcal{G}$, we have already introduced parameters which can be used to describe the fracture behavior. Another very useful quantity is the J-integral. Although this parameter in linear fracture mechanics is equivalent to K or $\mathcal{G}$, respectively, it is of outstanding importance. One reason for this is that J in contrast to K and $\mathcal{G}$, can be applied also to inelastic materials (cf. Chapter 5, elastic-plastic fracture mechanics).

4.6.5.1 Conservation integrals of *J* type

We consider a homogeneous, elastic body with strain energy density $U(\varepsilon_{ij})$ and suppose that no volume forces act onto the body ($f_i = 0$). The material can be arbitrarily nonlinear and anisotropic. For simplicity, we further assume small deformations (infinitesimal strains). Then, the J-integral vector is defined as

$$J_k = \int_{\partial V} b_{kj}\, n_j \,\mathrm{d}A = \int_{\partial V} (U\,\delta_{jk} - \sigma_{ij}\, u_{i,k})\, n_j \,\mathrm{d}A \tag{4.107}$$

where ∂V is a closed surface with the outward unit normal vector n_j (Fig. 4.35a). The quantity

$$b_{kj} = U\,\delta_{jk} - \sigma_{ij}\, u_{i,k} \tag{4.108}$$

is called *configurational stress tensor* or ESHELBY'S *stress tensor*, sometimes also *energy-momentum tensor* of elastostatics. It has the remarkable property that its divergence vanishes under the presumed circumstances. This can be shown by differentiating it with respect to x_j and incorporating (1.46), (1.19), (1.25):

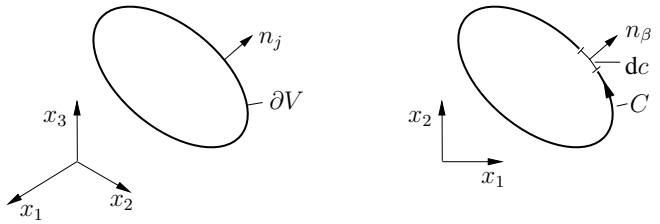

Fig. 4.35 J-Integral

$$\begin{aligned} b_{kj,j} &= \frac{\partial U}{\partial \varepsilon_{mn}} \frac{\partial \varepsilon_{mn}}{\partial x_j} \delta_{jk} - \sigma_{ij,j}\, u_{i,k} - \sigma_{ij}\, u_{i,kj} \\ &= \sigma_{mn}\, u_{m,nk} - \sigma_{ij}\, u_{i,kj} = 0 \,. \end{aligned} \tag{4.109}$$

Hence, according to the divergence theorem

$$J_k = 0 \tag{4.110}$$

for an arbitrary closed surface ∂V containing a defect-free material without singularities or discontinuities of b_{kj}. If the material is inhomogeneous or if V contains discontinuities or singularities as, for example, a crack or point defect, then J_k in general is not zero. Equation (4.110) can be regarded as a special conservation law of elastostatics which advantageously can be applied in various situations.

If we apply (4.110), as an example of elementary strength of materials, to a beam which is solely loaded at its supports A and B by bending moments M and shear forces V, we obtain

$$-\frac{M_A^2}{2EI} + \frac{M_B^2}{2EI} + V_A w'_A + V_B w'_B = 0 \,.$$

Here, EI is the bending stiffness and w' is the derivative of the beam deflection.

There exist two further surface integrals with similar properties as J_k:

$$\begin{aligned} L_k &= \int_{\partial V} \epsilon_{klm} (x_l\, b_{mj} + u_l\, \sigma_{mj})\, n_j \, \mathrm{d}A \,, \\ M &= \int_{\partial V} \left[b_{ij}\, x_i + \frac{1}{2}\, \sigma_{ij}\, (2-\alpha)\, u_i \right] n_j \, \mathrm{d}A \,. \end{aligned} \tag{4.111}$$

Here, L_k is a vector and M is a scalar quantity, ϵ_{klm} is the permutation tensor and $\alpha = 3$ in the three-dimensional and $\alpha = 2$ in the two-dimensional case. Analogous to (4.110), the divergence theorem yields

$$L_k = 0 \tag{4.112}$$

for an arbitrary closed surface ∂V including a defect-free, isotropic, homogeneous material. It can be shown that $J_k = 0$ and $L_k = 0$ apply also for finite deformations. Contrary, the conservation law

$$M = 0 \tag{4.113}$$

is valid only in the special case of a linear elastic material and infinitesimal strains.

For plane problems, the field quantities depend only on x_1 and x_2. In this case, the surface integrals degenerate to contour integrals along a closed curve C (Fig. 4.35b). The J-integral vector is then given by

$$J_\alpha = \int_C (U\,\delta_{\alpha\beta} - \sigma_{i\beta}\,u_{i,\alpha})\,n_\beta\,\mathrm{d}c \tag{4.114}$$

where Greek subscripts attain the values $1, 2$.

4.6.5.2 Generalized forces

We will now discuss the mechanical meaning of the J-integral (4.107) when a discontinuity surface A_D is embedded within V (Fig. 4.36a). Such a discontinuity is present if b_{kj} or one of the terms U, σ_{ij}, or $u_{i,k}$, respectively, experiences a jump across the surface A_D. That is the case when, for instance, A_D is the boundary of an elastic body which is loaded by the boundary tractions $t_i = \sigma_{ij}n_j$, i.e., there is no material on the left-hand side of A_D in Fig. 4.36a. We now assume that the boundary A_D is shifted by a constant increment $\mathrm{d}s_k$ (translation of A_D) while the external load t_i remains unchanged. Such a displacement can be visualized by material being "taken away" or "added". On account of $\mathrm{d}s_k$, the total energy of the system changes by $\mathrm{d}\Pi$. The latter consists of the strain energy

$$\mathrm{d}\Pi^{int} = \int_{A_D} U\,\mathrm{d}s_k\,n_k\,\mathrm{d}A$$

stored in the layer of thickness $\mathrm{d}s_k n_k$ and of the difference of the potentials of external forces

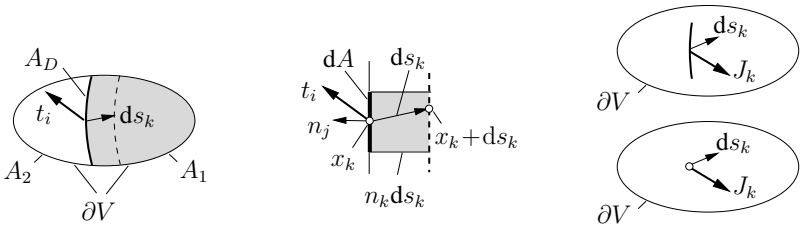

Fig. 4.36 Generalized forces

$$\mathrm{d}\Pi^{ext} = -\int_{A_D} t_i\, u_i(x_k + \mathrm{d}s_k)\,\mathrm{d}A + \int_{A_D} t_i\, u_i(x_k)\,\mathrm{d}A = -\int_{A_D} \sigma_{ij}\, u_{i,k}\,\mathrm{d}s_k\, n_j\,\mathrm{d}A$$

where $u_i(x_k + \mathrm{d}s_k) = u_i(x_k) + u_{i,k}\,\mathrm{d}s_k$ (Fig. 4.36b). Thus, we obtain

$$\mathrm{d}\Pi = \mathrm{d}\Pi^{int} + \mathrm{d}\Pi^{ext} = \mathrm{d}s_k \int_{A_D} (U\,\delta_{jk} - \sigma_{ij}\, u_{i,k})\, n_j\,\mathrm{d}A\,.$$

According to (4.110), the corresponding integral over the closed surface $A_1 + A_D$ is equal to zero: $\int_{A_1} \ldots + \int_{A_D} \ldots = 0$. Consequently, since $\partial V = A_1 + A_2$ with $\int_{A_2} \ldots = 0$, the energy change can be written as

$$\mathrm{d}\Pi = -\mathrm{d}s_k \int_{A_1} (U\delta_{jk} - \sigma_{ij}u_{i,k})n_j\mathrm{d}A = -\mathrm{d}s_k \int_{\partial V} (U\delta_{jk} - \sigma_{ij}u_{i,k})n_j\mathrm{d}A \quad (4.115)$$

or

$$\boxed{\mathrm{d}\Pi = -J_k\mathrm{d}s_k}\,. \quad (4.116)$$

The result (4.116) applies not only for this specific example but it can be generalized to arbitrary discontinuity surfaces (surface defects) and singularities such as dislocations (line defects) and point defects (Fig. 4.35c). In other words, the energy change of an elastic system due to a translation of a discontinuity or singularity (surface, line, or point defect) can be described by means of the "path-independent" integral J_k where the integration domain (surface ∂V) must contain the defect but otherwise is arbitrary. In this energetic sense, J_k can be interpreted as a force acting on the defect. It is referred to as a *generalized force*, *material force*, or as *configurational force*.

Analogous to J_k, the path-independent integral L_k can be interpreted as a *generalized moment* or *configurational moment* acting on the defect. It leads to the energy change of the system when the defect experiences a rotation. Finally, the M-integral characterizes the system's energy change due to a self-similar growth of the defect (e.g., the radial increase of a spherical cavity).

As a simple example, we consider a bi-material bar of constant cross section A under tension (see Fig. 4.37) with Young's modulus undergoing a jump at the interface A_D. The configurational force acting at A_D can be determined by using the dashed integration contour. With the strain energy density $U = \sigma^2/2E$, the force $N = \sigma A$ and Hooke's law $u_{1,1} = \sigma/E$ we obtain

$$\begin{aligned} J_1 &= \left(\frac{N^2}{2EA} - \sigma A\, u_{1,1}\right)_{②} - \left(\frac{N^2}{2EA} - \sigma A\, u_{1,1}\right)_{①} \\ &= \frac{N^2}{2A}\left[\frac{1}{E_1} - \frac{1}{E_2}\right]\,, \\ J_2 &= J_3 = 0 \end{aligned} \quad (4.117)$$

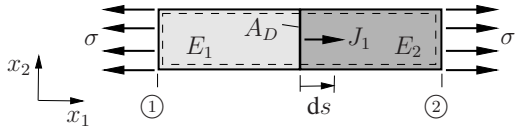

Fig. 4.37 Bi-material bar under tension

where only surfaces perpendicular to x_1 provide a nonzero contribution. Thus, when the interface A_D is shifted by $\mathrm{d}s$, the system undergoes the energy change

$$\mathrm{d}\Pi = -J_1 \mathrm{d}s = \frac{N^2}{2A}\left[\frac{1}{E_2} - \frac{1}{E_1}\right]\mathrm{d}s\ . \tag{4.118}$$

This example can be regarded as a simplified model of a phase transformation in a single crystal. In this case, the interface between two phases (phase boundary) with different elastic properties is displaced.

4.6.5.3 *J*–integral as a crack-tip loading parameter

In what follows, we apply the J-integral vector to the plane problem of a crack with traction-free crack faces (Fig. 4.38a). For this purpose we choose an arbitrary open contour C which starts and ends at the opposite crack faces and encloses the crack tip. Then, according to (4.115) and (4.116), J_1 and J_2, respectively, characterize the energy change (energy release) of the system when the crack faces (= discontinuity line) enclosed by the contour together with the crack tip (= singularity) are shifted in x_1- and x_2-direction, respectively. While a displacement in x_2-direction is only virtually realizable, a displacement $\mathrm{d}a$ in x_1-direction corresponds to a kinematically possible crack advance. The respective contour integral

$$J = J_1 = \int_C \left(U\,\delta_{1\beta} - \sigma_{i\beta}\,u_{i,1}\right) n_\beta\,\mathrm{d}c = \int_C \left(U\,\mathrm{d}y - t_i\,u_{i,x}\,\mathrm{d}c\right) \tag{4.119}$$

is denoted as *J-integral* where the subscript 1 usually is omitted.

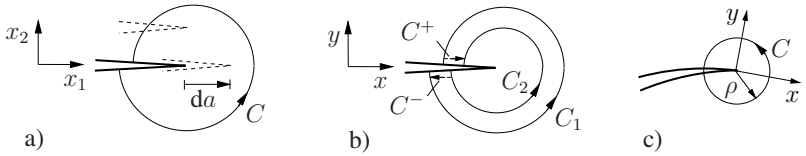

Fig. 4.38 J-integral

In its energetic interpretation, J corresponds the energy release rate during crack growth in an elastic body:

$$J = \mathcal{G} = -\frac{\mathrm{d}\Pi}{\mathrm{d}a} \,. \tag{4.120}$$

Due to this relation, J can be applied as a fracture parameter. A fracture criterion

$$\boxed{J = J_c} \tag{4.121}$$

is fully equivalent to the energy criterion (4.99). In case of a linear elastic material, (4.120) with (4.86) yields

$$J = \frac{1}{E'}(K_I^2 + K_{II}^2) + \frac{1}{2G}K_{III}^2 \tag{4.122}$$

where $E' = E/(1-\nu^2)$ for plane strain and $E' = E$ for plane stress. Hence, (4.121) is equivalent also to the K-concept provided that a pure mode-I or a pure mode-II or a pure mode-III prevails.

The relevance of J as a fracture parameter can be substantiated without utilizing the energy interpretation. For this purpose, we choose two different contours C_1 and C_2 for the determination of J, see Fig. 4.38b. Then, according to (4.110), for the closed contour $C_1 + C^+ + C_2 + C^-$, taking the contour directions into account, $\int_{C_1} \ldots + \int_{C^+} \ldots - \int_{C_2} \ldots + \int_{C^-} \ldots = 0$ holds. The integrals $\int_{C^+} \ldots$ and $\int_{C^-} \ldots$ vanish under the made assumptions (straight traction-free crack faces) since $\int U \mathrm{d}y = 0$ and $t_i = 0$. It finally remains $\int_{C_1} \ldots = \int_{C_2} \ldots$. Thus, the J-integral is *path independent*. It is a characteristic parameter for the state in the vicinity of the crack tip, no matter whether the contour runs through this area or not. It applies in the linear as well as in the nonlinear elastic case.

The path independence of J can advantageously be utilized for the calculation of the crack-tip loading for specific configurations. For instance, it is advisable to choose for numerical calculations with finite elements or boundary elements integration paths sufficiently far away from the crack tip. A cumbersome and precise computation of the field in the crack-tip region then is not necessary. In this manner, the numerical determination of K-factors in many cases is accomplished by use of the relation

$$J = \mathcal{G} = \frac{1}{E'}K_I^2 \tag{4.123}$$

via the calculation of the J-integral.

The path independence of the J-integral is ensured only under the mentioned circumstances. If the crack faces are loaded or the crack is curved, J is in general *path dependent*. Incidentally, this applies to J_2 already for the traction-free straight crack. A "path independent" crack-tip parameter, which characterizes the crack-tip state, is obtained under such circumstances only when the contour is shrunk directly to the crack tip (Fig. 4.38c):

$$J = J_1 = \lim_{\rho \to 0} \int_C (U \mathrm{d}y - t_i u_{i,x} \mathrm{d}c) \,. \tag{4.124}$$

Then, equation (4.122) in the linear elastic case still is valid as before. This can be proofed by choosing a circle as the contour in (4.124) and introducing the crack-tip field solution according to Section 4.2.1. In the same manner, the y-component of the generalized force at the crack tip can be determined:

$$J_2 = -\frac{1}{E'} K_I K_{II} \ . \tag{4.125}$$

The J-integral can also be applied to three-dimensional problems where the crack loading varies along the crack front. As an example, we consider the case of a plane crack with a straight crack front as shown in Fig. 4.39. The generalized force component in x_1-direction, acting on an element Δl of the crack front, is determined appropriately by integrating (4.107) over the whole surface (including the lateral surfaces) of the disc-shaped body, generated by the contour C in the x_1, x_2-plane. In the limit case $\Delta l \to 0$, the integrals over the opposite lateral surfaces cancel each other and only the contour integral (4.119) remains. However, it is now dependent on the position along the crack front: $J = J(x_3)$. With the same arguments as in the plane case, the path independence of J also can be shown here.

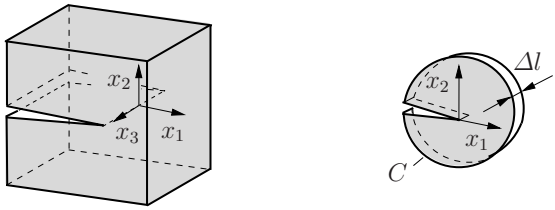

Fig. 4.39 J for three-dimensional crack problem

A necessary prerequisite for the applicability of the J-integral as a crack-tip parameter is an open contour which encloses solely the corresponding crack tip. Contrary, if a closed contour around the whole crack is chosen, then J_k, according to Section 4.6.5.2, describes the energy change of the system on account of a translation of the entire crack. Analogous statements apply to L_k and M for a rotation and a self-similar crack growth, respectively. Such crack "movements", apart from some exceptions, are kinematically impossible. Therefore these integrals are of minor importance in fracture mechanics.

4.7 Small-scale yielding

4.7.1 Plastic zone size, Irwin's crack length correction

In linear elastic fracture mechanics it is assumed that the plastic zone is small compared to the K-dominated region (see Section 4.3). This condition is known as *small-scale yielding*. Here, the plastic zone covers the whole region where the material response deviates from a linear elastic behavior. The determination of the size and shape of this zone in case of a "nonlinear" material is, in general, not an easy task. Therefore, in a first step, we will provide only an estimate on the basis of the elastic crack-tip field solution for mode-I with the material behavior in the plastic zone assumed to be perfectly plastic.

A simple approximation for the extension of the plastic zone ahead of a crack tip goes back to G. IRWIN. It can be obtained by replacing the elastic stress distribution ahead of the crack by the elastic-plastic stress distribution, as depicted in Fig. 4.40a. The latter is assumed to be constant within the plastic zone. In the elastic domain, the stress is represented by the elastic crack-tip field solution which is shifted to the right. We now require that Tresca's yield condition $\sigma_1 - \sigma_3 = \sigma_{_Y}$ is fulfilled at the boundary between the elastic and plastic domain. With $\sigma_1 = \sigma_y = K_I/\sqrt{2\pi x}$ and $\sigma_3 = 2\,\nu\,\sigma_1$ for plane strain and $\sigma_3 = 0$ for plane stress, respectively, this conditions yields

$$\sigma_y = \alpha\sigma_{_Y}\ , \qquad 1/\alpha = \begin{cases} 1-2\nu & \text{(plane strain)} \\ 1 & \text{(plane stress)} \end{cases}$$

and after substitution

$$x_1 = \frac{1}{2\pi}\left(\frac{K_I}{\alpha\sigma_{_Y}}\right)^2 .$$

The distance x_2 can be found from the condition that the forces resulting from the purely elastic stress distribution and from the elastic-plastic stress distribution must be equal:

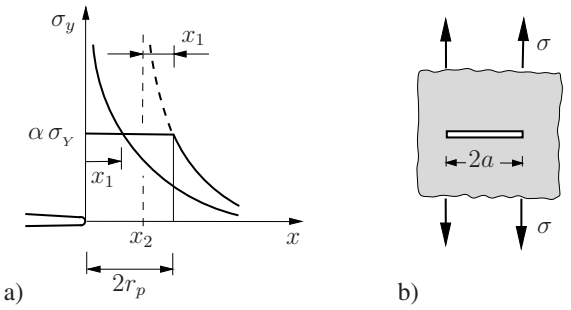

Fig. 4.40 Estimation of plastic zone size

$$\int_0^{\infty} \frac{K_I}{\sqrt{2\pi x}}\,\mathrm{d}x = \alpha\sigma_{_Y}(x_1 + x_2) + \int_{x_1+x_2}^{\infty} \frac{K_I}{\sqrt{2\pi(x - x_2)}}\,\mathrm{d}x\ .$$

From this condition it follows that $x_2 = x_1$. Thus, the length $2r_p = x_1 + x_2$ of the plastic zone is given by

$$2r_p = \begin{cases} \dfrac{1}{3\pi}\left(\dfrac{K_I}{\sigma_{_Y}}\right)^2 & \text{(plane strain)}\ , \\[2ex] \dfrac{1}{\pi}\left(\dfrac{K_I}{\sigma_{_Y}}\right)^2 & \text{(plane stress)} \end{cases} \tag{4.126}$$

Here, for plane strain the value $\alpha = \sqrt{3}$, i.e., $\nu = 0.21$ has been chosen. According to (4.126), for the same crack loading (i.e., same K_I) the plastic zone in plane strain is significantly smaller than in plane stress. This is confirmed also experimentally.

Equation (4.126) provides the opportunity to rewrite the size condition (4.77), which must be fulfilled for the determination of a valid fracture toughness K_{Ic}, in a different form. Assuming a plane strain state, we obtain for the critical case at crack initiation ($K_I = K_{Ic}$) by substituting (4.126):

$$r_{pc} \lessapprox 0.02\ \{a,\, W-a,\, B\}\ . \tag{4.127}$$

This relation provides an impression of the admissible size of the plastic zone within the framework of linear fracture mechanics. Thereby, the right-hand side can be extended by possibly appearing further geometric parameters.

The length $x_2 = r_p$ characterizes the translation of the elastic crack-tip field due to plastic deformation. Exactly the same crack-tip field occurs in the purely elastic case if the crack is fictitiously extended by r_p. Having this in mind, G. IRWIN suggested to account for yielding in the fracture criterion by using an *effective crack length* which is corrected by r_p:

$$a_{\text{eff}} = a + r_p\ . \tag{4.128}$$

This approach is called *Irwin's crack length correction*. For example, when (4.128) is applied to the crack shown in Fig. 4.40b, we obtain with $K_I = \sigma\sqrt{\pi a}$ and (4.126) for a plane stress state

$$a_{\text{eff}} = a + \frac{1}{2\pi}\left(\frac{K_I}{\sigma_{_Y}}\right)^2 = a\left[1 + \frac{1}{2}\left(\frac{\sigma}{\sigma_{_Y}}\right)^2\right]\ . \tag{4.129}$$

Introducing this result into the K-criterion, the critical stress follows as

$$\sigma_c = \frac{K_{Ic}}{\sqrt{\pi a_{\text{eff}}}} = \frac{K_{Ic}}{\sqrt{\pi[a + (1/2\pi)(K_{Ic}/\sigma_{_Y})^2]}}\ . \tag{4.130}$$

4.7.2 Qualitative remarks on the plastic zone

Precise statements on the shape of the plastic zone as well as on the stresses and deformations appearing in it can be made only after the solution of the corresponding elastic-plastic boundary value problem. Such a solution, even for simple material models (e.g., elastic - perfectly plastic) and plane strain (or plane stress) problems, is possible only by using numerical methods.

A rough impression of the shape of the plastic zone can be obtained when the boundary of this zone is identified with the contour along which the stresses of the elastic crack-tip field just fulfill the yield condition. In this manner, taking for instance the von Mises yield condition (1.77b)

$$(\sigma_1 - \sigma_2)^2 + (\sigma_2 - \sigma_3)^2 + (\sigma_3 - \sigma_1)^2 = 6k^2 = 2\sigma_Y^2 \ ,$$

and the principal stresses (4.23), (4.24) for mode I, the contour is determined as

$$r_p(\varphi) = \frac{K_I^2}{2\pi\sigma_Y^2} \cos^2\frac{\varphi}{2} \begin{cases} [3\sin^2\frac{\varphi}{2} + (1-2\nu)^2] & \text{plane strain} \\ [3\sin^2\frac{\varphi}{2} + 1] & \text{plane stress} \ . \end{cases} \tag{4.131}$$

For comparison, the contours resulting from von Mises' and from Tresca's yield condition are displayed in Fig. 4.41a where Poisson's ratio $\nu = 1/4$ has been chosen for plane strain. Both hypotheses show a distinct difference in size between plane strain and plane stress.

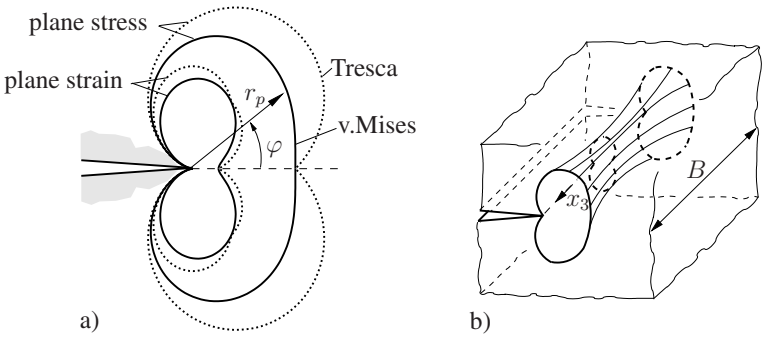

Fig. 4.41 Plastic zone

The result (4.131) forms the basis of the *dog bone model* for the shape of the plastic zone in "thick" plates ($B \gg r_p$) which is depicted in Fig. 4.41b. Here, it is assumed that in the surrounding of the crack front, approximately a plane strain state dominates in the interior ($\varepsilon_{33} \approx 0$), whereas the state at the surface approaches the plane stress state ($\sigma_{3i} \approx 0$). But three-dimensional numerical investigations show

that the size of the plastic zone at the surface generally is overestimated by this model.

In plane strain, according to (4.25), the maximum shear stresses occur predominantly in cross sections with the normal vector perpendicular to x_3. This suggests a slip mechanism for plastic deformation as shown in Fig. 4.42a. Corresponding slip processes lead to a blunting of an originally sharp crack tip and as a consequence to a "crack opening". Contrary to plane strain, $\tau_{\max}$ in plane stress occurs in cross sections under $45°$ to the x_1, x_2-plane. Accordingly, the slip mechanism as shown in Fig. 4.42b will take place in "thin" plates ($r_p \gg B$). This mechanism restricts the extension of the plastic zone in x_2-direction to the size of the plate thickness and promotes its strip-like evolution in x_1-direction (Fig. 4.42c). This mechanism is also responsible for the necking ahead of the crack tip which can be observed in this case.

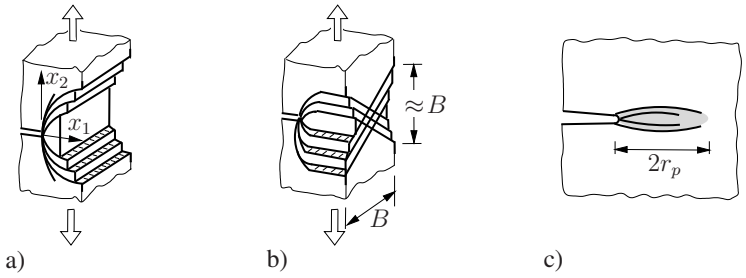

Fig. 4.42 Slip mechanism: a) plane strain, b) and c) plane stress

As has been discussed in Section 4.6, the fracture toughness K_{Ic} is directly connected with the energy needed for the fracture process: $K_{Ic}^2 \sim \mathcal{G}_c$. The latter includes the entire energy needed for the deformation process within the plastic zone. Herewith, the dependency of the fracture toughness on the thickness B, as shown in Fig. 4.23a, qualitatively can be explained. For $B \gg r_p$ (thick samples), approximately plane strain dominates along the crack front which allows only a constrained plastic deformation. This corresponds to a low energy dissipation and consequently to a low K_{Ic}. In contrast, for $B \ll r_p$ (thin samples), plane stress dominates with a larger plastic zone and lower deformation constraint. As a consequence, a higher plastic energy dissipation and therefore also a higher K_{Ic}-value occurs.

4.8 Stable crack growth

We consider a straight crack under pure mode-I conditions. At crack initiation and subsequent crack growth the fracture criterion must be fulfilled which, according to (4.99), may be expressed as $\mathcal{G} = \mathcal{G}_c$. The crack resistance $\mathcal{G}_c$ is rarely constant, but in most cases, as shown in Fig. 4.43a, a monotonously increasing function of the

crack advance $\Delta a = a - a_0$:

$$\mathcal{G}_c = R(\Delta a) \ . \tag{4.132}$$

The function $R(\Delta a)$ is known as the *crack-resistance curve* or the so-called *R-curve*. For instance, the crack resistance of a metal, starting from the initiation value $\mathcal{G}_{ci}$ at initial crack length a_0, may increase up to a multiple of $\mathcal{G}_{ci}$ during crack growth of one or two millimeters. One of the reasons for this is the "motion" of the plastic zone in the course of crack advance. During this process, the material particles experience quite complex stress histories (loading, unloading) and the size and shape of the plastic zone change. A detailed description of this process can be omitted when determining the $R(\Delta a)$-curve from experiments. The R-curve then is regarded as a material-specific function which uniquely characterizes quasi-static crack growth.

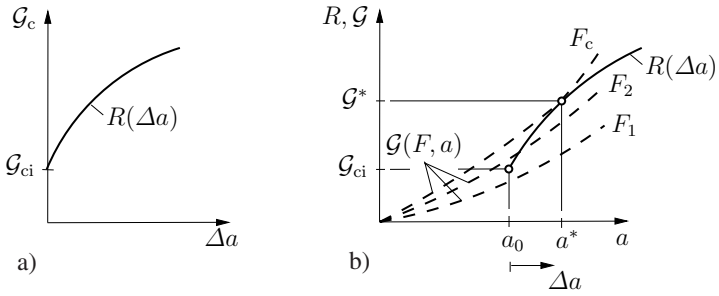

Fig. 4.43 Stable crack growth

Due to the rise of R, it is possible to increase the crack load beyond its initiation value. As a consequence, the crack growth is determined through the equilibrium condition

$$\mathcal{G}(F,a) = R(\Delta a) \tag{4.133}$$

between crack extension force and crack resistance force (Fig. 4.43b). Here, the parameter F denotes the dependence of the crack extension force on the external load. The equilibrium state is *stable* under fixed loading condition, provided that the crack resistance increases more rapidly with increasing crack length than the crack extension force:

$$\left.\frac{\partial \mathcal{G}}{\partial a}\right|_{F=\text{const}} < \frac{\mathrm{d}R}{\mathrm{d}a} \ . \tag{4.134}$$

Under these circumstances, the external load must be increased to drive the crack forward. This is indicated in Fig. 4.43b by the family of $\mathcal{G}$-curves for different external loads ($F_1 < F_2 < \ldots$). The limit of *stable crack growth* is reached when the critical condition

$$\left.\frac{\partial \mathcal{G}}{\partial a}\right|_{F=\text{const}} = \frac{\mathrm{d}R}{\mathrm{d}a} \tag{4.135}$$

is met. When the load is further increased, the equilibrium condition (4.133) is no longer fulfilled and the crack starts to propagate dynamically. The critical load F_c and the corresponding value $\mathcal{G}^*$ depend on the crack geometry and the loading type as well as on the R-curve.

The statements made above, can also be derived in a more formal manner. For this purpose we assume that the system's "total energy" Π^* consist of the total potential Π and the fracture surface energy Γ, i.e., $\Pi^*(a) = \Pi(a) + \Gamma(a)$ (cf. Section 4.6.4). The equilibrium state of the system is characterized by the condition $\mathrm{d}\Pi^*/\mathrm{d}a = 0$. With $\mathcal{G} = -\mathrm{d}\Pi/\mathrm{d}a$ and $R = \mathrm{d}\Gamma/\mathrm{d}a$ this corresponds to equation (4.133). Information about the stability is provided by the second derivative. The equilibrium state of the system is stable for $\mathrm{d}^2\Pi^*/\mathrm{d}a^2 > 0$ while at $\mathrm{d}^2\Pi^*/\mathrm{d}a^2 = 0$ the transition to instability occurs. These are exactly the statements (4.134) and (4.135).

Stable crack growth can not only be investigated on the basis of the energy concept. Because of the equivalence of K, $\mathcal{G}$, and J in linear fracture mechanics, it can be done on the basis of any of these parameters.

In what follows, we will determine $\mathrm{d}\mathcal{G}/\mathrm{d}a$ for the body depicted in Fig. 4.44 which contains a crack and is loaded via a spring by a given displacement u_F. With the compliances $C(a)$ and C_F of the body and spring, the following relations between the acting force and the displacements hold:

$$F = \frac{u_F}{C(a) + C_F} , \qquad u_P = CF = \frac{C}{C + C_F}\, u_F . \tag{4.136}$$

Therefore, the potential is

$$\Pi = \frac{1}{2} F u_P + \frac{1}{2} F(u_F - u_P) = \frac{1}{2}\, \frac{u_F^2}{C(a) + C_F} ,$$

and by differentiation we obtain

$$\mathcal{G} = -\frac{\mathrm{d}\Pi}{\mathrm{d}a} = \frac{u_F^2}{2}\, \frac{C'}{(C + C_F)^2} , \tag{4.137a}$$

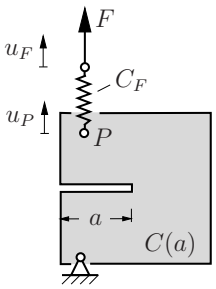

Fig. 4.44 Stability of crack growth

$$\frac{\mathrm{d}\mathcal{G}}{\mathrm{d}a} = -\frac{\mathrm{d}^2\Pi}{\mathrm{d}a^2} = \frac{u_F^2}{2}\,\frac{C''(C+C_F) - 2C'^2}{(C+C_F)^3} = \frac{F^2}{2}\left[C'' - \frac{2C'^2}{C+C_F}\right], \quad (4.137b)$$

where $C' = \mathrm{d}C/\mathrm{d}a$. Thus, not solely the properties of the body but also the type of the loading (C_F) enter the quantity $\mathrm{d}\mathcal{G}/\mathrm{d}a$ which essentially determines the stability of crack growth.

From (4.137b), we can derive results for the special cases $C_F = 0$ and $C_F \to \infty$. According to (4.136), the former corresponds to a loading by a displacement u_F prescribed in point P while the latter is related to a load which is independent of $C(a)$ (i.e., dead loading). We obtain

$$\frac{\mathrm{d}\mathcal{G}}{\mathrm{d}a} = \frac{F^2}{2}\begin{cases} C'' - \dfrac{2C'^2}{C} & \text{for } C_F = 0\,, \\[2ex] C'' & \text{for } C_F \to \infty\,. \end{cases} \quad (4.138)$$

Thus, for an increasing dead load of the body in point P (i.e., $C_F \to \infty$), the instability point is always reached earlier than for a loading by a prescribed displacement (i.e., $C_F = 0$).

As an example, the DCB specimen shown in Fig. 4.29 shall be considered. Introducing the compliance $C(a) = 8a^3/EBh^3$ (cf. Section 4.6.3), from (4.138) we obtain

$$\frac{\mathrm{d}\mathcal{G}}{\mathrm{d}a} = \begin{cases} -\dfrac{48F^2a}{EBh^3} & \text{for } C_F = 0\,, \\[2ex] +\dfrac{24F^2a}{EBh^3} & \text{for } C_F \to \infty\,. \end{cases} \quad (4.139)$$

Hence, for loading by prescribed displacements ($C_F = 0$), crack growth is always stable.

4.9 Mixed-mode loading

Until now, essentially fracture criteria and crack problems for pure mode-I loading have been considered. In such a case, we could assume that crack advance occurs in tangential direction at the crack tip, i.e., a straight crack propagates in its longitudinal direction. Now we want to discuss fracture criteria for *mixed-mode loading* where mode-I and mode-II are superimposed while mode III should not be present. Under such circumstances the critical state (onset of crack growth) is determined by the influence of both modes and crack propagation starts under a certain angle to the tangent at the crack tip (Fig. 4.45). For brittle materials, in most cases a propagation direction is observed where the new crack faces open as under pure mode-I loading.

If mode-I and mode-II prevail, the state at the crack tip can, within the scope of linear fracture mechanics, be characterized by the stress intensity factors K_I and K_{II}. A mixed-mode fracture criterion then can generally be expressed as (cf.

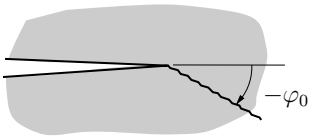

Fig. 4.45 Crack growth under mixed-mode loading

(4.29)):

$$f(K_I, K_{II}) = 0 \; . \tag{4.140}$$

Similar to the failure hypotheses in Chapter 2, it is possible to formulate arbitrarily many fracture criteria of the type (4.140). In fact, there exist a number of hypotheses which, depending on the material class and the dominating micro-mechanism, respectively, are more or less in good agreement with experimental results. In what follows, some frequently used fracture criteria are discussed which also make statements about the crack growth direction.

Energy criterion

According to (4.87) or (4.99), crack growth is initiated at

$$\mathcal{G} = \mathcal{G}_c \tag{4.141}$$

where $\mathcal{G} = (K_I^2 + K_{II}^2)/E'$. If we introduce the fracture toughness for mode I by means of $\mathcal{G}_c = K_{Ic}^2/E'$, equation (4.141) can be written as

$$K_I^2 + K_{II}^2 = K_{Ic}^2 \; . \tag{4.142}$$

This criterion is based on the assumption that crack propagation in any case occurs in tangential direction, independently of the magnitude of mode-II. For an isotropic material this is acceptable with sufficient accuracy only for $K_{II} \ll K_I$ or if the crack growth direction is prescribed by a "weakened zone" as for instance an interface. Thus, the criterion (4.142) is restricted to very special applications.

Criterion of maximum circumferential stress

This criterion dates back to F. ERDOGAN and G.C. SIH (1963) and is based on two assumptions: (a) the crack propagates in radial direction φ_0, perpendicular to the maximum circumferential stress $\sigma_{\varphi\max}$ and (b) crack advance is initiated when the near field stress $\sigma_{\varphi\max} = \sigma_\varphi(\varphi_0)$ at a distance r_c in front of the crack tip reaches the same critical value as in pure mode I. As a consequence, for the circumferential stress (see Section 4.2.1 and 4.2.2)

$$\sigma_\varphi = \frac{1}{4\sqrt{2\pi r_c}} \left[K_I \left(3\cos\frac{\varphi}{2} + \cos\frac{3\varphi}{2} \right) - K_{II} \left(3\sin\frac{\varphi}{2} + 3\sin\frac{3\varphi}{2} \right) \right] ,$$

the following conditions apply:

$$\left. \frac{\partial \sigma_\varphi}{\partial \varphi} \right|_{\varphi_0} = 0 \, , \qquad \sigma_\varphi(\varphi_0) = \frac{K_{Ic}}{\sqrt{2\pi r_c}} \, .$$

They lead to the equations

$$\begin{aligned} K_I \sin\varphi_0 + K_{II} \left(3\cos\varphi_0 - 1 \right) &= 0 \, , \\ K_I \left(3\cos\frac{\varphi_0}{2} + \cos\frac{3\varphi_0}{2} \right) - K_{II} \left(3\sin\frac{\varphi_0}{2} + 3\sin\frac{3\varphi_0}{2} \right) &= 4K_{Ic} \, . \end{aligned} \tag{4.143}$$

From the first one the deflexion angle φ_0 is obtained. Introducing this, the second equation determines when failure occurs. The corresponding results for $K_I, K_{II} \geq 0$ are shown in Fig. 4.46a,b. For example, the deflexion angle for pure mode II ($K_I = 0$) results as $\cos\varphi_0 = 1/3$, i.e., $\varphi_0 = -70.6°$ and the critical load is given by $K_{II} = \sqrt{3/4}\, K_{Ic} = 0.866\, K_{Ic}$.

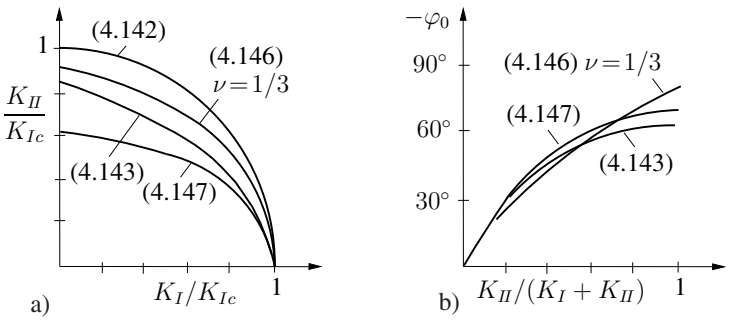

Fig. 4.46 Mixed-mode loading: a) fracture criteria, b) crack deflexion angle

S–criterion

The strain energy density in the vicinity of the crack tip for plane strain can be expressed with the crack-tip field solution (4.14) and (4.15) as

$$\begin{aligned} U &= \frac{1}{4G} \left[(1-\nu)(\sigma_x^2 + \sigma_y^2) - 2\nu\sigma_x\sigma_y + 2\tau_{xy}^2 \right] \\ &= \frac{1}{r} \left(a_{11} K_I^2 + 2a_{12} K_I K_{II} + a_{22} K_{II}^2 \right) = \frac{S}{r} \end{aligned} \tag{4.144}$$

where

$$\begin{aligned} 16\pi G a_{11} &= (3 - 4\nu - \cos\varphi)(1 + \cos\varphi) \,, \\ 16\pi G a_{12} &= 2\sin\varphi\,(\cos\varphi - 1 + 2\nu) \,, \\ 16\pi G a_{22} &= 4(1-\nu)(1-\cos\varphi) + (1+\cos\varphi)(3\cos\varphi - 1) \,. \end{aligned} \tag{4.145}$$

G.C. SIH (1973) assumed that (a) the crack grows into that radial direction φ_0 where the strength S of the singular strain energy density has a minimum and (b) the crack starts growing when $S(\varphi_0)$ reaches a material specific critical value S_c. The latter can be replaced by the fracture toughness K_{Ic} of pure mode I (then $\varphi_0 = 0$): $S_c = a_{11}(\varphi_0 = 0) K_{Ic}^2$. Hence, the directional criterion and the fracture criterion read

$$\begin{gathered} \left.\frac{\mathrm{d}S}{\mathrm{d}\varphi}\right|_{\varphi_0} = 0 \qquad \text{with} \qquad \left.\frac{\mathrm{d}^2 S}{\mathrm{d}\varphi^2}\right|_{\varphi_0} > 0 \,, \\ \left[a_{11} K_I^2 + 2a_{12} K_I K_{II} + a_{22} K_{II}^2\right]_{\varphi_0} = \frac{1-2\nu}{4\pi G}\, K_{Ic}^2 \,. \end{gathered} \tag{4.146}$$

The deflexion angle and the failure curve are depicted in Fig. 4.46. If we choose $\nu = 1/3$, from this hypothesis for pure mode II the deflexion angle $\cos\varphi_0 = 1/9$, i.e., $\varphi_0 = -83.62°$ results, and the critical loading is $K_{II} = \sqrt{9/11}\; K_{Ic} = 0.905\; K_{Ic}$.

The S-criterion can be modified in various ways. For instance, it might be appropriate to start not from the strain energy density U but from the volumetric strain energy density U_V or from the distortional energy density U_G. But we will not go into this in more detail.

Kink model

This model starts from the assumption that the crack tip under mixed mode loading in the initial phase forms a small kink within the K_I, K_{II}-dominated region (Fig. 4.47). In the second phase, when the kink becomes critical under a certain load, crack propagation starts in tangential direction from the kink tip. Physically, the kink can be regarded as a simplified model for possible radial micro cracks in the vicinity of the macroscopic crack tip. At the tip of the kink the field is again singular and it can be characterized by the stress intensity factors k_I, k_{II}. M.A. HUSSAIN, S.L. PU, and I. UNDERWOOD (1972) assumed that (a) the kink is formed at an angle φ_0 for which the respective energy release rate $\mathcal{G} = (k_I^2 + k_{II}^2)/E'$ is maximum and (b) the crack starts to grow when this energy release rate reaches a critical value $\mathcal{G}_c$. Thus, the directional condition and the failure condition read

$$\left.\frac{\mathrm{d}\mathcal{G}}{\mathrm{d}\varphi}\right|_{\varphi_0} = 0 \,, \qquad \mathcal{G}(\varphi_0) = \mathcal{G}_c \tag{4.147}$$

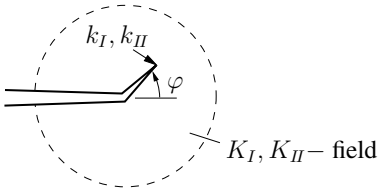

Fig. 4.47 Kink model

where $\mathcal{G}_c = K_{Ic}^2/E'$. The solution of these equations requires the determination of $k_I(\varphi)$, $k_{II}(\varphi)$ from the solution of the corresponding boundary value problem. This is possible only with numerical methods. Figure 4.46 shows the results for the deflexion angle and the failure curve. An approximate solution for $k_I(\varphi)$, $k_{II}(\varphi)$ can be written as

$$k_I \simeq C_{11}K_I + C_{12}K_{II} + D_1\sigma_T\sqrt{\pi\varepsilon}\,, \quad k_{II} \simeq C_{21}K_I + C_{22}K_{II} + D_2\sigma_T\sqrt{\pi\varepsilon} \tag{4.148a}$$

where ε denotes the length of the kink and

$$\begin{aligned} C_{11} &= \frac{1}{4}\left(3\cos\frac{\varphi}{2} + \cos\frac{3\varphi}{2}\right), & C_{12} &= -3\cos^2\frac{\varphi}{2}\sin\frac{\varphi}{2}\,, \\ C_{22} &= \frac{1}{4}\left(\cos\frac{\varphi}{2} + 3\cos\frac{3\varphi}{2}\right), & C_{21} &= \sin\frac{\varphi}{2}\cos^2\frac{\varphi}{2}\,, \\ D_1 &= \sin^2\varphi\,, & D_2 &= -\sin\varphi\cos\varphi\,. \end{aligned} \tag{4.148b}$$

The terms in (4.148a) which represent the contribution of the T-stress σ_T in many cases can be neglected. But they play a role in situations where the terms related to K_I, K_{II} more or less cancel each other.

The fracture criteria discussed above do not account for the microscopic failure mechanisms. These microscopic mechanisms can be quite different, depending on whether mode I or mode II dominates, which in turn may significantly affect the macroscopic fracture behavior. Therefore, the applicability of these criteria is restricted and they may not be overstrained regarding their physical interpretation. For instance, the mentioned criteria often fail for a pure mode-II loading. Due to the missing crack opening, the microscopic asperities of the opposite crack surfaces get in contact, which changes the state at the crack-tip. The actual crack-tip loading is then smaller than that expressed by K_{II} which is determined under the assumption of traction-free crack faces. In order to ensure traction-free crack surfaces, a certain minimum crack opening hence should always exist ($K_I > 0$). That means that all mentioned fracture criteria basically are physically meaningful only for $K_I \geq 0$. If crack closure occurs, a mode-I crack-tip field no longer exists and a pure mode-II crack-tip loading ($K_I = 0$) then is present. A typical example for this are cracks under a combined pressure and shear loading (i.e., shear cracks). Due to the mentioned friction effects, the fracture criteria are hardly applicable but the directional criteria for the crack deflexion angle under pure mode-II still remain valid.

Because the agreement of the various hypotheses with experimental results may be quite different for different materials, it has been proposed not to insist on a physically motivated fracture hypothesis, but to simply adopt a formal approach. One possibility for this is the following representation of the fracture criterion:

$$\left(\frac{K_I}{K_{Ic}}\right)^{\mu} + \left(\frac{K_{II}}{K_{IIc}}\right)^{\nu} = 1 \tag{4.149}$$

where the four parameters K_{Ic}, K_{IIc}, μ, and ν must be determined from experiments.

It should be noted that the different hypotheses differ only slightly from one another as long as the mode-II part is small ($K_{II} \ll K_I$). This applies especially for the deflexion angle φ_0. The criteria (4.143), (4.146), and (4.147) then all lead to the same result:

$$\varphi_0 \approx -2\,\frac{K_{II}}{K_I}\,. \tag{4.150}$$

As a simple example of a mixed mode loading, we consider an inclined crack under uniaxial tension (Fig. 4.48a). In this case the stress intensity factors are

$$K_I = \sigma\sqrt{\pi a}\,\cos^2\gamma\,, \qquad K_{II} = \sigma\sqrt{\pi a}\,\sin\gamma\cos\gamma\,. \tag{4.151}$$

If the criterion of maximum circumferential stress according to (4.143) is applied one obtains for the deflexion angle φ_0 and the critical stress σ_c the results shown in Fig. 4.48b,c. It is remarkable that σ_c varies only a little for sufficiently small γ.

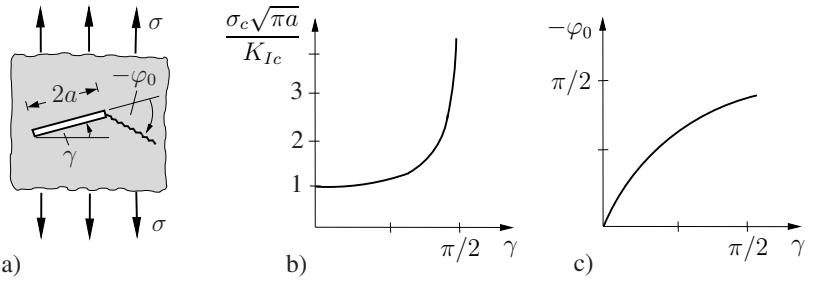

Fig. 4.48 Inclined crack under uniaxial tension

4.10 Crack initiation at cavities and notches

At *stress concentrators* like cavities, notches or corners, generally high stresses occur that frequently lead to the formation of a crack. When the maximum stresses are finite, as e.g. at an elliptic cavity (cf. Section 4.4.5) or at a blunt notch with fi-

nite notch radius, i.e. when no stress singularities are present, it seems reasonable to treat crack initiation by applying a classical failure hypothesis, see Chapter 2. However, the applicability of classical failure hypotheses turns out to be limited since they cannot describe the *size effect* which experimentally can be observed. Here, under size effect the dependence of the failure stress on the absolute size of the stress concentrator is understood. For example, it is well known that the maximum stress $\sigma_{\max}$ at the boundary of a circular cavity in an infinite plate under uniaxial tension σ is three times the applied stress: $\sigma_{\max} = 3\sigma$. According to the maximum stress hypothesis (2.2) failure should occur, independent on the size of the cavity, if the condition $\sigma_{\max} = \sigma_t$ is fulfilled, i.e. for an applied stress $\sigma = \sigma_t/3$, where σ_t is the tensile strength of the material. In a good approximation this is in fact the case for sufficiently large cavities. But when the cavity gets smaller and smaller, the tensile stress σ necessary for failure increases more and more until it reaches in the limit case of a microscopic cavity exactly the tensile strength σ_t. The reason for this apparently paradox is found in the microstructure of the material which generates local fluctuations of the stress state on the microscale, see also Chapter 8. When the characteristic size of the stress concentrators gets smaller and finally attains the characteristic size of the microstructure, the stress concentrator itself becomes an element of the microstructure. Then, from a macroscopic point of view, the difference gets lost between the stress fluctuations due to the microstructure and the disturbance of the stress state on account of the stress concentrator. In other words, the stress concentration at the microscopic cavity disappears in the microscopic "noise" of the stress state - the microscopic cavity is macroscopically no longer visible. This analogously applies for blunt notches whose absolute size is self-similarly reduced.

At V-shaped sharp notches or sharp corners, in any case stress singularities are present whose strength is characterized by a generalized stress intensity factor, i.e. for example in mode I by a K_I^* factor, see Section 4.2.1. Here, the direct application of classical failure hypotheses is not practical. They predict, on account of the stress singularity, failure even for the smallest external loading which contradicts experimental evidence. For this reason, in analogy to crack initiation, the usage of failure criteria of the type $K_I^* = K_{Ic}^*$ have been proposed. It is a considerable disadvantage of such an approach that the fracture toughness K_{Ic}^*, when generalized in this manner, depends on the opening angle of the notch and therefore represents no intrinsic material parameter. An additional disadvantage is, that in contrast to a crack, no relation between such a generalized K^*-concept and an energy criterion exists. In fact, it can be shown that the energy release rate $\mathcal{G}$ at crack initiation vanishes for a sharp as well as for a blunt notch. For this purpose we assume, similar to Section 4.6.2, that a small crack of length Δa evolves from the notch. We can determine the induced energy change from (4.83) simply by replacing the stresses ahead of a crack by the corresponding stresses ahead of the sharp notch (i.e. in mode I by (4.20)) or the blunt notch. For $\Delta a \to 0$ this leads in any case (except for a crack) to $\mathcal{G} = 0$.

A crack initiation criterion, that does not show the mentioned disadvantages, was proposed by D. LEGUILLON. It starts from the assumption that at initiation a crack of finite length Δa_c spontaneous develops. This happens if two necessary

conditions are fulfilled. First, a stress criterion $F(\sigma_{ij}) \geq 0$ must be satisfied over the entire length Δa_c for which usually the maximum stress criterion (2.2) in form of

$$\sigma_1 \geq \sigma_t \tag{4.152a}$$

is taken. Additionally, the energy criterion

$$\mathcal{G}^* = \mathcal{G}_c \tag{4.152b}$$

must be fulfilled where

$$\mathcal{G}^* = -\frac{\Delta \Pi}{\Delta a_c} \tag{4.153}$$

and $\mathcal{G}_c$ are the *incremental energy release rate* and the crack resistance, respectively.

The so-called *hybrid criterion* (4.152a,b) correctly describes failure in the two limit cases of a crack and of a homogeneous stress state. In case of a crack the stress criterion (4.152a) is always satisfied and crack initiation is controlled by the energy criterion (4.152b). In the other limit case of a homogeneous stress state in a sufficiently large body, failure is controlled solely by the stress criterion (4.152a). An advantage of LEGUILLON'S criterion is, that only the two well-known material parameters σ_t and $\mathcal{G}_c$ are involved. It also has been shown that the criterion can describe size effects in a satisfying manner. However, the practical application is not as simple as it looks at first glance and in most cases is only possible by using numerical methods like the FEM. The reason is that the initially unknown magnitude and direction of Δa_c as well as the critical external load must be iteratively determined for a certain notch configuration.

On account of the two involved material parameters, LEGUILLON'S criterion belongs to the class of *two-parameter criteria*. Furthermore, because it assumes a finite crack advance at initiation, the term *finite fracture mechanics* is sometimes used. There exist a number of other two-parameter criteria. Also the cohesive zone models can be regarded as two-parameter models if the cohesive law is characterized by solely two parameters. This model will be discussed in more detail in Section 5.3.

4.11 Fatigue crack growth

When a component containing a crack is loaded statically, no crack growth takes place as long as the crack length or the loading, respectively, remains below a critical value. In contrast, when the loading is oscillating, crack growth in "small steps" can be observed already for loading amplitudes far below the critical static load (cf. Section 3.2.1). Such a crack growth is called *fatigue crack growth*. Usually, fatigue crack growth is characterized by the *crack growth rate* $\mathrm{d}a/\mathrm{d}N$ where N is the number of load cycles. The physical reasons for fatigue crack growth are the complex inelastic processes occurring during periodic loading inside the process zone (plastic zone). In metals, a material particle in this zone experiences cyclic plastic deformation under tension and compression (plastic hysteresis). With the deforma-

tion also the eigenstress fields vary and the damage of the material increases, e.g., by void formation and growth, until total separation takes place.

In what follows, we restrict the attention to a cyclic mode-I loading. If the conditions of linear fracture mechanics are fulfilled (small-scale yielding), fatigue crack growth can be described by use of the K-concept. A periodic loading then is characterized by a periodically varying stress intensity factor with the difference ΔK between maximum and minimum K-factor (Fig. 4.49a) denoted as the *cyclic stress intensity factor*. Measurements of the crack growth rate for a material in dependence of ΔK lead to results as qualitatively shown in Fig. 4.49b. Below a threshold value ΔK_0, the crack does not propagate. This value usually is smaller than $K_{Ic}/10$. The middle part of the curve between ΔK_0 and K_{Ic}, in a logarithmic representation, can be approximated by a straight line with slope m. Accordingly, crack growth is empirically described by the equation

$$\frac{\mathrm{d}a}{\mathrm{d}N} = C\,(\Delta K)^m \tag{4.154}$$

which after P.C. PARIS (1963) is called *Paris' law*. The constants C and m depend on the material and various influence factors such as temperature, environmental medium, or the mean stress intensity factor. For metals, exponents within the range $m \approx 2 \ldots 4$ are typical.

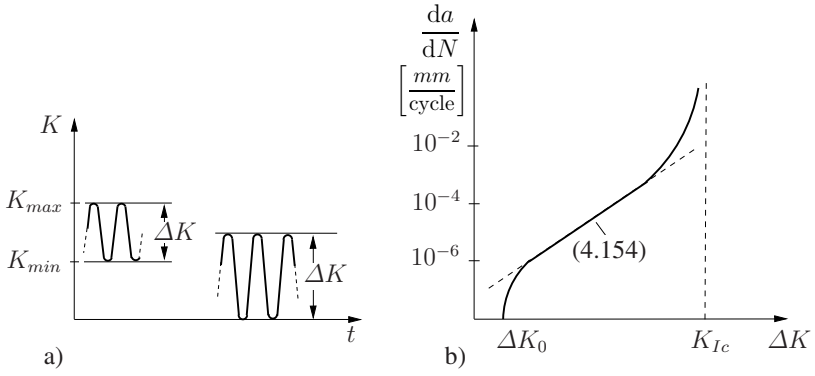

Fig. 4.49 Fatigue crack growth

There are many different approaches which allow to fit experimental data better than (4.154). Among others, R.G. FOREMAN's representation (1967)

$$\frac{\mathrm{d}a}{\mathrm{d}N} = \frac{C\,(\Delta K)^m}{(1-R)K_{Ic} - \Delta K} \tag{4.155}$$

sometimes is applied where $R = K_{\min}/K_{\max}$. Furthermore, there exist a number of models for a simplified description of the fatigue crack propagation process which in detail is very complex. One of these models, for example, starts from the assumption

that the crack advance during each cycle is proportional to the size of the plastic zone. Since $r_p \propto K_I^2$ (see (4.126)), this leads to $\mathrm{d}a/\mathrm{d}N \propto (\Delta K)^2$, i.e., to an exponent of $m = 2$.

Knowledge of the crack growth rate $\mathrm{d}a/\mathrm{d}N$ allows to predict the life time of a component containing a crack. For this purpose, the number N_c of cycles is determined until the crack reaches its critical length a_c. As an example of the procedure, we consider a component which is periodically loaded by a constant cyclic stress $\Delta\sigma$. This leads to a cyclic stress intensity factor $\Delta K = \Delta\sigma\sqrt{\pi a}\, F(a)$ where $F(a)$ depends on the geometry of the component including the actual crack configuration (cf. Section 4.4.1, Table 4.1). If Paris' law (4.154) is used, we obtain by integration the number of cycles necessary for a crack growth from the initial length a_i to the length a:

$$N(a) = \frac{1}{C\,(\Delta\sigma)^m} \int_{a_i}^{a} \frac{\mathrm{d}\overline{a}}{\left[\sqrt{\pi\overline{a}}\; F(\overline{a})\right]^m} \quad . \tag{4.156}$$

The critical number of cycles N_c finally follows by introducing the critical crack length a_c.

4.12 Interface cracks

Up to now, we have considered only cracks in homogeneous materials. But also cracks in the interface between two materials with different elastic constants are of considerable practical interest. They are called *interface cracks* or *bimaterial cracks*. Typical examples are cracks in material compounds, in adhesive joints or cracks in the interfaces of composite materials (laminates, fiber-matrix materials, etc.). The K-concept cannot be directly applied to such cracks because the crack-tip field in this case has not the same form as for a homogeneous material. Furthermore, it is not a priori clear to what extent parameters such as $\mathcal{G}$ or J can be used in fracture criteria for such cracks.

To begin with, we consider the field at the tip of a bimaterial crack which lies in the interface between two materials with the elastic constants E_1, ν_1 and E_2, ν_2

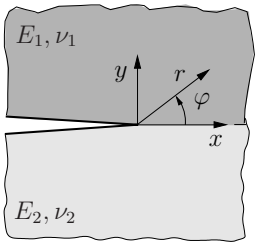

Fig. 4.50 Tip of a bimaterial crack

(Fig. 4.50). Here, we can restrict our attention to plane strain since a plane stress state can hardly be realized in the vicinity of the tip of an interface crack. In order to determine the crack-tip field, we use again the complex method (cf. Section 4.2.1) which now must be applied separately for the upper (1) and the lower (2) half planes. For the solution we use the functions

$$\Phi_1(z) = A_1 z^\lambda, \quad \Psi_1(z) = B_1 z^\lambda, \qquad \Phi_2(z) = A_2 z^\lambda, \quad \Psi_2(z) = B_2 z^\lambda \tag{4.157}$$

where in contrast to the homogeneous material (see Section 4.2.1) the exponent λ can now be complex. Since the displacements at the crack tip must be non-singular and the strain energy shall be limited, we consider $\mathrm{Re}\,\lambda > 0$. The boundary and transition conditions

$$(\sigma_\varphi + \mathrm{i}\,\tau_{r\varphi})^{(1)}_{\varphi=\pi} = 0\,, \qquad (\sigma_\varphi + \mathrm{i}\,\tau_{r\varphi})^{(1)}_{\varphi=0} = (\sigma_\varphi + \mathrm{i}\,\tau_{r\varphi})^{(2)}_{\varphi=0}\,,$$
$$(\sigma_\varphi + \mathrm{i}\,\tau_{r\varphi})^{(2)}_{\varphi=-\pi} = 0\,, \qquad (u + \mathrm{i}\,v)^{(1)}_{\varphi=0} = (u + \mathrm{i}\,v)^{(2)}_{\varphi=0}$$

lead to a homogeneous system of equations for the four complex constants $A_1 \ldots B_2$ (four real and four imaginary parts). From the condition that the 8×8 determinant of the coefficients must be zero, one obtains the equation for the eigenvalues which has the solution

$$\lambda = \begin{cases} 1/2 + n + \mathrm{i}\,\varepsilon \\ n \end{cases} \qquad n = 0, 1, 2, \ldots \tag{4.158}$$

where

$$\varepsilon = \frac{1}{2\pi} \ln \frac{\mu_2\kappa_1 + \mu_1}{\mu_1\kappa_2 + \mu_2} \tag{4.159}$$

with $\mu_i = E_i/2(1+\nu_i)$ and $\kappa_i = 3 - 4\nu_i$. The constant ε is known as the so-called *bimaterial constant*. At the crack tip $r \to 0$, the field dominates which corresponds to the eigenvalue with the lowest real part, i.e.

$$\lambda = 1/2 + \mathrm{i}\,\varepsilon\,. \tag{4.160}$$

Hence, according to Kolosov's formulae (1.118a) or (1.119) and taking into account $r^{\mathrm{i}\,\varepsilon} = \mathrm{e}^{\mathrm{i}\,\varepsilon \ln r}$, the stresses and the displacements show a behavior of the type

$$\sigma_{ij} \sim r^{-1/2} \cos(\varepsilon \ln r)\,, \qquad u_i \sim r^{1/2} \cos(\varepsilon \ln r) \tag{4.161}$$

where the cosine may be also replaced by the sine. Thus, the typical $1/\sqrt{r}$-type singular behavior of the stresses and the $\sqrt{r}$-behavior of the displacements is present also at the bimaterial crack tip. But now these quantities oscillate increasingly when approaching the crack tip (oscillating singularity).

We will not derive the complete crack-tip field but restrict the analysis to the stresses in the interface and to the crack opening:

$$
\begin{aligned}
(\sigma_y + \mathrm{i}\,\tau_{xy})_{\varphi=0} &= \frac{K\,(r/2a)^{\mathrm{i}\,\varepsilon}}{\sqrt{2\pi r}}\,, \\
(v^+ - v^-) + \mathrm{i}\,(u^+ - u^-) &= \frac{c_1 + c_2}{2\cosh\pi\varepsilon}\,\frac{K\,(r/2a)^{\mathrm{i}\,\varepsilon}}{1 + 2\,\mathrm{i}\,\varepsilon}\,\sqrt{\frac{r}{2\pi}}\,.
\end{aligned}
\tag{4.162a}
$$

Here, $2a$ is an arbitrary reference length (e.g., the crack length),

$$
K = K_1 + \mathrm{i}\,K_2 \tag{4.162b}
$$

is the complex stress intensity factor and

$$
c_1 = (1 + \kappa_1)/\mu_1\,, \qquad c_2 = (1 + \kappa_2)/\mu_2\,. \tag{4.162c}
$$

Accordingly, the crack-tip field is uniquely characterized by the modified complex stress intensity factor $\overline{K} = K\,(2a)^{-\mathrm{i}\,\varepsilon}$. If we introduce through

$$
|K| = \sqrt{K_1^2 + K_2^2}\,, \qquad \tan\psi = K_2/K_1 \tag{4.163}
$$

its absolute value $|K|$ and phase angle ψ, it can also be written as

$$
\overline{K} = |K|\,\mathrm{e}^{\mathrm{i}\,\psi}\,(2a)^{-\mathrm{i}\,\varepsilon}\,. \tag{4.164}
$$

In addition to the stress intensity factors K_1 and K_2, also the reference length $2a$ occurs which is weighted by the bimaterial constant ε. For this reason, a decomposition into pure mode I and mode II is impossible. Consequently, the stress intensity factors K_1 and K_2 also cannot simply be related to these modes. This can clearly be recognized when representing the stresses in the interface according to (4.162a) in real form:

$$
\left\{ \begin{array}{c} \sigma_y \\ \tau_{xy} \end{array} \right\} = \frac{1}{\sqrt{2\pi r}} \left\{ \begin{array}{l} K_1 \cos[\varepsilon \ln (r/2a)] - K_2 \sin[\varepsilon \ln (r/2a)] \\ K_1 \sin[\varepsilon \ln (r/2a)] + K_2 \cos[\varepsilon \ln (r/2a)] \end{array} \right\}\,. \tag{4.165}
$$

The stress intensity factor K_1 is not only associated with the normal stresses in the interface but also with the shear stresses. In the same manner, both the shear and normal stresses are associated with K_2. Thus, at a bimaterial crack tip, both modes are (strictly speaking) inseparably connected to each other. Only in the limit case of the homogeneous material ($c_1 = c_2$, $\varepsilon = 0$), K_1 and K_2 reduce to K_I and K_{II} and both modes then are separable.

From (4.162a) it can be seen that the crack opening oscillates increasingly when approaching the crack tip. Since a penetration of the crack faces is physically impossible, they must get into contact behind the crack tip. As a consequence, the presented solution is meaningful to describe the crack-tip field only outside the contact region.

We now will determine the energy release rate $\mathcal{G} = -\mathrm{d}\Pi/\mathrm{d}a$ during crack growth in the interface (see also Section 4.6.2, equation (4.83)). It can be obtained

from

$$\frac{\mathrm{d}\Pi}{\mathrm{d}a} = -\lim_{\Delta a \to 0} \frac{1}{2\Delta a} \int_0^{\Delta a} \left[\sigma_y \left(v^+ - v^-\right) + \tau_{xy} \left(u^+ - u^-\right)\right] \mathrm{d}x$$

in conjunction with (4.162a) and (4.162c). We get

$$\mathcal{G} = \frac{(c_1 + c_2)\left(K_1^2 + K_2^2\right)}{16 \cosh^2(\pi\varepsilon)} \,. \tag{4.166}$$

Thus, $\mathcal{G}$ is uniquely determined by both stress intensity factors. Hence, only the "absolute value" $(K_1^2 + K_2^2)^{1/2}$ and not the separate components K_1 and K_2 can be determined from $\mathcal{G}$.

It can be show that the energy release rate of a bimaterial crack can be determined from the J-integral

$$J = \mathcal{G} = \int_C (U \,\mathrm{d}y - t_i u_{i,x} \mathrm{d}c) \tag{4.167}$$

as it is valid for a crack in a homogeneous material. The integral is path independent as long as the crack is straight, has traction-free crack faces, and the elastic constants do not vary in x-direction.

As a simple example of an interface crack for which a closed form solution can be found, we consider a crack in an infinite domain under internal pressure, see Fig. 4.51a. Since the complex potentials are rather involved, only Φ_1' is exemplarily given here:

$$\Phi_1' = \frac{\sigma}{1 + \mathrm{e}^{2\pi\varepsilon}} \left[\left(\frac{z+a}{z-a} \right)^{\mathrm{i}\,\varepsilon} \frac{z - 2\,\mathrm{i}\,\varepsilon\, a}{\sqrt{z^2 - a^2}} - 1 \right] \,.$$

The stress intensity factors at the right crack tip are

$$K = (1 + 2\,\mathrm{i}\,\varepsilon)\,\sigma\sqrt{\pi a} \qquad \text{or} \qquad \begin{cases} K_1 = \sigma\sqrt{\pi\, a}\,, \\ K_2 = 2\,\varepsilon\,\sigma\sqrt{\pi\, a}\,. \end{cases} \tag{4.168}$$

If homogeneous fields in both materials are superimposed, with tension σ in y-direction and appropriate constant stresses σ_1, σ_2 in x-direction, the loading case shown in Fig. 4.51b is obtained. Here, the same stress intensity factors (4.168) apply as for internal pressure. If the shear stress τ acts at infinity instead of tension (Fig. 4.51c), one obtains

$$K_1 = -2\,\varepsilon\,\tau\sqrt{\pi a}\,, \qquad K_2 = \tau\sqrt{\pi\, a}\,. \tag{4.169}$$

It should be noted that in this case, because of $K_1 < 0$ and $K_2 > 0$ and according to (4.165), pressure prevails in the interface. Therefore the crack tip will be closed. Finally, for the configuration shown in Fig. 4.51d, the stress intensity factors are (see also Table 4.1, No. 4)

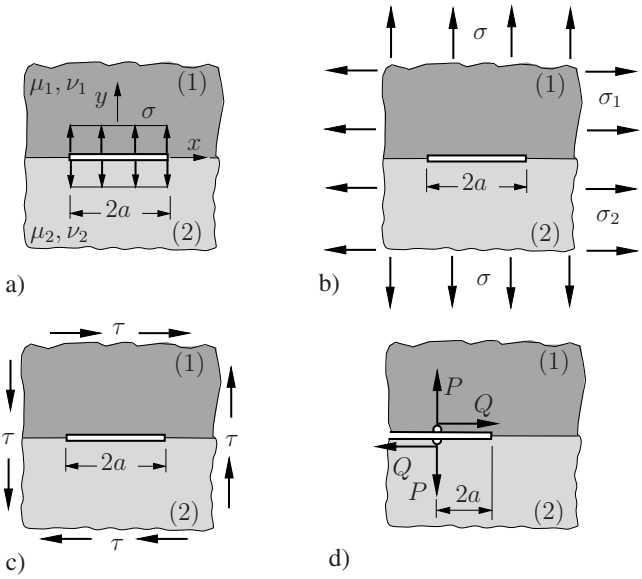

Fig. 4.51 Interface cracks

$$K_1 = \frac{P}{\sqrt{\pi\, a}} \cosh \pi\varepsilon \;, \qquad K_2 = \frac{Q}{\sqrt{\pi\, a}} \cosh \pi\varepsilon \;. \tag{4.170}$$

By means of the examples in Fig. 4.51a,b, we can estimate the length of the contact zone at the crack tip. For this purpose, we identify the contact length with the maximum distance r_c where the crack opening $\delta = v^+ - v^-$ due to the oscillation becomes zero for the first time. This leads, according to (4.162a), to the condition $\mathrm{Re}\,[K\,(r_c/2a)^{\mathrm{i}\,\varepsilon}/(1 + 2\mathrm{i}\,\varepsilon)] = 0$. Introducing (4.168) gives $\mathrm{Re}\,[r_c/2a]^{\mathrm{i}\,\varepsilon} = \cos[\varepsilon \ln(r_c/2a)] = 0$ and from that we obtain

$$r_c/2a = \exp\left(-\pi/2\,\varepsilon\right) . \tag{4.171}$$

An extreme value which ε attains for $\mu_2 \to \infty$ and $\nu_1 = 0$, is $\varepsilon_{\max} = 0.175$. But in most cases of practical interest, the bimaterial constant is far lower: $\varepsilon \ll 1$. For example, $\varepsilon = 0.039$ for the material combination Ti/Al_2O_3, $\varepsilon = 0.028$ for the combination Cu/Al_2O_3 and $\varepsilon = 0.004$ for Au/MgO. If we insert $\varepsilon = 0.05$ into (4.171), we obtain $r_c/2a \approx 2 \cdot 10^{-14}$, i.e., the contact zone is negligibly small. As already mentioned, this is not the case for a pure shear loading. But if a small amount of tension is superimposed which leads to crack opening, the contact zone becomes small again.

The crack-tip field of a bimaterial crack is uniquely determined by the modified complex K-factor (4.164) or by its real and imaginary parts, respectively. Therefore it seems obvious to formulate a fracture criterion formally as: $\overline{K} = \overline{K}_c$. However, in doing so some difficulties arise. For instance, the transfer of $\overline{K}$-factors is not an easy task. This can be recognized when two cracks with different lengths $2a^*$ and

$2a$ but with the same ε are considered. The crack-tip fields, and by this the crack-tip loadings, of both cracks are equal only if the conditions

$$|K^*|\,\mathrm{e}^{\mathrm{i}\,\psi^*}\,(2a^*)^{-\mathrm{i}\,\varepsilon} = |K|\,\mathrm{e}^{\mathrm{i}\,\psi}\,(2a)^{-\mathrm{i}\,\varepsilon} \tag{4.172a}$$

or

$$|K|^* = |K|\,, \qquad \psi^* = \psi - \varepsilon \ln a/a^* \tag{4.172b}$$

are fulfilled. Consequently, the phase angles (i.e., K_2/K_1) for both configurations must be different. Further difficulties consist in the transferability of experimentally determined $\overline{K}_c$-values to situations which differ from the experimental one as well as in their ε-dependent dimension.

On account of the mentioned reasons, frequently a pragmatic approach is adopted. In many cases of practical relevance, because of $\varepsilon \ll 1$, it is admissible to assume $\overline{K} \approx K$ or $K_1 \approx K_I$ and $K_2 \approx K_{II}$, respectively. The crack-tip state, in a good approximation, is described by the usual mode-I and mode-II stress intensity factors as for a homogeneous material. Equivalent to this is a characterization of the crack tip loading by $K_I^2 + K_{II}^2$ and K_{II}/K_I or by the energy release rate $\mathcal{G}$ and the phase angle ψ, respectively. The fracture criterion then can be expressed as

$$\mathcal{G}(\psi) = \mathcal{G}_c^{(i)}(\psi) \qquad \text{with} \qquad \tan\psi = \frac{K_{II}}{K_I}\,. \tag{4.173}$$

Here, the interface fracture toughness $\mathcal{G}_c^{(i)}$ generally shows a strong dependence on ψ. If we apply this fracture criterion to the examples in Fig. 4.51a,b, it leads in conjunction with (4.166) and (4.168) for a given loading σ to the critical crack length

$$a_c = \frac{18\cosh^2(\pi\varepsilon)\,\mathcal{G}_c^{(i)}(0)}{\pi(1+4\varepsilon^2)(c_1+c_2)\,\sigma^2}\,. \tag{4.174}$$

With $\varepsilon \ll 1$, it can be simplified to $a_c \approx 18\,\mathcal{G}_c^{(i)}(0)/\pi(c_1+c_2)\,\sigma^2$.

As a typical example, relevant in applications, we consider the delamination of two layers (1) and (2) which is accompanied by the propagation of an interface crack (Fig. 4.52a). A similar problem has already been considered in Section 4.6.2. As a generalization, now a finite thickness h_2 of layer (2) is assumed which, as h_1, shall be small compared with all other length parameters: $h_1, h_2 \ll a$. Due to an *eigenstrain* ε_0 of layer (2), e.g., on account of heating, eigenstresses occur in the system. They can be characterized by the forces N and moments M_1 and $M_2 = M_1 + (h_1+h_2)N/2$ resulting in both layers. Here, the eigenstrain ε_0 describes the strain difference of both layers if each of them can deform freely and unconstrained. The energy release rate $\mathcal{G}$ can be determined exactly by using elementary beam theory. From this, the following expressions are obtained for $x \gg h_1, h_2$ in a first step

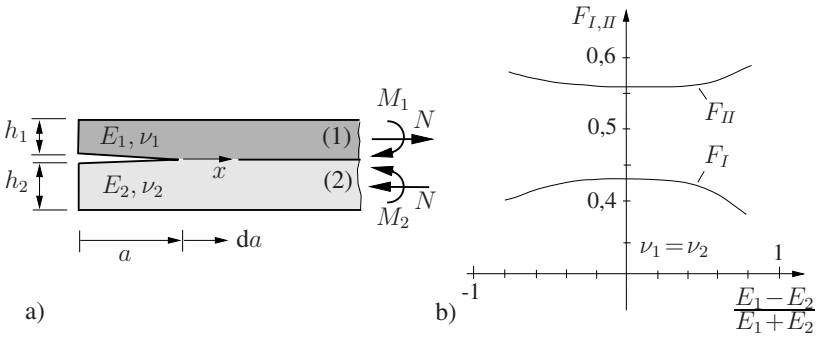

Fig. 4.52 Delamination

$$N = f\,\frac{E_1'\,h_1\,\varepsilon_0}{B}\,, \qquad f = \left[1 + eH + 3\,\frac{(1+H)^2\,eH}{1+eH^3}\right]^{-1}\,, \tag{4.175}$$

$$M_1 = -\frac{(1+H)eH^3}{2(1+eH^3)}\,h_2 N\,, \qquad M_2 = \frac{(1+H)}{2(1+eH^3)}\,h_2 N\,,$$

where B is the width of the layers and the abbreviations $e = E_1/E_2$ and $H = h_1/h_2$ have been used. With

$$\mathrm{d}\Pi = \mathrm{d}\Pi^i = -\frac{1}{2}\left[12\,\frac{M_1^2}{E_1'\,h_1^3} + 12\,\frac{M_2^2}{E_2'\,h_2^3} + \frac{N^2}{E_1'\,h_1} + \frac{N^2}{E_2\,h_2}\right] B\,\mathrm{d}a\,,$$

and the reference stress $\sigma = E_1'\,\varepsilon_0$, one finally obtains

$$\mathcal{G} = f\,\frac{(1-\nu_1^2)\,\sigma^2\,h_1}{2\,E_1}\,. \tag{4.176}$$

In the limit case $h_1/h_2 \to 0$ this result reflects with $f \to 1$ just the result (4.89) of Section 4.6.2 while the limit case of two equal layers ($e = 1$, $H = 1$) leads to $f = 0.2$.

The stress intensity factors cannot be determined in such a simple manner. For this purpose, in fact the solution of the elastic boundary value problem in the surrounding of the crack tip is necessary. In general, the solution can be represented as

$$K_I = F_I\,N\,\sqrt{h_1}\,, \qquad K_{II} = F_{II}\,N\,\sqrt{h_1} \tag{4.177}$$

where F_I and F_{II} are dependent on $H = h_1/h_2$ and the elastic constants. For the special case of a thin layer on a thick substrate ($h_1/h_2 \to 0$) and $\nu_1 = \nu_2$, the functions F_I and F_{II} are shown in Fig. 4.52b.

Due to the different material properties, a mixed-mode loading through K_I and K_{II} is present at a bimaterial crack even if the geometric configuration and external loading is symmetric. This might lead to the effect that a possible crack growth

does not take place in the interface but that instead the crack deflects into one of the two materials. The particular behavior of the crack depends on the phase angle ψ as well as on the different fracture toughnesses of the interface and the individual materials. By means of the example in Fig. 4.53a, this briefly shall be discussed using qualitative considerations. For this purpose we assume $\mu_1 < \mu_2$ and $\nu_1 = \nu_2$, i.e., that material (1) is "softer" than material (2). Under these circumstances, external tension causes shear stresses in the interface which lead to a negative K_{II} and consequently to a negative phase angle ψ at the right crack tip (Fig. 4.53b). If we now assume that as a result of a disturbance, the crack has slightly grown into material (1), we can apply the crack deflection hypotheses from Section 4.9. All of them predict a positive deflexion angle φ_0 for the corresponding situation, i.e., a crack propagation away from the interface into the softer material (1) (cf. (4.150)). If we apply the same consideration to a hypothetic small crack advance into material (2), we again obtain a positive deflection angle φ_0 which drives the crack back to the interface. All in all, the crack tends to deflect out of the interface and to propagate into the softer material (Fig. 4.53c). However, this occurs only if the fracture toughness of the soft material is not higher than that of the interface: $\mathcal{G}_c^{(1)} \leq \mathcal{G}_c^{(i)}$.

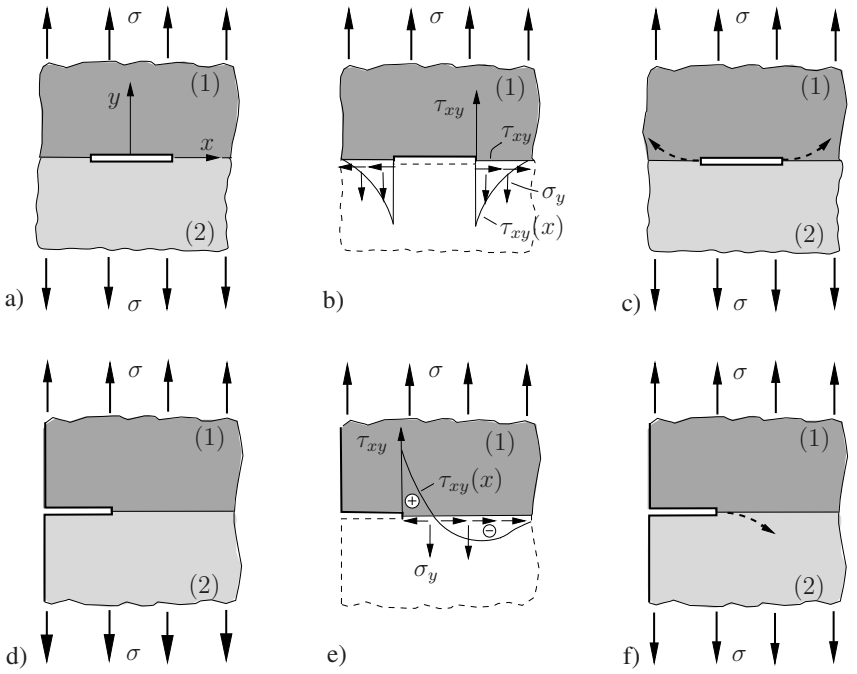

Fig. 4.53 Crack deflection

A different behavior can be observed for the bimaterial crack shown in Fig. 4.53d where the same material properties are assumed as before. In this case the external tension causes a shear stress distribution in the interface which leads to

a positive K_{II} (Fig. 4.53e). Accordingly, the crack will tend to propagate into the "stiffer" material as long as the fracture toughness there is not higher than in the interface (Fig. 4.53f).

4.13 Piezoelectric materials

4.13.1 Basic principles

Piezoelectric materials are characterized by the property that deformations occur not only as a result of mechanical forces but also due to applied electric fields. This phenomenon is called *electrostriction* . Conversely, deformations induce electric fields in such materials which is denoted the *piezoelectric effect* . Due to their wide application as actuating elements or sensors, especially ferroelectric ceramics are of significant technical importance. In ferroelectric materials a macroscopic piezoelectric effect occurs only after a polarization through a sufficiently high electric field. Therefore, they then behave transversely isotropic, i.e., there exists a principal direction which coincides with the direction of polarization. Without going into details, the fundamental equations shall briefly be discussed which are necessary for the solution of fracture mechanics problems. We will restrict our attention to the *small signal range* which in good approximation can be characterized by a linear material behavior with a constant polarization. In this case, all relevant relations are fully analogous to those we have already discussed for usual, purely elastic materials. However, auxiliary terms now appear due to the coupling of the mechanical and the electrical problem. Moreover, the anisotropic material behavior leads to a certain inflation of the equations.

The linear coupled electromechanical behavior of the piezoelectric materials can be described by the constitutive equations (cf. (1.35a))

$$\sigma_{ij} = C_{ijkl}\,\varepsilon_{kl} - e_{kij}\,E_k\,, \qquad D_i = e_{ikl}\,\varepsilon_{kl} + \epsilon_{ik}\,E_k\,. \tag{4.178}$$

Here, D_i is the dielectric displacement, E_k is the electrical field strength, and e_{kij} and ϵ_{ij} are the tensors of the piezoelectric and dielectric material constants (one should not mix up the strains ε_{ij} with the material constants ϵ_{ik} and e_{ijk} with the permutation symbol!). In case of transversely isotropic ferroelectrics whose polarization direction coincides with the x_3-direction, the material law can also be written in the matrix form

$$\begin{bmatrix}\sigma_{11}\\ \sigma_{22}\\ \sigma_{33}\\ \sigma_{23}\\ \sigma_{31}\\ \sigma_{12}\end{bmatrix} = \begin{bmatrix} c_{11} & c_{12} & c_{13} & 0 & 0 & 0\\ c_{12} & c_{11} & c_{13} & 0 & 0 & 0\\ c_{13} & c_{13} & c_{33} & 0 & 0 & 0\\ 0 & 0 & 0 & c_{44} & 0 & 0\\ 0 & 0 & 0 & 0 & c_{44} & 0\\ 0 & 0 & 0 & 0 & 0 & c_{66}\end{bmatrix} \begin{bmatrix}\varepsilon_{11}\\ \varepsilon_{22}\\ \varepsilon_{33}\\ 2\,\varepsilon_{23}\\ 2\,\varepsilon_{31}\\ 2\,\varepsilon_{12}\end{bmatrix} - \begin{bmatrix} 0 & 0 & e_{31}\\ 0 & 0 & e_{31}\\ 0 & 0 & e_{33}\\ 0 & e_{15} & 0\\ e_{15} & 0 & 0\\ 0 & 0 & 0\end{bmatrix} \begin{bmatrix}E_1\\ E_2\\ E_3\end{bmatrix} \tag{4.179a}$$

$$\begin{bmatrix} D_1 \\ D_2 \\ D_3 \end{bmatrix} = \begin{bmatrix} 0 & 0 & 0 & 0 & e_{15} & 0 \\ 0 & 0 & 0 & e_{15} & 0 & 0 \\ e_{31} & e_{31} & e_{33} & 0 & 0 & 0 \end{bmatrix} \begin{bmatrix} \varepsilon_{11} \\ \varepsilon_{22} \\ \varepsilon_{33} \\ 2\,\varepsilon_{23} \\ 2\,\varepsilon_{31} \\ 2\,\varepsilon_{12} \end{bmatrix} + \begin{bmatrix} \epsilon_{11} & 0 & 0 \\ 0 & \epsilon_{11} & 0 \\ 0 & 0 & \epsilon_{33} \end{bmatrix} \begin{bmatrix} E_1 \\ E_2 \\ E_3 \end{bmatrix} \tag{4.179b}$$

where $c_{66} = (c_{11} - c_{12})/2$.

According to (1.25) the strains ε_{ij} are related to the mechanical displacements. Furthermore, the electrical field strength can be derived from the electric potential ϕ. The respective equations are

$$\varepsilon_{ij} = \frac{1}{2}(u_{i,j} + u_{j,i}) \,, \qquad E_i = -\phi_{,i} \,. \tag{4.180}$$

In addition, the field equations

$$\sigma_{ij,j} = 0 \,, \qquad D_{i,i} = 0 \tag{4.181}$$

hold where we have assumed that no volume forces and distributed charges are present. Finally, the mechanical and electrical boundary conditions complete the description of a boundary value problem. The electrical boundary conditions involve a statement on the potential ϕ or the normal component D_n of the dielectric displacement at the boundary.

As a generalization of the strain energy density (cf. Section 1.3.1.2), the specific electro-mechanical potential (electric enthalpy density)

$$W = \frac{1}{2}\, C_{ijkl}\, \varepsilon_{ij} \varepsilon_{kl} - e_{kij}\, E_k\, \varepsilon_{ij} - \frac{1}{2}\, \epsilon_{ij}\, E_i E_j \tag{4.182}$$

can be introduced. Then there exists the surface integral

$$J_k = \int_{\partial V} (W \delta_{jk} - \sigma_{ij} u_{i,k} + D_j E_k) n_j \mathrm{d}A \tag{4.183}$$

with basically the same properties as the J-integral vector (4.107). If ∂V contains a defect, J_k characterizes the configurational force acting on the defect. It causes a change of the total energy $\mathit{\Pi}$ of the piezoelectric system when the defect is displaced by $\mathrm{d}s_k$: $\mathrm{d}\mathit{\Pi} = -J_k\, \mathrm{d}s_k$.

The basic equations of transversely isotropic piezoelectricity can be simplified in various cases. A plane strain state is present for a polarization in x_3-direction when the mechanical and electrical fields are independent, e.g., of x_2. With $u_2 = 0$, $\varepsilon_{22} = \varepsilon_{32} = \varepsilon_{12} = 0$, $E_2 = 0$, the constitutive law (4.179a,b) then reduces to

$$\begin{bmatrix} \sigma_{11} \\ \sigma_{33} \\ \sigma_{31} \\ D_1 \\ D_3 \end{bmatrix} = \begin{bmatrix} c_{11} & c_{13} & 0 & 0 & -e_{31} \\ c_{13} & c_{33} & 0 & 0 & -e_{33} \\ 0 & 0 & c_{44} & -e_{15} & 0 \\ 0 & 0 & e_{15} & \epsilon_{11} & 0 \\ e_{31} & e_{33} & 0 & 0 & \epsilon_{33} \end{bmatrix} \begin{bmatrix} \varepsilon_{11} \\ \varepsilon_{33} \\ 2\,\varepsilon_{31} \\ E_1 \\ E_3 \end{bmatrix} \tag{4.184}$$

and the field equations can be summarized as follows:

$$\begin{aligned} c_{11}u_{1,11} + (c_{13} + c_{44})u_{3,13} + c_{44}u_{1,33} + (e_{31} + e_{15})\phi_{,13} = 0\,, \\ c_{44}u_{3,11} + (c_{13} + c_{44})u_{1,31} + c_{33}u_{3,33} + e_{15}\phi_{,11} + e_{33}\phi_{,33} = 0\,, \\ e_{15}u_{3,11} + (e_{15} + e_{31})u_{1,13} + e_{33}u_{3,33} - \epsilon_{11}\phi_{,11} - \epsilon_{33}\phi_{,33} = 0\,. \end{aligned} \tag{4.185}$$

In particular, the longitudinal (out of plane) shear stress state, where $u_1 = u_3 = 0$, $E_3 = 0$ applies, proves to be relatively simple. Assuming again a polarization in x_3-direction, the constitutive law simplifies to

$$\begin{bmatrix} \sigma_{23} \\ \sigma_{12} \\ D_1 \\ D_2 \end{bmatrix} = \begin{bmatrix} c_{44} & 0 & 0 & -e_{15} \\ 0 & c_{44} & -e_{15} & 0 \\ 0 & e_{15} & \epsilon_{11} & 0 \\ e_{15} & 0 & 0 & \epsilon_{11} \end{bmatrix} \begin{bmatrix} 2\varepsilon_{23} \\ 2\,\varepsilon_{12} \\ E_1 \\ E_2 \end{bmatrix} \tag{4.186}$$

and the field equations reduce to

$$c_{44}\Delta u_3 + e_{15}\Delta\phi = 0\,, \qquad e_{15}\Delta u_3 - \epsilon_{11}\Delta\phi = 0 \tag{4.187}$$

where $\Delta(.) = \partial^2(.)/\partial x_1^2 + \partial^2(.)/\partial x_3^2$

4.13.2 The crack in a ferroelectric material

In the following we consider a crack in a ferroelectric material, initially with an arbitrary polarization direction (Fig. 4.54). Without going into the analysis, under the assumption that the dielectric displacement along the crack faces vanishes (impermeable boundaries: $D_2^- = D_2^+ = 0$), the crack-tip field ($r \to 0$) displays a behavior

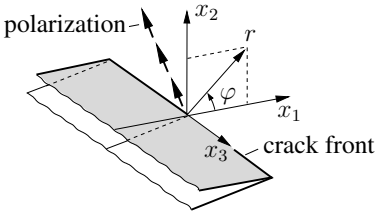

Fig. 4.54 Crack in a ferroelectric material

of the same type as for the purely elastic material:

$$\sigma_{ij} \sim r^{-1/2}\,, \qquad u_i \sim r^{1/2}\,, \qquad D_i \sim r^{-1/2}\,, \qquad \phi \sim r^{1/2}\,. \tag{4.188}$$

Accordingly, at the crack front (crack tip), the dielectric displacement, exactly as the stresses, has a singularity of the type $r^{-1/2}$. The field can be fully described by means of the henceforth four "stress intensity factors" K_I, K_{II}, K_{III}, and K_D. For simplicity, only field quantities in front of the crack tip ($\varphi = 0$) are given here, where reference is made to the coordinate system shown in Fig. 4.54:

$$\sigma_{22} = \frac{K_I}{\sqrt{2\pi r}}\,, \qquad \sigma_{12} = \frac{K_{II}}{\sqrt{2\pi r}}\,, \qquad \sigma_{13} = \frac{K_{III}}{\sqrt{2\pi r}}\,, \qquad D_2 = \frac{K_D}{\sqrt{2\pi r}}\,. \tag{4.189}$$

It can be recognized that K_D describes the strength of the singular dielectric displacement. With the K-factors, the energy release rate (crack extension force) for straight crack propagation, can be represented as

$$\mathcal{G} = J = -\frac{\mathrm{d}\Pi}{\mathrm{d}a} = C_{MN} K_M K_N \qquad (M, N = I, II, III, D) \tag{4.190}$$

where the summation has to be taken over M and N. Here, $J = J_1$ is the x_1-component of the configurational force J_k according to (4.183) and C_{MN} are material constants which depend on the polarization.

A technically important special case is a polarization perpendicular to the crack faces as shown in Fig. 4.55a. It should be noted that contrary to the previous sections, the x_3-axis now is perpendicular to the crack face. In case of plane strain, when the fields are independent on x_2 and, moreover, the configuration is symmetric with respect to the x_1-axis, K_{II} and K_{III} vanish. Then a mode-I crack opening is present and the following quantities behind the crack tip ($\varphi = \pm\pi$) can be obtained for $r \to 0$:

$$u_3^{\pm} = \pm 4\sqrt{\frac{r}{2\pi}}\left(\frac{K_I}{c_T} + \frac{K_D}{e}\right), \qquad \phi^{\pm} = \pm 4\sqrt{\frac{r}{2\pi}}\left(-\frac{K_D}{\epsilon} + \frac{K_I}{e}\right)\,. \tag{4.191}$$

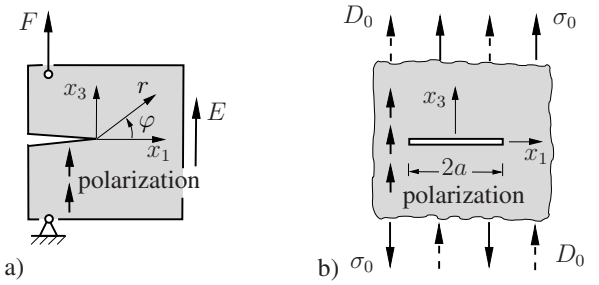

Fig. 4.55 Electromechanical crack loading

Here, c_T, ϵ, and e denote combined elastic, dielectric, and piezoelectric material properties which can be expressed by means of the material constants (4.184). The energy release rate herewith results as

$$\begin{aligned}\mathcal{G} = \mathcal{G}_m + \mathcal{G}_e &= \left[K_I \left(\frac{K_I}{c_T} + \frac{K_D}{e}\right)\right] + \left[K_D \left(-\frac{K_D}{\epsilon} + \frac{K_I}{e}\right)\right] \\ &= \frac{K_I^2}{c_T} - \frac{K_D^2}{\epsilon} + 2\,\frac{K_I K_D}{e}\,.\end{aligned} \tag{4.192}$$

The two parts $\mathcal{G}_m$ and $\mathcal{G}_e$ can be interpreted as mechanical and electrical parts of the energy release rate.

Due to the electromechanical coupling, in general both stress intensity factors K_I and K_D occur under a purely mechanical or purely electrical loading. Specific loading conditions in a few special cases can involve only one K-factor. One example is an impermeable finite crack in an infinite domain (see Fig. 4.55b). Due to a loading solely by σ_0 or solely by D_0, the following stress intensity factors are obtained:

$$K_I = \sigma_0\sqrt{\pi a}\,, \qquad K_{IV} = D_0\sqrt{\pi a}\,. \tag{4.193}$$

The state at the crack tip which is loaded symmetrically, is uniquely characterized by K_I and K_D. Therefore, a fracture criterion for this case can formally be written as

$$f(K_I, K_{IV}) = 0. \tag{4.194}$$

Among others, the following criteria have been proposed:

$$\begin{aligned}&(A) \qquad \mathcal{G} = \mathcal{G}_c\,, \\ &(B) \qquad \mathcal{G}_m = \mathcal{G}_{mc}\,, \\ &(C) \qquad K_I = K_{Ic}\end{aligned} \tag{4.195}$$

where criterion (A) often is preferred. But independently of the chosen criterion, the determination of both sides of (4.195), i.e., the acting crack-tip load and the critical values are afflicted with uncertainties. One reason for this is the electric boundary condition which often is not known sufficiently accurate along crack faces in real materials.

4.14 Problems

Problem 4.1 A crack tip field is given by the complex functions

$$\Phi(z) = A\sqrt{z}\,, \qquad \Psi(z) = -(\frac{1}{2}A - \overline{A})\sqrt{z}\,, \qquad A \text{ purely imaginary.}$$

a) Determine the stresses $\sigma_x, \sigma_y, \tau_{xy}$.

b) Which type of opening mode is present and how is A related to the stress intensity factor?

Solution: Pure mode II with $K_I = 0$ and $K_{II} = -\sqrt{2\pi}\ \mathrm{Im}A$.

Problem 4.2 A crack in an infinite region is loaded by a remote linearly varying stress $\sigma_y^\infty = \sigma_0(b/a - x/a)$.

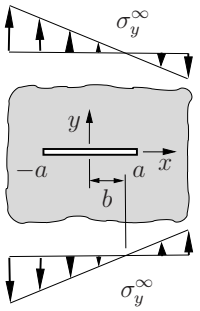

Fig. 4.56

a) Determine the K-factors by using the basic solution for a crack subjected to point forces.

b) What is the condition for $K_I^+ = 0$, and what does this mean?

Solution:

a) $K_I^\pm = \sigma_0\sqrt{\pi a}\left(\dfrac{b}{a} \mp \dfrac{1}{2}\right)$

b) $K_I^+ = 0$ for $b = a/2$. Under this loading condition there exists no stress singularity at the right crack tip.

Problem 4.3 A crack grows along the interface in a bi-material bar of width B under tension.

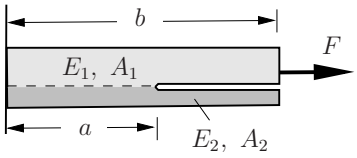

Fig. 4.57

a) Determine the energy release rate by using simple bar theory.

b) Calculate K_{II} for the case $E_1 = E_2$ under the assumption that pure mode II and plane stress is present.

Solution: a) $\mathcal{G} = \dfrac{F^2 A_2 E_2}{2BA_1E_1(A_1E_1 + A_2E_2)}$, b) $K_{II} = \sqrt{\dfrac{F^2 A_2}{2BA_1(A_1 + A_2)}}$

Problem 4.4 Calculate for both configurations, shown in Fig. 4.58, the energy release rates and the K_I-factors. In case a) use beam theory and assume plane stress, in case b) assume $h \ll a$ and plane strain.

Solution: a) $\mathcal{G} = \dfrac{3\,uEh^3}{4\,a^4}$, $K_I = \dfrac{\sqrt{3}\,u\,Eh^{3/2}}{2\,a^2}$

b) $\mathcal{G} = \dfrac{2\,u^2E}{b(1-\nu^2)}$, $K_I = uE\sqrt{\dfrac{2h}{b(b-h)(1-\nu^2)}}$

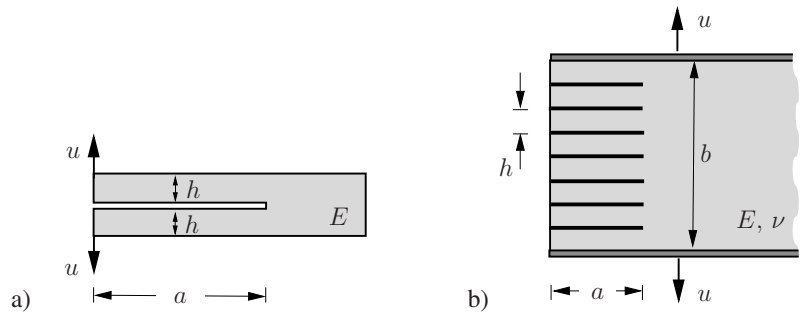

Fig. 4.58

Problem 4.5 The configuration shown in Fig. 4.59 contains an interface crack between the thin elastic layer and the substrate (coefficients of thermal expansion k_l and k_s). The initially stress-free system experiences a temperature change ΔT.

Determine the energy release rate under the assumptions that the thin layer is in a plane strain state and does not influence the thermal strains of the substrate.

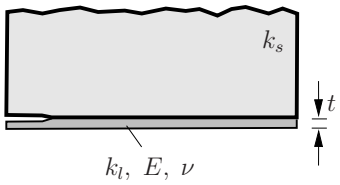

Fig. 4.59

Solution: $\mathcal{G} = \dfrac{E\,t}{2(1-\nu)}\,(k_s - k_l)^2\,\Delta T^2\,.$

Problem 4.6 Calculate the crack deflection angle φ for the two configurations shown in Fig. 4.60. Use the criterion of maximum circumferential stress and assume $\tau_0 = \sigma_0/2$.

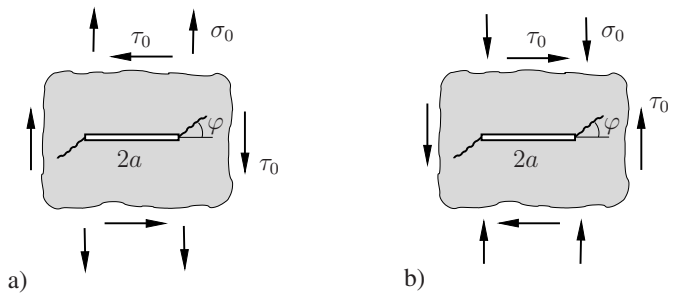

Fig. 4.60

Solution: a) $\varphi = 40.2°$ b) $\varphi = -70.6°$.

4.15 Further reading

Anderson, T.L. *Fracture Mechanics; Fundamentals and Application*. CRC Press, Boca Raton, 2004

Bazant, Z.P. and Planas, J. *Fracture and Size Effects in Concrete and Other Quasibrittle Materials*. CRC Press, Boca Raton, 1997

Broberg, K.B. *Cracks and Fracture*. Academic Press, London, 1999

Broek, D. *Elementary Engineering Fracture Mechanics*. Nijhoff, The Hague, 1982

Broek, D. *The Practical Use of Fracture Mechanics*. Kluwer, Dordrecht, 1988

Cherepanov, G.P. *Mechanics of Brittle Fracture*. McGraw-Hill, New York, 1979

Cotterell, B. and Mai, Y.-W. *Fracture Mechanics of Cementitious Materials*. Blackie Academic & Professional, 1996

Gdoutos, E.E. *Fracture Mechanics – An Introduction*. Kluwer, Dordrecht, 1993

Hellan, K. *Introduction to Fracture Mechanics*. McGraw-Hill, New York, 1985

Janssen, M., Zuidema, J. and Wanhill, R.J.H., Fracture Mechanics. DUP Blue Print, Delft 2002

Kachanov, M. *Elastic Solids with Many Cracks and Related Problems*. In *Advances in Applied Mechanics*, Vol. 30, pp. 259-445, Academic Press, 1993

Kanninen, M.F. and Popelar, C.H. *Advanced Fracture Mechanics*. Clarendon Press, Oxford, 1985

Knott, J.F. *Fundamentals of Fracture Mechanics*. Butterworth, London, 1973

Liebowitz, H. (ed.) *Fracture – A Treatise*, Vol. 2, Chapter 1-3. Academic Press, London, 1973

Miannay, D.P. *Fracture Mechanics*. Springer, New York, 1998

Murakami, Y. *Stress Intensity Factors Handbook*. Pergamon Press, New York, 1987

Pikley, W.D. *Peterson's Stress Concentration Factors*. John Wiley, New York, 1997

Qin, Q.-H. *Fracture Mechanics in Piezoelectric Materials*. WIT Press, Southampton, 2001

Sih, G.C. (ed.) *Mechanics of Fracture*, Vol. 2, Noordhoff, Leyden, 1975

Suresh, S. *Fatigue of Materials*. Cambridge University Press, Cambridge, 1998

Tada, H., Paris, P. and Irwin, G. *The Stress Analysis of Cracks Handbook*. Del. Research Corp., St. Louis, 1985

Weertmann, J. *Dislocation Based Fracture Mechanics*. World Scientific, Singapore, 1998

Chapter 5
Elastic-plastic fracture mechanics

5.1 Introduction

When a test specimen or a structural component consisting of a ductile material and containing a crack is loaded, plastic flow starts in the vicinity of the crack tip. As a consequence, the crack tip becomes increasingly blunted with increasing load and the crack opens. At the same time the plastic zone grows and may, depending on the material and geometry, extend over large regions or the entire specimen until at some critical load crack initiation takes place. In such a situation of *large-scale yielding* linear elastic fracture mechanics can no longer be applied and parameters and fracture concepts such as the K–concept based on linear elastic material behavior become meaningless. Fracture parameters and concepts then are needed which account for plastic flow of the material in larger regions outside the process zone.

Two alternative parameters characterizing the state at a crack tip are well established in elastic-plastic fracture mechanics. The first one is the *J–integral* proposed by J.R. RICE (1968) which in the present context represents the intensity of stress or strain rather than the energy release rate. The second one is the *crack-tip opening displacement (CTOD)* δ_t as a measure of the state of deformation at a crack tip, which dates back to A.H. COTTRELL and A.A. WELLS (1963). While J is essentially based on the deformation theory of plasticity (total strain theory, Section 1.3.3.3), the use of δ_t is experimentally motivated. It will, however, be shown that both quantities are directly related to each other.

In order to investigate problems of elastic-plastic fracture mechanics we will consider simple material models of rate-independent plasticity such as perfect plasticity or total strain theory. Furthermore, monotonic loading is assumed which means that global unloading or cyclic loading is precluded. Only under these restrictions do a few special cases of simple geometry allow for analytical solutions which form the basis for the above-mentioned fracture concepts. More involved material models or the analysis of real structures instead require the application of numerical methods. Analogous to linear elastic fracture mechanics we will focus here mainly on plane problems with straight cracks subjected to mode-I loading.

D. Gross and T. Seelig, *Fracture Mechanics: With an Introduction to Micromechanics*, Mechanical Engineering Series, DOI 10.1007/978-3-642-19240-1_5,

5.2 Dugdale model

Plastic zones ahead of a crack tip in thin plates of a ductile material typically display an elongated shape (Fig. 5.1a). Such a plastic zone results from through-the-thickness slip in planes inclined at $45°$ to the plane of the plate which leads to an extension of the zone in y-direction of the order of the plate thickness (see Section 4.7.2).

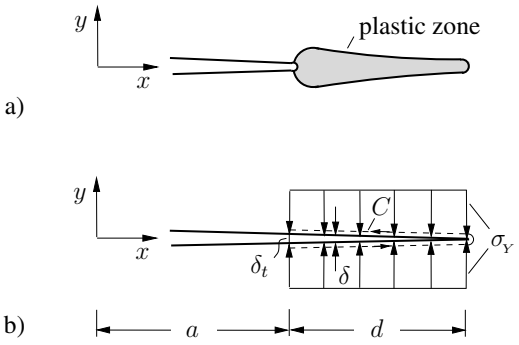

Fig. 5.1 Dugdale model

A simple model for the respective mode-I problem has been proposed by D.S. DUGDALE (1960). It is based on the assumptions that the material behavior inside the plastic zone is perfectly plastic and that the extension of the plastic zone in y-direction is small compared to its length d. The plastic zone then may be idealized as a line (strip) along which under plane stress conditions and according to the Tresca yield criterion the yield stress σ_Y prevails. The problem thus is reduced to that of an elastic medium containing a crack with its length fictitiously increased by the distance d along which the crack faces are subjected to the stress σ_Y (Fig. 5.1b). The unknown length d is determined from the condition that the stress must not exceed the yield stress σ_Y. Hence the stress singularity (K–factor) at the tip of the fictitious crack, i.e., at the tip of the plastic zone, must vanish. It has to be emphasized that the length of the plastic zone in this model is not restricted; it may be of the order of the crack length or any other characteristic length of the problem.

The relative displacement of the crack faces (i.e., the crack opening displacement) along the fictitious extension of the crack is denoted $\delta = v^+ - v^-$. It attains a value δ_t at the physical crack tip and vanishes at the tip of the plastic zone. If δ is interpreted to result from plastic deformations, δ_t may be taken as a measure of the state of deformation at the crack tip. An elastic-plastic criterion for the onset of crack growth then can be postulated in the form

$$\boxed{\delta_t = \delta_{tc}} \tag{5.1}$$

where the critical crack opening displacement δ_{tc} is a material parameter.

To determine the value of the J–integral a contour C along the lower and upper faces of the yield strip is considered (Fig. 5.1b). Employing (4.119) with $\mathrm{d}y = 0$ and $\tau_{xy} = 0$ we get

$$J = -\sigma_Y \int_a^{a+d} \frac{\partial}{\partial x} \left[v^+ - v^- \right] \mathrm{d}x = -\sigma_Y \left[\delta \right]_a^{a+d}$$

from which, using $\delta(a+d) = 0$ and $\delta(a) = \delta_t$, the simple expression

$$J = \sigma_Y \, \delta_t \tag{5.2}$$

is obtained. Within the framework of the Dugdale model therefore a fracture criterion

$$\boxed{J = J_c} \tag{5.3}$$

is equivalent to the δ_t–criterion (5.1). Here, $J_c = \sigma_Y \, \delta_{tc}$ is a material parameter characterizing the onset of crack growth.

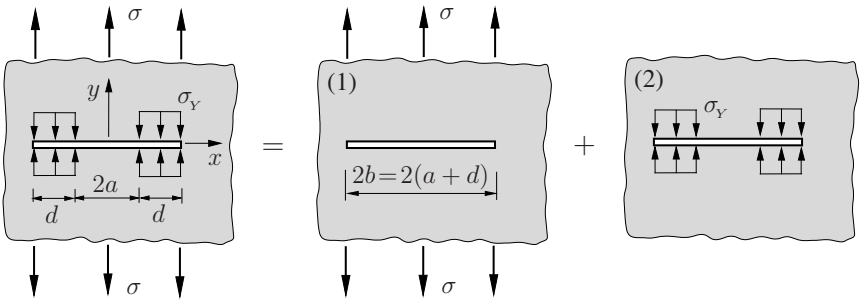

Fig. 5.2 Dugdale model of a crack subjected to uniaxial tension

Figure 5.2 illustrates the application of the Dugdale model to the situation of a crack of length $2a$ in an infinite domain subjected to uniaxial tension. The solution can be constructed by superposition of the two loading cases (1) "uniaxial tension" and (2) "crack face loading". According to the notation in Fig. 5.2 the respective stress intensity factors are (see Section 4.4.1)

$$K_I^{(1)} = \sigma \sqrt{\pi b} \, , \qquad K_I^{(2)} = -\frac{2}{\pi} \sigma_Y \sqrt{\pi b} \, \arccos \frac{a}{b}$$

and the displacements in y-direction at the physical crack tip ($x = a$) can be written as

$$v^{(1)}(a) = \frac{2\sigma}{E'} \sqrt{b^2 - a^2} \, ,$$

$$v^{(2)}(a) = \frac{4\sigma_Y}{\pi E'} \left[-\sqrt{b^2 - a^2} \, \arccos \frac{a}{b} + a \ln \frac{b}{a} \right] .$$

From the condition $K_I^{(1)} + K_I^{(2)} = 0$ the length of the plastic zone is determined as

$$d = b - a = a \left[\left(\cos \frac{\pi\sigma}{2\sigma_Y} \right)^{-1} - 1 \right] . \tag{5.4}$$

Using this result one obtains the following expression for the crack-tip opening displacement (note that $v^- = -v^+$ due to symmetry):

$$\delta_t = 2 \left[v^{(1)}(a) + v^{(2)}(a) \right] = \frac{8\,\sigma_F}{\pi E'}\, a \ln \left(\cos \frac{\pi\sigma}{2\,\sigma_Y} \right)^{-1} . \tag{5.5}$$

Correspondingly, the J–integral reads

$$J = \sigma_Y \delta_t = \frac{8\,\sigma_Y^2}{\pi E'}\, a \ln \left(\cos \frac{\pi\sigma}{2\,\sigma_Y} \right)^{-1} . \tag{5.6}$$

The size of the plastic zone according to (5.4) which is in good agreement with experimental findings for $\sigma \widetilde{<} 0.9\,\sigma_Y$ is depicted in Fig. 5.3a. The limit $\sigma \to \sigma_Y$ corresponds to $d \to \infty$ which means a plastification of the entire ligament. At this *limit load* failure takes place by *plastic collapse*.

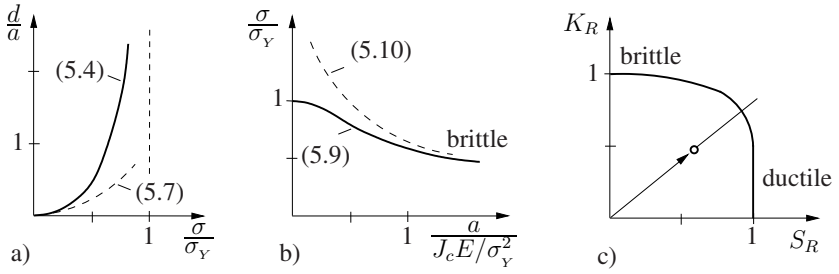

Fig. 5.3 a) plastic zone size, b) failure load, c) failure assessment curve

For sufficiently low loading ($\sigma \ll \sigma_Y$) the plastic zone remains small. Then small-scale yielding conditions prevail and linear elastic fracture mechanics is valid. In this case

$$\left(\cos \frac{\pi\sigma}{2\sigma_Y} \right)^{-1} \approx 1 + \frac{1}{2} \left(\frac{\pi\sigma}{2\,\sigma_Y} \right)^2 \qquad \text{with} \qquad \sigma\sqrt{\pi a} = K_I$$

and from (5.4) the size of the plastic zone follows as

$$d = 2r_p^D = \frac{a}{2} \left(\frac{\pi\sigma}{2\sigma_Y} \right)^2 = \frac{\pi}{8} \left(\frac{K_I}{\sigma_Y} \right)^2 . \tag{5.7}$$

The letter D here indicates its derivation from the Dugdale model. Analogously, δ_t and J reduce to

$$\delta_t = \frac{K_I^2}{E' \sigma_Y} , \qquad J = \frac{K_I^2}{E'} . \tag{5.8}$$

That means that in case of small-scale yielding the fracture criteria (5.1) and (5.3) of elastic-plastic fracture mechanics reduce to the fracture criteria of linear elastic fracture mechanics (K-concept). The size of the plastic zone according to (5.7) then is of the same order of magnitude as Irwin's approximation (4.126) for plane stress.

In the general case of arbitrarily large plastic zones insertion of (5.6) into the fracture criterion (5.3) yields

$$\frac{8}{\pi} \ln \left(\cos \frac{\pi \sigma}{2 \sigma_Y} \right)^{-1} = \frac{J_c E}{\sigma_Y^2} \frac{1}{a} . \tag{5.9}$$

For the special case of linear elastic fracture mechanics ($\sigma \ll \sigma_Y$) this reduces to

$$\pi \left(\frac{\sigma_{\text{lin}}}{\sigma_Y} \right)^2 = \frac{J_c E}{\sigma_Y^2} \frac{1}{a} . \tag{5.10}$$

For given material parameters J_c, E, σ_Y these relations describe the dependence of the failure load σ on the crack length a in the general elastic-plastic case and the linear elastic case, respectively. Figure 5.3b shows that for small a ductile failure prevails; the failure load is close to the plastic limit load. In case of large a, on the other hand, failure takes place in a brittle manner according to linear elastic fracture mechanics.

A representation of the failure condition which is independent of the crack length is obtained by inserting (5.9) into (5.10). Using the notation $\sigma/\sigma_{\text{lin}} = K_I/K_{Ic} = K_R$ and $\sigma/\sigma_Y = S_R$ the *failure assessment curve* (Fig 5.3c) is given by

$$K_R = S_R \left[\frac{8}{\pi^2} \ln \left(\cos \frac{\pi}{2} S_R \right)^{-1} \right]^{-1/2} . \tag{5.11}$$

It may be interpreted as a failure criterion in the elastic-plastic range between the two limit cases of brittle fracture ($K_R = 1$) and plastic collapse ($S_R = 1$). By virtue of the proportionality of K_I and σ a loading process corresponds to the radial outward motion of a point in the diagram of Fig. 5.3c. The distance between the point and the limit curve then is a measure of the safety against failure.

Although, strictly speaking, being valid only for the example of Fig. 5.2, the relation (5.11), because of its simplicity, is frequently applied also to other crack configurations and technical components. Thereby σ and σ_Y are replaced by some load P and the plastic limit load P_L, respectively, and (5.11) is assumed to be universally valid.

Despite its simplicity the Dugdale model is capable of describing the essential phenomena of elastic-plastic fracture. Although originally developed for the situation of thin plates in plane stress, it is frequently applied also to plane strain or, in

modified form, to three-dimensional problems (e.g., penny-shaped cracks) where it yields practically reasonable results. The basic idea of modeling a plastic zone by a yield strip is suitable for various modifications. One may, for instance, consider multiple yield strips inclined against each other or take into account a hardening material behavior by a nonuniform stress distribution along the yield strip.

5.3 Cohesive zone models

In the Dugdale model, the plastic zone is reduced to a strip in which the opposite crack faces act on each other via the constant stress σ_Y. The basic idea of an interaction of the crack faces by distributed forces can be generalized to many other fracture processes where the debonding process is localized in a narrow band, the so-called *cohesive zone*. The corresponding models are known as *cohesive zone models*. Over the past years they have found wide acceptance because they allow an appropriate description of many fracture processes that have a strip-shaped process zone. Examples of their fields of application are ductile metals, fiber reinforced materials, ceramics, concrete and fracture processes along the interface between two materials.

The first cohesive model was proposed in 1959 by G.I. BARENBLATT for the description of perfect brittle fracture of a linear elastic body. Even though the model offers no advantages compared with the K-concept, it shall be briefly discussed here because it exemplifies the general approach. In Barenblatt's model, the process zone ahead of the physical crack tip is regarded as a cohesive zone of length d where the separation of the material, i.e. of the crack faces extended by d, takes place (Fig. 5.4a). Along the distance d intermolecular *cohesive stresses* σ^{coh} are acting which depend of the separation δ and whose distribution is qualitatively depicted in Fig. 5.4b (see also Fig. 3.1). Now the following three assumptions are made: 1. the cohesive zone is small compared with all other dimensions, i.e. $d \ll a$, 2. the distribution of separation δ and cohesive stress σ^{coh} in the cohesive zone is for a given material always the same and independent of the external load, 3. the

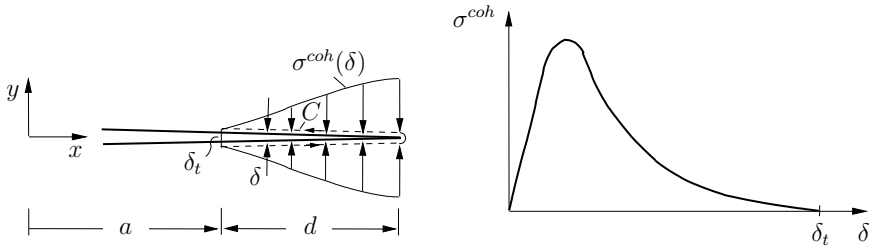

Fig. 5.4 Barenblatt model

opposite crack faces smoothly join each other at the end of the cohesive zone. The last condition is equivalent to the requirement of a vanishing stress intensity factor at the fictitious crack tip, i.e. the stresses remain finite everywhere. This can be expressed as $K_I + K_I^{coh} = 0$ where K_I and K_I^{coh} are the K-factors due to the external load and due to the cohesive stresses, respectively. Using load case 4 of Table 4.1, K_I^{coh} can be written as

$$K_I^{coh} = -\frac{\sqrt{2}}{\sqrt{\pi}}\,T \qquad \text{with} \qquad T = \int_a^{a+d} \frac{\sigma^{coh}(x)}{\sqrt{x}}\,\mathrm{d}x\,, \tag{5.12}$$

where T is the *cohesive modulus*, introduced by Barenblatt. It can be regarded as a measure of the state of the process zone. Since $d \ll a$, the K-factors $K_I(a)$ and $K_I(a+d)$ due to the external load are equal, which leads with $K_I + K_I^{coh} = 0$ to the simple relation

$$T = \frac{\sqrt{2}}{\sqrt{\pi}}\,K_I\,. \tag{5.13}$$

Therefore, the failure concept based on Barenblatt's cohesive modulus ($T = T_c$) and the K-concept ($K_I = K_{Ic}$) are fully equivalent. The equivalence to Griffith's energy release rate concept also can be easily shown. For this purpose it is practical to determine the J-Integral where, as in the Dugdale model, the contour C is chosen along the crack faces of the cohesive zone. As a result we obtain from (4.119)

$$J = -\int_a^{a+d} \sigma^{coh}(x)\frac{\mathrm{d}}{\mathrm{d}x}[v^+ - v^-]\mathrm{d}x = -\int_a^{a+d} \sigma^{coh}(x)\frac{\mathrm{d}\delta}{\mathrm{d}x}\mathrm{d}x = \int_0^{\delta_t} \sigma^{coh}(\delta)\mathrm{d}\delta\,. \tag{5.14}$$

Because of $J = \mathcal{G}$, the energy release rate is uniquely given by the area below the $\sigma^{coh}(\delta)$-curve.

In contrast to Barenblatt's model for brittle fracture, the length of the cohesive process zone is not small in many other fracture processes. Furthermore, the material not necessarily needs to be elastic, but, for instance, can be elastic-plastic or viscoelastic. Figure 5.5 schematically shows the process zone for different materials. This zone generally is characterized by *bridges* between the crack faces which transfer the cohesive forces. Their dependence on the separation δ is expressed by a material specific cohesive law $t(\delta)$ where the cohesive stress here is denoted by t (Fig. 5.5f). The cohesive law $t(\delta)$ describes the local constitutive behavior inside the cohesive zone in terms of a traction-separation relation. On account of the microscopic fracture processes, this constitutive law differs considerably from that of the surrounding material. Through the cohesive law, the specific work of separation

$$\mathcal{G}_c = \int_0^{\delta_c} t(\delta)\,\mathrm{d}\delta \tag{5.15}$$

is uniquely determined (see Fig. 5.5f). It represents the energy release rate and the J-integral if the surrounding material behaves elastic (see also (5.14)).

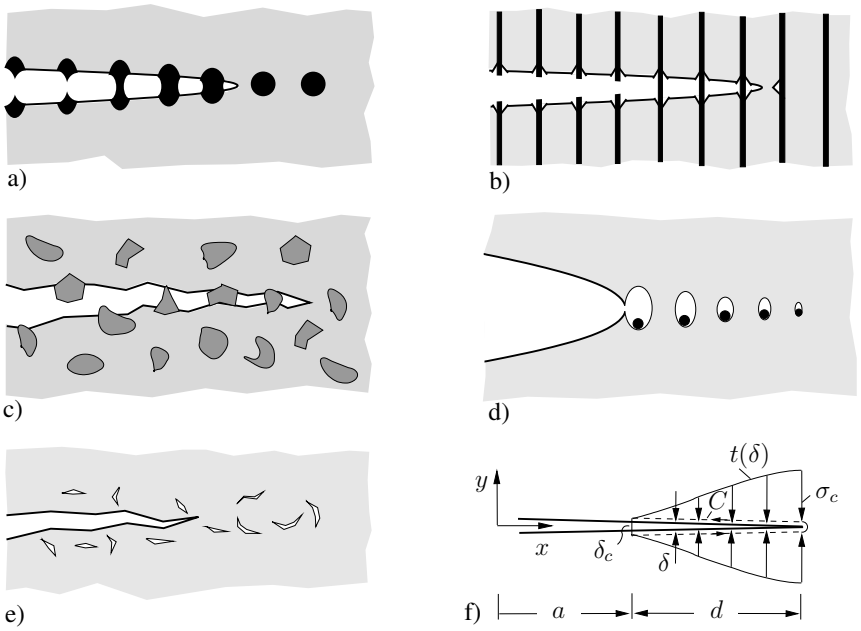

Fig. 5.5 Cohesive zones (schematic): a) metal-particle reinforced ceramics; b) fiber-matrix composite; c) heterogeneous ceramics, concrete; d) ductile material with void formation; e) brittle material with microcracks; f) cohesive zone model

Depending on the material and the characteristic fracture process, different approximations for the cohesive law are used. For example, for brittle metals or particle-matrix composites an exponential law of the type

$$t = \mathrm{e}\,\sigma_c \frac{\delta}{\delta_0}\,\mathrm{e}^{-\delta/\delta_0} \qquad \text{with} \qquad \mathrm{e} \approx 2.72 \tag{5.16}$$

has been proposed (Fig. 5.6a). It mimics the debonding process of atomic layers according to Fig. 3.1. Here, σ_c is the ultimate stress and δ_0 the associated separation. For this approach, the specific fracture-surface work according to (5.15) is given by $\mathcal{G}_c = \mathrm{e}\,\sigma_c\,\delta_0$. It is a disadvantage of the exponential law that, strictly speaking, the cohesive stress vanishes only for $\delta \to \infty$. Other cohesive laws are given, for example, by the trapezoidal shaped or the bilinear function as shown in Figs. 5.6b-d. They have been proposed for crack growth modeling in elastic-plastic materials or in the interface of adhesive joints (Fig. 5.6b), for the delamination of layered materials (Fig. 5.6c) and for the failure of concrete or cementitious materials (Fig. 5.6d).

The cohesive law is uniquely determined by a small number of parameters, which, in best case (e.g. exponential law (5.16)), can be reduced to two. In the latter case they can be experimentally determined relatively simple from two characteris-

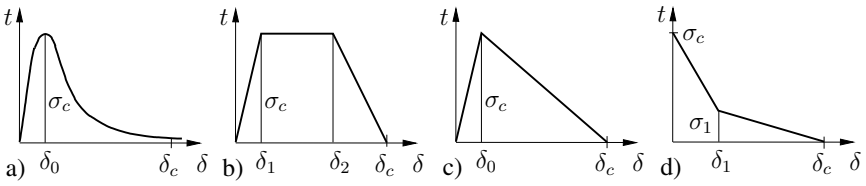

Fig. 5.6 Cohesive laws

tic material parameters: a) the ultimate stress (strength) σ_c and b) the specific work of separation $\mathcal{G}_c$.

In a general loading situation, not only a mode-I separation δ_n normal to the separation plane takes place. The material points opposite to each other also experience a relative displacement δ_t tangential to the separation plane as in mode II and mode III. In such a case it is expedient to formulate the cohesive law in vectorial form: $\boldsymbol{t}=\boldsymbol{f}(\boldsymbol{\delta})$ where $\boldsymbol{t}= t_n\boldsymbol{e}_n + t_t\boldsymbol{e}_t$ and $\boldsymbol{\delta}= \delta_n\boldsymbol{e}_n + \delta_t\boldsymbol{e}_t$. Yet, this shall not be further discussed here.

Cohesive zone models are very well suited for the numerical treatment of fracture processes within the framework of the finite element method. Here, the cohesive zone is discretized by using so-called cohesive elements. These elements are characterized by a vanishing initial thickness and their behavior is given by the material specific traction-separation law.

Finally it shall be mentioned that cohesive laws may be derived from micromechanical damage models which are exemplarily discussed in Sections 9.3 and 9.4.

5.4 Crack-tip field

Similar to linear elastic fracture mechanics, the field in the vicinity of a crack tip plays a key role also in elastic-plastic fracture mechanics. Crack-tip fields for different material models are investigated in the following. For simplicity we partly restrict our attention to the simplest case of mode III.

5.4.1 Perfectly plastic material

5.4.1.1 Antiplane shear, mode III

A state of antiplane shear is characterized by the displacement w and stresses $\tau_{xz},\ \tau_{yz}$ being the only nonvanishing components. For a perfectly plastic material the stresses have to fulfill the yield condition

$$\tau_{xz}^2 + \tau_{yz}^2 = \tau_Y^2 \quad \text{with} \quad \tau_Y = const. \tag{5.17}$$

According to Section 1.5.3 the curves along which τ_Y is attained (= α-lines) are always straight lines while in sections normal to these curves the shear stress vanishes. Therefore, a slip-line field as shown in Fig. 5.7 in the vicinity of a crack tip satisfies the boundary conditions of traction-free crack faces. In polar coordinates r, φ (note: φ coincides with the angle ϕ in Section 1.5.3) the stresses inside the fan ($|\varphi| \leq \pi/2$) are

$$\tau_{\varphi z} = \tau_Y \ , \qquad \tau_{rz} = 0 \ . \tag{5.18}$$

Along an α-line the displacement increment $\mathrm{d}w$ is constant which means that inside the fan $\mathrm{d}w = \mathrm{d}w(\varphi)$ holds and hence $\mathrm{d}\gamma_{rz} = \partial(\mathrm{d}w)/\partial r = 0$. The strain increment $\mathrm{d}\gamma_{\varphi z} = \partial(\mathrm{d}w)/r\partial\varphi$ can be determined if we consider $\mathrm{d}\gamma_{\varphi z}(R)$ to be known along the boundary $R(\varphi)$ of the plastic zone:

$$\mathrm{d}\gamma_{\varphi z}(r,\varphi) = \frac{R(\varphi)}{r}\,\mathrm{d}\gamma_{\varphi z}(R) \ . \tag{5.19}$$

Assuming an undeformed initial state and setting $w(\varphi = 0) = 0$ one obtains by integration

$$\gamma_{\varphi z} = \frac{1}{r}\frac{\partial w}{\partial \varphi} = \frac{R(\varphi)}{r}\,\gamma_{\varphi z}(R) \ , \qquad w = \int_0^{\varphi} R(\varphi)\gamma_{\varphi z}[R(\varphi)]\mathrm{d}\varphi \ . \tag{5.20}$$

The relations (5.17) through (5.20) are generally valid inside the fan, i.e., they apply also for arbitrarily large plastic zones. They indicate that the stresses are bounded by the yield stress whereas the strains display an $1/r$– singularity at the crack tip.

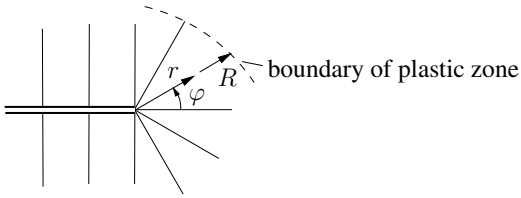

Fig. 5.7 α-lines in mode III

The stresses (5.18) may also be represented in a somewhat different way. In cartesian coordinates they are $\tau_{xz} = -\tau_Y \sin\varphi$ and $\tau_{yz} = \tau_Y \cos\varphi$, and along a circle with its center M located at a distance r^* ahead of the crack tip (Fig. 5.8) the following representation in terms of the angle φ^* holds

$$\tau_{xz} = -\tau_Y \sin\frac{\varphi^*}{2} \ , \qquad \tau_{yz} = \tau_Y \cos\frac{\varphi^*}{2} \ . \tag{5.21}$$

Up to a factor these are exactly the stresses which according to the elastic crack-tip solution (4.6) prevail along a circle around a crack tip at M if in (4.6) the distance r and the angle φ are replaced by the quantities r^* and φ^*. This correlation can

be employed to construct an exact solution for the case of small-scale yielding. The plastic zone then is embedded in an elastic domain inside which the elastic near-field solution holds. Along the boundary between the two domains the stresses from the elastic and plastic solution must coincide. This can be accomplished by setting (5.21) equal to (4.6) and taking into account the different notations: $\tau_{_Y} = K_{III}/\sqrt{2\pi r^*}$. Hence the plastic zone is a circular domain ahead of the crack tip with the radius

$$r_p = r^* = \frac{1}{2\pi}\left(\frac{K_{III}}{\tau_{_Y}}\right)^2 . \tag{5.22}$$

Note that the same result for r_p is obtained by estimating the size of the plastic zone from the elastic near-field solution according to Irwin (see Section 4.7.1).

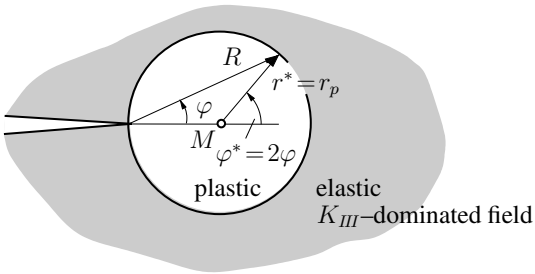

Fig. 5.8 Plastic zone inside elastic near tip field

Using (5.22) the boundary $R(\varphi)$ of the plastic zone and the strain $\gamma_{\varphi z}(R)$ prevailing along it are

$$R(\varphi) = 2r_p\cos\varphi = \frac{1}{\pi}\left(\frac{K_{III}}{\tau_{_Y}}\right)^2\cos\varphi\ , \qquad \gamma_{\varphi z}(R) = \frac{\tau_{_Y}}{G}\ . \tag{5.23}$$

From (5.19) and (5.20) it thus follows that

$$\gamma_{\varphi z} = \frac{1}{r}\,\frac{K_{III}^2}{\pi G\tau_{_Y}}\cos\varphi\ , \qquad w = \frac{K_{III}^2}{\pi G\tau_{_Y}}\sin\varphi \tag{5.24}$$

holds inside the plastic zone. The crack-tip opening displacement δ_t is given by the relative displacement of the two crack faces at the crack tip:

$$\delta_t = w(\frac{\pi}{2}) - w(-\frac{\pi}{2}) = \frac{2}{\pi}\,\frac{K_{III}^2}{G\tau_{_Y}}\ . \tag{5.25}$$

5.4.1.2 Plane strain, mode I

The plastic crack-tip field under plane strain conditions can likewise be obtained from slip line theory according to Section 1.5.3. Due to symmetry only the upper

half plane ($y \geq 0$) needs to be considered (Fig. 5.9a). Along the traction-free crack faces as well as along the x-axis ahead of the crack tip (mode-I symmetry) the boundary condition $\tau_{xy} = 0$ holds. Hence the slip lines there terminate at an angle of $45°$. The connection between the resulting regions A and C is established by the fan B (quarter circle). After L. PRANDTL (1875-1953), who presented this solution for the first time, the corresponding slip line field is called a *Prandtl–field*. Using (1.125) and the notation given in Fig. 5.9a the "starting" (boundary) value $\sigma_m = k$ is obtained at the crack face ($\phi = 3\pi/4$, $\sigma_y = 0$, $\tau_{xy} = 0$). Along a β-line passing through A, B, and C ($\phi^A = 3\pi/4,\ \phi^B = \varphi,\ \phi^C = \pi/4$) Hencky's equations (1.126) yield

$$\sigma_m^A = k\ , \qquad \sigma_m^B = k(1 + 3\pi/2 - 2\varphi)\ , \qquad \sigma_m^C = k(1 + \pi)\ . \tag{5.26}$$

From (1.125) therefore the stresses in the various regions are

$$\begin{pmatrix} \sigma_x \\ \sigma_y \\ \tau_{xy} \end{pmatrix} = \frac{\sigma_Y}{\sqrt{3}} \left(\begin{array}{c|c|c} & \text{region A} & \text{region B} & \text{region C} \\ \hline 2 & 1 + 3\pi/2 - 2\varphi - \sin 2\varphi & \pi \\ 0 & 1 + 3\pi/2 - 2\varphi + \sin 2\varphi & 2 + \pi \\ 0 & \cos 2\varphi & 0 \end{array} \right)\ , \tag{5.27}$$

where $k = \sigma_Y / \sqrt{3}$ has been inserted. The angular variations of the components in polar coordinates are depicted in Fig. 5.9b.

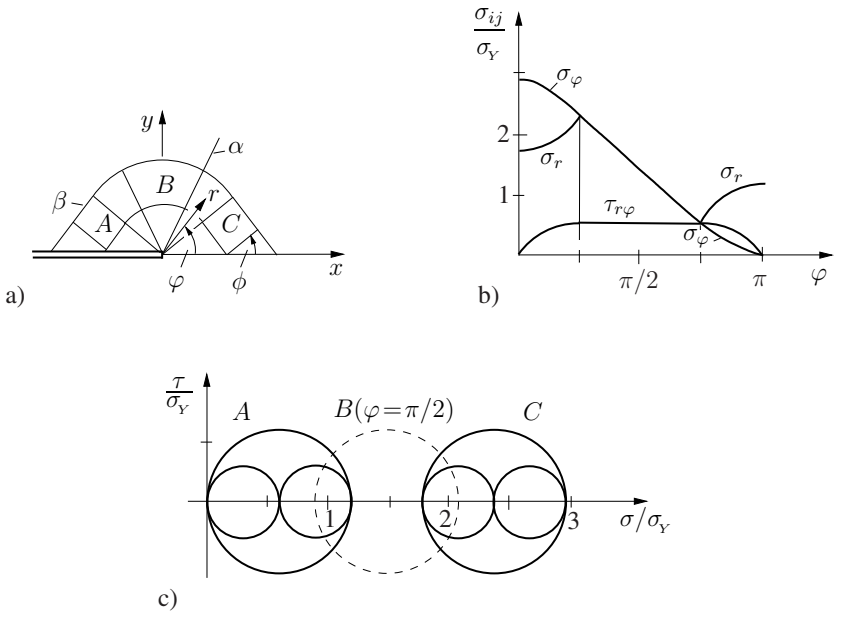

Fig. 5.9 Crack tip field in perfectly plastic material

Because of $\sigma_z = \sigma_m$ the crack-tip stress field is completely determined by (5.27) and (5.26). Mohr's circles corresponding to the three regions are shown in Fig. 5.9c. Obviously, a high hydrostatic stress component prevails in the region C ahead of the crack tip. This can be taken as an indication that microscopic void growth is promoted there.

Along slip lines the variations of shear strain are maximum while length changes of material elements in the direction of the slip lines vanish. It can be shown that this behavior gives rise to a representation of the strain field inside the fan B of the form

$$\varepsilon_{ij} = \frac{1}{r}\,\widetilde{\varepsilon}_{ij}(\varphi)\ . \tag{5.28}$$

Like in the corresponding mode-III case it contains an $1/r$–singularity. The complete determination of ε_{ij} in the entire plastic zone and of the crack-opening displacement requires the knowledge of ε_{ij} along one boundary (for instance, along the boundary between the elastic and plastic region). This has not yet been found by analytical methods.

The crack tip field (5.27) shall primarily describe the situation at a crack tip under mode-I tensile loading. But the solution remains unaltered if in addition a possible T-stress is taken into account. In such a case only the dimension of the region where this solution dominates may change. This can qualitatively be understood when for a fixed mode-I tensile load the stress state at a material point in the elastic region at some distance ahead of the crack tip is considered along with the plastic zone directly surrounding the crack tip. If now an increasing negative T-stress (pressure) is superposed, the maximum shear stress at this point increases until plastic flow sets in. This means that the size of the plastic zone increases when a negative T-stress is present while a positive T-stress leads to a smaller plastic zone size.

The solution (5.27) allows to directly compute the plastic limit load P_L for the crack configuration depicted in Fig. 5.10. Corresponding to the shown slip line field which is valid for $b \gg a$ the stress $\sigma_y = \sigma_Y\,(2+\pi)/\sqrt{3}$ prevails between the two crack tips. Therefore the limit load is

$$P_L = \sigma_y 2aB = \frac{2(2+\pi)}{\sqrt{3}}\,aB\sigma_Y\ . \tag{5.29}$$

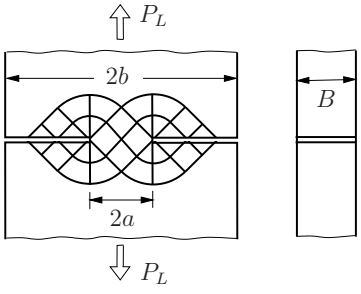

Fig. 5.10 Plastic limit load

It appears pertinent here to briefly discuss another important solution for a crack-tip field in perfectly plastic material. The effect mentioned before that the high hydrostatic stresses ahead of a crack tip cause void growth in a ductile material becomes even more pronounced when the somewhat more realistic situation of a blunted crack tip is considered (Fig. 5.11). The stress distribution in this case can likewise be computed from slip-line theory and is in cartesian coordinates for $y = 0$ given by

$$\sigma_y = \frac{2\sigma_Y}{\sqrt{3}} \left[1 + \ln\left(1 + \frac{x}{r}\right)\right] , \qquad \sigma_x = \frac{2\sigma_Y}{\sqrt{3}} \ln\left(1 + \frac{x}{r}\right) . \tag{5.30}$$

The slip-lines now are logarithmic spirals which terminate from the traction-free boundary at angles of $45°$. In contrast to the corresponding purely elastic solution, the vertical stress σ_y increases with increasing distance from the crack tip and the maximum hydrostatic stress in the plastic region (bounded from outside by the elastic field) is attained at some distance ahead of the crack tip. That means that void growth can be expected to occur inside the material somewhere ahead of the crack tip. The extension of the plastic region and the precise location of the peak hydrostatic stress can not be determined from slip-line theory (rigid-plastic material) alone; therefore an elastic-plastic analysis is required.

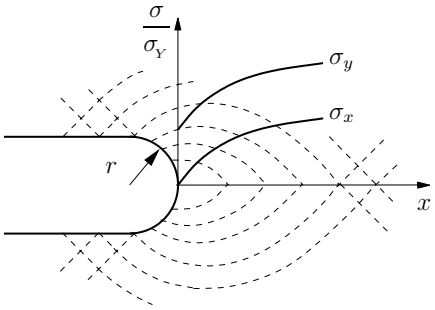

Fig. 5.11 Blunted crack tip in a perfectly plastic material

The approximation of the material behavior as a perfectly plastic one is not fully satisfactory. Though the analysis yields some information about the singular character of the strain field at the crack tip it does not provide a parameter to be used in a fracture criterion. Furthermore, a hardening behavior as observed for many materials can not be described. A material model which overcomes these deficiencies is discussed in the following Section.

5.4.2 Total strain theory, HRR−field

In the framework of total strain theory (see Section 1.3.3.3) we consider a hardening material with the uniaxial stress-strain behavior approximated by the *Ramberg–Osgood law* (Fig. 5.12a)

$$\frac{\varepsilon}{\varepsilon_0} = \frac{\sigma}{\sigma_0} + \alpha \left(\frac{\sigma}{\sigma_0} \right)^n . \tag{5.31}$$

For sufficiently small α the parameters ε_0 and σ_0 can be understood as the strain and stress at the onset of yield while n is the *hardening exponent*. The limit case $n = 1$ corresponds to a fully linear behavior, whereas an elastic perfectly plastic material is obtained for $n \to \infty$. The two terms on the right-hand side can be interpreted as the elastic and plastic parts of strain: $\varepsilon^e/\varepsilon_0 = \sigma/\sigma_0$, $\varepsilon^p/\varepsilon_0 = \alpha(\sigma/\sigma_0)^n$.

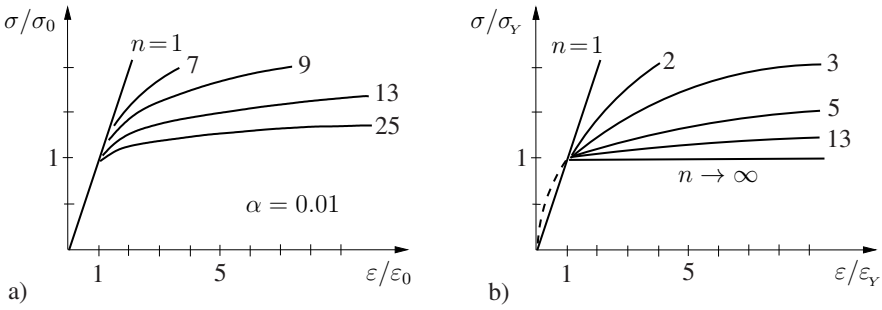

Fig. 5.12 Power law

In the vicinity of a crack tip the material is in the plastic range ($\varepsilon/\varepsilon_0 \gg 1$). Because of the strain singularity expected to prevail at the crack tip, the elastic strains there can be neglected compared to the plastic strains, i.e., $\varepsilon_{ij} = \varepsilon^p_{ij}$. Hence (5.31) reduces to

$$\frac{\varepsilon}{\varepsilon_0} = \alpha \left(\frac{\sigma}{\sigma_0} \right)^n \tag{5.32}$$

and the general constitutive law of total strain theory (1.86) can be written as

$$\varepsilon_{kk} = 0 , \qquad e_{ij} = \frac{3}{2} \frac{\varepsilon_\mathrm{e}}{\sigma_\mathrm{e}} s_{ij} . \tag{5.33}$$

Using (5.32) as the relation between ε_e and σ_e in (5.33) yields

$$\varepsilon_{ij} = e_{ij} = \frac{3}{2} \alpha \varepsilon_0 \left(\frac{\sigma_\mathrm{e}}{\sigma_0} \right)^n \frac{s_{ij}}{\sigma_\mathrm{e}} \tag{5.34}$$

where the uniaxial equivalent strain and stress are defined as $\varepsilon_\mathrm{e} = (\frac{2}{3}\varepsilon_{ij}\varepsilon_{ij})^{1/2}$ and $\sigma_\mathrm{e} = (\frac{3}{2}s_{ij}s_{ij})^{1/2}$, respectively.

The constitutive law (5.34) may also be obtained from the stress-strain relation (see Fig. 5.12b)

$$\frac{\varepsilon}{\varepsilon_{_Y}} = \begin{cases} \sigma/\sigma_{_Y} & \text{for} \quad \sigma \le \sigma_{_Y} \\ (\sigma/\sigma_{_Y})^n & \text{for} \quad \sigma \ge \sigma_{_Y} \end{cases} \tag{5.35}$$

where the power law $\varepsilon/\varepsilon_{_Y} = (\sigma/\sigma_{_Y})^n$ holds in the plastic range. For the three-dimensional generalization (5.34) one has to assume an incompressible material behavior and set $\varepsilon_{_Y}/\sigma_{_Y}^n = \alpha\varepsilon_0/\sigma_0^n$.

In the framework of total strain theory a plastic material behavior is described like a nonlinear elastic material which in the present case is in addition incompressible. This can be verified by comparing (5.31–5.34) with (1.55 ff). Correspondingly, all relations from nonlinear elasticity are also valid for total strain theory. For instance, from (1.58) the strain energy density in the vicinity of a crack tip is

$$\begin{aligned} U &= \frac{n}{n+1}\, s_{ij}e_{ij} = \frac{n}{n+1}\, \frac{\sigma_0}{(\alpha\varepsilon_0)^{1/n}} \left(\frac{2}{3}\varepsilon_{ij}\varepsilon_{ij}\right)^{\frac{1+n}{2n}} \\ &= \frac{n}{n+1}\, \alpha\varepsilon_0\sigma_0 \left(\frac{\sigma_{\mathrm{e}}}{\sigma_0}\right)^{1+n} . \end{aligned} \tag{5.36}$$

An important consequence of the equivalence of total strain theory and elasticity theory is the path-independence of the J–integral (4.119) evaluated for a crack tip with straight and traction-free crack faces (see Section 4.6.5.3). This property allows to determine in a simple manner the asymptotic behavior of field quantities when approaching the crack tip. Therefore we consider a circular integration contour C close to the crack tip ($r \to 0$) as depicted in Fig. 5.13. With $\mathrm{d}c = r\mathrm{d}\varphi$ the J–integral can be written as

$$J = \int_{-\pi}^{+\pi} [U n_1 - \sigma_{i\beta} u_{i,1} n_\beta]\, r\mathrm{d}\varphi \, . \tag{5.37}$$

Path-independence, i.e., independence from r requires that the term in brackets behaves like $1/r$ for $r \to 0$. Since both terms in brackets are of the type $\sigma_{ij}\varepsilon_{ij}$ the following relations must hold:

$$\sigma_{ij}\varepsilon_{ij} \sim \frac{\hat{f}(\varphi)}{r} = \frac{J}{r}\, \tilde{f}(\varphi) \, , \qquad U \sim \frac{\hat{U}(\varphi)}{r} = \frac{J}{r}\, \tilde{U}(\varphi) \, .$$

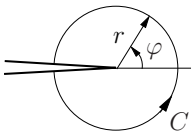

Fig. 5.13 Integration contour for J–integral

From (5.34) and (5.36) one obtains for the stresses

$$\sigma_{ij} = C \left(\frac{J}{r} \right)^{\frac{1}{n+1}} \tilde{\sigma}_{ij}(\varphi) \tag{5.38}$$

where C is some constant. It is practical to replace C by a new dimensionless constant I chosen in such a way that $\tilde{\sigma}_{ij}(\varphi)$ as well as the J/r term become dimensionless: $C = \sigma_0/(I\alpha\varepsilon_0\sigma_0)^{1/(n+1)}$. For $r \to 0$ the field quantities then may be represented as

$$\begin{aligned}
\sigma_{ij} &= \sigma_0 \left(\frac{J}{I\alpha\varepsilon_0\sigma_0 r} \right)^{\frac{1}{n+1}} \tilde{\sigma}_{ij}(\varphi) \,, \\
\varepsilon_{ij} &= \alpha\varepsilon_0 \left(\frac{J}{I\alpha\varepsilon_0\sigma_0 r} \right)^{\frac{n}{n+1}} \tilde{\varepsilon}_{ij}(\varphi) \,, \\
u_i - u_{i0} &= \alpha\varepsilon_0 r \left(\frac{J}{I\alpha\varepsilon_0\sigma_0 r} \right)^{\frac{n}{n+1}} \tilde{u}_i(\varphi) \,,
\end{aligned} \tag{5.39}$$

where u_{i0} is some rigid body motion. Using $\tilde{\sigma} = (\frac{3}{2}\tilde{\sigma}_{ij}\tilde{\sigma}_{ij})^{1/2}$ and inserting into (5.37) yields the relation

$$\begin{aligned}
I = \int_{-\pi}^{+\pi} \Bigg\{ & \left[\frac{n}{n+1}\, \tilde{\sigma}^{1+n} - \frac{1}{1+n} \left(\tilde{\sigma}_r \tilde{u}_r + \tilde{\tau}_{r\varphi}\tilde{u}_\varphi + \tilde{\tau}_{rz}\tilde{u}_z \right) \right] \cos\varphi \\
& + \left[\tilde{\sigma}_r(\tilde{u}_r' - \tilde{u}_\varphi) + \tilde{\tau}_{r\varphi}(\tilde{u}_\varphi' + \tilde{u}_r) + \tilde{\tau}_{rz}\tilde{u}_z' \right] \sin\varphi \Bigg\} \mathrm{d}\varphi \,.
\end{aligned} \tag{5.40}$$

The primes here denote derivatives with respect to φ.

The dominating field at a crack tip (5.39) displays stress and strain singularities which depend on the hardening exponent n. For $n = 1$ the already known $1/\sqrt{r}$–singularity of linear elastic fracture mechanics occurs while $n \to \infty$ leads to nonsingular stresses and a strain singularity of the type $1/r$. The angular variations $\tilde{\sigma}_{ij}$, $\tilde{\varepsilon}_{ij}$, $\tilde{u}_i$ in (5.39) can not be determined from these simple considerations. Similar to linear elastic fracture mechanics they have to be computed from a boundary value problem. In the present nonlinear case, however, this requires a numerical solution (see below). The dominating crack-tip field then is fixed up to the parameter J which characterizes the magnitude or "intensity" of the field. Using the initials of J.W. HUTCHINSON, J.R. RICE, and G.F. ROSENGREN who investigated this field for the first time it is called the *HRR–field*.

It has to be emphasized that although the derivation of the HRR-field (5.39) is based on total strain theory it is also valid in the framework of the incremental theory of plasticity. This follows from the fact that the crack-tip field is solely determined by the single parameter J so that the power law (5.32) leads to proportional loading. In this case the total strain theory and the incremental theory are equivalent (Section 1.3.3.3).

Figure 5.14a shows the r–dependence of the stresses for various values of n. It can be seen that the domain of high stress, i.e., the domain inside which the HRR-field actually dominates, becomes smaller with increasing n. The deformation of the crack tip is likewise dependent on the hardening parameter (Fig. 5.14b); with increasing n the crack-opening profile becomes more and more blunted.

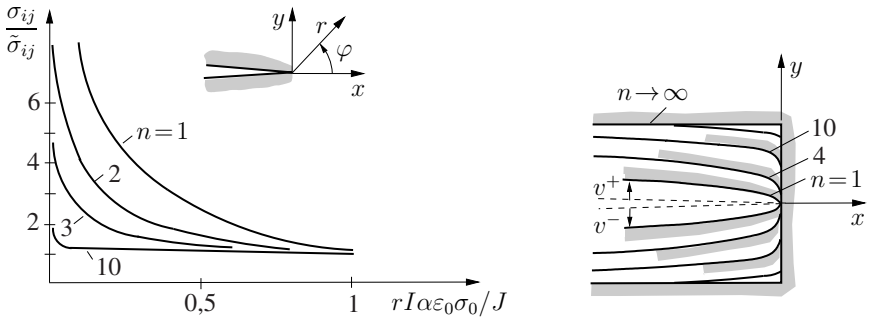

Fig. 5.14 HRR–field: a) stress distribution, b) crack-opening profile

In the following it is briefly outlined for the case of plane strain how the complete near tip solution can be obtained. For this purpose the problem is formulated in terms of the stresses by elimination of the strains. Inserting the constitutive law (5.34) into the compatibility condition

$$\frac{1}{r}\frac{\partial^2}{\partial r^2}(r\varepsilon_\varphi)+\frac{1}{r^2}\frac{\partial^2\varepsilon_r}{\partial\varphi^2}-\frac{1}{r}\frac{\partial\varepsilon_r}{\partial r}-\frac{2}{r^2}\frac{\partial}{\partial r}\left(r\frac{\partial\varepsilon_{r\varphi}}{\partial\varphi}\right)=0 \tag{5.41}$$

yields

$$\begin{aligned}-\frac{1}{r}\frac{\partial^2}{\partial r^2}\left[r\sigma^{n-1}(\sigma_r-\sigma_\varphi)\right]+\frac{1}{r^2}\frac{\partial^2}{\partial\varphi^2}\left[\sigma^{n-1}(\sigma_r-\sigma_\varphi)\right]\\ -\frac{1}{r}\frac{\partial}{\partial r}\left[\sigma^{n-1}(\sigma_r-\sigma_\varphi)\right]-\frac{4}{r^2}\frac{\partial}{\partial r}\left[r\frac{\partial}{\partial\varphi}(\sigma^{n-1}\tau_{r\varphi})\right]=0\end{aligned} \tag{5.42}$$

where

$$\sigma=\left[\frac{3}{4}(\sigma_r-\sigma_\varphi)^2+3\tau_{r\varphi}^2\right]^{1/2}. \tag{5.43}$$

It is appropriate to introduce the *Airy stress function* $\phi(r,\varphi)$ from which the stresses are derived according to

$$\sigma_r=\frac{1}{r}\frac{\partial\phi}{\partial r}+\frac{1}{r^2}\frac{\partial^2\phi}{\partial\varphi^2}\,,\qquad \sigma_\varphi=\frac{\partial^2\phi}{\partial r^2}\,,\qquad \tau_{r\varphi}=-\frac{\partial}{\partial r}\left(\frac{1}{r}\frac{\partial\phi}{\partial\varphi}\right)\,. \tag{5.44}$$

Equations (5.44) identically satisfy the equilibrium conditions. Now a separation ansatz is chosen for ϕ of the type

$$\phi = A\, r^s \tilde{\phi}(\varphi) \qquad \text{where} \qquad s = \frac{2n+1}{n+1} \tag{5.45}$$

such that the asymptotic character of the crack-tip field (5.39) is accounted for. Then (5.42) leads to the following nonlinear ordinary differential equation for the function $\tilde{\phi}$

$$\begin{aligned} \frac{n(n+2)}{(n+1)^2}\,\tilde{\sigma}^{n-1}\left[\frac{2n+1}{(n+1)^2}\,\tilde{\phi}+\tilde{\phi}''\right] + \left\{\tilde{\sigma}^{n-1}\left[\frac{2n+1}{(n+1)^2}\,\tilde{\phi}+\tilde{\phi}''\right]\right\}'' \\ + \frac{4n}{(n+1)^2}\left[\tilde{\sigma}^{n-1}\tilde{\phi}'\right]' = 0 \end{aligned} \tag{5.46}$$

where

$$\tilde{\sigma} = \left\{\frac{3}{4}\left[\frac{2n+1}{(n+1)^2}\tilde{\phi}+\tilde{\phi}''\right]^2 + 3\left[\frac{n}{n+1}\tilde{\phi}'\right]^2\right\}^{1/2} . \tag{5.47}$$

The mode-I crack-tip field is symmetric with respect to $\varphi = 0$, i.e.: $\tau_{r\varphi}(0) = 0$, $\partial\sigma_\varphi/\partial\varphi|_{\varphi=0} = 0$, $\partial\sigma_r/\partial\varphi|_{\varphi=0} = 0$. Furthermore, the crack faces are assumed to be traction-free: $\sigma_\varphi(\pi) = 0$, $\tau_{r\varphi}(\pi) = 0$. For $\tilde{\phi}$ this leads to the boundary conditions

$$\tilde{\phi}'(0) = 0\,, \qquad \tilde{\phi}'''(0) = 0\,, \qquad \tilde{\phi}(\pi) = 0\,, \qquad \tilde{\phi}'(\pi) = 0\,. \tag{5.48}$$

A solution of (5.46)–(5.48) in closed form is not known, yet it may be obtained with high accuracy by numerical integration. In Fig. 5.15 the angular variation of the stresses is depicted for two different values of n. Comparison with Fig. 4.6b and Fig. 5.9b shows that for $n = 2$ it is still close to that of a linear elastic material while for $n = 10$ a strong similarity to that of a perfectly material can be seen. From the now known functions $\tilde{\sigma}_{ij}$, $\tilde{u}_i$ the factor I finally can be computed from (5.40); some

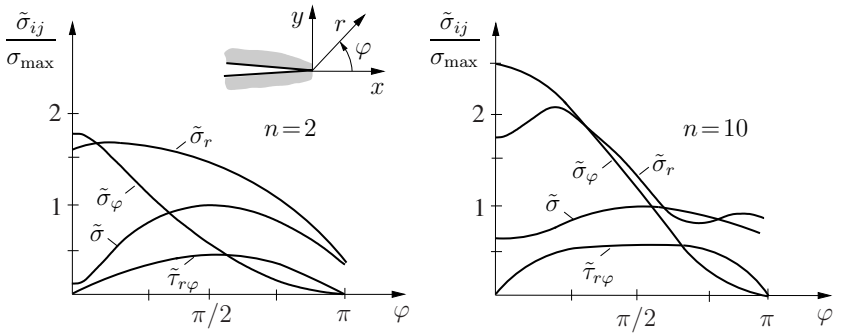

Fig. 5.15 HRR–field: angular variation of stresses

values are given in Table 5.1. It has to be mentioned that analogous analyses can be performed for mode-II loading as well as for plane stress.

n	2	3	5	10	∞
I	5.94	5.51	5.02	4.54	3.72
D	1.72	1.33	1.08	0.93	0.79

Table 5.1 Values of $I(n)$ and $D(n)$ for plane strain

5.5 Fracture criterion

In order to formulate a fracture criterion of elastic-plastic fracture mechanics the same fundamental ideas can be adopted as in case of the K–concept (Section 4.3). According to (5.39) the parameter J describes the intensity of the otherwise completely determined crack-tip field. The latter dominates inside a domain with an outer boundary schematically by denoted R in Fig. 5.16a. From inside the crack-tip region the validity of the field (5.39) is limited by a domain of radius r_N which can not be described by total strain theory. For instance, large deformations and local unloading may occur inside this region. It furthermore contains the process zone (radius ρ) where the fracture process with its material specific micromechanisms (e.g., void growth) takes place. Figure 5.16b schematically shows the correspondence of the different regions with respective ranges of the σ-ε-diagram. Now, if the J–determined domain II is large compared to the enclosed region III ($R \gg r_N,\ \rho$) then the state inside the process zone is controlled by the surrounding field, i.e., by J. Therefore J can be regarded as a measure of the "loading" of the crack-tip region. Crack propagation initiates once this loading attains a material-dependent

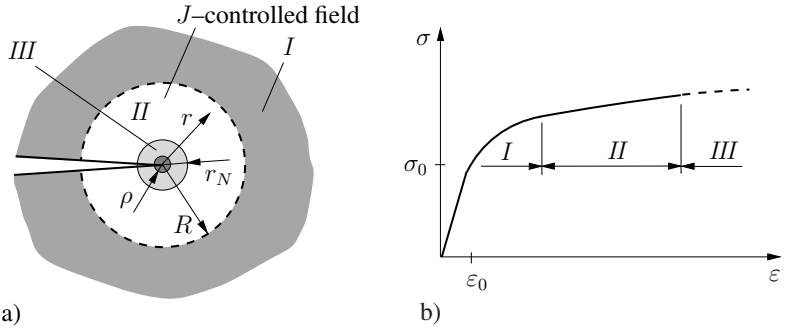

Fig. 5.16 Different crack-tip regions and deformation regimes

critical value J_c:

$$\boxed{J = J_c} \,. \tag{5.49}$$

Basis of the fracture criterion (5.49) are the total strain theory of plasticity as well as the assumption of existence of a dominating crack-tip field. This has important consequences to be emphasized here. The total strain theory is equivalent to the incremental theory of plasticity only in case of monotonically increasing loading (Section 1.3.3.3); it can not properly describe unloading processes. Numerical simulations have confirmed that the respective situation is in fact found with good approximation in the vicinity of a stationary crack tip. Crack propagation, in contrast, always gives rise to unloading processes. Therefore, the condition (5.49) is first of all valid only for crack initiation. Circumstances under which it may also be applied to crack propagation are discussed in Section 5.8.

The dominance of the crack-tip field (5.39) is guaranteed only if the material displays sufficient hardening (see Fig. 5.14a). With decreasing hardening the domain of dominance becomes smaller and it vanishes for a perfectly plastic material. Then J can no longer be regarded as a parameter which controls the crack-tip state.

The use of J as a fracture parameter is not directly tied to the HRR–field since elastic-plastic material behavior in the framework of total strain theory may also be approximated by a bilinear stress-strain dependence instead of a power law. This results in a dominating singular crack-tip field which is different from the HRR–field, yet with an intensity again determined by J.

As already mentioned the crack-opening displacement δ_t is, besides J, occasionally used as a fracture parameter. This approach is based on the idea that δ_t is a measure of plastic strain at the crack tip which in turn controls the fracture process. Accordingly, crack propagation initiates once the crack-opening displacement attains a critical value δ_{tc}:

$$\boxed{\delta_t = \delta_{tc}} \,. \tag{5.50}$$

If one assumes that the state of deformation at the crack tip may be sufficiently well described by the HRR–field then δ_t and J are equivalent parameters and can transformed into each other. This can be seen from equations (5.39) where the strains and displacements are directly connected to J. Ignoring the rigid body motion, the displacement of some point P on the upper crack face is (Fig. 5.17)

$$v_P = \alpha\varepsilon_0 r_P \left(\frac{J}{I\alpha\varepsilon_0\sigma_0 r_P}\right)^{\frac{n}{n+1}} \tilde{v}(\pi) \,, \qquad u_P = \alpha\varepsilon_0 r_P \left(\frac{J}{I\alpha\varepsilon_0\sigma_0 r_P}\right)^{\frac{n}{n+1}} \tilde{u}(\pi) \,.$$

If one defines δ_t by the intersection of two straight lines inclined by 45° to the x–axis with the crack-opening profile it follows that

$$v_P = \frac{\delta_t}{2} = r_P - u_P \,.$$

From these three equations one obtains by elimination of r_P the relation

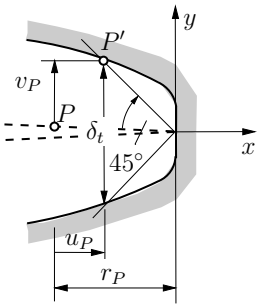

Fig. 5.17 Crack-opening displacement δ_t

$$\delta_t = (\alpha\varepsilon_0)^{1/n}\, D\, \frac{J}{\sigma_0} \tag{5.51}$$

where

$$D = \frac{2}{I}\,[\tilde{v}(\pi) + \tilde{u}(\pi)]^{1/n}\,\tilde{v}(\pi)\ . \tag{5.52}$$

Some values of D are given in Table 5.1. For a perfectly plastic material ($n \to \infty$) this yields $\delta_t = 0.79\ J/\sigma_0$ which is quite close to equation (5.2) based on the Dugdale model. One has, however, to note that this equation has been derived for plane stress. Furthermore, in this case (5.51) is strictly speaking no longer valid since it assumes the dominance of the HRR–field at least for $r < r_P$ or $r \lesssim \delta_t$. For a perfectly plastic material this dominance is not given.

Though J and δ_t are equivalent parameters the use of J and hence the fracture criterion (5.49) offer several advantages. Firstly, the crack-tip loading J is easier to compute than δ_t. Secondly, the experimental determination of the material parameter δ_{tc} is, in contrast to J_c, connected with difficulties. Another disadvantage of the crack-tip opening displacement is that its definition suffers from some arbitrariness. In the following we will therefore focus only on J.

5.6 Determination of *J*

The computation of J for a technical component that contains a crack and large plastic zones generally requires numerical methods. Especially the Finite Element Method (FEM) and to some extend also the Boundary Element Method (BEM) are employed for the solution of respective elastic-plastic boundary value problems. In doing so, several properties of J are exploited (see Section 4.6.5.3). For instance, J can be computed from a path-independent integral if the integration contour lies inside a region where the material behaves either purely elastic or according to the total strain theory of plasticity (i.e., no local unloding). Then it is often advantageous to choose a contour far away from the crack tip, possibly in a purely elastic region.

This circumvents the costly determination of field quantities in the vicinity of the crack tip with high accuracy which would require a rather fine discretization.

Another possibility is based on the meaning of J as an energy release rate. The latter can be determined from simulating crack advance by the release of a finite element node and computing the work done by the nodal force. Of course, the material then has to be described as nonlinear elastic. For further details the reader is referred to the extensive literature.

Besides the purely numerical calculation of J it is in some cases possible to derive approximate analytical solutions or to determine J by experimental methods. The latter approach is discussed in the following section. Approximate solutions may be found especially in the *Ductile Fracture Handbook* (see literature list, Section 5.11).

5.7 Determination of J_c

The determination of J_c is performed in standardized experiments. For this purpose specimens containing a crack of definite length a (e.g., CT-specimens, Fig. 4.22) are loaded until crack initiation (or often beyond) and the load-displacement curve is measured (Fig. 5.18a). The area below the curve $F(u_F, a)$ then is the work W^a done by the force F where the parameter a indicates that F depends on the chosen crack length a. The work W^a is equal to the strain energy Π^i if one assumes that under monotonic loading (i.e., no local unloading) the elastic-plastic material can be described as a nonlinear elastic one:

$$\Pi^i(u_F, a) = W^a = \int_0^{u_F} F(\bar{u}_F, a)\,\mathrm{d}\bar{u}_F \,. \tag{5.53}$$

Then J can be defined as $J = -\mathrm{d}\Pi/\mathrm{d}a$ where $\Pi = \Pi^i + \Pi^a$. If the crack length is changed by $\mathrm{d}a$ for fixed displacement $u_F = const.$ one has $\mathrm{d}\Pi^a = 0$ and $\mathrm{d}\Pi = \mathrm{d}\Pi^i$ such that

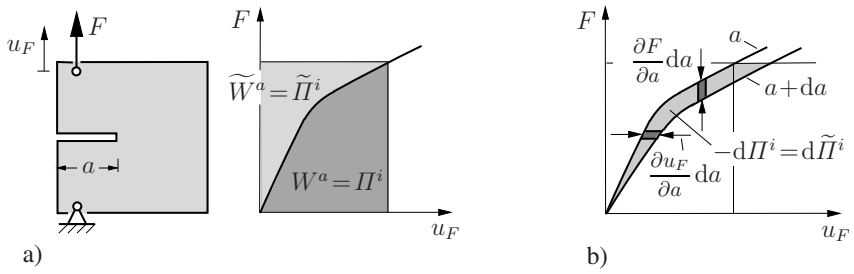

Fig. 5.18 Definition and determination of J

$$J = -\left.\frac{\mathrm{d}\Pi^i}{\mathrm{d}a}\right|_{u_F} = -\frac{\partial \Pi^i}{\partial a} = -\int_0^{u_F} \left.\frac{\partial F}{\partial a}\right|_{\bar{u}_F} \mathrm{d}\bar{u}_F \,. \tag{5.54}$$

The subscript here emphasizes which quantity is kept constant during differentiation. As illustrated in Fig. 5.18b J can formally be determined according to (5.54) from the load-displacement curves for two specimens differing by the crack lengths a and $a + \mathrm{d}a$.

A method for the determination of J_c which is based on the above result has been proposed by J.A. BEGLEY and J.D. LANDES (1972). Thereby, load-displacement curves $F(u_F, a_i)$ are measured for a series of specimens with different crack lengths a_1, a_2, a_3, ... (Fig. 5.19a). From these curves stepwise approximations for $\Pi^i(a, u_F)$ and for $J(u_F, a_j) \approx -\Delta\Pi^i/\Delta a$ can be obtained (Fig. 5.19b,c). From the known crack initiation value u_{Fc} for a particular crack length (e.g., for a_2) then J_c is found. The disadvantage of this so-called *multi-specimen technique* is its large experimental expense and the lack of accuracy.

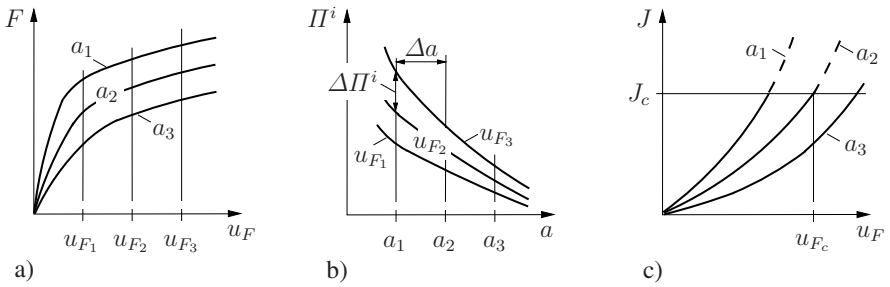

Fig. 5.19 Determination of J_c from the multi-specimen technique

An alternative method which requires testing only of a single specimen dates back to J.R. RICE. For its derivation we start from the complementary energy (see Section 1.4 and Fig. 5.18a)

$$\widetilde{\Pi}^i(F, a) = \widetilde{W}^a = \int_0^F u_F(\bar{F}, a)\, \mathrm{d}\bar{F} \qquad \text{where} \qquad \Pi^i + \widetilde{\Pi}^i = u_F F \,. \tag{5.55}$$

Differentiating

$$\Pi^i(u_F, a) = u_F F - \widetilde{\Pi}^i(F, a)$$

and using $(\partial\widetilde{\Pi}^i/\partial F)_a = u_F$ and $F = F(u_F, a)$ yields

$$\left.\frac{\partial \Pi^i}{\partial a}\right|_{u_F} = u_F \left.\frac{\partial F}{\partial a}\right|_{u_F} - \left.\frac{\partial \widetilde{\Pi}^i}{\partial F}\right|_a \cdot \left.\frac{\partial F}{\partial a}\right|_{u_F} - \left.\frac{\partial \widetilde{\Pi}^i}{\partial a}\right|_F = -\left.\frac{\partial \widetilde{\Pi}^i}{\partial a}\right|_F \tag{5.56}$$

such that from (5.54) the representation

$$J = + \left. \frac{\partial \widetilde{\Pi}^i}{\partial a} \right|_F = + \int_0^F \left. \frac{\partial u_F}{\partial a} \right|_{\bar{F}} \mathrm{d}\bar{F} \tag{5.57}$$

is obtained. This relation can be illustrated also from the area increment in Fig. 5.18b. It is, of course, not only valid for loading of a specimen or component by a single force but holds in corresponding form also for loading by some bending moment.

In the following we consider a specimen as depicted in Fig. 5.20a with its ends subjected to a bending moment and experiencing a relative rotation by an angle θ. In this case (5.57) reads

$$J = \int_0^M \left. \frac{\partial \theta}{\partial a} \right|_{\bar{M}} \mathrm{d}\bar{M} \, . \tag{5.58}$$

The rotation angle θ generally depends on the loading M, the geometric parameters a, b, l and the material behavior. If, by neglecting the linear elastic range, the latter is characterized solely by σ_Y and a hardening parameter n (see Fig. 5.12) normalization of all quantities yields

$$\theta = \theta \left(\frac{M}{M_0}, n, \frac{a}{b}, \frac{l}{b} \right) \qquad \text{where} \qquad M_0 = \frac{\sigma_Y b^2}{4} \, . \tag{5.59}$$

Here, the reference moment M_0 is the limit moment for a perfectly plastic material. For $a \gg b$ and $l \gg b$ and if by $n \gg 1$ the hardening is not very pronounced, θ is within a first approximation independent of the latter three parameters:

$$\theta \approx \theta \left(\frac{M}{M_0} \right) \, . \tag{5.60}$$

With $a = W - b$ and $\mathrm{d}a = -\mathrm{d}b$ one obtains

$$\left. \frac{\partial \theta}{\partial a} \right|_M = - \left. \frac{\partial \theta}{\partial b} \right|_M = - \frac{\mathrm{d}\theta}{\mathrm{d}(\frac{M}{M_0})} \cdot \frac{4M}{\sigma_Y} \left(- \frac{2}{b^3} \right)$$

$$\left. \frac{\partial \theta}{\partial M} \right|_a = \left. \frac{\partial \theta}{\partial M} \right|_b = - \frac{\mathrm{d}\theta}{\mathrm{d}(\frac{M}{M_0})} \cdot \frac{4M}{\sigma_Y b^2}$$

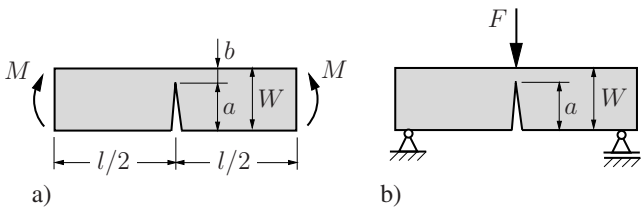

Fig. 5.20 Determination of J_c with a single specimen

and after elimination of $\mathrm{d}\theta/\mathrm{d}(\frac{M}{M_0})$

$$\left.\frac{\partial\theta}{\partial a}\right|_M = \frac{2M}{b}\cdot\left.\frac{\partial\theta}{\partial M}\right|_a .$$

Insertion into (5.58) finally yields

$$J = \frac{2}{b}\int_0^\theta M(\bar{\theta})\mathrm{d}\bar{\theta} = \frac{2}{b}\,W^a . \tag{5.61}$$

That means that up to a factor of $2/b$ the current loading J of the crack is given by the work W^a done by the moment. If bending of a specimen of thickness B is instead of a moment M produced by some force F (see Fig. 5.20b) it follows from (5.61) that

$$J = \frac{2}{B(W-a)}\int_0^{u_F} F(\bar{u}_F)\mathrm{d}\bar{u}_F \tag{5.62}$$

where it has to be noted that in (5.61) J was given per unit specimen thickness. From the known initiation value u_{Fc}, therefore J_c can easily be determined from the area below the load-displacement curve.

As already mentioned, the approximation (5.62) is only valid for deeply cracked specimens ($a \gg b$) subjected to bending loading. The negligence of the elastic range of the material behavior furthermore requires that over the major part of the remaining specimen cross section the plastic strains are large compared to the elastic strains. Hence the remaining cross section has to be sufficiently plastified prior to the onset of crack growth.

In order to obtain geometry-independent J_c-values from measurements certain size requirements have to be fulfilled, similar to linear elastic fracture mechanics. For CT-specimens and 3-point-bending specimens the following conditions have to be satisfied:

$$W-a,\ B > 25\,\frac{J_c}{\sigma_Y} . \tag{5.63}$$

Because of the direct proportionality of J_c/σ_Y and δ_{tc} (see (5.2), (5.51)) that means that all relevant dimensions need to be large compared to the crack-tip opening displacement at the instant of crack initiation. In addition to (5.63) the material must display a sufficient hardening to assure the dominance of a J-controlled crack-tip field (see Section 5.5).

5.8 Crack propagation

5.8.1 J–controlled crack growth

The loading of a crack in ductile metals under large-scale yielding conditions can be increased to a multitude of the initiation value and this increase is accompanied by a crack advance of a few millimeters (see also Section 4.8). Due to this crack advance unloading processes take place, especially in parts of the plastic zone behind the crack tip, which can not be properly described by the deformation theory of plasticity. Hence also the requirements for the application of J are not fulfilled. For small amounts of crack advance, however, J can, under certain conditions, nevertheless represent a meaningful measure of the crack-tip loading state. In such a case the fracture criterion

$$J = J_R(\Delta a) \tag{5.64}$$

holds also in the course of crack growth. Here, J_R is the crack resistance (subscript R) which depends on the amount of crack advance Δa. $J_R(\Delta a)$ is called the *J–resistance curve* of a material and its typical shape is schematically depicted in Fig. 5.21a. The steep initial increase for $J < J_c$ is solely due to blunting of the crack tip by plastic deformations; it is called the *blunting line*. If we assume that the crack extension caused by blunting is approximately half the crack-tip opening displacement ($\Delta a \approx \delta_t/2$), the use of $J = \sigma_Y \delta_t$ (see (5.2) and (5.51)) yields the coarse estimate for the blunting line

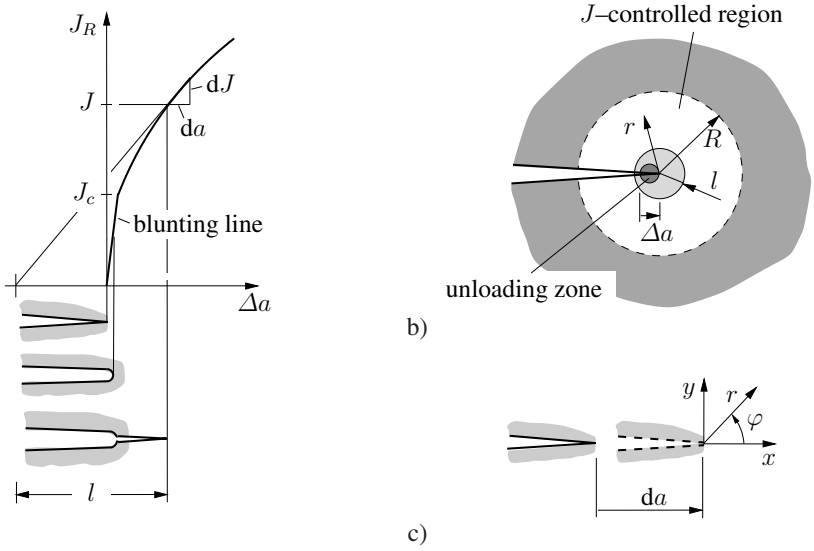

Fig. 5.21 J–controlled crack growth

$$J \approx 2\sigma_Y \Delta a \ . \tag{5.65}$$

For $J \geq J_c$ the blunting line is followed by the actual J_R–curve where crack extension takes place by material separation.

Figure 5.21b illustrates the situation at the crack tip for a crack extension by Δa. A J–controlled state can obviously prevail if the essential character of the crack-tip field found at a stationary crack is only slightly disturbed by the crack advance. For this to hold it is necessary that the characteristic size of the unloading zone, i.e., the crack extension itself, is small compared to the dimension of the J–controlled region: $\Delta a \ll R$. More specific results concerning the requirement of nearly proportional loading can be obtained if the change of the crack-tip field is estimated from the HRR–field. Therefore we assume that the stress field (5.38)

$$\sigma_{ij}(J, r, \varphi) = C \left(\frac{J}{r} \right)^{\frac{1}{n+1}} \tilde{\sigma}_{ij}(\varphi)$$

moves with the propagating crack tip (Fig. 5.21c). Due to an increase of the loading by $\mathrm{d}J$ and a crack-tip translation by $\mathrm{d}a$ a material point experiences the stress change

$$\mathrm{d}\sigma_{ij} = \frac{\partial \sigma_{ij}}{\partial J} \, \mathrm{d}J - \frac{\partial \sigma_{ij}}{\partial x} \, \mathrm{d}a \ .$$

Using

$$\frac{\partial}{\partial x} = \cos\varphi \, \frac{\partial}{\partial r} - \sin\varphi \, \frac{\partial}{r \partial \varphi}$$

this can be written in the from

$$\mathrm{d}\sigma_{ij} = C \left(\frac{J}{r} \right)^{\frac{1}{n+1}} \left\{ \frac{\mathrm{d}J}{J} \left[\frac{\tilde{\sigma}_{ij}(\varphi)}{n+1} \right] + \frac{\mathrm{d}a}{r} \left[\frac{\tilde{\sigma}_{ij}(\varphi)}{n+1} \cos\varphi + \frac{\partial \tilde{\sigma}_{ij}}{\partial \varphi} \sin\varphi \right] \right\}. \tag{5.66}$$

The first term in the braces characterizes a stress increase proportional to the load increment $\mathrm{d}J$, i.e., proportional loading. This does not apply for the second term which is caused by crack growth. If we note that the two terms are of the same order of magnitude the second term can be neglected for those values of r for which the condition

$$\frac{\mathrm{d}a}{r} \ll \frac{\mathrm{d}J}{J} \tag{5.67}$$

holds. Then (5.66) describes nearly proportion loading. By $J/l = \mathrm{d}J/\mathrm{d}a$ we introduce a loading-dependent length l which for sufficiently steep increase $\mathrm{d}J/\mathrm{d}a$ is of the same order of magnitude as the crack advance (Fig. 5.21a). Therefore, J–dominance *and* proportional loading hold inside the annular region given by (see Fig. 5.21b)

$$l \ll r < R \ . \tag{5.68}$$

Hence J–controlled crack growth can be expected as long as $l \ll R$. Since the spatial extension R of the dominant crack-tip field has to be small compared to any relevant geometric dimension b of a specimen (e.g., the remaining cross section in

Fig. 5.20) and (5.64) must hold during crack propagation the above condition may also be expressed by

$$l \ll b \qquad \text{or} \qquad \frac{b}{J_R}\,\frac{\mathrm{d}J_R}{\mathrm{d}a} \gg 1\ . \tag{5.69}$$

5.8.2 *Stable crack growth*

Considerations concerning the stability of J–controlled crack growth are analogous to those in Section 4.8. According to (5.64) the amount of crack advance is determined from the "equilibrium condition"

$$J(F,a) = J_R(\Delta a)\ .$$

The equilibrium state is stable if the condition

$$\frac{\partial J}{\partial a} < \frac{\mathrm{d}J_R}{\mathrm{d}a} \tag{5.70}$$

holds. Then the increase of crack resistance with increasing crack length exceeds the change of the crack driving force caused by crack propagation. To maintain crack growth in such a case it is necessary to increase J (Fig. 5.22a). Typically this requires an increase of the external load F. With prescribed load the limit for stable crack growth is reached at

$$\left.\frac{\mathrm{d}J}{\mathrm{d}a}\right|_F = \frac{\mathrm{d}J_R}{\mathrm{d}a}\ . \tag{5.71}$$

If the dimensionless *tearing modulus*

$$T = \frac{E}{\sigma_Y^2}\,\frac{\mathrm{d}J}{\mathrm{d}a} \tag{5.72}$$

according to P.C. PARIS is introduced, the stability condition (5.70) can be written in the form

$$T < T_R\ . \tag{5.73}$$

Now we want to derive $\mathrm{d}J/\mathrm{d}a$ for the configuration given in Fig. 5.22b where loading of the cracked body takes place via a linear spring with prescribed end displacement u_F. In contrast to the respective example in Section 4.8 here the body can not be assumed to be linear elastic. It is appropriate to start from (5.57) and with

$$u_F(F,a) = C_F F + u_P(F,a) \qquad \text{and} \qquad \frac{\partial u_F}{\partial a} = \frac{\partial u_P}{\partial a}$$

we get

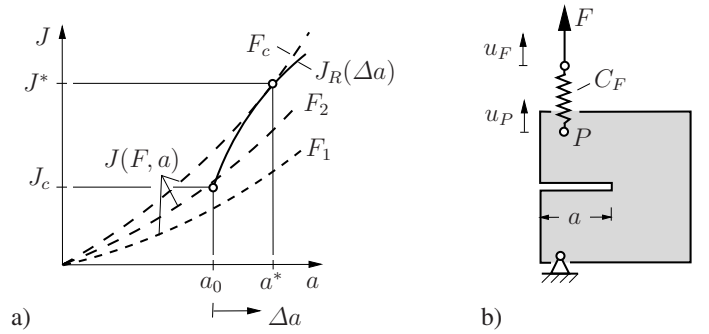

Fig. 5.22 Stable crack growth

$$J(F,a) = \int_0^F \left.\frac{\partial u_P}{\partial a}\right|_{\bar{F}} \mathrm{d}\bar{F} \,. \tag{5.74}$$

Differentiation yields

$$\frac{\mathrm{d}J}{\mathrm{d}a} = \frac{\partial J}{\partial F}\,\frac{\mathrm{d}F}{\mathrm{d}a} + \frac{\partial J}{\partial a} \,. \tag{5.75}$$

If the condition (fixed displacement u_F)

$$\frac{\mathrm{d}u_F}{\mathrm{d}a} = \frac{\partial u_F}{\partial F}\,\frac{\mathrm{d}F}{\mathrm{d}a} + \frac{\partial u_F}{\partial a} = 0 \quad \rightsquigarrow \quad \frac{\mathrm{d}F}{\mathrm{d}a} = -\frac{\partial u_F/\partial a}{\partial u_F/\partial F} = -\frac{\partial u_P/\partial a}{C_F + \partial u_P/\partial F}$$

and the relation following from (5.74)

$$\frac{\partial J}{\partial F} = \frac{\partial u_P}{\partial a}$$

are inserted into (5.75) this finally leads to

$$\left.\frac{\mathrm{d}J}{\mathrm{d}a}\right|_{u_F} = \left.\frac{\partial J}{\partial a}\right|_F - \frac{\left(\frac{\partial u_P}{\partial a}\right)^2}{C_F + \frac{\partial u_P}{\partial F}} \,. \tag{5.76}$$

For the special cases of a prescribed displacement u_F in P ($C_F = 0$) or dead loading ($C_F \to \infty$) one obtains

$$\frac{\mathrm{d}J}{\mathrm{d}a} = \begin{cases} \left.\dfrac{\partial J}{\partial a}\right|_F - \dfrac{\partial u_P/\partial a}{\partial u_P/\partial F} & \text{for } C_F = 0 \,, \\[2ex] \left.\dfrac{\partial J}{\partial a}\right|_F & \text{for } C_F \to \infty \,. \end{cases} \tag{5.77}$$

The actual determination of $\mathrm{d}J/\mathrm{d}a$ for particular geometries is in general possible only with numerical methods. In case of the deeply cracked 3-point-bending

specimen, as shown in Fig. 5.20b, subjected to prescribed displacement u_F, however, a simple relation can be found. Starting point is the approximation (5.62)

$$J(u_F, a) = \frac{2}{W-a} \int_0^{u_F} F(\bar{u}_F, a) \mathrm{d}\bar{u}_F \ ,$$

where J is taken per unit specimen thickness. Using (5.54) it follows that

$$\left.\frac{\mathrm{d}J}{\mathrm{d}a}\right|_{u_F} = \frac{2}{(W-a)^2} \int_0^{u_F} F(\bar{u}_F, a) \mathrm{d}\bar{u}_F + \frac{2}{W-a} \int_0^{u_F} \frac{\partial F}{\partial a} \mathrm{d}\bar{u}_F = -\frac{J}{W-a} \ . \tag{5.78}$$

Because of $\mathrm{d}J/\mathrm{d}a < 0$ crack growth under these circumstances is always stable.

5.8.3 Steady-state crack growth

5.8.3.1 Crack opening angle

The extension of a crack with large plastic zones is often possible far beyond the limits of J-controlled growth. Even steady-state conditions may develop in the vicinity of the crack tip after a sufficient amount of crack advance. Neither during the transition between J-controlled and steady-state crack growth nor in the steady-state regime can the crack-tip loading be characterized by J. Other control parameters of the crack-tip state then have to be used which are supposed to remain constant for steady-state crack growth. Based on experimental results it has been proposed to employ the crack opening angle. This measure of deformation can be introduced in two different ways:

1) The *crack-tip opening angle* $CTOA$ is the current opening angle between the crack faces in the vicinity of the crack tip (Fig. 5.23a). This definition bears the advantage that $CTOA$ and J are equivalent as long as a J–controlled state prevails because then the displacement and correspondingly the angle are uniquely determined by J. A disadvantage of $CTOA$, however, is that this quantity is difficult to measure.

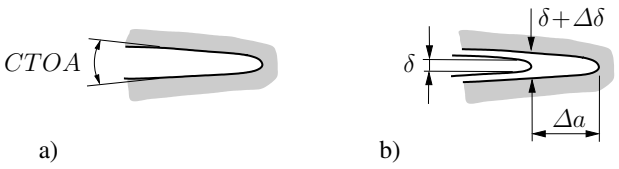

Fig. 5.23 Crack opening angle

2) The *crack opening angle* COA according to Fig. 5.23b is the change $\Delta\delta$ of the crack opening displacement at the original crack tip related to the crack advance Δa:

$$COA = \frac{\Delta\delta}{\Delta a} \,. \tag{5.79}$$

This parameter is easy to measure but its physical significance is questionable.

5.8.3.2 Crack-tip field

So far it has not been accomplished to a satisfactory extent to describe the entire evolution of the elastic-plastic crack-tip field, starting from the situation at a stationary crack tip via the transition regime until steady-state crack propagation. For the steady-state case, however, solutions can be found which are based on simple material models.

As an example we consider a crack which propagates at constant speed $\dot{a}$ in a perfectly plastic material. For simplicity we restrict the analysis to the mode-III case. Furthermore, we assume that the crack-tip motion is slow enough (quasistatic) for inertia forces to be neglected. The basic equations with respect to a fixed x, y–coordinate system are given in Section 1.5.3. It is appropriate to transform these equations to a x', y'–coordinate system which moves together with the crack tip (Fig. 5.24).

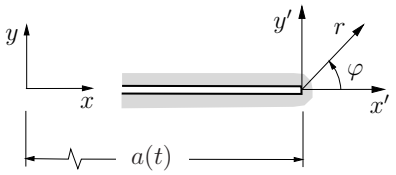

Fig. 5.24 Crack growth: moving coordinate system

The relation between moving and fixed coordinates is given by

$$x' = x - a(t) \,, \qquad y' = y \tag{5.80}$$

where $a(t)$ is the crack length which depends on time t. For some arbitrary field quantity $F(x, y, t) = F(x'[x, a(t)], y'[y], t)$ it follows that

$$\frac{\partial F}{\partial x} = \frac{\partial F}{\partial x'} \,, \quad \frac{\partial F}{\partial y} = \frac{\partial F}{\partial y'} \,, \qquad \dot{F} = \left.\frac{\partial F}{\partial t}\right|_{x,y} = \left.\frac{\partial F}{\partial t}\right|_{x',y'} - \dot{a}\,\frac{\partial F}{\partial x'} \,. \tag{5.81}$$

If we assume steady-state conditions the time derivative in the moving system vanishes and

$$\dot{F} = -\dot{a}\,\frac{\partial F}{\partial x'} \,. \tag{5.82}$$

Since from (5.81) the spatial derivatives are equal in both systems the yield condition and the equilibrium condition (1.127) maintain their form in the moving system. Only x and y have to be replaced by x' and y', respectively. As a consequence, the slip lines and the stress distribution can be adopted unaltered from the respective boundary value problem for a stationary crack in Section 5.4.1.1. Therefore, also for the moving crack

$$\tau_{\varphi z} = \tau_Y \ , \qquad \tau_{rz} = 0 \tag{5.83}$$

hold inside the fan (see Fig. 5.7). The corresponding strain increments (see (5.19)) can also be adopted; here they are related to the time increment $\mathrm{d}t$:

$$\dot\gamma_{\varphi z}(\varphi, r) = \frac{\mathrm{d}\gamma_{\varphi z}}{\mathrm{d}t} = \frac{R(\varphi)}{r}\,\dot\gamma_{\varphi z}(R) \ , \qquad \dot\gamma_{rz} = 0 \ . \tag{5.84}$$

Therein $\dot\gamma_{\varphi z}(R)$ is regarded to be known along $R(\varphi)$, e.g., from the outer elastic field. For the integration of (5.84) use is made of (5.82). To simplify the analysis we assume $R(\varphi) = R_0$ and $\dot\gamma_{\varphi z}(R_0) = C\dot a/R_0$. The cartesian components of the strain rate then are

$$\dot\gamma_{xz} = -\frac{C\dot a}{r}\sin\varphi \ , \qquad \dot\gamma_{yz} = +\frac{C\dot a}{r}\cos\varphi \ .$$

With

$$\sin\varphi = y'/r \ , \qquad \cos\varphi = x'/r \ , \qquad r^2 = x'^2 + y'^2$$

and (5.82) it follows that

$$\frac{\partial\gamma_{xz}}{\partial x'} = \frac{Cy'}{x'^2 + y'^2} \ , \qquad \frac{\partial\gamma_{yz}}{\partial x'} = -\frac{Cx'}{x'^2 + y'^2}$$

and after integration

$$\gamma_{xz} = C(\pi/2 - \varphi) + f_1(y') \ , \quad \gamma_{yz} = -C\ln\frac{r}{r_0} + f_2(y') \ , \tag{5.85}$$

where $f_1,\ f_2,\ r_0$ remain undetermined. If we consider only the logarithmic term in γ_{yz} which dominates for $r \to 0$ the near tip strains can be represented as

$$\gamma_{rz} = -C\ln r\sin\varphi \ , \qquad \gamma_{\varphi z} = -C\ln r\cos\varphi \ . \tag{5.86}$$

At a moving crack tip they display a logarithmic singularity which is weaker than the $1/r$–singularity at a stationary crack.

The respective analysis for a moving mode I crack is much more complicated. Analogous to mode-III it yields a logarithmic strain singularity and bounded stresses. It turns out, however, that the Prandtl–field according to Section 5.4.1.2 is not valid in the entire crack-tip region. In contrast to the stationary crack here a wedge–shaped unloading region occurs in which the material behaves elastically (Fig. 5.25). Similar unloading regions are obtained if the material is described by a modified Ramberg-Osgood law with elastic unloading. Then not only the strains but

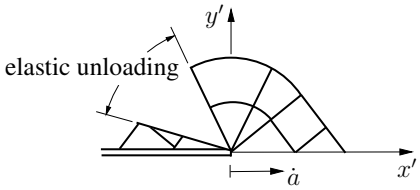

Fig. 5.25 Mode-I crack propagation in perfectly plastic material

also the stresses display a logarithmic crack-tip singularity which depends on the hardening exponent.

5.8.3.3 Energy flux and *J*–integral

If inertia forces are neglected and only mechanical energy terms are considered, then from (4.94) - (4.96) the energy flux $-P^*$ across the boundary A_P into the process zone is

$$-P^* = -\frac{\mathrm{d}W_\sigma}{\mathrm{d}t} = P - \dot{E} \quad \text{where} \quad P = \int_{\partial V} t_i\, \dot{u}_i \,\mathrm{d}A\,, \quad E = \int_V U^* \mathrm{d}V. \tag{5.87}$$

Here, ∂V denotes the total surface of the material volume V except the surface A_P which is the boundary of the process zone. The specific work of deformation is described by

$$U^* = \int_0^{\varepsilon_{kl}} \sigma_{ij}\,\mathrm{d}\varepsilon_{ij} = \int_0^t \sigma_{ij}\,\frac{\partial \varepsilon_{ij}}{\partial \tau}\,\mathrm{d}\tau = \int_0^t \sigma_{ij}\,\dot{u}_{i,j}\,\mathrm{d}\tau\,. \tag{5.88}$$

Only for an elastic material it is independent of the deformation path and equal to the strain energy density U (see Section 1.3.1.2).

In the following we consider the plane mode-I problem of a propagating straight crack with traction-free crack faces and a process zone represented by a point at the crack tip (Fig. 5.26). If the energy flux rate $\mathcal{G}^*$ is introduced via $\mathrm{d}W_\sigma/\mathrm{d}t = \dot{a}\,\mathrm{d}W_\sigma/\mathrm{d}a = -\dot{a}\,\mathcal{G}^*$ and if the notation is changed according to $A_P \to C_P$, $A \to C + C^+ + C^-$, $V \to A$ then one obtains from (5.87) for the energy flux across the boundary C_P

$$\dot{a}\,\mathcal{G}^* = \int_C t_i\,\dot{u}_i\,\mathrm{d}c - \frac{\mathrm{d}}{\mathrm{d}t}\int_A U^*\mathrm{d}A\,. \tag{5.89}$$

Here it has already been taken into account that the crack faces $C^\pm$ are traction-free. The contour C_P with radius ρ is in the limit taken to be vanishingly small ($\rho \to 0$). The star at the energy flux rate $\mathcal{G}^*$ indicates that in contrast to the energy release rate

$\mathcal{G}$ the energy flux is not necessarily connected with a change of the potential energy of an elastic system because here the material behavior is arbitrary, e.g., inelastic.

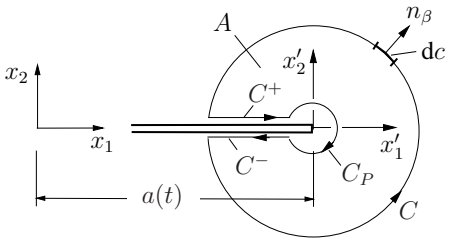

Fig. 5.26 Integration contours for energy flux into crack tip

Since the contour C_P moves with the crack tip (whereas C is fixed) the area A changes with time. In the temporal derivative of the work of deformation therefore the flux across C_P has to be accounted for (Reynold's transport theorem):

$$\frac{\mathrm{d}}{\mathrm{d}t}\int\limits_A U^*\mathrm{d}A = \int\limits_A \frac{\mathrm{d}U^*}{\mathrm{d}t}\,\mathrm{d}A + \dot{a}\int\limits_{C_P} U^* n_1\,\mathrm{d}c\,. \tag{5.90}$$

Using $\mathrm{d}U^*/\mathrm{d}t = \sigma_{ij}\,\dot{u}_{i,j} = (\sigma_{ij}\,\dot{u}_i)_{,j} - \sigma_{ij,j}\,\dot{u}_i$, the equilibrium condition $\sigma_{ij,j} = 0$ and the divergence theorem (where the crack faces $C^\pm$ yield no contribution since $t_i = 0$) this can be written as follows:

$$\begin{aligned}\frac{\mathrm{d}}{\mathrm{d}t}\int\limits_A U^*\mathrm{d}A &= \int\limits_A (\sigma_{ij}\,\dot{u}_i)_{,j}\,\mathrm{d}A + \dot{a}\int\limits_{C_P} U^* n_1\,\mathrm{d}c \\ &= \int\limits_C \sigma_{ij}\,\dot{u}_i\,n_j\,\mathrm{d}c + \int\limits_{C_P}\sigma_{ij}\,\dot{u}_i\,n_j\,\mathrm{d}c + \dot{a}\int\limits_{C_P} U^* n_1\,\mathrm{d}c\,.\end{aligned}$$

Insertion into (5.89) yields

$$\dot{a}\,\mathcal{G}^* = -\int\limits_{C_P}(\dot{a}\,U^* n_1 + t_i\,\dot{u}_i)\,\mathrm{d}c\,. \tag{5.91}$$

In order to obtain a more appropriate representation we employ a transformation to the moving x_1', x_2'–coordinate system and consider from now on the contour C and the area A likewise to move with the crack tip. The velocity $\dot{u}_i$ in (5.91) then has to be computed according to (5.81). Thereby we may assume that the displacement $u_i(r,\varphi,t)$ is regular (bounded) at the crack tip ($r \to 0$) while its spatial derivatives (strains) are singular. Hence the second "convective" term (see right-hand side of (5.81)) locally always dominates and $\dot{u}_i = -\dot{a}\,u_{i,1}$ like in the stationary case ("local stationarity"). The energy flux rate thus reads

$$\mathcal{G}^* = -\int_{C_P} (U^* n_1 - t_i\, u_{i,1})\, \mathrm{d}c \ . \tag{5.92}$$

If we now apply the divergence theorem to the area A with boundary $C + C_P + C^+ + C^-$ ($C^\pm$ again yields no contribution) and if we introduce by

$$J^* = \int_C (U^* n_1 - t_i\, u_{i,1})\, \mathrm{d}c = \int_C (U^* \delta_{1\beta} - \sigma_{i\beta}\, u_{i,1})\, n_\beta\, \mathrm{d}c \tag{5.93}$$

the modified J–integral, it follows that

$$\mathcal{G}^* = J^* - \int_A (U^*_{,1} - \sigma_{ij}\, u_{i,j1})\, \mathrm{d}A \ . \tag{5.94}$$

According to (5.94) the energy flux rate can in general *not* be represented by a path-independent contour integral J^*; an additional area integral rather has to be considered. If, however, the contour C is shrunk to the crack tip the area integral vanishes and

$$\mathcal{G}^* = \lim_{\rho \to 0} \int_C (U^* n_1 - t_i\, u_{i,1})\, \mathrm{d}c \ . \tag{5.95}$$

This coincides with (5.92); the difference in sign is due to the different orientation of the integration paths.

In the special case of stationary conditions the area integral in (5.94) always vanishes. This is so because from (5.82) and (5.88) it follows that $U^*_{,1} = -\dot{U}^*/\dot{a} = -\sigma_{ij}\, \dot{u}_{i,j}/\dot{a} = \sigma_{ij}\, u_{i,j1}$ and hence we get

$$\mathcal{G}^* = J^* \ . \tag{5.96}$$

Irrespective of the material behavior the energy flux rate can then be expressed by the J^*–integral (5.93) where the contour C is arbitrary (path-independence). This integral differs from the J–integral (4.119) in that J^* contains the specific work of deformation U^* instead of the strain energy density U.

As an example we consider crack propagation in a perfectly plastic material. In this case the stresses in the vicinity of the crack tip ($r \to 0$) are bounded while the strains display a logarithmic singularity: $\sigma_{i\beta} \sim \sigma_Y$, $u_{i,1} \sim \ln r$ (see Section 5.8.3.2). If the contour C is chosen according to Fig. 5.27 one obtains the following result from (5.95)

$$\mathcal{G}^* \sim \lim_{\varepsilon \to 0} 2\sigma_Y \int_{-\varepsilon}^{+\varepsilon} \ln|x'|\mathrm{d}x' = \lim_{\varepsilon \to 0} 2\sigma_Y\, [x'(\ln x' - 1)]_{-\varepsilon}^{+\varepsilon} = 0 \ . \tag{5.97}$$

That means that in a perfectly plastic material *no* energy flux takes place into the crack tip. Hence no energy is available for some dissipative process of material separation in the process zone. The source of this "paradox" obviously is the too

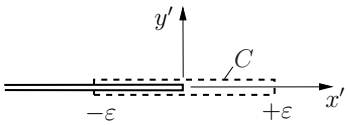

Fig. 5.27 Determination of $\mathcal{G}^*$

strong simplification of the process zone being only a point in conjunction with a perfectly plastic material behavior.

5.9 Essential work of fracture

Under large scale yielding conditions, size requirements such as (5.69) for the characterization of a material's fracture resistance in terms of J_c are often difficult to fulfill. This is especially so when tests (for practical reasons) are performed on thin sheets and when the material is very ductile and displays not much hardening. The definition and measurement of the crack tip opening displacement (Section 5.5) or the crack (tip) opening angle (Section 5.8.3.1), on the other hand, suffer from some arbitrariness. In contrast to these local quantities, the *essential work of fracture* (EWF) concept is based on global energetic considerations and tackles the problem of fracture toughness characterization not from initiation (and some period beyond) but from the other extreme of a completely fractured specimen. It has been developed by K.B. BROBERG, B. COTTERELL, J.K. REDDELL and Y.-W. MAI and is mainly used as a pragmatic approach of obtaining fracture toughness data for thin ductile metal sheets or ductile polymers.

The work expended during complete fracture of a specimen, i.e., the total fracture work W_f, is given by the area under the recorded load displacement curves in Fig. 5.28a. It depends on the specimen geometry (e.g., the ligament length l) and hence cannot be taken as a measure of the material's fracture toughness. The key assumption underlying the essential work of fracture concept is that W_f can be partitioned into two parts which scale differently with the ligament length l. A prerequisite for this is that prior to fracture the whole ligament has yielded and that the plastic zone (bright grey in Fig. 5.28b) fully comprises the fracture process zone (dark grey in Fig. 5.28b). The total work of fracture for a specimen of thickness B then can be written as

$$W_f = w_e B\, l + \beta\, w_p B\, l^2 \tag{5.98}$$

where the first term on the right hand side is the work dissipated in the fracture process zone (Bl = area of fracture surface) and the second term is the work not directly associated with fracture but dissipated in the surrounding plastic zone. The size of the latter in the specimen plane is proportional to l^2, and β is a shape factor. In (5.98) w_p is the specific (per volume) plastic work while w_e is called the specific

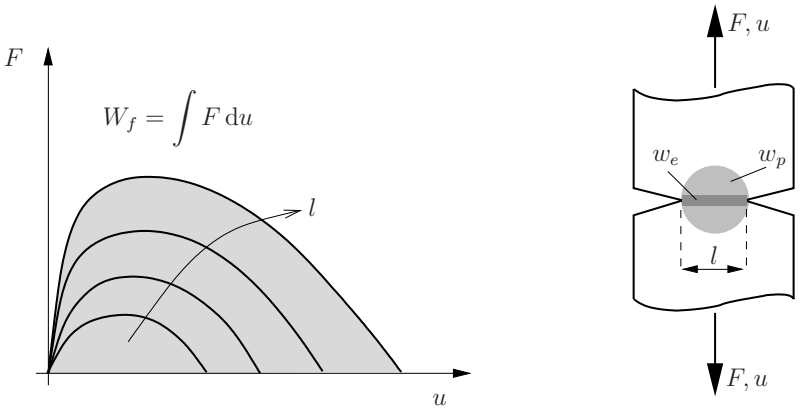

Fig. 5.28 a) Self-similar load displacement curves for ductile fracture, b) plastic zone and fracture ligament in double-edge notch tension (DENT) specimen

(per area) *essential work of fracture* since it is consumed per unit fracture area in the immediate fracture process (Fig. 5.28b).

In thin specimens of ductile materials yielding and fracture take place approximately under plane stress conditions and the situation sketched in Fig. 5.28b is typically met. The in-plane width of the fracture process zone then is of the order of the specimen thickness B since the fracture process involves through-thickness-slip and necking down of the ligament (see also Fig. 4.42b). That means that w_e depends on the specimen thickness. For a given thickness, however, it is approximately constant and independent of the specimen geometry. In order to determine w_e a series of *geometrically similar* specimens of different size, i.e. different ligament lengths, but fixed thickness have to be tested which leads to self-similar load displacement curves as sketched in Fig. 5.28a. If the resulting values of the total fracture work W_f are divided by the fracture area Bl and are plotted against the ligament length l

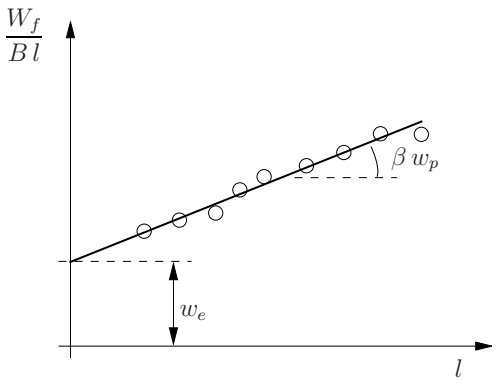

Fig. 5.29 Determination of essential work of fracture w_e from measured data (○)

(see Fig. 5.29) an approximately linear relation is obtained according to

$$\frac{W_f}{B\,l} = w_e + \beta\, w_p\, l\ . \tag{5.99}$$

The specific essential work of fracture w_e hence is found as the ordinate intercept for $l \to 0$.

5.10 Problems

Problem 5.1 The stresses for the depicted Dugdale crack can be derived from Westergaard's stress function

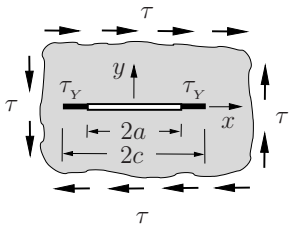

$$Z(z) = \frac{2\tau_{_Y}}{\pi}\tan^{-1}\sqrt{\frac{(c/a)^2-1}{1-(c/z)^2}}\ .$$

Determine the stresses along the x-axis and show that there are no stress singularities at $x = \pm c$.

Fig. 5.30

Solution: $\tau_{xy}(x,0) = \dfrac{2\tau_{_Y}}{\pi}\tan^{-1}\sqrt{\dfrac{(c/a)^2-1}{1-(c/x)^2}}$

Problem 5.2 Evaluate the Dugdale model (yield stress $\sigma_{_Y}$) for the semi-infinite crack shown in Figure 5.31a under an external load given by the applied stress intensity factor K_I^{app}.

Determine a) the length d of the yield strip,
b) the crack tip opening (CTOD) δ_t,
c) the J-integral.

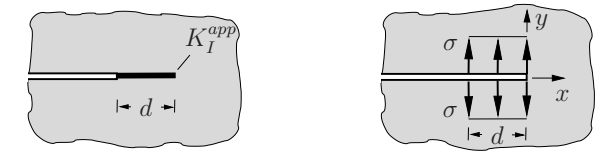

Fig. 5.31

Remark: Use Westergaard's stress function for a semi-infinite crack under a constant strip load according to Figure 5.31b:

$$Z(z) = \frac{2\sigma}{\pi}\left[\sqrt{\frac{d}{z}} - \tan^{-1}\sqrt{\frac{d}{z}}\right], \quad \bar{Z} = \frac{2\sigma}{\pi}\, d\left[\sqrt{\frac{z}{d}} - (1+z/d)\tan^{-1}\sqrt{\frac{d}{z}}\right].$$

Solution: $d = \frac{\pi}{8}\left(\frac{K_I^{app}}{\sigma_F}\right)^2, \qquad \delta_t = \frac{(K_I^{app})^2}{E'\sigma_Y}, \qquad J = \frac{(K_I^{app})^2}{E'}.$

5.11 Further reading

Anderson, T.L. *Fracture Mechanics – Fundamentals and Application*. CRC Press, Boca Raton, 2004

Broberg, K.B. *Cracks and Fracture*. Academic Press, London, 1999

Ductile Fracture Handbook. Electric Power Research Institute, Palo Alto, 1989

Hellan, K. *Introduction to Fracture Mechanics*. McGraw-Hill, New York, 1985

Hutchinson, J.W. *Nonlinear Fracture Mechanics*. Department of Solid Mechanics, Technical University of Denmark, 1979

Kanninen, M.F. and Popelar, C.H. *Advanced Fracture Mechanics*. Clarendon Press, Oxford, 1985

Knott, J.F. *Fundamentals of Fracture Mechanics*. Butterworth, London, 1973

Miannay, D.P. *Fracture Mechanics*. Springer, New York, 1998

Rice, J.R. *Mathematical Analysis in the Mechanics of Fracture.* In *Fracture – A Treatise*, Vol. 2, ed. H. Liebowitz, pp. 191-311. Academic Press, London, 1968

Chapter 6
Creep fracture

6.1 Introduction

Various materials display a time-dependent behavior which is the source of phenomena such as *creep* or *relaxation*. These processes typically take place *quasistatically*, i.e., so slow that inertia forces do not play any role. If a component made of such a material contains a crack and is loaded, time-dependent deformations occur especially in the vicinity of the crack tip due to the locally high stresses. This may cause a delay of crack initiation until some critical crack-tip deformation is attained. Creep of the material at the crack tip, however, may also lead directly to *creep crack growth*.

Typical examples for materials showing such a behavior are polymers at room temperature or steels above approximately 30% of their melting temperature. Despite similar macroscopic phenomena the micromechanisms underlying fracture of these materials are distinctly different. Thermally induced creep of metals is connected with void growth at grain boundaries. In the vicinity of a macroscopic crack tip this leads to the formation of microcracks and ultimate fracture takes plays by their coalescence. Fracture of glassy polymers (e.g., PMMA) in contrast, is preceded by the formation of an elongated *craze* zone ahead of the crack tip. This thin and porous layer of about a micron thickness and up to several millimeters length consist of fibrils of highly stretched macromolecules in the direction of maximum principal stress (perpendicular to the craze zone). Fracture then takes place by scission of the macromolecules or their pull-out from the bulk material. While the macroscopic behavior of polymers outside the process zone can usually be described as linear viscoelastic the adequate modeling of the creep of metals generally requires nonlinear constitutive laws. As in case of plasticity, we will keep the description as simple as possible (see Section 1.3.2.1).

As already mentioned, creep is especially pronounced at a crack tip. In certain cases the time-dependent inelastic behavior is restricted even to the immediate vicinity of the crack tip, whereas the material can otherwise be regarded as linear elastic. *Small-scale creep* conditions prevail if the creep zone is sufficiently small; the

D. Gross and T. Seelig, *Fracture Mechanics: With an Introduction to Micromechanics*, Mechanical Engineering Series, DOI 10.1007/978-3-642-19240-1_6,

crack-tip state then can be characterized by parameters of linear elastic fracture mechanics such as K_I. These parameters, however, may now be time-dependent. Parameters of linear elastic fracture mechanics can also be employed in case of creep in larger regions (e.g., creep of a whole component) provided that the material can be described as linear viscoelastic. In case of nonlinear material behavior parameters based on integral quantities are useful and frequently applied, for instance the C– or C^*–integral, which are closely related to the J–integral of elastic-plastic fracture mechanics.

6.2 Fracture of linear viscoelastic materials

6.2.1 Crack-tip field, elastic-viscoelastic analogy

To begin with, in the present section we focus our attention on stationary cracks in linear viscoelastic media. Solutions of respective boundary value problems can often be directly derived from the solution of the corresponding elastic problem. The Laplace-transformed solution of a viscoelastic boundary value problems is obtained when in the elastic solution the elastic constants are replaced by Laplace-transformed creep or relaxation functions (see Section 1.3.2.1). If the solution of the elastic problem does not contain any elastic constants then the viscoelastic solution likewise does not depend on creep or relaxation functions, hence it entirely coincides with the elastic solution.

This holds, for instance, for the stress field at the tip of a stationary crack. The respective equations in (4.6), (4.14), and (4.15) from linear elastic fracture mechanics are also valid in the viscolelastic case where the stress intensity factors may now depend on time according to the external loading. The displacements at the crack tip, however, which in the elastic solution depend on elastic constants can not be directly transferred to the viscoelastic case. Another example are bodies subjected to prescribed tractions along their entire boundary. Also in this case the viscoelastic and elastic stress distributions are equal. For multiply connected domains (e.g., containing internal cracks) one has to ensure in addition that the loading on interior boundaries is in equilibrium. K–factors for cracked viscoelastic bodies under prescribed loading hence can be directly adopted from the elastic case.

The determination of viscoelastic stresses and deformations is strongly facilitated if one assumes that Poisson's ratio ν is constant (like in elasticity) which approximately applies to many polymers. Two important situations then are distinguished:

1.) If a body is subjected to prescribed forces of the type $F_i = \hat{F}_i\, f(t)$ where the temporal variation is the same for all forces, then the viscoelastic and elastic stresses are equal: $\sigma_{ij} = \hat{\sigma}_{ij}\, f(t)$. This also holds for the stress intensity factors. The viscoelastic deformations are obtained from the elastic ones by replacing the shear modulus according to:

$$\frac{1}{G} \to \int_{-\infty}^{t} J_d(t-\tau)\frac{\mathrm{d}f(\tau)}{\mathrm{d}\tau}\,\mathrm{d}\tau\ . \tag{6.1}$$

(Note, that in this section $J_d(t)$ and $J(t)$ denote creep functions and are not to be confused with the J-integral!)

2.) If a body is subjected to prescribed displacements of the type $u_i^R = \hat{u}_i^R\, u(t)$ along part of its boundary while the remaining part of the boundary is traction-free then the viscoelastic and elastic deformations are equal: $u_i = \hat{u}_i\, u(t)$. The viscoelastic stresses and stress intensity factors follow from the respective elastic quantities by replacing the shear modulus according to:

$$G \to \int_{-\infty}^{t} G(t-\tau)\frac{\mathrm{d}u(\tau)}{\mathrm{d}\tau}\,\mathrm{d}\tau\ . \tag{6.2}$$

If (6.1) is applied to the crack-tip field (see (4.6), (4.14), (4.15)) it turns out that the viscoelastic and elastic displacements differ only by their temporal variation; the spatial distribution remains the same.

In the special case where the loading (forces or displacements) is applied at time $t = 0$ and kept constant afterwards it follows from (6.1) or (6.2), respectively, that

$$1/G \to J_d(t)\ , \qquad G \to G(t)\ . \tag{6.3}$$

The relaxation function $G(t)$ then varies between the *instantaneous modulus* $G(0) = G_g$ and the *equilibrium modulus* $G(\infty) = G_e$ (see Fig. 1.6). The same holds for the creep function $J_d(t)$. Hence the upper and lower limits of the stresses and deformations are readily obtained.

As an example, we consider the configuration depicted in Fig. 6.1a (see also DCB–specimen, Section 4.6.3) with the viscoelastic behavior approximated by the *linear standard material*. The latter can be illustrated by the rheological ("spring-dashpot") model in Fig. 6.1b. If we assume $J_e = 3J_g$ and $G_e = G_g/3$ with $J_g = 1/G_g$ the creep and relaxation functions are

$$J(t) = J_g(3 - 2\mathrm{e}^{-t/\tau_J})\ , \qquad G(t) = \frac{G_g}{3}(1 + 2\mathrm{e}^{-t/\tau_G})\ . \tag{6.4}$$

Here, τ_G and $\tau_J = \tau_G G_g/G_e = 3\tau_G$ denote the relaxation time and the retardation time of the material. The elastic solution of the problem in plane stress yields for the stress intensity factor K and the crack opening displacement (CTOD) $\delta = v^+ - v^-$ the results

$$K_I = 2\sqrt{3}\,\frac{Fa}{Bh^{3/2}} = \frac{\sqrt{3}}{2}\,\frac{u_F G(1+\nu)h^{3/2}}{a^2}\ , \qquad \delta = \frac{4K_I}{G(1+\nu)}\sqrt{\frac{r}{2\pi}}\ . \tag{6.5}$$

If the viscoelastic body is loaded by a constant force F at time $t = 0$ the K–factor is constant as well. The temporal variation of the CTOD is obtained from (6.5) by

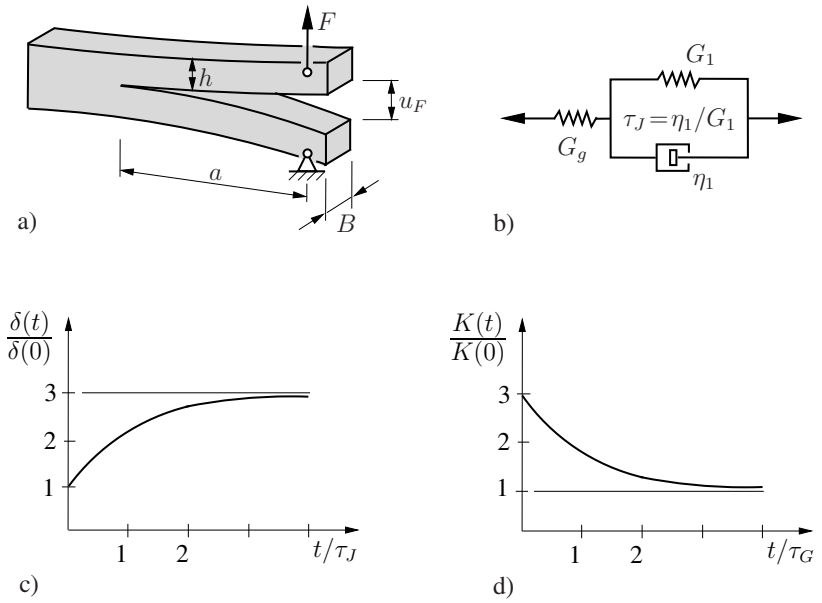

Fig. 6.1 a) DCB-specimen, b) standard material, c) $F = const$, d) $u_F = const$

replacing $1/G$ by $J(t)$:

$$K_I = 2\sqrt{3}\,\frac{Fa}{Bh^{3/2}}\,, \qquad \frac{\delta(t)}{\delta(0)} = \frac{J(t)}{J(0)} = 3 - 2\mathrm{e}^{-t/\tau_J}\,. \tag{6.6}$$

Accordingly, δ increases with time and tends for $t \to \infty$ to three times its instantaneous value (Fig. 6.1c).

In contrast, if loading takes place by a constant displacement u_F at $t = 0$ the CTOD remains constant and changes with time. Its variation follows from (6.5) after replacing G by $G(t)$:

$$\delta = 2\sqrt{3}\,\frac{u_F h^{3/2}}{a^2}\sqrt{\frac{r}{2\pi}}\,, \qquad \frac{K(t)}{K(0)} = \frac{G(t)}{G(0)} = 1 + 2\mathrm{e}^{-t/\tau_G}\,. \tag{6.7}$$

In this case the K–factor decreases and tends for $t \to \infty$ to one third of its instantaneous value (Fig. 6.1d).

6.2.2 Fracture concept

The spatial structure of the stress and displacement field at a crack tip in a viscoelastic material is the same as in the elastic case but their temporal variation is generally different. While the stresses are determined by $K(t)$ the displacements

are controlled by $\delta(t)$. In the example of the preceding section the displacements and thus $\delta(t)$ were increasing at constant stress (K =*const*). Conversely, the stresses and $K(t)$ decreased with time at fixed displacements (δ =*const*). Hence the crack tip and the actual loading of the crack tip are not solely governed by the stress intensity factor but by the current values of K and δ.

Moreover, because of the time-dependent material behavior it can not be expected that the state in the process zone is determined only by the current crack-tip field. It rather depends on the history of the crack-tip loading as confirmed by experimental investigations. The latter show, for instance, a clear dependence of the fracture load on the loading rate for many viscoelastic materials. The loading rate is regarded to be high if the time T of load increase until failure is small compared to the characteristic relaxation time: $T \ll \tau_G$. In that case creep and relaxation effects do not play any role and the material behaves according to instantaneous elasticity. Damage mechanisms such as void growth at the crack tip hardly occur and fracture takes place in a brittle manner. If, however, the loading rate is low ($T \gg \tau_G$) the material in the process zone relaxes or creeps and the damage process at the crack tip can take place as if it were temporally unrestricted.

Whether and when a critical state in the process zone is reached thus depends on the temporal variation of the crack-tip loading. The fracture criterion then may formally be written as

$$\mathcal{F}[K(t), \delta(t)] = 0 \tag{6.8}$$

where the symbol $\mathcal{F}$ denotes the dependence on the loading history. Because of the lack of experimental data this dependence is often ignored. It is then replaced by the simplifying assumption that the state in the process zone is solely characterized by the current crack tip deformation, i.e., by δ. This hypothesis is supported by the observation that deformation is often also a suitable measure of the damage state in a viscoelastic material. Instead of δ which depends on the distance r from the crack tip (see (6.5)) it is more appropriate to use a well-defined crack-tip opening displacement δ_t (e.g., by $45°$ intersections with the crack opening profile, see Fig. 5.17. The simplified fracture criterion then reads

$$\boxed{\delta_t = \delta_{tc}} \,. \tag{6.9}$$

It states that crack initiation takes place when $\delta_t(t)$ attains a material-dependent critical value δ_{tc}.

From the fracture criterion (6.9) the *initiation time* t_i (time of failure) can be determined at which crack propagation starts after the instant of loading. As an example, we consider again the DCB–specimen subjected to constant load and with the constitutive law of a linear standard material (Fig. 6.1a,c). The temporal variation of δ_t is given by (6.6). Insertion into (6.9) yields the initiation time

$$t_i = -\tau_J \ln \frac{3\delta_t(0) - \delta_{tc}}{2\delta_t(0)} \,. \tag{6.10}$$

The use of the parameters $\delta_t(t)$ or $K(t)$ in the fracture concept requires that the size condition holds. That means that the region where the crack-tip field determined by these parameters dominates must be large compared to the process zone (see Section 4.3). Frequently the process zone is simply regarded as a *plastic zone* where yielding takes place and the stresses are bounded. The term *small-scale yielding* from linear elastic fracture mechanics then is also used in the viscoelastic case.

6.2.3 Crack propagation

Crack initiation in viscoelastic materials need not directly lead to failure of a component. The reason is that the crack initially grows very slowly, i.e., it *creeps*. In a component under fixed loading the crack growth rate subsequently increases and only at some critical crack length the crack becomes "unstable" (unlimited crack speed).

This process is investigated here for a crack in plane stress where similar to the Dugdale model the process zone is modelled by a strip with yield stress σ_0 (Fig. 6.2). Under the assumption of small-scale yielding the strip length d has to be small compared to all other dimensions, i.e., the crack length can be regarded to be infinitely large compared to d. In case of an elastic material the following relations hold for the strip length d, the crack opening δ inside the strip, and the crack-tip opening displacement δ_t (see (5.7), (5.8))

$$d = \frac{\pi}{8}\left(\frac{K_I}{\sigma_0}\right)^2 , \tag{6.11}$$

$$\delta(r) = \frac{4\sigma_0 d}{\pi(1+\nu)G}\left[\sqrt{\frac{r}{d}} + \left(1-\frac{r}{d}\right)\operatorname{artanh}\sqrt{\frac{r}{d}}\right] , \tag{6.12}$$

$$\delta_t = \delta(d) = \frac{K_I^2}{2(1+\nu)G\sigma_0} . \tag{6.13}$$

With the crack-tip loading prescibed by K_I these quantities are uniquely determined.

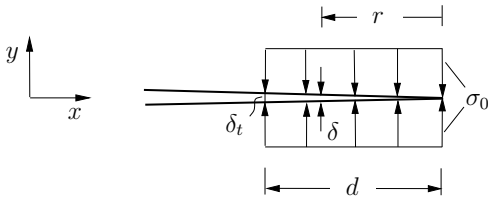

Fig. 6.2 Crack tip under small-scale yielding

The corresponding viscoelastic solution for a stationary (i.e., noncreeping) crack subjected at time $t = 0$ to some load K_I which is afterwards kept constant can directly be derived from (6.11) through (6.13). According to (6.3) therefore only $1/G$ has to be replaced by the creep function $J_d(t)$. This does not affect the strip length d, whereas the crack opening displacement inside the strip and at the crack tip now is time-dependent:

$$\delta(r,t) = \frac{4\sigma_0 d}{\pi(1+\nu)} J_d(t) \left[\sqrt{\frac{r}{d}} + \left(1 - \frac{r}{d}\right) \operatorname{artanh} \sqrt{\frac{r}{d}} \right] , \tag{6.14}$$

$$\delta_t(t) = \frac{K_I^2}{2(1+\nu)\sigma_0} J_d(t) . \tag{6.15}$$

Crack initiation takes place when δ_t attains the critical value δ_{tc} after the initiation time t_i.

In the following we consider the quasistatically growing crack according to Fig. 6.3 where during the time t_1 the whole yield strip moves through some point x. Since small-scale yielding is assumed the strip length d and the crack growth rate $\dot{a}$ can be taken constant during this time interval such that $d = \dot{a}\, t_1$. The crack opening displacement $\delta(x,t)$ inside the strip is computed using (6.14) and by modelling the motion of the strip in the time interval $0 \le \tau \le t$ by a succession of infinitesimally neighboring configurations:

$$\delta(x,t) = \frac{4\sigma_0 d}{\pi(1+\nu)} \int_0^t J_d(t-\tau) \frac{\partial}{\partial \tau} \left[\sqrt{\frac{\dot{a}\,\tau}{d}} + \left(1 - \frac{\dot{a}\,\tau}{d}\right) \operatorname{artanh} \sqrt{\frac{\dot{a}\,\tau}{d}} \right] \mathrm{d}\tau . \tag{6.16}$$

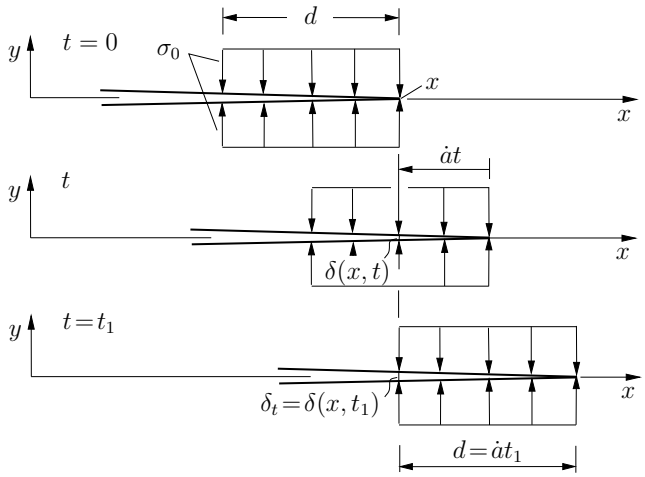

Fig. 6.3 Crack propagation

With $\delta_t = \delta(x, t_1)$ and the new variable $\xi = 1 - \dot{a}\,\tau/d$ the crack-tip opening displacement is given by the representation

$$\delta_t = \frac{4\sigma_0 d}{\pi(1+\nu)} \int_0^1 J_d\left(\frac{\xi d}{\dot{a}}\right) \left[\frac{1}{\sqrt{1-\xi}} - \operatorname{artanh}\sqrt{1-\xi}\right] \mathrm{d}\xi\,. \tag{6.17}$$

From this relation in conjunction with the fracture criterion (6.9) which must hold during crack propagation the crack growth rate $\dot{a}$ can be calculated. In many cases it is sufficient to approximate the creep function by the power law

$$J_d(t) = J_g + J_n t^n \tag{6.18}$$

where J_g is the instantaneous compliance and J_n and n are constants. Insertion into (6.17) together with (6.9) yields

$$\frac{\pi\delta_{tc}(1+\nu)}{4\sigma_0 d} = J_g + J_n P_n \left(\frac{d}{\dot{a}}\right)^n\,, \tag{6.19}$$

where

$$P_n = \int_0^1 \xi^n \left[\frac{1}{\sqrt{1-\xi}} - \operatorname{artanh}\sqrt{1-\xi}\right] \mathrm{d}\xi \tag{6.20}$$

is a constant. By solving (6.19) for $\dot{a}$ with (6.11) and

$$K_{Ig}^2 = \frac{2(1+\nu)}{J_g}\delta_{tc}\sigma_0 \tag{6.21}$$

one finally obtains

$$\dot{a} = \frac{\pi}{8}\left(\frac{J_n P_n}{J_g}\right)^{1/n} \frac{K_{Ig}^2}{\sigma_0^2} \frac{\left[\dfrac{K_I}{K_{Ig}}\right]^{2(n+1)/n}}{\left[1 - \left(\dfrac{K_I}{K_{Ig}}\right)^2\right]^{1/n}}\,. \tag{6.22}$$

For some given loading K_I of the crack and known material parameters thereby the crack growth rate $\dot{a}$ is determined. According to (6.22) it increases without limit ($\dot{a} \to \infty$) when K_I tends to K_{Ig}. The limit value K_{Ig} may be interpreted as the "instantaneous fracture toughness"; according to (6.21) it depends only on the instantaneous compliance J_g and not on the whole creep function (6.18). Figure 6.4 shows $\dot{a}$ as a function of K_I for $n = 1/2$.

Equation (6.22) allows to compute the creep time t_c needed by a crack to grow from its initial length a_0 to the critical length a_g at which $\dot{a}$ tends to infinity. This is illustrated from the simple example of an infinite plate with a crack under tensile loading σ depicted in Fig. 6.5. In this case $K_I = \sigma\sqrt{\pi a}$ and $K_{Ig} = \sigma\sqrt{\pi a_g}$. Hence

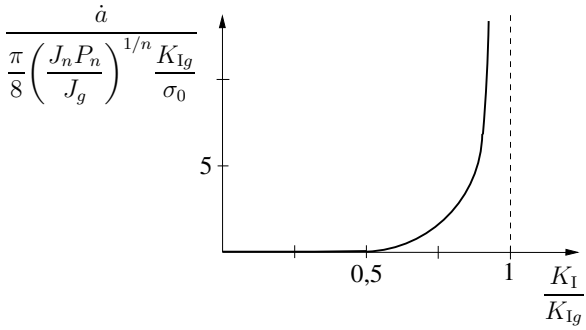

Fig. 6.4 Crack growth rate ($n = 1/2$)

the critical crack length is

$$a_g = \frac{K_{Ig}^2}{\pi\sigma^2} \tag{6.23}$$

and (6.22) yields

$$\dot{a} = \frac{\pi}{8}\left(\frac{J_n P_n}{J_g}\right)^{1/n} \frac{K_{Ig}^2}{\sigma_0^2} \frac{[a/a_g]^{(n+1)/n}}{[1-a/a_g]^{1/n}} \,. \tag{6.24}$$

Separation of variables and integration from the initial crack length a_0 to the critical crack length a_g leads to

$$t_c = \frac{8}{\pi^2}\left(\frac{J_g}{J_n P_n}\right)^{1/n} \left(\frac{\sigma_0}{\sigma}\right)^2 \int_{a_0/a_g}^{1} \frac{[1-a/a_g]^{1/n}}{[a/a_g]^{(n+1)/n}} \,\mathrm{d}(a/a_g) \,. \tag{6.25}$$

According to (6.25) the creep time t_c decreases with increasing loading σ and initial crack length a_0; the result is shown in Fig. 6.5 for $n = 1/2$.

It has to be noted that creep crack growth here has been regarded to take place quasistatically because of the low crack speed. However, for $\dot{a} \to \infty$ the assumption

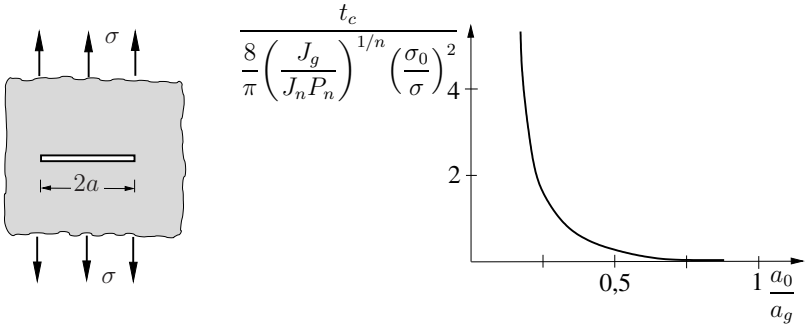

Fig. 6.5 Creep time (n=1/2)

of creep crack growth and the above results are no longer valid. One then has to consider fast crack growth where inertia forces can not be neglected (see Chapter 7).

6.3 Creep fracture of nonlinear materials

6.3.1 Secondary creep, constitutive law

Creep of metals under constant load is divided into three stages (see Section 1.3.2.2). Immediately upon loading primary creep sets in which is characterized by a decreasing strain rate. This regime is followed by secondary creep where steady-state conditions prevail and the creep rate is constant. During tertiary creep the creep rate then increases due to progressive damage of the material until ultimate failure.

Investigations in the present section focus on the initiation and growth of cracks in bodies undergoing secondary creep. Depending on the situation the creep region can be restricted to the vicinity of the crack tip (= small-scale creep) or it may encompass the entire body.

The material behavior is approximated by a nonlinear *Maxwell model* with the uniaxial constitutive law given by

$$\dot{\varepsilon} = \frac{\dot{\sigma}}{E} + B\sigma^n \ . \tag{6.26}$$

According to the spring-dashpot model shown in Fig. 6.6a the strain rate is additively composed by the elastic part $\dot{\varepsilon}^e = \dot{\sigma}/E$ and the nonlinear viscous part (creep rate) $\dot{\varepsilon}^v = B\sigma^n$ where B and $n > 1$ are constant material parameters. The creep curve corresponding to a constant stress σ applied at time $t = 0$ is depicted in Fig. 6.6b. In this case stationary conditions prevail with $\dot{\sigma} = 0$ and $\dot{\varepsilon}^e = 0$ and (6.26) reduces to Norton's creep law

$$\dot{\varepsilon} = \dot{\varepsilon}^v = B\sigma^n \tag{6.27}$$

(see (1.65)). The instantaneous behavior ($t \to 0$) is purely elastic. Subsequently the creep strain increases linearly with t and at time $t = 1/(EB\sigma^{n-1})$ the creep

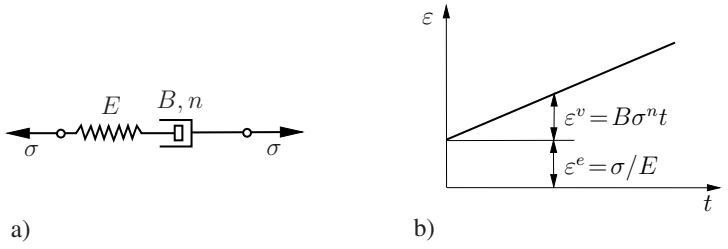

Fig. 6.6 Material behavior at secondary creep

strain equals the elastic strain ($\varepsilon^v = \varepsilon^e$). After a sufficient amount of time we have $\varepsilon^v \gg \varepsilon^e$ and the elastic strain can be neglected; for larger stress σ this state is reached earlier. The constitutive law (6.26) reduces to (6.27) even in case of a temporally varying stress provided that $B\sigma^n \gg \dot{\sigma}/E$. This holds when σ is very large (e.g., at a crack tip) and does not change too fast.

Using (1.38) and (1.71) the three-dimensional generalization of (6.26) reads

$$\dot{\varepsilon}_{ij} = \dot{\varepsilon}^e_{ij} + \dot{\varepsilon}^v_{ij} = -\frac{\nu}{E}\dot{\sigma}_{kk}\delta_{ij} + \frac{1+\nu}{E}\dot{\sigma}_{ij} + \frac{3}{2}B\,\sigma_{\mathrm{e}}^{n-1}s_{ij} \tag{6.28}$$

where $s_{ij} = \sigma_{ij} - \frac{1}{3}\delta_{ij}\sigma_{kk}$ and $\sigma_{\mathrm{e}} = (\frac{3}{2}s_{ij}s_{ij})^{1/2}$. Here it has been assumed that the creep strain can be derived from a flow potential and that creep takes place incompressibly ($\dot{\varepsilon}^v_{kk} = 0$). If the elastic strains are negligible (6.28) reduces to

$$\dot{\varepsilon}_{ij} = \frac{3}{2}B\,\sigma_{\mathrm{e}}^{n-1}s_{ij}\ . \tag{6.29}$$

In this case the analogy between nonlinear elastic behavior and creep according to Section 1.3.2.2 holds. That means that all relations and solutions obtained for a nonlinear elastic material with (1.57) or (5.34), respectively, can be transferred to creep processes with the constitutive law (6.29) simply by replacing the strains by strain rates.

It should be mentioned here that a nonlinear material behavior of the type (6.26) or (6.28) is in the literature often referred to as a *viscoplastic* behavior.

6.3.2 Stationary crack, crack-tip field, loading parameters

We consider a stationary crack in a component with the material behavior according to (6.28). The loading is arbitrary, i.e., it may be time-dependent or constant. The stress field at the crack tip ($r \to 0$) is expected to be singular of the type $\sigma_{ij}(r,\varphi,t) = r^{\lambda}\tilde{\sigma}_{ij}(\varphi,t)$ where the exponent $\lambda < 0$ is unknown. By insertion into (6.28) one realizes that the elastic strain is negligible compared to the creep strain. Hence the material behavior in the vicinity of the crack tip can be described by (6.29) and the solution for the crack-tip field is analogous to the corresponding elastic solution. The latter is given by the HRR-field discussed in Section 5.4.2. By changing the notation $\alpha\varepsilon_0\sigma_0^n \to B$, $\varepsilon_{ij} \to \dot{\varepsilon}_{ij}$, $u_i \to \dot{u}_i$, $J \to C(t)$ one thus obtains from (5.39):

$$\begin{aligned}\sigma_{ij} &= \left(\frac{C(t)}{IBr}\right)^{\frac{1}{n+1}}\tilde{\sigma}_{ij}(\varphi)\ ,\\ \dot{\varepsilon}_{ij} &= B\left(\frac{C(t)}{IBr}\right)^{\frac{n}{n+1}}\tilde{\varepsilon}_{ij}(\varphi)\ ,\end{aligned} \tag{6.30a}$$

$$\dot{u}_i - \dot{u}_{i0} = Br \left(\frac{C(t)}{IBr} \right)^{\frac{n}{n+1}} \tilde{u}_i(\varphi) \; . \tag{6.30b}$$

The parameter $I(n)$ and the angular functions $\tilde{\sigma}_{ij}(\varphi)$ are given by the respective quantities in Section 5.4.2 and the structure of the field (6.30a,b) corresponds exactly to the HRR-field. Here, the time-dependent loading parameter is $C(t)$; in analogy to (5.37) it can be expressed by the contour integral

$$C(t) = \lim_{r \to 0} \int_{-\pi}^{+\pi} [D \, n_1 - \sigma_{i\beta} \, \dot{u}_{i,1} \, n_\beta] \, r \mathrm{d}\varphi \tag{6.31}$$

(see Fig. 5.13) where the specific strain energy rate D is given by (1.72). The integration contour has to lie entirely inside the crack-tip field since only there the constitutive law (6.29) is valid. Hence the $C(t)$-integral is in general not path-independent. The determination of $C(t)$ for a particular crack configuration and given loading requires the solution of the time-dependent boundary value problem for the complete component with the constitutive law (6.28). Generally, this is possible only by numerical methods. The field quantities in the vicinity of the crack tip then allow the computation of the crack-tip loading parameter from (6.31).

In the following we assume that the loading of the component is constant in time. As a consequence, a state of stationary creep develops in the component after sufficiently long time ($\dot{\sigma}_{ij} = 0$ for $t \to \infty$) and the elastic strains can be neglected. Then (6.29) and the analogy with the elastic case hold not only at the crack tip but throughout the entire body. Hence the crack-tip field is again given by (6.30a,b) where the loading parameter is now time-dependent:

$$C^* = C(t \to \infty) \; . \tag{6.32}$$

It can be computed from the contour integral

$$C^* = \int_C [D \, n_1 - \sigma_{i\beta} \, \dot{u}_{i,1} \, n_\beta] \, \mathrm{d}c \tag{6.33}$$

which in contrast to (6.31) is path-independent like the J-integral. Some further relation can be transferred from the elastic problem. For instance, from the representation (5.54) for J the analogous representation for C^*

$$C^* = - \frac{\mathrm{d}\dot{\Pi}^i}{\mathrm{d}a} \bigg|_{\dot{u}_F} \tag{6.34}$$

is obtained where

$$\dot{\Pi}^i = \int_0^{\dot{u}_F} F \mathrm{d}\dot{u}_F \; . \tag{6.35}$$

Moreover, all solutions for specific crack problems can of course be adopted (see Section 5.7).

Now the evolution of the crack-tip field in a component subjected to some constant load at time $t = 0$ is investigated. The instantaneous behavior is purely elastic and at the crack tip hence a K-controlled field initially prevails with a region of dominance characterized by R_K in Fig. 6.7a. Inside this elastic crack-tip field a creep zone develops for $t > 0$ with a characteristic radius ρ and a $C(t)$-controlled field with a radius of dominance R_C (Fig. 6.7b). Both ρ and R_C increase with time. Outside the creep zone the creep strains are so small that they can be neglected compared to the elastic strains. Small-scale creep conditions prevail as long as $\rho \ll R_K$, for instance, up to some time t_1. During this short period the crack-tip loading can be characterized by the constant K-factor. For $t > t_1$ and an increasing creep zone the situation turns into large-scale creep and the crack-tip state is controlled by the field governed by $C(t)$; see Fig. 6.7c. For $t \to \infty$ a state of stationary creep develops throughout the whole component and the crack-tip loading is given by C^* (Fig. 6.7d).

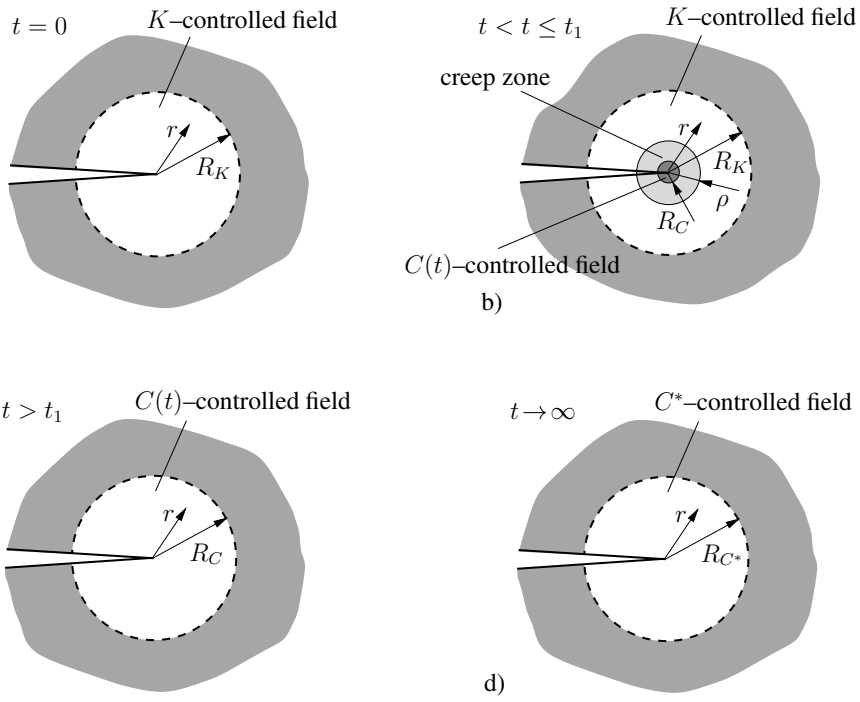

Fig. 6.7 Temporal evolution of the crack-tip field

The evolution of the creep zone during the short period of small-scale creep can easily be estimated. We assume for this purpose that the boundary ρ of the creep zone is approximately determined from the condition $\varepsilon_{\mathrm{e}}^{v} = \varepsilon_{\mathrm{e}}^{e}$ for the equivalent

strain on the ligament and that outside the creep zone the temporally constant stress distribution of the K-controlled field prevails. From the constitutive law (see Section 6.3.1) then the characteristic time

$$t = \frac{1}{EB\,\sigma_{\mathrm{e}}^{n-1}} \,. \tag{6.36}$$

follows. At this time the creep zone reaches some point where the so far constant equivalent stress σ_{e} is given by the K-field. In the following we neglect the transition region in Fig. 6.7b between the K-controlled and the C-controlled field by setting $R_C = \rho$. The stresses then are given by (4.22) outside the creep zone and by (6.30a) inside the creep zone:

$$\sigma_{\mathrm{e}}(r) \sim \begin{cases} \dfrac{K}{\sqrt{r}} & r \geq \rho \\[2ex] \left(\dfrac{C(t)}{Br}\right)^{\frac{1}{n+1}} & r \leq \rho \,. \end{cases} \tag{6.37}$$

At the boundary $r = \rho$ between the two regions they must be of the same order of magnitude:

$$\frac{K}{\sqrt{\rho}} \sim \left(\frac{C(t)}{B\rho}\right)^{\frac{1}{n+1}} \,. \tag{6.38}$$

Using (6.36) and (6.37) this leads to the following time dependencies of the size $\rho(t)$ of the creep zone and of $C(t)$

$$\rho(t) = \alpha_1 K^2 (EBt)^{\frac{2}{n-1}} \,, \qquad C(t) = \alpha_2 \frac{K^2}{Et} \tag{6.39}$$

where α_i are dimensionless constants of order unity. A rough estimate of the time t_1 until which small-scale creep prevails may be obtained by setting $C(t_1) \approx C^*$:

$$t_1 = \alpha_2 \frac{K^2}{EC^*} \,. \tag{6.40}$$

Finally, we briefly investigate the onset of crack growth. Therefore, we make use of the simple fracture criterion (6.9) $\delta_t = \delta_{tc}$ where δ_t denotes the crack opening displacement at some distance r_c from the crack tip. For sufficiently high loading crack initiation takes place already in the initial stage of small-scale creep. From (6.30a,b) and (6.39) then

$$\dot{\delta}_t = 2Br_c\tilde{u}_2(\pi) \left(\frac{\alpha_2 K^2}{EIBr_c t}\right)^{\frac{n}{n+1}} \,. \tag{6.41}$$

Time integration and insertion into the fracture criterion yields the initiation time

$$t_i = \left(\frac{\delta_{tc}}{2Br_c\tilde{u}_2(\pi)}\right)^{n+1} \left(\frac{EIBr_c}{\alpha_2 K^2}\right)^n \tag{6.42}$$

which is inversely proportional to K^{2n}. For sufficiently low loading, in contrast, crack initiation takes place when a state of stationary creep has developed in the component and the crack-tip loading parameter is C^*. Equation (630b) then yields

$$\dot{\delta}_t = 2Br_c\tilde{u}_2(\pi)\left(\frac{C^*}{IBr_c}\right)^{\frac{n}{n+1}} , \tag{6.43}$$

and time integration in conjunction with the fracture criterion leads to the initiation time

$$t_i = \frac{\delta_{tc}}{2Br_c\tilde{u}_2(\pi)}\left(\frac{IBr_c}{C^*}\right)^{\frac{n}{n+1}} . \tag{6.44}$$

In this case it is inversely proportional to $C^{*\frac{n}{n+1}}$.

6.3.3 Creep crack growth

6.3.3.1 Hui-Riedel field

After initiation crack propagation proceeds by creep. In order to describe this process we first analyze the crack-tip field. Steady-state conditions and a plane stress state are assumed. For the derivation which is similar to that of the HRR-field (see Section 5.4.2) it is appropriate to employ a coordinate system moving with the crack as depicted in Fig. 5.24. If the constitutive law (6.28) is inserted into the compatibility condition (5.41) and use is made of (5.81) one obtains

$$\begin{aligned} &\frac{\dot{a}}{E}\frac{\partial}{\partial x_1'}\left[\Delta(\sigma_r+\sigma_\varphi)\right] \\ &+\frac{B}{4}\left\{\frac{1}{r}\frac{\partial^2}{\partial r^2}\left[r\sigma^{n-1}(2\sigma_\varphi-\sigma_r)\right]+\frac{1}{r^2}\frac{\partial^2}{\partial\varphi^2}\left[\sigma^{n-1}(2\sigma_r-\sigma_\varphi)\right]\right. \\ &\left.-\frac{1}{r}\frac{\partial}{\partial r}\left[\sigma^{n-1}(2\sigma_r-\sigma_\varphi)\right]-\frac{3}{r^2}\frac{\partial}{\partial r}\left[r\frac{\partial}{\partial\varphi}(\sigma^{n-1}\tau_{r\varphi})\right]\right\}=0 \end{aligned} \tag{6.45}$$

where

$$\sigma = \left(\sigma_r^2+\sigma_\varphi^2-\sigma_r\sigma_\varphi+\tau_{r\varphi}^2\right)^{1/2} \tag{6.46}$$

and

$$\frac{\partial}{\partial x_1'} = \cos\varphi\frac{\partial}{\partial r}-\sin\varphi\frac{\partial}{r\partial\varphi} , \qquad \Delta = \frac{\partial^2}{\partial r^2}+\frac{1}{r^2}\frac{\partial^2}{\partial\varphi^2}+\frac{1}{r}\frac{\partial}{\partial r} . \tag{6.47}$$

The Airy stress function $\phi(r,\varphi)$ with the definitions (5.44) is introduced which identically satisfies the equilibrium conditions. With the representation

$$\phi = A\, r^s\, \tilde{\phi}(\varphi) \tag{6.48}$$

for the crack-tip field it then follows from (6.45) that

$$\frac{\dot{a}}{E}\, r^{s-3} D_1(\tilde{\phi}) + BA^{n-1} r^{n(s-2)} D_2(\tilde{\phi}) = 0 \tag{6.49}$$

where

$$\begin{aligned}
D_1 &= [(s-4)\cos\varphi - \sin\varphi\, \frac{\partial}{\partial\varphi}] \left[(s-2)^2(s^2\tilde{\phi}+\tilde{\phi}'') + (s^2\tilde{\phi}+\tilde{\phi}'')''\right] \,, \\
D_2 &= \Big\{ n(s-2)[1+n(s-2)]\tilde{\sigma}^{n-1}[s(2s-3)\tilde{\phi} - \tilde{\phi}''] \\
&\quad + [\tilde{\sigma}^{n-1}(s(1-s)\tilde{\phi} + 2\tilde{\phi}'')]'' - n(s-2)\tilde{\sigma}^{n-1}[s(1-s)\tilde{\phi} + 2\tilde{\phi}''] \\
&\quad + 3[1+n(s-2)](s-1)(\tilde{\sigma}^{n-1}\tilde{\phi}')' \Big\} \,, \\
\tilde{\sigma} &= \left[s^2(3-3s+s^2)\tilde{\phi}^2 + s(3-s)\tilde{\phi}\tilde{\phi}' + \tilde{\phi}''^2 + (s-1)^2\tilde{\phi}'^2 \right]^{1/2} \,.
\end{aligned} \tag{6.50}$$

The first term on the left-hand side of (6.49) describes the elastic part and the second one represents the creep part of the crack-tip field. In order to determine the unknown exponent s we proceed from the hypothesis that the first term, i.e., the elastic strain, is negligible. This leads to exactly the same relations as in case of a stationary (non-propagating) crack. According to (6.30) the corresponding crack-tip field then is of the HRR-type with $\sigma_{ij} \sim r^{-1/(n+1)}$ and $\phi \sim r^{(2n+1)/(n+1)}$; the exponent s in this case is $s = \frac{2n+1}{n+1}$. This is inserted into (6.49) in order to verify the above hypothesis. The first term then is of the type $r^{-(n+2)/(n+1)}$ and the second one is of the type $r^{-n/(n+1)}$. For $r \to 0$ the first term dominates which contradicts the assumption. In contrast to the situation of a stationary crack hence the elastic strains can not be neglected in case of a propagating crack.

Conversely, we now assume that the creep part in (6.49) can be neglected compared to the elastic part. This leads to an elastic crack-tip field with $\sigma_{ij} \sim r^{-1/2}$, $\phi \sim r^{3/2}$ and $s = 3/2$. If this again is inserted into (6.49) to check the hypothesis it turns out that the first term is of the type $r^{-3/2}$ while the second one is of the type $r^{-n/2}$. For $n < 3$ the first term indeed dominates at the crack tip ($r \to 0$) in agreement with the assumption. In this case hence the elastic crack-tip field prevails which is given by (4.14) for mode I (see Section 4.2.2). However, $n \geq 3$ leads to a contradiction to the assumption since then both terms are of the same order of magnitude ($n = 3$) or, respectively, the second term dominates ($n > 3$).

From the preceding considerations it can be concluded that for $n > 3$ both terms in (6.49) must have the same asymptotic behavior for $r \to 0$. Therefore, it follows that $s - 3 = n(s-2)$ or $s = \frac{2n-3}{n-1}$. The amplitude A may now without loss of generality be fixed by $A = (\dot{a}/EB)^{1/(n-1)}$. Thereby (6.49) reduces to the fifth

order ordinary differential equation

$$D_1(\tilde{\phi}) + D_2(\tilde{\phi}) = 0 \tag{6.51}$$

for the unknown function $\tilde{\phi}(\varphi)$. Four boundary conditions are for mode I given by (5.48); a further condition is the regularity of the solution at $\varphi = 0$. The solution of (6.51) subject to these boundary conditions can be obtained by numerical integration. Then the stress function and hence the stresses and strains in the crack-tip region ($r \to 0$) are uniquely determined. They are of the general form

$$\begin{aligned} \sigma_{ij} &= \left(\frac{\dot{a}}{EB\,r}\right)^{\frac{1}{n-1}} \tilde{\sigma}_{ij}(\varphi) \,, \\ \varepsilon_{ij} &= \frac{1}{E}\left(\frac{\dot{a}}{EB\,r}\right)^{\frac{1}{n-1}} \tilde{\varepsilon}_{ij}(\varphi) \,. \end{aligned} \tag{6.52}$$

Named after C.Y. HUI and H. RIEDEL who intensively studied creep crack growth this field is called *Hui-Riedel field*. In contrast to the situation of a stationary crack (HRR-field) the stresses and strains of the Hui-Riedel field display the same asymptotic behavior.

In Fig. 6.8 the angular distribution of the stresses and strains is depicted for the case $n = 5$. It should be noted that the quantities $\tilde{\sigma}$, $\tilde{\varepsilon}$, $\tilde{\varepsilon}_\varphi$ are unbounded when approaching the crack faces ($\varphi \to \pm\pi$). This has to be understood to result from the strain history a material point close to the x-axis experiences during the passage of the crack tip. Another important feature of the field (6.52) is that its amplitude is determined solely by the crack-tip speed $\dot{a}$ and the material parameter EB. In contrast to the HRR-field here the amplitude does not explicitly depend on the external loading or the geometry of the body.

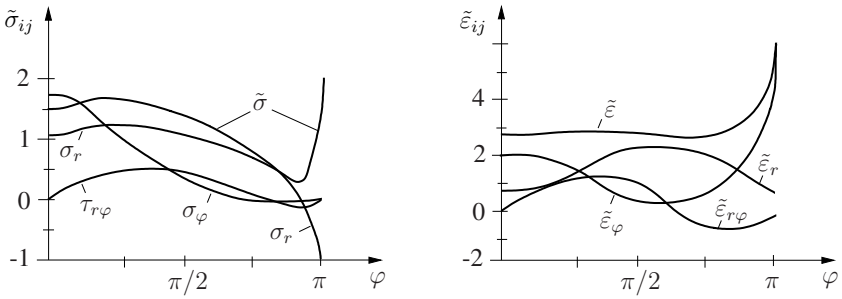

Fig. 6.8 Hui-Riedel field, angular distribution of field quantities (plane stress, $n = 5$)

In deriving the crack-tip field we have assumed steady-state conditions, i.e., $\dot{a} = const$. This is not strictly necessary; rather the results are valid also in the transient case ($\dot{a} \neq const$). This can be seen from the time derivative of (6.48) which is ac-

cording to (5.81) in the general (transient) case given by $\dot{\phi} = (\partial\phi/\partial t) - \dot{a}(\partial\phi/\partial x_1')$. Using (6.47) the first term is of the type r^s while the second one is of the type r^{s-1}. Correspondingly, the asymptotic behavior of $\dot{\phi}$ for $r \to 0$ is in the transient case as well as under steady-state conditions solely governed by the second term, i.e., by the relation (5.81) used above.

Analogous considerations can of course be performed for plane strain and for mode II. The structure of the crack-tip field (6.52) then remains the same.

6.3.3.2 Small-scale creep

In the following we consider crack propagation under the condition of small-scale creep. Furthermore, we assume $n > 3$ and, as in the preceding section, a plane stress state. The situation which then prevails in the vicinity of a crack tip is schematically sketched in Fig. 6.9. The creep zone with a characteristic radius ρ is embedded in the K-controlled field with a radius of dominance $R_K \gg \rho$. Inside the creep zone, close to the crack tip, the Hui-Riedel field is found with a radius of dominance R_{HR}.

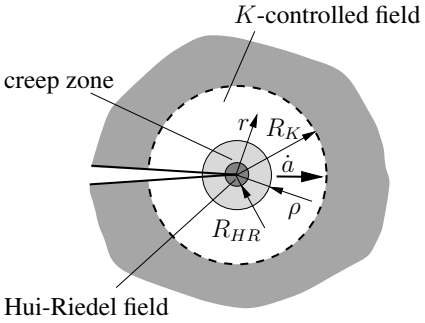

Fig. 6.9 Crack propagation in case of small-scale creep, $n > 3$

The exact determination of the field in the transition region between the K-controlled field and the Hui-Riedel field is only possible by numerical methods. Here we are satisfied with an approximate solution which nevertheless allows to study all essential features. We proceed in a similar way as in case of small-scale creep at a stationary crack (see Section 6.3.2). In order to compute the size ρ of the creep region we first assume that this boundary is approximately determined from the condition $\varepsilon_{\mathrm{e}}^v = \varepsilon_{\mathrm{e}}^e$ for the equivalent strain on the ligament and that outside this boundary the stress distribution of the K-controlled field is valid.

From the latter the equivalent stress on the ligament is in plane stress given by $\sigma_{\mathrm{e}} = K/\sqrt{2\pi r}$. Using (6.26) and noting that $(.)^{\cdot} = -\dot{a}\,\partial(.)/\partial r$ (on the ligament $x_1 = r$) then leads to

$$\begin{aligned} \varepsilon_{\mathrm{e}}^{e} &= \frac{\sigma_{\mathrm{e}}}{E} = \frac{K}{E\sqrt{2\pi r}} \,, \\ -\dot{a}\,\frac{\partial {\varepsilon_{\mathrm{e}}}^{v}}{\partial r} &= B\,\sigma_{\mathrm{e}}^{n} = \frac{BK^{n}}{(2\pi r)^{n/2}} \quad \rightarrow\ \varepsilon_{\mathrm{e}}^{v} = \frac{2BK^{n}}{(2\pi)^{n/2}(n-2)\dot{a}r^{(n-2)/2}} \,. \end{aligned} \tag{6.53}$$

The integration of $\varepsilon_{\mathrm{e}}^{v}$ here is performed in the limits from $R_K \rightarrow \infty$ to r. Equating the two equivalent strains at $r = \rho$ yields

$$\rho = \left[\frac{2}{(2\pi)^{(n-1)/2}(n-2)}\ \frac{EBK^{n-1}}{\dot{a}}\right]^{\frac{2}{n-3}} \tag{6.54}$$

and

$$\varepsilon_{\mathrm{e}}^{v}(\rho) = \varepsilon_{\mathrm{e}}^{e}(\rho) = \frac{1}{E}\ \left[\pi(n-2)\frac{\dot{a}}{EBK^{2}}\right]^{\frac{1}{n-3}} \,. \tag{6.55}$$

In the following we again neglect the transition region between the K-controlled field and the Hui-Riedel field by setting $\rho = R_{HR}$. From (6.53) and (6.52) the creep strain then is given by

$$\varepsilon_{\mathrm{e}}^{v}(r) = \varepsilon_{\mathrm{e}}^{v}(\rho) \begin{cases} \left(\dfrac{\rho}{r}\right)^{\frac{n-2}{2}} & r \geq \rho \\ \left(\dfrac{\rho}{r}\right)^{\frac{1}{n-1}} & r \leq \rho \,. \end{cases} \tag{6.56}$$

In order to describe crack propagation a fracture criterion has to be employed. We assume therefor that crack advance proceeds in such a way that the creep strain $\varepsilon_{\mathrm{e}}^{v}$ at some distance r_c ahead of the crack tip attains a critical value: $\varepsilon_{\mathrm{e}}^{v}(r_c) = \varepsilon_c$. It should be noted that in this criterion only the creep strain appears and not the total strain. Physically this can be motivated from the creep strain being a measure of the accumulated void volume which in turn characterizes the state of damage of the material. By inserting (6.56) together with (6.54), (6.55) in this fracture criterion one obtains

$$\frac{1}{\bar{K}} = \begin{cases} \left(\dfrac{\rho}{r_c}\right)^{\frac{n-3}{2}} & r_c \geq \rho \\ \left(\dfrac{\rho}{r_c}\right)^{-\frac{n-3}{2(n-1)}} & r_c \leq \rho \end{cases} \tag{6.57}$$

or

$$\dot{\bar{a}} = \begin{cases} \bar{K}^{n} & r_c \geq \rho \\ 1 & r_c \leq \rho \,, \end{cases} \tag{6.58}$$

where

$$\dot{\bar{a}} = \frac{n-2}{2}\ \frac{\dot{a}}{E^{n}B\,r_c\,\varepsilon_c^{n-1}} \,, \qquad \bar{K} = \frac{K}{E\varepsilon_c\sqrt{2\pi r_c}} \tag{6.59}$$

denote the dimensionless crack-tip speed and stress intensity factor, respectively.

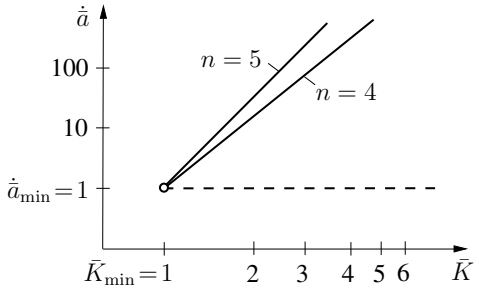

Fig. 6.10 Crack-tip speed

Two solutions for the crack-tip speed are given by (6.59); they are depicted by the solid and dashed lines in Fig. 6.10. In addition it can be seen from (6.57) that the conditions $r_c \geq \rho$ or $r_c \leq \rho$ in any case yield $\bar{K} \geq 1$. The minimum K-factor for which crack propagation is possible hence is $\bar{K} = 1$ or

$$K_{\min} = E\varepsilon_c\sqrt{2\pi r_c};. \tag{6.60}$$

It corresponds to a minimum crack-tip speed $\dot{\bar{a}} = 1$ or

$$\dot{a}_{\min} = \frac{2}{n-2}\, E^n B\, r_c\, \varepsilon_c^{n-1}\,. \tag{6.61}$$

We now consider the solution $\dot{\bar{a}} = 1$ and assume that at constant K the crack-tip speed $\dot{a}$ is slightly increased by some perturbation. According to (6.54) the creep zone becomes smaller which may lead to $r_c > \rho$. But then the second solution for $\dot{\bar{a}}$ is valid and the crack-tip speed "jumps" to the corresponding higher value. In this sense the lower branch ($\dot{\bar{a}} = 1$) of the solution is *unstable*. The physically relevant solution hence is given by the upper branch $\dot{\bar{a}} = \bar{K}^n$, i.e., by the relation

$$\dot{a} = \frac{2}{n-2}\,\frac{B\, r_c}{\varepsilon_c}\left(\frac{K}{\sqrt{2\pi r_c}}\right)^n\,. \tag{6.62}$$

Thus, the crack-tip speed increases according to K^n.

6.4 Further reading

Bazant, Z.P. and Planas, J. *Fracture and Size Effects in Concrete and Other Quasibrittle Materials*. CRC Press, Boca Raton, 1997

Bernasconi, G. and Piatti, G. *Creep of Engineering Materials and Structures*. Applied Science Publishers, London, 1978

Gittus, J. *Creep, Viscoelasticity and Creep Fracture in Solids*. Applied Science Publishers, London, 1975

Kanninen, M.F. and Popelar, C.H. *Advanced Fracture Mechanics*. Clarendon Press, Oxford, 1985

Riedel, H. *Fracture at High Temperature*. Springer, Berlin, 1987

Williams, J.G. *Fracture Mechanics of Polymers*. John Wiley & Sons, New York, 1987

Chapter 7
Dynamic fracture mechanics

7.1 Introduction

So far, our investigations of crack initiation and propagation have always been based on the assumption of quasistatic conditions. This is no longer justified when inertia forces or high strain rates significantly affect the fracture behavior. It is, for instance, well known that a material is more likely to fail under impulsive dynamic loading than in case of a slowly applied load. One reason for this is the different material behavior: plastic or viscous flow is increasingly suppressed at higher loading rates and a material often behaves more brittle in the dynamic case than in the static case. This and possibly different failure mechanisms in the process zone may lead to a change of the fracture toughness. Another reason is due to the fact that the inertia forces in case of dynamic loading can cause higher stresses in the vicinity of a crack tip than in the corresponding quasistatic case.

If a crack propagates through a material it often reaches a very high speed (e.g. more than 1000 m/s) after a short acceleration phase. In case of such a fast crack advance the inertia forces and high strain rates play an important role and strongly influence the fracture behavior. Various aspects of this behavior are well known from the failure of technical components as well as from laboratory experiments. For instance, a fast running crack typically does not exceed a certain *limit speed*. Depending on the actual conditions it may *branch*, once or several times, or it may become *unstable* with respect to the propagation direction. The latter means that even under fully symmetric conditions the crack tends to deviate from a straight path. Another (often desired) dynamic effect is the *crack arrest*, i.e., the crack may slow down until it finally stops growing.

The understanding of the above-mentioned phenomena and their appropriate quantitative description is only possible in the framework of a dynamic fracture theory. Some foundations are presented in the following sections. In the spirit of linear elastic fracture mechanics we thereby restrict the considerations to fracture of brittle materials which can be described by linear elasticity theory. The investigations focus on two typical problems: a) the stationary (i.e., nonpropagating) crack under

D. Gross and T. Seelig, *Fracture Mechanics: With an Introduction to Micromechanics*, Mechanical Engineering Series, DOI 10.1007/978-3-642-19240-1_7,

dynamic loading and b) the fast running crack. With regard to the fracture concept (criterion) we will employ already established quantities such as the K-factors or the energy release rate.

7.2 Some foundations of elastodynamics

The basic equations of linear elastodynamics are given by the balance of momentum (1.20), the kinematic relations (1.25), and the elasticity law (1.37). Inserting these into each other yields in case of vanishing body forces ($f_i = 0$) the *Navier-Lamé equations*

$$(\lambda + \mu)u_{j,ji} + \mu u_{i,jj} = \rho \ddot{u}_i \quad . \tag{7.1}$$

The introduction of a scalar potential ϕ and a vector potential ψ_k with

$$u_1 = \phi_{,1} + \psi_{3,2} - \psi_{2,3} \, , \quad u_2 = \phi_{,2} + \psi_{1,3} - \psi_{3,1} \, , \quad u_3 = \phi_{,3} + \psi_{2,1} - \psi_{1,2} \, , \tag{7.2}$$

leads to the *Helmholtz wave equations*

$$c_1^2 \, \phi_{,ii} = \ddot{\phi} \, , \qquad c_2^2 \, \psi_{k,ii} = \ddot{\psi}_k \tag{7.3}$$

where

$$c_1^2 = \frac{\lambda + 2\mu}{\rho} \, , \qquad c_2^2 = \frac{\mu}{\rho} \, . \tag{7.4}$$

The scalar potential ϕ describes the volume change (dilatation) and the vector potential ψ_k characterizes pure distortions at constant volume. Correspondingly, c_1 is the speed of *dilatational (longitudinal) waves* and c_2 that of *distortional (shear, transversal) waves*. Typical values for some materials are given in Table 7.1. By these wave speeds signals (dilatations or distortions) propagate through a solid body unless they impinge on some boundary.

Material	c_1 [m/s]	c_2 [m/s]	c_R [m/s]
steel	6000	3200	2940
aluminum	6300	3100	2850
glass	5800	3300	3033
PMMA	2400	1000	920

Table 7.1 Typical wave speeds

The representation simplifies in case of plane problems. For plane strain with $u_3 = 0$ and $\psi_1 = \psi_2 = 0$ and the notation $\psi = \psi_3$ equation (7.3) reduces to the two wave equations

$$c_1^2 \, \phi_{,ii} = \ddot{\phi} \, , \qquad c_2^2 \, \psi_{,ii} = \ddot{\psi} \, . \tag{7.5}$$

The case of plane stress is governed by the same relations; only the elastic constants in the wave speeds need to be changed (see Section 1.5.1).

Besides the transversal and longitudinal waves so-called *Rayleigh waves* or *surface waves* play an important role in dynamic fracture. These are waves which propagate along a free surface of a body and rapidly (exponentially) decay towards its interior. In a body in plane strain that occupies the upper half plane with the boundary $x_2 = 0$ they can be represented by

$$\phi = A \exp^{-\alpha x_2} \cos k(x_1 - c_R t) \,, \qquad \psi = B \exp^{-\beta x_2} \cos k(x_1 - c_R t) \,. \quad (7.6)$$

Here, c_R denotes the unknown speed of the Rayleigh waves and k is the wave number. Inserting (7.6) into (7.5) yields the values of α and β. From the boundary conditions $\sigma_{22}(x_1, 0) = 0$, $\sigma_{12}(x_1, 0) = 0$ then the ratio A/B of the amplitudes is obtained as well as the governing relation for c_R:

$$R(c_R) = 4\sqrt{1 - \left(\frac{c_R}{c_1}\right)^2}\sqrt{1 - \left(\frac{c_R}{c_2}\right)^2} - \left[2 - \left(\frac{c_R}{c_2}\right)^2\right]^2 = 0 \,. \quad (7.7)$$

$R(c_R)$ is called the *Rayleigh function*. Equation (7.7) may also be written in the form

$$\left(\frac{c_R}{c_2}\right)^6 - 8\left(\frac{c_R}{c_2}\right)^4 + \frac{8(2-\nu)}{1-\nu}\left(\frac{c_R}{c_2}\right)^2 - \frac{8}{1-\nu} = 0 \,. \quad (7.8)$$

Like c_1 and c_2 the Rayleigh wave speed c_R depends only on material constants and not on the wave number or wave length. For Poisson's ratio in the range $0 \le \nu \le 0.5$ it follows that $0.864 \le c_R/c_2 \le 0.955$. The data given in Table 7.1 are based on the value $\nu = 0.25$ for which $c_R = 0.919\, c_2$.

Particularly simple is the situation of antiplane shear where one may start directly from (7.1). With $u_1 = u_2 = 0$ and setting $w = u_3$ one obtains

$$c_2^2\, w_{,ii} = \ddot{w} \,. \quad (7.9)$$

Hence the motion of the continuum is described by a single equation with the characteristic wave speed c_2; Rayleigh waves do not occur in this case.

7.3 Dynamic loading of a stationary crack

7.3.1 Crack-tip field, K*-concept*

The crack-tip field of a dynamically loaded stationary crack does not differ from that in case of static loading. This can be shown directly from the field equations (7.1). For this purpose we assume that the stresses are singular at the crack tip ($r \to 0$) while the displacements are nonsingular and can be represented by $u_i = r^\lambda \tilde{u}_i(\varphi, t)$

where $0 < \lambda < 1$. Because of the second spatial derivatives the terms on the left hand side of (7.1) then are of the type $r^{\lambda-2}$ whereas the right-hand side is of the type r^{λ}. Hence the inertia forces can be neglected for $r \to 0$ and the crack-tip field is in the dynamic case governed by the same equations as in the static case. It therefore coincides with the static crack-tip field discussed in Section 4.2. As the only difference the stress intensity factors now depend on time: $K_I = K_I(t)$ etc. In general, they cannot be adopted from the static case but have to be computed from the solution of the dynamic (initial) boundary value problem where inertia forces are taken into account.

Since the crack-tip field is uniquely determined by the K-factors it is appropriate to employ the K-concept also in case of dynamic loading of a crack. Accordingly, mode-I crack initiation takes place when the condition

$$K_I(t) = K_{Ic} \tag{7.10}$$

is met. The application of this criterion, however, is complicated by two facts. As already mentioned the fracture toughness K_{Ic} depends on the loading rate $\dot{K}_I$ or, respectively, on some characteristic loading time τ: $K_{Ic} = K_{Ic}(\tau)$. Its determination, especially in case of impulsive loading, requires an enormous experimental effort which is possible only in a few well-equipped laboratories. Hence only a rather limited amount of reliable material data is available up to now. On the other hand, (7.10) is only valid if the dominance region of the K-field is sufficiently large compared to all other characteristic dimensions. In the dynamic case this region of dominance depends on time and it can be smaller than in the static case. Due to the finite wave speed it takes some time after an impulsive loading of a crack until a sufficiently large dominating crack-tip field has built up.

7.3.2 Energy release rate, energetic fracture criterion

The energy release rate is defined as the decrease of the total energy of a body due to crack advance. Since in the dynamic case the kinetic energy K has to be taken into account it reads

$$\mathcal{G} = -\frac{\mathrm{d}(\Pi + K)}{\mathrm{d}a} \,. \tag{7.11}$$

In the present situation of a stationary crack ($\dot{a} = 0$) the crack advance is considered to take place "quasistatically" (i.e., virtually).

Because of the kinetic energy which additionally appears in (7.11) the relations for $\mathcal{G}$ cannot be adopted from the static case (Sections 4.6.2 – 4.6.5) in a straightforward manner. Instead of giving a detailed derivation here, we make use of the result for the more general situation of a running crack presented in Section 7.4.3. Accordingly, the relation (7.34) for the energy release rate reduces in the plane problem of a straight stationary crack ($\dot{a} = 0$) with traction-free crack faces to

$$\mathcal{G} = \int_C (U\delta_{1\beta} - \sigma_{i\beta}\, u_{i,1}) n_\beta \,\mathrm{d}c + \int_A \sigma_{ij,j}\, u_{i,1} \,\mathrm{d}A \,. \tag{7.12}$$

Here, A is the area enclosed by some arbitrary contour C which encompasses the crack tip from one crack face to the other (Fig. 7.1a). In contrast to the static case the energy release rate (7.12) is no longer given solely by the path-independent J-integral but also contains an additional integral over the enclosed area A (see also Section 4.6.5.3). The latter vanishes only if the contour is shrunk to the crack tip (Fig. 7.1b):

$$\mathcal{G} = \lim_{C\to 0} \int_C (U\delta_{1\beta} - \sigma_{i\beta}\, u_{i,1}) n_\beta \,\mathrm{d}c \,. \tag{7.13}$$

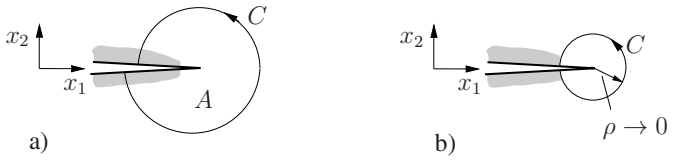

Fig. 7.1 Contours around stationary crack tip related to the energy release rate

The above relations are also valid in the general nonlinear elastic case since no particular elasticity law is employed. If linear elastic material behavior is assumed the crack-tip fields for a stationary crack are equal in the static and the dynamic case, as discussed above. From (7.13) it then follows immediately that the relation known from statics

$$\mathcal{G} = \frac{1}{E'}\left(K_I^2 + K_{II}^2\right) + \frac{1}{2G} K_{III}^2 \tag{7.14}$$

is valid also in the dynamic case. Correspondingly, for pure mode I with $\mathcal{G} = K_I^2/E'$ the K-concept and the energetic criterion

$$\mathcal{G} = \mathcal{G}_c \tag{7.15}$$

are equivalent, like in statics. Here, $\mathcal{G}_c(\tau)$ is the energy required for crack propagation; it can depend on the loading rate or on the characteristic loading time τ, respectively. It should be mentioned that (7.12) in conjunction with (7.14) are well suited for the determination of dynamic K-factors by means of experimental methods.

7.3.3 Examples

Various methods can be utilized for the determination of dynamic stress intensity factors. Experimental and numerical techniques are of primary importance while

analytical methods are applicable only in a few special cases. Experimental methods allow for the determination of the temporal variation $K_I(t)$ of the crack-tip loading as well as the initiation value $K_{Ic}(\tau)$, and the so-called *method of caustics* has proven to be particularly useful for this. The crack-tip loading $K_I(t)$ can be computed with numerical methods where the boundary element method (BEM), the finite element method (FEM), and the finite difference method (FDM) are successfully employed. Results for three examples are discussed in the following which have been obtained with these methods.

As a first example we consider the rotational-symmetric problem of a circular (penny-shaped) crack in an unbounded domain which is loaded by a stress wave. The latter impinges perpendicularly on the crack and is characterized by the loading time τ and the amplitude σ_0 (Fig. 7.2). After arrival of the wave at time $t = 0$ the stress intensity factor $K_I(t)$ first increases monotonically until it attains a maximum and then tends to the corresponding static value $K_I^{\text{stat}} = 2\sigma_0\sqrt{\pi a}/\pi$ in an oscillating manner. The decay can be explained from the fact that due to the reflection and scattering of waves energy is radiated into the unbounded domain (i.e., towards infinity). These waves do no longer contribute to the loading of the crack. For $\tau = 0$ the peak value of $K_I(t)$ is about 25 % higher than K_I^{stat}. It is attained approximately at time $t_R = 2a/c_R$ which is needed by Rayleigh waves to travel across the diameter $2a$ of the crack. With increasing loading time τ the maximum K_I value becomes smaller. A noticable "dynamic overshoot" only occurs for loading times in the range $\tau c_2/a \lesssim 1$. For instance, in a steel plate which contains a crack of length $2a = 20\,\text{mm}$ this takes place for $\tau \approx 6 \cdot 10^{-6}\,\text{s}$. Such a short loading time is observed only in rare situations.

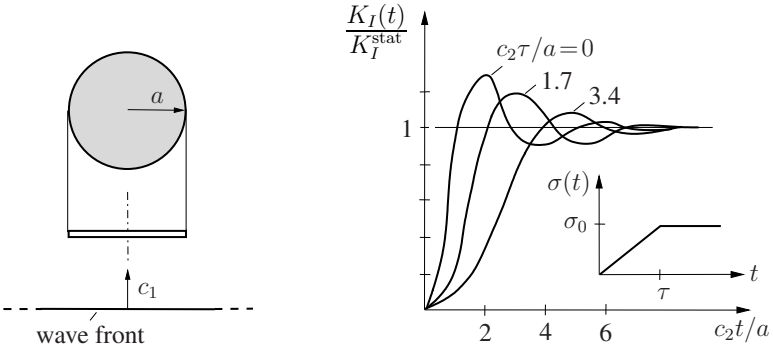

Fig. 7.2 Impulsive loading of a circular (penny-shaped) crack in an infinite domain

In the second example (Fig. 7.3) a straight crack is located in a rectangular plate which is subjected to an ideal impact $\sigma_0 H(t)$ on the two opposite boundaries parallel to the crack. Here, $H(t)$ denotes the Heaviside function. In the present case the profile of the wave impinging on the crack is influenced also by the boundaries of the plate. Furthermore, in contrast to the preceding example energy radiation towards infinity here does not take place by virtue of the bounded domain. The $K_I(t)$

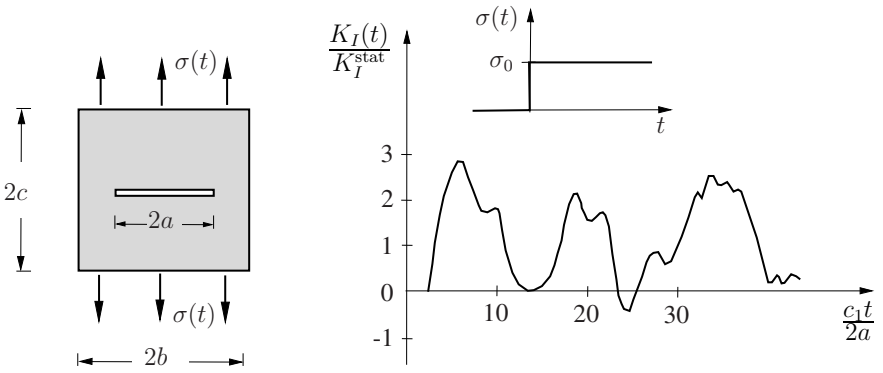

Fig. 7.3 Impact loading of a crack in a rectangular plate (plane stress, $\nu = 0.25$; $a : b : c = 9.5 : 100 : 60$)

variation is qualitatively an oscillation with a period which is essentially determined by the travel time of a wave over the distance $2c$. Local peaks superimposed on this oscillation can also be explained from travel times of waves propagating at different speeds (c_1, c_2, c_R). Since there is no damping (e.g., due to energy radiation) the oscillation of $K_I(t)$ does not decay.

As a final example we consider an impact-loaded 3-point-bending specimen as it is used for the determination of K_{Ic} values (Fig. 7.4). For a prescribed value of the impact velocity the variation $F(t)$ of the loading has been measured; the latter gives rise to the depicted $K_I(t)$ variation (Fig. 7.4). It can be seen that the temporal variations $F(t)$ and $K_I(t)$ are completely different, especially in the initial phase. Hence the current value of K_I cannot be determined from the current value of F. Also, it should be noted that for such a type of loading a repeated loss of contact between the specimen and the impactor as well as between the specimen and the support takes place due to the motion of the specimen.

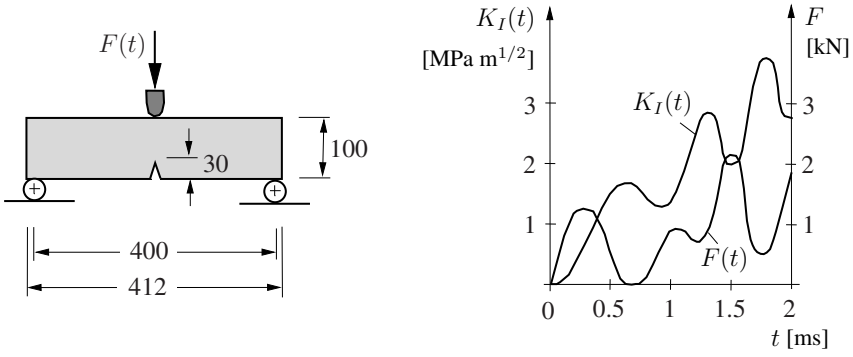

Fig. 7.4 Impact loading of 3-point-bending specimen

7.4 Crack propagation

7.4.1 Crack-tip field

Now we consider a crack which propagates at some speed $\dot{a}$ and acceleration $\ddot{a}$ (Fig. 7.5). The dynamic crack-tip field is investigated first for pure mode III (antiplane shear) as the simplest case. The respective problem is described by the equation of motion (7.9) which for the present purpose is transformed to the coordinate system x', y' that moves with the crack tip (cf. Section 5.8.3.2). Using $x' = x - a(t)$, $y' = y$ one obtains for an arbitrary field quantity (here the displacement w)

$$\frac{\partial^2 w}{\partial x^2} = \frac{\partial^2 w}{\partial x'^2}, \quad \frac{\partial^2 w}{\partial y^2} = \frac{\partial^2 w}{\partial y'^2}, \quad \ddot{w} = \frac{\partial^2 w}{\partial t^2} - 2\dot{a}\frac{\partial^2 w}{\partial x' \partial t} - \ddot{a}\frac{\partial w}{\partial x'} + \dot{a}^2 \frac{\partial^2 w}{\partial x'^2} \,. \quad (7.16)$$

At the crack tip ($r \to 0$) a nonsingular displacement field of the type $w(r, \varphi, t) = r^\lambda \tilde{w}(\varphi, t)$ with $0 \le \lambda < 1$ and a singular stress field is expected. Because of

$$\frac{\partial}{\partial x'} = \cos\varphi \frac{\partial}{\partial r} - \sin\varphi \frac{\partial}{r\partial\varphi} \quad , \qquad \frac{\partial}{\partial y'} = \sin\varphi \frac{\partial}{\partial r} + \cos\varphi \frac{\partial}{r\partial\varphi}$$

the last term in $\ddot{w}$ dominates for $r \to 0$ compared to the first three terms and we get $\ddot{w} = \dot{a}^2 \partial^2 w / \partial x'^2$. Thus the equation of motion governing the crack-tip field reads

$$\frac{\partial^2 w}{\partial x'^2} + \frac{1}{\alpha_2^2} \frac{\partial^2 w}{\partial y'^2} = 0 \qquad \text{where} \qquad \alpha_2^2 = 1 - \frac{\dot{a}^2}{c_2^2} \,. \quad (7.17)$$

By introducing of the new coordinates (contraction of the y-coordinate)

$$x_2 = r_2 \cos\varphi_2 = x' = r\cos\varphi \,, \quad y_2 = r_2 \sin\varphi_2 = \alpha_2 y' = \alpha_2 r \sin\varphi \,, \quad (7.18)$$

equation (7.17) can be transformed into Laplace's equation

$$\frac{\partial^2 w}{\partial x_2^2} + \frac{\partial^2 w}{\partial y_2^2} = 0 \,. \quad (7.19)$$

The easiest way for its solution is the use of complex variables (see Sections 1.5.2 and 4.2.1) which leads to

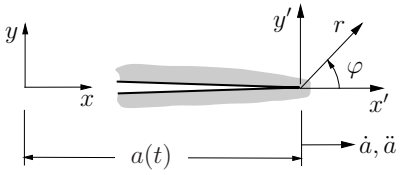

Fig. 7.5 Running crack

$$\begin{aligned} Gw &= \mathrm{Re}\ \Omega(z_2) \quad , \\ \tau_{xz} - \mathrm{i}\frac{\tau_{yz}}{\alpha_2} &= \Omega'(z_2) \end{aligned} \tag{7.20}$$

where $z_2 = x_2 + \mathrm{i}\, y_2 = r_2 \mathrm{e}^{\mathrm{i}\varphi_2}$. The subsequent steps are analogous to the static case. The dominating part of the solution which satisfies the boundary conditions is described by $\Omega = A z_2^{1/2}$. If the stress intensity factor is defined (as in statics) by

$$K_{III} = \lim_{r\to 0} \sqrt{2\pi r}\ \tau_{yz}(\varphi = 0) \tag{7.21}$$

one finally obtains the crack-tip field

$$\left\{ \begin{array}{c} \tau_{xz} \\ \\ \tau_{yz} \end{array} \right\} = \frac{K_{III}}{\sqrt{2\pi r_2}} \left\{ \begin{array}{c} -\frac{1}{\alpha_2} \sin\frac{\varphi_2}{2} \\ \\ \cos\frac{\varphi_2}{2} \end{array} \right\} , \qquad w = \frac{2K_{III}}{G\alpha_2} \sqrt{\frac{r_2}{2\pi}} \sin\frac{\varphi_2}{2} \ . \tag{7.22}$$

Its general structure is similar to the static case with a stress singularity of the type $r^{-1/2}$. The angular distribution of the field quantities, however, depends on α_2, i.e., on the crack-tip speed $\dot{a}$. In the limit case of a stationary crack ($\dot{a} = 0$) with $\alpha_2 = 1$ and $r_2 = r$, $\varphi_2 = \varphi$ the static crack-tip field (cf. Eq. (4.6)) is recovered.

For mode I the procedure is fully analogous to the just described mode III case. The transformation of (7.5) to the moving coordinate system yields for $r \to 0$

$$\frac{\partial^2\phi}{\partial x'^2} + \frac{1}{\alpha_1^2}\frac{\partial^2\phi}{\partial y'^2} = 0 \ , \quad \frac{\partial^2\psi}{\partial x'^2} + \frac{1}{\alpha_2^2}\frac{\partial^2\psi}{\partial y'^2} = 0 \quad \text{where} \quad \alpha_i^2 = 1 - \frac{\dot{a}^2}{c_i^2} \ . \tag{7.23}$$

If in the first equation the coordinates

$$x_1 = r_1 \cos\varphi_1 = x' = r\cos\varphi \ , \qquad y_1 = r_1 \sin\varphi_1 = \alpha_1 y' = \alpha_1 r \sin\varphi \tag{7.24}$$

are introduced and in the second one the coordinates (7.18) the two Laplace equations

$$\frac{\partial^2\phi}{\partial x_1^2} + \frac{\partial^2\phi}{\partial y_1^2} = 0 \ , \qquad \frac{\partial^2\psi}{\partial x_2^2} + \frac{\partial^2\psi}{\partial y_2^2} = 0 \tag{7.25}$$

are obtained. Their solution for the symmetric (mode I) crack-tip field can be written in the form $\phi = A\ \mathrm{Re}\ z_1^{3/2}$, $\psi = B\ \mathrm{Im}\ z_2^{3/2}$ where $z_1 = x_1 + \mathrm{i}y_1 = r_1 \mathrm{e}^{\mathrm{i}\varphi_1}$, $z_2 = x_2 + \mathrm{i}y_2 = r_2 \mathrm{e}^{\mathrm{i}\varphi_2}$ and the real constants A, B are determined from the boundary conditions (traction-free crack faces). Introducing the definition of the stress intensity factor

$$K_I = \lim_{r\to 0} \sqrt{2\pi r}\ \sigma_y(\varphi = 0) \tag{7.26}$$

leads to

$$\left\{\begin{array}{c}\sigma_x\\ \\ \sigma_y\\ \\ \tau_{xy}\end{array}\right\} = \frac{K_I f}{\sqrt{2\pi}} \left\{\begin{array}{c}(1+2\alpha_1^2-\alpha_2^2)\frac{\cos(\varphi_1/2)}{\sqrt{r_1}} - \frac{4\alpha_1\alpha_2}{1+\alpha_2^2}\frac{\cos(\varphi_2/2)}{\sqrt{r_2}}\\ \\ -(1+\alpha_2^2)\frac{\cos(\varphi_1/2)}{\sqrt{r_1}} + \frac{4\alpha_1\alpha_2}{1+\alpha_2^2}\frac{\cos(\varphi_2/2)}{\sqrt{r_2}}\\ \\ 2\alpha_1\frac{\sin(\varphi_1/2)}{\sqrt{r_1}} - 2\alpha_1\frac{\sin(\varphi_2/2)}{\sqrt{r_2}}\end{array}\right\} \tag{7.27a}$$

$$\left\{\begin{array}{c}u\\ \\ v\end{array}\right\} = \frac{K_I 2f}{G\sqrt{2\pi}} \left\{\begin{array}{c}\sqrt{r_1}\,\cos\frac{\varphi_1}{2} - \sqrt{r_2}\,\frac{2\alpha_1\alpha_2}{1+\alpha_2^2}\cos\frac{\varphi_2}{2}\\ \\ -\alpha_1\sqrt{r_1}\,\sin\frac{\varphi_1}{2} + \sqrt{r_2}\,\frac{2\alpha_1}{1+\alpha_2^2}\sin\frac{\varphi_2}{2}\end{array}\right\} \tag{7.27b}$$

where

$$f = \frac{1+\alpha_2^2}{R(\dot{a})} = \frac{1+\alpha_2^2}{4\alpha_1\alpha_2 - (1+\alpha_2^2)^2}\,. \tag{7.28}$$

Here, $R(\dot{a})$ denotes the Rayleigh function defined in (7.7). The stresses and displacements display the same dependence on r as in the static case. Their magnitude and angular distribution, however, depend on the crack-tip speed $\dot{a}$; the acceleration $\ddot{a}$ has no influence. Hence the crack-tip field is uniquely determined once the K-factor and the crack-tip speed are known. This can also be seen from the results for the stress σ_y ahead of the crack tip ($\varphi = 0$) and the crack opening displacement $\delta = v(\pi) - v(-\pi)$:

$$\sigma_y = \frac{K_I}{\sqrt{2\pi r}} \quad , \qquad \delta = \frac{K_I}{G}\sqrt{\frac{r}{2\pi}}\,\frac{4\alpha_1(1-\alpha_2^2)}{R(\dot{a})}\,. \tag{7.29}$$

While σ_y is solely determined by K_I, the crack opening displacement δ at fixed K increases with increasing crack speed and tends to infinity for $\dot{a} \to c_R$. One should, however, note that for a specific crack configuration the dynamic stress intensity factor is itself a decreasing function of the crack speed. This issue is further discussed at the end of Section 7.4.2.

From the crack-tip field several conclusions can be drawn with regard to the behavior of a fast running crack. Figure 7.6a indicates that the stress ratio σ_y/σ_x ahead of the crack tip ($\varphi = 0$) decreases with increasing crack speed. Correspondingly, the propensity for material separation in planes perpendicular to the crack propagation direction increases. When the crack speed approaches the Rayleigh wave speed the stress ratio tends to zero and crack propagation in the direction $\varphi = 0$ becomes impossible. Therefore, the Rayleigh wave speed can be considered as an upper bound for the crack-tip speed.

For various values of the crack-tip speed the angular distribution of the circumferential stress σ_φ at the crack tip is depicted in Fig. 7.6b. While for a sufficiently low crack speed the maximum stress prevails at $\varphi = 0$ this maximum shifts to $\varphi \gtrsim \pi/3$ for $\dot{a} \gtrsim 0.6\ c_2$. If one assumes that crack advance proceeds in the direction of maxi-

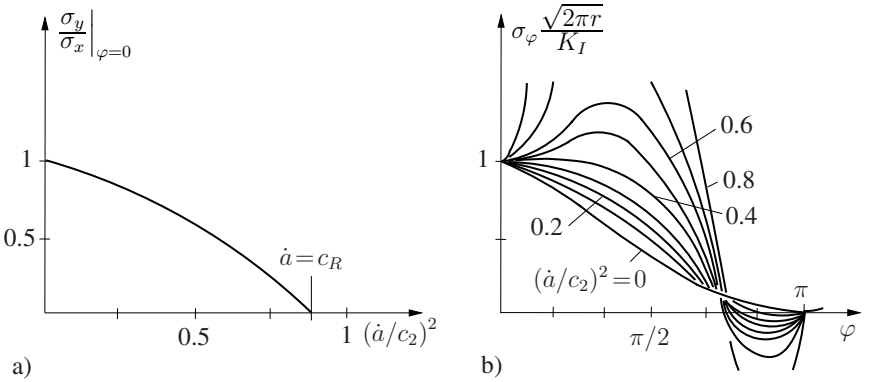

Fig. 7.6 Influence of the crack speed on the crack-tip stress field ($\nu = 1/4$)

mum circumferential stress this can be taken as an indication that for $\dot{a} \widetilde{>} 0.6\ c_2$ the crack becomes unstable with regard to its original propagation direction. This stability threshold, first emphasized by E.H. YOFFE (1951), can be regarded as another upper bound for the crack-tip speed.

Finally, in the same manner as for mode I, the mode II crack-tip field can be determined. It reads

$$\left\{\begin{array}{c}\sigma_x\\ \\ \sigma_y\\ \\ \tau_{xy}\end{array}\right\} = \frac{K_{II} f}{\sqrt{2\pi}} \left\{\begin{array}{c} -2\alpha_2 \dfrac{1+2\alpha_1^2-\alpha_2^2}{1+\alpha_2^2} \dfrac{\sin(\varphi_1/2)}{\sqrt{r_1}} + 2\alpha_2 \dfrac{\sin(\varphi_2/2)}{\sqrt{r_2}} \\ 2\alpha_2 \dfrac{\sin(\varphi_1/2)}{\sqrt{r_1}} - 2\alpha_2 \dfrac{\sin(\varphi_2/2)}{\sqrt{r_2}} \\ \dfrac{4\alpha_1\alpha_2}{1+\alpha_2^2} \dfrac{\cos(\varphi_1/2)}{\sqrt{r_1}} - (1+\alpha_2^2) \dfrac{\cos(\varphi_2/2)}{\sqrt{r_2}} \end{array}\right\} \tag{7.30a}$$

$$\left\{\begin{array}{c}u\\ \\ v\end{array}\right\} = \frac{K_{II} 2f}{G\sqrt{2\pi}} \left\{\begin{array}{c} \sqrt{r_1}\, \dfrac{2\alpha_2}{1+\alpha_2^2} \sin\dfrac{\varphi_1}{2} - \sqrt{r_2}\, \alpha_2\, \sin\dfrac{\varphi_2}{2} \\ -\sqrt{r_1}\, \dfrac{2\alpha_2\alpha_2}{1+\alpha_2^2}\, \cos\dfrac{\varphi_1}{2} + \sqrt{r_2}\, \cos\dfrac{\varphi_2}{2} \end{array}\right\} . \tag{7.30b}$$

7.4.2 Energy release rate

The energy release rate $\mathcal{G}$ for the problem of a straight running crack with traction-free crack faces shall be investigated now. We proceed exactly as in Section 5.8.3.3 except that here the kinetic energy has to be accounted for and the material is assumed elastic. The energy flux $-P^*$ into the process zone at the crack tip then is generally given by

$$-P^* = P - \dot{E} - \dot{K} \tag{7.31}$$

where E is the strain energy and K the kinetic energy. When applied to the situation sketched in Fig. 7.7 the energy flux $-P^* = \dot{a}\mathcal{G}$ across the contour C_P reads (cf. (5.89))

$$\dot{a}\mathcal{G} = \int_C t_i \dot{u}_i \mathrm{d}c - \frac{\mathrm{d}}{\mathrm{d}t}\int_A U \mathrm{d}A - \frac{\mathrm{d}}{\mathrm{d}t}\int_A \frac{1}{2}\rho \dot{u}_i \dot{u}_i \mathrm{d}A \,. \tag{7.32}$$

Here, U is the strain energy density and $\rho\dot{u}_i\dot{u}_i/2$ is the specific kinetic energy; the contour C_P is taken to be vanishingly small ($C_P \to 0$). Analogous to the procedure in Section 5.8.3.3, applying Reynold's transport theorem, the relation $\mathrm{d}U/\mathrm{d}t = \sigma_{ij}\dot{u}_{i,j} = (\sigma_{ij}\dot{u}_i)_{,j} - \sigma_{ij,j}\dot{u}_i$, the equation of motion $\sigma_{ij,j} = \rho\ddot{u}_i$ and the divergence theorem after some steps leads to

$$\dot{a}\mathcal{G} = -\int_{C_P} \left[\dot{a}\Big(U + \frac{1}{2}\rho\dot{u}_i\dot{u}_i\Big)n_1 + t_i\dot{u}_i\right]\mathrm{d}c \,. \tag{7.33}$$

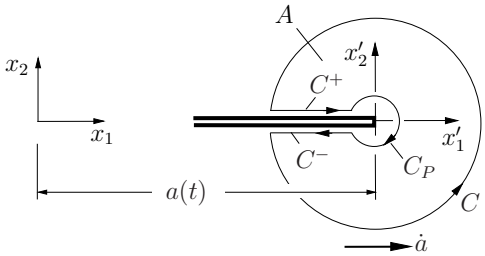

Fig. 7.7 Moving crack tip and contours considered in energy release rate calculation

Now we perform the transition to the moving coordinate system x_1', x_2' and consider A and C to be as well moving with the crack tip. Since it can be assumed that u_i is regular at the crack tip while $u_{i,1}$ is singular (cf. (7.27b)) it follows from (5.81) that at the crack tip $\dot{u}_i = -\dot{a}u_{i,1}$. Inserting this into (7.32) leads to

$$\mathcal{G} = -\int_{C_P} \left[\Big(U + \frac{1}{2}\dot{a}^2\rho\, u_{i,1}u_{i,1}\Big)n_1 - t_i u_{i,1}\right]\mathrm{d}c \,. \tag{7.34}$$

By applying the divergence theorem to the area A with boundary $C + C_P + C^+ + C^-$ (C^+, C^- yield no contribution) together with $t_i = \sigma_{ij}n_j$ one finally obtains for the energy release rate

$$\boxed{\mathcal{G} = \int_C \Big[(U + \frac{1}{2}\dot{a}^2\rho u_{i,1}u_{i,1})n_1 - t_i u_{i,1}\Big]\mathrm{d}c + \int_A (\sigma_{ij,j}u_{i,1} - \dot{a}^2\rho u_{i,11}u_{i,1})\mathrm{d}A} \,. \tag{7.35}$$

The relation (7.35) simplifies in various special cases. For a crack which propagates at constant speed $\dot{a}$ under steady-state conditions the area integral vanishes because of $\sigma_{ij,j} = \rho\ddot{u}_i$ and $\ddot{u}_i = \dot{a}^2 u_{i,11}$ (see also (7.16)) and we get

$$\mathcal{G} = \int_C \Big[\Big(U + \frac{1}{2}\dot{a}^2\rho u_{i,1}u_{i,1}\Big)n_1 - t_i u_{i,1}\Big]\,\mathrm{d}c\,. \tag{7.36}$$

In the special case $\dot{a} = 0$ (7.35) reduces to (7.12). If, in addition, static conditions prevail ($\sigma_{ij,j} = 0$) the J-integral (4.119) is recovered from $\mathcal{G}$.

The contour C in (7.35) can be chosen arbitrarily. If it is contracted to the crack tip the area integral vanishes and we obtain

$$\mathcal{G} = \lim_{C\to 0}\int_C \Big[\Big(U + \frac{1}{2}\dot{a}^2\rho u_{i,1}u_{i,1}\Big)n_1 - t_i u_{i,1}\Big]\,\mathrm{d}c\,. \tag{7.37}$$

From this the interrelation between $\mathcal{G}$ and K_I for mode I can be established by inserting (7.27a,b) and (7.28):

$$\mathcal{G} = \frac{\alpha_1(1-\alpha_2^2)}{2GR(\dot{a})}\,K_I^2 = \frac{\alpha_1(1-\alpha_2^2)}{4\alpha_1\alpha_2 - (1+\alpha_2^2)^2}\,\frac{K_I^2}{2G}\,. \tag{7.38}$$

Hence the energy release rate is uniquely determined by the stress intensity factor and the crack-tip speed . According to (7.7) the function $R(\dot{a})$ vanishes for the Rayleigh wave speed. That means that for $K_I \neq 0$ the energy release rate $\mathcal{G}$ apparently tends to infinity when the crack speed approaches the Rayleigh wave speed. Conversely, at finite $\mathcal{G}$ the stress intensity factor tends to zero for $\dot{a} \to c_R$.

However, the dynamic stress intensity factor K_I is itself a function of the crack speed. If one compares for a given crack configuration, i.e. for the same geometry and loading, the stress intensity factor at a stationary crack tip with that at a running crack tip ($\dot{a} > 0$), one obtains

$$K_I^{\mathrm{dyn}} = k(\dot{a})K_I^{\mathrm{stat}}\quad . \tag{7.39}$$

Here,

$$k(\dot{a}) \approx \frac{1-\dot{a}/c_R}{\sqrt{1-\dot{a}/c_1}} \tag{7.40}$$

is a universal function which is equal to 1 for $\dot{a} = 0$ and tends to zero for $\dot{a} \to c_R$. Inserting (7.39) with (7.40) into (7.38) leads to the expression

$$\mathcal{G}^{\mathrm{dyn}} = g(\dot{a})\,\mathcal{G}^{\mathrm{stat}} \tag{7.41}$$

for the energy release rate where $g(\dot{a})$ decreases monotonically from $g(\dot{a}=0) = 1$ to $g(\dot{a} = c_R) = 0$. That means that the energy release rate (and hence the energy flux into the crack tip) decreases with increasing crack speed and vanishes for $\dot{a} \to c_R$.

The Rayleigh wave speed c_R therefore represents an upper bound for dynamic crack propagation under mode I conditions.

In case of a running crack under mixed-mode loading by K_I, K_{II}, and K_{III} the general relation

$$\mathcal{G} = \frac{1}{2G}\left[\frac{(1-\alpha_2^2)(\alpha_1 K_I^2 + \alpha_2 K_{II}^2)}{4\alpha_1\alpha_2 - (1+\alpha_2^2)^2} + \frac{K_{III}^2}{\alpha_2}\right] . \tag{7.42}$$

holds which for $\dot{a} = 0$ reduces to (7.14).

7.4.3 *Fracture concept, crack-tip speed, crack branching, crack arrest*

In the framework of linear fracture mechanics the K-concept can be applied also to fast crack propagation. Accordingly, at any instant of crack advance under mode-I conditions the fracture criterion

$$K_I(t) = K_{Id} \tag{7.43}$$

must be fulfilled. Here, K_{Id} denotes the *dynamic fracture toughness* which is assumed to be a material parameter that, in a first approximation, depends only on the crack-tip speed: $K_{Id} = K_{Id}(\dot{a})$. This dependence is qualitatively depicted in Fig. 7.8. Starting from the initiation value K_{Ic} the fracture toughness in most cases first shows only a weak dependence on the crack-tip speed while it rapidly increases at higher values of $\dot{a}$. One possible explanation for this behavior could be a change in the micromechanisms of material separation in the process zone. This is supported by the well-known observation that the roughness of the fracture surface strongly increases with increasing crack speed. Another reason lies in the fact that (different from the static case) the crack-tip field or the state in the process zone, respectively, is not uniquely characterized by the stress intensity factor; according

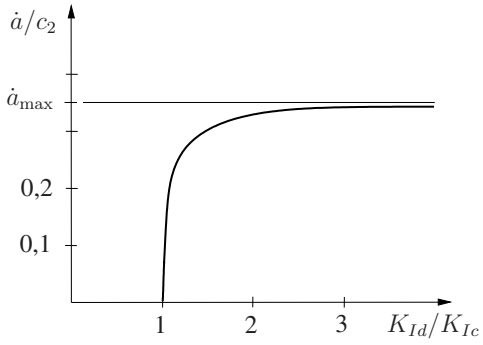

Fig. 7.8 Typical dependence of fracture toughness on crack-tip speed

to Section 7.4.1 the stresses and deformations depend also on the crack-tip speed. During crack advance also the energetic fracture condition

$$\mathcal{G}(t) = \mathcal{G}_d(\dot{a}) \tag{7.44}$$

must be satisfied where $\mathcal{G}_d(\dot{a})$ is the material specific fracture resistance which depends on the crack-tip speed. Due to the relation (7.38) between $\mathcal{G}$ and K_I the fracture conditions (7.43) and (7.44) are equivalent.

From measurements it is known that the crack-tip speed under mode I conditions even in very brittle materials does not exceed a maximum value of about $\dot{a}_{max} \approx 0.5\, c_2$. An exception are fracture experiments where via special devices such as a laser beam, energy is directly supplied to the crack tip. Despite various possible explanations the issue of this limit crack-tip speed is not yet fully understood. One reason, for instance, could be the instability of the straight crack advance at crack speeds above $\dot{a} \gtrsim 0.6 c_2$ (see Section 7.4.1). This is supported by the increasing roughness (or waviness) of the fracture surface with increasing crack-tip speed as well as by an enhanced tendency for the formation of secondary cracks. The latter are microcracks which form in the neighborhood of the main crack or depart (branch off) from it. The increasing roughness of the fracture surface and the formation of secondary cracks also provide an explanation for the enhanced dynamic fracture toughness since especially the formation of microcracks is a mechanism which may strongly contribute to energy dissipation. An objection to the "instability hypothesis", however, arises from the fact that the measured maximum crack speeds are significantly lower than the theoretical instability threshold. Another, more qualitative attempt of explanation is based on the discrete nature of bond breaking. According to this, a crack advances by "jumps" along discrete material elements of a characteristic length l_M. In order to transfer the entire information about the preceding jump to the next element (maximum distance $2l_M$) a characteristic time $\tau \approx 2l_M/c_2$ of wave propagation is required (one may also insert c_R instead of c_2). If one assumes that after this time the next jump takes place one obtains, irrespective of the precise value of the microstructural length l_M, an average (approximate) speed of crack propagation of $\dot{a} \approx l_M/\tau \approx c_2/2$.

A phenomenon frequently observed in conjunction with dynamic fracture is crack branching (Fig. 7.9a). It is most likely to occur at a crack-tip speed close to the limit speed $\dot{a}_{max}$, but it may (depending on the material) take place also at lower values of $\dot{a}$. Crack branching is typically preceded by an increasing roughness of the fracture surface and by the formation of secondary cracks which may be interpreted as "branching attempts". Likewise the issue of a limiting crack speed, a generally accepted explanation for crack branching and a reliable branching criterion are still lacking. Theoretical reasoning is mostly based on the analysis of the crack-tip field of a single fast running crack or of a crack that has just branched. Crack branching has, for instance, also been related to the directional instability which occurs at $\dot{a} \approx 0.6\, c_2$. Yet, this is not suitable to explain branching at lower crack speeds and the observed significantly smaller branching angle of about $\alpha \approx 28°$. The latter, however, can be explained from the plausible hypothesis that upon branching both

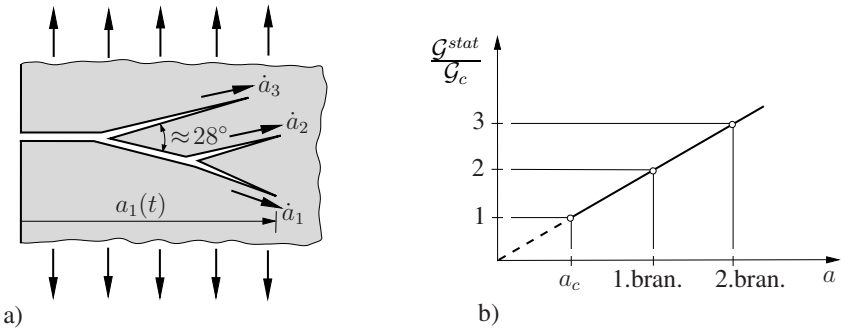

Fig. 7.9 Crack branching

crack tips propagate under pure mode-I conditions. Even for a quasistatic analysis this hypothesis yields results which agree well with experimental observations.

A prerequisite for crack branching is a sufficient energy flux into the process zone, i.e., a sufficiently large energy release rate $\mathcal{G}$, which enables the formation and subsequent propagation of two cracks. The determination of $\mathcal{G}$ typically is cumbersome since this quantity generally depends on the geometry of the specimen, on time, on the current crack length, and the crack speed. A simple and coarse approximation for $\mathcal{G}$ can be obtained from the corresponding static problem by neglecting the inertia forces. For instance, in case of an edge-crack subjected to uniaxial loading (see Table 4.1, No. 5) this leads to $\mathcal{G} \approx \mathcal{G}^{stat} = (K_I^{stat})^2/E' = 1.26\,\pi\sigma^2 a$. If, in addition, one assumes that branching of the crack takes place when $\mathcal{G}$ attains integer multiples of the value $\mathcal{G}_c$ required for crack initiation the result depicted in Fig. 7.9b is obtained. This result, however, is only of qualitative nature.

Of great practical importance – since desired in technical components – is the *crack arrest*. This takes place when in the course of crack propagation the stress intensity factor decreases to such an extent that the fracture condition (7.43) is no longer fulfilled; the crack then stops growing. The condition for arrest can be written in the form

$$K_I(t) = K_{Ia} \tag{7.45}$$

where $K_{Ia} = \min[K_{Id}(\dot{a})]$ is called the *crack arrest toughness*. Since crack arrest in a component is a dynamic process its treatment generally requires the complete dynamic analysis of the structure (including inertia forces and wave phenomena). It has, however, turned out that in many practical cases a quasistatic analysis yields sufficiently accurate results.

As outlined at the end of Section 7.4.2, mode-I cracks cannot grow faster than the Rayleigh wave speed for energetic reasons since the energy release rate vanishes for $\dot{a} > c_R$. This is not the case for mode-II shear cracks. While in this case the energy release rate likewise goes to zero for $\dot{a} \to c_R$, it again attains a positive value for $\dot{a} = \sqrt{2}c_2$. In the range $c_R < \dot{a} < \sqrt{2}c_2$ the crack tip singularity depends on the crack speed and is weaker than $r^{-1/2}$ so that the energy release rate is zero. That means that mode II shear cracks may propagate at a so-called *intersonic* speed,

i.e. above c_R and c_2 and below c_1. Recent experimental results and observations from shallow crustal earthquakes provide evidence of intersonic crack propagation.

7.4.4 Examples

The investigation of fast crack propagation is generally quite laborious, irrespective of whether experimental, numerical, or analytical methods are utilized. A significant simplification, however, results when it can be assumed that the crack advance takes place at constant speed $\dot{a}$ and under steady-state conditions. The transformation of the wave equations (7.5) for plane strain to the coordinate system x', y' that moves at the speed $\dot{a} = const$ then leads with $\partial(\cdot)/\partial t = 0$ and $\ddot{a} = 0$ to exactly the Laplace equations (7.25) discussed in Section 7.4.1. Their solution can generally be written in the form $\phi = \mathrm{Re}\, \Phi(z_1)$, $\psi = \mathrm{Re}\, \Psi(z_2)$.

As an example the classical *Yoffe problem* (E.H. YOFFE, 1951) is considered first. It consists of a straight crack of constant length which moves at constant speed in an unbounded domain subjected to uniaxial tension σ (Fig. 7.10a). The crack hence opens at the leading tip and (physical unrealistically) closes again at its end. The corresponding static problem has been studied in Section 4.4.1. For Φ and Ψ the representations

$$\Phi'(z_1) = A_1 \sqrt{z_1^2 - a^2} + A_2 z_1 \,, \qquad \Psi'(z_2) = \mathrm{i}\, B_1 \sqrt{z_2^2 - a^2} + \mathrm{i}\, B_2 z_2 \,, \tag{7.46}$$

are chosen from which the displacements and stresses can be computed using (7.2) and the elasticity law. The boundary conditions $\sigma_y = 0$, $\tau_{xy} = 0$ for $|x'| < a$ (traction-free crack faces) and $\sigma_y = \sigma$, $\sigma_x = 0$ for $z_i \to \infty$ yield the constants

$$\begin{aligned} A_1 &= \frac{\sigma}{G} \frac{1+\alpha_2^2}{R(\dot{a})} \,, & A_2 &= \frac{\sigma}{G} \left[\frac{2(\alpha_1^2 - \alpha_2^2)}{R(\dot{a})} - \frac{1}{1+\alpha_2^2} \right] \,, \\ B_1 &= \frac{\sigma}{2} \frac{2\alpha_1}{R(\dot{a})} \,, & B_2 &= \frac{\sigma}{2} \left[\frac{(\alpha_1^2 - \alpha_2^2)(1+\alpha_2^2)}{\alpha_2 R(\dot{a})} - \frac{1}{2\alpha_2} \right] \,. \end{aligned} \tag{7.47}$$

The symmetry conditions $v = 0$, $\tau_{xy} = 0$ for $|x'| > a$ are automatically fulfilled. Thus the stresses and displacements in the entire domain are uniquely determined. In particular, the stress σ_y ahead of the crack tip and the displacements v of the upper and lower crack faces are obtained as

$$\sigma_y = \sigma \frac{x'}{\sqrt{x'^2 - a^2}} \quad , \qquad v^{\pm} = \pm \frac{\sigma}{G} \frac{\alpha_1 (1 - \alpha_2^2)}{R(\dot{a})} \sqrt{a^2 - x'^2} \,. \tag{7.48}$$

While σ_y is independent of $\dot{a}$ (i.e., it shows the same behavior as in the static case) the crack opening increases with increasing crack speed and tends to infinity for $\dot{a} \to c_R$. Correspondingly, the K-factor is given by the static value $K_I = \sigma\sqrt{\pi a}$

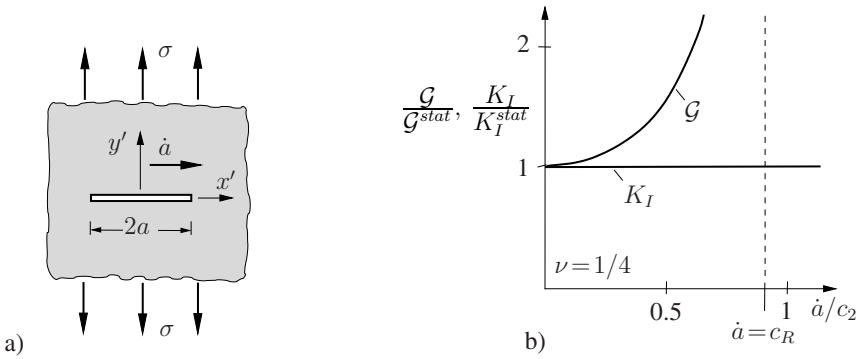

Fig. 7.10 Yoffe's problem

whereas the energy release rate according to (7.38) shows an unlimited growth with the crack speed (Fig. 7.10b).

As a second example the steady-state propagation of a semi-infinite crack in an infinitely long strip as sketched in Fig. 7.11a is investigated. Loading is specified by a prescribed constant relative displacement 2δ of the horizontal boundaries of the strip. In this case the energy release rate can easily be computed from (7.36). For this purpose a contour C is chosen with its vertical parts located far away from the crack tip in the undisturbed regions to the right and left, respectively (Fig. 7.11a). There the stress and deformation states in plane strain are given by

$$x_1' \gg h: \qquad \varepsilon_{22} = \frac{\delta}{h}, \quad \sigma_{22} = \frac{2G\delta(1-\nu)}{h(1-2\nu)}, \quad u_{i,1} = 0$$

$$x_1' \ll -h: \qquad \varepsilon_{22} = \sigma_{22} = u_{i,1} = 0\,.$$

With $U = \frac{1}{2}\sigma_{22}\,\varepsilon_{22}$ only the vertical part of C ahead of the crack tip yields a contribution to $\mathcal{G}$ (the contributions from the horizontal parts of C cancel each other) and one obtains

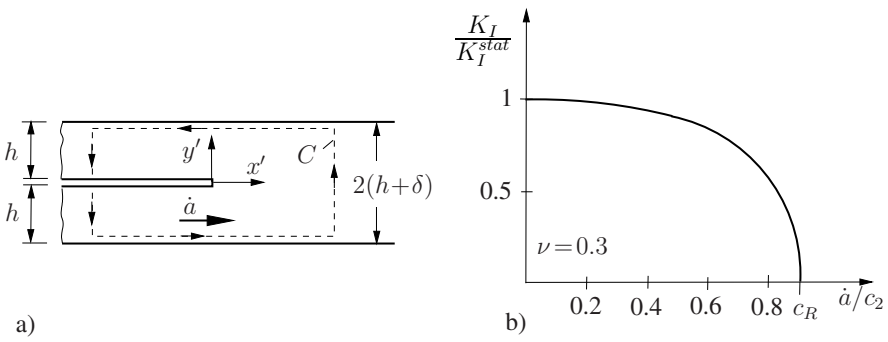

Fig. 7.11 Steady-state crack propagation in an infinite strip

$$\mathcal{G} = 2h\,U|_{x_1' \gg h} = \frac{2(1-\nu)}{1-2\nu}\,\frac{G\delta^2}{h}\,. \tag{7.49}$$

Accordingly, the energy release rate is independent of the crack speed and the result (7.49) hence is also valid for the stationary crack ($\dot{a} = 0$). The stress intensity factor follows from (7.38) and reads

$$K_I(\dot{a}) = 2G\delta\sqrt{\frac{(1-\nu)R(\dot{a})}{h(1-2\nu)(1-\alpha_2^2)\alpha_1}}\,. \tag{7.50}$$

It decreases with increasing crack speed and tends to zero for $\dot{a} \to c_R$ (Fig. 7.11b). It should be noted that from similar considerations the energy release rate for fast running cracks in long pipes can be computed which is an application of great practical importance.

The following example is concerned with the nonstationary growth of an edge-crack in a rectangular plate loaded by an idealized impact $\sigma H(t)$. Figure 7.12 shows results from numerical analyses in plane stress for three different fracture criteria. In case (a) the K-criterion (7.43) has been employed where $K_{Id}(\dot{a})$ is given by the relation

$$K_{Id}^{(a)} = K_{Ic}\left[1 + 2.5(\dot{a}/c_2)^2 + 3.9\cdot 10^4(\dot{a}/c_2)^{10}\right] \tag{7.51}$$

with $K_{Ic} = 0.69\,\mathrm{MPa}\sqrt{\mathrm{m}}$. This relation is an approximation to experimental data for Araldite (a brittle amorphous material). Case (b) is also based on the K-criterion where now, for simplicity, the fracture toughness is taken independent of the crack speed: $K_{Id}^{(b)} = K_{Ic}$. Finally, in case (c) the energetic fracture criterion (7.44) has been used where $\mathcal{G}_d$ is assumed to be independent of the crack speed: $\mathcal{G}_d^{(c)} = \mathcal{G}_c = K_{Ic}^2/E$. Using (7.38) the energetic criterion can be transformed into the K-criterion; the fracture toughness is in this case given by

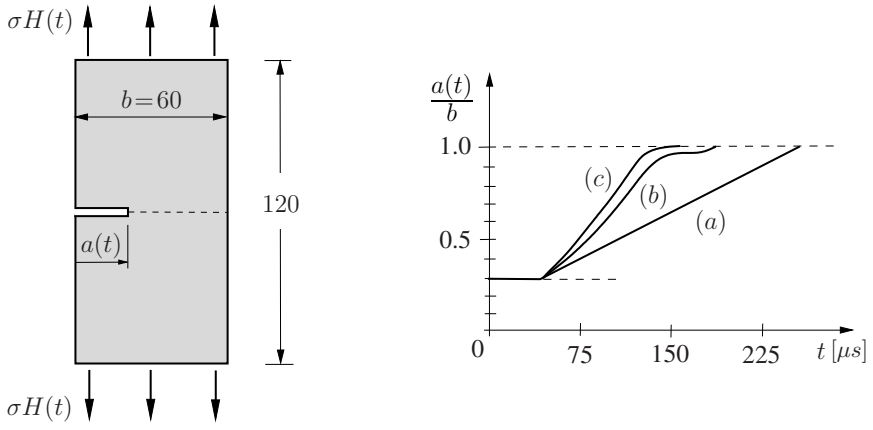

Fig. 7.12 Dynamic propagation of an edge-crack; a(0)=29.5 mm

$$K_{Id}^{(c)} = K_{Ic}\sqrt{\frac{R(\dot a)}{(1-\nu)\alpha_1(1-\alpha_2^2)}}\,. \tag{7.52}$$

Hence the three cases differ only by the $K_{Id}(\dot a)$-dependence and in the entire range of the crack speed we have $K_{Id}^{(c)} \le K_{Id}^{(b)} \le K_{Id}^{(a)}$. Accordingly, crack propagation through the plate is fastest for (c) and slowest for (a). The attained maximum crack speeds are $\dot a^{(c)} \approx \dot a^{(b)} = 0.74\,c_2$ and $\dot a^{(a)} = 0.37\,c_2$. The first two are unrealistically high while the last one is in the range of experimental observations. It should be noted that the crack speed in the most realistic case (a) is almost constant despite the strongly varying stress field.

It has already been mentioned that upon impact loading of a component which contains a crack, stress waves may repeatedly interact with the crack tip due to their multiple reflections. This leads to complex temporal variations of the stress intensity factors (cf. Fig. 7.3) and a mixed-mode loading state according to Section 4.9 generally prevails at the crack tip. The crack path then typically displays a curvilinear trajectory which is determined by the characteristic details of the dynamic loading which affect the crack-tip loading state at each current position of the crack tip. This is illustrated here by means of a numerical example where crack advance (including the direction) proceeds "freely", i.e., only controlled by a fracture criterion according to Section 4.9. We consider a rectangular plate (Fig. 7.13) with the symmetry slightly disturbed by the location of the initial (edge-) crack. Loading is specified by an ideal impact $\sigma H(t)$ on the vertical boundaries and by different temporal variations $\sigma_a(t)$ or $\sigma_b(t)$, respectively, on the horizontal boundaries. Figure 7.13 shows the crack trajectories determined from numerical simulations for two different loading rates ($\dot\sigma_a(t) \ll \dot\sigma_b(t)$). The incremental computation of the crack path is based on the fracture criterion of maximum circumferential stress (Section 4.9) and the relation (7.51) for the fracture toughness. Instead of the relations (4.143) which are valid only in the static case, the evaluation of the fracture criterion in the present situation of a fast running crack has to account for the dynamic crack-tip field $\sigma_\varphi(K_I,\, K_{II},\, \dot a,\, \varphi)$ according to (7.27).

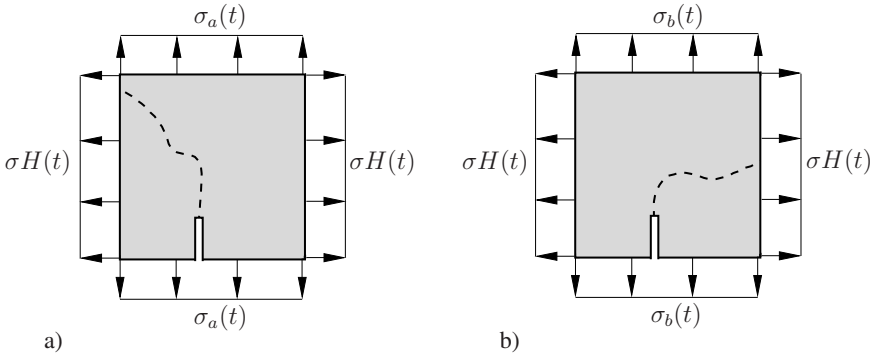

Fig. 7.13 Crack paths resulting from repeated stress wave loading; $\dot\sigma_a \ll \dot\sigma_b$

The two entirely different crack paths in Fig. 7.13 can be explained from the superposition of stress waves emanating from the boundaries of the plate. These superpositions cause sudden changes of the crack-tip stress field at distinct times. Which stress state exactly results and to which crack propagation direction this leads hence depends in a complicated manner on the type of the boundary loading ($\sigma_a(t)$ or $\sigma_b(t)$) that determines the wave profile.

7.5 Fragmentation

In the absence of a macroscopic initial crack, a sufficiently high dynamic loading often causes breaking of a solid body into a multitude of pieces (*fragments*). This process, which takes place in very short time, is called *fragmentation*. It can qualitatively be explained by the conversion of kinetic energy into fracture surface energy. In such a fracture process, the average size and number of resulting fragments are sometimes an important issue. Its thorough analysis requires to take statistical aspects into account, such as the distribution of initial defects (e.g. microcracks) in the material. Nevertheless, already a purely deterministic approach based on energetic considerations (GRADY, 1982) provides some interesting insight. This is illustrated in the following by means of a simple example.

We consider the axisymmetric problem of a thin-walled ring (or cylinder) which is loaded by a sufficiently high internal pressure so that the material moves outward in radial direction with velocity v_0 (Fig. 7.14). At a current radius r the strain rate in circumferential direction is $\dot{\varepsilon}_0 = v_0/r$. We assume that the ring breaks into n equal pieces of length l with $nl = 2\pi r$. Moreover, it can be assumed (supported by experimental observations) that at the instant of fragmentation the kinetic energy of the ring is significantly larger than the stored elastic energy and that the radial velocity v_0 does not change much. The kinetic energy of the material's motion in tangential direction in each fragment relative to its center of mass is considered as the source to supply the fracture energy. With the circumferential strain rate $\dot{\varepsilon}_0$ and the (circumferential) coordinate s measured from the fragment's center of mass (see Fig. 7.14) the respective relative velocity can be written as $v_{\mathrm{rel}} = \dot{\varepsilon}_0 s$. The corresponding portion T^* of kinetic energy per fragment hence reads

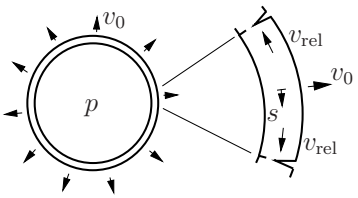

Fig. 7.14 Fragmentation of a ring subjected to internal pressure

$$T^* = \frac{1}{2}\,\varrho A\dot{\varepsilon}_0^2 \int_{-l/2}^{l/2} s^2\,\mathrm{d}s = \frac{1}{24}\,\varrho A\dot{\varepsilon}_0^2 l^3 \tag{7.53}$$

where ϱ is the mass density and A the cross section of the ring. With the specific fracture surface energy γ of the material, the fracture energy per fragment is $\Gamma = \gamma A$. Setting this equal to the kinetic energy portion T^* yields the following relation for the length l of a fragment as a function of specific fracture energy, mass density and circumferential strain rate:

$$l = \left(\frac{24\gamma}{\varrho\dot{\varepsilon}_0^2}\right)^{1/3} . \tag{7.54}$$

According to this, the fragment size l is directly proportional to $\gamma^{1/3}$ and inversely proportional to $\dot{\varepsilon}_0^{2/3}$. Despite the simplifying assumptions this scaling law for the fragment size agrees quite well with experimental findings. Similar considerations can be worked out for other geometrical configurations.

7.6 Further reading

Achenbach, J.D., *Dynamic effects in brittle fracture*. In *Mechanics Today* Vol. 1, ed. S. Nemat-Nasser, Pergamon Press, New York, 1972

Broberg, K.B., *Cracks and Fracture*. Academic Press, London, 1999

Freund, L.B., *Dynamic Fracture Mechanics*. Cambridge University Press, Cambridge, 1993

Gdoutos, E.E., *Fracture Mechanics – An Introduction*. Kluwer, Dordrecht, 2010

Kanninen, M.F. and Popelar, C.H., *Advanced Fracture Mechanics*. Clarendon Press, Oxford, 1985

Klepaczko, J.R. (ed.), *Crack Dynamics in Metallic Materials*. CISM courses and lectures no. 310, Springer, Wien, 1990

Liebowitz, H. (ed.), *Fracture – A Treatise*, Vol. 2, Chap. 5. Academic Press, London, 1968

Meyers, M.A., *Dynamic Behavior of Materials*. Wiley-Interscience, 1994

Ravi-Chandar, K., *Dynamic Fracture*. Elsevier Science, Amsterdam, 2004

Sih, G.C.(ed.), *Dynamic Crack Propagation*. Noordhoff, Leyden, 1973

Sih, G.C. (ed.), *Mechanics of Fracture*, Vol. 4, Noordhoff, Leyden, 1977

Weertmann, J., *Dislocation Based Fracture Mechanics*. World Scientific, Singapore, 1998

Zhang, Ch. and Gross, D., *On Wave Propagation in Elastic Solids with Cracks*. WIT Press, Southampton, 1997

Chapter 8
Micromechanics and homogenization

8.1 Introduction

On close inspection, e.g., through a microscope, all real materials show a multitude of heterogeneities even if they macroscopically appear to be homogeneous. These deviations from homogeneity may exist in form of cracks, voids, particles, or regions of a foreign material, layers or fibers in a laminate, grain boundaries, or irregularities in a crystal lattice. Here they shall be referred to as *defects* in a generalized sense. Subject of micromechanical investigations is the behavior of these heterogeneities or defects as well as their effect on the overall properties and performance of a material. For instance, heterogeneities of any kind can locally act as stress concentrators and thereby lead to the formation and coalescence of microcracks or voids as a source of progressive material damage (see Section 3.1.2 and Chapter 9).

Defects occur on different *length scales* which are characteristic for a certain material and for the respective type of defect (Fig. 8.1). An important task of micromechanics hence is to link mechanical relations on different length scales. Starting from a *macroscopic* level, defects and their spatial distribution prevailing on a smaller length scale – the *microscale* – are regarded as the *microstructure* of a material. What is meant by the macroscopic level and the microscopic level in a certain case depends on the problem at hand and is an issue of modelling. As illustrated in Fig. 8.1, a microstructure in form of many cracks on the millimeter scale may, for instance, be identified in a technical component. The apparently homogeneous material between the individual cracks, however, can itself be regarded as the macroscopic level with respect to an even finer polycrystalline microstructure with a characteristic length scale (grain size) in the range of microns. And a single grain, on the other hand, can represent the macroscopic level when focusing on the microstructure of the crystal lattice with numerous discrete dislocations. Such an approach bears the advantage that a complex material behavior which is difficult to describe in a purely phenomenological manner is traced back to elementary processes on the microscale. Micromechanical problems can be treated in the framework of continuum mechanics. Via the additional consideration of a finer length

D. Gross and T. Seelig, *Fracture Mechanics: With an Introduction to Micromechanics*, Mechanical Engineering Series, DOI 10.1007/978-3-642-19240-1_8,

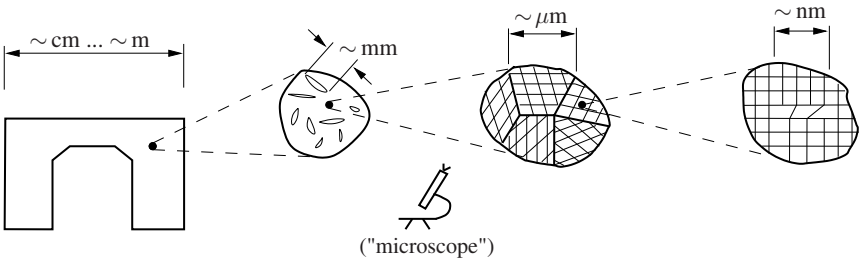

Fig. 8.1 Macroscopic and microscopic levels, characteristic length scales

scale (the microscopic level) a spatial distribution of defects (the microstructure) then is related to a material point on the macroscopic level.

The investigation of defects may be subdivided according to two essential problems. Point of interest can be the behavior of a defect on its *own* length scale which also comprises the interaction with further defects (see, e.g., Section 4.4.4). On the other hand, one may examine the influence of many defects on the *macroscopic* material behavior on a larger length scale. In this latter case the entire behavior of the microstructure is interpreted as the mechanical state of a material point on the macroscopic level which thereby is ascribed *effective* material properties. Such a micro-to-macro transition formally proceeds by appropriate averaging processes and is called *homogenization*. Microstructural changes then lead to changes of the overall (*effective*) properties of the material. A microstructural evolution such as the growth of microcracks or microvoids which gives rise to a reduction of macroscopic stiffness or strength is referred to as *damage* and is, because of its importance for fracture mechanics and failure, separately treated in Chapter 9.

The present chapter serves to introduce fundamental concepts and methods of micromechanics. Besides the characterization of typical defects and their local action the issue of the transition from the microscopic to the macroscopic level and the derivation of effective material properties from a given microstructure is investigated. We will mainly focus on linear elastic material behavior, yet a brief introduction into the treatment of elastic-plastic and thermoelastic materials is also given.

Early theoretical studies of the performance of materials with microstructure date back to J.C. MAXWELL (1831-1879), LORD RAYLEIGH, (1842-1919) and A. EINSTEIN (1879-1955). While the former two were concerned with the determination of the overall electric conductivity of a heterogeneous material the latter investigated the effective viscosity of a fluid which contains a suspension of solid spherical particles. In solid mechanics emphasis was orginally placed on the determination of the elastic constants of a polycrystal from those of a single crystal with first theoretical considerations by W. VOIGT (1850-1919) and A. REUSS (1900-1968). Important contributions were supplied, among others, by E. KRÖNER (1919-2000) and R. HILL (1921-2011) in the second half of the last century. Their theoretical concepts and analytical approximations, which also apply to modern composite materials, were later on extended and generalized to inelastic material behavior. Moreover, they serve as foundations for the treatment of the "inverse problem", i.e., the design

of new composite materials having an optimized microstructure with regard to the overall performance.

8.2 Selected defects and fundamental solutions

Defects in an elastic material inevitably give rise to inhomogeneous stress and strain fields by which the defects can be characterized. One may distinguish between defects which are themselves the source of a so-called *eigenstrain* or *eigenstress* field (e.g., dislocations, inclusions) and those which only under the action of some external load induce a perturbation of the uniform (i.e., spatially constant) field such as particles of a foreign material, voids, or cracks. In the latter case of *material inhomogeneities* it is possible and practical to decompose the total strain and stress field into two parts: (1) a uniform field as it would prevail in a defect-free material, and (2) the deviation induced by the defects. The second part then is referred to as the *equivalent eigenstrain* or *eigenstress*, respectively. This decomposition allows to establish a formal equivalence between an inhomogeneous material and some homogeneous material with a certain eigenstrain or eigenstress distribution, irrespective of its physical origin.

In the following we will discuss some typical defects by means of fundamental solutions in an unbounded linear elastic medium and start by analysing the effect of eigenstrains in a homogeneous material.

8.2.1 Eigenstrain

8.2.1.1 Center of dilatation

A center of dilatation is the idealization of an "infinitely" small (point-like) region which undergoes an "infinitely" strong radial expansion (eigenstrain). It gives rise to a singular strain and stress field which in an isotropic medium is spherically symmetric with tension in circumferential and pressure in radial direction. A center of dilatation may also be interpreted as a spherical region of radius a inside which a pressure p prevails (Fig. 8.2). The displacement and stress field in the surrounding material can be represented in spherical coordinates (r, φ, ϑ) as

$$\begin{aligned} u_r &= p\,\frac{a^3}{4\mu r^2}\,, \quad u_\varphi = u_\vartheta = 0\,, \\ \sigma_{rr} &= -p\,\frac{a^3}{r^3}\,, \quad \sigma_{\varphi\varphi} = \sigma_{\vartheta\vartheta} = p\,\frac{a^3}{2r^3}\,, \quad \sigma_{r\varphi} = \sigma_{r\vartheta} = \sigma_{\varphi\vartheta} = 0\,. \end{aligned} \tag{8.1}$$

A center of dilatation may, for instance, be taken as a simple model for the effect of an interstitial atom (point defect) on the surrounding elastic crystal lattice.

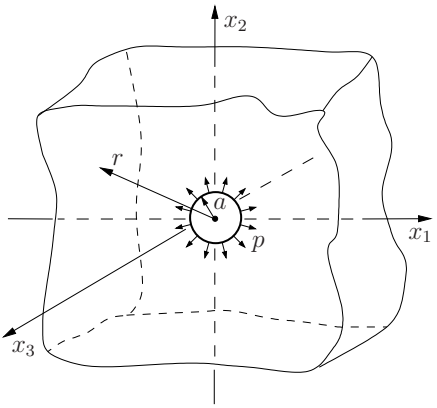

Fig. 8.2 Center of dilatation

8.2.1.2 Straight edge and screw dislocation

Dislocations are line defects in crystalline solids (see Section 3.1.2). In continuum mechanics they can be characterized by a constant jump $\boldsymbol{b}$, referred to as the *Burgers vector*, which the displacement field undergoes along some contour encircling the dislocation line (x_3-axis in Fig. 8.3; see also Fig. 3.2).

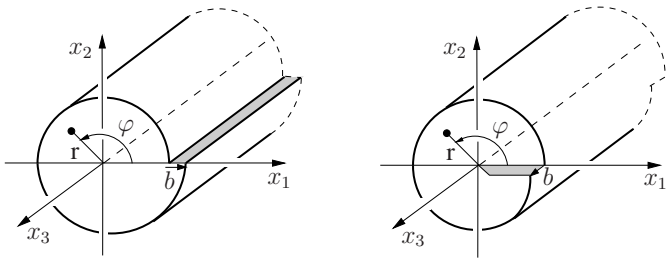

Fig. 8.3 a) Straight edge dislocation, b) straight screw dislocation

In case of a straight edge dislocation according to Fig. 8.3a with a Burgers vector of magnitude b the displacement and stress field in an isotropic, linear elastic medium can be written as

$$
\begin{aligned}
&u_1 = \frac{D}{2\mu}\left(2(1-\nu)\varphi + \frac{x_1 x_2}{r^2}\right), \quad u_2 = \frac{D}{2\mu}\left(-(1-2\nu)\ln r + \frac{x_2^2}{r^2}\right), \\
&\sigma_{11} = -Dx_2\frac{3x_1^2 + x_2^2}{r^4}, \quad \sigma_{12} = Dx_1\frac{x_1^2 - x_2^2}{r^4}, \quad \sigma_{22} = Dx_2\frac{x_1^2 - x_2^2}{r^4}
\end{aligned}
\tag{8.2}
$$

where $D = b\mu/2\pi(1-\nu)$ and $r^2 = x_1^2 + x_2^2$. The respective fields induced by a straight screw dislocation (Fig. 8.3b) are given by the simpler representation

$$u_3 = \frac{b}{2\pi}\,\varphi\ , \qquad \sigma_{13} = -\frac{b\mu}{2\pi}\,\frac{x_2}{r^2}\ , \qquad \sigma_{23} = \frac{b\mu}{2\pi}\,\frac{x_1}{r^2}\ . \tag{8.3}$$

8.2.1.3 Inclusion

In contrast to the foregoing examples of point or line defects now we consider the situation of a spatial distribution of eigenstrain $\varepsilon^t_{ij}(\boldsymbol{x})$. Those strains may, for instance, result from phase transformations in solids where atomic rearrangements change the geometry of the lattice. Since they are not caused by stress, eigenstrains are also referred to as *stress-free transformation strains* (superscript t). Formally, all kinds of strain which may prevail in a material in the absence of stress can be interpreted as eigenstrains; typical examples are thermal or plastic strains (see (1.44) and Section 1.3.3). In the framework of infinitesimal deformations the total strains ε_{ij} are the sum of elastic strains $\varepsilon^e_{ij} = C^{-1}_{ijkl}\,\sigma_{kl}$ and the eigenstrains: $\varepsilon_{ij} = \varepsilon^e_{ij} + \varepsilon^t_{ij}$. Then the stresses are given by

$$\sigma_{ij} = C_{ijkl}\,(\varepsilon_{kl} - \varepsilon^t_{kl})\ . \tag{8.4}$$

If nonvanishing eigenstrains prevail only in some bounded subregion Ω of the homogeneous material this region is called an *inclusion* and the surrounding material the *matrix* (Fig. 8.4). It has to be emphasized that the elastic properties of an inclusion and the matrix are the same; otherwise the region Ω is called an *inhomogeneity* (Section 8.2.2).

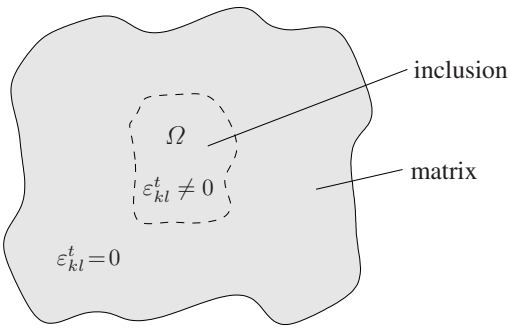

Fig. 8.4 Inclusion in matrix

In the general case of an arbitrary inclusion geometry Ω and an arbitrary eigenstrain field $\varepsilon^t_{kl}(\boldsymbol{x})$ it is not possible to represent the stress distribution and the total strain and displacement field in closed form. Some special cases are discussed in the following section.

8.2.1.4 Eshelby's result

The probably most important analytical solution of micromechanics has been found by J.D. ESHELBY (1916-1981). It is valid for an unbounded domain which contains an *ellipsoidal* inclusion Ω with principal axes a_i (Fig. 8.5):

$$(x_1/a_1)^2 + (x_2/a_2)^2 + (x_3/a_3)^2 \leq 1 \; .$$

If the eigenstrains in the inclusion are constant, $\varepsilon^t_{kl} = const$, then the remarkable result holds that the total strains ε_{kl} inside the inclusion Ω are constant as well. Via the fourth-order *Eshelby tensor* S_{ijkl} they depend linearly on the eigenstrains:

$$\boxed{\varepsilon_{ij} = S_{ijkl}\, \varepsilon^t_{kl} = const \qquad \text{in} \quad \Omega} \; . \tag{8.5}$$

Using (8.4) the stresses inside Ω which then are likewise constant can be represented as

$$\sigma_{ij} = C_{ijmn}\, (S_{mnkl} - I_{mnkl})\, \varepsilon^t_{kl} = const \qquad \text{in} \quad \Omega \tag{8.6}$$

where

$$I_{mnkl} = \frac{1}{2}(\delta_{mk}\delta_{nl} + \delta_{ml}\delta_{nk}) \tag{8.7}$$

is the symmetric fourth-order unit tensor. The Eshelby tensor is symmetric in the first and second pair of indices, but in general it is not symmetric with regard to an exchange of these pairs:

$$S_{ijkl} = S_{jikl} = S_{ijlk} \; , \qquad S_{ijkl} \neq S_{klij} \; . \tag{8.8}$$

In case of an isotropic material its components depend only on Poisson's ratio ν, the ratios of the principal axes a_i, and their orientation with respect to some cartesian coordinate system. Because of the length of the respective expressions they

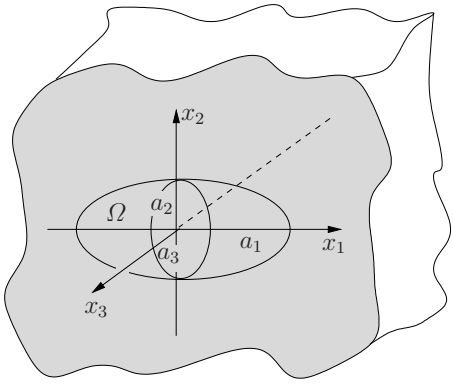

Fig. 8.5 Ellipsoidal inclusion Ω in an unbounded domain

are not given here and the reader is referred to the literature (e.g., MURA, 1982; KACHANOV et al., 2003) for their representation.

Outside the inclusion Ω the stresses and strains are not constant; with increasing distance r from the inclusion they asymptotically decay according to $\varepsilon_{ij}\,,\ \sigma_{ij} \sim r^{-3}$ for $r \to \infty$, as in case of a center of dilatation. The result (8.5) by ESHELBY (1957) holds for an arbitrary anisotropic material. Yet, only in case of an isotropic material is a closed-form representation of the tensor S_{ijkl} and the fields outside Ω possible. The Eshelby solution for ellipsoidal inclusions is of fundamental importance for analytical homogenization techniques; it will by intensively employed in later sections.

Starting from the general ellipsoid various special cases can be derived. For instance, the two-dimensional solution for an infinitely long cylinder of elliptic cross section in plane strain is obtained from the limit process $a_3 \to \infty$ (Fig. 8.6). The exterior strain and stress fields in the x_1, x_2-plane then display an asymptotic behavior of $\varepsilon_{ij}\,,\ \sigma_{ij} \sim r^{-2}$ for $r \to \infty$. The nonvanishing components of the Eshelby tensor in case of an isotropic material are for the orientation of the principal axes of Ω according to Fig. 8.6 given by

$$
\begin{aligned}
S_{1111} &= \frac{1}{2(1-\nu)} \left\{ \frac{a_2^2 + 2a_1a_2}{(a_1+a_2)^2} + (1-2\nu)\frac{a_2}{a_1+a_2} \right\} , \\
S_{2222} &= \frac{1}{2(1-\nu)} \left\{ \frac{a_1^2 + 2a_1a_2}{(a_1+a_2)^2} + (1-2\nu)\frac{a_1}{a_1+a_2} \right\} , \\
S_{1122} &= \frac{1}{2(1-\nu)} \left\{ \frac{a_2^2}{(a_1+a_2)^2} - (1-2\nu)\frac{a_2}{a_1+a_2} \right\} , \\
S_{2211} &= \frac{1}{2(1-\nu)} \left\{ \frac{a_1^2}{(a_1+a_2)^2} - (1-2\nu)\frac{a_1}{a_1+a_2} \right\} , \\
S_{1212} &= \frac{1}{2(1-\nu)} \left\{ \frac{a_1^2 + a_2^2}{2(a_1+a_2)^2} + \frac{1-2\nu}{2} \right\} , \\
S_{1133} &= \frac{\nu}{2(1-\nu)} \frac{2a_2}{a_1+a_2} , \qquad S_{2233} = \frac{\nu}{2(1-\nu)} \frac{2a_1}{a_1+a_2} , \\
S_{1313} &= \frac{a_2}{2(a_1+a_2)} , \qquad S_{2323} = \frac{a_1}{2(a_1+a_2)} .
\end{aligned}
\tag{8.9}
$$

For a spherical inclusion $(a_i = a)$ in an isotropic material the dependence on the principal axes and their orientation vanishes (geometric isotropy) and the Eshelby tensor reduces to

$$
S_{ijkl} = \alpha \frac{1}{3} \delta_{ij}\delta_{kl} + \beta \left(I_{ijkl} - \frac{1}{3} \delta_{ij}\delta_{kl} \right) \tag{8.10}
$$

where

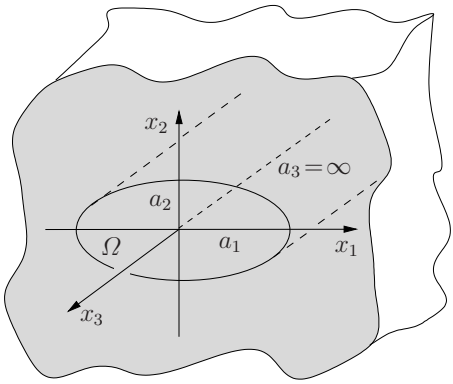

Fig. 8.6 Elliptic cylinder

$$\alpha = \frac{1+\nu}{3(1-\nu)} = \frac{3K}{3K+4\mu}\,, \qquad \beta = \frac{2(4-5\nu)}{15(1-\nu)} = \frac{6(K+2\mu)}{5(3K+4\mu)} \tag{8.11}$$

are scalar parameters. The entire (i.e., elastic and geometric) isotropy of the problem then allows the decomposition into volumetric and deviatoric strains which highlights the meaning of the parameters α and β:

$$\varepsilon_{kk} = \alpha\, \varepsilon^t_{kk}\,, \qquad e_{ij} = \beta\, e^t_{ij} \qquad \text{in } \Omega\,. \tag{8.12}$$

As a simple example we consider the thermal expansion due to a constant temperature increase ΔT in some spherical region of radius a. This can be described by the eigenstrains

$$\varepsilon^t_{ij} = \begin{cases} k\Delta T\, \delta_{ij}\,, & r \le a \\ 0\,, & r > a \end{cases} \tag{8.13}$$

where k is the coefficient of thermal expansion. According to (8.12) the strains inside the inclusion $(r \le a)$ are $\varepsilon_{kk} = 3\alpha k\, \Delta T\,,\ e_{ij} = 0$ or in spherical coordinates $(r,\, \varphi,\, \vartheta)$

$$\varepsilon_r = \varepsilon_\varphi = \varepsilon_\vartheta = \frac{1+\nu}{3(1-\nu)}\, k\, \Delta T\,. \tag{8.14}$$

Outside the inclusion $(r > a)$ the solution is

$$\varepsilon_r = -2\,\frac{1+\nu}{3(1-\nu)} \left(\frac{a}{r}\right)^3 k\, \Delta T\,, \qquad \varepsilon_\varphi = \varepsilon_\vartheta = \frac{1+\nu}{3(1-\nu)} \left(\frac{a}{r}\right)^3 k\, \Delta T\,. \tag{8.15}$$

8.2.1.5 Defect energies

Due to the stress and strain fields caused by defects on the microscopic level of a material the overall energy content of the material is affected. The evolution of defects (e.g., translation or growth) hence gives rise to energy changes which in turn can be related to the action of so-called *generalized (material)* forces (see Section 4.6.5.2). Of special importance in this context are those parts of the energy which express the interaction of external (imposed) fields with the fields induced by the defects.

In the following we consider an arbitrary inclusion Ω in some finite volume V with boundary ∂V on which the load t_i^0 is prescribed (Fig. 8.7); volume forces are neglected here. Because of the linearity of the problem all fields can additively be decomposed into a part due to the external load (indicated by the superscript 0) and a part (without superscript) caused by the eigenstrain $\varepsilon_{ij}^t(\boldsymbol{x})$ of the inclusion. The total potential hence reads

$$\begin{aligned} \Pi &= \frac{1}{2}\int_V (\sigma_{ij}^0 + \sigma_{ij})(\varepsilon_{ij}^0 + \underbrace{\varepsilon_{ij} - \varepsilon_{ij}^t}_{\varepsilon_{ij}^e})\,\mathrm{d}V - \int_{\partial V} t_i^0(u_i^0 + u_i)\,\mathrm{d}A \\ &= \underbrace{\frac{1}{2}\int_V \sigma_{ij}^0\varepsilon_{ij}^0\,\mathrm{d}V - \int_{\partial V} t_i^0 u_i^0\,\mathrm{d}A}_{\Pi^0} + \underbrace{\frac{1}{2}\int_V \sigma_{ij}(\varepsilon_{ij} - \varepsilon_{ij}^t)\,\mathrm{d}V}_{\Pi^t} \\ &\quad + \underbrace{\frac{1}{2}\int_V (\sigma_{ij}^0(\varepsilon_{ij} - \varepsilon_{ij}^t) + \sigma_{ij}\varepsilon_{ij}^0)\,\mathrm{d}V}_{=0 \quad (*)} \underbrace{- \int_{\partial V} t_i^0 u_i\,\mathrm{d}A}_{\Pi^i}\,. \end{aligned} \tag{8.16}$$

That the term $(*)$ vanishes can be shown as follows. First, by inserting the elasticity law, the terms below the integral can be combined. Application of the divergence theorem then yields a surface integral and a volume integral, the integrands of which

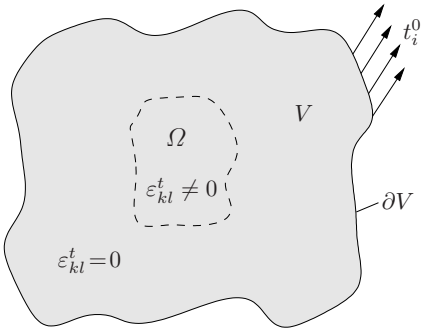

Fig. 8.7 Inclusion Ω in bounded domain under external load

both vanish since eigenstrains alone do not cause tractions on ∂V (i.e., $t_i|_{\partial V} = 0$) and because of the equilibrium condition $\sigma_{ij,j} = 0$:

$$(*) = \frac{1}{2}\int_V [\varepsilon^0_{kl} \underbrace{C_{ijkl}(\varepsilon_{ij} - \varepsilon^t_{ij})}_{\sigma_{kl}} + \sigma_{ij}\varepsilon^0_{ij}]\,\mathrm{d}V = \int_V \sigma_{ij}\varepsilon^0_{ij}\,\mathrm{d}V$$
$$= \int_{\partial V} t_i u^0_i\,\mathrm{d}A - \int_V \sigma_{ij,j} u^0_i\,\mathrm{d}V = 0\,.$$

The term Π^0 in the total potential (8.17) denotes the energy solely due to the external load and is irrelevant in the present context. The energy Π^t which results solely from the eigenstrain is called the *self energy* of the defect; it can be further transformed according to

$$\Pi^t = \frac{1}{2}\int_V \sigma_{ij}(\varepsilon_{ij} - \varepsilon^t_{ij})\,\mathrm{d}V = \underbrace{\frac{1}{2}\int_V \sigma_{ij}\varepsilon_{ij}\,\mathrm{d}V}_{=0,\ \text{cf. } (*)} - \frac{1}{2}\int_V \sigma_{ij}\varepsilon^t_{ij}\,\mathrm{d}V = -\frac{1}{2}\int_\Omega \sigma_{ij}\varepsilon^t_{ij}\,\mathrm{d}V\,. \tag{8.17}$$

In the special case of an ellipsoidal inclusion in an unbounded domain and a constant eigenstrain the stress σ_{ij} inside Ω is also constant. Using (8.6) the term Π^t then reduces to

$$\Pi^t = -\frac{1}{2}\,\sigma_{ij}\varepsilon^t_{ij} V_\Omega = -\frac{1}{2}\,C_{ijmn}(S_{mnkl} - I_{mnkl})\varepsilon^t_{ij}\varepsilon^t_{kl} V_\Omega \tag{8.18}$$

where V_Ω denotes the volume of the inclusion.

The *interaction energy* Π^i of the inclusion is defined as $\Pi^i = \Pi - \Pi^0 - \Pi^t$ and hence is equal to the remaining term in (8.17). It expresses the work done by the displacements induced by the eigenstrain on the external load and can be written as follows

$$\Pi^i = -\int_{\partial V} t^0_i u_i\,\mathrm{d}A = -\int_V \sigma^0_{ij}\varepsilon_{ij}\,\mathrm{d}V = -\int_V \varepsilon^0_{ij} C_{ijkl} \underbrace{(\varepsilon^e_{kl} + \varepsilon^t_{kl})}_{\varepsilon_{kl}}\,\mathrm{d}V$$
$$= \underbrace{-\int_V \varepsilon^0_{ij}\sigma_{ij}\,\mathrm{d}V}_{=0,\ \text{cf. } (*)} - \int_V \sigma^0_{ij}\varepsilon^t_{ij}\,\mathrm{d}V = -\int_\Omega \sigma^0_{ij}\varepsilon^t_{ij}\,\mathrm{d}V\,. \tag{8.19}$$

using similar steps as above. In case of a constant eigenstrain and a uniform external load ($\sigma^0_{ij} = const$) it simplifies to

$$\Pi^i = -\sigma^0_{ij}\varepsilon^t_{ij} V_\Omega\,. \tag{8.20}$$

The relation between the energy due to the presence of a defect and the generalized force acting on the defect is exemplified here by means of a center of dilatation (Section 8.2.1.1) in an unbounded domain subjected to a constant far-field loading σ^0_{ij}. When located at point $\boldsymbol{x} = \boldsymbol{\xi}$ the eigenstrain of a center of dilatation can be written using *Dirac's delta function* $\delta(.)$ as

$$\varepsilon^t_{ij}(\boldsymbol{x}) = q\,\delta(\boldsymbol{x} - \boldsymbol{\xi})\,\delta_{ij} \tag{8.21}$$

where q denotes its *intensity*. Insertion into (8.19) yields the dependence of the interaction energy on the location of the defect:

$$\Pi^i(\boldsymbol{\xi}) = -\int_V \sigma^0_{ij}(\boldsymbol{x})\varepsilon^t_{ij}(\boldsymbol{x})\,\mathrm{d}V = -q\int_V \sigma^0_{jj}(\boldsymbol{x})\delta(\boldsymbol{x} - \boldsymbol{\xi})\,\mathrm{d}V = -q\,\sigma^0_{jj}(\boldsymbol{\xi}) \tag{8.22}$$

In case of a center of dilatation it depends only on the hydrostatic part σ^0_{jj} of the stress field induced by the external load. Analogous to Section 4.6.5.2 the generalized force $\boldsymbol{F}$ acting on the center of dilatation is determined from the energy $\mathrm{d}\Pi = -F_k \mathrm{d}\xi_k$ released by a translation $\mathrm{d}\boldsymbol{\xi}$ of the defect. In the present case only the interaction energy changes with a translation of the defect and we get

$$F_k = -\frac{\partial \Pi^i}{\partial \xi_k} = q\,\frac{\partial \sigma^0_{jj}(\boldsymbol{\xi})}{\partial \xi_k}\,. \tag{8.23}$$

The generalized force on the center of dilatation hence is proportional to the gradient of the hydrostatic part of the external stress field (Fig. 8.8).

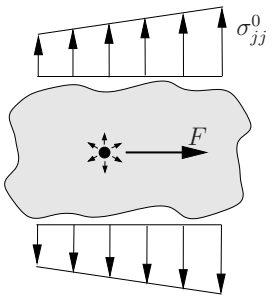

Fig. 8.8 Generalized force on a center of dilatation

The above example can be taken as a simple model for the stress-assisted diffusion of an interstitial atom in a crystal lattice. According to this, the generalized force causes a preferential migration of the interstitial atom towards regions subjected to a higher hydrostatic stress, i.e., with larger distances between the lattice atoms.

8.2.2 Inhomogeneities

8.2.2.1 Concept of equivalent eigenstrain

Now we focus on the second class of defects which instead of eigenstrains in a homogeneous material are characterized by inhomogeneous, i.e., spatially varying, material properties. We proceed in that we first describe these defects by an *equivalent eigenstrain* in some homogeneous *comparison material* in order to then apply again Eshelby's result. Therefore, we consider a domain V with the inhomogeneous material behavior described by the spatially dependent elasticity tensor $C_{ijkl}(\boldsymbol{x})$ and with displacements $\hat{u}_i$ prescribed on the boundary ∂V (Fig. 8.9a). If volume forces are neglected this boundary value problem is governed by the equations

$$\sigma_{ij,j} = 0 \,, \qquad \sigma_{ij} = C_{ijkl}(\boldsymbol{x})\,\varepsilon_{kl} \,, \qquad u_i|_{\partial V} = \hat{u}_i \,. \tag{8.24}$$

In addition we consider the geometrically identical domain V subjected to the same boundary conditions, yet consisting of a *homogeneous comparison material* with the constant material properties C^0_{ijkl} (Fig. 8.9b). The fields in this problem are indicated by the superscript 0:

$$\sigma^0_{ij,j} = 0 \,, \qquad \sigma^0_{ij} = C^0_{ijkl}\,\varepsilon^0_{kl} \,, \qquad u^0_i|_{\partial V} = \hat{u}_i \,. \tag{8.25}$$

If the *difference fields*

$$\tilde{u}_i = u_i - u^0_i \,, \qquad \tilde{\varepsilon}_{ij} = \varepsilon_{ij} - \varepsilon^0_{ij} \,, \tag{8.26}$$

are formed, it follows for the stress difference that

$$\begin{aligned} \tilde{\sigma}_{ij} = \sigma_{ij} - \sigma^0_{ij} \;&=\; C_{ijkl}(\boldsymbol{x})\,\varepsilon_{kl} - C^0_{ijkl}\Big(\underbrace{\varepsilon_{kl} - \tilde{\varepsilon}_{kl}}_{\varepsilon^0_{ij}}\Big) \\ &= C^0_{ijkl}\Big[\,\tilde{\varepsilon}_{kl} + \underbrace{C^{0\,-1}_{klmn}[\,C_{mnpq}(\boldsymbol{x}) - C^0_{mnpq}\,]\,\varepsilon_{pq}}_{-\varepsilon^*_{kl}}\,\Big] \,. \end{aligned} \tag{8.27}$$

The difference fields hence are governed by the equations

$$\tilde{\sigma}_{ij,j} = 0 \,, \qquad \tilde{\sigma}_{ij} = C^0_{ijkl}\Big(\tilde{\varepsilon}_{kl} - \varepsilon^*_{kl}\Big) \,, \qquad \tilde{u}_i|_{\partial V} = 0 \tag{8.28}$$

which describe a boundary value problem in a *homogeneous* material C^0_{ijkl} with *eigenstrain* $\varepsilon^*_{kl}(\boldsymbol{x})$ and vanishing displacements on the boundary ∂V (Fig. 8.9c). Here,

$$\varepsilon^*_{ij} = -\,C^{0\,-1}_{ijkl}\Big[\,C_{klmn}(\boldsymbol{x}) - C^0_{klmn}\,\Big]\,\varepsilon_{mn} \tag{8.29}$$

denotes the *equivalent eigenstrain*, i.e., equivalent to the heterogeneity of the material. Using an arbitrary homogeneous comparison material, the originally complex

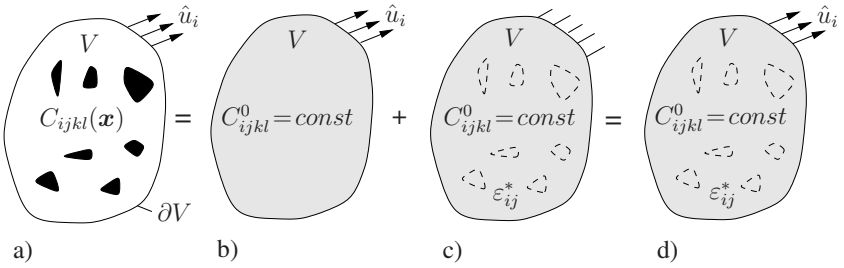

Fig. 8.9 a) Heterogeneous material, b) homogeneous comparison material, c) equivalent eigenstrain, d) homogenized original problem

problem of Fig. 8.9a thus has been transformed into the simpler problem of Fig. 8.9d with a homogeneous material and distributed eigenstrains. The latter still depend on the strain field of the original problem, but this dependence is only via the deviation $C_{ijkl}(\boldsymbol{x}) - C^0_{ijkl}$ in the elastic properties. Such an approach which may also be understood as a kind of *filtering* is advantageous in several regards. For instance, we already know fundamental solutions for eigenstrain problems in a homogeneous material such as Eshelby's result which now can be formally applied to material inhomogeneities. Also, the difference $C_{ijkl}(\boldsymbol{x}) - C^0_{ijkl}$ in (8.29) means that with an appropriately chosen C^0_{ijkl} an error in the approximation of $\varepsilon_{ij}(\boldsymbol{x})$ in the solution of the boundary value problem (8.28) may have a smaller effect than in the original problem (8.24). The quantity

$$\tau_{ij}(\boldsymbol{x}) = \left[C_{ijkl}(\boldsymbol{x}) - C^0_{ijkl} \right] \varepsilon_{kl}(\boldsymbol{x}) \tag{8.30}$$

in (8.29) which is called *stress polarization* emphasizes this connection. It describes the deviation of the "true" stress $\sigma_{ij} = C_{ijkl}\,\varepsilon_{kl}$ from the stress which would result from the "true" strain ε_{kl} in the homogeneous comparison material. The stress polarization τ_{ij} plays an important role in the framework of a variational formulation in Section 8.3.3.2.

The method of subtraction of a boundary value problem for a homogeneous (i.e., defect-free) material was basically already applied in Section 4.4.1 in the decomposition into two subproblems (Fig. 4.9). The fictitious crack loading introduced there in the subproblem (2) may also be interpreted as an eigenstress and the displacement jump, as will become more clear later on, as an eigenstrain.

If in addition to the material inhomogeneity $C_{ijkl}(\boldsymbol{x})$ a "true" eigenstrain $\varepsilon^t_{ij}(\boldsymbol{x})$ according to Section 8.2.1.3 prevails, the above procedure leads to an equivalent eigenstrain in the homogeneous comparison material of

$$\varepsilon^*_{ij} = -\,C^{0\,-1}_{ijkl} \left[\left(C_{klmn}(\boldsymbol{x}) - C^0_{klmn} \right) \varepsilon_{mn} - C_{klmn}(\boldsymbol{x})\,\varepsilon^t_{mn} \right] . \tag{8.31a}$$

In view of the frequently occurring tensorial expressions we will in the following besides the index notation for clarity also make use of the symbolic notation:

σ_{ij}, ε_{ij}, $C_{ijkl} \rightarrow \boldsymbol{\sigma}$, $\boldsymbol{\varepsilon}$, $\boldsymbol{C}$ (see Chapter 1). In this notation, for instance equation (8.31a) attains the form:

$$\boldsymbol{\varepsilon}^* = -\boldsymbol{C}^{0\,-1} : \left[\left(\boldsymbol{C}(\boldsymbol{x}) - \boldsymbol{C}^0 \right) : \boldsymbol{\varepsilon} - \boldsymbol{C}(\boldsymbol{x}) : \boldsymbol{\varepsilon}^t \right] . \tag{8.31b}$$

To distinguish it from the second-order unit tensor $\boldsymbol{I}$ the fourth-order unit tensor (8.7) is represented by the symbol $\mathbf{1}$. The interchange of the first and second pair of indices of a fourth-order tensor is indicated by a superscript T (transposition): $A_{mnij}\, B_{mnkl} = (\boldsymbol{A}^T : \boldsymbol{B})_{ijkl}$.

8.2.2.2 Ellipsoidal inhomogeneities

As an important special case which allows to apply Eshelby's result we consider an ellipsoidal material inhomogeneity Ω in an unbounded matrix (Fig. 8.10a). Now the elastic properties are piecewise constant and given by the elasticity tensors $\boldsymbol{C}_{\mathrm{I}}$ inside Ω (inhomogeneity) and $\boldsymbol{C}_{\mathrm{M}}$ in the surrounding matrix. At infinity the homogeneous strain field $\boldsymbol{\varepsilon}^0 = const$ is prescribed and the matrix material is chosen as the homogeneous comparison material: $\boldsymbol{C}^0 = \boldsymbol{C}_{\mathrm{M}}$. Using (8.26) and (8.29) the equivalent eigenstrain in Ω then is

$$\boldsymbol{\varepsilon}^*(\boldsymbol{x}) = -\,\boldsymbol{C}_{\mathrm{M}}^{-1} : \left(\boldsymbol{C}_{\mathrm{I}} - \boldsymbol{C}_{\mathrm{M}} \right) : \left(\tilde{\boldsymbol{\varepsilon}}(\boldsymbol{x}) + \boldsymbol{\varepsilon}^0 \right) . \tag{8.32}$$

Since outside Ω we have $\boldsymbol{\varepsilon}^* = \mathbf{0}$ the difference strain $\tilde{\boldsymbol{\varepsilon}}(\boldsymbol{x})$ in (8.28) can be determined from Eshelby's result

$$\tilde{\boldsymbol{\varepsilon}} = \boldsymbol{S} : \boldsymbol{\varepsilon}^* = const . \tag{8.33}$$

That the prerequisite for its application of a constant eigenstrain indeed holds is confirmed by insertion of (8.33) into (8.32). Solving for $\boldsymbol{\varepsilon}^*$ then yields the equivalent

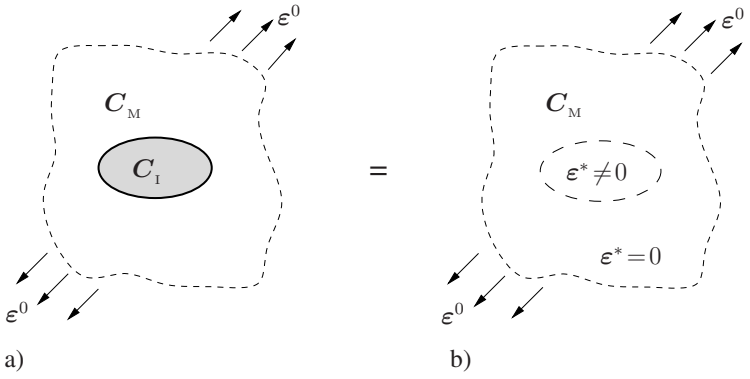

Fig. 8.10 a) Ellipsoidal inhomogeneity, b) homogeneous material with eigenstrain

eigenstrain due to a constant strain $\boldsymbol{\varepsilon}^0$ imposed at infinity at (Fig. 8.10b):

$$\boldsymbol{\varepsilon}^* = -\left[\boldsymbol{S} + (\boldsymbol{C}_{\mathrm{I}} - \boldsymbol{C}_{\mathrm{M}})^{-1} : \boldsymbol{C}_{\mathrm{M}}\right]^{-1} : \boldsymbol{\varepsilon}^0 \qquad \text{in} \quad \Omega \,. \tag{8.34}$$

Using (8.33) and (8.34) the total strain $\boldsymbol{\varepsilon} = \boldsymbol{\varepsilon}^0 + \tilde{\boldsymbol{\varepsilon}}$ inside the inhomogeneity Ω as a function of the external load $\boldsymbol{\varepsilon}^0$ reads

$$\boldsymbol{\varepsilon} = \underbrace{\left[\mathbf{1} + \boldsymbol{S} : \boldsymbol{C}_{\mathrm{M}}^{-1} : (\boldsymbol{C}_{\mathrm{I}} - \boldsymbol{C}_{\mathrm{M}})\right]^{-1}}_{\boldsymbol{A}_{\mathrm{I}}^{\infty}} : \boldsymbol{\varepsilon}^0 \; = const \,. \tag{8.35a}$$

The fourth-order tensor $\boldsymbol{A}_{\mathrm{I}}^{\infty}$ which describes the relation between the strain $\boldsymbol{\varepsilon}$ inside the inhomogeneity and the external load $\boldsymbol{\varepsilon}^0$ is called *influence tensor*. Using (8.35a) the stress $\boldsymbol{\sigma} = \boldsymbol{C}_{\mathrm{I}} : \boldsymbol{\varepsilon}$ inside Ω which is also constant can now be expressed, for instance, as a function of the stress $\boldsymbol{\sigma}^0 = \boldsymbol{C}_{\mathrm{M}} : \boldsymbol{\varepsilon}^0$ applied at infinity:

$$\boldsymbol{\sigma} = \boldsymbol{C}_{\mathrm{I}} : \boldsymbol{A}_{\mathrm{I}}^{\infty} : \boldsymbol{C}_{\mathrm{M}}^{-1} : \boldsymbol{\sigma}^0 \,. \tag{8.35b}$$

As an example we compute $\boldsymbol{\sigma}$ for a spherical isotropic inhomogeneity embedded in an isotropic matrix and, for simplicity, consider only the hydrostatic part. Using (8.35b) we need only replace $\boldsymbol{S}$ in $\boldsymbol{A}_{\mathrm{I}}^{\infty}$ by $\alpha(\nu_{\mathrm{M}})$ from (8.11) and $\boldsymbol{C}_{\mathrm{I}}$ and $\boldsymbol{C}_{\mathrm{M}}$ by the bulk moduli $3K_{\mathrm{I}}$ and $3K_{\mathrm{M}}$, respectively:

$$\sigma_{ii} = 3K_{\mathrm{I}} \left[1 + \alpha \, \frac{3K_{\mathrm{I}} - 3K_{\mathrm{M}}}{3K_{\mathrm{M}}}\right]^{-1} \frac{\sigma_{ii}^0}{3K_{\mathrm{M}}} \qquad \text{in} \quad \Omega \,. \tag{8.36}$$

According to (8.11) the parameter representing the Eshelby tensor attains a value of $\alpha = 2/3$ for $\nu_{\mathrm{M}} = 1/3$. For a "stiff" inhomogeneity with $K_{\mathrm{I}} \gg K_{\mathrm{M}}$ it then follows from (8.36) that the hydrostatic stress inside Ω is $\sigma_{ii} \approx 1.5\, \sigma_{ii}^0$. In case of a "soft" inhomogeneity ($K_{\mathrm{I}} \ll K_{\mathrm{M}}$), in contrast, we get $\sigma_{ii} \ll \sigma_{ii}^0$.

Outside the ellipsoidal inhomogeneity the stresses and strains are not constant and the difference fields $\tilde{\boldsymbol{\sigma}}$, $\tilde{\boldsymbol{\varepsilon}}$, $\tilde{\boldsymbol{u}}$ in the equivalent eigenstrain problem (8.28) display the same asymptotic behavior as the solution of the inclusion problem discussed in Section 8.2.1.4.

8.2.2.3 Cavities and cracks

A special case of material inhomogeneities are cavities (voids) and cracks in an otherwise homogeneous medium. Formally, one may consider these defects to consist of a material of vanishing stiffness and set $\boldsymbol{C}_{\mathrm{I}} = \mathbf{0}$ in the relations obtained above for general inhomogeneities in order to derive respective results for ellipsoidal cavities and (in the limit of one vanishing principal axis) for cracks. Only the strains inside the defects have to be interpreted in a proper way (see Section 8.3.1.2). It seems, however, more illustrative to directly treat the boundary value problem for

these defects in a homogeneous material subjected to a constant far field loading. One then has to consider boundary conditions on the void surface or crack and in the following we assume these boundaries to be traction-free. With regard to quantities needed later on, it suffices here to know only the displacements on the respective defect surfaces. In the sequel they are given for three important cases. If required, the complete stress and strain fields may be found in the literature (e.g., MURA, 1982; KACHANOV et al., 2003).

a) Circular hole (2D)
In case of an unbounded isotropic plate in plane stress with a circular hole of radius a subjected to uniform far field loading σ^0_{ij} (Fig. 8.11a) the displacements along the hole ($r = a$) are in polar coordinates given by

$$u_r(a,\varphi) = \frac{a}{E}\Big[\sigma^0_{11}(3\cos^2\varphi - \sin^2\varphi) + \sigma^0_{22}(3\sin^2\varphi - \cos^2\varphi) + 8\sigma^0_{12}\sin\varphi\cos\varphi\Big]$$
$$u_\varphi(a,\varphi) = \frac{4a}{E}\Big[-\sigma^0_{11}\sin\varphi\cos\varphi + \sigma^0_{22}\sin\varphi\cos\varphi + \sigma^0_{12}(\cos^2\varphi - \sin^2\varphi)\Big]. \tag{8.37}$$

b) Straight crack (2D)
Along a straight crack of length $2a$ in an unbounded isotropic plate in plane stress subjected to a constant load σ^0_{ij} at infinity (Fig. 8.11b) the displacement field undergoes a jump $\Delta\boldsymbol{u}$. In a cartesian x_1, x_2-coordinate system it can be represented as follows (see Section 4.4.1)

$$\Delta u_i(x_1) = \frac{4\,\sigma^0_{i2}}{E}\sqrt{a^2 - x_1^2} \qquad (i,j = 1,2)\,. \tag{8.38}$$

c) Circular ('penny-shaped') crack (3D)
The displacement jump across a penny-shaped crack of radius a oriented perpendicular to the local x_3-axis (Fig. 8.11c) reads

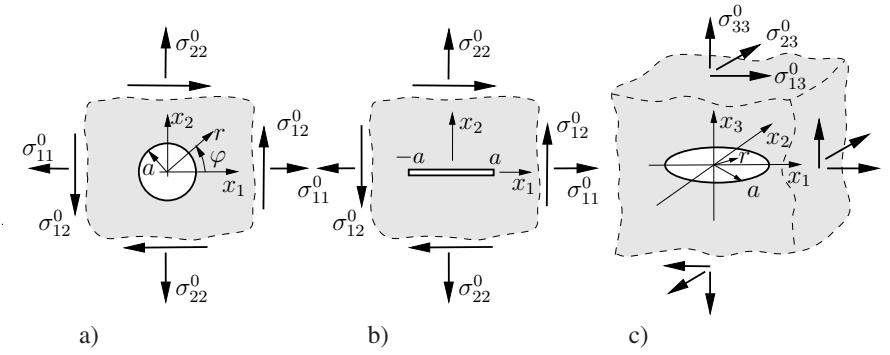

Fig. 8.11 a) Circular hole, b) straight crack, c) penny-shaped crack (3D)

$$\begin{aligned} \Delta u_i(r) &= \frac{16(1-\nu^2)}{\pi E(2-\nu)}\,\sigma^0_{i3}\,\sqrt{a^2-r^2} \qquad (i=1,2)\,, \\ \Delta u_3(r) &= \frac{8(1-\nu^2)}{\pi E}\,\sigma^0_{33}\,\sqrt{a^2-r^2} \end{aligned} \tag{8.39}$$

where $r = \sqrt{x_1^2 + x_2^2}$.

8.3 Effective elastic properties

As already mentioned a macroscopically homogeneous material may have a heterogeneous microstructure on the microscopic level. Now we want to investigate how this microstructure affects the material behavior on the macroscopic level, i.e., on a larger length scale. For an explicit description of the material's heterogeneity we will employ the idealized defects or inhomogeneities discussed above. Under certain conditions which will be made more precise in the sequel it is possible to "smear out" the fine-scale heterogeneous microstructure and describe the material on the macroscale as homogeneous with spatially constant *effective* properties. The latter then account for the microstructure in an averaged sense. This micro-to-macro transition is called *homogenization*. Effective properties in this sense are, for instance, Young's modulus and Poisson's ratio of steel as experimentally determined with standard testing specimens. In many technical applications these properties are well suited to describe the behavior of a material which microscopically has a very complex composition (e.g., anisotropic crystallites, grain boundaries, dislocations, etc.). Measuring material properties, of course, makes only sense if the result does not depend on the chosen testing specimen; the later has to be *representative* of the material. Analogous requirements hold when macroscopic effective material properties are theoretically derived from a given microstructure as will be discussed in the following.

8.3.1 Foundations

8.3.1.1 Representative volume element (RVE)

In the framework of a deterministic and continuum mechanical approach the process of homogenization and the role of the macroscopic and microscopic level with their characteristic length scales can be illustrated by Fig. 8.12. At some arbitrary point $\boldsymbol{x}^{\mathrm{macro}}$ on the macroscopic level (e.g., a technical component) where the material shall be described as homogeneous with constant effective properties, a sufficient magnification ("microscope") reveals the spatially extended fine-scale microstructure.

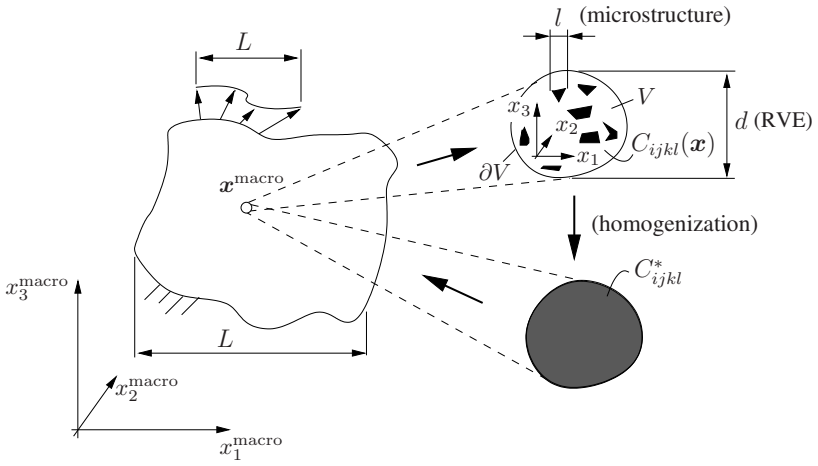

Fig. 8.12 Homogenization and characteristic length scales

We assume that the material behavior on the microscale is known and linear elastic. If an additional coordinate system is introduced there, the microstructure can be described by the dependence of the elasticity tensor $C_{ijkl}(\boldsymbol{x})$ on the microscale coordinates x_i. Analogous to the measurement of macroscopic material properties from a representative testing specimen we now consider a volume V on the microscopic level which has to be *representative* of the entire material. This volume is employed in the homogenization process to ascribe macroscopic properties to the material in terms of a spatially constant *effective elasticity tensor* C^*_{ijkl}. To assure that this result is independent of the point $\boldsymbol{x}^{\text{macro}}$ the entirety of the microstructural details which are described by $C_{ijkl}(\boldsymbol{x})$ and contribute to C^*_{ijkl} has to be independent of the location on the macroscale. This prerequisite to a homogenization is also referred to as a *statistically homogeneous* distribution of the defects (heterogeneities) throughout the material. Furthermore, C^*_{ijkl} must not depend on the size or shape of the chosen volume V. That means that in case of an irregular microstructure (defect distribution) the volume V has to contain a sufficiently large number of defects and its dimension d hence has to be much larger than the characteristic length scale l of the microstructure. The latter is given, for instance, by the typical size or distance of individual defects (Fig. 8.12). With this "wave length" l of varying elastic properties $C_{ijkl}(\boldsymbol{x})$ also the stress and strain fields fluctuate on the microscale. On the other hand, the volume V has to be small enough that it can approximately be regarded as a point on the macroscopic level (Fig. 8.12). A characteristic length L on this level is given by the geometry, by the spatial variation of the loading, or by the stress and strain fields ("macro fields") resulting in the macroscopically homogeneous material. In order to allow in a certain situation the selection of some volume V which is suitable for the homogenization of the material the characteristic length scales have to satisfy the size condition

$$\boxed{l \ll d \ll L} \,. \tag{8.40}$$

Then the volume V is called a *representative volume element* (RVE).

Obviously the restriction of d from two sides according to (8.40) can preclude the existence of an RVE and thereby a meaningful homogenization. Such a situation, for instance, prevails at a macroscopic crack tip where the strains in a homogeneous material are singular and hence strongly vary over an arbitrarily small distance L. The size d of an RVE according to (8.40) then would have to be infinitely small and would necessarily violate the distance to the microstructural length scale (l) of any real material. One usually assumes that this takes place only in the process zone (see Section 4.10). Similar arguments hold in case of micro-electro-mechanical systems (MEMs) where components are often so small that "classical" material properties measured from standard (i.e., large) testing specimens are not suitable for their mechanical description. These examples both refer to the right-hand side of the inequality (8.40) which will, as the condition of statistical homogeneity of the material, in the following be assumed to be fulfilled. The left-hand side of the inequality, i.e., the requirement for a minimum size d of an RVE, will be discussed in Section 8.3.1.3 in conjunction with the specific homogenization process which also allows for a quantitative assessment. For practical applications, typical values of $d \approx 0.1\,\text{mm}$ in case of ceramics and polycrystalline metals or $d \approx 100\,\text{mm}$ in case of concrete may be considered (see also Fig. 8.1).

Caution is also required in the description of so-called *functionally gradient materials* (FGMs) with spatially varying macroscopic properties. In this case the distribution of microstructural details displays a spatial variation such that the condition of a statistically homogeneous microstructure which is necessary for the definition of effective properties strictly speaking does not hold. The use of effective properties then has to be seen as a pragmatic approximation.

The prerequisite of statistical homogeneity of a locally irregular microstructure is no longer necessary in the special case of a strictly periodic defect arrangement. Then a *unit cell* of this arrangement is already representative of the entire heterogeneous material.

8.3.1.2 Averaging

Via the two-scale consideration according to Fig. 8.12 a material point on the macroscopic level is related to a volume V on the microscopic level where stresses and strains prevail as fluctuating micro-fields. The *macro-stresses* and *macro-strains* which characterize the mechanical state of the macroscopic material point are defined as the volumetric averages of the microscopic fields

$$\langle \sigma_{ij} \rangle = \frac{1}{V} \int\limits_V \sigma_{ij}(\boldsymbol{x})\, \mathrm{d}V \,, \qquad \langle \varepsilon_{ij} \rangle = \frac{1}{V} \int\limits_V \varepsilon_{ij}(\boldsymbol{x})\, \mathrm{d}V \tag{8.41}$$

where the symbol $\langle\cdot\rangle$ is used as an abbreviation. Employing the divergence theorem the macroscopic quantities (8.41) can also be expressed by integrals over the boundary ∂V of the averaging domain V. If vanishing volume forces are assumed the equilibrium condition $\sigma_{ik,k} = 0$ and $x_{j,k} = \delta_{jk}$ yield the following identity for the stresses:

$$(x_j\,\sigma_{ik})_{,k} = x_{j,k}\,\sigma_{ik} + x_j\,\sigma_{ik,k} = \sigma_{ij}\ .$$

Insertion into (8.41) leads to the representation of the macro-stresses

$$\langle\sigma_{ij}\rangle = \frac{1}{V}\int_V (x_j\,\sigma_{ik})_{,k}\,\mathrm{d}V = \frac{1}{V}\int_{\partial V} x_j\,\sigma_{ik}\,n_k\,\mathrm{d}A = \frac{1}{V}\int_{\partial V} t_i\,x_j\,\mathrm{d}A\ . \tag{8.42}$$

The macro-strains can also be written as

$$\langle\varepsilon_{ij}\rangle = \frac{1}{2V}\int_V (\,u_{i,j} + u_{j,i}\,)\,\mathrm{d}V = \frac{1}{2V}\int_{\partial V} (\,u_i\,n_j + u_j\,n_i\,)\,\mathrm{d}A\ . \tag{8.43}$$

In the derivation of (8.42) and (8.43) the differentiability of the microscopic fields in the entire domain V, which is necessary for the applicability of the divergence theorem, was tacitely assumed. Although this condition is not fulfilled in case of heterogeneous materials with discontinuously varying properties the representations (8.42) and (8.43) of the macroscopic quantities by boundary integrals are generally valid. They hold independent of the material behavior and also in case of microstructures which contain cavities or cracks. In order to show that this is true we consider an internal interface S inside a volume V according to Fig. 8.13a which separates two subdomains V_1 and V_2 with different properties; across the interface S the stresses and displacements are generally not differentiable. Therefore, the divergence theorem has to be applied separately to the two subdomains where S appears once as the boundary of V_2 (with outer unit normal n_j) and also as the inner boundary of V_1 (with outer unit normal $-n_j$). For the stresses this leads to

$$\int_V \sigma_{ij}\mathrm{d}V = \int_{V_1} \sigma_{ij}\mathrm{d}V + \int_{V_2} \sigma_{ij}\mathrm{d}V = \int_{\partial V} t_i\,x_j\mathrm{d}A + \int_S (\,t_i^{(2)} - t_i^{(1)}\,)\,x_j\mathrm{d}A \tag{8.44}$$

and for the displacement gradient it follows that

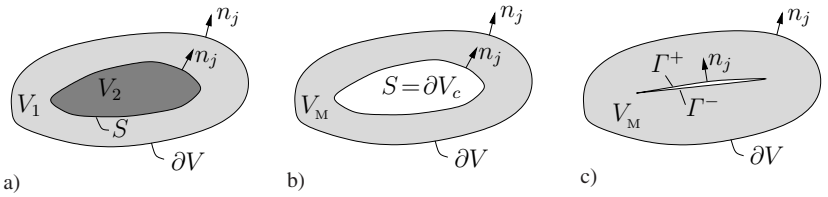

Fig. 8.13 Volume V with a) internal interface S, b) cavity, c) crack $\Gamma = \Gamma^+ + \Gamma^-$

$$\int_V u_{i,j}\mathrm{d}V = \int_{V_1} u_{i,j}\mathrm{d}V + \int_{V_2} u_{i,j}\mathrm{d}V = \int_{\partial V} u_i\, n_j \mathrm{d}A + \int_S (u_i^{(2)} - u_i^{(1)}) n_j \mathrm{d}A. \quad (8.45)$$

Here, $t_i^{(1,2)}$ and $u_i^{(1,2)}$ denote the traction and the displacement vectors of V_1 and V_2 along the interface S. Because of $t_i^{(1)} = t_i^{(2)}$ (equilibrium) and $u_i^{(1)} = u_i^{(2)}$ (continuity) at the interface, the integrals over S in (8.44) and (8.45) vanish. The representations

$$\boxed{\langle \sigma_{ij} \rangle = \frac{1}{V} \int_{\partial V} t_i\, x_j \,\mathrm{d}A\,, \qquad \langle \varepsilon_{ij} \rangle = \frac{1}{2V} \int_{\partial V} (\, u_i\, n_j + u_j\, n_i\,)\,\mathrm{d}A} \quad (8.46)$$

of the macroscopic quantities hence are valid even in case of discontinuous material properties. Since this holds true independent of the actual material behavior and geometry of the subdomain V_2 this result also comprises the special case of cavities which is obtained in the limit of a vanishing stiffness of the material inside V_2 (Fig. 8.13b). By a further limit process $S \to \Gamma$ towards an infinitely thin domain V_2 (Fig. 8.13c) also the situation of cracks is included.

Often a volume V of a heterogeneous material consists of n subdomains V_α ($\alpha = 1, ..., n$) with volume fractions $c_\alpha = V_\alpha / V$ and $\sum_{\alpha=1}^{n} c_\alpha = 1$ where the elastic properties $\boldsymbol{C}_\alpha$ are piecewise constant. In case of such a microstructure consisting of *discrete phases* we have

$$\langle \boldsymbol{\sigma} \rangle = \sum_{\alpha=1}^{n} c_\alpha \langle \boldsymbol{\sigma} \rangle_\alpha\,, \qquad \langle \boldsymbol{\varepsilon} \rangle = \sum_{\alpha=1}^{n} c_\alpha \langle \boldsymbol{\varepsilon} \rangle_\alpha \quad (8.47)$$

where

$$\langle \boldsymbol{\sigma} \rangle_\alpha = \frac{1}{V_\alpha} \int_{V_\alpha} \boldsymbol{\sigma}\,\mathrm{d}V\,, \qquad \langle \boldsymbol{\varepsilon} \rangle_\alpha = \frac{1}{V_\alpha} \int_{V_\alpha} \boldsymbol{\varepsilon}\,\mathrm{d}V \quad (8.48)$$

are the *phase averages* of the stresses and strains. They are related to each other by

$$\langle \boldsymbol{\sigma} \rangle_\alpha = \boldsymbol{C}_\alpha : \langle \boldsymbol{\varepsilon} \rangle_\alpha \qquad \text{inside} \quad V_\alpha\,. \quad (8.49)$$

In case of microstructures which contain only cavities or cracks it is practical to represent the macroscopic quantities (8.46) in a somewhat different form. Therefore, we first consider the situation of cavities and transform the average strain $\langle \varepsilon_{ij} \rangle_{\mathrm{M}}$ in the surrounding matrix material of volume $V_{\mathrm{M}} = c_{\mathrm{M}} V$ using the divergence theorem (see Fig. 8.13b). We get

$$\langle \varepsilon_{ij} \rangle_{\mathrm{M}} = \frac{1}{2V_{\mathrm{M}}} \int_{V_{\mathrm{M}}} (u_{i,j} + u_{j,i}) \, \mathrm{d}V$$
$$= \frac{1}{2V_{\mathrm{M}}} \int_{\partial V} (u_i n_j + u_j n_i) \, \mathrm{d}A \; - \; \frac{1}{2V_{\mathrm{M}}} \int_{\partial V_c} (u_i n_j + u_j n_i) \, \mathrm{d}A$$

where ∂V_c denotes the cavity surface. If the first integral on the right-hand side is replaced by (8.43) the macro-strains can be written as

$$\boxed{\langle \varepsilon_{ij} \rangle = c_{\mathrm{M}} \langle \varepsilon_{ij} \rangle_{\mathrm{M}} + \underbrace{\frac{1}{2V} \int_{\partial V_c} (u_i n_j + u_j n_i) \, \mathrm{d}A}_{\langle \varepsilon_{ij} \rangle_c}} \, . \tag{8.50a}$$

In case of cracks the limit process $\partial V_c \to \Gamma = \Gamma^+ + \Gamma^-$ (see Fig. 8.13c) and the abbreviation $\Delta u_i = u_i^+ - u_i^-$ lead to

$$\boxed{\langle \varepsilon_{ij} \rangle = c_{\mathrm{M}} \langle \varepsilon_{ij} \rangle_{\mathrm{M}} + \underbrace{\frac{1}{2V} \int_{\Gamma} (\Delta u_i n_j + \Delta u_j n_i) \, \mathrm{d}A}_{\langle \varepsilon_{ij} \rangle_c}} \, . \tag{8.50b}$$

The macro-strains in case of cavities or cracks hence consist of the average matrix strain and the quantity $\langle \boldsymbol{\varepsilon} \rangle_c$ which represents the average strain of the defect phase (c for *cavity* or *crack*):

$$\langle \boldsymbol{\varepsilon} \rangle = c_{\mathrm{M}} \langle \boldsymbol{\varepsilon} \rangle_{\mathrm{M}} + \langle \boldsymbol{\varepsilon} \rangle_c \, . \tag{8.51}$$

In contrast, the macro-stress is in case of traction-free cavities or cracks solely given by the average matrix stress:

$$\langle \boldsymbol{\sigma} \rangle = c_{\mathrm{M}} \, \langle \boldsymbol{\sigma} \rangle_{\mathrm{M}} \, . \tag{8.52}$$

In a material which contains only cracks the volume fraction of the matrix phase is $c_{\mathrm{M}} = 1$.

If the matrix material is homogeneous with $\boldsymbol{C}_{\mathrm{M}} = const$ and $\langle \boldsymbol{\sigma} \rangle_{\mathrm{M}} = \boldsymbol{C}_{\mathrm{M}} : \langle \boldsymbol{\varepsilon} \rangle_{\mathrm{M}}$ elimination of the average matrix stress and strain using (8.47) and (8.50a) leads to

$$\langle \boldsymbol{\sigma} \rangle = \boldsymbol{C}_{\mathrm{M}} : \Big(\langle \boldsymbol{\varepsilon} \rangle - \langle \boldsymbol{\varepsilon} \rangle_c \Big) \qquad \text{or} \qquad \langle \boldsymbol{\varepsilon} \rangle = \boldsymbol{C}_{\mathrm{M}}^{-1} : \langle \boldsymbol{\sigma} \rangle + \langle \boldsymbol{\varepsilon} \rangle_c \, , \tag{8.53}$$

respectively. According to this representation $\langle \boldsymbol{\varepsilon} \rangle_c$ appears in the relation between macro-stresses and macro-strains (established here by the elastic properties of the matrix !) in the same way as the eigenstrain in (8.4).

8.3.1.3 Effective elastic constants

Analogous to the elasticity law on the microscopic level

$$\sigma_{ij}(\boldsymbol{x}) = C_{ijkl}(\boldsymbol{x})\,\varepsilon_{kl}(\boldsymbol{x}) \tag{8.54}$$

the *effective elasticity tensor* C^*_{ijkl} is defined by the linear relation between the macro-stresses and macro-strains (8.41):

$$\boxed{\langle\sigma_{ij}\rangle = C^*_{ijkl}\,\langle\varepsilon_{kl}\rangle}\,. \tag{8.55}$$

The interpretation of C^*_{ijkl} as a *material property* is subjected to several conditions. It is, for instance, appropriate to require the equality of the average strain energy density $\langle U\rangle$ in the volume V when expressed by means of the microscopic or macroscopic quantities:

$$\langle U\rangle = \langle\frac{1}{2}\,\varepsilon_{ij}\,C_{ijkl}\,\varepsilon_{kl}\rangle \;=\; \frac{1}{2}\langle\varepsilon_{ij}\rangle C^*_{ijkl}\langle\varepsilon_{kl}\rangle\;. \tag{8.56}$$

Using (8.54) and (8.55) this requirement, known as the *Hill-condition* (HILL, 1963), can also be written in the form

$$\boxed{\langle\sigma_{ij}\,\varepsilon_{ij}\rangle \;=\; \langle\sigma_{ij}\rangle\langle\varepsilon_{ij}\rangle}\,. \tag{8.57}$$

For the *fluctuations* $\tilde{\sigma}_{ij}(\boldsymbol{x}) = \sigma_{ij}(\boldsymbol{x}) - \langle\sigma_{ij}\rangle$ and $\tilde{\varepsilon}_{ij}(\boldsymbol{x}) = \varepsilon_{ij}(\boldsymbol{x}) - \langle\varepsilon_{ij}\rangle$ of the microscopic fields around their averages it then follows that

$$\langle\tilde{\sigma}_{ij}\,\tilde{\varepsilon}_{ij}\rangle = 0\;. \tag{8.58}$$

That means that on average the stress fluctuations must not do any work on the strain fluctuations. Using the divergence theorem and the equilibrium condition $\sigma_{ik,k} = 0$ this can be expressed in terms of quantities on the boundary of the averaging domain:

$$\frac{1}{V}\int\limits_{\partial V}\Big(\,u_i - \langle\varepsilon_{ij}\rangle x_j\,\Big)\Big(\,\sigma_{ik} - \langle\sigma_{ik}\rangle\,\Big)\,n_k\,\mathrm{d}A = 0\;. \tag{8.59}$$

Written in this form, the Hill-condition can be interpreted to state that the microfields fluctuating along the boundary of an RVE have to be energetically equivalent to their averages (Fig. 8.14). As already discussed in Section 8.3.1.1 this can only be expected to hold if the averaging domain V is sufficiently large with respect to the heterogeneities.

In order to compute the fields $\sigma_{ij}(\boldsymbol{x})$ and $\varepsilon_{ij}(\boldsymbol{x})$ in some volume V on the microscopic level, the equilibrium condition $\sigma_{ij,j} = 0$ and the elasticity law (8.54) have to be complemented by boundary conditions on ∂V, i.e., a boundary value problem has to be formulated. The domain V of the heterogeneous material is regarded to be equivalent to the same domain of a homogeneous (effective) medium

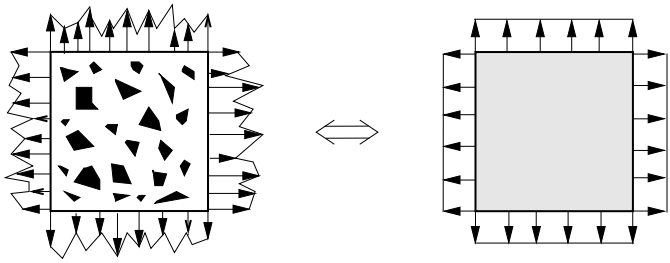

Fig. 8.14 RVE with fluctuating microscopic fields and averages

and at the same time represents a macroscopic material point which experiences only homogeneous stress and strain states. It is therefore appropriate to prescribe those homogeneous states as boundary conditions on ∂V; this can be done in two ways:

a) *Linear displacements*: $u_i = \varepsilon^0_{ij}\, x_j$ on ∂V where $\varepsilon^0_{ij} = const$.

In this case it follows from (8.43) with $\int\limits_{\partial V} x_i\, n_j \,\mathrm{d}A = V\delta_{ij}$ that

$$\boxed{\langle \varepsilon_{ij} \rangle = \varepsilon^0_{ij}} \,. \tag{8.60a}$$

b) *Uniform tractions*: $t_i = \sigma^0_{ij}\, n_j$ on ∂V where $\sigma^0_{ij} = const$.

Equation (8.42) then yields

$$\boxed{\langle \sigma_{ij} \rangle = \sigma^0_{ij}} \,. \tag{8.60b}$$

Homogeneous strains ε^0_{ij} prescribed on the boundary of an arbitrary domain of a heterogeneous material hence are equal to the volume average of the strains throughout this domain. Analogously, if a homogeneous stress state σ^0_{ij} is prescribed on the boundary ∂V it is equal to the average stress in the domain V provided that volume forces are not present. In case of a homogeneous material both types of boundary conditions are equivalent and induce homogeneous (i.e., spatially constant) fields throughout the volume. The relations (8.60a) and (8.60b) are often referred to as the *'average strain theorem'* and the *'average stress theorem'*.

Using (8.59) one can verify that both types of boundary conditions satisfy the Hill-condition identically, i.e., irrespective of the domain V. This is not surprising since the consequence of the Hill-condition that the fluctuating fields on the boundary of an RVE can be replaced by homogeneous fields is anticipated in the above boundary conditions (a) or (b). Moreover, when the boundary conditions (a) or (b) are imposed the Hill-condition in the form (8.57) or (8.59) is satisfied independent of any relation between the fields σ_{ij} and ε_{ij}. Hence it can be generalized and applied to arbitrary statically admissible stress fields $\sigma^{(1)}_{ij}$ and kinematically admissible strain fields $\varepsilon^{(2)}_{ij}$:

$$\boxed{\langle \sigma_{ij}^{(1)} \varepsilon_{ij}^{(2)} \rangle = \langle \sigma_{ij}^{(1)} \rangle \langle \varepsilon_{ij}^{(2)} \rangle} \,. \tag{8.61}$$

This relation which will be repeatedly used later on follows directly from the general work theorem (1.95) when boundary conditions of the type (a) or (b) are prescribed.

Because of the uniqueness of the solution of linear elastic boundary value problems the fields inside the domain V depend *linearly* on the "loading" parameters ε_{ij}^0 or σ_{ij}^0 in the boundary conditions (a) or (b). The fields therefore can be represented in the following form:

$$\text{a)} \quad \varepsilon_{ij}(\boldsymbol{x}) = A_{ijkl}(\boldsymbol{x})\, \varepsilon_{kl}^0 \qquad \text{for} \qquad u_i = \varepsilon_{ij}^0\, x_j \quad \text{on} \ \partial V \,, \tag{8.62a}$$

$$\text{b)} \quad \sigma_{ij}(\boldsymbol{x}) = B_{ijkl}(\boldsymbol{x})\, \sigma_{kl}^0 \qquad \text{for} \qquad t_i = \sigma_{ij}^0\, n_j \quad \text{on} \ \partial V \,. \tag{8.62b}$$

Here, $A_{ijkl}(\boldsymbol{x})$ and $B_{ijkl}(\boldsymbol{x})$ denote the components of the so-called *influence tensors* $\boldsymbol{A}(\boldsymbol{x})$ and $\boldsymbol{B}(\boldsymbol{x})$. The fourth-order influence tensors represent the complete solution of the respective boundary value problems and depend on the microstructure in the entire domain V. With respect to its first two indices $A_{ijkl}(\boldsymbol{x})$ satisfies the compatibility conditions (1.30), exactly as ε_{ij} does. Correspondingly, $B_{ijkl}(\boldsymbol{x})$ satisfies the equilibrium condition $B_{ijkl,j}(\boldsymbol{x}) = 0$. Averaging (8.62a) and (8.62b) over V using (8.60a) and (8.60b) in addition reveals that the average value of these functions is the fourth-order unit tensor (8.7):

$$\langle \boldsymbol{A} \rangle = \boldsymbol{1} \,, \qquad\qquad \langle \boldsymbol{B} \rangle = \boldsymbol{1} \,. \tag{8.63}$$

According to (8.54) and (8.55) the following relations in symbolic notation hold for the effective elasticity tensor $\boldsymbol{C}^*$ and the effective compliance tensor $\boldsymbol{C}^{*\,-1}$, respectively:

$$\boldsymbol{C}^* : \langle \boldsymbol{\varepsilon} \rangle = \langle \boldsymbol{\sigma} \rangle = \langle \boldsymbol{C} : \boldsymbol{\varepsilon} \rangle \qquad , \qquad \boldsymbol{C}^{*\,-1} : \langle \boldsymbol{\sigma} \rangle = \langle \boldsymbol{\varepsilon} \rangle = \langle \boldsymbol{C}^{-1} : \boldsymbol{\sigma} \rangle \,. \tag{8.64}$$

In case of the boundary condition (a) insertion of (8.62a) leads to the representation

$$\boldsymbol{C}^{*\,(\mathrm{a})} = \langle \boldsymbol{C} : \boldsymbol{A} \rangle \tag{8.65a}$$

and insertion of (8.62b) in case (b) yields

$$\boldsymbol{C}^{*\,(\mathrm{b})} = \langle \boldsymbol{C}^{-1} : \boldsymbol{B} \rangle^{-1} \,. \tag{8.65b}$$

From inserting (8.62a) and (8.62b) in the energy relation (8.56) one obtains the alternative representations

$$\boldsymbol{C}^{*\,(\mathrm{a})} = \langle \boldsymbol{A}^T : \boldsymbol{C} : \boldsymbol{A} \rangle \qquad \text{and} \qquad \boldsymbol{C}^{*\,(\mathrm{b})} = \langle \boldsymbol{B}^T : \boldsymbol{C}^{-1} : \boldsymbol{B} \rangle^{-1} \tag{8.66}$$

from which the symmetry of the effective elasticity tensor with respect to the first and second pair of indices becomes obvious.

By the superscripts (a) and (b) it shall be emphasized that these averages which are computed for an arbitrary volume V in general depend on the type of boundary condition prescribed on ∂V. Therefore, $\boldsymbol{C}^{*\,(\mathrm{a})}$ or $\boldsymbol{C}^{*\,(\mathrm{b})}$ can strictly speaking not be regarded as effective *material properties* because the volume V need not automatically satisfy the requirements of an RVE. The distance between $\boldsymbol{C}^{*\,(\mathrm{a})}$ and $\boldsymbol{C}^{*\,(\mathrm{b})}$ (in the sense of an appropriate norm) can be taken as a measure for the quality of the averaging domain. Only if the domain V guarantees that $\boldsymbol{C}^{*\,(\mathrm{a})} = \boldsymbol{C}^{*\,(\mathrm{b})} = \boldsymbol{C}^{*}$ can $\boldsymbol{C}^{*}$ be interpreted as a unique macroscopic material property. Clearly, this must also hold for any larger domain which comprises V.

An important problem of micromechanics is the derivation of explicit representations for the influence tensors $\boldsymbol{A}(\boldsymbol{x})$ or $\boldsymbol{B}(\boldsymbol{x})$, and hence for the micro-fields, as well as for the effective elastic constants. By employing the fundamental solutions presented in Section 8.2 along with suitable approximations various different methods will be discussed in the following.

8.3.2 Analytical approximations

8.3.2.1 General relations

According to (8.65a) or (8.65b) the effective elastic constants $\boldsymbol{C}^{*}$ can be represented as the *weighted averages* of the microscopic elastic properties $\boldsymbol{C}(\boldsymbol{x})$ where the influence tensor, e.g., $\boldsymbol{A}(\boldsymbol{x})$, serves as a weighting function. In case of a real microstructure, however, neither the exact function $\boldsymbol{C}(\boldsymbol{x})$ is known nor can the corresponding influence tensor in general be written in closed form. Thus appropriate approximations have to be made with regard to the available information in modeling the microstructure as well as in the representation of the influence tensors.

It is therefore practical to restrict the considerations first to microstructures consisting of discrete phases with piecewise constant elastic properties according to (8.49) which for many materials actually applies (e.g., polycrystals, composites). Using (8.60a), (8.60b) with prescribed macro-strains $\langle\boldsymbol{\varepsilon}\rangle = \boldsymbol{\varepsilon}^{0}$ or prescribed macro-stresses $\langle\boldsymbol{\sigma}\rangle = \boldsymbol{\sigma}^{0}$ it then follows from (8.62a), (8.62b) for the phase averages that

$$\langle\boldsymbol{\varepsilon}\rangle_{\alpha} = \boldsymbol{A}_{\alpha} : \langle\boldsymbol{\varepsilon}\rangle \qquad \text{or} \qquad \langle\boldsymbol{\sigma}\rangle_{\alpha} = \boldsymbol{B}_{\alpha} : \langle\boldsymbol{\sigma}\rangle \;, \tag{8.67}$$

respectively, where

$$\boldsymbol{A}_{\alpha} = \langle\boldsymbol{A}\rangle_{\alpha} \qquad \text{and} \qquad \boldsymbol{B}_{\alpha} = \langle\boldsymbol{B}\rangle_{\alpha} \;. \tag{8.68}$$

The constant influence tensors $\boldsymbol{A}_{\alpha}$ and $\boldsymbol{B}_{\alpha}$ express the dependence of the average (over the volume of phase α) of some field on the prescribed macroscopic quantity. Equations (8.65a) and (8.65b) then reduce to

$$\boldsymbol{C}^{*(\mathrm{a})} = \sum_{\alpha=1}^{n} c_\alpha \boldsymbol{C}_\alpha : \boldsymbol{A}_\alpha \qquad \text{and} \qquad \boldsymbol{C}^{*(\mathrm{b})} = \left(\sum_{\alpha=1}^{n} c_\alpha \boldsymbol{C}_\alpha^{-1} : \boldsymbol{B}_\alpha \right)^{-1} \tag{8.69}$$

where only the influence tensors $\boldsymbol{A}_\alpha$ or $\boldsymbol{B}_\alpha$ of $n-1$ phases are needed for the representation of the effective elastic constants $\boldsymbol{C}^*$ because

$$\sum_{\alpha=1}^{n} c_\alpha \boldsymbol{A}_\alpha = \boldsymbol{1} \qquad \text{and} \qquad \sum_{\alpha=1}^{n} c_\alpha \boldsymbol{B}_\alpha = \boldsymbol{1} \; . \tag{8.70}$$

For simplicity, we consider in the following a material which consists of two phases only; the methods discussed, however, apply also to the general case. If one phase is referred to as the matrix (M) and the other as the inhomogeneity (I) it follows from (8.69) and (8.70) that

$$\boxed{\boldsymbol{C}^{*\,(\mathrm{a})} = \boldsymbol{C}_{\mathrm{M}} + c_{\mathrm{I}} (\boldsymbol{C}_{\mathrm{I}} - \boldsymbol{C}_{\mathrm{M}}) : \boldsymbol{A}_{\mathrm{I}}} \tag{8.71a}$$

or

$$\boxed{\boldsymbol{C}^{*\,(\mathrm{b})} = \left(\boldsymbol{C}_{\mathrm{M}}^{-1} + c_{\mathrm{I}} (\boldsymbol{C}_{\mathrm{I}}^{-1} - \boldsymbol{C}_{\mathrm{M}}^{-1}) : \boldsymbol{B}_{\mathrm{I}} \right)^{-1}} \, , \tag{8.71b}$$

respectively. These relations are not directly applicable to the special case of a homogeneous matrix which as the second "phase" contains cavities or cracks. In this case the linear dependence of the average defect strain $\langle \boldsymbol{\varepsilon} \rangle_c$ defined in (8.50a), (8.50b) on the prescribed macro-quantities $\boldsymbol{\varepsilon}^0$ or $\boldsymbol{\sigma}^0$ is expressed by influence tensors $\boldsymbol{D}$ and $\boldsymbol{H}$:

$$\langle \boldsymbol{\varepsilon} \rangle_c = \boldsymbol{D} : \langle \boldsymbol{\varepsilon} \rangle \quad \text{for } \langle \boldsymbol{\varepsilon} \rangle = \boldsymbol{\varepsilon}^0 \quad , \quad \langle \boldsymbol{\varepsilon} \rangle_c = \boldsymbol{H} : \langle \boldsymbol{\sigma} \rangle \quad \text{for } \langle \boldsymbol{\sigma} \rangle = \boldsymbol{\sigma}^0 \; . \tag{8.72}$$

Using (8.53) and (8.64) the effective elasticity tensors then are given by

$$\boxed{\boldsymbol{C}^{*\,(\mathrm{a})} = \boldsymbol{C}_{\mathrm{M}} : (\boldsymbol{1} - \boldsymbol{D})} \qquad \text{or} \qquad \boxed{\boldsymbol{C}^{*\,(\mathrm{b})} = \left[\boldsymbol{C}_{\mathrm{M}}^{-1} + \boldsymbol{H} \right]^{-1}} \, . \tag{8.73}$$

By virtue of the fact that cavities or cracks cause a reduction of the effective stiffness of a material the influence tensor $\boldsymbol{D}$ may be interpreted as a measure of *damage* (see Chapter 9) while $\boldsymbol{H}$ describes an additional compliance.

In the following some approximations, models, and methods are discussed which allow for an approximate computation of effective elastic constants.

8.3.2.2 Voigt and Reuss approximation

In a homogeneous material the boundary conditions (8.60a) or (8.60b) lead to homogeneous (spatially constant) stress and strain fields. In case of a heterogeneous material the simplest approximation hence is to assume one of the micro-fields to be constant, in accordance with the boundary conditions (a) or (b).

If according to W. VOIGT (1889) the strains inside V are taken to be constant ($\boldsymbol{\varepsilon} = \langle \boldsymbol{\varepsilon} \rangle = const$) it follows from (8.62a) that the influence tensor is $\boldsymbol{A} = \mathbf{1}$. From (8.65a) or (8.69) the effective elasticity tensor then is approximated by the *average stiffness*:

$$\boxed{\boldsymbol{C}^*_{(\mathrm{Voigt})} = \langle \boldsymbol{C} \rangle = \sum_{\alpha=1}^{n} c_\alpha \boldsymbol{C}_\alpha} \; . \tag{8.74a}$$

Analogously, in the approximation due to A. REUSS (1929) a constant stress field is assumed ($\boldsymbol{\sigma} = \langle \boldsymbol{\sigma} \rangle = const$) which corresponds to $\boldsymbol{B} = \mathbf{1}$ in (8.62b). With (8.65b) or (8.69) this leads to the approximation of the effective compliance tensor by the *average compliance*

$$\boxed{\boldsymbol{C}^{*\,-1}_{(\mathrm{Reuss})} = \langle \boldsymbol{C}^{-1} \rangle = \sum_{\alpha=1}^{n} c_\alpha \boldsymbol{C}_\alpha^{-1}} \; . \tag{8.74b}$$

In the special case of discrete phases of an *isotropic* material the above approximations lead to the effective bulk and shear moduli

$$K^*_{(\mathrm{Voigt})} = \sum_{\alpha=1}^{n} c_\alpha K_\alpha \; , \qquad \mu^*_{(\mathrm{Voigt})} = \sum_{\alpha=1}^{n} c_\alpha \mu_\alpha \tag{8.75a}$$

or

$$K^{*\,-1}_{(\mathrm{Reuss})} = \sum_{\alpha=1}^{n} \frac{c_\alpha}{K_\alpha} \; , \qquad \mu^{*\,-1}_{(\mathrm{Reuss})} = \sum_{\alpha=1}^{n} \frac{c_\alpha}{\mu_\alpha} \; . \tag{8.75b}$$

One should note that according to these models the macroscopic behavior of the material is approximated to be isotropic although in reality an anisotropy may result from the geometric arrangement of the phases (e.g., fiber-reinforced materials).

In case of a matrix containing cavities or cracks the vanishing stiffness or infinite compliance, respectively, of the defect phase leads to the Voigt and Reuss approximations

$$\boldsymbol{C}^*_{(\mathrm{Voigt})} = c_{\mathrm{M}} \boldsymbol{C}_{\mathrm{M}} \qquad \text{and} \qquad \boldsymbol{C}^*_{(\mathrm{Reuss})} = 0 \; . \tag{8.76}$$

If, in contrast, one of the phases is rigid (e.g., $\boldsymbol{C}_{\mathrm{I}} \to \infty$) one obtains

$$\boldsymbol{C}^*_{(\mathrm{Voigt})} \to \infty \qquad \text{and} \qquad \boldsymbol{C}^*_{(\mathrm{Reuss})} = \frac{1}{c_{\mathrm{M}}} \boldsymbol{C}_{\mathrm{M}} \; . \tag{8.77}$$

The approximations of effective elastic properties by the average stiffness or the average compliance are often referred to as *rules of mixtures*. They are exact only in one-dimensional special cases of different materials arranged "in parallel" (Voigt) or "in series" (Reuss). In general the assumption of constant strains leads to a violation of local equilibrium (e.g., at phase boundaries) and the assumption of constant stress precludes the compatibility of deformation. Despite these obvious deficiencies the simple approximations by Voigt and Reuss bear the advantage that they yield exact bounds for the true effective elastic constants of a heterogeneous ma-

terial. In Section 8.3.3.1 it will be shown that $K^*_{(\mathrm{Reuss})} \leq K^* \leq K^*_{(\mathrm{Voigt})}$ and $\mu^*_{(\mathrm{Reuss})} \leq \mu^* \leq \mu^*_{(\mathrm{Voigt})}$. Since the Voigt and Reuss approximations are often far apart from each other a pragmatic approach to improve the approximation of effective constants is to take their mean values

$$K^* \approx \frac{1}{2}\left(K^*_{(\mathrm{Reuss})} + K^*_{(\mathrm{Voigt})}\right), \qquad \mu^* \approx \frac{1}{2}\left(\mu^*_{(\mathrm{Reuss})} + \mu^*_{(\mathrm{Voigt})}\right). \quad (8.78)$$

8.3.2.3 Non-interacting (dilute) defect distribution

Using the exact fundamental solutions presented in Section 8.2.2 it is possible to develop micromechanical models which satisfy the local equilibrium and guarantee the compatibility of deformation. In doing so we consider a two-phase material which consists of a homogeneous matrix with $\boldsymbol{C}_{\mathrm{M}} = const$ and one kind of equal defects (second phase). With regard to the available fundamental solutions the latter will be approximated by ellipsoidal elastic inhomogeneities with $\boldsymbol{C}_{\mathrm{I}} = const$, by circular holes (2D) or by straight (2D) or penny-shaped (3D) cracks.

The simplest situation prevails when the inhomogeneities or defects are so dilutely distributed in the homogeneous matrix that their interaction among each other and with the boundary of the RVE can be neglected ("dilute distribution"). As illustrated in Fig. 8.15 each defect then can be considered in an unbounded domain subjected to a uniform far-field loading $\boldsymbol{\varepsilon}^0 = \langle \boldsymbol{\varepsilon} \rangle$ or $\boldsymbol{\sigma}^0 = \langle \boldsymbol{\sigma} \rangle$. The characteristic dimension of the defects therefore has to be small compared to their distance or to the distance from the boundary of the RVE. Although the solutions obtained under these idealizations are themselves only valid for very small volume fractions ($c_{\mathrm{I}} \ll 1$) they form the basis for important generalizations.

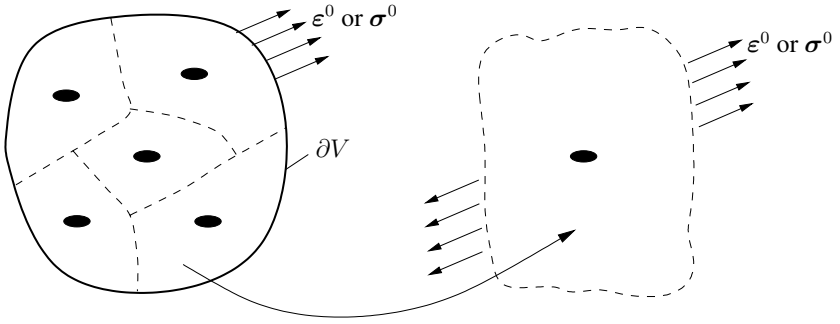

Fig. 8.15 Model of dilute defect distribution

a) Ellipsoidal inhomogeneities

In case of an ellipsoidal inhomogeneity Ω (Section 8.2.2.2) the strain inside the inhomogeneity is constant ($\boldsymbol{\varepsilon} = \langle \boldsymbol{\epsilon} \rangle_{\mathrm{I}}$ in Ω) and given by the influence tensor $\boldsymbol{A}^{\infty}_{\mathrm{I}}$ introduced in (8.35a). According to (8.71a) hence the effective elasticity tensor of

a material which contains a dilute distribution of ellipsoidal inhomogeneities with equal orientation and aspect ratio reads

$$\boldsymbol{C}^{*\,(\mathrm{a})}_{(\mathrm{DD})} = \boldsymbol{C}_{\mathrm{M}} + c_{\mathrm{I}}(\,\boldsymbol{C}_{\mathrm{I}} - \boldsymbol{C}_{\mathrm{M}}\,) : \boldsymbol{A}^{\infty}_{\mathrm{I}} \tag{8.79a}$$

where $c_{\mathrm{I}} \ll 1$ is the volume fraction of inhomogeneities and (DD) stands for "dilute distribution". Insertion of (8.35a) yields the representation

$$\boxed{\boldsymbol{C}^{*\,(\mathrm{a})}_{(\mathrm{DD})} = \boldsymbol{C}_{\mathrm{M}} + c_{\mathrm{I}}(\,\boldsymbol{C}_{\mathrm{I}} - \boldsymbol{C}_{\mathrm{M}}\,) : \left[\boldsymbol{1} + \boldsymbol{S}_{\mathrm{M}} : \boldsymbol{C}^{-1}_{\mathrm{M}} : (\boldsymbol{C}_{\mathrm{I}} - \boldsymbol{C}_{\mathrm{M}})\right]^{-1}} \tag{8.79b}$$

where the Eshelby tensor $\boldsymbol{S}_{\mathrm{M}}$ depends on the matrix material. In case of different kinds of ellipsoidal inhomogeneities, e.g., of different orientations, one has to start from (8.69) where the individual influence tensors $\boldsymbol{A}^{\infty}_{\alpha}$ represent the different orientations via the respective Eshelby tensors.

The superscript (a) in (8.79a,b) indicates that this result is valid only for the case (a) of prescribed macro-strains. If the model of a dilute defect distribution is evaluated for prescribed macro-stresses (b) an effective elasticity tensor $\boldsymbol{C}^{*\,(\mathrm{b})}_{(\mathrm{DD})}$ is obtained which differs from (8.79b) for finite values of c_{I}.

In contrast to the Voigt or Reuss approximations the overall behavior described by (8.79a,b) may even in case of an isotropic material of both phases be anisotropic due to a preferred orientation of the ellipsoids which is accounted for by the Eshelby tensor. Only in case of spherical isotropic inhomogeneities in an isotropic matrix is the macroscopic (effective) behavior isotropic and (8.79b) can be split into the volumetric and deviatoric parts using (8.10) and (8.12):

$$\begin{aligned} K^{*}_{(\mathrm{DD})} &= K_{\mathrm{M}} + c_{\mathrm{I}}\,\frac{(K_{\mathrm{I}} - K_{\mathrm{M}})\,K_{\mathrm{M}}}{K_{\mathrm{M}} + \alpha\,(K_{\mathrm{I}} - K_{\mathrm{M}})}\,, \\ \mu^{*}_{(\mathrm{DD})} &= \mu_{\mathrm{M}} + c_{\mathrm{I}}\,\frac{(\mu_{\mathrm{I}} - \mu_{\mathrm{M}})\,\mu_{\mathrm{M}}}{\mu_{\mathrm{M}} + \beta\,(\mu_{\mathrm{I}} - \mu_{\mathrm{M}})}\,. \end{aligned} \tag{8.80}$$

Corresponding to the model of a matrix which contains a small volume fraction (dilute distribution) of defects the effective elastic constants are given by those of the matrix plus an additional term which is *linear* in c_{I}. According to (8.11) the parameters α and β in the Eshelby tensor depend via Poisson's ratio $\nu_{\mathrm{M}} = (3K_{\mathrm{M}} - 2\mu_{\mathrm{M}})/(6K_{\mathrm{M}} + 2\mu_{\mathrm{M}})$ of the matrix material on both moduli K_{M} and μ_{M} and hence describe a coupling of the volumetric and shear stiffness. The effective Young's modulus can be computed from $E^{*} = 9K^{*}\mu^{*}/(3K^{*} + \mu^{*})$.

Finally, we consider the special case of rigid spherical inhomogeneities ($K_{\mathrm{I}},\ \mu_{\mathrm{I}} \to \infty$) in an incompressible matrix ($K_{\mathrm{M}} \to \infty$). With $\beta = 2/5$ from (8.11) a macroscopically incompressible material ($K^{*}_{(\mathrm{DD})} \to \infty$) is obtained from (8.80) with

$$\mu^{*}_{(\mathrm{DD})} = \mu_{\mathrm{M}}\left(1 + \frac{5}{2}\,c_{\mathrm{I}}\right)\,. \tag{8.81}$$

In view of the analogy between linear elasticity and a Newtonian (linearly viscous) fluid this result corresponds exactly to the relation for the effective viscosity of a suspension of a viscous fluid with rigid particles derived by A. EINSTEIN (1906).

b) Circular holes (2D)
As a second application of the model of a dilute defect distribution we now consider an infinitely extended plate in plane stress which contains circular holes of equal radius a (Fig. 8.16). Because of the neglected interaction the average strain $\langle \varepsilon_{ij} \rangle_c$ of each individual hole due to a uniform external loading σ^0_{ij} can be obtained from (8.50a) by integration of the fundamental solution (8.37) along the boundary of the hole

$$\langle \varepsilon_{ij} \rangle_c = \frac{1}{2A} \int_0^{2\pi} (u_i n_j + u_j n_i) \, a \, \mathrm{d}\varphi \tag{8.82}$$

where $u_1 = u_r \cos\varphi - u_\varphi \sin\varphi$, $u_2 = u_r \sin\varphi + u_\varphi \cos\varphi$, $n_1 = \cos\varphi$, $n_2 = \sin\varphi$. In this two-dimensional problem averaging is performed with respect to the area A of the plate, hence instead of the surface integral in (8.50a) a contour integral has to be evaluated. From the relation (8.72) between the average defect strain and external loading $\boldsymbol{\sigma}^0$ the additional compliance tensor $\boldsymbol{H}^\infty$ is obtained. The latter is employed in (8.73) to represent the effective elasticity tensor in case of a dilute distribution of holes:

$$\boxed{\boldsymbol{C}^{*\,(\mathrm{b})}_{(\mathrm{DD})} = \left[\boldsymbol{C}_{\mathrm{M}}^{-1} + \boldsymbol{H}^\infty \right]^{-1}} \, . \tag{8.83}$$

The nonvanishing components of $\boldsymbol{H}^\infty$ read

$$\begin{aligned} H^\infty_{1111} &= H^\infty_{2222} = \frac{3c}{E} \, , \qquad H^\infty_{1122} = H^\infty_{2211} = -\frac{c}{E} \, , \\ H^\infty_{1212} &= H^\infty_{2121} = H^\infty_{1221} = H^\infty_{2112} = \frac{4c}{E} \end{aligned} \tag{8.84}$$

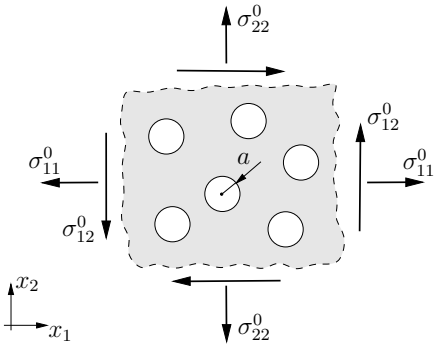

Fig. 8.16 Plate with circular holes

where $c = \pi a^2/A$ denotes the area fraction of holes and E is Young's modulus of the matrix material. From $C^{-1}_{1111} = 1/E$ and $C^{-1}_{1212} = 1/2\mu$ the effective Young's modulus and the effective shear modulus are obtained:

$$E^*_{(\mathrm{DD})} = \frac{E}{1+3c} \approx E(1-3c), \quad \mu^*_{(\mathrm{DD})} = \frac{E}{2(1+\nu+4c)} \approx \mu(1 - \frac{4c}{1+\nu}). \quad (8.85)$$

As expected, both effective stiffnesses decrease with increasing area fraction of holes.

c) Straight cracks (2D)
Exactly as in case of a circular hole the average strain of a straight crack of length $2a$ subjected to a uniform external loading (Fig. 8.11b) can be obtained from (8.50b) using the fundamental solution (8.38):

$$\begin{aligned} \langle \varepsilon_{11} \rangle_c &= 0 \\ \langle \varepsilon_{12} \rangle_c &= \frac{1}{2A} \int_{-a}^{a} \Delta u_1(x_1)\, \mathrm{d}x_1 \;=\; \frac{a^2}{A}\,\frac{\pi}{E}\,\sigma^0_{12} \;=\; f\,\frac{\pi}{E}\,\sigma^0_{12} \\ \langle \varepsilon_{22} \rangle_c &= \frac{1}{A} \int_{-a}^{a} \Delta u_2(x_1)\, \mathrm{d}x_1 \;=\; f\,\frac{2\pi}{E}\,\sigma^0_{22}\,. \end{aligned} \quad (8.86)$$

In analogy to the volume fraction or area fraction of a defect the *crack density parameter* $f = a^2/A$ has been introduced here; in view of the assumed dilute distribution its value has to be small: $f \ll 1$. The nonvanishing components of the additional compliance tensor $\boldsymbol{H}^{\infty}$ read

$$H^{\infty}_{1212} = H^{\infty}_{2121} = H^{\infty}_{1221} = H^{\infty}_{2112} = f\,\frac{\pi}{E}\,, \qquad H^{\infty}_{2222} = f\,\frac{2\pi}{E}\,. \quad (8.87)$$

In case of a plate which consists of a homogeneous isotropic matrix material with *parallel* cracks of equal length $2a$ (Fig. 8.17a) the effective elastic constants according to (8.83) are

$$\begin{aligned} E^*_{1\,(\mathrm{DD})} &= E\,, \qquad E^*_{2\,(\mathrm{DD})} \;=\; \frac{E}{1+2\pi f} \;\approx\; E\,(1-2\pi f)\,, \\ \mu^*_{12\,(\mathrm{DD})} &= \frac{E}{2(1+\nu+\pi f)} \;\approx\; \mu\,(1 - \frac{\pi f}{1+\nu})\,. \end{aligned} \quad (8.88)$$

Due to the uniform crack orientation the overall material behavior here is *anisotropic* with a reduced stiffness normal to the cracks.

If, in contrast, the crack orientations are *statistically equal distributed* (Fig. 8.17b) the additional compliance tensor (8.87) can, within the model of a dilute defect distribution, be averaged over all orientations:

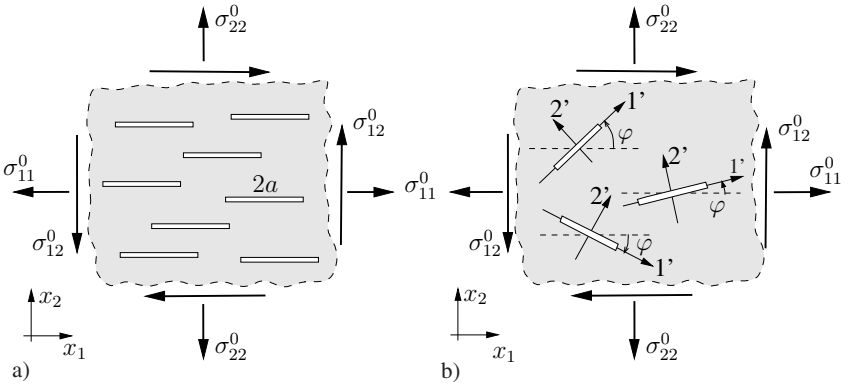

Fig. 8.17 a) Parallel and b) statistically equal distributed crack orientation

$$H^{\infty}_{ijkl} = \frac{1}{2\pi}\int_0^{2\pi} H^{\infty}_{i'j'k'l'}(\varphi)\,\mathrm{d}\varphi \;\rightsquigarrow\; H^{\infty}_{1111} = H^{\infty}_{1212} = H^{\infty}_{2121} = H^{\infty}_{2222} = f\frac{\pi}{E}\,. \tag{8.89}$$

Since macroscopically there is no preferred direction the effective material behavior is isotropic with

$$E^*_{(\mathrm{DD})} = \frac{E}{1+\pi f} \approx E\,(1-\pi f), \quad \mu^*_{(\mathrm{DD})} = \frac{E}{2(1+\nu+\pi f)} \approx \mu(1-\frac{\pi f}{1+\nu})\,. \tag{8.90}$$

d) Penny-shaped cracks (3D)

Starting from the fundamental solution (8.39) for a penny-shaped crack of radius a in an unbounded domain and following the same procedure as before the additional compliance tensor in case of a uniform loading σ^0_{ij} is obtained from (8.50b) and (8.72). In a local coordinate system with the x_3-axis normal to the crack its nonvanishing components read

$$H^{\infty}_{3333} = f\frac{16(1-\nu^2)}{3E}\,, \qquad H^{\infty}_{1313} = H^{\infty}_{2323} = f\,\frac{32(1-\nu^2)}{3E(2-\nu)} \tag{8.91}$$

where now (3D) the crack density parameter is given by $f = a^3/V$. The effective elastic constants of a material which consists of an isotropic matrix with a dilute distribution of *parallel* and equally sized penny-shaped cracks can be written as

$$\begin{aligned}
&E^*_{1\,(\mathrm{DD})} = E^*_{2\,(\mathrm{DD})} = E\,, \quad \nu^*_{12\,(\mathrm{DD})} = \nu\,, \quad \mu^*_{12\,(\mathrm{DD})} = \mu = \frac{E}{2(1+\nu)}\,,\\
&E^*_{3\,(\mathrm{DD})} = \frac{3E}{3+f16(1-\nu^2)}\,,\\
&\mu^*_{13\,(\mathrm{DD})} = \mu^*_{23\,(\mathrm{DD})} = \mu\left[1+f\frac{16(1-\nu)}{3(2-\nu)}\right]^{-1}\,,
\end{aligned} \tag{8.92}$$

$$\nu^*_{13\,(\mathrm{DD})} = \nu^*_{23\,(\mathrm{DD})} = \nu \left[1 + f\frac{16(1-2\nu)(\nu^2-1)}{3\nu(2-\nu)}\right]\left[1 + f\frac{16(1-\nu^2)}{3}\right]^{-1}.$$

It should be noted that the parameters $E^*_{1\,(\mathrm{DD})}$, $\nu^*_{12\,(\mathrm{DD})}$, and $\mu^*_{12\,(\mathrm{DD})}$ are not independent but are solely determined by two elastic constants. Hence the overall material behavior is characterized by five independent elastic constants and is isotropic in the x_1, x_2-plane; this kind of anisotropy is termed *transversely isotropic* (see (1.41), (1.42)).

If all crack orientations occur equally often the macroscopic behavior is isotropic. Averaging of (8.91) over all orientations

$$H^\infty_{ijkl} = \frac{1}{4\pi}\int_0^{2\pi}\int_0^{\pi} H^\infty_{i'j'k'l'}(\varphi,\,\vartheta)\,\cos\vartheta\,\mathrm{d}\vartheta\,\mathrm{d}\varphi$$

then yields

$$\begin{aligned} H^\infty_{1111} &= H^\infty_{2222} = H^\infty_{3333} = \frac{f}{E}\,\frac{16(1-\nu^2)(10-3\nu)}{45(2-\nu)} \\ H^\infty_{1122} &= H^\infty_{2233} = H^\infty_{3311} = -\frac{f}{E}\,\frac{16\nu(1-\nu^2)}{45(2-\nu)} \\ H^\infty_{1212} &= H^\infty_{2323} = H^\infty_{3131} = \frac{f}{E}\,\frac{32(1-\nu^2)(5-\nu)}{45(2-\nu)} \end{aligned} \tag{8.93}$$

from which the effective elastic constants

$$\begin{aligned} E^*_{(\mathrm{DD})} &= E\left[1 + f\,\frac{16(1-\nu^2)(10-3\nu)}{45(2-\nu)}\right]^{-1} \approx E\left[1 - f\,\frac{16(1-\nu^2)(10-3\nu)}{45(2-\nu)}\right], \\ \mu^*_{(\mathrm{DD})} &= \mu\left[1 + f\,\frac{32(1-\nu)(5-\nu)}{45(2-\nu)}\right]^{-1} \approx \mu\left[1 - f\,\frac{32(1-\nu)(5-\nu)}{45(2-\nu)}\right] \end{aligned} \tag{8.94}$$

are obtained.

8.3.2.4 Mori-Tanaka model

The approximation of a dilute distribution of non-interacting defects is equivalent to the assumption that in a sufficient distance from each defect the constant strain field $\boldsymbol{\varepsilon}^0$ or stress field $\boldsymbol{\sigma}^0$ of the external loading prevails. This assumption is the starting point for a refinement of the model to account for an interaction and hence a finite volume fraction of defects. In the Mori-Tanaka model (1973) therefore the strain or stress field in the matrix is, in a sufficient distance from a defect, approximated by the constant field $\langle\boldsymbol{\varepsilon}\rangle_{\mathrm{M}}$ or $\langle\boldsymbol{\sigma}\rangle_{\mathrm{M}}$ (Fig. 8.18). The loading of each defect then depends

on the existence of further defects via the average matrix strain $\langle\boldsymbol{\varepsilon}\rangle_{\mathrm{M}}$ or the average matrix stress $\langle\boldsymbol{\sigma}\rangle_{\mathrm{M}}$. Fluctuations of the local fields, however, are neglected in this approximation of defect interaction.

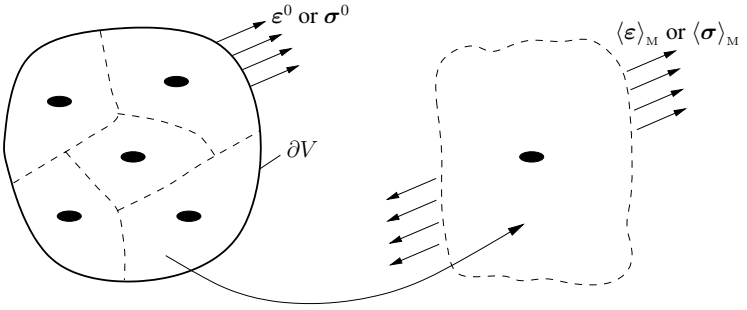

Fig. 8.18 Defect interaction in the Mori-Tanaka model

In view of the idealized consideration of a single defect in an unbounded matrix, yet subjected to some *effective loading* $\langle\boldsymbol{\varepsilon}\rangle_{\mathrm{M}}$ or $\langle\boldsymbol{\sigma}\rangle_{\mathrm{M}}$, the Mori-Tanaka model formally equals that of a dilute distribution (see Fig. 8.15) and allows for the application of the already known influence tensors $\boldsymbol{A}_{\mathrm{I}}^{\infty}$ and $\boldsymbol{H}^{\infty}$ to represent the average defect strain:

$$\langle\boldsymbol{\varepsilon}\rangle_{\mathrm{I}} = \boldsymbol{A}_{\mathrm{I}}^{\infty} : \langle\boldsymbol{\varepsilon}\rangle_{\mathrm{M}} \qquad \text{or} \qquad \langle\boldsymbol{\varepsilon}\rangle_{c} = \boldsymbol{H}^{\infty} : \langle\boldsymbol{\sigma}\rangle_{\mathrm{M}} \,. \tag{8.95}$$

In order to determine the effective material properties the average defect strain needs to be represented as a function of the macroscopic quantities $\langle\boldsymbol{\varepsilon}\rangle = \boldsymbol{\varepsilon}^0$ or $\langle\boldsymbol{\sigma}\rangle = \boldsymbol{\sigma}^0$, respectively (see (8.67)). Therefore, the matrix quantities $\langle\boldsymbol{\varepsilon}\rangle_{\mathrm{M}}$ and $\langle\boldsymbol{\sigma}\rangle_{\mathrm{M}}$ are eliminated. Using $\langle\boldsymbol{\varepsilon}\rangle = c_{\mathrm{M}}\langle\boldsymbol{\varepsilon}\rangle_{\mathrm{M}} + c_{\mathrm{I}}\langle\boldsymbol{\varepsilon}\rangle_{\mathrm{I}}$ and (8.95) in case of ellipsoidal inhomogeneities leads to $\langle\boldsymbol{\varepsilon}\rangle_{\mathrm{I}} = \boldsymbol{A}_{\mathrm{I}\,(\mathrm{MT})} : \langle\boldsymbol{\varepsilon}\rangle$ where

$$\boldsymbol{A}_{\mathrm{I}\,(\mathrm{MT})} = \left[c_{\mathrm{I}}\boldsymbol{1} + c_{\mathrm{M}}\boldsymbol{A}_{\mathrm{I}}^{\infty\,-1}\right]^{-1} = \left[\boldsymbol{1} + c_{\mathrm{M}}\,\boldsymbol{S}_{\mathrm{M}} : \boldsymbol{C}_{\mathrm{M}}^{-1} : (\boldsymbol{C}_{\mathrm{I}} - \boldsymbol{C}_{\mathrm{M}})\right]^{-1} \tag{8.96a}$$

is the influence tensor of the Mori-Tanaka model. In case of cavities or cracks (8.95) and $\langle\boldsymbol{\sigma}\rangle = c_{\mathrm{M}}\langle\boldsymbol{\sigma}\rangle_{\mathrm{M}}$ lead to $\langle\boldsymbol{\varepsilon}\rangle_{c} = \boldsymbol{H}_{(\mathrm{MT})} : \langle\boldsymbol{\sigma}\rangle$ with the additional compliance tensor

$$\boldsymbol{H}_{(\mathrm{MT})} = \frac{1}{c_{\mathrm{M}}}\,\boldsymbol{H}^{\infty} \,. \tag{8.96b}$$

According to (8.71a) and (8.73) hence the effective elastic constants for the two kinds of defects are given by

$$\boxed{\boldsymbol{C}^{*}_{(\mathrm{MT})} = \begin{cases} \boldsymbol{C}_{\mathrm{M}} + c_{\mathrm{I}}(\boldsymbol{C}_{\mathrm{I}} - \boldsymbol{C}_{\mathrm{M}}) : \boldsymbol{A}_{\mathrm{I}\,(\mathrm{MT})} & \text{(ellipsoids)} \\ \left[\boldsymbol{C}_{\mathrm{M}}^{-1} + \boldsymbol{H}_{(\mathrm{MT})}\right]^{-1} & \text{(cavities, cracks)} \end{cases}} \,. \tag{8.97}$$

From (8.96a) and (8.97) it can be seen that the Mori-Tanaka model, in contrast to the model of a dilute distribution, correctly covers the extreme cases of $c_{\mathrm{I}} = 0$ and $c_{\mathrm{I}} = 1$ (homogeneous material) and therefore can formally be applied for arbitrary volume fractions c_{I}. Yet, the fundamental assumption of a distinct matrix phase and a defect subjected to a homogeneous far-field loading can only be realized for small or large values of c_{I}; in the latter case the inhomogeneity attains the role of the matrix phase. In case of cavities (8.96b) and (8.97) yield a loss of the macroscopic stress-carrying capacity ($\boldsymbol{C}^{*}_{(\mathrm{MT})} \to 0$) only in the limit $c_{\mathrm{M}} \to 0$ which is not realistic (see Section 8.3.2.5).

It can be shown that the approximations for the effective material properties obtained from the Mori-Tanaka model are independent of the type of prescribed macroscopic quantities $\boldsymbol{\varepsilon}^0$ or $\boldsymbol{\sigma}^0$. For small values of the defect volume fraction ($c_{\mathrm{I}} \ll 1$) they asymptotically approach the results for a dilute distribution.

In the special case of an isotropic matrix which contains isotropic spherical inhomogeneities the Mori-Tanaka model yields irrespective of the spatial arrangement of the defects an isotropic overall behavior with effective elastic constants (see (8.80))

$$\begin{aligned} K^{*}_{(\mathrm{MT})} &= K_{\mathrm{M}} + c_{\mathrm{I}} \frac{(K_{\mathrm{I}} - K_{\mathrm{M}})\, K_{\mathrm{M}}}{K_{\mathrm{M}} + \alpha\,(1 - c_{\mathrm{I}})\,(K_{\mathrm{I}} - K_{\mathrm{M}})} \,, \\ \mu^{*}_{(\mathrm{MT})} &= \mu_{\mathrm{M}} + c_{\mathrm{I}} \frac{(\mu_{\mathrm{I}} - \mu_{\mathrm{M}})\, \mu_{\mathrm{M}}}{\mu_{\mathrm{M}} + \beta\,(1 - c_{\mathrm{I}})\,(\mu_{\mathrm{I}} - \mu_{\mathrm{M}})} \,. \end{aligned} \tag{8.98}$$

A macroscopic anisotropy which might result from the geometric arrangement of the inhomogeneities hence can not be described by this model (like in case of the dilute distribution). It should further be noted that in contrast to (8.80) now the effective constants (8.98) depend nonlinearly on the volume fraction c_{I} of inhomogeneities. In the limit case of rigid spheres ($K_{\mathrm{I}},\, \mu_{\mathrm{I}} \to \infty$) in an incompressible matrix ($K_{\mathrm{M}} \to \infty,\, \beta = 2/5$) they reduce to (see (8.81))

$$\mu^{*}_{(\mathrm{MT})} = \mu_{\mathrm{M}} \Big(1 + \frac{5}{2} \frac{c_{\mathrm{I}}}{1 - c_{\mathrm{I}}} \Big) \,. \tag{8.99}$$

In the 2D-example of a plate in plane stress with circular holes of an area fraction c according to Fig. 8.16 the Mori-Tanaka model yields by insertion of (8.84) into (8.96b), (8.97)

$$E^{*}_{(\mathrm{MT})} = E\, \frac{1 - c}{1 + 2c} \,, \qquad \mu^{*}_{(\mathrm{MT})} = \mu\, \frac{(1 - c)(1 + \nu)}{1 + \nu + c\,(3 - \nu)} \,. \tag{8.100}$$

Cracks, because of their vanishing volume ($c_{\mathrm{M}} = 1$), have no effect on the average stress: $\langle \boldsymbol{\sigma} \rangle_{\mathrm{M}} = \langle \boldsymbol{\sigma} \rangle$. For a material with straight (2D) or penny-shaped cracks the Mori-Tanaka model thus leads to the same effective elastic constants as the model of a dilute defect distribution in case of prescribed macro-stress (see (8.88), (8.90), (8.92), or (8.94)). Accordingly, the Mori-Tanaka model when applied to cracks does not predict a total loss of the macroscopic stress-carrying capacity, even in case of an arbitrary high value of the crack density.

8.3.2.5 Self-consistent method

Analytical methods for the approximation of effective material properties are typically based on the consideration of a single defect in an unbounded domain because of the limited availability of closed-form solutions. In doing so, the interaction of defects has in the previous section been accounted for by an appropriate approximation of the loading of individual defects; a sufficient distance among these defects in a homogeneous matrix therefore was required. This latter assumption, however, does often not hold. For instance, in a polycrystal the inhomogeneities prevail in form of single crystal grains which are in direct contact with each other without any distinct matrix phase. With focus on this particular situation the self-consistent method has been developed. It is based on the approximation ("smearing") of the entire surrounding of each individual defect by an infinite matrix with elastic properties given by the unknown effective properties which are to be determined (Fig. 8.19). Inside the defect the solution of the respective boundary value problem (single defect subjected to some loading $\varepsilon^0 = \langle\varepsilon\rangle$ or $\boldsymbol{\sigma}^0 = \langle\boldsymbol{\sigma}\rangle$) is formally obtained from the solution for a dilute defect distribution by replacing the matrix properties by the effective properties (see also Fig. 8.15). Correspondingly, the average defect strain and the influence tensors are for ellipsoidal inhomogeneities given by

$$\begin{aligned} \langle\boldsymbol{\varepsilon}\rangle_{\mathrm{I}} &= \boldsymbol{A}_{\mathrm{I\,(SK)}} : \langle\boldsymbol{\varepsilon}\rangle \,, \\ \boldsymbol{A}_{\mathrm{I\,(SK)}} &= \boldsymbol{A}_{\mathrm{I}}^{\infty}(\boldsymbol{C}_{\mathrm{M}} = \boldsymbol{C}^*) = \left[\mathbf{1} + \boldsymbol{S}^* : \boldsymbol{C}^{*\,-1} : (\,\boldsymbol{C}_{\mathrm{I}} - \boldsymbol{C}^*\,)\right]^{-1} \end{aligned} \tag{8.101a}$$

and in case of cavities and cracks by

$$\langle\boldsymbol{\varepsilon}\rangle_c = \boldsymbol{H}_{(\mathrm{SK})} : \langle\boldsymbol{\sigma}\rangle \,, \qquad \boldsymbol{H}_{(\mathrm{SK})} = \boldsymbol{H}^{\infty}(\boldsymbol{C}_{\mathrm{M}} = \boldsymbol{C}^*) \,. \tag{8.101b}$$

The effective elastic properties then follow by insertion into (8.71a) or (8.73). They are subject to the requirement to coincide with the effective matrix properties $\boldsymbol{C}^*$ used in the representation of the influence tensors (8.101a), (8.101b) which explains the notion *self-consistence*. Thus the self-consistent method yields an implicit repre-

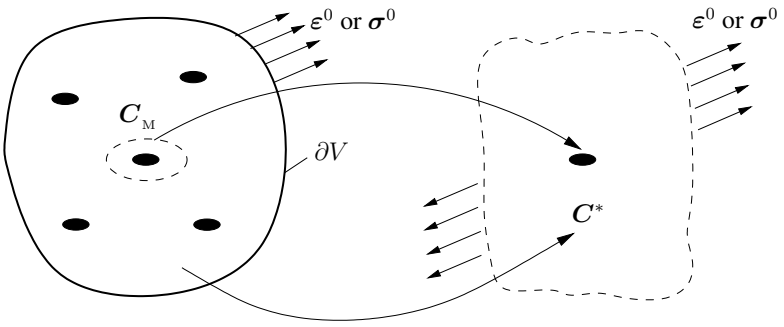

Fig. 8.19 Model of the self-consistent method

sentation of the effective elasticity tensor in form of nonlinear algebraic equations. Using (8.71a) and (8.73) the latter read

$$\boxed{\boldsymbol{C}^*_{(\mathrm{SK})} = \begin{cases} \boldsymbol{C}_{\mathrm{M}} + c_{\mathrm{I}}(\,\boldsymbol{C}_{\mathrm{I}} - \boldsymbol{C}_{\mathrm{M}}\,) : \boldsymbol{A}_{\mathrm{I}}^{\infty}(\boldsymbol{C}^*_{(\mathrm{SK})}) & \text{(ellipsoids)} \\ \left[\boldsymbol{C}_{\mathrm{M}}^{-1} + \boldsymbol{H}^{\infty}(\boldsymbol{C}^*_{(\mathrm{SK})})\right]^{-1} & \text{(cavities, cracks)} \end{cases}} \,. \tag{8.102}$$

Like the Mori-Tanaka model, the self-consistent method also yields a unique result which is independent of the prescribed macroscopic quantities and correctly covers the limit cases of a homogeneous material. Moreover, it should be noted that in the self-consistent method a macroscopic anisotropy which may result from the relative defect orientation or arrangement has to be accounted for already in the effective behavior adopted in the fundamental solution $\boldsymbol{A}_{\mathrm{I}}^{\infty}(\boldsymbol{C}^*_{(\mathrm{SK})})$ or $\boldsymbol{H}^{\infty}(\boldsymbol{C}^*_{(\mathrm{SK})})$. A typical example are parallel cracks where already an individual defect has a distinguished orientation; but also preferred orientations in the spatial arrangement of isotropic defects give rise to a macroscopic anisotropy. Only in case of a complete (i.e., material and geometric) isotropy of the microstructure is the overall behavior isotropic. This holds, for instance, for an isotropic distribution of spherical inhomogeneities in an isotropic matrix. In this special case insertion of the parameters $\alpha^*(\nu^*)$, $\beta^*(\nu^*)$ of the isotropic Eshelby tensor (8.11) leads to the following equations for the effective bulk and shear moduli:

$$\begin{aligned} 0 &= \frac{c_{\mathrm{M}}}{K^*_{(\mathrm{SK})} - K_{\mathrm{I}}} + \frac{c_{\mathrm{I}}}{K^*_{(\mathrm{SK})} - K_{\mathrm{M}}} - \frac{3}{3K^*_{(\mathrm{SK})} + 4\mu^*_{(\mathrm{SK})}} \,, \\ 0 &= \frac{c_{\mathrm{M}}}{\mu^*_{(\mathrm{SK})} - \mu_{\mathrm{I}}} + \frac{c_{\mathrm{I}}}{\mu^*_{(\mathrm{SK})} - \mu_{\mathrm{M}}} - \frac{6\left(K^*_{(\mathrm{SK})} + 2\mu^*_{(\mathrm{SK})}\right)}{5\mu^*_{(\mathrm{SK})}\left(3K^*_{(\mathrm{SK})} + 4\mu^*_{(\mathrm{SK})}\right)} \,. \end{aligned} \tag{8.103}$$

From this representation it is obvious that in the self-consistent method none of the involved phases plays the role of a surrounding matrix; this corresponds to the situation of a polycrystalline or interpenetrating microstructure.

In the special case of rigid spherical particles ($K_{\mathrm{I}} \to \infty\,,\ \mu_{\mathrm{I}} \to \infty$) in an incompressible matrix ($K_{\mathrm{M}} \to \infty$) the self-consistent method yields in contrast to (8.81) and (8.99)

$$\mu^*_{(\mathrm{SK})} = \frac{2\,\mu_{\mathrm{M}}}{2 - 5\,c_{\mathrm{I}}} \,. \tag{8.104}$$

Hence a macroscopically rigid material ($\mu^*_{(\mathrm{SK})} \to \infty$) is predicted already at a volume fraction of spherical particles of $c_{\mathrm{I}} = 2/5$. Also the case of spherical voids ($K_{\mathrm{I}} \to 0\,,\ \mu_{\mathrm{I}} \to 0$) in an incompressible matrix ($K_{\mathrm{M}} \to \infty$) can be directly derived from (8.103) which leads to

$$K^*_{(\mathrm{SK})} = \frac{4\,\mu_{\mathrm{M}}(1 - 2\,c_{\mathrm{I}})(1 - c_{\mathrm{I}})}{c_{\mathrm{I}}(3 - c_{\mathrm{I}})} \,, \qquad \mu^*_{(\mathrm{SK})} = \frac{3\,\mu_{\mathrm{M}}(1 - 2\,c_{\mathrm{I}})}{3 - c_{\mathrm{I}}} \,. \tag{8.105}$$

From this result it can be seen that the self-consistent method applied to a porous material predicts the entire loss of macroscopic stress carrying capacity ($K^*_{(\mathrm{SK})} \to 0$, $\mu^*_{(\mathrm{SK})} \to 0$) at a void volume fraction of 50%, i.e., $c_{\mathrm{I}} = 1/2$. The limit behavior described by (8.104) and (8.105) is qualitatively correct since statistically already at a volume fraction well below 1 "bridges" of rigid particles or voids prevail in a real material which extend throughout the whole microstructure and determine the overall performance. This statistical effect is called *percolation* and is subject of the *percolation theory* to be found in the special literature (see also Section 3.1.4). The apparent strength of the self-consistent method to account for this effect, however, is weakened by the fact that the prerequisite for a homogenization of statistical homogeneity of an RVE is violated by the existence of the above-mentioned bridges (percolation).

Another drawback of the self-consistent method lies in its mixing of the microscopic and macroscopic level which strictly should be separated. A single defect, "visible" only on the microscale, is embedded into an effective medium which is defined only on the macroscopic level. In order to reduce this inconsistency the so-called *generalized self-consistent method* considers the defect and the infinitely extended effective medium to be separated by a layer of the true matrix material. Yet, this rather complicated method is not further treated here.

The result (8.102) of the self-consistent method shall now be evaluated for the situation of circular holes and cracks. In case of a plate containing isotropically distributed circular holes (macroscopic isotropy) therefore only the Young's modulus E of the matrix material in (8.84) needs to be replaced by $E^*_{(\mathrm{SK})}$ which leads to

$$E^*_{(\mathrm{SK})} = E\,(1-3\,c)\,, \qquad \mu^*_{(\mathrm{SK})} = \frac{E\,(1-3\,c)}{2\,[1+c+\nu(1-3\,c)]}\,. \tag{8.106}$$

The total loss of effective stiffness of the plate hence is predicted already at an area fraction of holes of $c = 1/3$. Experimental data or those based on percolation theory, however, are approximately twice that value (see Fig. 8.21).

As already mentioned, the application of the self-consistent method to materials with parallel cracks requires the somewhat cumbersome determination of the fundamental solution for a single crack in an anisotropic medium because of the resulting overall anisotropy. Referring for this case to the special literature we restrict ourselves here to the situation of statistically equal distributed crack orientations where the overall material behavior is isotropic. In case of straight cracks of length $2a$ in a plate under plane stress only E in (8.89) has to replaced by $E^*_{(\mathrm{SK})}$. The effective Young's modulus and shear modulus then are given by

$$E^*_{(\mathrm{SK})} = E\,(1-\pi f)\,, \qquad \mu^*_{(\mathrm{SK})} = \frac{E\,(1-\pi f)}{2\,[1+\nu(1-\pi f)]}\,. \tag{8.107}$$

Accordingly, a total loss of macroscopic stiffness is predicted at $f = 1/\pi$. At this value the area πa^2 covered by a crack by varying its orientation is equal to the reference area A of the material. For the three-dimensional problem of penny-shaped

cracks with randomly distributed orientation the isotropic additional compliance tensor $\boldsymbol{H}_{(\mathrm{SK})} = \boldsymbol{H}^{\infty}(\boldsymbol{C}^{*}_{(\mathrm{SK})})$ is obtained from (8.93) by substituting E and ν by $E^{*}_{(\mathrm{SK})}$ and $\nu^{*}_{(\mathrm{SK})}$ which, using (8.102), leads to coupled nonlinear equations for the effective elastic constants:

$$\begin{aligned} \frac{\nu^{*}_{(\mathrm{SK})}}{E^{*}_{(\mathrm{SK})}} &= \frac{\nu}{E} + f\,\frac{16\nu^{*}_{(\mathrm{SK})}(1-\nu^{*2}_{(\mathrm{SK})})}{45(2-\nu^{*}_{(\mathrm{SK})})E^{*}_{(\mathrm{SK})}}\,, \\ \frac{1+\nu^{*}_{(\mathrm{SK})}}{E^{*}_{(\mathrm{SK})}} &= \frac{1+\nu}{E} + f\,\frac{32(1-\nu^{*2}_{(\mathrm{SK})})(5-\nu^{*}_{(\mathrm{SK})})}{45(2-\nu^{*}_{(\mathrm{SK})})E^{*}_{(\mathrm{SK})}}\,. \end{aligned} \tag{8.108}$$

8.3.2.6 Differential scheme

In contrast to the self-consistent method where the entire volume fraction of each phase is embedded in the effective matrix in a single step, the differential scheme is based on a succession of this embedding by infinitesimal steps. This can be associated with the actual manufacturing of a heterogeneous material by the stepwise incorporation of one phase (inhomogeneity) into an originally homogeneous material (matrix) where it is irrelevant which of the phases attains the role of the originally homogeneous material. Since in each step only an infinitesimal volume $\mathrm{d}V$ of the defect phase with elasticity tensor $\boldsymbol{C}_{\mathrm{I}}$ is embedded into the infinitely extended homogeneous matrix, the model of a dilute distribution and the respective relations for the effective properties are exact. In an arbitrary step the matrix is characterized by the effective properties $\boldsymbol{C}^{*}(c_{\mathrm{I}})$ which correspond to the up to then embedded volume fraction $c_{\mathrm{I}} = V_{\mathrm{I}}/V$. This procedure is illustrated in Fig. 8.20 for an ellipsoidal inhomogeneity. By conservation of the total volume V, an infinitesimal volume $\mathrm{d}V$ of the defect phase is incorporated while the same volume of effective matrix mate-

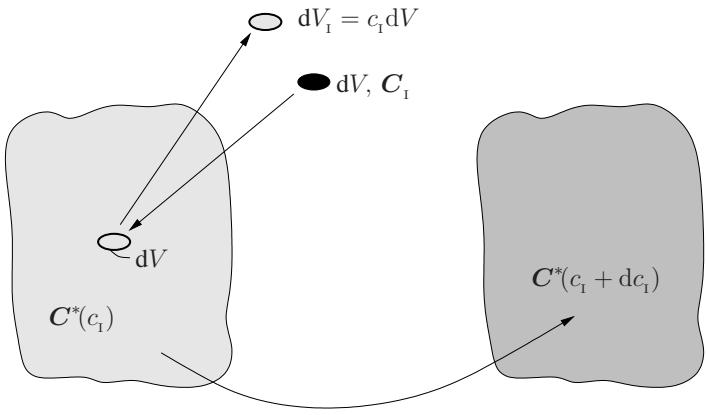

Fig. 8.20 Differential scheme

rial has to be removed. Thereby the volume fraction of the inhomogeneity changes to $c_{\mathrm{I}} + \mathrm{d}c_{\mathrm{I}}$ and its volume balance during this step can be written as

$$(c_{\mathrm{I}} + \mathrm{d}c_{\mathrm{I}})\, V = c_{\mathrm{I}}\, V - c_{\mathrm{I}}\, \mathrm{d}V + \mathrm{d}V \qquad \rightsquigarrow \qquad \frac{\mathrm{d}V}{V} = \frac{\mathrm{d}c_{\mathrm{I}}}{1 - c_{\mathrm{I}}}\ . \tag{8.109}$$

Since only an infinitesimal volume $\mathrm{d}V$ (volume fraction $\mathrm{d}V/V$) is embedded, the relation (8.79a) of the model of a dilute distribution is exact and, applied to the current situation, reads

$$\boldsymbol{C}^*(c_{\mathrm{I}} + \mathrm{d}c_{\mathrm{I}}) = \underbrace{\boldsymbol{C}^*(c_{\mathrm{I}})}_{\text{Matrix}} + \frac{\mathrm{d}V}{V}\Big(\boldsymbol{C}_{\mathrm{I}} - \underbrace{\boldsymbol{C}^*(c_{\mathrm{I}})}_{\text{Matrix}}\Big) : \boldsymbol{A}_{\mathrm{I}}^{\infty}\ . \tag{8.110}$$

Here, the influence tensor depends on the effective matrix material: $\boldsymbol{A}_{\mathrm{I}}^{\infty}(\boldsymbol{C}^*(c_{\mathrm{I}}))$. Using $\boldsymbol{C}^*(c_{\mathrm{I}} + \mathrm{d}c_{\mathrm{I}}) = \boldsymbol{C}^*(c_{\mathrm{I}}) + \mathrm{d}\boldsymbol{C}^*(c_{\mathrm{I}})$ and (8.109) one obtains

$$\boxed{\frac{\mathrm{d}\boldsymbol{C}^*(c_{\mathrm{I}})}{\mathrm{d}c_{\mathrm{I}}} = \frac{1}{1 - c_{\mathrm{I}}}\left(\boldsymbol{C}_{\mathrm{I}} - \boldsymbol{C}^*(c_{\mathrm{I}})\right) : \boldsymbol{A}_{\mathrm{I}}^{\infty}}\ . \tag{8.111}$$

The differential scheme hence leads to a nonlinear ordinary differential equation for the effective elasticity tensor as a function of the volume fraction c_{I} of the embedded phase. The original material (second phase) appears only in the initial condition: $\boldsymbol{C}^*(c_{\mathrm{I}} = 0) = \boldsymbol{C}_{\mathrm{M}}$. In case of total (i.e., material and geometric) isotropy one obtains from (8.111) the following system of coupled differential equations for the effective bulk and shear modulus

$$\begin{aligned}
\frac{\mathrm{d}K^*_{(\mathrm{DS})}}{\mathrm{d}c_{\mathrm{I}}} &= \frac{K_{\mathrm{I}} - K^*_{(\mathrm{DS})}}{1 - c_{\mathrm{I}}}\,\frac{3K^*_{(\mathrm{DS})} + 4\mu^*_{(\mathrm{DS})}}{3K_{\mathrm{I}} + 4\mu^*_{(\mathrm{DS})}}\ , \\
\frac{\mathrm{d}\mu^*_{(\mathrm{DS})}}{\mathrm{d}c_{\mathrm{I}}} &= \frac{\mu_{\mathrm{I}} - \mu^*_{(\mathrm{DS})}}{1 - c_{\mathrm{I}}}\,\frac{5\mu^*_{(\mathrm{DS})}\left(3K^*_{(\mathrm{DS})} + 4\mu^*_{(\mathrm{DS})}\right)}{\mu^*_{(\mathrm{DS})}\left(9K^*_{(\mathrm{DS})} + 8\mu^*_{(\mathrm{DS})}\right) + 6\mu_{\mathrm{I}}\left(K^*_{(\mathrm{DS})} + 2\mu^*_{(\mathrm{DS})}\right)}
\end{aligned} \tag{8.112}$$

with initial conditions $K^*_{(\mathrm{DS})}(c_{\mathrm{I}} = 0) = K_{\mathrm{M}}\,,\ \mu^*_{(\mathrm{DS})}(c_{\mathrm{I}} = 0) = \mu_{\mathrm{M}}$.

For the example of rigid spheres (I) in an incompressible matrix (M) (8.112) reduces to

$$\frac{\mathrm{d}\mu^*_{(\mathrm{DS})}}{\mathrm{d}c_{\mathrm{I}}} = \frac{1}{1 - c_{\mathrm{I}}}\,\frac{5\,\mu^*_{(\mathrm{DS})}}{2} \tag{8.113}$$

with the solution

$$\mu^*_{(\mathrm{DS})}(c_{\mathrm{I}}) = \frac{\mu_{\mathrm{M}}}{(1 - c_{\mathrm{I}})^{5/2}}\ . \tag{8.114}$$

Contrary to the self-consistent method (see (8.104)) the differential scheme yields the overall rigidity of the material only for $c_{\mathrm{I}} \to 1$.

Table 8.1 Effective elastic constants

1	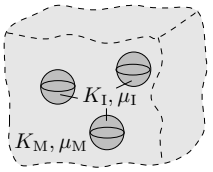	spherical inhomogeneities $K^* = K_{\rm M} + c_{\rm I} \dfrac{(K_{\rm I} - K_{\rm M})\, K_{\rm M}}{K_{\rm M} + \alpha\,(1 - c_{\rm I})\,(K_{\rm I} - K_{\rm M})}$ $\mu^* = \mu_{\rm M} + c_{\rm I} \dfrac{(\mu_{\rm I} - \mu_{\rm M})\, \mu_{\rm M}}{\mu_{\rm M} + \beta\,(1 - c_{\rm I})\,(\mu_{\rm I} - \mu_{\rm M})}$
2	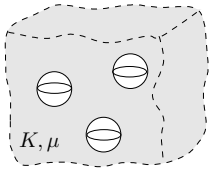	spherical voids $K^* = K\Big(1 - \dfrac{c}{1 - \alpha(1-c)}\Big)$ $\mu^* = \mu\Big(1 - \dfrac{c}{1 - \beta(1-c)}\Big)$
3	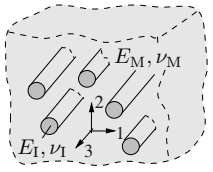	unidirectional fibers (inhomogeneities) $E_3^* = c_{\rm I} E_{\rm I} + (1 - c_{\rm I}) E_{\rm M}\,, \quad \mu_{12}^* = \dfrac{2 + c_{\rm I}}{5(1 - c_{\rm I})}\, E_{\rm M}$ $\mu_{13}^* = \mu_{23}^* = \dfrac{2(1 + c_{\rm I})}{5(1 - c_{\rm I})}\, E_{\rm M}\,, \quad \nu_{31}^* = \nu_{32}^* = 1/4$ $\dfrac{1}{E_{1,2}^*} = \dfrac{1}{4}\Big(\dfrac{1}{\mu_{12}^*} + \dfrac{5(1 - c_{\rm I})}{2E_{\rm M}(2 + c_{\rm I})} + \dfrac{1}{4E_3^*}\Big)$ for $\nu_{\rm I} = \nu_{\rm M} = 1/4\,, \quad E_{\rm I} \gg E_{\rm M}\,, \quad c_{\rm I} < 1$
4	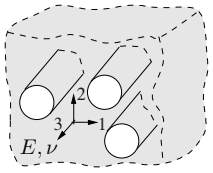	unidirectional hollow cylinders (plane strain) $E_{1,2}^* = \dfrac{(1 - c)E}{1 + c(2 - 3\nu^2)}\,, \quad \mu_{12}^* = \dfrac{(1 - c)\mu}{1 + 3c - 4\nu c}$
5	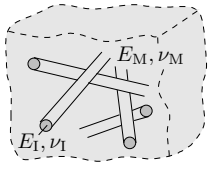	isotropically oriented fibers $E^* = \dfrac{c_{\rm I}}{6}\, E_{\rm I} + \dfrac{1 + c_{\rm I}/4 + c_{\rm I}^2/6}{1 - c_{\rm I}}\, E_{\rm M}\,, \quad \nu^* = \dfrac{1}{4}$ for $\nu_{\rm I} = \nu_{\rm M} = 1/4\,, \quad E_{\rm I} \gg E_{\rm M}\,, \quad c_{\rm I} < 1$

Table 8.1 Effective elastic constants (cont.)

6	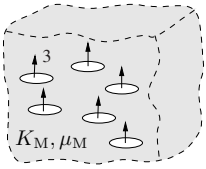	parallel penny-shaped cracks (3D) $E^*_{1,2} = E\,, \quad E^*_3 = \dfrac{3E}{3 + f16(1-\nu^2)}\,, \quad \nu^*_{12} = \nu$ $\nu^*_{13} = \nu^*_{23} = \nu\left[1 + f\dfrac{16(1-2\nu)(\nu^2-1)}{3\nu(2-\nu)}\right]\dfrac{E^*_3}{E}$ $\mu^*_{12} = \dfrac{E}{2(1+\nu)}\,, \quad \mu^*_{13} = \mu^*_{23} = \mu\left[1 + f\dfrac{16(1-\nu)}{3(2-\nu)}\right]^{-1}$
7	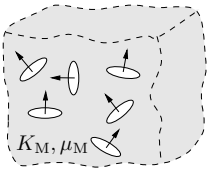	isotropically oriented penny-shaped cracks (3D) $E^* = E\left[1 + f\,\dfrac{16(1-\nu^2)(10-3\nu)}{45(2-\nu)}\right]^{-1}$ $\mu^* = \mu\left[1 + f\,\dfrac{32(1-\nu)(5-\nu)}{45(2-\nu)}\right]^{-1}$
8	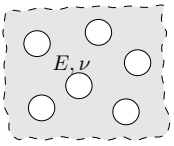	circular holes (2D, plane stress) $E^* = E\,\dfrac{1-c}{1+2c}\,, \quad \mu^* = E\,\dfrac{1-c}{2(1+\nu+c\,(3-\nu))}$
9	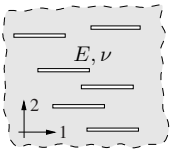	parallel cracks (2D, plane stress) $E^*_1 = E\,, \quad E^*_2 = \dfrac{E}{1+2\pi f}\,, \quad \mu^*_{12} = \dfrac{E}{2(1+\nu+\pi f)}$
10	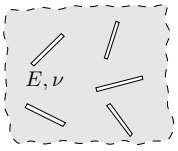	isotropically oriented cracks (2D, plane stress) $E^* = \dfrac{E}{1+\pi f}\,, \quad \mu^* = \dfrac{E}{2(1+\nu+\pi f)}$

When the differential scheme is applied to materials with cracks or holes the latter have to be treated as the embedded phase. In case of circular holes in a plate according to Fig. 8.16 we start directly from the relations (8.85) for a dilute distribution written in the form

$$\frac{1}{E^*_{(\mathrm{DD})}} = \frac{1}{E} + c\,\frac{3}{E}\,, \qquad \frac{1}{2\mu^*_{(\mathrm{DD})}} = \frac{1}{2\mu} + c\,\frac{4}{E}\,. \tag{8.115}$$

Following the same procedure as above the incremental increase $\mathrm{d}c$ of the area fraction c of holes then leads to the differential equations

$$\frac{\mathrm{d}E^{*\,-1}_{(\mathrm{DS})}}{\mathrm{d}c} = \frac{1}{1-c}\,\frac{3}{E^*_{(\mathrm{DS})}}\,, \qquad \frac{\mathrm{d}\mu^{*\,-1}_{(\mathrm{DS})}}{\mathrm{d}c} = \frac{1}{1-c}\,\frac{8}{E^*_{(\mathrm{DS})}} \tag{8.116}$$

with initial conditions $E^*_{(\mathrm{DS})}(c=0) = E\,,\ \mu^*_{(\mathrm{DS})}(c=0) = \mu$. The first differential equation can be solved directly and the second one after insertion of $E^*_{(\mathrm{DS})}(c)$. They lead to the solutions

$$E^*_{(\mathrm{DS})}(c) = E\,(1-c)^3\,, \qquad \mu^*_{(\mathrm{DS})}(c) = \mu\,\frac{3(1+\nu)(1-c)^3}{4+(3\nu-1)(1-c)^3}\,. \tag{8.117}$$

Similar to the foregoing example the differential scheme yields the total loss of macroscopic stiffness only for $c \to 1$.

Like the situation of holes, the differential scheme can be applied to homogenize materials with cracks. Without going into the details of the derivation we present here only the results for the 2D case of isotropically distributed cracks of equal length in a plate under plane stress where f denotes the crack density:

$$E^*_{(\mathrm{DS})}(f) = E(1-f)^\pi\,, \qquad \mu^*_{(\mathrm{DS})}(f) = \mu\,\frac{(1+\nu)(1-f)^\pi}{1+\nu(1-f)^\pi}\,. \tag{8.118}$$

Again the total loss of macroscopic stiffness of the material is reached only in the limit $f \to 1$. For small values of f (8.118) tends asymptotically to the result (8.90) of the dilute distribution.

In order to provide some comparison of the different homogenization methods discussed so far, their results are collectively presented in Fig. 8.21 in terms of the effective Young's modulus of a plate with circular holes. Also shown are experimental data and the percolation threshold which both indicate a total loss of macroscopic stiffness ($E^* \to 0$) at an area fraction of holes well below 1. Only the self-consistent method (SC) is able to predict this behavior. In accordance with the underlying assumptions the model of a dilute defect distribution (DD) is valid only at very small values of c.

For various cases of isotropic or transversely isotropic microstructures effective elastic constants are listed in Table 8.1 where the presentation has been kept as simple as possible. Again, it has to be emphasized that these relations for effective

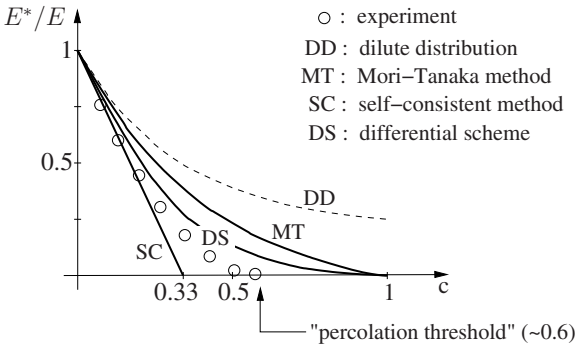

Fig. 8.21 Effective Young's modulus of a plate containing isotropically distributed circular holes

properties are only approximations the quality of which decreases with increasing defect concentration (c_1, c, f).

8.3.3 Energy methods and bounds

In the previous sections effective elastic properties of a heterogeneous medium have been determined by solving a boundary value problem for an RVE. Various simplifying assumptions therefore had to be made. For instance, the RVE has been taken infinitely large and the effect of distributed inhomogeneities has always been described using the fundamental solution for a single defect. Different assumptions within the micromechanical models lead to different approximative solutions for the effective properties which may strongly deviate from each other and in some cases display an even qualitatively differing behavior (see, e.g., Fig. 8.21). Moreover, no information is provided by the micromechanical models with regard to the accuracy of their results. This lack of accuracy results also from the fact that only a rather limited amount of information about the microstructure (e.g., only the volume fraction of defects) is accounted for in the simple micromechanical models. It is therefore desirable to determine an exact range within which the effective properties of a heterogeneous material are definitely located. This is accomplished by means of extremum principles of elasticity theory which allow to derive strict upper and lower bounds for the effective properties from energetic expressions.

8.3.3.1 Voigt and Reuss bounds

Besides their simplicity the Voigt and Reuss approximations introduced in Section 8.3.2.2 bear the advantage that they are upper and lower bounds for the effective elastic properties of a heterogeneous material. This can be shown from the *principle of minimum potential energy* (1.99) which states that among all kine-

matically admissible strain fields the true strains render the total potential energy a minimum. If displacements are prescribed along the entire boundary ∂V of some volume the potential of the boundary loads vanishes and the total potential energy in case of a kinematically admissible (i.e., not necessarily true!) strain field $\hat{\boldsymbol{\varepsilon}}$ reads $\hat{\Pi}(\hat{\boldsymbol{\varepsilon}}) = \hat{\Pi}^i(\hat{\boldsymbol{\varepsilon}}) = \frac{1}{2}\int_V \hat{\boldsymbol{\varepsilon}} : \boldsymbol{C} : \hat{\boldsymbol{\varepsilon}}\,\mathrm{d}V = \frac{V}{2}\langle \hat{\boldsymbol{\varepsilon}} : \boldsymbol{C} : \hat{\boldsymbol{\varepsilon}}\rangle$. In case of the special boundary condition of *linear* displacements $\boldsymbol{u}|_{\partial V} = \boldsymbol{\varepsilon}^0 \cdot \boldsymbol{x}$ where $\boldsymbol{\varepsilon}^0 = const = \langle \boldsymbol{\varepsilon}\rangle$ the (true) strain energy according to the HILL-condition (8.56) is $\Pi = \frac{V}{2}\langle \boldsymbol{\varepsilon}\rangle : \boldsymbol{C}^* : \langle \boldsymbol{\varepsilon}\rangle$. From the extremum principle $\hat{\Pi}(\hat{\boldsymbol{\varepsilon}}) \geq \Pi$ it then follows that

$$\langle \hat{\boldsymbol{\varepsilon}} : \boldsymbol{C} : \hat{\boldsymbol{\varepsilon}}\rangle \geq \langle \boldsymbol{\varepsilon}\rangle : \boldsymbol{C}^* : \langle \boldsymbol{\varepsilon}\rangle \tag{8.119}$$

for all strain fields $\hat{\boldsymbol{\varepsilon}}$ which satisfy the above boundary condition. Such a strain field is, for instance, given by the VOIGT approximation $\hat{\boldsymbol{\varepsilon}} = const = \langle \boldsymbol{\varepsilon}\rangle$. Insertion into (8.119) yields

$$\langle \boldsymbol{\varepsilon}\rangle : \langle \boldsymbol{C}\rangle : \langle \boldsymbol{\varepsilon}\rangle \geq \langle \boldsymbol{\varepsilon}\rangle : \boldsymbol{C}^* : \langle \boldsymbol{\varepsilon}\rangle$$

or

$$\langle \boldsymbol{\varepsilon}\rangle : \big(\langle \boldsymbol{C}\rangle - \boldsymbol{C}^*\big) : \langle \boldsymbol{\varepsilon}\rangle \geq 0\,. \tag{8.120}$$

In the sense of a quadratic form in $\langle \boldsymbol{\varepsilon}\rangle$ hence the average elasticity tensor $\langle \boldsymbol{C}\rangle$ is larger than $\boldsymbol{C}^*$ and therefore represents an *upper bound* for the effective elasticity tensor.

Analogously, one may start from the *principle of minimum complementary energy* (1.104) where stress fields $\hat{\boldsymbol{\sigma}}$ in order to be admissible have to satisfy equilibrium and prescribed traction boundary conditions. In case of pure traction boundary conditions the complementary energy is given by $\hat{\tilde{\Pi}}(\hat{\boldsymbol{\sigma}}) = \frac{V}{2}\langle \hat{\boldsymbol{\sigma}} : \boldsymbol{C}^{-1} : \hat{\boldsymbol{\sigma}}\rangle$. If, moreover, the boundary tractions are *uniform* $\boldsymbol{t}|_{\partial V} = \boldsymbol{\sigma}^0 \cdot \boldsymbol{n}$ where $\boldsymbol{\sigma}^0 = const = \langle \boldsymbol{\sigma}\rangle$ the (true) complementary energy according to the HILL-condition is $\tilde{\Pi} = \frac{V}{2}\langle \boldsymbol{\sigma}\rangle : \boldsymbol{C}^{*-1} : \langle \boldsymbol{\sigma}\rangle$. From $\hat{\tilde{\Pi}}(\hat{\boldsymbol{\sigma}}) \geq \tilde{\Pi}$ it follows that

$$\langle \hat{\boldsymbol{\sigma}} : \boldsymbol{C}^{-1} : \hat{\boldsymbol{\sigma}}\rangle \geq \langle \boldsymbol{\sigma}\rangle : \boldsymbol{C}^{*-1} : \langle \boldsymbol{\sigma}\rangle \tag{8.121}$$

for all admissible fields $\hat{\boldsymbol{\sigma}}$. One such field is the REUSS approximation $\hat{\boldsymbol{\sigma}} = const = \langle \boldsymbol{\sigma}\rangle$ which yields

$$\langle \boldsymbol{\sigma}\rangle : \big(\langle \boldsymbol{C}^{-1}\rangle - \boldsymbol{C}^{*-1}\big) : \langle \boldsymbol{\sigma}\rangle \geq 0\,. \tag{8.122}$$

In the sense of a quadratic form in $\langle \boldsymbol{\sigma}\rangle$ the Reuss approximation (8.74b) hence represents a lower bound for $\boldsymbol{C}^*$.

When combined the two results state that the effective elasticity tensor always lies in between the VOIGT and REUSS bounds:

$$\boxed{\boldsymbol{C}^*_{(\mathrm{Voigt})} = \langle \boldsymbol{C}\rangle \;\geq\; \boldsymbol{C}^* \;\geq\; \langle \boldsymbol{C}^{-1}\rangle^{-1} = \boldsymbol{C}^*_{(\mathrm{Reuss})}}\,. \tag{8.123}$$

In case of materials with discrete isotropic phases which are isotropically distributed the effective behavior is likewise isotropic and (8.123) can be written in terms of the effective bulk and shear moduli. For a two-phase material we get

$$
\begin{aligned}
K^*_{(\mathrm{Voigt})} = c_{\mathrm{I}} K_{\mathrm{I}} + c_{\mathrm{M}} K_{\mathrm{M}} \;\geq K^* \geq\; \frac{K_{\mathrm{I}} K_{\mathrm{M}}}{c_{\mathrm{I}} K_{\mathrm{M}} + c_{\mathrm{M}} K_{\mathrm{I}}} = K^*_{(\mathrm{Reuss})} \\
\mu^*_{(\mathrm{Voigt})} = c_{\mathrm{I}} \mu_{\mathrm{I}} + c_{\mathrm{M}} \mu_{\mathrm{M}} \;\geq \mu^* \geq\; \frac{\mu_{\mathrm{I}} \mu_{\mathrm{M}}}{c_{\mathrm{I}} \mu_{\mathrm{M}} + c_{\mathrm{M}} \mu_{\mathrm{I}}} = \mu^*_{(\mathrm{Reuss})} \,.
\end{aligned}
\tag{8.124}
$$

The Voigt and Reuss bounds are valid irrespective of the actual microstructure. The underlying approximations of a constant stress or strain field in general violate the compatibility of deformation or the local equilibrium, respectively (see Section 8.3.2.2). In a real microstructure, however, the compatibility of deformation and the local equilibrium are always satisfied, hence the extreme values of the bounds can not be attained. As a consequence, the effective properties of all real microstructures are located truly inside these bounds.

8.3.3.2 Hashin-Shtrikman variational principle and bounds

The Voigt and Reuss bounds which are derived from classical extremum principles of elasticity theory are typically rather far apart from each other which can limit their value considerably. Closer bounds are obtained from a variational principle that has been established by HASHIN and SHTRIKMAN (1962) particularly for heterogeneous materials. In contrast to the total stress and strain fields employed in the above approach now appropriate auxiliary fields are considered which represent only the deviation from some reference solution. In that way the error made in an approximation has a smaller effect on the final result. One such auxiliary field is, for instance, the *stress polarization* $\boldsymbol{\tau}(\boldsymbol{x})$ introduced in Section 8.2.2.1.

In the following we consider a volume V of the heterogeneous material subjected to the boundary condition $\boldsymbol{u}|_{\partial V} = \boldsymbol{\varepsilon}^0 \cdot \boldsymbol{x}$ such that $\boldsymbol{\varepsilon}^0 = const = \langle \boldsymbol{\varepsilon} \rangle$. The stress polarization (8.30) describes the deviation of the true stress from the stress which would be induced by the true strain $\boldsymbol{\varepsilon}(\boldsymbol{x})$ in some homogeneous comparison material with elasticity tensor $\boldsymbol{C}^0$. Using the strain fluctuation $\tilde{\boldsymbol{\varepsilon}}(\boldsymbol{x}) = \boldsymbol{\varepsilon}(\boldsymbol{x}) - \boldsymbol{\varepsilon}^0$ it can be written as

$$
\boldsymbol{\tau}(\boldsymbol{x}) = \Big[\boldsymbol{C}(\boldsymbol{x}) - \boldsymbol{C}^0 \Big] : \Big[\boldsymbol{\varepsilon}^0 + \tilde{\boldsymbol{\varepsilon}}(\boldsymbol{x}) \Big] \,. \tag{8.125}
$$

From the governing equations (8.28) for the fluctuations

$$
\nabla \cdot \tilde{\boldsymbol{\sigma}} = \boldsymbol{0} \,, \qquad \tilde{\boldsymbol{\sigma}} = \boldsymbol{C}^0 : \Big(\tilde{\boldsymbol{\varepsilon}} - \boldsymbol{\varepsilon}^* \Big) \,, \qquad \tilde{\boldsymbol{u}}|_{\partial V} = \boldsymbol{0} \tag{8.126}
$$

one can compute $\tilde{\boldsymbol{\varepsilon}}(\boldsymbol{x})$ which depends upon the equivalent eigenstrain $\boldsymbol{\varepsilon}^*(\boldsymbol{x})$. According to (8.29), (8.30) the latter is linearly related to the stress polarization by $\boldsymbol{\tau}(\boldsymbol{x}) = -\boldsymbol{C}^0 : \boldsymbol{\varepsilon}^*(\boldsymbol{x})$, hence the solution of (8.126) may formally be written as $\tilde{\boldsymbol{\varepsilon}}[\boldsymbol{\tau}(\boldsymbol{x})]$. Insertion into (8.125) yields an equation for $\boldsymbol{\tau}(\boldsymbol{x})$ which thus depends on the macrostrain $\boldsymbol{\varepsilon}^0$:

$$
- \Big[\boldsymbol{C}(\boldsymbol{x}) - \boldsymbol{C}^0 \Big]^{-1} : \boldsymbol{\tau}(\boldsymbol{x}) + \tilde{\boldsymbol{\varepsilon}}[\boldsymbol{\tau}(\boldsymbol{x})] + \boldsymbol{\varepsilon}^0 = \boldsymbol{0} \,. \tag{8.127}
$$

From the calculus of variations it can be shown that (8.127) is equivalent to the *Hashin-Shtrikman variational principle*

$$F(\hat{\boldsymbol{\tau}}) = \frac{1}{V}\int_V \left\{-\hat{\boldsymbol{\tau}} : (\boldsymbol{C}-\boldsymbol{C}^0)^{-1} : \hat{\boldsymbol{\tau}} + \hat{\boldsymbol{\tau}} : \tilde{\boldsymbol{\varepsilon}}[\hat{\boldsymbol{\tau}}] + 2\hat{\boldsymbol{\tau}} : \boldsymbol{\varepsilon}^0\right\} \mathrm{d}V \\ = \text{stationary} \tag{8.128}$$

where $F(\hat{\boldsymbol{\tau}})$ has to be varied with respect to $\hat{\boldsymbol{\tau}}$. Accordingly, among all possible functions $\hat{\boldsymbol{\tau}}$ the true stress polarization $\boldsymbol{\tau}$ renders the expression (functional) $F(\hat{\boldsymbol{\tau}})$ stationary.

In order to gain information about the effective properties $\boldsymbol{C}^*$ we first compute the stationary value of $F(\hat{\boldsymbol{\tau}})$. This is done by inserting the true $\boldsymbol{\tau}$ according to (8.125) and (8.127) into (8.128). Using the Hill-condition the stationary value is found to be $F(\boldsymbol{\tau}) = \boldsymbol{\varepsilon}^0 : (\boldsymbol{C}^* - \boldsymbol{C}^0) : \boldsymbol{\varepsilon}^0$. It can be shown that this value is a maximum if for arbitrary $\boldsymbol{\tau}$ the relation $\boldsymbol{\tau}(\boldsymbol{x}) : \left[\boldsymbol{C}(\boldsymbol{x}) - \boldsymbol{C}^0\right] : \boldsymbol{\tau}(\boldsymbol{x}) \geq 0$ holds, i.e., if the difference $\boldsymbol{C}(\boldsymbol{x}) - \boldsymbol{C}^0$ is positive definite. Conversely, $F(\hat{\boldsymbol{\tau}})$ attains a minimum at $\hat{\boldsymbol{\tau}} = \boldsymbol{\tau}$ if $\boldsymbol{C}(\boldsymbol{x}) - \boldsymbol{C}^0$ is negative definite. It is useful to modify the integral expression (8.128) somewhat. Because of the boundary condition $\tilde{\boldsymbol{u}}|_{\partial V} = \boldsymbol{0}$ in (8.126) the average value of the strain fluctuation must vanish for arbitrary $\hat{\boldsymbol{\tau}}$: $\frac{1}{V}\int_V \tilde{\boldsymbol{\varepsilon}}\,\mathrm{d}V = \boldsymbol{0}$. Then also $\frac{1}{V}\int_V \langle\hat{\boldsymbol{\tau}}\rangle : \tilde{\boldsymbol{\varepsilon}}\,\mathrm{d}V = \boldsymbol{0}$ holds and the second term below the integral in (8.128) can be extended to $(\hat{\boldsymbol{\tau}} - \langle\hat{\boldsymbol{\tau}}\rangle) : \tilde{\boldsymbol{\varepsilon}}$. Hence (8.128) can be written as

$$\boxed{F(\hat{\boldsymbol{\tau}}) \begin{Bmatrix}\leq\\ \geq\end{Bmatrix} \boldsymbol{\varepsilon}^0 : (\boldsymbol{C}^* - \boldsymbol{C}^0) : \boldsymbol{\varepsilon}^0 \quad \text{for} \quad \boldsymbol{C} - \boldsymbol{C}^0 \begin{Bmatrix}\text{pos. def.}\\ \text{neg. def.}\end{Bmatrix}} \tag{8.129a}$$

where

$$F(\hat{\boldsymbol{\tau}}) = \frac{1}{V}\int_V \left\{-\hat{\boldsymbol{\tau}} : (\boldsymbol{C}-\boldsymbol{C}^0)^{-1} : \hat{\boldsymbol{\tau}} + (\hat{\boldsymbol{\tau}} - \langle\hat{\boldsymbol{\tau}}\rangle) : \tilde{\boldsymbol{\varepsilon}}[\hat{\boldsymbol{\tau}}] + 2\hat{\boldsymbol{\tau}} : \boldsymbol{\varepsilon}^0\right\} \mathrm{d}V. \tag{8.129b}$$

For an appropriate choice of the comparison material $\boldsymbol{C}^0$ and some approximation of $\hat{\boldsymbol{\tau}}$ thus $F(\hat{\boldsymbol{\tau}})$ according to (8.129b) yields an upper or lower bound for the expression $\boldsymbol{\varepsilon}^0 : (\boldsymbol{C}^* - \boldsymbol{C}^0) : \boldsymbol{\varepsilon}^0$. The evaluation of these bounds, however, requires the determination of $\tilde{\boldsymbol{\varepsilon}}$ depending on $\hat{\boldsymbol{\tau}}$; this is possible only in special cases.

A special case of great practical importance is a material which consists of n discrete phases with partial volumes $V_\alpha = c_\alpha V$ and piecewise constant elastic properties $\boldsymbol{C}_\alpha$. In this case it seems appropriate to choose a piecewise constant approximation for the stress polarization: $\hat{\boldsymbol{\tau}}(\boldsymbol{x}) = \boldsymbol{\tau}_\alpha = const$ in V_α. With the average value of the latter $\langle\hat{\boldsymbol{\tau}}\rangle = \sum_{\alpha=1}^{n} c_\alpha \boldsymbol{\tau}_\alpha$ and the phase averages of the strain fluctuations $\tilde{\boldsymbol{\varepsilon}}_\alpha = \langle\tilde{\boldsymbol{\varepsilon}}\rangle_\alpha$ the expression $F(\hat{\boldsymbol{\tau}})$ reduces to

$$
\begin{aligned}
F(\boldsymbol{\tau}_\alpha) \;=& -\sum_{\alpha=1}^{n} c_\alpha \boldsymbol{\tau}_\alpha : (\boldsymbol{C}_\alpha - \boldsymbol{C}^0)^{-1} : \boldsymbol{\tau}_\alpha \\
&+ \sum_{\alpha=1}^{n} c_\alpha (\boldsymbol{\tau}_\alpha - \langle \hat{\boldsymbol{\tau}} \rangle) : \tilde{\boldsymbol{\varepsilon}}_\alpha \;+\; 2 \langle \hat{\boldsymbol{\tau}} \rangle : \boldsymbol{\varepsilon}^0 \; .
\end{aligned}
\tag{8.130}
$$

In the eigenstrain problem (8.126) for the determination of the strain fluctuation $\tilde{\boldsymbol{\varepsilon}}$ the individual phases appear only as regions V_α of constant eigenstrain $\boldsymbol{\varepsilon}^*_\alpha = -\boldsymbol{C}^{0\,-1} : \boldsymbol{\tau}_\alpha$ in the homogeneous comparison material (inclusions). It can be shown that in case of isotropy of all phases and their isotropic distribution in an infinitely extended domain the average strain $\tilde{\boldsymbol{\varepsilon}}_\alpha$ of each phase in (8.126) is equal to the (constant) strain inside a spherical inclusion of eigenstrain $\boldsymbol{\varepsilon}^*_\alpha = -\boldsymbol{C}^{0\,-1} : \boldsymbol{\tau}_\alpha$. Using the isotropic Eshelby-tensor $\boldsymbol{S}$ according to (8.10) hence the following relation holds

$$
\tilde{\boldsymbol{\varepsilon}}_\alpha = \boldsymbol{S} : \boldsymbol{\varepsilon}^*_\alpha = -\boldsymbol{S} : \boldsymbol{C}^{0\,-1} : \boldsymbol{\tau}_\alpha
\tag{8.131}
$$

which represents the required solution $\tilde{\boldsymbol{\varepsilon}}[\boldsymbol{\tau}]$ of (8.126). Insertion into (8.130) renders $F(\boldsymbol{\tau}_\alpha)$ an explicit function of the n parameters $\boldsymbol{\tau}_\alpha$. In order to obtain bounds from (8.129a) which are as close as possible the parameters $\boldsymbol{\tau}_\alpha$ have to be chosen in such a way that $F(\boldsymbol{\tau}_\alpha)$ becomes extremal. The necessary conditions

$$
\frac{\partial F}{\partial \boldsymbol{\tau}_\alpha} = 0
\tag{8.132}
$$

yield the n equations

$$
\boldsymbol{\tau}_\alpha : (\boldsymbol{C}_\alpha - \boldsymbol{C}^0)^{-1} + (\boldsymbol{\tau}_\alpha - \langle \hat{\boldsymbol{\tau}} \rangle) : \boldsymbol{S} : \boldsymbol{C}^{0\,-1} = \boldsymbol{\varepsilon}^0
\tag{8.133}
$$

for the determination of the "optimal" parameters $\boldsymbol{\tau}_\alpha(\boldsymbol{\varepsilon}^0)$. The latter depend linearly on $\boldsymbol{\varepsilon}^0$ and after insertion into $F(\boldsymbol{\tau}_\alpha)$ the left-hand side of the inequality in (8.129a) is a quadratic expression in $\boldsymbol{\varepsilon}^0$. In the sense of a quadratic form in $\boldsymbol{\varepsilon}^0$ (8.129a) thus leads to upper and lower bounds for $\boldsymbol{C}^*$; these bounds are referred to as the *Hashin-Shtrikman bounds*.

As an important special case we consider a heterogeneous material which consists of two isotropic phases with elastic constants $\boldsymbol{C}_{\mathrm{M}}$ and $\boldsymbol{C}_{\mathrm{I}}$ or K_{M}, μ_{M} and K_{I}, μ_{I}, respectively. If we assume $K_{\mathrm{M}} < K_{\mathrm{I}}$ and $\mu_{\mathrm{M}} < \mu_{\mathrm{I}}$ it is possible to choose the elastic properties of one of the phases as those of the homogeneous comparison material which guarantees the positive definiteness of $\boldsymbol{C} - \boldsymbol{C}^0$. Another advantage of this choice is that the stress polarization of one of the phases according to (8.133) vanishes. First we consider the case $\boldsymbol{C}^0 = \boldsymbol{C}_{\mathrm{M}}$ such that $\boldsymbol{\tau}_{\mathrm{M}} = 0$ and $\langle \boldsymbol{\tau} \rangle = c_{\mathrm{I}} \boldsymbol{\tau}_{\mathrm{I}}$. Using (8.130) then (8.129b) reduces to

$$
\begin{aligned}
F(\boldsymbol{\tau}_{\mathrm{I}}) &= -c_{\mathrm{I}} \boldsymbol{\tau}_{\mathrm{I}} : \Big[(\boldsymbol{C}_{\mathrm{I}} - \boldsymbol{C}_{\mathrm{M}})^{-1} : \boldsymbol{\tau}_{\mathrm{I}} + c_{\mathrm{M}} \boldsymbol{S}_{\mathrm{M}} : \boldsymbol{C}_{\mathrm{M}}^{-1} : \boldsymbol{\tau}_{\mathrm{I}} - 2\boldsymbol{\varepsilon}^0 \Big] \\
&\leq \boldsymbol{\varepsilon}^0 : (\boldsymbol{C}^* - \boldsymbol{C}_{\mathrm{M}}) : \boldsymbol{\varepsilon}^0 \; .
\end{aligned}
\tag{8.134}
$$

Exploiting the symmetry of the elasticity tensors and of the Eshelby-tensor and using (8.96a) the extremal condition $\partial F/\partial \boldsymbol{\tau}_{\mathrm{I}} = 0$ yields

$$\boldsymbol{\tau}_{\mathrm{I}} = \left[(\boldsymbol{C}_{\mathrm{I}}-\boldsymbol{C}_{\mathrm{M}})^{-1}+ c_{\mathrm{M}}\boldsymbol{S}_{\mathrm{M}}:\boldsymbol{C}_{\mathrm{M}}^{-1}\right]^{-1} : \boldsymbol{\varepsilon}^0 = \boldsymbol{A}_{\mathrm{I}\,(\mathrm{MT})} : (\boldsymbol{C}_{\mathrm{I}}-\boldsymbol{C}_{\mathrm{M}}):\boldsymbol{\varepsilon}^0. \quad (8.135)$$

The fact that the right-hand side can be written in terms of the influence tensor (8.96a) indicates a remarkable interrelation between the Mori-Tanaka model and the Hashin-Shtrikman variational principle in the special case of isotropy. Insertion of (8.135) into (8.134) leads to $F(\boldsymbol{\tau}_{\mathrm{I}}) = c_{\mathrm{I}}\boldsymbol{\tau}_{\mathrm{I}} : \boldsymbol{\varepsilon}^0 = \langle\boldsymbol{\tau}\rangle : \boldsymbol{\varepsilon}^0$ where the latter expression is valid also for an n-phase material. The inequality (8.134) can be transformed into

$$\boldsymbol{\varepsilon}^0 : \left(\boldsymbol{C}_{\mathrm{M}} + c_{\mathrm{I}}\left[(\boldsymbol{C}_{\mathrm{I}} - \boldsymbol{C}_{\mathrm{M}})^{-1} + c_{\mathrm{M}}\boldsymbol{S}_{\mathrm{M}} : \boldsymbol{C}_{\mathrm{M}}^{-1}\right]^{-1}\right) : \boldsymbol{\varepsilon}^0 \le \boldsymbol{\varepsilon}^0 : \boldsymbol{C}^* : \boldsymbol{\varepsilon}^0 \quad (8.136)$$

and yields the *lower Hashin-Shtrikman bound*

$$\boldsymbol{C}^*_{(\mathrm{HS}^-)} = \boldsymbol{C}_{\mathrm{M}} + c_{\mathrm{I}}\left[(\boldsymbol{C}_{\mathrm{I}} - \boldsymbol{C}_{\mathrm{M}})^{-1} + c_{\mathrm{M}}\boldsymbol{S}_{\mathrm{M}} : \boldsymbol{C}_{\mathrm{M}}^{-1}\right]^{-1} \quad (8.137a)$$

for the effective elasticity tensor. It coincides with the result (8.96a), (8.97) of the Mori-Tanaka model .

If the stiffer material is chosen as the comparison material ($\boldsymbol{C}^0 = \boldsymbol{C}_{\mathrm{I}}$) the analogous procedure leads to the *upper Hashin-Shtrikman bound*

$$\boldsymbol{C}^*_{(\mathrm{HS}^+)} = \boldsymbol{C}_{\mathrm{I}} + c_{\mathrm{M}}\left[(\boldsymbol{C}_{\mathrm{M}} - \boldsymbol{C}_{\mathrm{I}})^{-1} + c_{\mathrm{I}}\boldsymbol{S}_{\mathrm{I}} : \boldsymbol{C}_{\mathrm{I}}^{-1}\right]^{-1} . \quad (8.137b)$$

It corresponds to the Mori-Tanaka result if the properties of the matrix material and the inhomogeneity are exchanged. The effective elasticity tensor hence is subject to the restriction (in the sense of a quadratic form)

$$\boxed{\boldsymbol{C}^*_{(\mathrm{HS}^+)} \ge \boldsymbol{C}^* \ge \boldsymbol{C}^*_{(\mathrm{HS}^-)}} . \quad (8.138)$$

Because of the isotropy assumed for the phase properties and the macroscopic distribution it follows that

$$K^*_{(\mathrm{HS}^+)} \ge K^* \ge K^*_{(\mathrm{HS}^-)} \qquad \text{and} \qquad \mu^*_{(\mathrm{HS}^+)} \ge \mu^* \ge \mu^*_{(\mathrm{HS}^-)} \quad (8.139)$$

where

$$\begin{aligned}
K^*_{(\mathrm{HS}^-)} &= K_{\mathrm{M}} + c_{\mathrm{I}}\left(\frac{1}{K_{\mathrm{I}} - K_{\mathrm{M}}} + \frac{3\,c_{\mathrm{M}}}{3K_{\mathrm{M}} + 4\mu_{\mathrm{M}}}\right)^{-1}, \\
K^*_{(\mathrm{HS}^+)} &= K_{\mathrm{I}} + c_{\mathrm{M}}\left(\frac{1}{K_{\mathrm{M}} - K_{\mathrm{I}}} + \frac{3\,c_{\mathrm{I}}}{3K_{\mathrm{I}} + 4\mu_{\mathrm{I}}}\right)^{-1}, \\
\mu^*_{(\mathrm{HS}^-)} &= \mu_{\mathrm{M}} + c_{\mathrm{I}}\left(\frac{1}{\mu_{\mathrm{I}} - \mu_{\mathrm{M}}} + \frac{6\,c_{\mathrm{M}}\,(K_{\mathrm{M}} + 2\mu_{\mathrm{M}})}{5\,\mu_{\mathrm{M}}(3K_{\mathrm{M}} + 4\mu_{\mathrm{M}})}\right)^{-1},
\end{aligned} \quad (8.140)$$

$$\mu^*_{(\mathrm{HS}^+)} = \mu_{\mathrm{I}} + c_{\mathrm{M}} \left(\frac{1}{\mu_{\mathrm{M}} - \mu_{\mathrm{I}}} + \frac{6\, c_{\mathrm{I}}\, (K_{\mathrm{I}} + 2\mu_{\mathrm{I}})}{5\, \mu_{\mathrm{I}} (3K_{\mathrm{I}} + 4\mu_{\mathrm{I}})} \right)^{-1} .$$

The range described by the Hashin-Shtrikman bounds (8.139), (8.140) inside which the effective elastic properties of a heterogeneous material can be found is much more narrow than that given by the Voigt and Reuss bounds (8.124). For special microstructures it can furthermore by shown that the effective bulk modulus can indeed attain the value of the upper or (by exchange of the properties of matrix and inhomogeneity) the lower Hashin-Shtrikman bound. This is the case, for instance, in the so-called *composite spheres model* where the entire space is filled with spherical inhomogeneities of different size, each surrounded by a matrix shell the radius of which is chosen in a fixed ratio to the radius of the enclosed sphere (see e.g., R.M. CHRISTENSEN, 1979). Since they can actually be attained, the bounds $K^*_{(\mathrm{HS}^+)}$ and $K^*_{(\mathrm{HS}^-)}$ are the best possible, i.e. closest, bounds that can be found solely in terms of phase properties and volume fractions.

For the special case of a two-phase material with $K_{\mathrm{I}} = 10K_{\mathrm{M}}$ and $\mu_{\mathrm{I}} = 10\mu_{\mathrm{M}}$ the Hashin-Shtrikman and Voigt-Reuss bounds are shown in Fig. 8.22 in terms of the effective bulk modulus as a function of the volume fraction c_{I} along with approximations according to the self-consistent method and the differential scheme. Respective results for the effective shear modulus display a qualitatively similar behavior. As expected, the range of possible effective material properties described by the Hashin-Shtrikman bounds is significantly closer than that given by the Voigt-Reuss bounds. The Hashin-Shtrikman bounds are equal the two results of the Mori-Tanaka model obtained when the properties of matrix and inhomogeneity are exchanged. These two solutions are for small or large volume fractions asymptotically approached by the result of the self-consistent method which does not consider a dis-

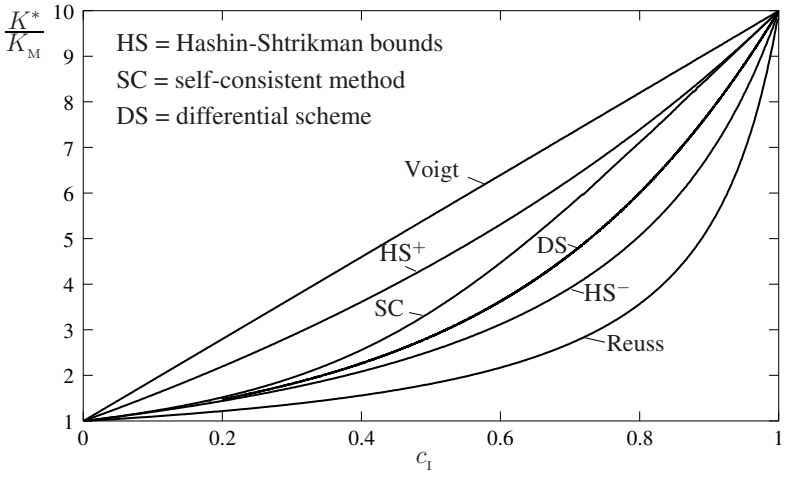

Fig. 8.22 Effective bulk modulus for $K_{\mathrm{I}} = 10K_{\mathrm{M}}$, $\mu_{\mathrm{I}} = 10\mu_{\mathrm{M}}$

tinguished matrix phase. For small values of c_{I} this asymptotic behavior corresponds to the solution (not shown here) in case of a dilute distribution of inhomogeneities.

In the limit case of one rigid phase $(K_{\text{I}} \to \infty\,,\ \mu_{\text{I}} \to \infty)$ an infinitely high upper Hashin-Shtrikman bound results from (8.140), exactly as the Voigt bound (8.77). Correspondingly, the lower Hashin-Shtrikman bound as well as the Reuss bound (8.76) is zero in case of a material with voids.

The evaluation of the Hashin-Shtrikman variational principle in case of an n-phase material can be performed analogous to the above procedure. It is, however, much more laborious since it requires the determination of $n-1$ parameters $\boldsymbol{\tau}_\alpha$. Various generalizations of this method with regard to anisotropic, periodic, or stochastic microstructures as well as to nonlinear material behavior can be found in the special literature.

8.4 Homogenization of elastic-plastic materials

Real materials often show an inelastic behavior and have to be described by nonlinear stress-strain relations. The micromechanical models and homogenization techniques discussed so far then are no longer applicable since they are based on the assumption of a linear elastic material behavior and the availability of respective fundamental solutions. More far-reaching considerations hence are necessary for the investigation of micro-heterogeneous inelastic materials. In the following we focus on the case of rate-independent plasticity (see Section 1.3.3).

Micromechanics allows to grasp the notion of plasticity in a rather general context and consider a variety of different microscopic processes which all are the source of the macroscopic phenomenon of permanent *plastic* deformations. Examples are the various multiscale mechanisms of metal plasticity such as dislocation glide and grain boundary sliding but also frictional sliding along distributed microcracks in brittle rock. Within this introductory treatment, however, we will restrict to a material description in the framework of phenomenological elasto-plasticity according to Section 1.3.3. This still allows to investigate important classes of materials such as metal matrix composites or metal-infiltrated ceramics as well as the role of porosity in the course of damage of ductile materials (see Chapter 9).

8.4.1 Foundations

We consider a volume V on the microscopic level of a heterogeneous material (Fig. 8.23a) where the constitutive equations according to Section 1.3.3 hold. The elastic-plastic material behavior (microstructure) then is characterized in terms of the spatially varying elasticity tensor $\boldsymbol{C}(\boldsymbol{x})$ and the likewise spatially varying *yield condition*

$$F\Big(\boldsymbol{\sigma}(\boldsymbol{x}),\, \boldsymbol{x}\Big) \le 0\,. \tag{8.141}$$

The latter describes the set of all admissible stress states which in addition must satisfy the equilibrium condition $\nabla \cdot \boldsymbol{\sigma}(\boldsymbol{x}) = \mathbf{0}$. Via the elasticity law they are related to the elastic strains $\boldsymbol{\varepsilon}^e(\boldsymbol{x})$ which according to (1.73) are additively composed with the plastic strains $\boldsymbol{\varepsilon}^p(\boldsymbol{x})$ to the total strains:

$$\boldsymbol{\sigma} = \boldsymbol{C}(\boldsymbol{x}) : \boldsymbol{\varepsilon}^e = \boldsymbol{C}(\boldsymbol{x}) : \left(\boldsymbol{\varepsilon} - \boldsymbol{\varepsilon}^p \right) . \tag{8.142}$$

These equations are supplemented by the *flow rule* (1.82) for the plastic strain increments $\dot{\boldsymbol{\varepsilon}}^p$ in the framework of the incremental theory or by (1.86) in the framework of deformation theory.

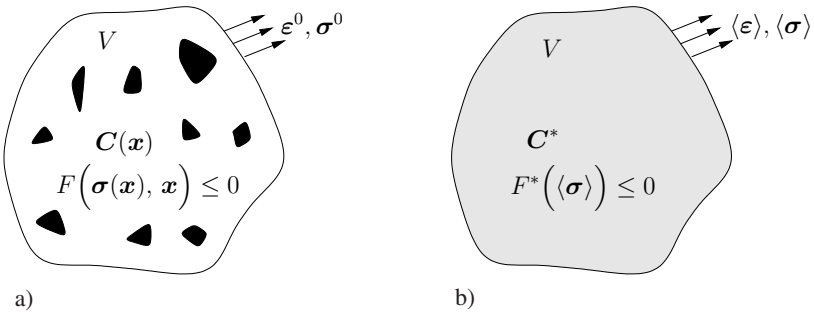

Fig. 8.23 a) Micro-heterogeneous elastic-plastic material, b) homogenized material

In order to describe the macroscopic *effective* behavior of the material, in the following we are looking for relations between the macroscopic stresses $\langle\boldsymbol{\sigma}\rangle$ and strains $\langle\boldsymbol{\varepsilon}\rangle$ (or their increments, respectively) defined as volume averages over the domain V according to (8.41). Analogous to the situation of elastic materials homogeneous boundary conditions $\boldsymbol{\varepsilon}^0$ or $\boldsymbol{\sigma}^0$ are therefore prescribed (Fig. 8.23a). One of the macroscopic quantities then is in either case already known from the relations (8.60a) or (8.60b) which are independent of the material behavior.

8.4.1.1 Plastic and elastic macrostrains

As already mentioned, the macroscopic strains $\langle\boldsymbol{\varepsilon}\rangle$ are defined as volume averages of the microscopic strains $\boldsymbol{\varepsilon}(\boldsymbol{x})$. Such a simple relation, however, does not hold for the plastic and elastic parts of the macroscopic strains. We want to investigate how the spatially distributed plastic and elastic strains $\boldsymbol{\varepsilon}^p(\boldsymbol{x})$ and $\boldsymbol{\varepsilon}^e(\boldsymbol{x})$ on the microscopic level are transferred to the macroscale. In addition to the original problem we therefore consider a purely *elastic comparison problem* for the heterogeneous volume subjected to the same boundary conditions, yet with vanishing plastic strains. The corresponding fields are indicated with a tilde. They are statically and kinematically admissible and can for both types of homogeneous boundary conditions be represented in terms of the influence tensors introduced in (8.62a) and (8.62b):

$$\begin{aligned} &\text{a)}\ \boldsymbol{u}|_{\partial V} = \boldsymbol{\varepsilon}^0 \cdot \boldsymbol{x} \ : \qquad \tilde{\boldsymbol{\varepsilon}}^{(\mathrm{a})}(\boldsymbol{x}) = \boldsymbol{A}(\boldsymbol{x}) : \boldsymbol{\varepsilon}^0 \,, \qquad \langle \tilde{\boldsymbol{\varepsilon}}^{(\mathrm{a})} \rangle = \langle \boldsymbol{\varepsilon} \rangle = \boldsymbol{\varepsilon}^0 \,, \\ &\text{b)}\ \boldsymbol{t}|_{\partial V} = \boldsymbol{\sigma}^0 \cdot \boldsymbol{n} \ : \qquad \tilde{\boldsymbol{\sigma}}^{(\mathrm{b})}(\boldsymbol{x}) = \boldsymbol{B}(\boldsymbol{x}) : \boldsymbol{\sigma}^0 \,, \qquad \langle \tilde{\boldsymbol{\sigma}}^{(\mathrm{b})} \rangle = \langle \boldsymbol{\sigma} \rangle = \boldsymbol{\sigma}^0 \,. \end{aligned} \tag{8.143}$$

The stresses are given by $\tilde{\boldsymbol{\sigma}}^{(\mathrm{a})} = \boldsymbol{C} : \tilde{\boldsymbol{\varepsilon}}^{(\mathrm{a})}$ or $\tilde{\boldsymbol{\sigma}}^{(\mathrm{b})} = \boldsymbol{C} : \tilde{\boldsymbol{\varepsilon}}^{(\mathrm{b})}$, respectively. If in case of the boundary condition (a) the elasticity law (8.142) is multiplied by $\tilde{\boldsymbol{\varepsilon}}^{(a)}(\boldsymbol{x})$ and the volume average over V is taken one obtains

$$\langle \boldsymbol{\sigma} : \tilde{\boldsymbol{\varepsilon}}^{(\mathrm{a})} \rangle = \langle \boldsymbol{\varepsilon} : \overbrace{\boldsymbol{C} : \underbrace{\boldsymbol{A} : \boldsymbol{\varepsilon}^0}_{\tilde{\boldsymbol{\varepsilon}}^{(\mathrm{a})}}}^{\tilde{\boldsymbol{\sigma}}^{(\mathrm{a})}} \rangle - \langle \boldsymbol{\varepsilon}^p : \boldsymbol{C} : \boldsymbol{A} : \boldsymbol{\varepsilon}^0 \rangle \,.$$

Since the fields $\tilde{\boldsymbol{\varepsilon}}^{(\mathrm{a})}$ and $\tilde{\boldsymbol{\sigma}}^{(\mathrm{a})}$ as well as $\boldsymbol{\varepsilon}$ and $\boldsymbol{\sigma}$ are kinematically and statically admissible the above relation, using (8.61) and (8.65a), can be transformed according to

$$\langle \boldsymbol{\sigma} \rangle : \boldsymbol{\varepsilon}^0 = \langle \boldsymbol{\varepsilon} \rangle : \langle \boldsymbol{C} : \boldsymbol{A} \rangle : \boldsymbol{\varepsilon}^0 - \langle \boldsymbol{\varepsilon}^p : \boldsymbol{C} : \boldsymbol{A} \rangle : \boldsymbol{\varepsilon}^0 = \langle \boldsymbol{\varepsilon} \rangle : \boldsymbol{C}^* : \boldsymbol{\varepsilon}^0 - \langle \boldsymbol{\varepsilon}^p : \boldsymbol{C} : \boldsymbol{A} \rangle : \boldsymbol{\varepsilon}^0 \,.$$

Since this holds for arbitrary $\boldsymbol{\varepsilon}^0$ one obtains the macroscopic stress-strain relation

$$\boxed{\langle \boldsymbol{\sigma} \rangle = \boldsymbol{C}^* : \Big(\langle \boldsymbol{\varepsilon} \rangle - \boldsymbol{\mathcal{E}}^p \Big)} \tag{8.144}$$

with the representation

$$\boxed{\boldsymbol{\mathcal{E}}^p = \boldsymbol{C}^{*\,-1} : \langle \boldsymbol{\varepsilon}^p : \boldsymbol{C} : \boldsymbol{A} \rangle} \tag{8.145a}$$

for the macroscopic plastic strain. Correspondingly, the macroscopic elastic strain is given by

$$\boxed{\boldsymbol{\mathcal{E}}^e = \langle \boldsymbol{\varepsilon} \rangle - \boldsymbol{\mathcal{E}}^p = \boldsymbol{C}^{*\,-1} : \langle \boldsymbol{\varepsilon}^e : \boldsymbol{C} : \boldsymbol{A} \rangle} \,. \tag{8.145b}$$

Thus the macroscopic elastic and plastic strains are indeed not the ordinary volume averages but the *weighted averages* of the respective microfields where the elastic heterogeneity in terms of the tensors $\boldsymbol{C}$ and $\boldsymbol{A}$ serves as the weighting factor. Only in case of an elastically homogeneous material ($\boldsymbol{C} = const$, $\boldsymbol{A} = \boldsymbol{1}$) or for homogeneous elastic and plastic strains is $\boldsymbol{\mathcal{E}}^p = \langle \boldsymbol{\varepsilon}^p \rangle$ and $\boldsymbol{\mathcal{E}}^e = \langle \boldsymbol{\varepsilon}^e \rangle$.

In case of the boundary condition (b) the analogous procedure utilizing the elastic comparison field $\tilde{\boldsymbol{\sigma}}^{(\mathrm{b})}$ leads to the somewhat shorter representation

$$\boldsymbol{\mathcal{E}}^{p,e} = \langle \boldsymbol{\varepsilon}^{p,e} : \boldsymbol{B} \rangle \tag{8.146}$$

where the effective elasticity tensor is given by (8.65b). For a representative volume element (RVE) both representations must coincide.

8.4.1.2 Elastic energy and dissipation

When after some amount of plastic flow a micro-heterogeneous elastic-plastic material is macroscopically unloaded ($\langle\boldsymbol{\sigma}\rangle \to \mathbf{0}$), a complete local unloading ($\boldsymbol{\sigma}(\boldsymbol{x}) \to \mathbf{0}$) generally does not take place in all points $\boldsymbol{x}$ of the microscopic level. Elastic energy remains stored in an inhomogeneous residual stress field (eigenstress field). For a closer inspection of this effect we consider a material which behaves *elastic-perfectly plastic* on the microscopic level. Energy storage then is possible only by elastic strains and the strain energy density reads

$$U(\boldsymbol{x}) = \frac{1}{2}\,\boldsymbol{\varepsilon}^e : \boldsymbol{C}(\boldsymbol{x}) : \boldsymbol{\varepsilon}^e \,. \tag{8.147}$$

Considering the boundary condition (b) of prescribed macrostress $\langle\boldsymbol{\sigma}\rangle = \boldsymbol{\sigma}^0$ we introduce an auxiliary field $\boldsymbol{\sigma}^r(\boldsymbol{x})$ which describes the deviation of the true stress $\boldsymbol{\sigma}(\boldsymbol{x})$ of the elastic-plastic problem from the stress $\tilde{\boldsymbol{\sigma}}^{(\mathrm{b})}(\boldsymbol{x})$ in a purely elastic comparison problem:

$$\boldsymbol{\sigma}^r(\boldsymbol{x}) = \boldsymbol{\sigma}(\boldsymbol{x}) - \tilde{\boldsymbol{\sigma}}^{(\mathrm{b})}(\boldsymbol{x}) = \boldsymbol{\sigma}(\boldsymbol{x}) - \boldsymbol{B}(\boldsymbol{x}) : \boldsymbol{\sigma}^0 \,. \tag{8.148}$$

In case of macroscopic unloading ($\boldsymbol{\sigma}^0 = \mathbf{0}$) this auxiliary field is equal to the residual stress prevailing in the volume V. Obviously this field has the properties

$$\nabla\cdot\boldsymbol{\sigma}^r = \mathbf{0} \quad \text{in } V\,, \qquad \boldsymbol{\sigma}^r\cdot\boldsymbol{n} = \mathbf{0} \quad \text{on } \partial V\,, \qquad \langle\boldsymbol{\sigma}^r\rangle = 0 \tag{8.149}$$

and vanishes only for vanishing plastic strains $\boldsymbol{\varepsilon}^p$ throughout the volume V. Using (8.148) the elastic strain field in (8.147) can be replaced by

$$\boldsymbol{\varepsilon}^e = \boldsymbol{C}^{-1}(\boldsymbol{x}) : \boldsymbol{\sigma} = \boldsymbol{C}^{-1}(\boldsymbol{x}) : \big(\boldsymbol{B}(\boldsymbol{x}) : \boldsymbol{\sigma}^0 + \boldsymbol{\sigma}^r\big) \,. \tag{8.150}$$

Volume averaging over V then leads to

$$\begin{aligned}\langle U\rangle &= \frac{1}{2}\,\big\langle \big(\boldsymbol{C}^{-1}\colon\boldsymbol{B} : \boldsymbol{\sigma}^0 + \boldsymbol{C}^{-1}\colon\boldsymbol{\sigma}^r\big) : \boldsymbol{C} : \big(\boldsymbol{C}^{-1}\colon\boldsymbol{B} : \boldsymbol{\sigma}^0 + \boldsymbol{C}^{-1}\colon\boldsymbol{\sigma}^r\big)\big\rangle \\ &= \frac{1}{2}\,\boldsymbol{\sigma}^0 \colon \underbrace{\langle \boldsymbol{B}^T\colon\boldsymbol{C}^{-1}\colon\boldsymbol{B}\rangle}_{\boldsymbol{C}^{*\,-1},\ \text{see (8.66)}} : \boldsymbol{\sigma}^0 \;+\; \frac{1}{2}\,\langle\boldsymbol{\sigma}^r\colon\boldsymbol{C}^{-1}\colon\boldsymbol{\sigma}^r\rangle + \underbrace{\langle\boldsymbol{\sigma}^r\colon\boldsymbol{C}^{-1}\colon\underbrace{\boldsymbol{B}:\boldsymbol{\sigma}^0}_{\tilde{\boldsymbol{\sigma}}^{(\mathrm{b})}}\rangle}_{\tilde{\boldsymbol{\varepsilon}}^{(\mathrm{b})}} \,.\end{aligned}$$

The last expression in brackets vanishes because of (8.149) and (8.61) and the average strain energy density in V reads

$$\boxed{\langle U\rangle \;=\; \frac{1}{2}\underbrace{\boldsymbol{\sigma}^0 : \boldsymbol{C}^{*\,-1} : \boldsymbol{\sigma}^0}_{\boldsymbol{\mathcal{E}}^e\,:\,\boldsymbol{C}^*\,:\,\boldsymbol{\mathcal{E}}^e} + \frac{1}{2}\,\langle\boldsymbol{\sigma}^r : \boldsymbol{C}^{-1} : \boldsymbol{\sigma}^r\rangle} \,. \tag{8.151}$$

The first term describes the energy due to the macroscopic elastic strains while the second term represents the effect of the heterogeneous residual stress field.

If the material behavior on the microscopic level is perfectly plastic the work done by the stresses on the plastic strains is entirely dissipated and the average dissipation (power) in some volume V reads

$$\mathcal{D} = \langle \boldsymbol{\sigma} : \dot{\boldsymbol{\varepsilon}}^p \rangle \, . \tag{8.152}$$

Using the incremental forms of (8.61) and (8.149) and the auxiliary field

$$\dot{\boldsymbol{\sigma}}^r(\boldsymbol{x}) = \dot{\boldsymbol{\sigma}}(\boldsymbol{x}) - \boldsymbol{B}(\boldsymbol{x}) : \dot{\boldsymbol{\sigma}}^0 = \underbrace{\boldsymbol{C}(\boldsymbol{x}) : \left(\dot{\boldsymbol{\varepsilon}}(\boldsymbol{x}) - \dot{\boldsymbol{\varepsilon}}^p(\boldsymbol{x}) \right)}_{\dot{\boldsymbol{\sigma}}(\boldsymbol{x})} - \boldsymbol{B}(\boldsymbol{x}) : \underbrace{\boldsymbol{C}^* : \left(\langle \dot{\boldsymbol{\varepsilon}} \rangle - \dot{\boldsymbol{\mathcal{E}}}^p \right)}_{\dot{\boldsymbol{\sigma}}^0}$$

the following relation can be derived

$$\boxed{\mathcal{D} = \langle \boldsymbol{\sigma} \rangle : \dot{\boldsymbol{\mathcal{E}}}^p - \frac{1}{2} \langle \boldsymbol{\sigma}^r : \boldsymbol{C}^{-1} : \boldsymbol{\sigma}^r \rangle^{\cdot}} \, . \tag{8.153}$$

It states that the power of the macroscopic stresses done on the macroscopic plastic strains is only partly dissipated; the remaining part is stored as the elastic energy of the residual stress field.

The results (8.51) and (8.153) obtained here for the boundary condition (b) of prescribed macrostress $\boldsymbol{\sigma}^0$ can also be derived in case of prescribed macrostrain $\boldsymbol{\varepsilon}^0$. Instead of (8.148) one then has to make use of the auxiliary strain field

$$\boldsymbol{\varepsilon}^r(\boldsymbol{x}) = \boldsymbol{\varepsilon}^e(\boldsymbol{x}) - \boldsymbol{A}(\boldsymbol{x}) : \boldsymbol{\mathcal{E}}^e \tag{8.154}$$

and its incremental form. If the volume V considered for averaging is statistically representative (RVE) both approaches are equivalent and the auxiliary fields are related to each other by $\boldsymbol{\sigma}^r(\boldsymbol{x}) = \boldsymbol{C}(\boldsymbol{x}) : \boldsymbol{\varepsilon}^r(\boldsymbol{x})$.

8.4.1.3 Macroscopic yield condition

If at some point on the microscopic level plastic flow takes place with $\dot{\boldsymbol{\varepsilon}}^p \neq \boldsymbol{0}$ the stress state $\boldsymbol{\sigma}$ at this point is according to (8.141) located on the yield surface $F = 0$. For stress states inside the yield surface ($F < 0$) the material behaves elastically. Again we consider a microscopically *elastic-perfectly plastic* material where the yield surface is not altered by plastic flow (i.e., no hardening on the microscopic level). However, the size and shape of the yield surface may spatially vary on the microscale due to the heterogeneous material properties. In order to investigate which consequences this has for the macroscopic stress $\langle \boldsymbol{\sigma} \rangle$ we consider some volume V subjected to the boundary condition $\langle \boldsymbol{\sigma} \rangle = \boldsymbol{\sigma}^0$ (Fig. 8.23).

First, we proceed from a situation where nowhere in V plastic flow has taken place: $\boldsymbol{\varepsilon}^p(\boldsymbol{x}) = \boldsymbol{0}$. The stress field throughout V then is purely elastic and can

according to (8.62b) be written as $\boldsymbol{\sigma}(\boldsymbol{x}) = \boldsymbol{B}(\boldsymbol{x}) : \langle\boldsymbol{\sigma}\rangle$. Insertion into the yield condition (8.141) for every point $\boldsymbol{x}$ yields the following (infinitely many) conditions for the macroscopic stress state $\langle\boldsymbol{\sigma}\rangle$

$$F\Big(\boldsymbol{B}(\boldsymbol{x}) : \langle\boldsymbol{\sigma}\rangle,\, \boldsymbol{x}\Big) \equiv F_x^*\Big(\langle\boldsymbol{\sigma}\rangle\Big) \leq 0 \qquad \text{for every } \boldsymbol{x} \text{ in } V \tag{8.155}$$

which may formally be combined to the *macroscopic yield condition*

$$\boxed{F^*\Big(\langle\boldsymbol{\sigma}\rangle\Big) \leq 0}\,. \tag{8.156}$$

The set of all admissible macroscopic stress states satisfying (8.156) is the *intersection* of all $\langle\boldsymbol{\sigma}\rangle$ for which (8.155) holds in every point $\boldsymbol{x}$ of V. For an illustration we consider two such points $\boldsymbol{x}_a$ and $\boldsymbol{x}_b$ and represent the corresponding yield surfaces by contours in the 1,2-plane of the principal stress space (Fig. 8.24). The shaded re-

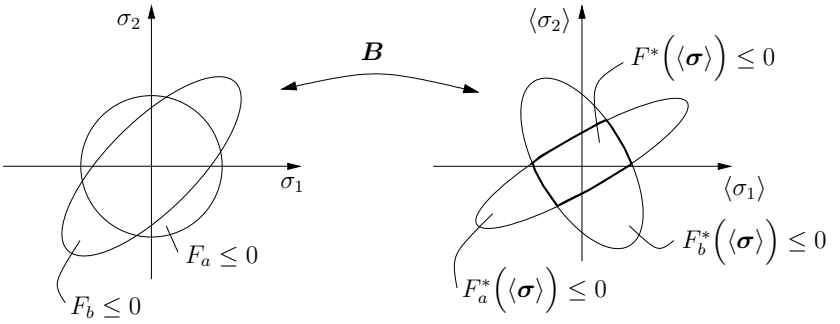

Fig. 8.24 Elastic domains and yield surfaces on the microscopic (left) and macroscopic (right) level

gion characterizes the set of all macroscopic stress states $\langle\boldsymbol{\sigma}\rangle$ for which the resulting microstress fields $\boldsymbol{\sigma}(\boldsymbol{x})$ satisfy the condition (8.141) at *both* points $\boldsymbol{x}_a$ and $\boldsymbol{x}_b$. The influence tensor $\boldsymbol{B}$ transforms, as a linear mapping, the convex microscopic yield surfaces $F_{a,b} = 0$ into the likewise convex surfaces $F_{a,b}^* = 0$; being the intersection of the latter the shaded region of admissible macroscopic stress states is convex as well. Since macroscopic stress states which cause plastic flow are necessarily located on the boundary of the shaded region this boundary can be interpreted as the *macroscopic yield surface* $F^*(\langle\boldsymbol{\sigma}\rangle) = 0$.

Moreover, from (8.156) or (8.155) it is obvious that plastic flow is macroscopically not noticable if it takes place only in a single point on the microscopic level (say $\boldsymbol{x}_a$ *or* $\boldsymbol{x}_b$ in Fig. 8.24). Because of this it can be shown that the macroscopic yield surface initially must have a *vertex* at a stress state that causes macroscopic plastic flow (such as one of the intersection points of the surfaces $F_a^* = 0$ and $F_b^* = 0$ in Fig. 8.24). Despite this theoretical argument, however, it has to be mentioned that such a vertex is in practice hardly measurable.

In order to investigate the effect of preceding plastic flow on the macroscopic yield surface, now we consider a point $\boldsymbol{x}$ on the microscopic level at which some amount of plastic flow $\boldsymbol{\varepsilon}^p \neq \mathbf{0}$ has already taken place and where the local stress state $\boldsymbol{\sigma}$ is located on the yield surface (Fig. 8.25). The corresponding macroscopic stress state $\langle\boldsymbol{\sigma}\rangle$ is located on the macroscopic yield surface. Due to the plastic defor-

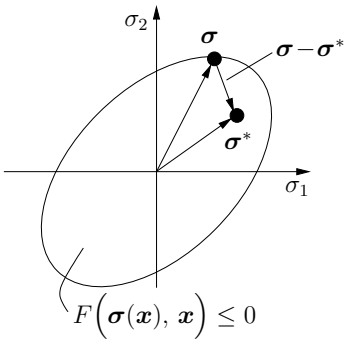

Fig. 8.25 Elastic unloading on the microscopic level

mation the auxiliary field (8.148) then is no longer zero: $\boldsymbol{\sigma}^r(\boldsymbol{x}) \neq \mathbf{0}$. Unloading at point $\boldsymbol{x}$ leads to a microscopic stress state $\boldsymbol{\sigma}^*$ inside the elastic range (Fig. 8.25). If unloading takes place at all points on the microscopic level the macroscopic stress state attains a value $\langle\boldsymbol{\sigma}\rangle^*$ inside the macroscopic elastic range. The relation between the change of the microstress field and the macroscopic stress state then can be expressed in terms of the influence tensor (8.62b):

$$\boldsymbol{\sigma}(\boldsymbol{x}) - \boldsymbol{\sigma}^*(\boldsymbol{x}) = \boldsymbol{B}(\boldsymbol{x}) : \Big(\langle\boldsymbol{\sigma}\rangle - \langle\boldsymbol{\sigma}\rangle^*\Big) \,. \tag{8.157}$$

Using the residual stress field (8.148) this can be written as

$$\boldsymbol{B}(\boldsymbol{x}) : \langle\boldsymbol{\sigma}\rangle^* = \boldsymbol{\sigma}^*(\boldsymbol{x}) - \boldsymbol{\sigma}^r(\boldsymbol{x}) \,. \tag{8.158}$$

This representation is valid for all stress states $\langle\boldsymbol{\sigma}\rangle^*$ inside the macroscopic yield surface, i.e., for those macrostresses which cause in every point $\boldsymbol{x}$ on the microscopic level a stress state $\boldsymbol{\sigma}^*$ located inside the local microscopic yield surface. Accordingly, the macroscopic yield surface (or the set of all stress states $\langle\boldsymbol{\sigma}\rangle^*$ in its interior, respectively) is determined from the admissible microstress states $\boldsymbol{\sigma}^*(\boldsymbol{x})$ through the *translation* by $\boldsymbol{\sigma}^r(\boldsymbol{x})$, the *linear transformation* by $\boldsymbol{B}(\boldsymbol{x})$, and the *intersection* with respect to all $\boldsymbol{x}$ in V. The translation by $\boldsymbol{\sigma}^r(\boldsymbol{x})$ means that the location of the macroscopic yield surface in stress space changes in response to the microscopic plastic deformation. Hence the macroscopic behavior of a microscopically heterogeneous elastic-perfectly plastic material displays *kinematic hardening* (see Section 1.3.3.1).

This phenomenon can be illustrated by means of the one-dimensional example of a purely elastic and an elastic-perfectly plastic bar in parallel (Fig. 8.26). For

simplicity the elastic stiffnesses of both bars are taken equal. The yield stress of bar (2) is denoted by k. The loading and unloading cycle depicted in Fig. 8.26 (solid line) shows the translation of the macroscopic elastic range as a consequence of plastic flow in bar (2). After macroscopic unloading $\langle\sigma\rangle = 0$, the inhomogeneous residual stress in the elastic bar (1) is $\sigma_1 = k$ whereas it is $\sigma_2 = -k$ in bar (2).

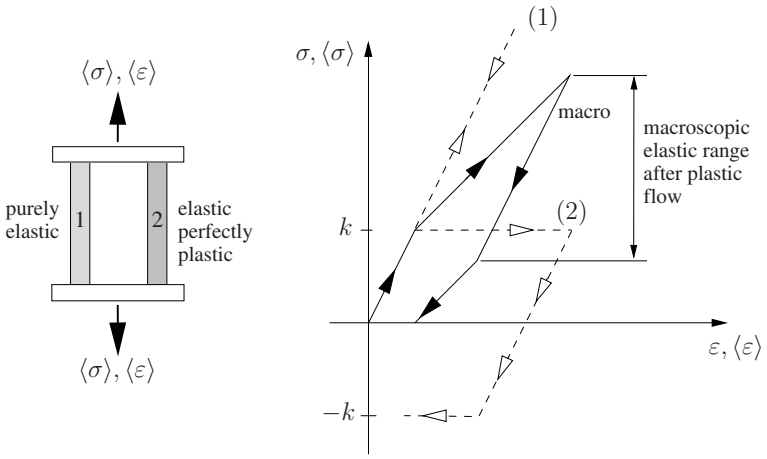

Fig. 8.26 Illustration of kinematic hardening

In the special case that the yield condition is in every point on the microscopic level given by the VON MISES yield condition (1.77) with the spatially varying yield stress $k(\boldsymbol{x})$ a coarse upper bound for the macroscopic yield stress can be derived. From

$$\frac{1}{2}\,\boldsymbol{s}(\boldsymbol{x}) : \boldsymbol{s}(\boldsymbol{x}) \leq k^2(\boldsymbol{x}) \qquad \text{at every} \quad \boldsymbol{x} \quad \text{in } V \tag{8.159}$$

it follows by averaging that

$$\frac{1}{2}\langle\boldsymbol{s}\rangle : \langle\boldsymbol{s}\rangle \leq \frac{1}{2}\langle\boldsymbol{s} : \boldsymbol{s}\rangle \leq \langle k^2\rangle \,. \tag{8.160}$$

The range of admissible macroscopic stress states hence is located inside the VON MISES cylinder of radius $\sqrt{2\langle k^2\rangle}$ (see also Fig. 1.7). This bound, however, is no longer meaningful if in some part of the microstructure the material is purely elastic ($k = \infty$). On the other hand, for a porous medium with porosity f and matrix yield stress $k = const$ it follows that the macroscopic stress states are bounded according to (cf. (8.52))

$$\frac{1}{2}\langle\boldsymbol{s}\rangle : \langle\boldsymbol{s}\rangle \leq (1-f)^2 k^2 \,. \tag{8.161}$$

In contrast to the overall deviatoric stress for which only bounds can be strictly derived (see above), the special case of overall hydrostatic loading of a porous perfectly plastic medium allows for an exact solution. The latter can be obtained from

the simple micromechanical model of a spherically symmetric thick-walled shell (hollow sphere) with inner and outer radii $r = a$ and $r = b$, respectively, subjected to purely radial loading $\sigma_r(r = b) = \Sigma_m$ on the outer boundary (Fig. 8.27). The inner boundary (void surface) is taken as traction-free, i.e. $\sigma_r = 0$ at $r = a$, and $f = (a/b)^3$ is the porosity in this cell model. If the matrix material is rigid perfectly-

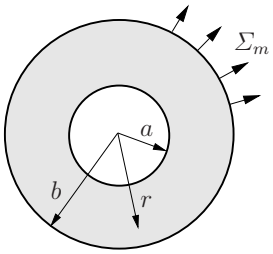

Fig. 8.27 Hollow sphere subjected to hydrostatic loading

plastic and obeys the VON MISES yield criterion $\sqrt{\frac{3}{2}\,\boldsymbol{s} : \boldsymbol{s}} = \sigma_{\mathrm{e}} \leq k$ with deviatoric stress $\boldsymbol{s}$, deformation of the shell can take place only if every material point is in a state of plastic flow. From the equilibrium condition and the yield condition

$$\frac{\mathrm{d}\sigma_r}{\mathrm{d}r} - \frac{2}{r}\,(\sigma_\varphi - \sigma_r) = 0 \quad , \qquad \sigma_\varphi - \sigma_r \equiv \sigma_{\mathrm{e}} = k = const \tag{8.162}$$

it then follows that

$$\sigma_r(r) = 2k \ln\left(\frac{r}{a}\right) \ , \qquad \sigma_\varphi(r) = \sigma_r(r) + k \ . \tag{8.163}$$

The boundary conditions yield

$$\Sigma_m = \frac{2k}{3} \ln\left(\frac{1}{f}\right) \quad \text{or} \quad 2f \cosh\left(\frac{3\Sigma_m}{2k}\right) - (1 + f^2) = 0 \tag{8.164}$$

where for the second equation in (8.164) the identity $\ln(x) = \mathrm{Arcosh}\left(\frac{x^2+1}{2x}\right)$ has been used. The problem that (8.164) is only exact for a spherical shell which is not space-filling can be overcome by considering an assemblage of shells of any size, all having the same porosity f, similar to the *Composite Spheres Model* (see Section 8.3.3.2). Space then can be entirely filled and all the shells exert the purely radial stress Σ_m on each other; hence (8.164) is an exact result for a space-filling porous medium (with rigid perfectly-plastic matrix) under purely hydrostatic loading. In real porous media, however, the void size usually is not randomly distributed. The solution (8.164) plays an important role in the so-called GURSON model presented in Section 9.4.2.

8.4.2 Approximations

The general results about the effective behavior of micro-heterogeneous elastic-plastic materials derived in the preceding section are based on the mere existence of the influence tensors $\boldsymbol{A}(\boldsymbol{x})$ or $\boldsymbol{B}(\boldsymbol{x})$ and the elastic auxiliary fields they are used to describe. Their explicit representations in terms of the Eshelby tensor are available only for the interior of ellipsoidal inhomogeneities in an otherwise homogeneous matrix. While this information was sufficient for the homogenization of purely elastic materials this is no longer the case if in addition spatially varying plastic strains have to be taken into account – even if those may formally be regarded as eigenstrains. The application of analytical homogenization methods to elastic-plastic materials hence requires further approximations. From the variety of different approaches which are discussed in the literature and are a subject of ongoing research only a few fundamental concepts can be presented here.

We therefore consider ellipsoidal inhomogeneities (I) in an infinitely extended matrix (M) where each phase has constant material properties characterized by elasticity laws

$$\boldsymbol{\sigma} = \boldsymbol{C}_\alpha : (\boldsymbol{\varepsilon} - \boldsymbol{\varepsilon}^p) \tag{8.165}$$

with $\alpha = \mathrm{I}, \mathrm{M}$ and flow rules (see also (1.82))

$$\dot{\boldsymbol{\varepsilon}}^p = \dot{\lambda}_\alpha \, \frac{\partial F_\alpha(\boldsymbol{\sigma})}{\partial \boldsymbol{\sigma}} \, . \tag{8.166}$$

Prior to the onset of plastic flow the stresses and strains inside the individual inhomogeneities are constant according to Eshelby's result. If only the inhomogeneities deform plastically the plastic strains evolving inside are likewise constant. Since they can be regarded as eigenstrains they occur analogous to $\boldsymbol{\varepsilon}^t$ in the relation (8.31a) for the equivalent eigenstrain and allow for a direct application of the Eshelby result. In the framework of the model of a dilute distribution or the Mori-Tanaka model no approximations then are necessary which go beyond those for a purely elastic material. The self-consistent method, however, which considers the inhomogeneity to be embedded in the effective, now elastic-plastic medium, requires modifications even in this simplest case; these shall not be further discussed here.

In the following we consider the situation, more important for practical applications, of inhomogeneities prevailing in a *ductile matrix* where inhomogeneous plastic deformations take place. The discussion of some typical approximations and their differences is restricted here to spherical inhomogeneities, isotropic elastic behavior of both phases, and the VON MISES yield condition (1.77).

8.4.2.1 Piecewise constant plastic strains

The simplest approach consists in assuming the plastic strain in each phase to be constant and hence equal to its average value:

$$\boldsymbol{\varepsilon}^p(\boldsymbol{x}) = \begin{cases} \langle \boldsymbol{\varepsilon}^p \rangle_{\mathrm{I}} & \text{in } V_{\mathrm{I}} \,, \\ \langle \boldsymbol{\varepsilon}^p \rangle_{\mathrm{M}} & \text{in } V_{\mathrm{M}} \,. \end{cases} \tag{8.167}$$

In addition we consider only the phase average of the stress in the local yield conditions (8.166):

$$\langle \dot{\boldsymbol{\varepsilon}}^p \rangle_{\mathrm{I}} = \dot{\lambda}_{\mathrm{I}} \, \frac{\partial F_{\mathrm{I}}(\langle \boldsymbol{\sigma} \rangle_{\mathrm{I}})}{\partial \langle \boldsymbol{\sigma} \rangle_{\mathrm{I}}} \,, \qquad \langle \dot{\boldsymbol{\varepsilon}}^p \rangle_{\mathrm{M}} = \dot{\lambda}_{\mathrm{M}} \, \frac{\partial F_{\mathrm{M}}(\langle \boldsymbol{\sigma} \rangle_{\mathrm{M}})}{\partial \langle \boldsymbol{\sigma} \rangle_{\mathrm{M}}} \,. \tag{8.168}$$

Due to these approximations the formal construction of the macroscopic yield condition $F^*(\langle \boldsymbol{\sigma} \rangle) \leq 0$ as discussed in Section 8.4.1.3 is not necessary and only the local conditions $F_\alpha(\langle \boldsymbol{\sigma} \rangle_\alpha) \leq 0$ need to be evaluated. Since therefore the phase averages of the stress fields are required the effective material behavior is *implicitly* described by a system of equations which involves macroscopic quantities and phase averages. In view of the approximation of constant plastic strains in each phase, the macroscopic plastic strains (8.145a) can be written as

$$\boldsymbol{\mathcal{E}}^p = \boldsymbol{C}^{*\,-1} : \Big(c_{\mathrm{I}} \langle \boldsymbol{\varepsilon}^p \rangle_{\mathrm{I}} : \boldsymbol{C}_{\mathrm{I}} : \boldsymbol{A}_{\mathrm{I}} + c_{\mathrm{M}} \langle \boldsymbol{\varepsilon}^p \rangle_{\mathrm{M}} : \boldsymbol{C}_{\mathrm{M}} : \boldsymbol{A}_{\mathrm{M}} \Big) \tag{8.169}$$

where c_{I} and c_{M} are the volume fractions and the relation $c_{\mathrm{M}} \boldsymbol{A}_{\mathrm{M}} = \boldsymbol{1} - c_{\mathrm{I}} \boldsymbol{A}_{\mathrm{I}}$ holds (see (8.70)). For the influence tensor $\boldsymbol{A}_{\mathrm{I}}$ of the inhomogeneity which according to (8.71a) determines also the effective elasticity tensor $\boldsymbol{C}^*$ any of the representations derived from different models in Section 8.3.2 may now be inserted. For completeness also the additional equations are given here from which, for instance, under prescribed macrostrains $\langle \boldsymbol{\varepsilon} \rangle = \boldsymbol{\varepsilon}^0$ all phase averages and the macrostresses can be determined:

$$\begin{aligned} &\langle \boldsymbol{\sigma} \rangle_\alpha = \boldsymbol{C}_\alpha : \Big(\langle \boldsymbol{\varepsilon} \rangle_\alpha - \langle \boldsymbol{\varepsilon}^p \rangle_\alpha \Big) \,, \qquad \langle \boldsymbol{\sigma} \rangle = \boldsymbol{C}^* : \Big(\langle \boldsymbol{\varepsilon} \rangle - \boldsymbol{\mathcal{E}}^p \Big) \,, \\ &\langle \boldsymbol{\sigma} \rangle = c_{\mathrm{I}} \langle \boldsymbol{\sigma} \rangle_{\mathrm{I}} + c_{\mathrm{M}} \langle \boldsymbol{\sigma} \rangle_{\mathrm{M}} \,, \qquad \langle \boldsymbol{\varepsilon} \rangle = c_{\mathrm{I}} \langle \boldsymbol{\varepsilon} \rangle_{\mathrm{I}} + c_{\mathrm{M}} \langle \boldsymbol{\varepsilon} \rangle_{\mathrm{M}} \,. \end{aligned} \tag{8.170}$$

The essential step in this simple approach which allows for the use of elastic fundamental solutions such as the Eshelby tensor is the assumption of piecewise constant plastic strains in the individual phases. Yet, the evaluation in case of stiff elastic particles (I) embedded in a soft ductile matrix (M) reveals the deficiency of this approach. It yields an effective behavior which in comparison to detailed finite element calculations or alternative homogenization techniques (Section 8.4.2.3, see Fig. 8.28) is far too stiff. The reason for this is the neglected concentration of plastic matrix flow in the immediate vicinity of the particles (stress concentrators). In the present model the particles are located in a less compliant surrounding than they are in reality, with the consequence that their stiffening effect on the overall behavior is overestimated.

8.4.2.2 Incremental theory

Now the assumption of piecewise constant plastic strains is given up and an incremental constitutive law, valid is the state of plastic flow, is chosen as the starting point. The *Prandtl-Reuss law* (1.83c)

$$\dot{\boldsymbol{e}} = \left[\frac{1}{2\mu_\alpha} \mathbf{1} + \frac{3}{2g_\alpha} \frac{\boldsymbol{s} \otimes \boldsymbol{s}}{\boldsymbol{s} : \boldsymbol{s}} \right] : \dot{\boldsymbol{s}} \tag{8.171}$$

is therefore employed for both phases where the deviator $\dot{\boldsymbol{e}}(\boldsymbol{x})$ and the purely elastic volumetric part add up to the total strain rate $\dot{\boldsymbol{\varepsilon}}(\boldsymbol{x})$. The symbol $\otimes$ denotes the dyadic product of two tensors: $(\boldsymbol{\sigma} \otimes \boldsymbol{\sigma})_{ijkl} = \sigma_{ij}\sigma_{kl}$. In terms of the elastic-plastic tangent tensors $\tilde{\boldsymbol{C}}_\alpha$ the relations between the stress and strain increments can be written as:

$$\dot{\boldsymbol{\sigma}} = \tilde{\boldsymbol{C}}_\alpha : \dot{\boldsymbol{\varepsilon}} \qquad (\alpha = \mathrm{I}, \mathrm{M}) \; . \tag{8.172}$$

It should be noted that the tangent tensors vary in space via the actual stress distribution: $\tilde{\boldsymbol{C}}_\alpha = \tilde{\boldsymbol{C}}_\alpha(\boldsymbol{s}(\boldsymbol{x}))$. The relation (8.172) between the stress and strain increments is formally analogous to the elasticity law (8.54). However, the tangent tensors are even in case of an elastically isotropic material *anisotropic* since they depend on the direction of plastic flow via the second part of (8.171).

In the following the stress dependence of the tangent tensors is approximated by a dependence only on the average stress in the respective phase. This leads to an incrementally linear material behavior with a spatially constant tangent stiffness in each phase:

$$\dot{\boldsymbol{\sigma}} = \tilde{\boldsymbol{C}}_\alpha \Big(\langle \boldsymbol{s} \rangle_\alpha \Big) : \dot{\boldsymbol{\varepsilon}} \; . \tag{8.173}$$

Now the Eshelby result can again be applied, yet requiring the Eshelby tensor for an anisotropic matrix material $\tilde{\boldsymbol{C}}_{\mathrm{M}}(\langle \boldsymbol{s} \rangle_{\mathrm{M}})$. The homogenization techniques presented in Section 8.3.2 finally lead to an *effective tangent tensor* $\tilde{\boldsymbol{C}}^*(\langle \boldsymbol{s} \rangle_\alpha)$ for the incremental description of the macroscopic material behavior:

$$\langle \dot{\boldsymbol{\sigma}} \rangle = \tilde{\boldsymbol{C}}^* \Big(\langle \boldsymbol{s} \rangle_\alpha \Big) : \langle \dot{\boldsymbol{\varepsilon}} \rangle \; . \tag{8.174}$$

In the course of an incremental evaluation the current values of the average deviatoric stress states $\langle \boldsymbol{s} \rangle_{\mathrm{I}}$ and $\langle \boldsymbol{s} \rangle_{\mathrm{M}}$ in both phases have to be determined which are needed to update the tangent tensors. Because of the anisotropy of the tangent tensors and the Eshelby tensor, changing in the course of loading, this method is rather costly. Yet, it leads to more realistic results since the plastic strain rates in the matrix phase

$$\dot{\boldsymbol{\varepsilon}}^p(\boldsymbol{x}) = \frac{3}{2g_{\mathrm{M}}} \left[\frac{\langle \boldsymbol{s} \rangle_{\mathrm{M}} \otimes \langle \boldsymbol{s} \rangle_{\mathrm{M}}}{\langle \boldsymbol{s} \rangle_{\mathrm{M}} : \langle \boldsymbol{s} \rangle_{\mathrm{M}}} \right] : \dot{\boldsymbol{s}}(\boldsymbol{x}) \tag{8.175}$$

are not taken to be constant.

8.4.2.3 Total strain theory

Significant simplifications result when only monotonous and *proportional* loading is considered (see Section 1.3.3.3). Because of the coaxiality of $\boldsymbol{\sigma}$, $\boldsymbol{s}$, and $\dot{\boldsymbol{\sigma}}$ then the relations $\boldsymbol{s}(\boldsymbol{s} : \dot{\boldsymbol{s}}) = (\boldsymbol{s} : \boldsymbol{s})\dot{\boldsymbol{s}} = \frac{2}{3}\,\sigma_{\mathrm{e}}^2\,\dot{\boldsymbol{s}}$ hold and integration of (8.171) leads to the *Hencky-Ilyushin law* (see also (1.86))

$$\boldsymbol{s} = 2\mu_\alpha^s\,\boldsymbol{e}\ . \tag{8.176}$$

It has the structure of a nonlinear elastic constitutive law with the *secant modulus* $\mu^s(\sigma_{\mathrm{e}}(\boldsymbol{x}))$. The latter depends on the stress state only via the one-dimensional equivalent stress $\sigma_{\mathrm{e}} = \sqrt{\frac{3}{2}\boldsymbol{s} : \boldsymbol{s}}$. In case of isotropic hardening with a yield stress $k(p) = k_0 + A\,p^{1/n}$ which depends only on the one-dimensional equivalent plastic strain $p \equiv \varepsilon_{\mathrm{e}}^p = \sqrt{\frac{2}{3}\,\boldsymbol{\varepsilon}^p : \boldsymbol{\varepsilon}^p}$ the secant modulus reads

$$\mu^s(\sigma_{\mathrm{e}}) = \frac{\mu\,\sigma_{\mathrm{e}}\,A^n}{\sigma_{\mathrm{e}}\,A^n + 3\mu(\frac{\sigma_{\mathrm{e}}}{\sqrt{3}} - k_0)^n} \tag{8.177}$$

for $\sigma_e \geq \sqrt{3}\,k_0$ where k_0 denotes the initial yield stress.

In order to eliminate the spatial dependence of the secant moduli in both phases the inhomogeneous stress fields are approximated by their phase averages. The equivalent stresses in both phases then can be written as $\Sigma_\alpha = \sqrt{\frac{3}{2}\langle\boldsymbol{s}\rangle_\alpha : \langle\boldsymbol{s}\rangle_\alpha}$. As a consequence, (8.176) reduces to an elasticity law with a constant secant modulus in each phase

$$\boldsymbol{s} = 2\mu_\alpha^s(\Sigma_\alpha)\,\boldsymbol{e}\ . \tag{8.178}$$

Since the stiffness of the matrix material now is spatially constant the Eshelby result for an ellipsoidal inhomogeneity can also be applied to this nonlinear problem. Via the secant shear modulus $\mu_{\mathrm{M}}^s(\Sigma_{\mathrm{M}})$ the Eshelby tensor depends on the current average matrix stress state or the equivalent stress Σ_{M} computed from it, respectively. In case of spherical inhomogeneities the parameters (8.11) of the isotropic Eshelby tensor (8.10) hence read

$$\alpha^s\,(\Sigma_{\mathrm{M}}) = \frac{3K_{\mathrm{M}}}{3K_{\mathrm{M}} + 4\mu_{\mathrm{M}}^s}\ , \qquad \beta^s\,(\Sigma_{\mathrm{M}}) = \frac{6(K_{\mathrm{M}} + 2\mu_{\mathrm{M}}^s)}{5(3K_{\mathrm{M}} + 4\mu_{\mathrm{M}}^s)}\ . \tag{8.179}$$

The homogenization can now be performed with any of the methods discussed in Section 8.3.2; in the representations for the effective stiffness only the shear moduli μ_{I} and μ_{M} have to be replaced by $\mu_{\mathrm{I}}^s(\Sigma_{\mathrm{I}})$ and $\mu_{\mathrm{M}}^s(\Sigma_{\mathrm{M}})$. This leads to a macroscopic constitutive law written in terms of the *effective secant moduli* K_s^* and μ_s^*:

$$\boxed{\langle\sigma_{kk}\rangle = 3K_s^*\langle\epsilon_{kk}\rangle\ , \qquad \langle\boldsymbol{s}\rangle = 2\mu_s^*\langle\boldsymbol{e}\rangle}\ . \tag{8.180}$$

The determination of K_s^* and μ_s^* requires the solution of a nonlinear system of equations since the current phase averages $\langle \boldsymbol{s} \rangle_\alpha$ have to be computed as functions of some prescribed macroscopic quantity. Therefore, it is practical to eliminate the phase averages of the strains from the general relations for the macroscopic quantities:

$$c_{\mathrm{I}} \langle \boldsymbol{s} \rangle_{\mathrm{I}} + c_{\mathrm{M}} \langle \boldsymbol{s} \rangle_{\mathrm{M}} = \langle \boldsymbol{s} \rangle \,, \qquad \frac{c_{\mathrm{I}} \langle \boldsymbol{s} \rangle_{\mathrm{I}}}{2\mu_{\mathrm{I}}^s(\Sigma_{\mathrm{I}})} + \frac{c_{\mathrm{M}} \langle \boldsymbol{s} \rangle_{\mathrm{M}}}{2\mu_{\mathrm{M}}^s(\Sigma_{\mathrm{M}})} = \langle \boldsymbol{e} \rangle \,. \tag{8.181}$$

As an example we consider an elastic-plastic composite material which consists of a ductile aluminum matrix and purely elastic spherical alumina particles with a volume fraction of $c_{\mathrm{I}} = 0.3$. The behavior of the matrix can be characterized by the typical material data $E_{\mathrm{M}} = 75\,\mathrm{GPa}$, $\nu_{\mathrm{M}} = 0.3$, $k_0 = 75\,\mathrm{MPa}$, $A = 400\,\mathrm{MPa}$, and $n = 3$ while that of the particles is given by $E_{\mathrm{I}} = 400\,\mathrm{GPa}$ and $\nu_{\mathrm{I}} = 0.2$. Figure 8.28 shows the stress-strain behavior of both phases as well as the overall behavior under uniaxial tension. From the values of the material parameters and the morphology of the composite (stiff particles in a soft matrix) it can be expected that the overall behavior is mainly determined by the matrix. The concentration of plastic matrix flow in the vicinity of the particles reduces their stiffening effect in comparison to a purely elastic composite. Besides the overall behavior of the composite based on the total strain theory, Fig. 8.28 also shows the $\langle\sigma\rangle, \langle\varepsilon\rangle$-curve obtained under the assumption of piecewise constant plastic strains (Section 8.4.2.1).

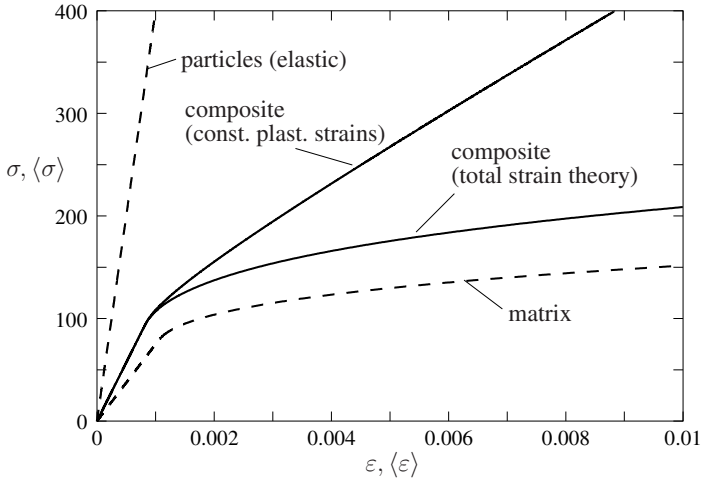

Fig. 8.28 Elastic-plastic composite, comparison of approximate methods

The homogenization has in both cases been performed using the Mori-Tanaka model. Obviously the assumption of piecewise constant plastic strains leads to an unrealistically weak influence of matrix plasticity on the overall behavior; this has already been mentioned in Section 8.4.2.1. The result based on total strain theory

which allows for inhomogeneous plastic strains, in contrast, captures the dominance of the ductile matrix in the overall behavior much better.

8.5 Thermoelastic material

Spatial fluctuations on the microscale of heterogeneous media are generally displayed not only by the elastic or plastic properties but also by other physical parameters. One of the most important ones is the thermal expansion coefficient $\boldsymbol{k}$ which according to (1.43) appears in the *Duhamel-Neumann law*

$$\boldsymbol{\sigma}(\boldsymbol{x}) = \boldsymbol{C}(\boldsymbol{x}) : \Big(\boldsymbol{\varepsilon}(\boldsymbol{x}) - \boldsymbol{\varepsilon}^{th}(\boldsymbol{x})\Big) = \boldsymbol{C}(\boldsymbol{x}) : \Big(\boldsymbol{\varepsilon}(\boldsymbol{x}) - \boldsymbol{k}(\boldsymbol{x})\Delta T(\boldsymbol{x})\Big) \tag{8.182}$$

of a micro-heterogeneous thermoelastic material. For the majority of practical applications it is justified to consider the temperature change ΔT to be constant throughout the microscale. The material behavior on the macroscopic level then can be characterized by the effective elasticity tensor $\boldsymbol{C}^*$ according to Section 8.3 and the *effective coefficient of thermal expansion* $\boldsymbol{k}^*$:

$$\langle\boldsymbol{\sigma}\rangle = \boldsymbol{C}^* : \Big(\langle\boldsymbol{\varepsilon}\rangle - \boldsymbol{\mathcal{E}}^{th}\Big) \qquad \text{where} \quad \boldsymbol{\mathcal{E}}^{th} = \boldsymbol{k}^*\Delta T\,. \tag{8.183}$$

Comparison of (8.182) and (8.183) with (8.4) or (8.142) and (8.144) reveals that thermal strains $\boldsymbol{\varepsilon}^{th} = \boldsymbol{k}\Delta T$ are equivalent to stress-free transformation strains $\boldsymbol{\varepsilon}^t$ or plastic strains $\boldsymbol{\varepsilon}^p$. This already repeatedly mentioned analogy can be exploited to determine $\boldsymbol{k}^*$. Accordingly, (8.145a) yields the macroscopic thermal strain

$$\boldsymbol{\mathcal{E}}^{th} = \boldsymbol{C}^{*-1} : \langle\boldsymbol{\varepsilon}^{th} : \boldsymbol{C} : \boldsymbol{A}\rangle \tag{8.184a}$$

and after insertion of $\boldsymbol{\mathcal{E}}^{th}$ and $\boldsymbol{\varepsilon}^{th}$ it follows that

$$\boxed{\boldsymbol{k}^* = \boldsymbol{C}^{*-1} : \langle\boldsymbol{k} : \boldsymbol{C} : \boldsymbol{A}\rangle}\,. \tag{8.184b}$$

Hence the effective coefficient of thermal expansion is the *weighted average* of its microscopic counterpart (weighted by the elastic heterogeneity in terms of $\boldsymbol{C}(\boldsymbol{x})$ and the influence tensor $\boldsymbol{A}(\boldsymbol{x})$). Only in case of an elastically homogeneous material ($\boldsymbol{C} = const,\ \boldsymbol{A} = \boldsymbol{1}$) is $\boldsymbol{k}^* = \langle\boldsymbol{k}\rangle$.

As a special case of practical importance we again consider a composite material which consists of two piecewise homogeneous phases with $\boldsymbol{C}_{\mathrm{M}}$, $\boldsymbol{C}_{\mathrm{I}}$, $\boldsymbol{k}_{\mathrm{M}}$, $\boldsymbol{k}_{\mathrm{I}}$ and volume fractions c_{M}, c_{I}. Using $c_{\mathrm{I}}\boldsymbol{A}_{\mathrm{I}} + c_{\mathrm{M}}\boldsymbol{A}_{\mathrm{M}} = \boldsymbol{1}$ one obtains from (8.184b)

$$\boldsymbol{k}^* = \boldsymbol{C}^{*-1} : \Big(\boldsymbol{k}_{\mathrm{M}} : \boldsymbol{C}_{\mathrm{M}} + c_{\mathrm{I}}(\boldsymbol{k}_{\mathrm{I}} : \boldsymbol{C}_{\mathrm{I}} - \boldsymbol{k}_{\mathrm{M}} : \boldsymbol{C}_{\mathrm{M}}) : \boldsymbol{A}_{\mathrm{I}}\Big)\,. \tag{8.185a}$$

If the influence tensor $\boldsymbol{A}_{\mathrm{I}}$ of the inhomogeneity is replaced by (8.71a) it follows that

$$\boldsymbol{k}^* = \boldsymbol{C}^{*-1} : \Big(\boldsymbol{k}_{\mathrm{M}} : \boldsymbol{C}_{\mathrm{M}} + (\boldsymbol{k}_{\mathrm{I}} : \boldsymbol{C}_{\mathrm{I}} - \boldsymbol{k}_{\mathrm{M}} : \boldsymbol{C}_{\mathrm{M}}) : (\boldsymbol{C}_{\mathrm{I}} - \boldsymbol{C}_{\mathrm{M}})^{-1} : (\boldsymbol{C}^* - \boldsymbol{C}_{\mathrm{M}}) \Big) . \quad (8.185b)$$

In this representation any of the approximations of the effective elasticity tensor $\boldsymbol{C}^*$ derived from the micromechanical models in Section 8.3.2 can now be inserted.

A problem that often occurs in practical applications is that of thermally induced eigenstresses in the course of heating up or cooling down a heterogeneous microstructure or composite. If the material is considered to be macroscopically unloaded $\langle \boldsymbol{\sigma} \rangle = \boldsymbol{0}$ it follows from (8.47) for the average stresses in both phases that $c_{\mathrm{I}} \langle \boldsymbol{\sigma} \rangle_{\mathrm{I}} = -c_{\mathrm{M}} \langle \boldsymbol{\sigma} \rangle_{\mathrm{M}}$ and the average strain is $\langle \boldsymbol{\varepsilon} \rangle = c_{\mathrm{I}} \langle \boldsymbol{\varepsilon} \rangle_{\mathrm{I}} + c_{\mathrm{M}} \langle \boldsymbol{\varepsilon} \rangle_{\mathrm{M}} = \boldsymbol{k}^* \Delta T$. By inserting the constitutive laws for both phases $\langle \boldsymbol{\sigma} \rangle_\alpha = \boldsymbol{C}_\alpha : (\langle \boldsymbol{\varepsilon} \rangle_\alpha - \boldsymbol{k}_\alpha \Delta T)$ one obtains for the average stresses

$$c_{\mathrm{I}} \langle \boldsymbol{\sigma} \rangle_{\mathrm{I}} = -c_{\mathrm{M}} \langle \boldsymbol{\sigma} \rangle_{\mathrm{M}} = \left(\boldsymbol{C}_{\mathrm{M}}^{-1} - \boldsymbol{C}_{\mathrm{I}}^{-1} \right)^{-1} : \left(c_{\mathrm{I}} \boldsymbol{k}_{\mathrm{I}} + c_{\mathrm{M}} \boldsymbol{k}_{\mathrm{M}} - \boldsymbol{k}^* \right) \Delta T . \quad (8.186)$$

Now we consider a material with both phases being elastically (K_α, μ_α) and thermally isotropic. The local thermal strains then are purely volumetric: $\boldsymbol{\varepsilon}^{th} = k_\alpha \Delta T \, \boldsymbol{I}$. If the material is elastically isotropic also on the macroscale then the effective coefficient of thermal expansion according to (8.185b) is likewise isotropic $\boldsymbol{k}^* = k^* \boldsymbol{I}$ and depends only on the effective bulk modulus:

$$k^* = \frac{k_{\mathrm{M}} K_{\mathrm{M}} (K_{\mathrm{I}} - K_{\mathrm{M}}) + (k_{\mathrm{I}} K_{\mathrm{I}} - k_{\mathrm{M}} K_{\mathrm{M}})(K^* - K_{\mathrm{M}})}{K^* (K_{\mathrm{I}} - K_{\mathrm{M}})} . \quad (8.187)$$

If in case of a microstructure with spherical inhomogeneities the Mori-Tanaka model (Section 8.3.2.4) is employed for the homogenization then (8.98) and the volumetric part $\alpha = (1+\nu)/3(1-\nu)$ of the isotropic Eshelby tensor (8.10), (8.11) lead to

$$k^*_{(\mathrm{MT})} = k_{\mathrm{M}} + c_{\mathrm{I}} \frac{K_{\mathrm{I}} (k_{\mathrm{I}} - k_{\mathrm{M}})}{K_{\mathrm{M}} + (\alpha + c_{\mathrm{I}}(1-\alpha))(K_{\mathrm{I}} - K_{\mathrm{M}})} . \quad (8.188)$$

Insertion into (8.186) yields the average values of the thermally induced stresses in both phases which are purely hydrostatic:

$$\langle \boldsymbol{\sigma} \rangle_{\mathrm{I}} = -\frac{c_{\mathrm{M}}}{c_{\mathrm{I}}} \langle \boldsymbol{\sigma} \rangle_{\mathrm{M}} = \frac{-3 K_{\mathrm{I}} K_{\mathrm{M}} c_{\mathrm{M}} (1-\alpha)(k_{\mathrm{I}} - k_{\mathrm{M}})}{K_{\mathrm{M}} + (\alpha + c_{\mathrm{I}}(1-\alpha))(K_{\mathrm{I}} - K_{\mathrm{M}})} \Delta T \, \boldsymbol{I} . \quad (8.189)$$

In the special case of a very stiff matrix ($K_{\mathrm{M}} \gg K_{\mathrm{I}}$) one obtains

$$\langle \boldsymbol{\sigma} \rangle_{\mathrm{I}} = -3 K_{\mathrm{I}} (k_{\mathrm{I}} - k_{\mathrm{M}}) \Delta T \, \boldsymbol{I} . \quad (8.190)$$

In case of an elastically homogeneous material ($K_{\mathrm{M}} = K_{\mathrm{I}} = K$), in contrast, it follows that

$$\langle \boldsymbol{\sigma} \rangle_{\mathrm{I}} = -3 K c_{\mathrm{M}} (1-\alpha)(k_{\mathrm{I}} - k_{\mathrm{M}}) \Delta T \, \boldsymbol{I} \quad (8.191)$$

which comprises the result (8.14) when the thermal expansion is restricted to the inhomogeneity ($k_{\mathrm{M}} = 0$) with a very small volume fraction ($c_{\mathrm{I}} \ll 1$, $c_{\mathrm{M}} \approx 1$):

$$\langle \boldsymbol{\varepsilon} \rangle_{\mathrm{I}} = \frac{\langle \boldsymbol{\sigma} \rangle_{\mathrm{I}}}{3K} + k_{\mathrm{I}} \, \Delta T \, \boldsymbol{I} = \alpha \, k_{\mathrm{I}} \, \Delta T \, \boldsymbol{I} \, . \tag{8.192}$$

As an example of practical relevance we consider a microstructure which results from the infiltration of aluminum into a porous ceramic matrix of alumina (Al_2O_3). Since the manufacturing proceeds at high temperatures cooling down the material to room temperature leads to thermally induced eigenstresses in both phases. Typical material data for the ceramic matrix (M) and the aluminum phase approximated here as spherical inhomogeneities (I) are: $K_{\mathrm{M}} = 220\,\mathrm{GPa}$, $\nu_{\mathrm{M}} = 0.2$, $k_{\mathrm{M}} = 8 \cdot 10^{-6}\mathrm{K}^{-1}$, $K_{\mathrm{I}} = 60\,\mathrm{GPa}$, $\nu_{\mathrm{I}} = 0.3$, $k_{\mathrm{I}} = 2.4 \cdot 10^{-5}\mathrm{K}^{-1}$. This leads to $\alpha(\nu_{\mathrm{M}}) = 0.5$ and for a volume fraction of aluminum of $c_{\mathrm{I}} = 0.25$ one obtains from (8.188) an effective coefficient of thermal expansion of $k^* \approx 10^{-5}\mathrm{K}^{-1}$. A temperature change in the course of cooling of $\Delta T = -400\,\mathrm{K}$ leads according to (8.189) to an average pressure of $\sigma_{\mathrm{M}} \approx -250$ MPa in the ceramic matrix (M) and to a hydrostatic tensile stress of $\sigma_{\mathrm{I}} \approx 750$ MPa in the infiltrated aluminum (I). Despite the strongly simplified approximation of the morphology by spherical aluminum particles these values correspond quite well to experimental findings. One should note that the average stress in the aluminum phase is much higher than the yield stress of aluminum. However, since the stress state is purely hydrostatic yielding does not occur in the course of cooling, instead cavities are formed in the aluminum phase.

8.6 Problems

Problem 8.1 The effective bulk modulus K^* of a heterogeneous, macroscopically isotropic material is know from measurements. The material consists microscopically of two isotropic phases with the elastic constants $K_{\mathrm{I}}, \mu_{\mathrm{I}}, K_{\mathrm{M}}, \mu_{\mathrm{M}}$. Compute from the Voigt-Reuss bounds and the Hashin-Shtrikman bounds the intervals of possible volume fractions c_{I} and $c_{\mathrm{M}} = 1 - c_{\mathrm{I}}$, respectively. Assume that the elastic constants are related to each other by $K_{\mathrm{I}} = 10K_{\mathrm{M}}$, $\mu_{\mathrm{I}} = 10\mu_{\mathrm{M}}$ and $K^* = 5K_{\mathrm{I}}$.

Solution: a) Voigt-Reuss bounds: $0.44 \le c_{\mathrm{I}} \le 0.88$,

b) Hashin-Shtrikman bounds: $0.56 \le c_{\mathrm{I}} \le 0.79$.

Problem 8.2 Apply Hashin-Shtrikman's variational principle to the 1D-example of a heterogeneous two-phase bar.

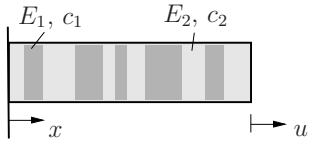

Fig. 8.29

Solution: Choosing first material 1 (E_1) and subsequently material 2 (E_2) as the comparison material, the identical result $E^* = E_1 E_2/(c_1 E_1 + c_2 E_2)$ is obtained as the upper and as the lower Hashin-Shtrikman bound. Consequently, this is the exact solution for the effective Young's modulus.

Problem 8.3 Two isotropic linear elastic materials (a) and (b) with Lamé's constants λ^a, μ^a, λ^b, μ^b are perfectly bonded. At some point P of the interface the strain state ε^a_{ij} in material (a) is assumed to be known.
Determine the strain state in material (b) at the point P.

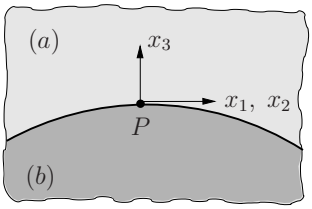

Fig. 8.30

Hint: Along the interface, the following relations hold with respect to the sketched cartesian coordinate system:

$$\sigma^a_{i3} = \sigma^b_{i3} \quad (i = 1,2,3)\,, \qquad \varepsilon^a_{11} = \varepsilon^b_{11}\,, \qquad \varepsilon^a_{12} = \varepsilon^b_{12}\,, \qquad \varepsilon^a_{22} = \varepsilon^b_{22}$$

Solution: The unknown strains in material (b) are

$$\varepsilon^b_{\gamma 3} = \frac{\mu^a}{\mu^b}\,\varepsilon^a_{\gamma 3} \quad (\gamma = 1,2)\,,$$
$$\varepsilon^b_{33} = \frac{1}{\lambda^b + 2\mu^b}\left[(\lambda^a + 2\mu^a)\,\varepsilon^a_{33} + (\lambda^a - \lambda^b)\,(\varepsilon^a_{11} + \varepsilon^a_{22})\right].$$

Problem 8.4 An isotropic linear elastic composite material with spherical particles I in a matrix M is subjected to an uniaxial macroscopic stress Σ.
Use the result of problem 8.3 together with Eshelby's solution (Sections 8.2.1.4 and 8.2.2.2) to compute the stress state in the matrix at some point P of the particle-matrix interface at the particle equator.

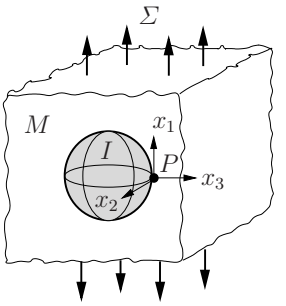

Fig. 8.31

Solution: For the special case of $K_{\mathrm{M}} = 2\mu_{\mathrm{M}}$, $K_{\mathrm{I}} = 2\mu_{\mathrm{I}}$, i.e. $\nu_{\mathrm{M}} = \nu_{\mathrm{I}} = 2/7$, the normalized stress components at point P are plotted in Fig. 8.32 as functions of the

stiffness ratio $\mu_{\mathrm{I}}/\mu_{\mathrm{M}}$.

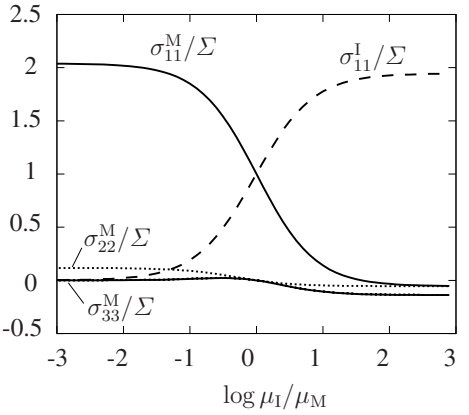

Fig. 8.32

8.7 Further reading

Aboudi, J., *Mechanics of Composite Materials - A Unified Micromechanical Approach*. Elsevier, Amsterdam, 1991

Christensen, R.M., *Mechanics of Composite Materials*. Dover Publ. Inc., 2005

Doghri, I. *Mechanics of Deformable Solids*. Springer, Berlin, 2000

Hashin, Z., Analysis of Composite Materials – A Survey. *J. Appl. Mech.* **50** (1983), 481-505

Hill, R., Elastic properties of reinforced solids: some theoretical principles. *J. Mech. Phys. Solids* **11** (1963), 357-372

Hill, R., The essential structure of constitutive laws for metal composites and polycrystals. *J. Mech. Phys. Solids* **15** (1967), 79-95

Jones, R.M., *Mechanics of Composite Materials*. Taylor & Francis, Philadelphia, 1999

Kachanov, M., Shafiro, B. and Tsukrov, I., *Handbook of Elasticity Solutions*. Kluwer Academic Publishers, Dordrecht, 2003

Kreher, W. and Pompe, W., *Internal Stresses in Heterogeneous Solids*. Akademie Verlag, Berlin, 1989

Le, K.C., *Introduction to Micromechanics*. Nova Science Publ. Inc., 2010

Li, S. and Wang, G., *Introduction to Micromechanics and Nanomechanics*. World Scientific, 2008

Mura, T., *Micromechanics of Defects in Solids*. Martinus Nijhoff Publishers, Dordrecht, 1987

Nemat-Nasser, S. and Hori, M., *Micromechanics – Overall Properties of Heterogeneous Materials*. North-Holland, Amsterdam, 1998

Qu, J. and Cherkaoui, M., *Fundamentals of Micromechanics of Solids*. John Wiley, 2006

Sanchez-Palencia, E. and Zaoui, A. (eds.), *Homogenization Techniques for Composite Materials*. Springer, Berlin, 1987

Suquet, P. (ed.), *Continuum Micromechanics*. CISM Lecture notes, Springer, Berlin, 1997

Torquato, S., *Random heterogeneous Materials: Microstructure and Macroscopic Properties*. Springer, Berlin, 2002

Van der Giessen, E., Background of micromechanics. In: Lemaitre, J. (ed.), *Handbook of Materials Behavior Models*, Vol. 3, Academic Press, 2001, 959-967

Yang, W. and Lee, W.B., *Mesoplasticity and its Applications*. Springer, Berlin, 1993

Zohdi, T.I. and Wriggers, P., *Introduction to Computational Micromechanics*. Springer, Berlin, 2008

Chapter 9
Damage mechanics

9.1 Introduction

Real materials often contain already in the initial state a multitude of defects such as microcracks or voids. In the course of a deformation process these internal cavities may grow and coalesce while at the same time further material separation takes place by the creation of new microdefects at stress concentrators (e.g. inclusions, grain boundaries, inhomogeneities). This causes a change of the macroscopic properties of the material and its strength decreases. Such a process of structural deterioration of a material which results from the creation, growth and coalescence of microdefects is called *damage*. In its final stage it leads to a complete loss of the material's integrity and to the formation of a macroscopic crack.

Material damage is classified according to the dominant macroscopic phenomenon as *brittle damage*, *ductile damage*, *creep damage*, and *fatigue damage*. The prevailing mechanism of brittle damage is the formation and growth of microcracks as it takes place for instance in ceramics, geomaterials, or concrete. In contrast, ductile damage and creep damage in metals is essentially due to the nucleation, growth, and coalescence of microvoids. The source of fatigue damage are microcracks which are formed at stress concentrators in the course of microplastic cyclic loading and which more and more grow and coalesce.

The description of the macroscopic behavior of a damaged material may still proceed in the framework of continuum mechanics. Macroscopic stresses and strains then have to be understood as volumetric averages over a *representative volume element* (RVE) inside which the damage process takes place (see also Section 8.3.1.1). The relevant characteristic length scales depend on the material at hand as well as on the damage mechanism. The state (extent) of damage is represented by a so-called *damage variable* (internal variable). The latter is governed by an evolution law which has to be formulated in a way to describe the evolution of damage in a physically adequate manner. For its derivation it is practical to employ micromechanical models which capture the essential features of the defects and allow for a detailed investigation of their growth. A respective damage theory can be con-

D. Gross and T. Seelig, *Fracture Mechanics: With an Introduction to Micromechanics*, Mechanical Engineering Series, DOI 10.1007/978-3-642-19240-1_9,

sidered as a link between classical continuum mechanics and fracture mechanics. It is in principle capable of describing the formation of a macroscopic crack in an initially crack-free material body.

The present chapter serves to present elementary concepts of damage mechanics. Thereby we focus only on the simplest cases of brittle and ductile damage in the course of monotonic loading.

9.2 Foundations

Damage variables can be introduced in various ways. A simple means of describing the state of damage consists in its geometric quantification and dates back to L.M. KACHANOV (1914-1993). In a cross section of the damaged body we therefore consider an area element $\mathrm{d}A$ with unit normal vector $\boldsymbol{n}$ (Fig. 9.1a). The area of the defects in this element is denoted by $\mathrm{d}A_D$ and the amount of damage then can be characterized by the area fraction

$$\omega(\boldsymbol{n}) = \frac{\mathrm{d}A_D}{\mathrm{d}A} \qquad \text{with} \qquad 0 \leq \omega \leq 1 \tag{9.1}$$

where $\omega = 0$ corresponds to the undamaged material and $\omega = 1$ formally describes the totally damaged material with a complete loss of stress carrying capacity (i.e., fracture). In real materials, however, already at values of $\omega \approx 0.2 \ldots 0.5$ processes take place which lead to total failure. If the damage is constant across a finite area, for instance, under uniaxial tension as in Fig. 9.1b, the relation (9.1) reduces to $\omega = A_D/A$. Obviously this simplest definition of damage is only suitable for void-like defects which have a spatial extension and hence a defect area $\mathrm{d}A_D$ in arbitrary cross sections. The influence of microcracks which are inclined to the cross section can not be properly described in this way.

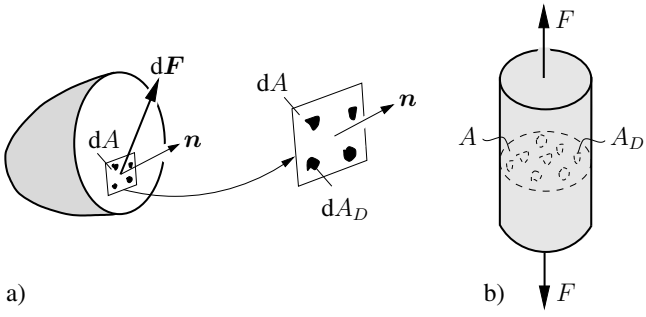

Fig. 9.1 Definition of damage

In the course of a deformation process the defects may grow in preferred directions which are determined by the stress state. In this case ω depends on $\boldsymbol{n}$ and the

damage is *anisotropic*. If, however, the defects and their spatial distribution do not display preferred orientations *isotropic damage* prevails and the state of damage can be characterized by a scalar. A sufficiently small amount of damage may often be considered isotropic as a first approximation.

If the force $\mathrm{d}\boldsymbol{F}$ acting on some cross section is divided by the area $\mathrm{d}A$, one obtains the common stress vector $\boldsymbol{t}$ according to (1.1). The *effective stress vector* $\tilde{\boldsymbol{t}}$ is defined as the force per unit effective (stress carrying) area $\mathrm{d}\tilde{A} = \mathrm{d}A - \mathrm{d}A_D = (1-\omega)\mathrm{d}A$:

$$\tilde{\boldsymbol{t}} = \boldsymbol{t}\,\frac{\mathrm{d}A}{\mathrm{d}\tilde{A}} = \frac{\boldsymbol{t}}{1-\omega}\,. \tag{9.2}$$

Correspondingly, in case of isotropic damage (ω independent of $\boldsymbol{n}$) the *effective stresses* are given by

$$\tilde{\sigma}_{ij} = \frac{\sigma_{ij}}{1-\omega}\,. \tag{9.3}$$

The effective stresses $\tilde{\sigma}_{ij}$ are the average stresses in the undamaged *matrix material*.

In order to formulate constitutive laws one often assumes that the effective stresses $\tilde{\sigma}_{ij}$ lead to the same strains in the damaged material as are induced by the classical stresses σ_{ij} in the undamaged material (*equivalent strain principle*). The stress-strain behavior of the damaged material can then be described by the constitutive law of the undamaged material if the stresses are replaced by the effective stresses. In the uniaxial case of a damaged linear elastic material, for instance, one obtains

$$\varepsilon = \frac{\tilde{\sigma}}{E} = \frac{\sigma}{(1-\omega)E} \tag{9.4}$$

where E is the Young's modulus of the undamaged material. The respective approach also applies to inelastic material behavior and the elastic strains in the framework of plasticity are obtained according to

$$\mathrm{d}\varepsilon^e = \frac{\mathrm{d}\tilde{\sigma}}{E} = \frac{\mathrm{d}\sigma}{(1-\omega)E} \qquad \text{or} \qquad \varepsilon^e = \frac{\tilde{\sigma}}{E} = \frac{\sigma}{(1-\omega)E}\,. \tag{9.5}$$

Hence the amount of damage can be determined by measuring the effective Young's modulus

$$E^* = (1-\omega)E \tag{9.6a}$$

of the damaged material (Fig. 9.2):

$$\omega = 1 - \frac{E^*}{E}\,. \tag{9.6b}$$

Comparison of the representation (9.6a) with the result (8.73)

$$\boldsymbol{C}^* = \boldsymbol{C} : (\boldsymbol{1} - \boldsymbol{D}) \tag{9.7}$$

from the micromechanical investigation of materials with cavities and cracks reveals that the damage variable ω is the uniaxial special case of the influence tensor $\boldsymbol{D}$

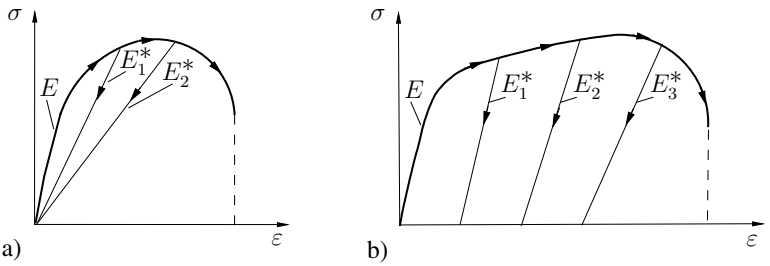

Fig. 9.2 Damage evolution: a) elastic, b) elastic-plastic

where the latter comprises also the situation of anisotropic damage due to preferred defect orientations. The boundary condition (on an RVE) of prescribed macrostrains (see (8.72), (8.73)) assumed in Section 8.3 for the derivation of (9.7) corresponds to the equivalent strain principle employed here.

Besides ω according to (9.1) or $\boldsymbol{D}$ according to (9.7) further quantities are utilized for the characterization of damage. Irrespective of the material behavior the generally anisotropic damage due to the presence of microcracks can be described by the *damage tensor*

$$\omega_{ij} = \frac{1}{2V} \int_{A_R} (n_i \Delta u_j + n_j \Delta u_i) \, \mathrm{d}A \; . \tag{9.8}$$

Here, V denotes a representative volume element, Δu_i is the displacement jump, n_i is the unit normal vector, and the integration has to be performed over the entire crack surface A_R, i.e., over all cracks within the volume V. The quantity (9.8) may also be interpreted as an 'eigenstrain' induced by the damage (see (8.50b),(8.53)). If the microcracks do not close completely upon unloading, (9.8) describes the residual (inelastic) strains.

Damage due to voids in ductile materials is often represented by the void volume fraction or *porosity*

$$f = \frac{V_p}{V} \tag{9.9}$$

where V_p is the total volume of voids within the volume V of some RVE. Analogously, the crack density parameter introduced in Section 8.3 may be used as a damage variable to describe damage due to microcracks.

9.3 Brittle damage

The dominant mechanism of brittle damage is the nucleation and growth of microcracks. These cracks usually have a preferred orientation given by the principal axes of the stress tensor. Under tensile loading cracks are observed to grow preferentially

normal to the maximum tensile stress (Fig. 9.3). Their characteristic length in the initial state, however, is typically determined by the microstructure of the material (e.g., grain size). In the course of loading and beyond some critical load the cracks start to grow and multiply which leads to a decreasing stiffness (e.g., Young's mod-

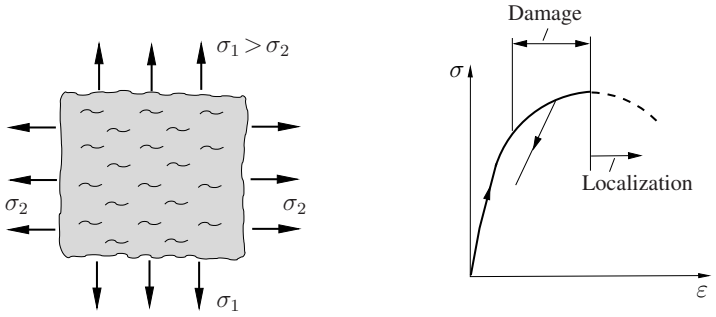

Fig. 9.3 Brittle damage under tensile loading

ulus) in the direction of loading. Although the undamaged matrix material behaves linear elastic the macroscopic behavior of the damaged material is nonlinear because of the increasing damage (Fig. 9.3). The deformation process proceeds in this way until the material becomes macroscopically *unstable* and a *localization* of damage takes place (see Section 9.6). Damage then is no longer uniformly distributed throughout the material; instead a single crack which dominates over the others continues to grow alone.

In case of compressive loading, cracks are often observed to grow into the direction of maximum compressive stress (Fig. 9.4a). They may originate from various mechanisms which give rise to local tensile stress fields. A typical example is a spherical cavity or inhomogeneity at the poles of which a local tensile stress is induced under global compressive load. Another mechanism involves shear cracks under mode-II loading which kink and afterwards grow under local mode-I conditions into the direction of overall compression (Fig. 9.4b). The macroscopic material

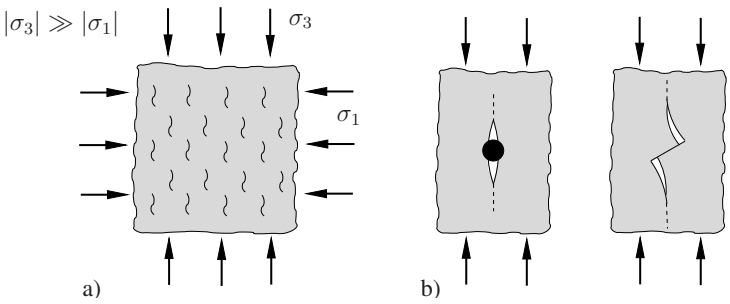

Fig. 9.4 Brittle damage under compressive loading

behavior again is nonlinear due to the increasing damage and in the course of deformation displays a material instability which leads to the localization of damage. This localization often takes place in form of *shear bands* which originate from the growth and coalescence of shear cracks and which are inclined at a certain angle to the overall compressive load.

In the following we consider a simple example of damage under uniaxial tension (Fig. 9.5). The RVE is modeled as a plane region of area ΔA which in the initial state contains only a single mode-I crack. Its length is sufficiently small compared to the distance to other cracks so that the interaction of the cracks need not be accounted

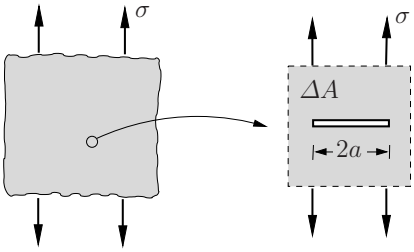

Fig. 9.5 2D model for damage under tensile loading

for (see Section 8.3.2.3). The macroscopic material behavior is described using the complementary energy $\widetilde{U}$ (see Section 1.3.1):

$$\widetilde{U} = \widetilde{U}^e(\sigma_{ij}) + \Delta\widetilde{U}(\sigma_{ij}, a) \; . \tag{9.10}$$

The first term denotes the energy of the undamaged material which according to (1.49) is in the present case given by $\widetilde{U}^e = \sigma^2/2E'$. The second term describes the energy change - related to the size of the RVE - caused by the presence of the microcracks and is computed from the energy release rate $\mathcal{G} = K_I^2/E'$ with $K_I = \sigma\sqrt{\pi a}$:

$$\Delta\widetilde{U} = \frac{2}{\Delta A}\int_0^a \mathcal{G}\mathrm{d}a = \frac{\pi}{E'\Delta A}\sigma^2 a^2 \; . \tag{9.11}$$

This leads to the complementary energy

$$\widetilde{U}(\sigma, a) = \frac{\sigma^2}{2E'}\left(1 + \frac{2\pi}{\Delta A}a^2\right) \tag{9.12}$$

and according to (1.48) one obtains by differentiation

$$\varepsilon(\sigma, a) = \frac{\partial\widetilde{U}}{\partial\sigma} = \frac{\sigma}{E'}\left(1 + \frac{2\pi}{\Delta A}a^2\right) \; . \tag{9.13}$$

The crack length a here has the meaning of an internal variable.

For a fixed crack length ($a = const$) the relation (9.13) describes a linear elastic material represented by the effective Young's modulus $E^* = E'/(1 + 2\pi a^2/\Delta A)$ (see Fig. 9.2a). The damage ω then is determined from (9.6b). In the following it is assumed that the cracks have an initial length $2a_0$ and beyond a certain loading σ_0 or strain ε_0 grow according to the fracture criterion $\mathcal{G}(\sigma, a) = R(\Delta a)$ (see Section 4.8). The latter may equivalently be written as

$$K_I(\sigma, a) = K_R(\Delta a) \qquad \text{or} \qquad \sigma\sqrt{\pi a} = K_R(\Delta a) \tag{9.14}$$

where K_R describes the crack resistance curve for a microcrack. This is the evolution law for the internal variable which together with (9.13) uniquely determines the material behavior:

$$\varepsilon(\sigma, a) = \frac{\sigma}{E'}\left(1 + \frac{2\pi}{\Delta A}a^2\right) \quad \begin{cases} a = const \text{ for } \sigma\sqrt{\pi a} < K_R(\Delta a) \\ \dot{a} > 0 \quad \text{for } \sigma\sqrt{\pi a} = K_R(\Delta a) \end{cases} \tag{9.15}$$

For an illustration the crack resistance curve is represented by $K_R = K_\infty[1 - (1 - K_0/K_\infty)e^{-\eta\Delta a/a_0}]$ where $K_0 = \sigma_0\sqrt{\pi a_0}$ is the initiation value and K_∞ is the plateau value of K_R; the latter is faster or slower attained depending on η. Figure 9.6 shows some macroscopic stress-strain curves obtained from this model.

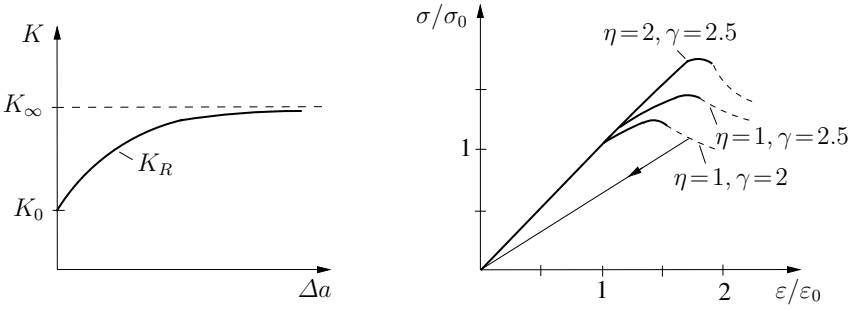

Fig. 9.6 Crack resistance curve and corresponding σ-ε behavior; $2\pi a_0^2/\Delta A = 0.05$, $\gamma = K_\infty/K_0$

9.4 Ductile damage

9.4.1 Void growth

Ductile damage in crystalline solids originates from the nucleation, growth, and coalescence of microvoids. These form preferentially at second-phase particles, grain

boundaries, and other obstacles to the motion of dislocations. They may also initiate from the cracking of brittle inclusions.

Various models exist for the description of void growth alone. Here we consider the model by McClintock (1968) which approximates a single void by a cylindrical hole in an unbounded domain subjected to a radial tensile stress σ_∞ (Fig. 9.7). The surrounding material is taken to be rigid perfectly plastic and a state of plane

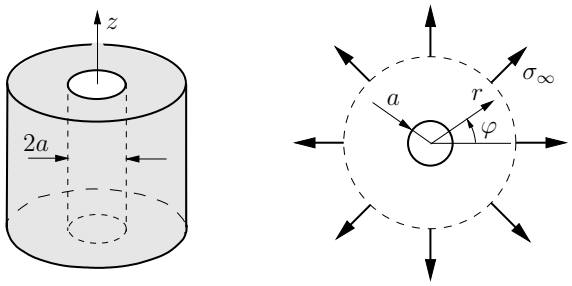

Fig. 9.7 McClintock model

strain is assumed with a prescribed strain rate $\dot{\varepsilon}_z = \dot{\varepsilon}_0$. In cylindrical coordinates and accounting for the rotational symmetry the equilibrium condition reads

$$\frac{\mathrm{d}\sigma_r}{\mathrm{d}r} - \frac{1}{r}(\sigma_\varphi - \sigma_r) = 0 \tag{9.16}$$

while the kinematic relations are given by

$$\dot{\varepsilon}_r = \frac{\mathrm{d}\dot{u}_r}{\mathrm{d}r}\,, \qquad \dot{\varepsilon}_\varphi = \frac{\dot{u}_r}{r} \qquad \rightarrow \qquad \dot{\varepsilon}_r = \frac{\mathrm{d}(r\dot{\varepsilon}_\varphi)}{\mathrm{d}r} \tag{9.17}$$

and the constitutive law follows from Section 1.3.3 to be

$$\begin{aligned} &\dot{\varepsilon}_r = \dot{\lambda}\, s_r\,, \qquad \dot{\varepsilon}_\varphi = \dot{\lambda}\, s_\varphi\,, \qquad \dot{\varepsilon}_z = \dot{\lambda}\, s_z \\ &\text{where} \qquad \dot{\lambda} = \frac{1}{\tau_F}\sqrt{\frac{1}{2}(\dot{\varepsilon}_r^2 + \dot{\varepsilon}_\varphi^2 + \dot{\varepsilon}_z^2)}\,, \qquad\qquad \dot{\varepsilon}_r + \dot{\varepsilon}_\varphi + \dot{\varepsilon}_z = 0 \end{aligned} \tag{9.18}$$

and $\tau_F = \sigma_F/\sqrt{3}$. By using (9.18) and integrating (9.17) the incompressibility condition leads to

$$\dot{\varepsilon}_\varphi + r\,\frac{\mathrm{d}\dot{\varepsilon}_\varphi}{\mathrm{d}r} + \dot{\varepsilon}_\varphi + \dot{\varepsilon}_0 = 0 \qquad \rightarrow \qquad \dot{\varepsilon}_\varphi = \frac{C_1}{r^2} - \frac{\dot{\varepsilon}_0}{2}\,.$$

If the void growth rate is introduced by $\dot{\varepsilon}_a = \dot{a}/a = \dot{u}_r(a)/a = \dot{\varepsilon}_\varphi(a)$ it follows that

$$\dot{\varepsilon}_\varphi = \frac{a^2}{r^2}(\dot{\varepsilon}_a + \dot{\varepsilon}_0/2) - \dot{\varepsilon}_0/2\,, \qquad \dot{\varepsilon}_r = -\frac{a^2}{r^2}(\dot{\varepsilon}_a + \dot{\varepsilon}_0/2) - \dot{\varepsilon}_0/2\,. \tag{9.19}$$

With the abbreviation

$$\xi = \frac{2a^2}{\sqrt{3}\,r^2}\;\frac{\dot\varepsilon_a + \dot\varepsilon_0/2}{\dot\varepsilon_0}$$

equation (9.19) yields

$$\sigma_\varphi - \sigma_r = s_\varphi - s_r = \frac{\tau_F(\dot\varepsilon_\varphi - \dot\varepsilon_r)}{\sqrt{\frac{1}{2}(\dot\varepsilon_r^2 + \dot\varepsilon_\varphi^2 + \dot\varepsilon_z^2)}} = \tau_F\;\frac{2\xi}{\sqrt{1+\xi^2}}\;.$$

Using this the equilibrium condition can be written in the following form and can be solved by integration:

$$\frac{\mathrm{d}\sigma_r}{\mathrm{d}\xi} = -\frac{\tau_F}{\sqrt{1+\xi^2}} \qquad \rightarrow \qquad \sigma_r = -\tau_F\,\mathrm{arsinh}\,\xi + C_2\;.$$

From the boundary conditions $\sigma_r(r\to\infty) = \sigma_\infty$ and $\sigma_r(r=a) = 0$ one finally obtains

$$\dot\varepsilon_a = \frac{\dot\varepsilon_0}{2}\left(\sqrt{3}\;\sinh\frac{\sigma_\infty}{\tau_F} - 1\right)\;. \tag{9.20}$$

Using (9.19) one may replace $\dot\varepsilon_0$ by the equivalent plastic strain rate at infinity: $\dot\varepsilon_{\mathrm{e}}^p = [\frac{3}{2}(\dot\varepsilon_z^2 + \dot\varepsilon_\varphi^2 + \dot\varepsilon_r^2)]^{1/2} = \dot\varepsilon_0$. With the hydrostatic stress at infinity $\sigma_m = \sigma_{kk}/3 = \sigma_r - s_r = \sigma_\infty + \tau_F/\sqrt{3}$ and by introducing the growth rate of the void volume by $\dot V_P/V_P = 2\dot\varepsilon_a + \dot\varepsilon_0$ the above result can be written in the form

$$\frac{\dot V_P}{V_P} = \sqrt{3}\;\dot\varepsilon_{\mathrm{e}}^p\;\sinh\frac{\sigma_m - \tau_F/\sqrt{3}}{\tau_F}\;. \tag{9.21}$$

It states that void growth ($\dot V_P > 0$) requires a sufficiently high hydrostatic stress σ_m and that the growth rate increases with σ_m.

A similar result follows from the model by RICE and TRACEY (1969) for the growth rate of a single spherical void in an unbounded domain of a perfectly plastic material:

$$\frac{\dot V_P}{V_P} = 0.85\,\dot\varepsilon_{\mathrm{e}}^p \exp\frac{3\sigma_m}{2\sigma_F}\;. \tag{9.22}$$

As in the previous model it is assumed that at infinity the strain rate $\dot\varepsilon_z = -2\dot\varepsilon_x = -2\dot\varepsilon_y = \dot\varepsilon_0$ prevails which corresponds to a state of uniaxial tension in an incompressible material: $\dot\varepsilon_{\mathrm{e}}^p = \dot\varepsilon_0$.

These results can be employed in the framework of damage mechanics if one assumes that the voids are sufficiently far away from each other so that their interaction may be neglected. They can, however, be also directly applied to elastic-plastic fracture mechanics. Ahead of a crack tip typically a high hydrostatic stress prevails. If it is approximated by (5.22) one obtains $\sigma_m \approx \tau_F(1+\pi)$ and it follows from (9.20) or (9.21) (which yield practically equal results) that $\dot V_P/V_P \approx 31\,\dot\varepsilon_{\mathrm{e}}^p$. This indicates pronounced void growth ahead of a crack tip in ductile materials.

9.4.2 Damage models

In order to investigate the damage behavior of a ductile material we now assume isotropic damage by distributed voids which can be characterized by the porosity f. The description of the elastic-plastic material behavior proceeds analogous to that of undamaged materials (see Section 1.3.3). According to (1.73) the strain rate is split into an elastic and a plastic part where the elastic part is governed by the elasticity law (1.39). The plastic part is determined from a yield condition and a flow rule. In contrast to an undamaged material now the yield condition depends not only on the stress state σ_{ij} but also on the damage variable f: $F(\sigma_{ij}, f) = 0$. Moreover, it can no longer be assumed that the hydrostatic stress σ_m or the invariant I_σ, respectively, has no influence on plastic flow; it rather controls void growth and the volumetric plastic strain (see Section 9.4.1). Correspondingly, the yield condition can be expressed as

$$F(I_\sigma, II_s, f) = 0 \tag{9.23}$$

where it has been assumed that F does not depend on III_s. The volumetric plastic strain caused by void growth is given by the volume change of the RVE: $\dot{V}/V = \dot{\varepsilon}^p_V = \dot{\varepsilon}^p_{kk}$. Noting that the matrix material is plastically incompressible this together with (9.9) yields the evolution law for the damage variable

$$\dot{f} = (1 - f)\, \dot{\varepsilon}^p_{kk} \; . \tag{9.24}$$

Among the various existing models which differ by the specific forms of the yield condition and details of the further evaluation only the model by GURSON (1977) is considered in the following. It is based on the yield condition

$$F(I_\sigma, II_s, f) = \frac{\sigma_{\mathrm{e}}^2}{\sigma_{_M}^2} + 2f \cosh \frac{3\sigma_m}{2\sigma_{_M}} - \left(1 + f^2\right) = 0 \tag{9.25}$$

where $\sigma_{\mathrm{e}} = (\frac{3}{2} s_{ij} s_{ij})^{1/2}$ is the macroscopic equivalent stress and $\sigma_{_M}$ denotes the yield stress of the matrix material. It should be noted that $\sigma_{_M}$ is an effective (spatially constant) yield stress which appropriately represents the in reality inhomogeneous state of plastic flow and hardening in the entire matrix material surrounding the voids. The Gurson yield condition (9.25) covers some important special cases. For purely hydrostatic loading ($\sigma_{\mathrm{e}} = 0$) (9.25) reduces to the exact analytical solution (8.164). On the other hand, under deviatoric loading ($\sigma_m = 0$) it coincides with the upper bound (8.161) by virtue of $\cosh(0) = 1$. And obviously (9.25) reduces to the von Mises yield condition (1.77) for $f = 0$ where the influence of hydrostatic stress vanishes. The macroscopic plastic strain rate is obtained from the flow rule

$$\dot{\varepsilon}^p_{ij} = \dot{\lambda}\, \frac{\partial F}{\partial \sigma_{ij}} \; . \tag{9.26}$$

It is furthermore assumed that the plastic work rate of the matrix stress – expressed in terms of the yield stress $\sigma_{_M}$ and the corresponding equivalent plastic strain rate

$\dot{\varepsilon}^p_{_M}$ – is equal to the respective work rate of the macroscopic stress:

$$\sigma_{ij}\,\dot{\varepsilon}^p_{ij} = (1-f)\sigma_{_M}\dot{\varepsilon}^p_{_M}\ . \tag{9.27}$$

From the knowledge of the uniaxial stress-strain curve of the undamaged material, i.e., from the relation $\dot{\varepsilon}^p_{_M}(\dot{\sigma}_{_M})$, thus the macroscopic material behavior is known.

It has been found that the behavior of a ductile damaged material can not be satisfactorily represented by the equations (9.24) to (9.27). For instance, they predict the loss of stress-carrying capacity at an unrealistically high value of the damage variable. One reason for this lies in the fact that in the above model the nucleation of voids as well as the increasing interaction of voids in the course of their growth and their final coalescence are not accounted for. Better results are obtained from the modified yield condition according to TVERGAARD and NEEDLEMAN (1984)

$$F(I_\sigma, II_s, f) = \frac{\sigma_e^2}{\sigma_{_M}^2} + 2q_1 f^* \cosh\frac{3q_1\sigma_m}{2\sigma_{_M}} - \left(1+(q_1 f^*)^2\right) = 0 \tag{9.28}$$

where q_1 and q_2 are material parameters. The function $f^*(f)$ is chosen in such a way that total material failure occurs at a realistic amount of damage ($f \approx 0.25$). In addition, the contribution of void nucleation (from second-phase particles) to the change of the porosity is taken into account. Strain-controlled nucleation of voids is described by

$$\dot{f}_{nucl} = \mathcal{D}(\varepsilon^p_{_M})\, f_N\, \dot{\varepsilon}^p_{_M}\ , \qquad \mathcal{D}(\varepsilon^p_{_M}) = \frac{1}{\sigma\sqrt{2\pi}}\exp\left[-\frac{(\varepsilon^p_{_M}-\varepsilon_N)^2}{2\sigma^2}\right] \tag{9.29}$$

where f_N is the volume fraction of particles at which voids nucleate. The function $\mathcal{D}$ is a normal distribution with the average value ε_N and the standard deviation σ (see also Section 10.2). The total change of porosity thus consists of the growth term (9.24) plus the nucleation term (9.29). It should be mentioned that a representation similar to (9.29) may be adopted for stress-controlled void nucleation (i.e., by fracture of particles).

Figure 9.8 shows the material behavior under uniaxial tension for a particular choice of material parameters. For the matrix material a power law behavior has

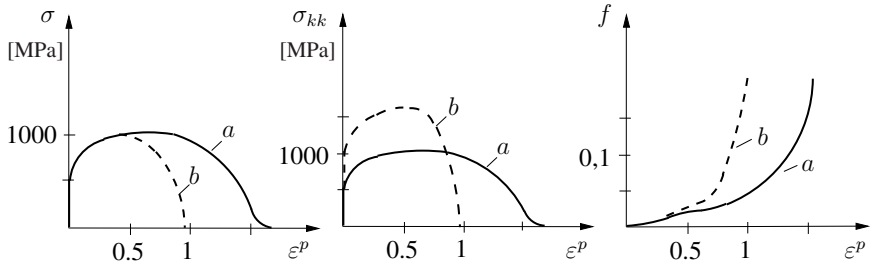

Fig. 9.8 Gurson model: uniaxial tension, (a) without, (b) with suppression of lateral strain

been assumed. Depicted are the variations of tensile stress σ, hydrostatic stress σ_{kk}, and damage f as functions of the plastic strain ε^p (the small elastic strains ε^e are neglected). It can be seen that with increasing plastic strain also the damage increases which gives rise first to a softening behavior and later to the total loss of stress-carrying capacity. A remarkable effect arises from the suppression of lateral strain (contraction of the specimen). This constraint promotes a stronger evolution of damage with the result that failure takes place at smaller macroscopic plastic strains.

9.4.3 Fracture concept

Damage models describe the material behavior until the total loss of the stress-carrying capacity. Local failure, i.e., fracture, takes place when the damage f attains a critical value f_c:

$$\boxed{f = f_c} \tag{9.30}$$

Such a local failure criterion can be employed in the treatment of various problems of fracture mechanics. For instance, it may be used to describe the formation of a crack after preceding damage. Furthermore, (9.30) can be employed as a fracture criterion which has to be satisfied at crack initiation and in the course of subsequent crack growth. This approach bears the advantage that fracture parameters such as J, δ_t, or J_R-curves are not needed.

Finally, a drawback of (continuum) damage mechanics should be emphasized: as repeatedly mentioned the increase of damage leads to an instability in the macroscopic material behavior (softening) which gives rise to the localization of deformation and damage (e.g., growth of only a single crack or void growth within a narrow band). Such a localization violates the requirements of an RVE discussed in Section 8.3.1 and micromechanically motivated damage models loose their validity. Damage variables then no longer have their originally ascribed physical meaning, they are only formal parameters. Another disadvantage of continuum damage mechanics consists in the dependence of numerical solutions of boundary value problems on the underlying discretization (finite element mesh) which often occurs also as a consequence of localization.

9.5 Material softening and strain localization

The afore mentioned influence of a damage-induced softening material behaviour on the localization of strain shall now be discussed more thoroughly. By *softening* the situation is denoted when the stress in a material decreases with increasing deformation, as sketched in Figs. 9.2 and 9.3 or computed from specific damage models in Figs. 9.6 and 9.8.

As long as an increase of deformation requires an increasing stress, a material behaviour is called *stable*; the stress and strain increments then fulfill the condition $\mathrm{d}\sigma\mathrm{d}\varepsilon > 0$, or $\mathrm{d}\sigma_{ij}\mathrm{d}\varepsilon_{ij} > 0$ in the 3D case, respectively. Conversely, a softening material behaviour with $\mathrm{d}\sigma\mathrm{d}\varepsilon < 0$ is called *unstable*; the resistance against deformation then decreases with increasing strain. Of particular interest is the transition where $\mathrm{d}\sigma\mathrm{d}\varepsilon = 0$ holds so that at vanishing stress change various changes of strain become possible; i.e. a *bifurcation* of deformation takes place.

Following DOGHRI (2000) this is exemplified using a simple one-dimensional material model with damage

$$\sigma = E(1-D)\varepsilon \quad , \tag{9.31}$$

where at some instant t the damage variable D is determined by the maximum value of strain attained throughout the prior history:

$$D(t) = \frac{1}{\varepsilon_f} \max_{\tau \le t} \varepsilon(\tau) \tag{9.32}$$

The ultimate strain at failure (fracture strain) is denoted by ε_f so that the damage variable lies in the range $0 \le D \le 1$. Under monotonically increasing strain it is given by $D = \varepsilon/\varepsilon_f$ and the stress-strain response

$$\sigma = E\left(1 - \frac{\varepsilon}{\varepsilon_f}\right)\varepsilon \tag{9.33}$$

displays a parabolic variation as depicted by the solid curve in Fig. 9.9.

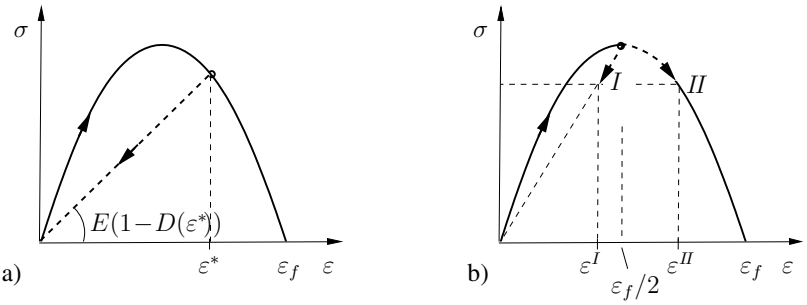

Fig. 9.9 a) Strain-controlled unloading, b) bifurcation of strain during reduction of stress

If at some arbitrary state ε^* the strain is reduced (strain-controlled unloading), the damage variable remains constant and the stress follows the dashed linear path with slope $E(1-D(\varepsilon^*))$ in Fig. 9.9a. From the total work (per volume) $\int_0^{\varepsilon^*} \sigma \mathrm{d}\varepsilon$ done by the stress up to ε^* (area below the solid curve) the portion below the linear unloading curve is recovered as elastic energy while the remaining (shaded) portion has been dissipated by the damage. If, in contrast, unloading proceeds by a con-

trolled reduction of stress (Fig. 9.9b) after the maximum of the $\sigma(\varepsilon)$ curve has been passed, i.e. in the range where $\mathrm{d}\sigma\mathrm{d}\varepsilon \leq 0$, two different strain changes towards states ε^I and ε^{II} are possible (bifurcation). The material then can respond either by elastic unloading (I) or by continued inelastic deformation with increasing damage (II).

In a spatially extended domain such as the tensile bar in Fig. 9.10a this leads to the coexistence of subdomains with different strain states, ε^I and ε^{II}, at the same stress. With the end displacement u and the total length $L = L^I + L^{II}$ of the bar, its macroscopic strain is given by

$$\langle\varepsilon\rangle = \frac{u}{L} = \frac{L^I}{L}\,\varepsilon^I + \frac{L^{II}}{L}\,\varepsilon^{II} \quad , \tag{9.34}$$

while the macroscopic stress is $\langle\sigma\rangle = \sigma$. The material response in the different subdomains is

$$\sigma = E(1 - D^I)\varepsilon^I \quad \text{where} \quad D^I = \frac{\varepsilon_f/2}{\varepsilon_f} = \frac{1}{2} \qquad \begin{array}{c}\text{(elastic unloading}\\ \text{from } \varepsilon_f/2)\end{array} \tag{9.35}$$

and

$$\sigma = E(1 - D^{II})\varepsilon^{II} = E\left(1 - \frac{\varepsilon^{II}}{\varepsilon_f}\right)\varepsilon^{II} \qquad \begin{array}{c}\text{(continued inelastic}\\ \text{deformation).}\end{array} \tag{9.36}$$

Inserting this into (9.34) yields

$$\langle\varepsilon\rangle = \frac{L^I}{L}\,\frac{2}{E}\,\langle\sigma\rangle + \frac{L^{II}}{L}\,\frac{\varepsilon_f}{2}\left(1 + \sqrt{1 - \frac{4}{\varepsilon_f E}\,\langle\sigma\rangle}\right). \tag{9.37}$$

The macroscopic (overall) response of the tensile bar is depicted in Fig. 9.10b for different lengths L^{II} of the subdomain in which continued straining and damage

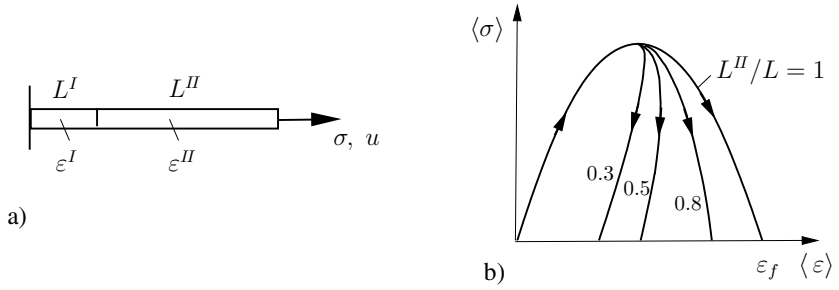

Fig. 9.10 a) Tensile bar, b) overall stress-strain response

takes place. Among the infinitely many solutions of the boundary value problem (infinitely many possible values of L^I and L^{II}, respectively) that one is energeti-

cally preferable (least dissipation and maximum energy release) where continued inelastic straining and damage proceeds in a vanishingly thin region, i.e. $L^{II} \to 0$. That means that a softening material behavior according to (9.31) and (9.32) leads to a *localization* of deformation. In case of the tensile bar this results in the formation of a crack.

In the following, the effect of a damage-induced softening material behaviour on the localization of deformation is discussed for the 3D continuum. The bifurcation of deformation preceding a strain localization then corresponds to the occurrence of a surface in the material across which the strain increment $\mathrm{d}\varepsilon_{ij}$, or the strain rate tensor $\dot{\varepsilon}_{ij}$, is discontinuous, i.e. experiences a jump

$$\Delta\dot{\varepsilon}_{ij} = \dot{\varepsilon}^{II}_{ij} - \dot{\varepsilon}^{I}_{ij} \neq 0 \quad . \tag{9.38}$$

Owing to local equilibrium, the stress vector $t_i = \sigma_{ij} n_j$ remains continuous

$$\Delta\dot{t}_i = \dot{t}^{II}_i - \dot{t}^{I}_i = 0 \quad , \tag{9.39}$$

where n_j denotes the unit normal vector on the surface. A possible jump of the strain rate tensor depends on two directions: the orientation n_i of the surface of discontinuity and the direction of the strain component undergoing a jump. This is accounted for by the representation

$$\Delta\dot{\varepsilon}_{ij} = \frac{1}{2}\left(n_i\, g_j + n_j\, g_i\right) \tag{9.40}$$

with some arbitrary vector g_i. If g_i is parallel to n_i a jump of longitudinal strain rate is described by $\Delta\dot{\varepsilon}_{ij}$ (as in the foregoing 1D example of a tensile bar) whereas the case of g_i normal to n_i corresponds to a jump in shear strain rate. We assume that the material behaviour is given in incremental form by

$$\dot{\sigma}_{ij} = \tilde{C}_{ijkl}\, \dot{\varepsilon}_{kl} \tag{9.41}$$

with the forth-order tangent tensor $\tilde{C}_{ijkl}$. Due to the symmetry of $\tilde{C}_{ijkl}$ with respect to the indices k and l this can also be written as

$$\dot{\sigma}_{ij} = \tilde{C}_{ijkl}\, \dot{u}_{k,l} \tag{9.42}$$

where $\dot{u}_{k,l}$ is the velocity gradient (see Section 1.2.1); according to (9.40) it undergoes a jump $\Delta\dot{u}_{i,j} = n_i g_j$. Inserting (9.42) into (9.39) yields

$$\left(\tilde{C}^{II}_{ijkl}\, \dot{u}^{II}_{k,l} - \tilde{C}^{I}_{ijkl}\, \dot{u}^{I}_{k,l}\right) n_j = 0 \quad , \tag{9.43}$$

where $\tilde{C}^{I}_{ijkl}$ and $\tilde{C}^{II}_{ijkl}$ characterize the different material behaviour (elastic unloading or continued inelastic straining) in the subdomains I and II on either side of the surface. At the instant of bifurcation the material behaviour in the two domains is still the same so that $\tilde{C}^{II}_{ijkl} = \tilde{C}^{I}_{ijkl} = \tilde{C}_{ijkl}$ holds. Inserting this together with the

representation $\dot{u}^{II}_{k,l} - \dot{u}^{I}_{k,l} = \Delta\dot{u}_{k,l} = g_k n_l$ into (9.43) leads to

$$\underbrace{\tilde{C}_{ijkl}\, n_j\, n_l}_{A_{ik}}\, g_k = 0 \quad . \tag{9.44}$$

This is a homogeneous linear system of equations for the unknown vector g_k where the matrix A_{ik} contains the components of the so-called *acoustic tensor*. A necessary condition for the existence of non-trivial solutions $g_k \neq 0$ is that the determinant of the acoustic tensor vanishes:

$$\det A_{ik} = 0 \quad . \tag{9.45}$$

Note, that $\det A_{ik}$ is a function of the current material behaviour $\tilde{C}_{ijkl}$ and the orientation n_i. The condition (9.45) is a prerequisite for the occurrence of a surface of discontinuity with respect to the strain rate tensor, i.e. for a bifurcation of deformation into states ε^{I}_{ij} and ε^{II}_{ij}. Since the inelastic deformation (softening) thereby takes place in an infinitely thin region, the consequence is the formation of a crack in case g_i is parallel to n_i or of a shear band if g_i is normal to n_i. The orientation n_i of this localization zone is determined by the first-time fulfillment of the condition (9.45) in the course of deformation.

9.6 Further reading

Bazant, Z.P. and Planas, J. *Fracture and Size Effects in Concrete and Other Quasibrittle Materials*. CRC Press, Boca Raton, 1997

Doghri, I. *Mechanics of Deformable Solids*. Springer, Berlin, 2000

Gurson, A.L. Continuum theory of ductile rupture by void nucleation and growth. *Journal of Engineering Materials and Technology* **99** (1977), 2-15

Hutchinson, J.W. *Micro-Mechanics of Damage in Deformation and Fracture*, The Technical University of Denmark, 1987

Kachanov, L.M. *Introduction to Continuum Damage Mechanics*. Martinus Nijhoff Publishers, Dordrecht, 1986

Kachanov, M. *Elastic Solids with Many Cracks and Related Problems*. In *Advances in Applied Mechanics*, Vol. 30, pp. 259-445, Academic Press, 1993

Krajcinovic, D. *Damage Mechanics*. Elsevier, Amsterdam, 1996

Lemaitre, J. *A Course on Damage Mechanics*. Springer, Berlin, 1992

Miannay, D.P. *Fracture Mechanics*. Springer, New York, 1998

Skrzypek, J. and Ganczarski, A. *Modeling of Material Damage and Fracture of Structures*. Springer, Berlin, 1999

Chapter 10
Probabilistic fracture mechanics

10.1 Introduction

The failure analysis of a structure proceeds on the basis of a fracture or failure criterion. A typical example is the criterion of brittle fracture $K_I = K_{Ic}$ which states that failure does not take place for $K_I < K_{Ic}$. Application of such a criterion in the deterministic sense requires all involved quantities to be exactly known. This, however, is not always the case. For instance, the in-service loading conditions of a technical component as well as the material's fracture toughness K_{Ic} may scatter. Also the location, size, and orientation of cracks is sometimes not precisely known. If these details are neglected and only 'averaged' quantities are employed the deterministic analysis may lead to rather vague results. If, on the other hand, the fluctuations are accounted for by considering an upper bound for K_I and a lower bound for K_{Ic} one obtains results which might be safe but probably are too conservative. It also has to be noted that these bounds likewise may not be exactly known. In any way, the risk of fracture remains unknown in the framework of a deterministic analysis. The same holds for all other failure criteria such as the classical failure hypotheses discussed in Chapter 2 or the life-time hypothesis according to the Paris law (Section 4.11).

In contrast to the deterministic analysis, the probabilistic approach takes into account the scatter and uncertainties of material properties, loading conditions, and defect distribution in an appropriate manner. Thereby it is assumed that the quantities entering a failure criterion are given in terms of probability distributions. This leads to statements with respect to the failure probability which determines the risk of fracture.

Statistical aspects also come into play when microstructural features of a material, which are relevant for its fracture behavior, are to be accounted for. In real materials usually a multitude of 'defects' such as microvoids, microcracks, inclusions, or inhomogeneities of different size, shape, and orientation are found which have a strong influence on the fracture process. Because of their large number the

D. Gross and T. Seelig, *Fracture Mechanics: With an Introduction to Micromechanics*, Mechanical Engineering Series, DOI 10.1007/978-3-642-19240-1_10,

effect of these defects on the macroscopic behavior is suitably described by means of statistical methods.

The present chapter deals only with the basic concepts of probabilistic fracture mechanics. It is restricted to brittle materials the strength properties of which may display especially strong scatter. Brittle materials often also show a pronounced decrease in strength with increasing volume of a testing specimen. The reason for this is the distribution of defects: the probability for the occurrence of a critical defect increases with the volume under consideration. This is the foundation of the statistical theory of brittle fracture developed by W. WEIBULL. In many situations it is employed for the assessment of the behavior of ceramics, fiber-reinforced materials, geological materials, concrete, or brittle metals.

10.2 Foundations

The frequency by which some quantity x occurs, for instance, the measured K_{Ic} value of a material or a crack length, is described by the *probability density* $f(x)$ (Fig. 10.1). If we assume that x attains only positive values the *probability distribution* is given by

$$F(x) = \int_0^x f(\bar{x})\mathrm{d}\bar{x} \; . \tag{10.1}$$

It determines the probability P that a random variable X lies in the interval $0 \leq X \leq x$:

$$P(X \leq x) = F(x) \; . \tag{10.2}$$

Since P can attain values between 0 and 1 the following relations hold:

$$\begin{aligned} P(X < \infty) &= \int_0^\infty f(x)\mathrm{d}x = 1 \; , \\ P(X \geq x) &= 1 - F(x) \; , \\ P(a \leq X \leq b) &= \int_a^b f(x)\mathrm{d}x = F(b) - F(a) \; . \end{aligned} \tag{10.3}$$

The *mean* (or *expectation*) *value* $\langle X \rangle$ of a random variable and the *variance* $varX$ are defined as

$$\begin{aligned} \langle X \rangle &= \int_0^\infty x f(x)\mathrm{d}x = \int_0^\infty [1 - F(x)]\mathrm{d}x \; , \\ varX &= \int_0^\infty [x - \langle X \rangle]^2 f(x)\mathrm{d}x \; . \end{aligned} \tag{10.4}$$

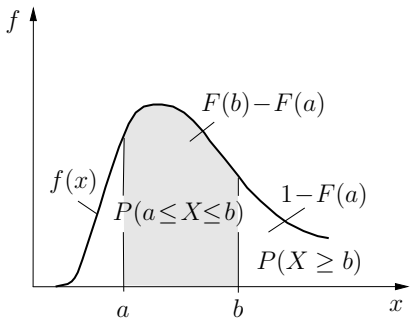

Fig. 10.1 Probability density and distribution

The latter can also be described as the average square deviation from the mean value $\langle X \rangle$. The square root of the variance is called the *standard deviation*: $\sigma = \sqrt{varX}$.

Among the various functions used to describe probability densities and distributions only a few a presented here. The *normal distribution* (Gaussian distribution) is given by (see Fig. 10.2a)

$$f(x) = \frac{1}{\sigma\sqrt{2\pi}} \exp\left(-\frac{(x-\mu)^2}{2\sigma^2}\right) \tag{10.5}$$

where μ denotes the mean value and σ the standard deviation. K_{Ic} and J_c values or other material parameters as well as their scatter are often described by normal distributions.

The *logarithmic normal distribution* or *lognormal distribution* (Fig. 10.2b) is defined by

$$f(x) = \frac{1}{\sigma\sqrt{2\pi x}} \exp\left(-\frac{(\ln x - \mu)^2}{2\sigma^2}\right) \tag{10.6}$$

with the mean value $\langle X \rangle = \mathrm{e}^{\mu+\sigma^2/2}$ and the variance $varX = \mathrm{e}^{2\mu+\sigma^2}(\mathrm{e}^{\sigma^2} - 1)$. It is in many cases employed to describe loading conditions and distributions of crack lengths and defects.

Of special importance is the *Weibull distribution*. Its density and probability distribution are given by (see Fig. 10.2c)

$$f(x) = \lambda\alpha x^{\alpha-1}\mathrm{e}^{-\lambda x^\alpha}\,, \qquad F(x) = 1 - \mathrm{e}^{-\lambda x^\alpha}\,. \tag{10.7}$$

This yields the mean value and variance

$$\langle X \rangle = \frac{\Gamma(1+\frac{1}{\alpha})}{\lambda^{1/\alpha}}\,, \qquad varX = \frac{\Gamma(1+\frac{2}{\alpha}) - [\Gamma(1+\frac{1}{\alpha})]^2}{\lambda^{2/\alpha}} \tag{10.8}$$

where Γ denotes the Gamma function. The Weibull distribution is very often applied to fatigue processes and for the characterization of the distribution of crack lengths and defects in brittle materials. In the special case $\alpha = 1$ it is also called *exponential distribution*.

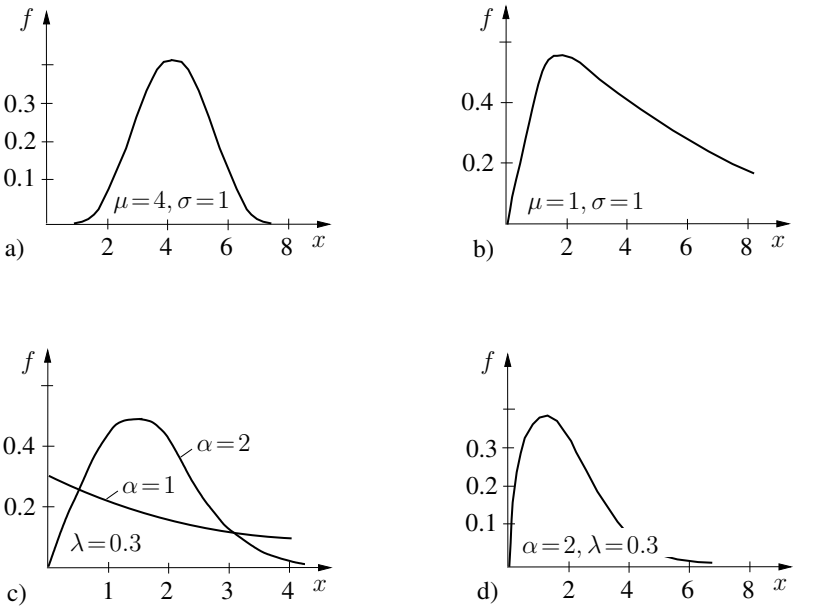

Fig. 10.2 Probability density: a) normal distribution, b) lognormal distribution, c) Weibull distribution, d) Gamma distribution

Finally, the *Gamma distribution* should be mentioned which is given by

$$f(x) = \lambda \frac{(\lambda x)^{\alpha-1}}{\Gamma(\alpha)} \mathrm{e}^{-\lambda x} \tag{10.9}$$

with $\langle X \rangle = \alpha/\lambda$ and $varX = \alpha/\lambda^2$ (Fig. 10.2d). It is likewise used to approximate the distribution of defect sizes. For $\alpha = 1$ it also reduces to the exponential distribution. The lognormal distribution, the Weibull distribution, and the Gamma distribution are nonsymmetric and therefore better suited for the characterization of failure-relevant properties than the symmetric normal distribution. An explanation for this is given in case of the Weibull distribution in the following section.

10.3 Statistical fracture concept of Weibull

10.3.1 Fracture probability

We consider an isotropic brittle material which is subjected to a uniform uniaxial stress σ and which contains internal defects (e.g., microcracks) but no macroscopic crack. The defects are assumed to be distributed in a statistically homogeneous manner, i.e., the probability of the occurrence of a defect of a particular kind, size, ori-

entation, etc. is everywhere the same. In addition it is assumed that total failure of the material (= fracture) takes place if a single defect becomes critical and starts to grow. This be possible only under tensile loading; defect growth under compressive loading is precluded for simplicity.

The probability that at a tensile stress σ a certain volume V does not contain a critical defect is denoted by $F^*(V)$. The respective probability for some other arbitrary volume V_1 (which does not contain V) is $F^*(V_1)$. If events in V and V_1 are independent of each other the probability that no critical defect is found in $V+V_1$ is given by

$$F^*(V+V_1) = F^*(V)F^*(V_1)\ . \tag{10.10}$$

Differentiation at fixed V_1 and subsequent division by (10.10) yields

$$\frac{\mathrm{d}F^*(V+V_1)}{\mathrm{d}V} = \frac{\mathrm{d}F^*(V)}{\mathrm{d}V}F^*(V_1)\ , \qquad \frac{\left[\dfrac{\mathrm{d}F^*(V+V_1)}{\mathrm{d}V}\right]}{F^*(V+V_1)} = \frac{\left[\dfrac{\mathrm{d}F^*(V)}{\mathrm{d}V}\right]}{F^*(V)}$$

or

$$\frac{\mathrm{d}}{\mathrm{d}V}\ln[F^*(V+V_1)] = \frac{\mathrm{d}}{\mathrm{d}V}\ln[F^*(V)] = -c\ .$$

Here, c is a constant which depends only on stress: $c = c(\sigma)$. Integration and noting that $F^*(0) = 1$ finally leads to the probability that no critical defect is contained in the volume V:

$$F^*(V) = \mathrm{e}^{-cV}\ . \tag{10.11}$$

Conversely, the probability that V contains a critical defect is $F(V) = 1-F^*(V) = 1-\mathrm{e}^{-c(\sigma)V}$. By virtue of the assumption that a single critical defect leads to failure, this is the fracture probability P_f:

$$\boxed{P_f = 1-\mathrm{e}^{-c(\sigma)V}}\ . \tag{10.12}$$

Accordingly, the fracture probability at constant c (i.e., constant σ) increases with increasing volume. The 'survival probability' (no failure) is given by $P_s = 1-P_f = \mathrm{e}^{-cV}$ and decreases with increasing volume.

Equation (10.12) is rather general since it does not contain any assumption with regard to the physical nature of the defects. Whether they are microcracks or other stress concentrators is irrelevant. In case of surface-like or bar-shaped bodies the volume has to be replaced by the area or length, respectively. Comparison with (10.7) shows that at fixed c (10.12) represents an exponential distribution. Thereby $c = 1/\bar{V}$ can be interpreted as the average concentration of defects. The smaller the average volume $\bar{V}$ per defect is, the faster the increase of P_f with V takes place. The assumptions underlying (10.12) are also referred to as *weakest link theory*. It corresponds to a chain which fails at the location of the weakest link when the tensile strength of the latter is exceeded.

The relation $c(\sigma)$ in (10.12) is an unknown function for which often the empirical representation according to Weibull

$$c(\sigma) = \begin{cases} \dfrac{1}{V_0}\left(\dfrac{\sigma - \sigma_u}{\sigma_0}\right)^m & \text{for } \sigma > \sigma_u \\ 0 & \text{for } \sigma \le \sigma_u \end{cases} \tag{10.13}$$

is chosen. Here, V_0 and σ_0 are normalization parameters and σ_u is the threshold stress below which the fracture probability is zero. For simplicity the latter is frequently set to zero. The material-specific exponent m is called *Weibull modulus*; some values are given in Table 10.1. Insertion of (10.13) into (10.12) yields the Weibull distribution (see (10.7)) for the fracture probability

$$\boxed{P_f = F(\sigma) = 1 - \exp\left[-\frac{V}{V_0}\left(\frac{\sigma - \sigma_u}{\sigma_0}\right)^m\right]} \tag{10.14}$$

where V now is taken to be fixed.

material	m
glass	2.3
SiC	4...10
Al_2O_3	8...20
graphite	12
cast iron	38

Table 10.1 Weibull modulus

The relation (10.14) holds only for a homogeneous uniaxial stress state. It can, however, easily be generalized to an inhomogeneous uniaxial stress state as it prevails, for instance, in a beam subjected to bending. For this purpose we apply (10.11) to a volume element ΔV_i in which the constant stress σ_i prevails: $c_i = c(\sigma_i)$. Then

$$F^*(\Sigma \Delta V_i) = \mathrm{e}^{-c_1 \Delta V_1} \mathrm{e}^{-c_2 \Delta V_2} \mathrm{e}^{-c_3 \Delta V_3} \ldots = \mathrm{e}^{-\Sigma c_i \Delta V_i}$$

describes the probability that in a sum of volume elements with different stresses no critical defect is found. Performing the limit process yields $F^*(V) = \exp[-\int c \mathrm{d}V]$ and using (10.13) one obtains for the fracture probability

$$P_f = F(\sigma) = 1 - F^* = 1 - \exp\left[-\frac{1}{V_0}\int_V \left(\frac{\sigma - \sigma_u}{\sigma_0}\right)^m \mathrm{d}V\right] . \tag{10.15}$$

10.3.2 Fracture stress

The fracture probability $F(\sigma)$ of a body subjected to uniform tension is given by (10.14). Setting $\sigma_u = 0$ one obtains from (10.7), (10.8) the mean fracture stress (= tensile strength) and variance

$$\begin{aligned} \bar{\sigma} = \langle\sigma\rangle &= \sigma_0 \left(\frac{V_0}{V}\right)^{\frac{1}{m}} \Gamma(1+1/m)\ , \\ var\,\sigma &= \sigma_0^2 \left(\frac{V_0}{V}\right)^{\frac{2}{m}} \left\{\Gamma(1+2/m) - [\Gamma(1+1/m)]^2\right\}\ . \end{aligned} \tag{10.16}$$

Accordingly, both quantities depend on the volume of the body. For one and the same material and two different volumes V_1 and V_2 one obtains

$$\frac{\bar{\sigma}_1}{\bar{\sigma}_2} = \left(\frac{V_2}{V_1}\right)^{1/m}\ , \qquad \frac{(var\,\sigma)_1}{(var\,\sigma)_2} = \left(\frac{V_2}{V_1}\right)^{2/m}\ . \tag{10.17}$$

For instance, $V_2/V_1 = 5$ and $m = 2$ leads to the values $\bar{\sigma}_1/\bar{\sigma}_2 = 2.24$ and $(var\,\sigma)_1/(var\,\sigma)_2 = 5$. Hence the mean fracture stress for the smaller volume V_1 is more than twice that of V_2; the variance, however, is also larger. It should be mentioned that the first equation in (10.17) allows for the determination of m by measuring the mean fracture stress for different volumes.

In order to investigate the influence of a nonuniform stress state we consider a beam of length l with a rectangular cross section (width b, height h) subjected to a constant bending moment. The stress distribution across the height of the beam is in this case given by $\sigma(z) = \sigma_{_B} 2z/h$ where $\sigma_{_B}$ is the maximum stress at the boundary. Insertion into (10.15) with $V = lbh$ yields for this case

$$P_f = F(\sigma_{_B}) = 1 - \exp\left[-\frac{V}{V_0}\left(\frac{\sigma_{_B}}{\sigma_0}\right)^m \frac{1}{2(m+1)}\right] \tag{10.18}$$

where it has to be noted that the integration is performed only over the tensile region (defects in the compressive part of the beam are considered to have no effect!). The mean fracture stress in case of bending (= bending strength) and the variance are obtained from (10.7) as

$$\begin{aligned} \bar{\sigma}_{_B} = \langle\sigma_{_B}\rangle &= \sigma_0 \left(\frac{V_0}{V}\right)^{\frac{1}{m}} \Gamma(1+1/m)[2(m+1)]^{1/m}\ , \\ var\,\sigma_{_B} &= \sigma_0^2 \left(\frac{V_0}{V}\right)^{\frac{2}{m}} \left\{\Gamma(1+2/m) - [\Gamma(1+1/m)]^2\right\} [2(m+1)]^{2/m}. \end{aligned} \tag{10.19}$$

Comparison with (10.16) shows that the dependence on the volume is still the same. However, the mean strength and the variance are larger in case of bending than under

uniform tension. If the quantities according to (10.16) are indicated by the subscript 'Z' one may write

$$\frac{\bar{\sigma}_B}{\bar{\sigma}_Z} = [2(m+1)]^{1/m} , \qquad \frac{var\,\sigma_B}{var\,\sigma_Z} = [2(m+1)]^{2/m} \tag{10.20}$$

from which, e.g., for $m = 5$ it follows that $\bar{\sigma}_B/\bar{\sigma}_Z = 1.64$.

10.3.3 Generalizations

The fracture concept according to Weibull can be generalized in various aspects. For instance, it may be extended to compressive stresses and multiaxial stress states. It is also possible to describe the actual defect structure by appropriate micromechanical models and thereby support the statistical concept. Furthermore, the Weibull concept can be applied to time-dependent fracture processes as they may occur in fiber-reinforced materials. In this case, c is represented instead of (10.13) by an approximation of the type $c = \alpha\, t^{\beta}$ where α and β depend on the stress σ and t denotes the time.

Here only one extension of the concept shall be discussed. It is based on the assumption that not already a single critical defect leads to failure but that a certain number $n > 1$ of critical defects is required. Thereby the observation is accounted for that often many defects (e.g., microcracks) grow before ultimate failure takes place. Starting point is the probability

$$P^*_{X=k} = \frac{1}{k!}\,(cV)^k\,\mathrm{e}^{-cV} \tag{10.21}$$

for the occurrence of exactly k independent critical defects in the volume V. It is called *Poisson distribution* and contains as a special case for $k = 0$ the probability (10.11) for the non-existence of a critical defect in V. The probability for the existence of less than n defects in V is obtained as the sum of the probabilities for the occurrence of 0 to $(n-1)$ defects:

$$P^*_{X<n-1} = \mathrm{e}^{-cV} \sum_{k=0}^{n-1} \frac{1}{k!}\,(cV)^k \, .$$

Therefore, the probability for the existence of n or more critical defects in V is

$$P_f = P_{X>n-1} = 1 - P^*_{X<n-1} = 1 - \mathrm{e}^{-cV} \sum_{k=0}^{n-1} \frac{1}{k!}\,(cV)^k \tag{10.22}$$

which hence is also the fracture probability. From the corresponding density $p_f = \mathrm{d}P_f/\mathrm{d}V = [c/(n-1)!](cV)^{n-1}\mathrm{e}^{-cV}$ one can recognize that this is a Gamma distribution (10.9). From (10.22) and by comparison with (10.12) one can further-

more see that the increase of the fracture probability with the volume is smaller that in case of the Weibull model and is slower for larger n. For instance, for $n = 3$ and $n = 10$ one obtains at $cV = 3$ the values $P_{f,3}(3) = 0.577$ and $P_{f,10}(3) = 0.001$, respectively, and at $cV = 10$ the values $P_{f,3}(10) = 0.997$ and $P_{f,10}(10) = 0.542$, respectively.

The dependence of the mean fracture stress on the volume and on the other parameters may be obtained using the approximation $cV_0 = (\sigma/\sigma_0)^n$ (see (10.13)) from (10.4) and (10.22):

$$\bar{\sigma} = \langle\sigma\rangle = \sigma_0 \left(\frac{V_0}{V}\right)^{\frac{1}{m}} \frac{\Gamma(n + 1/m)}{\Gamma(n)} \,. \tag{10.23}$$

The dependence on the volume is the same as in (10.16) or (10.19).

10.4 Probabilistic fracture mechanical analysis

The present section serves to explain in principle the procedure of a probabilistic fracture mechanical analysis. As an example we consider a plane component in which cracks of different size can be expected to occur in the course of loading. The component is subjected to uniaxial tension σ and the K-concept $K_I = K_{Ic}$ with $K_I = \sigma\sqrt{\pi a}\, G(a)$ is taken as the failure criterion where $G(a)$ is a geometry factor. We assume that at a certain instant the probability density $f_a(a)$ for the occurrence of different crack lengths is known from inspection. From this in conjunction with the above relations the probability density $f_{K_I}(K)$ for the stress intensity factors at a given loading σ can be determined. It is further assumed that the density distribution $f_{K_{Ic}}(K)$ for the fracture toughness of the material is also known from measurements. Both distributions are schematically depicted in Fig. 10.3.

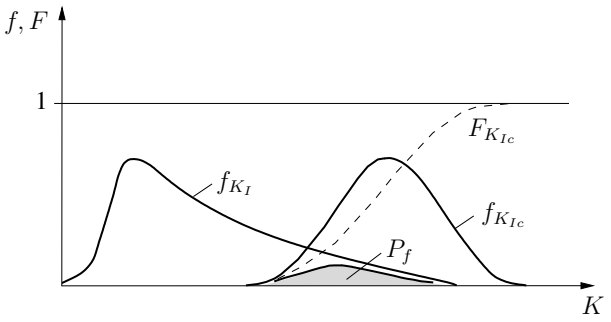

Fig. 10.3 Distributions of K_I and K_{Ic}

The probability that the fracture toughness is smaller than a certain value K is given by

$$P(K_{Ic} \le K) = F_{K_{Ic}}(K) = \int_0^K f_{K_{Ic}}(\bar{K})\,\mathrm{d}\bar{K}\ . \tag{10.24}$$

Correspondingly, $f_{K_I}(K)\,\mathrm{d}K$ is the probability for a crack-tip loading in the interval $K \le K_I \le K + \mathrm{d}K$. The product

$$\mathrm{d}P_f = F_{K_{Ic}}(K)\, f_{K_I}(K)\,\mathrm{d}K$$

then describes the probability that both applies, i.e., that the component fails. Integration over all possible levels of crack-tip loading finally yields the total failure probability:

$$P_f = \int_0^\infty F_{K_{Ic}}(K)\, f_{K_I}(K)\,\mathrm{d}K = \int_0^\infty \int_0^K f_{K_{Ic}}(\bar{K})\,\mathrm{d}\bar{K}\, f_{K_I}(K)\,\mathrm{d}K \tag{10.25}$$

It is represented by the shaded area in Fig. 10.3. When the distribution densities for the crack-tip loading and the fracture toughness change with time then P_f also changes. This may, for instance, take place when cracks grow in the course of cyclic loading or when the material undergoes aging.

The determination of the failure probability needs not be performed on the basis of stress intensity factors. Alternatively, one may directly start from the distribution density $f_a(a)$ of the crack lengths. Then the K_{Ic} distribution density has to be transformed into a density $f_{a_c}(a)$ of critical crack lengths. Another alternative approach consists in the direct determination of the failure probability

$$P_f = P(K_I \ge K \text{ and } K_{Ic} \le K) \quad \text{with} \quad 0 \le K < \infty \tag{10.26}$$

from *Monte-Carlo simulations*. Thereby randomly generated values for K_I and K_{Ic} are compared to each other and the number of events with $K_I \ge K_{Ic}$ divided by the total number of attempts yields P_f.

Finally, it should be mentioned that the probabilistic fracture mechanical analysis in real situations is often connected with difficulties. The main reason is the lack of data with regard to the exact distribution densities of crack lengths, loading or material parameters (e.g., K_{Ic}), as well as to their temporal evolution.

10.5 Further reading

Bazant, Z.P. and Planas, J. *Fracture and Size Effects in Concrete and Other Quasibrittle Materials*. CRC Press, Boca Raton, 1997

Broberg, K.B. *Cracks and Fracture*. Academic Press, London, 1999

Cotterell, B. and Mai, Y.-W. *Fracture Mechanics of Cementitious Materials*. Blackie Academic & Professional, 1996

Eggwertz, S. and Lind, N.C. (eds.) *Probabilistic Methods in the Mechanics of Solids and Structures*. Springer, Berlin, 1984

Krajcinovic, D. *Damage Mechanics*. Elsevier, Amsterdam, 1996

Liebowitz, H. (ed.) *Fracture – A Treatise*, Vol. 2, Chap. 6. Academic Press, London, 1968

Index

acoustic tensor, 316
adhesive bond, 97, 104, 128, 152
Airy's stress function, 162, 200
anisotropic damage, 303, 304
anisotropy, 15, 106, 136, 256, 262, 264, 266, 267, 291
anti-plane shear, 31, 64, 153, 209, 214
average – compliance, 256
– matrix strain, 250, 263
– matrix stress, 250, 263
– stiffness, 256
– strain energy density, 251, 283
– strain theorem, 252
– stress theorem, 252
averaging, 247

Barenblatt's model, 150
Betti's theorem, 30, 82
bimaterial – constant, 129
– crack, 128
blunt notch, 70
blunted crack tip, 116, 158
blunting line, 171
brittle – damage, 301, 304
– fracture, 2, 40, 56, 60, 64, 317
Broberg, 181
bulk modulus, 15, 243
–, effective, 256, 266, 269, 274, 279, 295, 296
Burgers vector, 54, 232

C*-integral, 186
C-integral, 186, 196
cavity, 53, 124, 243, 248, 305
center of dilatation, 231, 235, 239
channel crack, 103
circular hole, 244, 257, 259, 267, 272
Clapeyron's theorem, 30, 95
cleavage, 56
cluster, 57
COA, 176
cohesion, 43
cohesive – law, 151
– modulus, 151
– stress, 52, 106, 150
– zone model, 106, 150
compact tension specimen, 92
comparison material, 240
compatibility condition, 13, 31, 162, 199, 253
complementary – energy, 30, 168, 274, 306
– potential, 30
complex – method, 33, 75, 129
– stress intensity factor, 130
compliance, 99, 118, 192, 253, 255
– tensor, 15
composite material, 55, 103, 128, 151, 230, 254, 280, 293, 294, 297
composite-spheres model, 288, 279
configurational – force, 109, 137
– moment, 109
– stress tensor, 106
conservation – integral, 106
– law, 107
contact region, 130
contour integral, 110, 196
correspondence principle, 21
Cottrell, 145
Coulomb, 105
Coulomb-Mohr hypothesis, 43
crack, fatigue, 57
–, half-elliptical, 71
–, micro, 53
–, penny shaped, 71
–, stationary, 59
crack – arrest, 59, 207, 220, 222

D. Gross and T. Seelig, *Fracture Mechanics: With an Introduction to Micromechanics*, Mechanical Engineering Series, DOI 10.1007/978-3-642-19240-1,

– arrest toughness, 222
– branching, 207, 221
– closure, 70, 123
– coalescense, 89, 306
– deflection angle, 121–124, 135
– density parameter, 260, 304
– extension force, 96, 105, 117
– face, 63
– formation, 56, 95, 103
– front, 63
– growth, 59
– growth, stable, 116
– growth direction, 120
– growth rate, 126, 190, 191
– initiation, 59, 97, 116, 124, 125, 145, 165, 170, 185, 189, 190, 198, 207, 210
– interaction, 85
– length correction, 113
– length, effective, 114
– loading parameter, 73, 110, 195, 196, 199
– opening, 63, 70, 116, 129
– opening angle, 175, 181
– opening displacement, 146, 165, 187, 216
– opening mode, 63, 72
– opening profile, 162, 165
– orientation, 260
– propagation, 59, 94, 165, 171, 190
– resistance, 171
– resistance curve, 117, 307
– resistance force, 97, 105, 117
– speed, 207
– surface, 63
– tip, 1, 63
– tip field, 64, 91, 186, 195, 199, 209, 214
crack-tip – field, 67, 129, 139, 153, 176
– opening displacement, 145, 148, 181, 189
– speed, 201, 204, 215, 216, 219, 220
craze zone, 185
crazing, 55
creep, 21, 27, 59, 185
– compliance, 19
– crack growth, 59, 199
– damage, 301
– fracture, 60, 185
– function, 19, 186, 192
– strain, 21, 194, 203
– time, 192
- zone, 185, 197, 202, 204
criterion of maximum circumferential stress, 120
CT-specimen, 92, 167
CTOA, 175
CTOD, 145, 187
cyclic – loading, 59, 126, 145
– stress intensity factor, 127

damage, 229, 301
–, anisotropic, 303, 304
–, brittle, 301
–, creep, 301
–, ductile, 301
–, fatigue, 301
–, isotropic, 303, 310
– models, 310
– tensor, 304
– variable, 301
DCB specimen, 100, 119, 187, 189
defect, 1, 53, 229, 237, 244, 257, 262
– distribution, 246, 257, 259, 260, 264, 272
– energy, 237
– fraction, 57
– interaction, 263
– phase, 250, 256, 268
– strain, 255, 259, 263
deformation – plasticity, 23
– theory, 26, 145, 281
delamination, 99, 133, 152
deviatoric stress state, 9
dielectric – displacement, 136
– material constants, 136
differential scheme, 268
diffusion, 239
dilatational wave, 208
dilute distribution, 257, 262, 264, 268, 280
dimples, 57
discontinuity, 81
discrete phases, 249, 254, 256, 276
dislocation, 53, 80, 109, 229, 231, 232, 245, 280
displacement – jump, 80, 81, 241, 244, 304
– vector, 11
dissipation, 116, 221, 283, 284, 315
– rate, 22
distorsional – strain energy density, 18, 24
– wave, 208
dog bone model, 115
Drucker-Prager hypothesis, 46
ductile – damage, 301, 307
– fracture, 60
Dugdale model, 146, 166, 190
Duhamel-Neumann law, 17, 294
dynamic – crack growth, 59
– fracture toughness, 220
– loading, 207, 209, 226
– overshoot, 212
– stress intensity factor, 219

edge dislocation, 53, 81, 232

effective – bulk modulus, 269, 279, 295, 296
– coefficient of thermal expansion, 294
– compliance tensor, 253
– crack length, 114
– elastic constants, 251, 254
– elastic properties, 245
– elasticity tensor, 246, 251, 255, 266, 274, 278, 290, 294
– fracture surface energy, 61
– properties, 230, 245, 265, 268, 273, 276
– secant modulus, 292
– shear modulus, 267, 269, 279
– stiffness, 255, 267, 292
– strain, 18
– stress, 18, 303
– tangent tensor, 291
– viscosity, 230
– yield stress, 310
– Young's modulus, 267, 303, 307
eigenstrain, 133, 231, 233, 236, 238, 240, 250, 275, 289, 304
eigenstrain, equivalent, 240
eigenstress, 54, 231, 241, 283, 295
Einstein, 230
elastic – comparison problem, 281
– constants, 15
– potential, 28
– strain, 23, 159, 170, 195, 200, 281, 283, 303, 312
elastic-plastic – fracture, 145
– tangent tensor, 291
elastic-viscoelastic analogy, 21, 186
elasticity, 15
– law, 237, 251, 281, 289, 292
– tensor, 15, 31, 240, 246, 255, 258, 266, 268, 274, 278, 280, 282, 290, 294
elastodynamics, 208
electric enthalpy density, 137
electrical field, 136
electro-mechanical potential, 137
electrostriction, 136
ellipsoidal – inclusion, 234
– inhomogeneity, 242, 257
elliptic cylinder, 236
energy – balance, 27, 94, 100
– criterion, 97, 111, 120, 125, 126, 210
– dissipation, 116, 221
– flux, 27, 178, 217
– methods, 273
– principles, 27
– release, 94, 95
– release rate, 1, 96, 99, 125, 130, 140, 151, 208, 210, 217, 306
– release rate, incremental, 126
–, internal, 28
–, kinetic, 28
–, surface, 51
energy-momentum tensor, 106
equilibrium – condition, 10, 105, 173
– modulus, 187
equivalent – eigenstrain, 240, 243, 275, 289
– plastic strain, 47, 292
– strain, 18, 159, 198, 202
– strain principle, 303
– stress, 18, 24, 159, 292
Erdogan, 120
Eshelby tensor, 234
Eshelby's – result, 234, 241, 289
– stress tensor, 106
essential work of fracture, 181
expectation value, 318
exponential distribution, 319
extrusion, 57

failure – assessment curve, 149
– condition, 40, 149
– criterion, 125, 149
– hypotheses, 41
– probability, 326
– surface, 40
fast crack growth, 59
fatigue, 126
– crack, 57
– crack growth, 59, 126
– damage, 301
– fracture, 60
fault, 44
ferroelectric ceramics, 136
FGM, 247
fiber, 229
– matrix material, 128
– reinforced material, 256
finite fracture mechanics, 126
flow – potential, 22, 195
– rule, 25, 40, 48, 281, 289, 310
fluctuation, 125, 251, 263, 275, 294
Foreman, 127
fracture – concept, 188, 220, 312
– criterion, 73, 111, 119, 140, 146, 164, 171, 189, 203, 220, 307
– energy, 100, 104
– probability, 320
– stress, 323
– surface, 48, 57, 60, 101, 181, 221
– surface energy, 61, 101, 102, 118, 228
– surface roughness, 220
– toughness, 73, 92, 97, 116, 125, 135, 181, 192, 210, 220

– work, 106, 181, 182
fracture, brittle, 56, 60
–, ductile, 60
–, intercrystalline, 56
–, transcrystalline, 56
fragmentation, 227
functionally graded material, 247
fundamental solution, 76, 231, 254, 266, 273, 280, 290

Galilei, 2
gamma distribution, 320
Gaussian distribution, 319
general work theorem, 28, 253
generalized – force concept, 105
– forces, 108, 237
– moment, 109
Green's strain tensor, 12
Griffith, 2, 97, 151
Griffith's fracture criterion, 100, 102
Gurson – model, 288, 310
– yield condition, 310

half-elliptical crack, 71
hardening exponent, 159
Hashin-Shtrikman – bounds, 275
– variational principle, 275
heat flux, 28
Hencky's equations, 36, 156
Hencky-Ilyushin law, 26, 292
Hill-condition, 251, 274, 276
hollow sphere, 288
homogenization, 229
Hooke's law, 15
HRR-field, 159, 172, 195, 199
Hui-Riedel field, 199, 202
Hutchinson, 161
hybrid criterion, 126
hydrostatic – loading, 287, 310
– stress, 239, 243, 295, 309, 310
– stress state, 9

impact loading, 212, 225
imperfection, 53
inclusion, 53, 231, 233
–, ellipsoidal , 234
–, spherical, 235, 277
incompressible material, 18, 22, 258, 309
incremental – energy release rate, 126
– plasticity, 23
– theory, 25, 281, 291
inertia forces, 11, 207
infinitesimal strain tensor, 12
influence tensor, 243, 253, 255, 257, 263, 265, 281, 285, 289, 294
inhomogeneity, 233, 240
–, ellipsoidal, 242
–, spherical, 243, 258, 264, 266, 279, 289, 292, 295, 296
initiation time, 189, 191, 199
intrusion, 57
instantaneous – compliance, 192
– fracture toughness, 192
– modulus, 187
integral equation, 80
interaction energy, 238
intercrystalline fracture, 56
interface, 152
– crack, 98, 128
internal energy, 28, 102
intersonic crack propagation, 223
interstitial atom, 53, 231, 239
invariants of – strain tensor, 13
– stress deviator, 9
– stress tensor, 8
Irwin, 2, 73, 113, 149, 155
Irwin's crack length correction, 113
isotropic – damage, 303, 310
– hardening, 23, 24
isotropy, 15
–, transverse, 16

J-controlled crack growth, 171
J-integral, 106, 110, 131, 137, 145, 147, 151, 178, 186, 196, 211
J-integral vector, 108
J-resistance curve, 171

K-concept, 2, 72, 97, 125, 127, 128, 145, 149, 150, 164, 209, 220
K-factor, 66, 73, 186, 208
Kachanov, 85, 302
kinematic hardening, 23, 286
kinetic energy, 28, 210, 218
kink model, 122
Kolosov's formulas, 33, 75
Kröner, 230

Lamé constants, 15
Laplace transform, 20, 186
large scale – creep, 197
– yielding, 145, 181
Leguillon, 125
length scale, 2, 229, 245, 301
Lennard-Jones potential, 53
limit – load, 148, 149, 157
– speed, 207

line defect, 232
linear standard material, 187
load cycle, 126
localization, 57, 64, 305, 312
logarithmic – distribution, 319
– singularity, 177
– strain singularity, 180
lognormal distribution, 319
longitudinal – shear, 31, 64, 66, 138
– wave, 208

macro – strain, 247, 281
– stress, 247
macroscopic – level, 229, 245, 267
– material behavior, 230
– plastic strain, 282, 312
– strain, 301, 314
– stress, 301, 310, 311, 314
– yield condition, 284
– yield surface, 285
material force, 109, 237
matrix – material, 233, 303
– properties, 265
– strain, 250, 263
– stress, 250, 263
maximum shear stress, 9, 25, 33, 35, 71, 116, 157
Maxwell, 230
– model, 194
McClintock model, 308
mesoscale, 53
method of weight function, 82
micro – crack, 53, 56, 185, 221, 229, 301
– structure, 53
– to-macro transition, 230
– scale, 53, 229
– -scopic field, 247
– level, 229, 237, 245, 246, 251, 267, 280, 281, 284, 286
– structure, 1, 229, 245, 305
– void, 301
Mises – stress, 24
– yield condition, 25, 35, 115, 287, 310
– yield criterion, 24
mixed-mode loading, 73, 119, 134, 220, 226
Mohr's – circles, 9, 32, 43, 157
– failure hypothesis, 45
Monte-Carlo simulation, 326
Mori-Tanaka model, 262, 278, 289
multi-specimen technique, 168

natural strain increment, 14
Navier-Lamé equations, 208
near field, 67, 120
necking, 116, 182
nonlinear elastic material, 18
normal – distribution, 319
– fault, 45
– stress dominated fracture, 48, 60
normality rule, 25
Norton's creep law, 21, 194
notch, 70, 90, 124

octahedral – shear stress, 24, 46
– stresses, 9
opening mode, 141
orthotropy, 16
oscillating singularity, 129

Paris, 173
– law, 127
particle-matrix composite, 152
path – dependence, 196
– independence, 111, 131, 160, 180
– independent integral, 109
peel test, 104
penny-shaped crack, 71, 150, 212, 244, 261
percolation, 57, 267
– limit, 58
– threshold, 58
perfect plasticity, 145
perfectly – plastic, 23–26, 284, 286, 308
– plastic material, 35, 153, 309
Petroski-Achenbach approach, 84
phase – angle, 130
– average, 249, 254, 290, 293
– transformation, 110
piezoelectric – effect, 136
– material, 136
– material constants, 136
plane strain, 31, 35, 66, 155, 202, 208, 223, 235, 308
plane stress, 24, 31, 41, 61, 66, 146, 149, 164, 182, 187, 190, 199, 201, 209, 225, 244, 259, 264, 272
plastic – collapse, 148
– incompressibility, 23
– limit load, 149, 157
– macrostrain, 282
– strain, 23, 26, 47, 60, 159, 165, 233, 281, 289, 310
– strain, equivalent, 47
– strain increment, 23
– strain rate, 309
– tangent modulus, 26
– zone, 73, 115, 146, 190
– zone size, 113
plasticity, 13, 22, 48, 280, 303

–, deformation, 23
–, incremental, 23
point defect, 231
Poisson distribution, 324
Poisson's ratio, 15, 234, 245, 258
polarization, 136, 241
polymer, 54, 185
porosity, 280, 287, 304
potential – energy, 29, 273
–, Lennard-Jones, 53
power law, 19, 159, 192
Prandtl's creep law, 21
Prandtl-field, 156, 177
Prandtl-Reuss law, 26, 291
primary creep, 194
principal – strain hypothesis, 42
– strains, 13
– stress hypothesis, 41
– stresses, 8, 33, 71
principle of – maximum plastic work, 25
– minimum complementary energy, 30, 274
– minimum potential energy, 29, 273
– virtual complementary work, 29
– virtual displacements, 29, 105
– virtual forces, 29
– virtual work, 28
probabilistic fracture analysis, 325
probability – density, 318
– distribution, 318
process zone, 64, 73, 101, 106, 145, 150, 164, 178, 185, 189, 207, 217, 220, 247
proportional loading, 27, 161, 172, 292

R-curve, 117, 171
Ramberg-Osgood law, 159, 177
Rayleigh, 230
– function, 209
– wave, 209
– wave speed, 216, 219
reciprocity relation, 31
reference – configuration, 83
– displacement, 84
– load, 84
relaxation, 185
– function, 19, 186
– time, 187
representative volume element, 245, 301
residual – strain, 304
– stress, 283
resistance curve, 117
retardation time, 187
Reuss – approximation, 255, 273
– bound, 273, 275, 279
reverse fault, 45
Reynold's transport theorem, 179, 218
Rice, 145, 161, 168, 309
Rosengren, 161
rule of mixture, 256
RVE, 245, 301

S-criterion, 121
screw dislocation, 53, 232
secant modulus, 292
secondary creep, 194
self – consistency, 84, 87, 265
– consistent method, 265, 268, 269, 279, 289
– energy, 238
separation, 51, 56, 63, 73, 95, 127, 150, 172, 180, 216, 220, 301
– law, 106
– work, 151
shear – band, 306, 316
– dominated fracture, 48, 60
– lips, 60
– modulus, 15, 186
– modulus, effective, 256, 266, 267, 269, 274, 279
– modulus, secant, 292
– stress, maximum, 9
– wave, 208
Sih, 120, 122
singularity, 66, 69, 75, 109, 125, 139, 141, 146, 154, 157, 159, 215, 222
– logarithmic, 177, 180
– oscillating, 129
size – condition, 93, 114, 190, 246
– effect, 125
slip, 54
– band, 54, 57
– line field, 154, 177
– line fields, 35
– line theory, 35, 155
small – scale creep, 185, 194, 202
– scale yielding, 113, 127, 148, 190, 191
– signal range, 136
softening, 312
spherical – inclusion, 235, 277
– inhomogeneity, 243, 258, 264, 266, 279, 289, 292, 295, 296
– particle, 230
stable crack growth, 59, 116, 173
standard deviation, 319
stationary crack, 59, 165, 172, 176, 177, 195, 200, 209, 215, 219, 225
statistically homogeneous, 246, 320
steady-state – conditions, 175, 176, 194, 199, 202, 219, 223
– crack growth, 175, 176, 224

strain, 11
–, creep, 21, 194, 203
– deviator, 13
–, effective, 18
–, elastic, 23, 159, 170, 195, 200, 281, 283, 303, 312
– energy, 102, 103, 108, 129, 167, 218, 274
– energy density, 17, 28, 42, 106, 121, 137, 160, 178, 218, 251, 283
– energy density, distorsional, 18
– energy density, volumetric, 18
– energy hypothesis, 42
– energy rate density, 22
–, equivalent, 18, 159, 198, 202
– localization, 312
–, macroscopic, 247, 301, 314
–, plastic, 23, 26, 47, 60, 159, 165, 233, 281, 289, 310
–, principal, 13
– rate, 13, 177, 194, 207, 227, 291, 308, 315
– rate, plastic, 309, 310
– singularity, 154, 161, 177
– tensor, 11
– tensor, Green's, 12
– tensor, infinitesimal, 12
– theory, total, 23
–, thermal, 142, 294
–, volumetric, 13
–, thermal, 16
strength – hypothesis, 39
–, theoretical, 52
stress, 5
– concentration factor, 90
– concentrator, 124
–, deviatoric, 9
–, effective, 18, 303
–, equivalent, 18, 24, 159, 292, 310
– intensity factor, 66, 68, 139, 186, 210, 211
– intensity factor, cyclic, 127
– intensity factor, dynamic, 216
– intensity factor, complex, 130
–, macroscopic, 247, 301, 310, 311, 314
–, octahedral, 9
– polarization, 241, 275
–, principal, 8
– singularity, 161, 215
– state, hydrostatic, 9
– tensor, 7
–, ultimate, 40
– vector, 5
– vector, effective, 303
–, von Mises, 24
– wave, 212, 226
strike-slip fault, 45
subcritical crack growth, 59
substrate, 98, 103, 134, 142
summation convention, 6
superposition, 74, 86, 147, 227
surface – energy, 51, 61, 100, 102, 104, 227
– wave, 209

T-stress, 68, 123, 157
tearing modulus, 173
tension cut-off, 45
tertiary creep, 194
theoretical strength, 51
thermal – expansion coefficient, 17, 142, 236, 294
– strain, 16, 142, 294
thermally induced eigenstress, 296
thermoelastic material, 294
thin layer, 98, 103, 134, 142
time of failure, 189
total – potential, 29, 99, 104, 118, 237, 274
– strain theory, 23, 26, 145, 159, 292
Tracey, 309
transcrystalline fracture, 56
transformation – relation, 8, 32
– strain, 233, 294
transition temperature, 60
transmission factor, 85
transversal wave, 208
transverse isotropy, 16, 136, 262, 272
Tresca's yield condition, 25, 26, 113, 115, 146
two-parameter criterion, 126

ultimate stress, 40
unit cell, 247
unstable crack growth, 59, 190, 207, 217

V-notch, 69, 70, 125
vacancy, 53
van der Waals forces, 53, 55
virtual – complementary work, 30
– crack advance, 105, 210
– displacement, 29
– work, 29
– work principle, 28
viscoelasticity, 19, 185
void, 54, 127, 229, 230, 243, 266, 280, 301, 304, 317
– coalescence, 57, 229, 301, 307, 311
– formation, 55, 151
– growth, 127, 157, 158, 164, 185, 189, 307, 310, 312
– growth rate, 308, 309
– nucleation, 311
– size, 288

– surface, 288
– volume, 203
– volume fraction, 57, 267
Voigt – approximation, 255, 273
– bound, 273, 275, 279, 280
volume fraction, 249, 257, 264, 279, 290, 304, 311
volumetric – average, 247
– strain, 13
– strain energy density, 18

wave – equation, 208
– speed, 208
weakest link theory, 321
Weibull, 2, 318, 324
– distribution, 319, 322
– modulus, 322
Weibull's fracture concept, 320
weight function, 83
weighted average, 254, 282
Wells, 145
Westergaard's function, 35
work of separation, 151

yield – condition, 35, 153, 280, 288
– criterion, 23, 24
–, Gurson, 310
–, macroscopic, 284
–, von Mises, 25, 26, 287, 289, 310
–, Tresca's, 25
– strength, 40, 93
– stress, effective, 310
– strip, 146, 150
– surface, 23, 49
– surface, macroscopic, 285
Yoffe, 217
Young's modulus, 15, 245, 303
–, effective, 267, 303, 307